Artificial multicellular assemblies

Dynamics of spatially organized gene circuits

Aurore Dupin

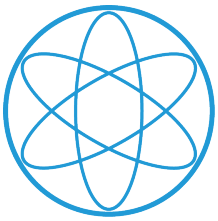

TECHNISCHE UNIVERSITÄT MÜNCHEN
FAKULTÄT FÜR PHYSIK
PHYSIK SYNTHETISCHER BIOSYSTEME – E14

Artificial multicellular assemblies

Complex dynamics in spatially organized gene circuits

Aurore Dupin

Vollständiger Abdruck der von der Fakultät für Physik der Technischen Universität München zur Erlangung des akademischen Grades eines

Doktors der Naturwissenschaften (rer. nat.)

genehmigten Dissertation.

Vorsitzende(r): Prof. Dr. Martin Zacharias

Prüfer der Dissertation:

1. Prof. Dr. Friedrich Simmel
2. Prof. Dr. Ulrich Gerland

Die Dissertation wurde am 13.08.2019 bei der Technischen Universität München eingereicht und durch die Fakultät für Physik am 09.10.2019 angenommen.

Contents

Abstract

From molecules forming cells to cells forming organisms, the interaction of parts in spatially organized environments allows for complex dynamics and functions to emerge. In synthetic biology, the field of artificial cells has so far only managed to reproduce unicellular organism-like systems. The hypothesis of this thesis is that spatial organization and specific interactions between artificial cells would allow complex dynamics to be actuated from gene circuits. Therefore, this thesis studies the assembly of artificial cells into multicellular systems with directed communication, and the implementation of synthetic gene circuits in them. Water-in-oil droplets are brought into two-dimensional structures of controlled geometries and where the droplets share direct interfaces. Diffusion of small chemicals through those interfaces is characterized, and the diffusion kinetics are shown to be tunable. Synthetic gene circuits placed in assemblies with dedicated signal droplets show non-trivial behaviour, including signal propagation and differentiation mimicking two embryogenesis models. Inducible signal-expression modules are developed and characterized. Thorough characterisation of building blocks and design rules for synthetic gene circuits is conducted. This thesis demonstrates the first assembly of artificial multicellular assemblies capable of spatially-resolved gene dynamics.

Zusammenfassung

Sowie aus Molekülen Zellen geformt werden und Zellen sich zu Organismen zusammenschliessen, so erlaubt der räumlich organisierte Zusammenschluss von vielen einfachen Teilen die Entstehung von komplexen Funktionen und Dynamiken. In der synthetischen Biologie ist es im Bereich der künstlichen Zellen bisher nur gelungen, einzellige, dem Organismus ähnliche Systeme zu reproduzieren. In dieser Arbeit soll die folgende Hypothese geprüft werden: durch die räumliche Anordnungen von künstlichen Zellen und mit spezifischen Interaktionen zwischen den künstlichen Zellen, können komplexe Dynamiken von genetischen Schaltkreisen ermöglicht werden. Die Arbeit befasst sich mit dem Zusammenfügen von künstlichen Zellen zu vielzelligen Systemen, der direkten Kommunikation zwischen den Zellen und mit der Implementierung von genetischen Schaltkreisen in den Zellen. Zellen bestehend aus Wasser-in-öl Tröpfchen wurden in kontrollierter Geometrie zu zweidimensionalen Strukturen zusammengebracht, wobei die Tröpfchen direkte Schnittstellen teilen. Die Diffusion von kleinen Molekülen über die Kontaktfläche von benachbarten Tröpfchen wurde charakterisiert und es wurde gezeigt, dass die Kinetik der Diffusion regelbar ist. Es wurde demonstriert, dass synthetische genetische Schaltkreise in einem Verbund von künstlichen Zellen nicht triviales Verhalten an den Tag legen können, was zum Beispiel für die Signalausbreitung oder Differenzierung von Zellen nützlich sein kann. Somit werden Mechanismen aus der Embryoalentwicklung in dem Verbund künstlicher Zellen nachgeahmt. Zudem wurden Module entwickelt und charakterisiert, die Signalmoleküle für genetische Schaltkreise exprimieren können. Es wurden weitere Bausteine und Designregeln für synthetische genetische Schaltkreise getestet und charakterisiert. In dieser Arbeit wurde das erste Mal ein mehrzelliges künstliches System zusammengebaut, welches es ermöglicht räumlich-aufgelöste Dynamik von genetischen Schaltkreisen zu studieren.

1 Introduction: Spatially organizing artificial cells

Artificial cells are being developed that can perform increasingly complex biological computation and serve as interfaces or study-platforms to better understand natural cells. One approach to synthetic biology is to design artificial cells from the bottom up, using building blocks from living cells and mimicking their organisation. However, living cells that inspire synthetic biologists today are the result of billions of years of evolution, and layers of complexity inherited from this evolution process must be shed off. Scientists therefore find themselves in the conundrum of reconstituting very simple cellular structures, mimicking what simple primordial cells may have resembled, in a bottom-up approach using tools that are complex, evolved, and whose functions are only partially understood.

Artificial cells have therefore been assembled, typically consisting of a simple membrane encapsulating a few biochemical reactions. The next frontier for this field of research is to engineer increasing complexity in artificial cells, either by adding complexity in the encapsulated reactions or by bringing simple artificial cells into larger assemblies capable of complex dynamics. The research conducted in this thesis is motivated by the idea that specific interactions between simple entities can allow for complex functionality to emerge. Indeed, when living cells are coordinated in multicellular organisms, they can demonstrate more complex behaviour than single cells. The aim of this thesis is to explore the implementation of multicellularity in artificial cells and the potentiality for complex dynamics to emerge in such systems.

The goal to assemble artificial multicellular assemblies (AMA) is motivated by two aspects. On the one hand, artificially-generated spatial dynamics are an investigation method into the spatial behaviours found at all scales in living systems, and might allow their control by synthetic means. On the other hand, compartmentalization of synthetic circuits provides modularity and programmability in artificial cells. Compartmentalization allows colocalizing or separating components and processes based on their mutual activation or toxicity, limiting diffusion of large species, and constraining communication to controllable diffusion paths. Establishing spatiotemporal patterns in multi-compartment structures allows mimicking the biological organisation of multicellu-

lar organisms, and therefore is a novel and promising platform to study spatial phenomena relating to embryo-development, structural organization of tissues or the emergence of multicellularity.

So far, patterns from gene circuits have been established in continuous, non compartmentalized environments on the one hand, and on the other hand gene circuits have been compartmentalized without considering their spatial organization or behaviour. This thesis is the first study of the response of compartmentalized and spatially organized gene circuits.

An appropriate method to generate spatially organized artificial cells should therefore allow for interesting spatial dynamics to emerge while retaining localization of most components in their compartment. I will first present reaction-diffusion circuits and their relevance to biology (Chapter 1.1). To address the current state of research in spatially resolved synthetic gene circuits, I will then review circuits with spatial dynamics that function in continuous, non-compartmentalized environments (Chapter 1.2). This will be followed by a review of compartmentalized gene circuits studies that do not address spatial behaviour (Chapter 1.3). So far, very little work has been conducted at the intersection of compartmentalization and spatial dynamics, and our work innovates by bringing the two fields of synthetic biology together. I will address studies where spatial patterns are created by genetically engineered cells, where the cells constitute the relevant compartments limiting diffusion (Chapter 1.4). I will then review artificial compartments assembling methods that would allow us to study spatial dynamics in AMA, and argue for the method we used, the droplet-interface-bilayer DIB method (Chapter 1.5). Finally, having defined the goals and the scope of this thesis, I will detail how the following chapters address the different aspects of creating spatially organized compartmentalized gene circuits with spatiotemporal dynamics (Chapter 1.6).

1.1 Reaction-diffusion systems

Reaction-diffusion systems are the basis for most spatial dynamic processes in biological organisms, such as pattern formation. They allow assemblies of cells, be it tissues or entire organisms, to achieve signalling, differentiation, and a myriad of other fundamental processes in multicellular organisms. This section presents the fundamental equations of reaction-diffusion (RD) systems (Chapter 1.1.1) but does not discuss analytical solutions to the equations, as this has been done in greater detail elsewhere (for example see [1]). The specific mathematical models used to describe the behaviour of the molecular circuits used in this thesis are presented in the corresponding chapters (Chapters 3 and 4 and Appendix A.2). This chapter discusses various RD systems relevant to patterning and signalling, and the two predominant theories for pattern formation in embryogenesis are discussed (Turing's theory is presented in Chapter 1.1.2

and compared with Wolpert's theory in Chapter 1.1.3).

1.1.1 General reaction-diffusion considerations

Reaction-diffusion systems, containing species i of concentrations u_i, are governed by dynamics described by:

$$\frac{\delta \vec{u}}{\delta t} = D\vec{\nabla}^2\vec{u} + \vec{r}(\vec{u}) \tag{1.1}$$

, where $\vec{u}$ is the vector of concentrations u_i, D is the matrix of diffusion coefficients, and $\vec{r}(\vec{u})$ is a function representing the reactions that affect species i.

The diffusion coefficient for species i can depend on the spatial direction when diffusion is non-homogeneous, and in some cases can also depend on the concentration of the species u_i (as was for example demonstrated for the apparent diffusion coefficient of 3OC6-HSL by Schwarz-Schilling *et al.* [2]). In the context of our multicellular assemblies, we nonetheless assume diffusion coefficients to not be concentration dependent, and to be homogeneous in space inside the droplets. However, we consider diffusion in our system as a two-step process, consisting of diffusion through the aqueous compartments and the permeation of the lipid bilayer interfaces (this is addressed in more details in Chapter 2.3.2). The diffusion flux $\vec{j_D}$ generated by a concentration gradient is given by Fick's law:

$$\vec{j_D} = -D\vec{\nabla}n \tag{1.2}$$

, where $\vec{\nabla}n$ is the gradient of the density of molecules. The permeation flux j_P across a membrane of thickness L is given by:

$$j_P = -P\Delta n \tag{1.3}$$

with P the permeability of the membrane and Δn the molecule density difference across the membrane. An equivalent diffusion coefficient across the membrane can be given by:

$$D_M = PL \tag{1.4}$$

but permeability will be primarily used in the following chapters.

For simplicity, the signal diffusion in linear arrangements of droplets was modelled in 1D (along the long axis of the assembly), for example in the case of the 3-droplets assemblies for characterization of signal diffusion kinetics (Chapter 2.3.2). However, for some molecules, particularly those where diffusion was limited by the aqueous diffusion step, the RD process in the droplet assemblies could not be reliably simulated with a 1D, 2D or 3D diffusion model (see Dupin and Simmel, 2018 [3], pulse model).

For the reactions term, we assume elementary reactions with a one-step mechanism when possible and apply the law of mass action. That is, for a reaction of the type:

$$\sum_i a_i A_i \underset{k_{off}}{\overset{k_{on}}{\rightleftharpoons}} \sum_i b_i B_i \tag{1.5}$$

, the rates can be equated to:

$$r_{on} = k_{on} \prod_i {A_i}^{a_i} \tag{1.6}$$

$$r_{off} = k_{off} \prod_i {B_i}^{b_i} \tag{1.7}$$

, and the equilibrium constant of Equation 1.5 is

$$K = \frac{k_{on}}{k_{off}} = \prod_i \frac{{B_i}^{b_i}}{{A_i}^{a_i}} \tag{1.8}$$

When necessary, we calculated apparent rates by splitting a reaction into its singular elementary steps and estimating the rates for each of these steps (see Chapter 3.2 for example). For more complex reactions such as transcription-translation, simplified models that have been shown to accurately predict kinetics were used (see Appendix A.1 for equations). In all cases, kinetic rates were fitted from experiments whenever possible.

1.1.2 Turing's symmetry-breaking RD systems

Alan Turing made one of the most significant contributions to the field of reaction-diffusion systems in a paper published in 1952, titled "The Chemical Basis of Morphogenesis" [4]. He posited that systems could be driven out of their chemical equilibrium by random disturbances amplified by diffusion and reactions. Such systems can then demonstrate stationary or dynamic patterns based on the diffusion and reaction kinetics. As Turing suggests and as was later demonstrated, such symmetric-breaking dynamics are at play in the development of embryos and in many other biological phenomena.

To intuitively understand how such systems can spontaneously diverge from equilibrium, a two cells, two chemicals system was presented by Turing as follows: the two chemicals X and Y are present in two cells between which diffusion occurs, with concentrations (X_1, Y_1) and (X_2, Y_2). The RD rate equations of the system are taken as follows (Figure 1.1.a), with D_X = 0.06 and D_Y = 0.18 the diffusion rates of the chemi-

cals:

$$\frac{dX_1}{dt} = 5X_1 - 6Y_1 + 1 + D_X(X_2 - X_1) \tag{1.9}$$

$$\frac{dY_1}{dt} = 6X_1 - 7Y_1 + 1 + D_Y(Y_2 - Y_1) \tag{1.10}$$

$$\frac{dX_2}{dt} = 5X_2 - 6Y_2 + 1 + D_X(X_1 - X_1) \tag{1.11}$$

$$\frac{dY_2}{dt} = 6X_2 - 7Y_2 + 1 + D_Y(Y_1 - Y_2) \tag{1.12}$$

If the system is initially at equilibrium, for example all concentrations are $X_1 = Y_1 = X_2 = Y_2 = 1$, it will remain there (Figure 1.1.b). However, if a small perturbation occurs so that $X_1 = 1+\epsilon$, $X_2 = 1-\epsilon$, $Y_1 = 1+3\epsilon$, $Y_2 = 1-3\epsilon$, the RD rate equations will drive the system out of equilibrium (eventually, this specific system will return to chemical equilibrium, but this is not generally the case for the RD systems considered by Turing) (Figure 1.1.e). When only reactions (Figure 1.1.c) or only diffusion (Figure 1.1.d) occur, the system will react to noise by quickly converging to equilibrium.

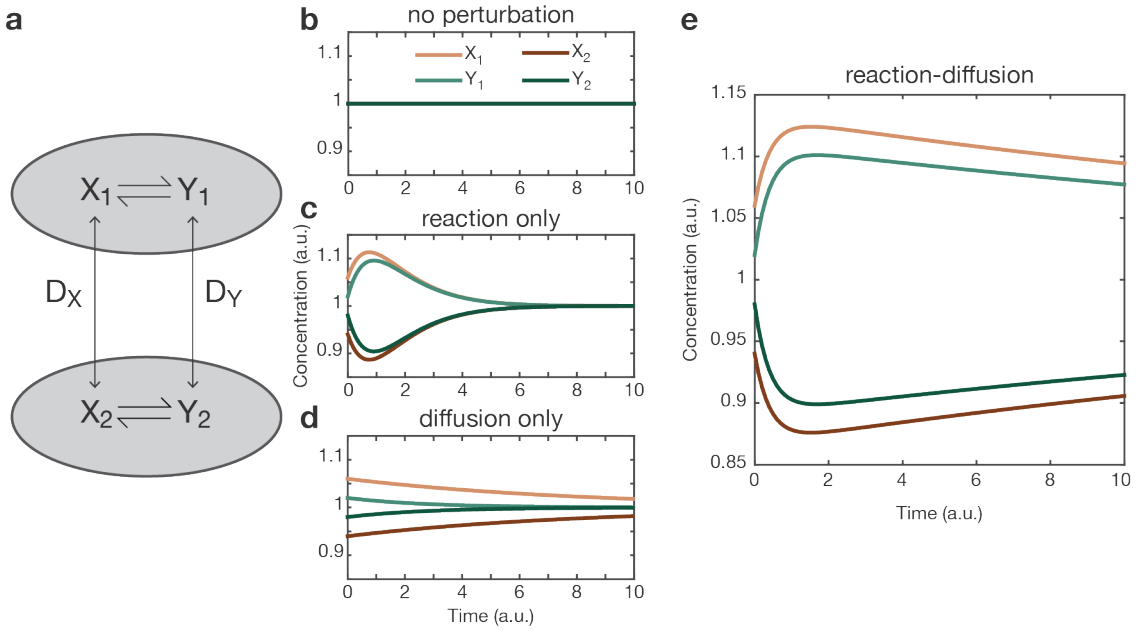

Figure 1.1. Turing's reaction-diffusion model of instabilities. **a**, the toy-model consists of two cells, 1 and 2, with two chemicals X and Y. In each cell X and Y react together, and each chemical can diffuse between the two cells. **b**, in the absence of perturbations, the system remains in chemical equilibrium. **c**, when only reactions occur in each cell but no diffusion occurs between the cells, an initial perturbation is shortly amplified before the system returns to equilibrium. **d**, when only diffusion occurs, an initial perturbation immediately leads the system to return to equilibrium. **e**, when both reaction and diffusion are present, a small perturbation is amplified for longer times than in the pure reaction case and the system takes longer to return to chemical equilibrium.

This toy-model provides a simple-to-check example of how combined reaction and diffusion circuits can lead to the emergence of non-trivial dynamics. Turing presented

an analysis of RD systems and classified their outcome into one homogeneous and five inhomogeneous (dynamically or stationary) equilibrium states. The outcome of RD systems into either one of these states depends on rate parameters and the geometry of the system. The existence of most of these states as a result of RD dynamics has been demonstrated to exist in biological organisms (as reviewed in more detail in [5]). The six states can be described as:

- (1) uniform stationary state,
- (2) uniform oscillatory state (found in circadian rhythms [6]),
- (3) stationary waves with short wavelength (typically seen when differentiating cells inhibit neighbours from differentiating, as in the *Drosophila* neurogenesis [7], we explored this class of reaction-diffusion system in Chapter 3.3),
- (4) oscillatory waves with short wavelength (to date not demonstrated in living organisms),
- (5) oscillatory waves with finite wavelength, *i.e.* traveling waves (of which calcium ion waves are one example [8], and which we explored in Chapter 3.2), and
- (6) stationary waves with finite wavelength, which have received the most attention and are commonly referred to as "Turing patterns" (such systems direct the formation of many surface patterns found in mature organisms, such as stripes on zebrafish [9], but are also believed to be involved in developmental mechanisms, such as the left-right asymmetry development in vertebrates [10]).

Mathematically speaking, only few of such RD systems can be solved analytically (when the number of components and dynamics are extremely simple), and in most cases, numerical methods are used to simulate the system's behaviour, as was done in this thesis.

1.1.3 Two classes of embryogenesis RD systems

Patterns in embryogenesis are believed to be formed by one of two mechanisms: Turing RD systems (described above, Figure 1.2.a) and pre-patterned gradients, a theory developed by Wolpert in the late 1960s [11] (Figure 1.2.b). According to this theory, a morphogen gradient imposed by a pre-existing asymmetry in the system provides positional information for the cells placed in it. That is, the morphogen levels in each point in space are interpreted by the cells through activation thresholds. Gene networks in the cells convert this positional information into a pattern that leads to large-scale organization and differentiation of the organism or of its tissues. As the pattern does not emerge spontaneously but following a pre-pattern, this process is believed to render

pattern formation more reliable and robust to biological noise such as embryo size.

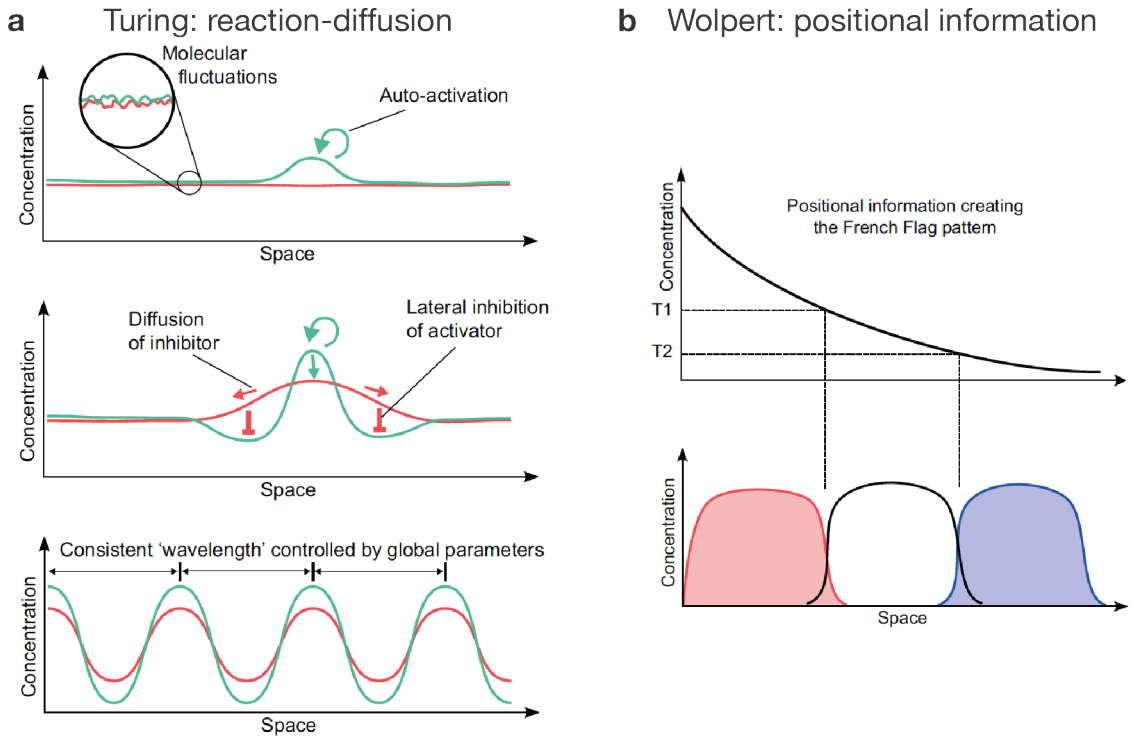

Figure 1.2. Two models of differentiation in embryogenesis. **a**, In the Turing model, perturbations of a chemical equilibrium are amplified through reaction-diffusion networks to form stable differentiated patterns. Lateral diffusion of components is crucial. **b**, in the Wolpert model, a pre-patterned gradient is read locally and induces spatial differentiation along the gradient. Lateral diffusion of components does not occur, as the pre-pattern provides all the information for differentiation. T1 and T2 correspond to two thresholds in the response of the genes to the morphogen concentration. Figure adapted with permission from [15].

Crick demonstrated in 1970 that a pre-existing gradient could reasonably be established by morphogen diffusion from a constant source [12]. Originally, the positional information theory considered that the morphogen gradient was static and other species did not diffuse in the system, although elucidation of specific pre-patterning mechanisms later demonstrated that the morphogen gradient is dynamic, and need only be stable for limited periods of time to induce the appropriate patterning [13]. The two archetypical examples of positional information pre-patterning are the development of the neural tube in vertebrates and of the *Drosophila* blastoderm [14]. We explored the implementation of a chemical gradient determining positional information and the response it induced in a gene circuit encapsulated in droplet assemblies in Chapter 3.4.

The theory of positional information for pattern formation was the dominant one in the second half of the 20th century, and Turing's theory was discarded for a variety of reasons, the most relevant one being that it was not believed to produce robust patterning that would lead to similar morphogenesis despite variations in size, protein expression levels, etc. The two mechanisms of patterning are visually exemplified in Figure

1.2. RD and positional information were considered to be incompatible mechanisms for pattern formation, as the first describes spontaneous symmetry-breaking from random fluctuations with component diffusion, and the second describes pre-existing symmetry breaking from a non-diffusing gradient.

However, since a few decades Turing patterns have seen revived interest in biology, as this mechanism has been demonstrated to play a crucial role in many developmental processes. New theories suggest that RD and positional information mechanisms are not mutually exclusive: positional information has been discussed to be a class of RD systems [5], and models for the interplay of the two mechanisms in major developmental processes have been presented [15]. To give two examples, in a combined Wolpert/Turing model, local diffusion of proteins in a morphogen gradient has been suggested to improve both the precision and robustness of a pattern [16]; and morphogen gradients can be established from a RD process which then imposes positional information, for example in the left-right asymmetry breaking process in vertebrates [15].

These developmental mechanisms demonstrate how critical reaction-diffusion systems are in multicellular organisms, where they control tissue-wide behaviour and the organization of complex structures and functions. The implementation of such RD systems in AMA would expand the complexity of dynamics that can be realized with synthetic gene circuits and artificial cells.

1.2 Spatial dynamics in continuous environments

The wavelength of patterns formed by RD systems will depend on the reaction and diffusion rates. In continuous environments, the designed gene circuits can create patterns in large length scales (µm to mm) due to a high local production rate of the patterning molecule and comparatively low diffusion coefficient. Complex dynamics often emerge from a signal diffusing from a localized source and inducing a downstream circuit, while other components are homogeneously distributed. Slowing down of diffusion rates through compartmentalization to achieve the expected dynamics and pattern lengthscale is therefore unnecessary.

Two independent studies have engineered front propagation dynamics from an autocatalytic reaction: using the autocatalytic polymerization of a short single-stranded DNA (ssDNA) in a DNA/enzymes purified environment (Zadorin *et al.* [17]), or using the autocatalytic synthesis of a transcription factor in an *in vitro* transcription-translation (IVTT) environment (Tayar *et al.* [18]). In the work from Zadorin *et al.* [17], all components (DNA template and polymerases) were homogeneously distributed in the 1D experimental chamber, and a DNA activator strand was then pipetted at one end of the chamber, inducing a propagating wave (Figure 1.3.a). Interestingly, the diffusion rate of

this species could be tuned by approximately 2-fold by having it transiently bind a complementary strand of adjustable molecular weight, and this in turn affected the velocity of the propagating wave. This system only relied on the diffusion of the single-stranded DNA activator, which was both the signal and the read-out, while the concentration of other components remained identical across the chamber, and therefore no localization of components was necessary. In the work from Tayar *et al.* [18], DNA genes were localized on the surface of microfabricated compartments between which diffusion was controlled by the dimensions of side communicating channels (Figure 1.3.b). The protein activator, constantly produced on the one end of the line of compartments, and the read-out protein, green fluorescent protein (GFP), were freely diffusing. However, their production was highly localized around the dense surface-bound DNA regions. In this study, the localization of the DNA in the compartments and a side flow channel creating a constant sink for expressed proteins served as an encapsulation proxy, although it is unclear how this affects the wave front propagation velocity or the entire spatial dynamics in comparison to a continuous environment. Other works on DNA-based pattern formation from reaction-diffusion circuits include the creation of a French flag pattern, a spatial differentiation relevant in embryo-development [19] and an edge detection circuit [20].

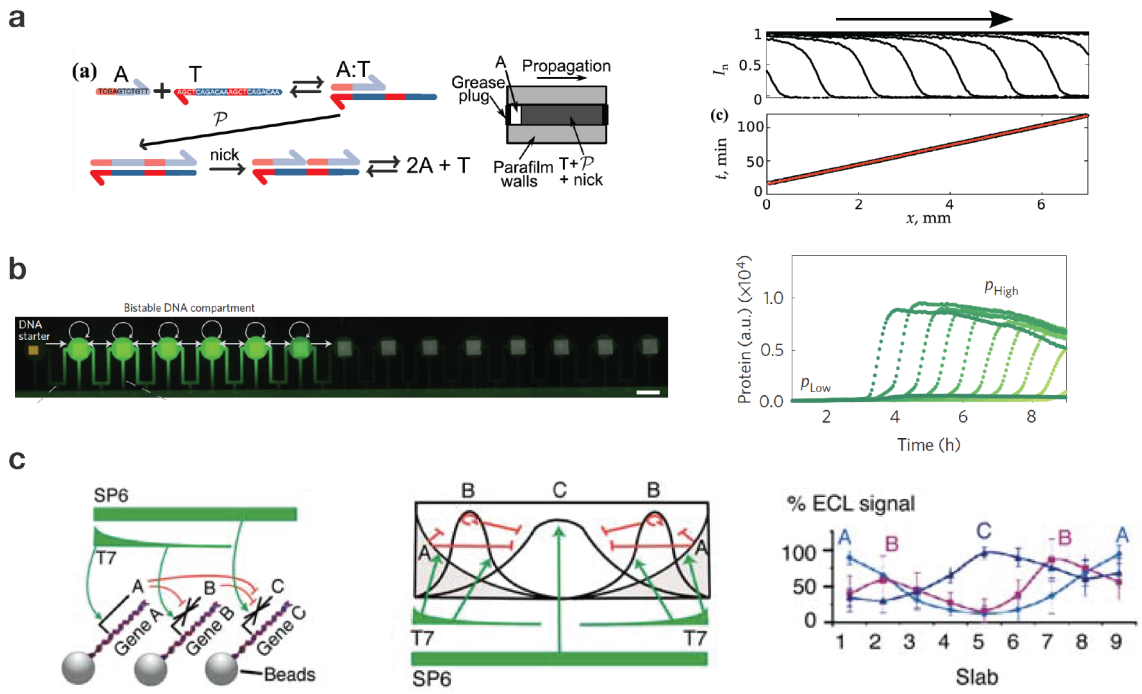

Figure 1.3. Spatial dynamics in continuous environments. **a**, Autocatalytic wave propagation in a continuous environment, with a DNA-based circuit. Figure adapted with permission from [17]. **b**, Autocatalytic wave propagation in set-up with localized DNA and limited diffusion, based on gene expression. Figure adapted with permission from [18]. **c**, Gene expression differentiation induced by a transcription activator gradient, imitating the early stages of differentiation in *Drosophila*. Figure adapted with permission from [21].

In a more biomimetic study, Isalan *et al.* [21] immobilized linear DNA genes on

magnetic beads and, by creating an external polymerase gradient, were able to reproduce some of the gene expression profile characteristics of the developing *Drosophila* embryo. In an IVTT environment, stable spatial differentiation was generated by mutual repression interactions under the overall control of the polymerase gradient (Figure 1.3.c). This synthetic circuit therefore implemented a positional information model of differentiation, as described in Chapter 1.1.3. In this study, modelling revealed that the activator (the polymerase) must diffuse about 10-fold faster than the repressor proteins for the pattern to emerge. This is achieved in the experimental system through localization of the repressor proteins on their target DNA, which effectively slows down their diffusion. The authors suggest that this might be achieved in the *Drosophila* embryo by trapping of certain proteins within the nuclei - effectively, a compartmentalization process.

These spatially dynamic gene circuits reproduce spatial-response systems known to serve key functions in biological organisms using synthetic components. Biological processes that have been mimicked are for example autocatalytic wave front propagation - a circuit that can relay a signal on longer distances than what the signal's diffusion alone would allow [18] - or pattern formation in a chemical gradient - a control mechanism for cell differentiation and embryo development in many embryogenesis processes [14].

1.3 Compartmentalized gene circuits

The use of compartmentalization in synthetic circuits generally serves the practical purpose of isolating incompatible reactions and colocalizing components that should interact together. But it also serves a conceptual purpose: synthetic circuits isolated in compartments permits the definition of a biological identity. In a continuous environment with no spatial organization, biological identity cannot be defined, and the program of synthetic biology to imitate living organisms remains limited to somewhat abstract homology of computation abilities. In contrast, when compartmentalization is introduced through encapsulation, localization or crowding, the concept of an artificial cell becomes concrete and specific, and the scope of what synthetic biology may reproduce from biology becomes clearer. Archetypical cellular behaviour can then be studied and quantified, for example cell-to-cell communication, predatory/prey behaviour or differentiation. The use of compartmentalization can moreover serve similar purposes in artificial cells as in biological organisms: it can allow for increased enzymatic kinetic rates due to local trapping (as seen in carboxysomes), compartments can segregate mutually incompatible processes (as found in the spatial segregation of transcription and translation in eukaryotes between nuclei and cytoplasm), to cite just a few examples.

Compartmentalization in the field of synthetic biology has been achieved in two distinguishable approaches: tight boundaries approaches, where compartments

bear a continuous, relatively impermeable boundary to the outer environment (Chapter 1.3.1) - such compartments are typically termed ”artificial cells” - and porous boundaries approaches, where compartments consist of highly dense regions (such as hydrogels) in which free diffusion is limited but which boundaries are highly porous (Chapter 1.3.2) - such compartments typically are not considered tight enough to be termed cells and considered ”artificial organelles”.

1.3.1 Compartments with tight boundaries: artificial cells

Droplets, lipid vesicles, polymersomes or proteinosomes are examples of compartments considered to be cell-like, as they have a continuous membrane that physically isolates the content of the compartment from its outer environment. Studies with such artificial cells usually characterize cell-to-cell communication by signal diffusion through an outer, well-mixed and dilute environment. Spatial parameters such as cell-to-cell distance or diffusion range of signals are rarely considered. Encapsulation often serves as a means to separate mutually toxic environments and to keep components form diffusing and being diluted.

Several studies have established communication between bacteria and *in vitro* transcription-translation (IVTT) environments. In these studies, the artificial environment is encapsulated in droplets or in vesicles, in part because the IVTT system typically works in a specific range of dilution, and would not function properly when well mixed with a bacterial culture. Moreover, communication could not be properly established and studied without a physical separation between the bacteria and the artificial environment - communication in itself encompasses the need for separate entities. Lentini *et al.* [22] encapsulated a cell-free protein expression system in lipid vesicles with signalling genetic circuits and demonstrated that these artificial cells could both sense chemicals produced by bacteria and produce chemicals that bacteria could sense, effectively creating a ”Turing test” where the bacteria communicated with the artificial cells through quorum sensing signals as they would with other cells. In a similar study by Schwarz-Schilling *et al.* [2], water-in-oil droplets were generated containing either IVTT or living bacteria, and the droplets were filled in capillaries to study droplet-to-droplet communication (Figure 1.4.a). With this strategy, an interesting spatial component could be implemented: in the capillaries, diffusion from droplet to droplet was effectively one dimensional, thus increasing coupling strength between neighbours, and dependent on the partitioning coefficient of the signal into the oil phase and on its diffusion in that phase. The response of the genetic circuit (an AND gate producing GFP in response to two chemicals, isopropyl β-D-1-thiogalactopyranoside IPTG and 3-oxohexanoyl-homoserine lactone 3OC6-HSL) to a gradient of the chemicals could be assessed in a one-shot experiment, where the capillaries were plugged into reservoirs of either of the chemicals. The diffusion kinetics of 3OC6-HSL played a crucial role in the response, as the paper demonstrated that two kinetic ranges of diffusion existed depending on this signal’s concentration.

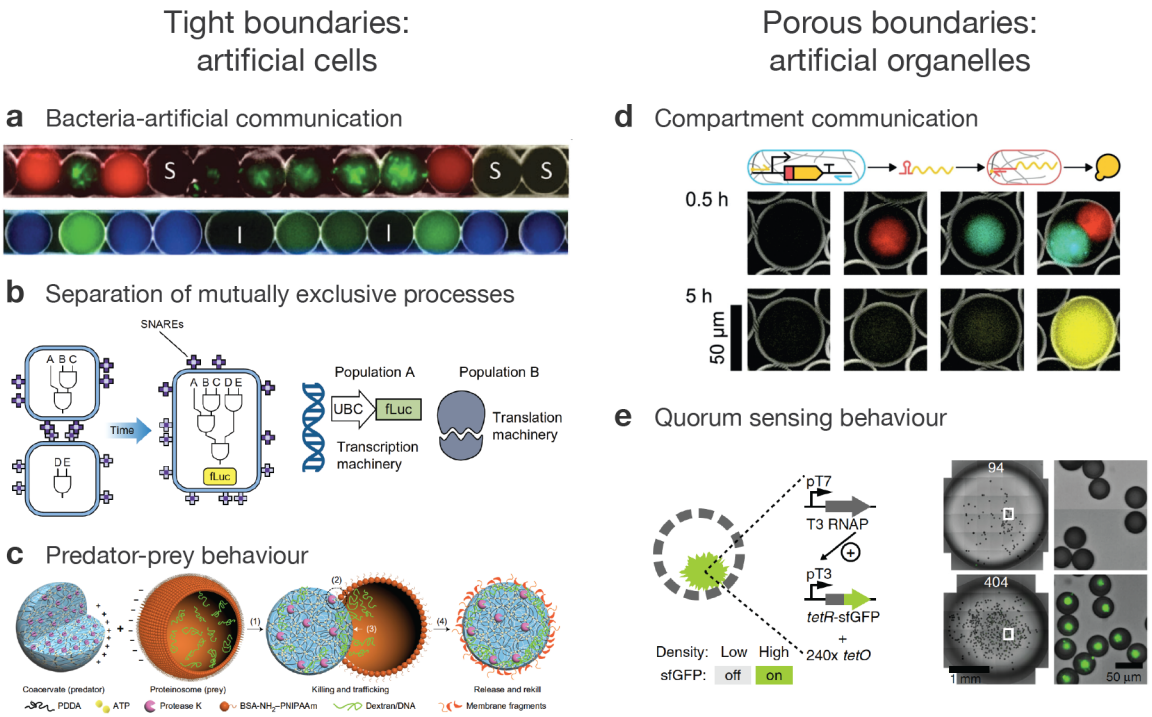

Figure 1.4. Different categories of artificial compartments. Tight boundaries compartments are termed artificial cells. These types of compartments can be shown to establish two-way communication with bacteria (**a**, figure adapted with permission from [2]), to perform mutually-exclusive processes such as mammalian transcription translation (**b**, figure adapted with permission from [23]), or to have predator-prey behaviour between communities of artificial cells (**c**, figure adapted with permission from [24]). Porous boundaries compartments are termed artificial organelles, and can be shown to establish inter-organelle communication (**d**, figure adapted with permission from [25]) or quorum sensing behaviour (**e**, figure adapted with permission from [26]).

A study based on encapsulated IVTT in vesicles showed the possibility to establish vesicle-to-vesicle communication in a well-mixed environment [23], but also demonstrated explicitly how encapsulation allowed orthogonal processes to be conducted. In eukaryotic cells, transcription is conducted in the nucleus and the mRNA is later exported into the cytoplasm to be translated. Accordingly, mammalian cell-extracts for transcription and for translation are mutually incompatible. In this study, the authors conducted transcription in one type of vesicle containing transcription cell-extract, and these were later fused with another type of vesicles containing translation cell-extract so that the full protein synthesis could be effectively conducted (Figure 1.4.b). Mutually incompatible processes could therefore be carried out sequentially.

Control over the content and membranes of artificial cells also allows the design of different populations of artificial cells that can then interact with each other following ecosystem dynamics. Using two types of protocells (coacervate microdroplets and proteinosomes), Qiao *et al.* [24] demonstrated predatory behaviour with electrostatic interaction of the two populations followed by protease-mediated degradation of the proteinosomes by the coacervates. The contents of the proteinosomes were then

transferred into the coacervate droplets (Figure 1.4.c). In this study, compartmentalization (through both membrane-free coacervates and protein-membrane vesicles) served to define two artificial cell populations, and to qualify enzymatic degradation as predatory behaviour - therefore mimicking population dynamics in living organisms. This study is a rare example of membrane-free coacervates being considered artificial cells (see Chapter 1.3.2).

Although artificial cells with tight boundaries provide an interesting platform for studying biological cellular dynamics and for building interfaces with living cells, the impermeability of their membranes imposes limitations. Communication between tight boundaries compartment is indeed often limited to small molecules that can still freely diffuse through the artificial cell's boundary. Although such compartments structurally resemble cells due to their continuous membranes, biological cells are capable of much more complex communication through chemical or protein signalling.

1.3.2 Compartments with porous boundaries: artificial organelles

Coarcevation, aggregation and cross-linking are interesting methods for localization, because such dense environments have porous boundaries and diffusion can be more readily tuned with mesh size than what can be achieved with a continuous membrane. Several studies from the lab of Wilhelm T.S. Huck have quantified how coacervates or hydrogels affect the diffusion and kinetic rates in IVTT systems [27], [28]. It is interesting to consider crowding for the construction of artificial cells, since the contents of most artificial cellular systems are typically more dilute than in cells (*e.g.* an IVTT reaction is about 30 times more dilute than a cell [29]). Furthermore, crowding and liquid-liquid phase separation seem to play an important role in cells, by creating "microcompartment" structures that affect diffusion and metabolic rates [30]. Although crowding can induce phase separation and significant trapping effects, it is not generally considered a sufficient physical boundary to define a coacervate or a hydrogel as a "cell". Studies on such crowded compartments often encapsulate them in water-in-oil emulsion, to provide identity and allow each coacervate or hydrogel to be studied independently.

For example, in a recent study [25], hydrogel beads in which IVTT was performed were termed "gel-based organelles". In this study, DNA was covalently attached to gel beads that were then encapsulated in water-in-oil droplets. Beads performed different functions depending on the DNA sequence bound to them: RNA transcription could be localized with a DNA template attached to the bead, or translation could be localized by pairing an mRNA to a complementary DNA on the bead, rendering the ribosome binding site accessible. Each of these processes occurred locally on the corresponding bead, and due to the porous property of the bead, RNA could diffuse from bead to bead while remaining contained in the water droplet, therefore acting as a signal between the beads (Figure 1.4.d).

In a similar study, Niederholtmeyer *et al.* [26] created DNA-hydrogels inside highly porous polymersomes (with pore diameters around 200 nm), which they termed respectively nucleus-mimic and cell-mimic. Such a porous artificial cell allowed localized transcription in the hydrogels, but delocalized translation and protein communication between cell-mimics. With this strategy, the authors established such behaviour as protein trapping in the nucleus-mimic or protein-based quorum sensing in a population of the cell-mimics (Figure 1.4.e). This is an interesting strategy to circumvent the complexity of engineering biomimicking cell-to-cell protein communication, which is handled in cells with a variety of complex mechanisms, from membrane protein mediated transport to vesicle fission and fusion (see for example [31] and [32]). However, in living organisms translation rarely occurs in large diffuse environments not contained by the cell membrane. One example where translation occurs in a diffuse environment is the developing *Drosophila* embryo, where nuclei initially divide in one millimetre-sized cell [33]. Such porous boundary-compartments as coacervates or hydrogels are therefore mainly considered as not physically separated enough to be termed cells, and are regarded rather as artificial organelles.

The complexity of dynamics that can be demonstrated in such tight or porous boundaries compartmentalized but well-mixed environments remains limited, however, because spatial arrangement of the compartments is not taken into consideration. At best, such artificial cells can be brought into large chambers, and overall large-scale diffusion can be characterized [26], but biological behaviour such as signalling on short and long ranges, direct cell-to-cell communication or differentiation of direct neighbouring cells are more difficult to implement.

1.4 Encapsulation and spatiotemporal patterns

In most biological systems, the aqueous diffusion constants of the various components involved in gene networks do not differ so much as to allow spatial patterns to emerge on the appropriate scales - for example, for single neighbouring cells to differentiate. An effective means to limit the diffusion of specific components is compartmentalization. The membranes of the compartments can drastically reduce the diffusion kinetics of large components but still permit the diffusion of smaller components. Similarly to biological cells, two important parameters for pattern formation and signalling in artificial multicellular assemblies are the reaction kinetics of the underlying reactions and the diffusion coefficient of the components involved. To our knowledge, we are the first to establish spatial dynamics at the cell length scale within artificial cells using synthetic gene circuits.

However, studies of spatial dynamics due to reaction-diffusion systems have been conducted in genetically modified *E. coli* cells. Selectively limiting diffusion is one

of the roles that cell boundaries play in living organisms, trapping proteins, DNA, sugar polymers and other large components, while small chemicals can either diffuse through the bilayer freely or diffuse through water channels formed by protein pores. Spatially dynamic circuits have correspondingly been built *in vivo*, using small chemicals (typically quorum sensing signals) to communicate and natural encapsulation. They offer insight into the spatial dynamics that could be built in artificial cells by implementing biomimicking diffusion and reaction conditions.

In a study from Danino *et al.* [34], the authors built an oscillator based on the production and degradation of a quorum sensing signal, 3-oxohexanoyl-homoserine lactone 3OC6-HSL. The machinery responsible for the production, degradation and readout of the signal was localized inside the cells, but the signal could freely diffuse, allowing oscillations to emerge passed a certain cell density. The synchrony of oscillations due to global 3OC6-HSL diffusion was shown to create propagating spatial waves that emerged spontaneously from points of high cell density, and whose spatial propagation was determined by the geometry of the chamber in which the cells were contained.

In other studies, genetically modified cells were plated with a predetermined pattern, and the spatial dynamics were consequently dependent on the initial distribution of the cells. For example, Basu *et al.* [35] created a band detector for 3OC6-HSL concentrations. Sender cells produced a 3OC6-HSL signal, creating a gradient around them. Receiver cells contained a genetic circuit with parallel and serial repression nodes, leading to GFP repression at high and low 3OC6-HSL concentrations. GFP expression was only possible at intermediate concentrations of 3OC6-HSL, and therefore at intermediate distances from the senders. This spatial behaviour was observed when cells were plated with a predetermined pattern - typically, receiver cells were homogeneously distributed on a plate and sender cells were spotted at specific points.

In both these studies, spatial dynamics could be observed over length scales of millimetres, three orders of magnitude higher than the length scale of bacterial cells. 3OC6-HSL is a fast-diffusing chemical, and it is naturally used in quorum sensing by bacterial populations. With chemicals showing slower diffusion, patterns at smaller length scales, down to one or a few cells, may be established. At this scale, cell-to-cell distance and the spatial arrangement of cells become crucial parameters for spatial dynamics. In multicellular tissues, cell-to-cell distance is minimal, and chemicals can diffuse over several cells without being significantly diluted in the outer medium. In developing embryos the position of an individual cell relative to the others can affect its fate for future development [36]. Therefore, we sought to build spatially organized artificial multicellular assemblies (AMA), with direct cell-to-cell contact and control over spatial arrangement.

1.5 Engineering multicellularity

As exemplified above, there are many different strategies for building artificial cells: for example droplets, vesicles, proteinosomes, polymersomes, coacervates or hydrogels. They have different properties in terms of stability, physical boundaries or biocompatibility. However, as all known cells and most cellular organelles are encompassed within lipid bilayer boundaries, lipid-based artificial cells potentially provide the best environment to implement biomimicking spatial dynamics and interfaces with living cells. Lipid bilayers are the support for the assembly of a variety of membrane-bound communication machineries, from water channels such as alpha-hemolysin (α-HL [37]), to complex DNA translocating pore assemblies such as the ϕ29 DNA packaging motor [38]. Although recent progress has been achieved, assembling artificial cells into multicellular assemblies remains a challenging task. I will review vesicle- and droplet-based methods for engineering multicellularity.

In a series of publications, Elani, Law and Ces used the "phase transfer method" to produce multicompartment liposomes: that is, vesicles containing several compartments bound through lipid interfaces. Water-in-oil droplets stabilized with a lipid monolayer were dropped above an oil-water interface covered with lipids. As the droplets went through the oil-water interface, they formed a lipid bilayer between them and a lipid bilayer on their outside, effectively becoming a multicompartment vesicle (Figure 1.5.a). The yield for forming two-compartment vesicles with this process was around 43 % [39]. The authors successively demonstrated *in vitro* transcription-translation (IVTT) reactions in the compartments [40] and spatially segregated an enzymatic pathway in three steps performed in three compartments, using the pore-mediated diffusion of glucose and the non-specific diffusion of hydrogen peroxide through bilayers to achieve substrate transfer from compartment to compartment [41]. The phase transfer method is however relatively labour-intensive and manual, and therefore is limited in both yield and total output.

Through an elegant dewetting process, Deng *et al.* [42] have demonstrated the microfluidic assembly of several multicompartment liposomes with much greater output than the phase transfer method (Figure 1.5.b). The yield of properly assembled vesicles with this method was around 62 %, and chemical communication could be demonstrated between compartments and through the outside bilayer of the vesicle. Both methods produce vesicles in an outer aqueous medium, so that they are adapted for biological environments. However, they do not allow control over spatial arrangement and are strongly limited in the number of compartments that can be assembled. Hence they are limited in mimicking biological organisms.

The lab of Hagan Bayley has developed a technique that allows tight control over spatial organization: the droplet-interface-bilayer method (DIB) [44]. In this method, water-in-oil droplets are produced in an oil bath containing lipids. The lipids assemble at the water/oil interface, and its full coverage is dependent on the surface area of the

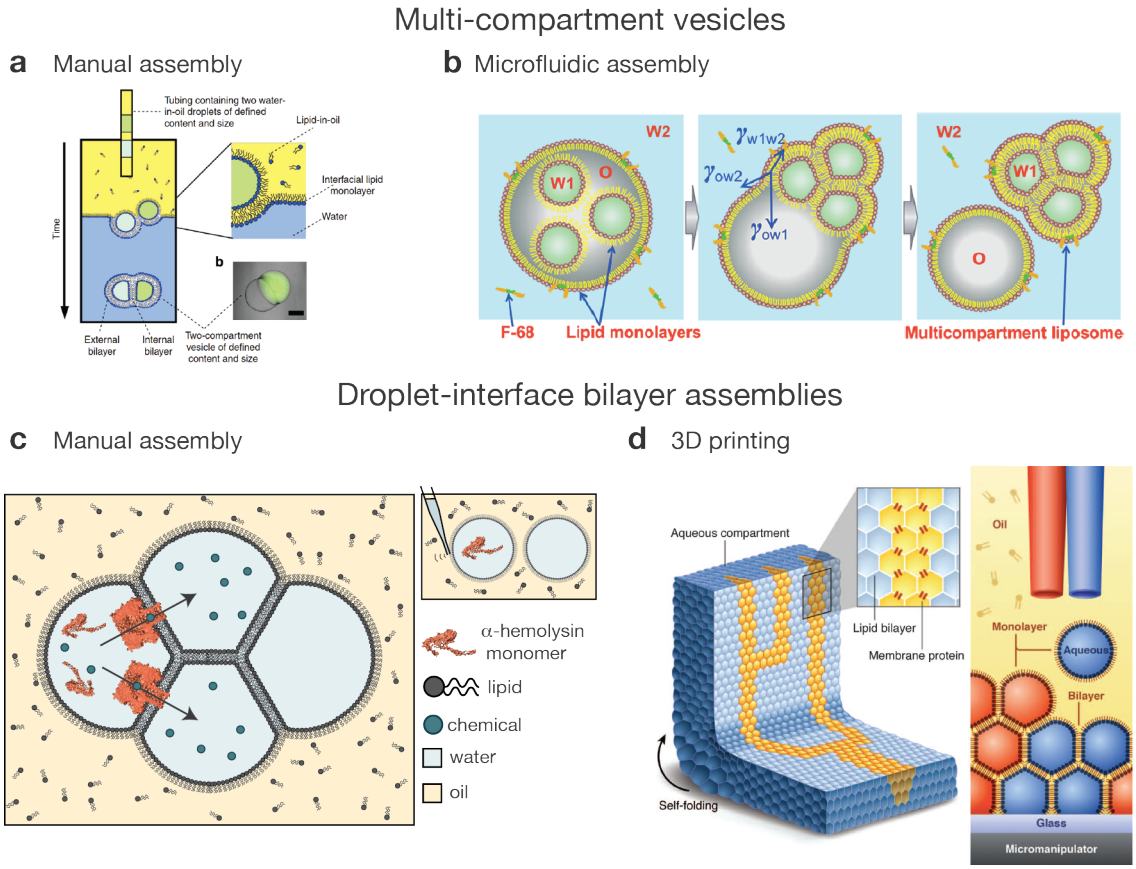

Figure 1.5. Engineering multicellularity. Forming vesicles composed of several interconnected compartments can be achieved via manual (**a**, figure adapted with permission from [41]) or microfluidic (**b**, figure adapted with permission from [42]) methods. Droplet interface bilayer assemblies can be built with manual methods, with micromanipulators or agarose-covered electrodes (**c**, figure adapted with permission from [3]) or printed with a 3D printer (**d**, figure adapted from [43]).

droplet, on the lipid composition, and on the solubility of the lipids in the oil. An oil mixture containing a high lipid-soluble oil (typically hexadecane) and a low lipid-soluble oil (typically silicone oil) allows for both the proper dispersion of the lipids in the oil phase and their fast assembly at the water/oil interface (see Chapter 2.1 for a discussion of lipid monolayer assembly and bilayer stability). Once each water droplet is coated with a lipid monolayer, two droplets can be brought together with a micromanipulator to form a bilayer (Figure 1.5.c) [44]. Bilayers assembled with this strategy are usually stable for days, and allow for the incorporation of pores. Such droplet assemblies have been successfully used to measure current-dependent translocation of double-stranded DNA through DNA nanopores [45], to assemble 3D networks and measure electrical current through protein pores across the network [46], and to induce protein expression with single-droplet resolution using a light-activated transcription activation [47]. As this method necessitates a micromanipulator and spatial organization is non-automatized (although some microfluidics methods have been investigated, see [48]), it remains labour intensive, and networks up to only hundreds of droplets could be built. This is a significant

improvement over the multicompartment vesicle techniques in terms of scale and spatial arrangement of the assembly, but downstream applications in biological or aqueous environments would demand the transfer of the water-in-oil network into an oil-in-water emulsion.

Recently, this technique was paired with 3D printing of droplets to achieve a fast assembly of large artificial tissues with spatial geometry control (Figure 1.5.d) [43]. Millimetre-sized assemblies of picoliter droplets (diameter around 5 µm) were produced in large oil-in-water droplets. Electrical current transduction across the assemblies through protein pores was demonstrated, and mechanical contraction due to osmolarity imbalance between droplets was shown to close a flat droplet assembly into a hollow sphere. The automatization of droplet positioning and the high-throughput given by 3D printing solve the limitations of the semi-manual technique. 3D printing of droplet assemblies is discussed in more detail in Chapter 2.3.4, however it should be noted that this strategy suffers from accumulating printing defaults that lead to geometrically imperfect assemblies, and imaging the core of such large 3D structures presents some difficulties. For experiments where spatial dynamics can be studied in length scales of tens of droplets, the semi-manual method allows for a more accurate control of geometry.

Droplet-interface-bilayer assembly of artificial multicellular assemblies is therefore the most versatile and accessible method for this work, as it has a low technical barrier to building a set-up, and it allows us to encapsulate a variety of gene circuits environments, with - most importantly - full control over content and spatial organization of every droplet in the assembly. The semi-manual technique is used for most of this thesis, and 3D printing is attempted in a later phase.

1.6 Implementing biomimetic complex dynamics in spatial organized assemblies of artificial cells

The field of synthetic biology has separately been interested in engineering molecular systems capable of spatial computation (see Chapter 1.2) and in compartmentalization and creation of artificial cells (see Chapter 1.3). This thesis aims to bring together these two research interests, by building artificial multicellular assemblies (AMA) in which spatially resolved dynamics can be implemented. By mimicking how spatial dynamics occur in tissues of cells or embryos, such an approach would allow the study and control of biologically relevant processes in an artificial context. I have shown that only a few strategies exist to spatially assemble artificial cells (Chapter 1.5), and I have described why droplet-interface-bilayer seems the most appropriate technique for our purpose. The following chapters describe the work conducted in this thesis, its main results and the insights gained. Technical and theoretical aspects regarding the assembly of multicellular droplet-interface-bilayer structures are addressed in Chapter 2, as

well as the characterization of a library of small chemicals as potential signals within the AMA. Chapters 3 and 4 describe the synthetic gene circuits that were designed and implemented in AMA, with Chapter 3 focusing on circuits where the signal was externally provided (signal-responsive circuits) and Chapter 4 exploring the expression of signals on site (signal-sending circuits). Other projects conducted during the thesis that did not directly involve AMA and other results are summarized in Chapter 5.

2 DIB multicellular assemblies

This chapter describes the method by which artificial cells were spatially organized with overall geometrical control, the droplet-interface-bilayer (DIB) technique, and how signalling was implemented in these assemblies. The assembly method and parameters affecting bilayer stability such as lipids and oil are addressed (Chapter 2.1). The use of protein pores to allow chemical diffusion across the bilayers is described (Chapter 2.2). Finally, a library of signalling molecules relevant to synthetic gene circuits and their diffusion mode are assessed (Chapter 2.3). Together, these elements constitute a toolbox from which reaction-diffusion circuits can be implemented.

2.1 Bilayer stability

Many parameters can affect the stability of bilayers in droplet multicellular assemblies, as for example the kinetics of lipid assembly, the volume of the droplets and the dimensions of the assemblies. This section first describes the method used for droplet printing (Chapter 2.1.1), and then addresses parameters affecting bilayer stability: the lipids and oil composition of the oil phase (Chapter 2.1.2), the energy of bilayer formation (Chapter 2.1.3) and the stability of droplet volume over time (Chapter 2.1.4).

2.1.1 Method for droplet printing

In this section, I shortly describe the set-up for droplet printing and assembling, so that the experimental results and theoretical considerations addressed thereafter can be concretely understood in the context of our platform. More details can be found in Appendix A.3.

Lipid-in-oil solutions were prepared as follows: lipid powders were dissolved in chloroform and mixed in a glass vial to reach the appropriate lipid composition. The chloroform was evaporated under a nitrogen stream, and the lipid film was dried for an

hour under vacuum. The lipid film was resuspended in 1:1 hexadecane:AR20 oil mix to reach the desired final lipid concentration. The mix was briefly vortexed and stored away from light for 2 to 6 months on average.

Experiment chambers consisted of rubber O-rings of about 7 mm in diameter glued onto glass slides. The chambers were washed before each experiment with soap, ethanol and double-distilled water and dried at 90 °C for at least 30 min, so that all contaminant proteins (and specifically, possibly remaining protein pores) were denatured.

The chamber was filled with 65 µL of the lipid/oil mix. Droplet solutions, such as sender, buffer and receiver, were prepared according to each experiment, and pipetted into heat-pulled glass capillaries with a tip diameter of around 30 µm. The glass capillary was then fixed onto a house-built micromanipulator (Figure 2.1), and connected to a microinjector pump, which provided pressure pulses in the range of 20 to 100 hPa for 0.1 s. A wipe was lightly pressed against the tip of the capillary to take out the residual air and allow the regular flow of the solution. The pipette was brought into the lipid/oil mix and pressure injections were applied to create droplets of 260 µm diameter or lower, 10 nL volume on average. The droplets sank to the bottom of the chamber and were incubated for 15 min on average, to allow a monolayer of lipids to form around them. The glass capillary, together with the micromanipulator, was then used to move the droplets in the chamber and bring them into contact, and they spontaneously formed bilayers. The chamber was closed with a glass slide to limit evaporation and shrinking of the droplets, as addressed in Chapter 2.1.4.

2.1.2 Lipids and bilayers

Lipids are the primary components of biological membranes, which define the identity and boundaries of cells and organelles. Lipid membranes limit the exchange of components between the compartment and its outer environment, while trans-membrane proteins mediate the transport of molecules and ions. Lipids are chemically composed of a hydrophilic head group, which can be polar, charged or zwitterionic and of a hydrophobic tail, usually made of two linear saturated or unsaturated carbon chains. Certain lipids have polycyclic structures in their hydrophobic tails: they are termed sterols. Chemical structures of lipids used in this study are shown in Figure 2.2. The amphiphilic property of lipids allows them to self-assemble into bilayers where the hydrophobic tails face each other and the hydrophilic head groups are oriented externally. These bilayers form the basic structure of all biological membranes. The hydrophobic core of the bilayer limits the diffusion of hydrophilic molecules due to repulsive interactions, and the ordering of lipids in the bilayer causes an entropic cost to the diffusion of large molecules across it, therefore rendering the bilayer impermeable to most molecules.

The ordering of lipids in a bilayer can be described with phase-transition dia-

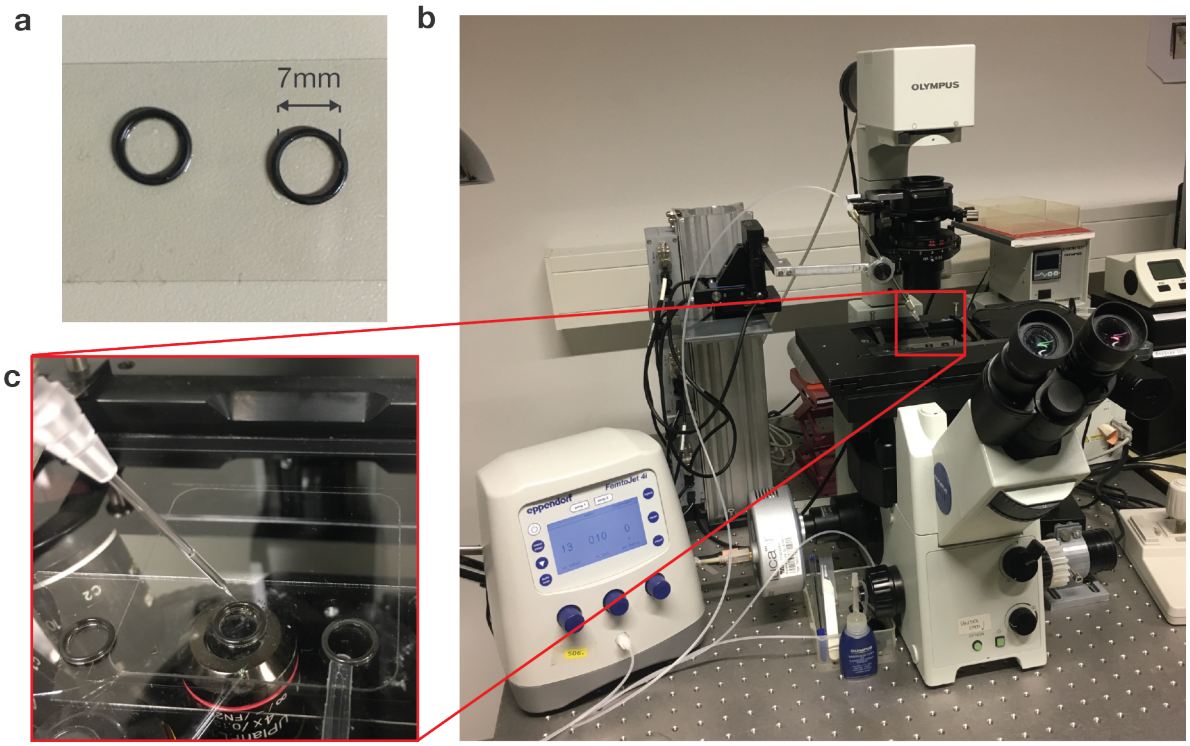

Figure 2.1. Set-up for the experimental realization of artificial multicellular assemblies (AMA). **a**, Chambers consist of rubber O-rings glued on glass slide and are tight to oil leakage. After assembling the droplets, the chamber is closed with a microscopy slide to avoid evaporation. **b**, Chambers are fixed on a transparent heating plate on the stage of the microscope. The glass pipette is mounted on a micromanipulator to the left of the stage and connected to a pressure pump (lower left). **c**, Close-up picture of the glass pipette above the chamber. Figure adapted with permission from [3].

grams, where the most common phases are a "solid" *i.e.* ordered state, a "liquid" *i.e.* disordered state, and a liquid-ordered state where the diffusion of the lipids is similar to the liquid-disordered state, but the packing and order of lipids is similar to a solid state [49]. The phase of the lipids depends on the temperature of the system, on the melting temperature of each lipid (temperature of the "solid" to "liquid" phase transition) and on the quantity and proportion of different lipids in the bilayer. The transition temperature and phase diagrams for a given lipid mixture are difficult to predict in most cases. Cholesterol, the most abundant sterol in mammals, can affect membrane permeability and fluidity due to its rigid and hydrophobic structure and induces the transition to liquid-ordered phase [50].

Natural lipid bilayers are usually composed of a large diversity of lipids and present an asymmetry in lipid composition both transversally and laterally. Transversally, each of the bilayer leaflets has a different lipid composition, which affects the bilayer's curvature: different lipids have different shapes, cylindrical, conical or inverted conical depending on the size ratio of head group to tail. The transversal difference in lipid composition also partially contributes to transmembrane potential. Laterally, lipids in natural

bilayers demonstrate phase-separation, leading to lateral differences in lipid composition and to the existence of ”rafts”, which can affect the local density of membranes proteins [49]. Due to the complexity of phase-separation processes in lipid membranes and the difficulty to control them, artificial lipid bilayers - and DIBs in particular - are often created with one type of lipids, or with mixtures of a few lipids at most.

Two methods exist to supply lipids to the water-oil interface in DIBs: lipids-in

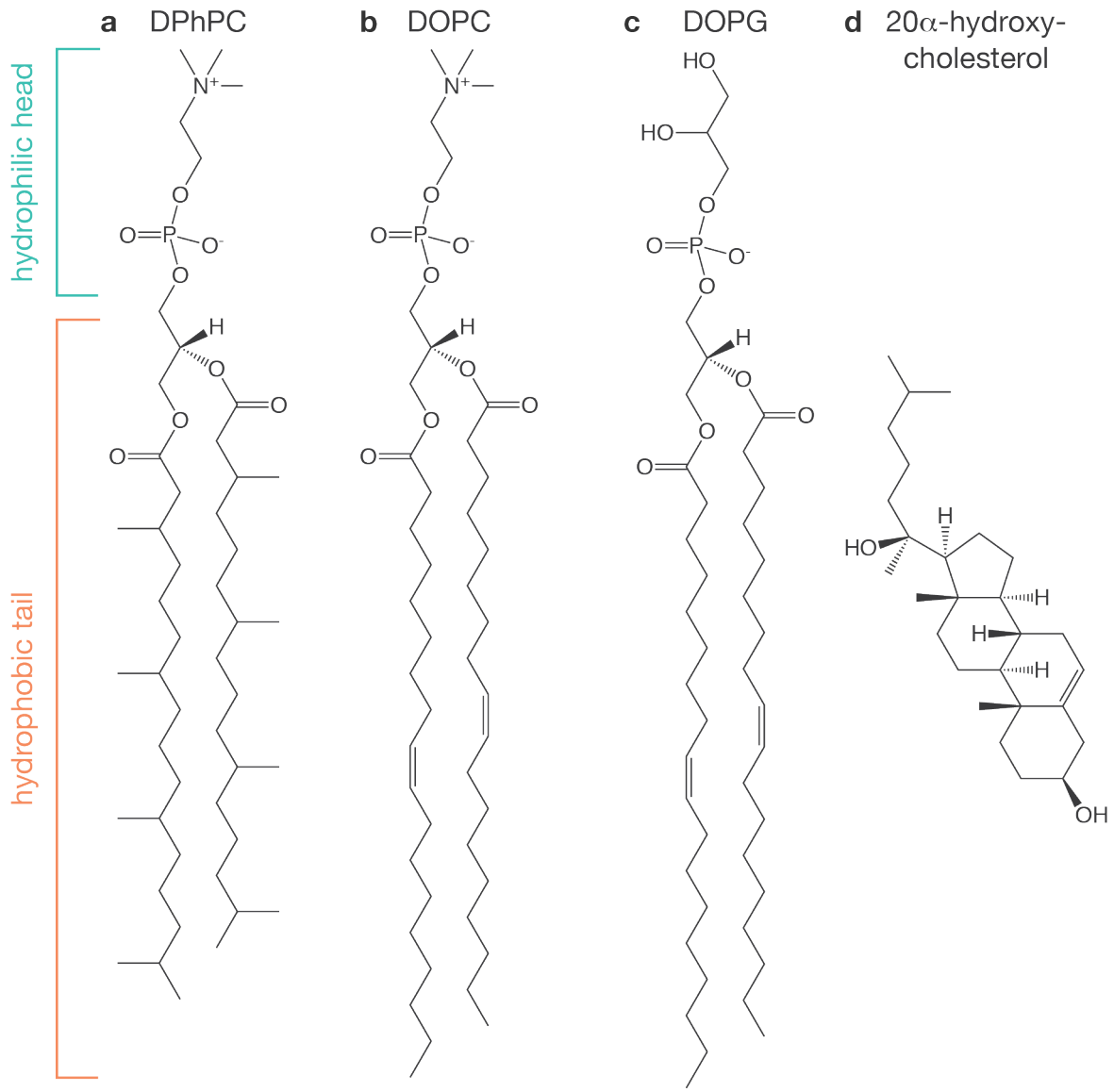

Figure 2.2. Lipids and sterols: building blocks of biological membranes. Lipids are composed of a hydrophilic head (shown in blue) and a hydrophobic tail (shown in orange), whereas sterols are dominantly hydrophobic. This figure displays the four components used for lipid bilayers in this thesis: **a**, 1,2-diphytanoyl-sn-glycero-3-phosphocholine (DPhPC), **b**, 1,2-dioleoyl-sn-glycero-3-phosphocholine (DOPC), **c**, 1,2-dioleoyl-sn-glycero-3-phospho-(1'-rac-glycerol) (DOPG) and **d**, 5-cholestene-3β,20α-diol or 20α-hydroxycholesterol (cholesterol).

and lipids-out [44]. In the lipids-in method, liposomes are loaded into the water phase of the droplets and adsorb at the water-oil interface to deliver lipids. With this method, asymmetric bilayers can be created, as every droplet can be loaded with liposomes of different lipid compositions. In the lipids-out method, lipids are dissolved into the oil phase and diffuse to the water-oil interface to form a monolayer. These two methods have different kinetics of adsorption, and quite intuitively, lipids-in will lead to a faster monolayer assembly as the lipids diffusion is more constrained in the droplet [51].

We found that the lipids-in method was unsuitable for our work, particularly when working with *E. coli* cell-extract. Lipid bilayers could not be formed reliably even with large incubation times, and we speculate that the protein content of the cell-extract interacted with the liposomes. The lipids-out method was therefore preferred. We initially found that 5.9 mM DPhPC dissolved in oil was sufficient to form stable bilayers for droplets containing DNA/RNA circuits and bacteria. However, bilayers could not be formed when encapsulating cell-extract: when the droplets were brought rapidly into contact, they tended to fuse, and when they were incubated for longer periods of time, the surface of the droplets became visibly irregular and they would no longer form bilayers. We speculate here again that proteins denature at the water-oil interface and affect the assembly of lipids. 6.4 mM DOPC led to fast and stable encapsulation of cell-extract, but when used for the encapsulation of DNA/RNA circuits and bacteria, the contact angle and the bilayer area between the droplets were too large to allow for a proper identification and tracking of single droplets within assemblies. We then investigated mixtures of lipids with fast monolayer assembly (such as DOPC), and with stabilizing effects such as negatively charged lipids (DOPG) and cholesterol. We tested the following lipid mixtures, keeping the total lipid molarity at 5 mM:

- 1.25 mM DOPC, 2.25 mM DPhPC, 1.25 mM DOPG, 0.25 mM cholesterol
- 2.25 mM DOPC, 2.25 mM DPhPC, 0.25 mM DOPG, 0.25 mM cholesterol
- 3 mM DOPC, 1.5 mM DPhPC, 0.25 mM DOPG, 0.25 mM cholesterol
- 4 mM DOPC, 0.5 mM DPhPC, 0.25 mM DOPG, 0.25 mM cholesterol

Only the last lipid mixture allowed for a fast formation of a monolayer and a long-term stability of the bilayers. Droplets could be assembled after 5 min to 15 min incubation, and the bilayers were stable for days. The lipid-oil mix itself was stable at room temperature for typically 2 months, and was discarded when bilayers were no longer stable. Our experiments were conducted either at 29 °C (*in vitro* transcription-translation) or at 37 °C (*in vitro* transcription, live cells), and we therefore did not address temperature-dependent destabilization or phase-transition of our bilayers. We also did not consider whether phase separation existed in our lipid bilayers, and do not expect that this affects cell-to-cell communication in our system.

2.1.3 Energy and bilayer formation

The formation of a bilayer between two water droplets is driven by a total free energy reduction ΔF, termed the adhesion energy, and by an entropy-driven exclusion of solvent molecules between the hydrophobic chains in the bilayer [52]. The geometry of two droplets forming a bilayer is represented in Figure 2.3.a. The contact angle is θ_0, the water-lipid-oil monolayer interfacial tension is γ_m and the water-lipid-water bilayer interfacial tension is γ_b. R_b, R_l and R_r indicate the radii of respectively the bilayer disc, the left droplet and the right droplet. The contact angle can be calculated from the radii:

$$2\theta_0 = sin^{-1}(\frac{R_b}{R_l}) + sin^{-1}(\frac{R_b}{R_r}) \tag{2.1}$$

Equilibrium of the forces on the droplet bilayer system imposes that [53]:

$$\gamma_b = 2\gamma_m cos\theta_0 \tag{2.2}$$

The adhesion energy, which quantifies the stabilization due to bilayer formation, can be deducted from the Young-Dupré equation [52]:

$$\Delta F = 2\gamma_m(1 - cos\theta_0) \tag{2.3}$$

Therefore two factors affect the formation of an energetically stable bilayer: the monolayer interfacial tension γ_m and the contact angle θ_0. Both may be affected by the composition of the oil phase and the lipids.

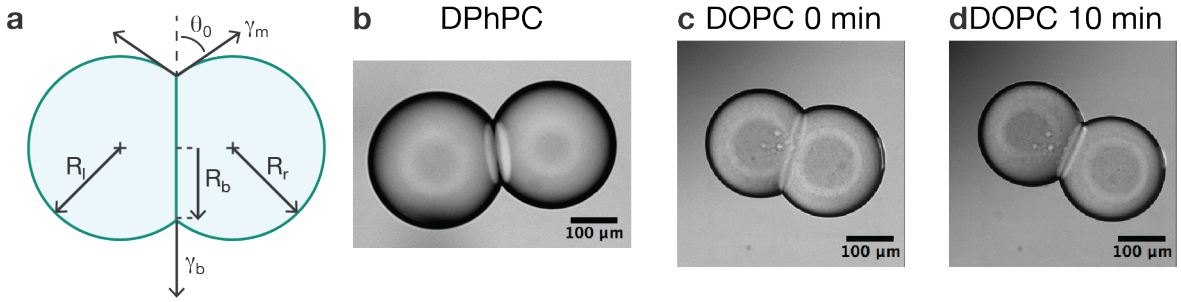

Figure 2.3. Lipid bilayers and contact angle. **a**, Sketch of the geometry of the bilayer and the principal factors that affect it: the water-lipid-oil monolayer interfacial tension γ_m, the water-lipid-water bilayer interfacial tension γ_b, the contact angle θ_0, the radii of the left droplet R_l, of the right droplet R_r, and of the bilayer disk R_b. **b**, Pair of droplets forming a bilayer with DPhPC lipids dissolved in the oil. **c**-**d**, Pairs of droplets forming bilayers with DOPC lipids dissolved in the oil after **c** ,0 min and **d**, 10 min incubation of the isolated droplets.

Generally, γ_m is greatly lowered by the presence of surfactants: the interfacial tension of a hexadecane/water interface is 44 mN.m^{-1} without surfactants and drops to 2.04 mN.m^{-1} when DPhPC lipids are present in the hexadecane [51]. All experiments discussed in this section use lipids-out methods. However, the oil composition seems

to only marginally affect γ_m: as reported in literature, DPhPC dissolved in hexadecane led to an oil/water interfacial tension of 1.18 mN.m^{-1}, while DPhPC dissolved in a 1:1 v:v mixture of hexadecane and silicone oil AR20 led to an interfacial tension of 1.03 mN.m^{-1} [54]. Similarly, the lipid composition seems to have only a small influence on γ_m: interfacial tension of the hexadecane/water interface was measured at 2.04 mN.m^{-1} with DPhPC, and at 1.8 mN.m^{-1} with DOPC [51].

The oil composition seems to affect more significantly the contact angle θ_0, thereby stabilizing the lipid bilayer. Taylor [54] measured an increase in the contact angle from 29.31 ° to 41.63 ° when changing the oil from hexadecane to 1:1 hexadecane:AR20, with DPhPC in both cases. Indeed, studies have shown that the use of a solvent where lipids are less soluble, such as a silicone oil, increases the adhesion energy of the bilayer [53]. For our experiments, we tested several oils: hexadecane, silicone oil AR20, mineral oil and squalene oil. We found that in our system, silicone oil AR20 and mineral oil were too viscous to allow a proper handling of the droplets, while with hexadecane or squalene oil the bilayers formed were unstable, particularly when encapsulating cell-extract. The final oil composition that was chosen for all subsequent experiments was **1:1 hexadecane:AR20**.

Lipids composition also affects the contact angle θ_0: we found that when changing lipids from DPhPC to DOPC (in 1:1 hexadecane:AR20), the contact angle increased from approximately 33.5 ° to 55.6 ° (Figure 2.3.b and c). Interestingly, when encapsulating cell-extract with DOPC, we also found differences in the contact angle based on the incubation time of the isolated droplets containing cell-extract: depending on whether bilayers were formed immediately or after 10 min incubation, the contact angle decreased from approximately 55.6 ° to 39.8 ° (Figure 2.3.c and d). As bilayers formed immediately were leading to more frequent fusion events, we kept the incubation time at around 10 to 15 min when encapsulating cell-extract. We also noticed that during cell-extract experiments, the contact angle seemed to reduce over the course of several hours (Figure A.1). This seems to confirm that proteins from the cell-extract denature at the water-oil interface and affect the stability of the bilayer, probably by affecting the ordering of the lipids.

Finally, we observed in our experiments that the formation of a lipid bilayer seemed to cause a temporary leakiness between the two droplets. We found that with chemicals that could not diffuse through bilayers, small amounts of these chemicals could be detected in a receiver droplet after bilayer formation with a sender droplet containing the chemical. This leakiness did not seem to continue after bilayer formation, and was negligible compared to chemical diffusion between droplets. However, whenever possible, we avoided this effect by introducing a buffer droplet between sender and receiver, as described in Chapter 2.3.1.

2.1.4 Stability of droplet volume

During the run of an experiment, droplet volumes tend to change due to two factors: water evaporation (predominantly due to Laplace pressure), which causes the droplets to shrink, and osmotic pressure between the droplets, which we will call internal osmotic pressure and causes one droplet to shrink and one droplet to grow. Droplet volume variation affects the area of the lipid bilayer, and therefore the kinetics of diffusion. This section will review these two causes for droplet volume change.

Droplet evaporation

Droplet evaporation is due to two factors: Laplace pressure and osmotic pressure on the water-oil interface. The flow of water from a droplet can then be summarized by [55]:

$$J_i^{out} = -\frac{dV_i}{dt} = \frac{p_f v_W}{R_{GP}T}(\Delta\Pi_i - P_i^L)S_i \tag{2.4}$$

where p_f is the water permeability through the oil-water monolayer, v_W is the water molar volume, R_{GP} is the gas constant, T is the temperature and S_i is the droplet's monolayer area. The osmotic pressure between the oil and the droplet i is:

$$\Delta\Pi_i = \Pi_{out} - \Pi_i^{in} = \Pi_{out} - \frac{C_i^{in}V_i(0)R_{GP}T}{V_i} \tag{2.5}$$

where C_i^{in} is the osmolarity of the droplet and $V_i(0)$ its initial volume. The Laplace pressure is:

$$P_i^L = 2\frac{\gamma_{m,i}(\Gamma_i)}{R_i} \tag{2.6}$$

where $\gamma_{m,i}$ is the oil-water interface tension, Γ_i is the density of occupied lipids sites on the monolayer, and R_i is the droplet radius.

When R_i decreases, P_i^L increases with a rate proportional to $\frac{1}{R_i}$, while Π_i^{in} increases with a rate proportional to $\frac{1}{(R_i)^6}$: Π_i^{in} depends on $C_i^{in} = \frac{n_i^{in}}{V_i}$, where n_i^{in} the number of moles causing osmolarity stays constant in the absence of any diffusive flux, therefore Π_i^{in} is proportional to $\frac{1}{(V_i)^2} = \frac{1}{(R_i)^6}$. Therefore the flow of water from the droplet is proportional to $-(\frac{1}{(R_i)^6}+\frac{1}{R_i})(R_i)^2$. The osmotic pressure term $\frac{1}{(R_i)^6}$ can be neglected, and as R_i decreases, J_i^{out} decreases proportionally to R_i. The water therefore evaporates with a rate that slows down until reaching an equilibrium where $\Delta\Pi_i = P_i^L$, which can be approximated to the following equilibrium radius:

$$R_i = \frac{2\gamma_{m,i}}{\Pi_{out}} \tag{2.7}$$

The evaporation of water can lead to an increase or a decrease in bilayer area, depending on the ratios of lipid desorption, adsorption and droplet evaporation [55]. In all our experiments, evaporation lead to a decrease of the bilayer area and an increase of the polar angles, suggesting that lipid desorption from the monolayer is faster than droplet evaporation. Although partitioning of water into the oil could not be avoided, evaporation could be limited to reaching the equilibrium mentioned in Equation 2.7 by sealing the chamber with a glass slide, thereby avoiding any further partitioning of the water into the air.

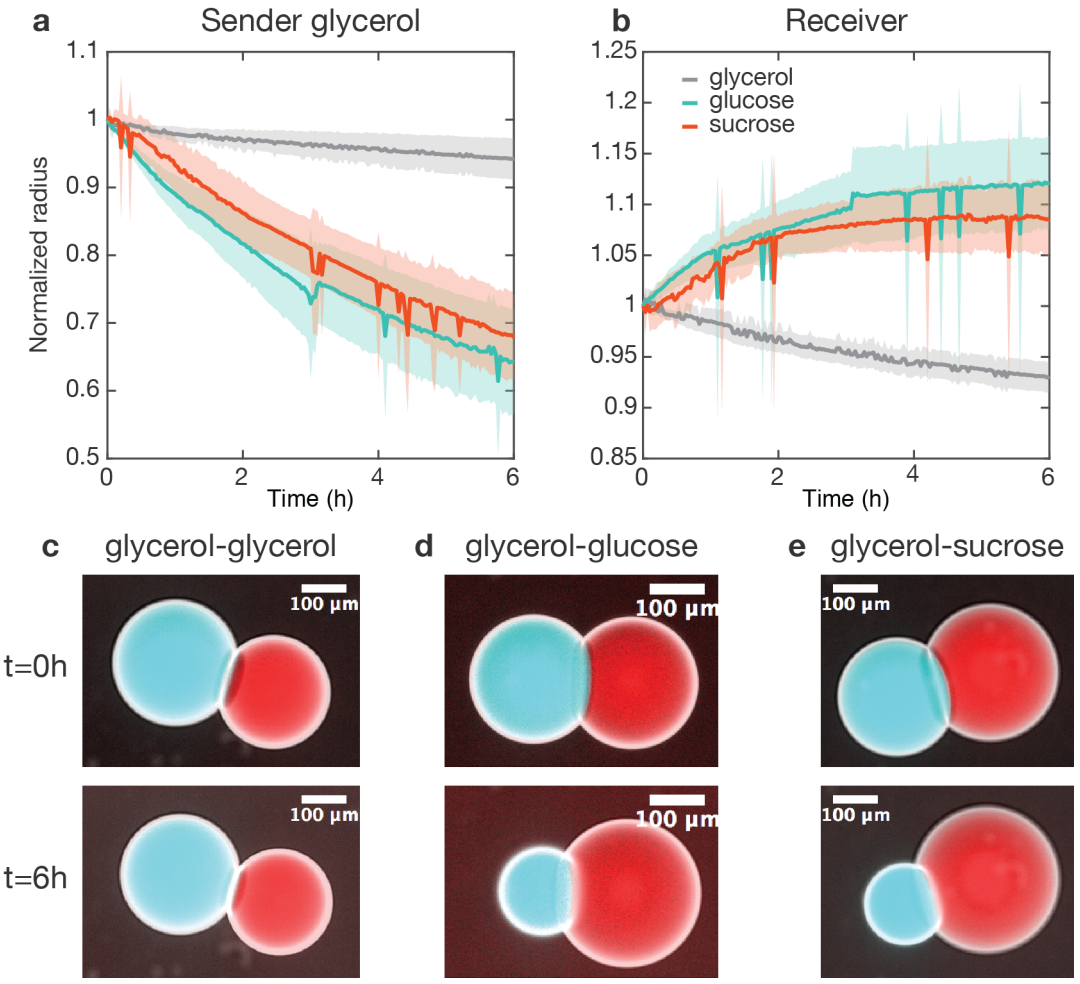

Figure 2.4. Osmolarity imbalance and volume shift. a-b The osmolarity of a glycerol-containing sender droplet is equilibrated in the receiver droplet with one of three sugars: bilayer-permeable glycerol (grey), bilayer-impermeable glucose (blue-green) or bilayer-impermeable sucrose (red). Sender and receiver volumes stay relatively constant in the glycerol-glycerol set-up, with slow droplet evaporation, whereas sender volumes (a) reduce drastically and receiver volumes (b) increase in the glycerol-glucose and glycerol-glucose setups. Mean and standard deviation of at least 6 assemblies are shown with thick lines and shaded area. c-e, Microscopy images at 0 h and 6 h for a glycerol-glycerol assembly (c), a glycerol-glucose assembly (d) and a glycerol-glucose assembly (e). Sender droplets containing glycerol are shown in cyan and receiver droplets containing glycerol, glucose or sucrose are shown in red.

Internal osmotic pressure

Internal osmotic pressure between two connected droplets annotated with l for left and r for right can be calculated with:

$$\Delta\Pi_{i,r} = R_{GP}T(C_l - C_r) = R_{GP}T(\frac{n_l}{V_l} - \frac{n_r}{V_r}) \tag{2.8}$$

If the two osmolarities C_l and C_r are not initially equal, water will flow between the droplets and their volumes will change until equilibrium is reached. In our circuits, we found that high osmolarity was caused by three factors:

- for DNA/RNA circuits, osmolarity was caused by the glycerol buffer enzymes such as T7 RNA Polymerase are stored in,
- for cell-extract circuits, osmolarity was imposed by the high salt and protein concentrations coming in the extract/buffer mix,
- for *in vivo E. coli* experiments, osmolarity was determined by the growth medium (M9 medium in most cases).

We therefore balanced the osmolarity across our assemblies by loading each droplet with equal amounts of either a self-made glycerol buffer, cell-extract/buffer mix, or M9 medium depending on the circuit chassis used.

We also performed experiments to monitor the droplet volume shift when osmolarity was equilibrated with different types of sugars: a glycerol/glycerol balance led to droplet volume stability, whereas a glycerol/sucrose balance or a glycerol/glucose balance led droplets containing glycerol to shrink (Figure 2.4). Glycerol is expected to easily cross bilayers, while glucose and sucrose should be trapped inside the droplets. Therefore, the equilibration of the glycerol concentration over the droplet pair while glucose or sucrose remains localized causes an osmolarity imbalance and a volume shift. While we aimed to keep droplet volumes constant in this work, volume change is an exciting control parameter to dynamically induce or stop concentration-dependent circuits, and it is an outlook of this work to explore such processes.

2.2 Protein pores

Since lipid bilayers form tight interfaces impermeable to most molecules, strategies must be devised to allow the diffusion of signalling molecules across the droplet assemblies. Transporters are a class of membrane proteins that serve this purpose in cells, allowing chemicals of a variety of sizes to pass the cell membrane. Three main categories of transporters have been described [56]:

- channels, which form simple water channels across the bilayer and allow molecules

matching certain size and chemical criteria to diffuse (these channels can be constitutively open or gated with membrane potential, mechanical strain or a ligand);

- solute carriers, which bind the translocating molecule and operate a conformational change to carry it across the bilayer;
- active transporters, which can move larger molecules across the cell wall, such as peptides or nucleic acids.

As protein pores operating with complex mechanisms are proportionally more complex to purify and assemble on artificial bilayers, we focused on employing well-characterized water channels. The toxin α-hemolysin is one of the best-characterized protein pores, and the most used for establishing diffusion across DIBs. This pore was used to mediate signal diffusion throughout the work described in this thesis and is described in Chapter 2.2.1. Other pores have been shown to insert in DIBs, although they are less systematically used, and they are presented in Chapter 2.2.2.

2.2.1 α-hemolysin

α-hemolysin (α-HL) is the most employed protein pore in studies of diffusion across lipid bilayers. Historical reasons might play a role, but α-HL is indeed an extremely practical and reliable pore. As a toxin secreted by the bacteria *Staphylococcus aureus*, it has evolved to rapidly form pores on cell membranes with high assembly efficiency. Targeted cells are lysed as the α-HL pore allows the flow of salts and low molecular weight molecules in the cells, affecting osmotic balance. The crystal structure of α-HL was resolved in 1996 [37]. The pore is translated as a 33.4 kDa monomer that is highly soluble in water, in contrast to most membrane proteins. Seven monomers assemble to form a mushroom-shaped pore 10 nm in length and in diameter, with a large chamber capping a 5.2 nm long, 2.6 nm outer-diameter channel (Figure 2.5.a) where hydrophobic residues are laying the outer side of the channel and hydrophilic residues are facing the inner side (Figure 2.5.c). The barrel ends in a ring of hydrophilic amino acids facing outwards, which gives the pore the appropriate hydrophilic-hydrophobic-hydrophilic geometry for stability in a lipid bilayer.

α-HL presents a slight anion selectivity and is blocked by divalent and trivalent cations, and this is likely due to interactions with positively charged residues present at the two most narrow points of the channel, at the neck and the base of the channel (Figure 2.5.b and d). The pore's narrowest inner diameter is 1.4 nm, and this is assumed to give it a size-selectivity for translocating globular chemicals of around 2 kDa, although the specific geometry and the tightness of solvation layers around each chemical will play a role in its diffusion in the α-HL barrel, as studies on the translocation of long DNA and RNA oligonucleotides demonstrates [57]. α-HL has been shown to assemble on a

variety of natural and synthetic membranes, and is extremely stable once formed, being resistant to heat, proteases and low concentrations of surfactants [37].

There is no consensus on the concentration of α-HL monomers required to induce pore formation. Early experiments on lysis of mammalian cells suggest that membrane composition may affect not only the minimum concentration leading to pore formation but possibly the mechanism of pore formation itself, as lytic concentrations varied by 3 orders of magnitude depending on the cells studied, from 1 nM to 1 µM [58]. Based on this study, α-HL was later reported to form pores at concentrations as low as 2 nM, and was estimated to assemble on synthetic lipid bilayers with a concentration of pore monomers in solution of around 200 nM [77]. In experiments where we expressed α-HL in droplets, models suggested the incorporation of pores in lipid bilayers to be a noisy process occurring at varying critical concentrations, which might control droplet-to-droplet variability of downstream processes (see Chapter 3.3 and [3], differentiation model. In most experiments, we circumvented this issue by using excess amounts of α-HL and assuming full coverage of the bilayer (see Chapter 2.3.2). It is however an outlook of this work to titrate α-HL monomer concentration in droplets and measure its effect on chemical diffusion.

Because α-HL is well characterized, simple to use, easy to express on site, efficient in pore formation, and allows comparison with other lipid bilayer synthetic biology studies, we used this pore in the vast majority of our work.

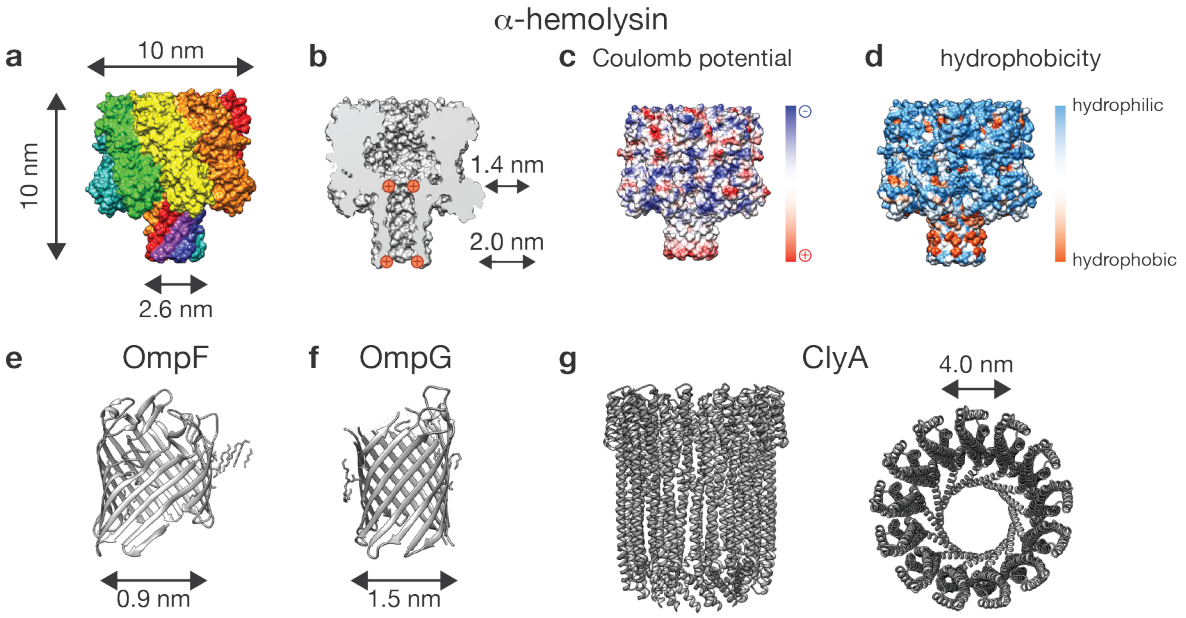

Figure 2.5. Protein pores. a-d, Structure and dimensions of α-HL, with each of the 7 monomers coloured differently (a), cross-section with inner diameters and charge of amino acids in the constriction sites of the channel (b), Coulomb surface potential indicating the local charges of amino acids (c) and hydrophobicity of the surface (d). e-g, Structure and dimensions of the inner channel of the pores OmpF (e), OmpG (f), and ClyA (g).

2.2.2 Alternative pores for DIB insertion

Although α-HL provides an interesting selectivity for chemical diffusion (see Chapter 2.3), we were also interested in translocating larger molecules such as small DNA/RNA oligos or peptides, as such intermediately-sized molecules frequently serve as signals in living organisms. Overall, having a library of pores with different diameters and different chemical selectivity could be an interesting toolbox to engineer selective diffusion paths across a droplet assembly. Although a few alternative pores were tested, this library could not be established in this thesis, but it is a clear and exciting outlook for the expansion of the artificial multicellular assembly (AMA) platform. In this section, we present interesting pores that were previously tested in DIB assemblies: pores of fixed structures and dimensions, and toxic peptides forming pores of varying sizes.

Structurally defined pores

Outer membrane proteins (Omp) are a class of pore proteins in bacteria that regulate the influx of nutrients. Most Omp consist of a β-barrel that has hydrophobic amino acids in its central belt, with side chains pointing into the membrane, and hydrophilic amino acids on the edges and on the inner part of the barrel. These pores can have closed and open conformations with loops folding into the barrel and constricting its diameter. Due to their relatively simple structure, they are believed to limit diffusion rather based on size than on chemical selectivity. We were interested in two pores from this family, OmpF (37 kDa) with an inner diameter of around 0.9 nm [59] (Figure 2.5.e), and OmpG (35 kDa) with an inner diameter of around 1.5 nm [60] (Figure 2.5.f). OmpG was employed in early DIB experiments to study asymmetric lipid bilayers [61]. Both these proteins have a smaller or equivalent diameter to α-HL, but we expected the chemical selectivity to be less restrictive, and the less constricted structure of the pore to allow the diffusion of polynucleotides.

We obtained purified OmpF from a collaborator [62], and when testing it in our systems, we found that OmpF gave no advantage compared to α-HL: for the chemicals we tested, it did not allow translocation, probably because of the narrow diameter of the pore (Figure 2.6.a).

When using OmpG, we aimed to express it *in situ* in droplets, as purification of functional membrane proteins is notoriously difficult. For this purpose, we constructed a DNA sequence with a gene coding for OmpG, whose RNA was tagged with a fluorescent aptamer [63], and followed by a reporter fluorescent protein mRaspberry (sequence in Appendix A.5). Our goal was to read out the expression levels of both transcription and translation steps and to image the localization of translation, as some ribosomes are known to be membrane-bound during translation. This membrane-localized translation has been shown to depend on the protein being translated, and nascent polypeptides can interact with membranes during their translation [64]. Transcription of Broccoli and translation of mRaspberry could be measured in cell-extract, as well as expression of

mRaspberry *in vivo* (Figure 2.6.b and c). OmpG expression was difficult to detect *in vivo* (Figure 2.6.d), as membrane proteins tend to form inclusion bodies that cannot be resolved on gels and the pore could not be purified from bacteria cultures using standard techniques. However, expression of the construct in droplets did not lead to any detectable Broccoli or mRaspberry expression, suggesting that transcription-translation was weakened in droplets. As OmpG did not present striking advantages compared to α-HL, and OmpF had failed to yield any interesting specificity, experiments with both porins were not pursued further.

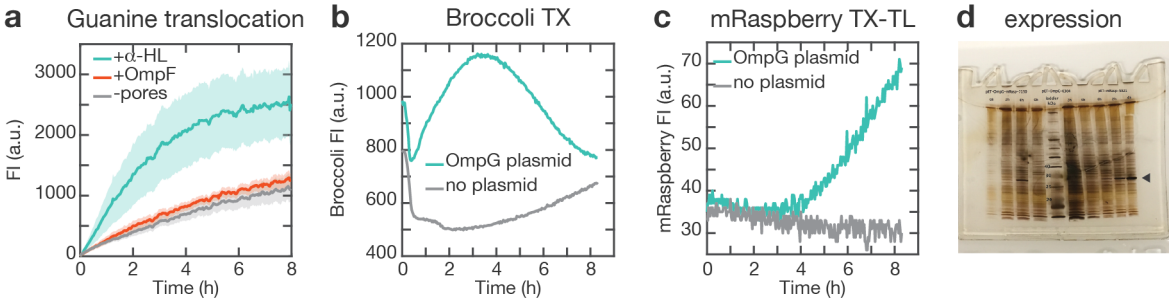

Figure 2.6. Testing of OmpF and OmpG. a, In most translocation experiments where OmpF was tested, it did not allow for a significantly faster translocation of chemicals compared to the absence of pores. Thick lines indicate mean and shaded area indicate standard deviation of at least three separate droplet assemblies. **b-c**, Transcription and translation of the OmpG construct in bulk cell-extract. OmpG was tagged with a Broccoli fluorescent aptamer that allowed the detection of transcription of the gene (**b**), and with a mRaspberry reporter that allowed tracking of translation under the same promoter (**c**). At both levels of expression, above background signals were detected (blue: OmpG plasmid, grey: negative control without plasmid). **d**, Expression of OmpG and mRaspberry in BL21star(DE3) *E. coli* cells induced with IPTG. SDS-PAGE gel is stained with silver staining. Samples were taken at 0 h, 2 h and 4 h after induction for pET-OmpG-mRasp (the full construct) and two controls coding each for only one protein: pET-OmpG and pET-mRasp. OmpG weighs 35.8 kDa and mRaspberry weighs 25.5 kDa. The band of mRaspberry is indicated by an arrow. No band can be detected for OmpG.

Cytolysin A (ClyA) is a pore-forming toxin expressed by *E. coli*, which assembles on bilayers from water-soluble monomers, similarly to other pore-forming toxins. In the case of ClyA, 13 monomers of 34 kDa assemble into a conical shaped pore with a diameter at the narrowest point of 40 Å[65] (Figure 2.5.g). Due to this large diameter, ClyA is an excellent candidate for spontaneous translocation of oligonucleotides and proteins, and indeed it has already been engineered for the voltage-dependent translocation of such macromolecules [66], [67]. ClyA pores were recently used to measure conductance in a droplet-hydrogel bilayer set-up [68]. However, this pore is not commercially available and we did not have the opportunity to test it during this work.

Peptide-based pores

Streptolysin O. (SLO, 69 kDa) is a toxin found in group A streptococci. It does not assemble into a pore of precise structure, rather the water-soluble monomers form rod structures that insert into the bilayer and assemble into large arcs and rings, creating pores of up to 30 nm diameter [69] and causing cell lysis. Cholesterol is an important membrane binding partner for proper functionality of SLO. In DIB assemblies, SLO was

used to translocate DNA in a voltage-dependent manner and subsequently perform logic computation [70]. As this pore is commercially available, we attempted to use it in our experiments, but could not detect diffusion, indicating that pore assembly did not occur. In the future, cholesterol concentration in the lipid mix could be screened to assess proper pore formation. However, the diameter of SLO pores would allow virtually all molecules - proteins, DNA, possibly even ribosomes - to freely diffuse from one compartment to the next, causing the compartments contents to mix. Identity of single compartments is a crucial feature in our systems to allow spatial resolution of processes such as signalling and differentiation (this is addressed in more details in Chapter 3), therefore the use of SLO might counter the encapsulating and localizing approach of this work.

Melittin (2.8 kDa) is a pore-forming peptide found in bee venom. The peptide monomers were shown to assemble in two stoichiometries leading to two inner diameters of the pores: 10 to 30 Å[71], and 35 to 45 Å[72]. Melittin was recently used in multi-compartment vesicle experiments [42]. The pore sizes seem to be a good alternative to α-HL, with a slightly higher diameter that still allows compartments to retain their identity (for example their DNA content).

α-HL pores offer a rich chemical selectivity for the diffusion of small metabolite signals (see Chapter 2.3), and it was an important element in reaction-diffusion circuits in this work (see Chapters 2.1 and 2.3). Other pores such as melittin and ClyA may allow larger molecules to diffuse through the droplet assemblies, inviting the design of new exciting reaction-diffusion circuits and should be assessed in future work.

2.3 Characterizing signalling chemicals

In order to engineer reaction-diffusion synthetic circuits, communication between artificial cells in assemblies must be established. For this purpose, we assessed the diffusion of a library of chemicals relevant for synthetic gene circuits in a simplified droplet assembly. The assessed diffusion behaviour and its α-HL pore dependency for all tested chemicals are first presented (Chapter 2.3.1). Modelling of diffusion and membrane permeation in this artificial-cell assembly system is then discussed, and a simple but effective model is constructed (Chapter 2.3.2). The possibility to control diffusion dynamics through ”source-and-sink” mechanisms or Donnan potential is briefly discussed (Chapter 2.3.3). Finally, the development of 3D-printing strategies in the context of this thesis is described (Chapter 2.3.4).

2.3.1 Signalling molecules and diffusion behaviour

The chemicals whose diffusion we were interested in assessing were at first all chemicals involved in synthetic gene circuits: small metabolites, DNA, RNA and proteins. Due to the hydrophobicity barrier of the lipid bilayer and the narrow diameter of the α-HL pores (1.4 nm), it was quite evident that large DNA and RNA molecules, as well as proteins, could not diffuse across bilayers, and this was validated in control experiments for the diffusion of other chemicals (read-out circuits, consisting of DNA, RNA and proteins, did not diffuse out of their compartments for instance). Indeed, the local trapping of macromolecules in droplets is what gave each compartment its identity, and allowed us to later on measure cellular-like behaviour such as differentiation. We therefore focused on assessing the diffusion of small chemicals that could serve as interesting inducers for synthetic gene circuits, such as aptamer ligands or riboswitch regulators. As most of these chemicals were not fluorescent on their own, we designed a read-out synthetic circuit for each of the chemicals tested, either with *in vitro* transcription, *in vitro* transcription-translation or with genetically modified *E. coli* cells (experimental conditions are listed in Appendix A.3).

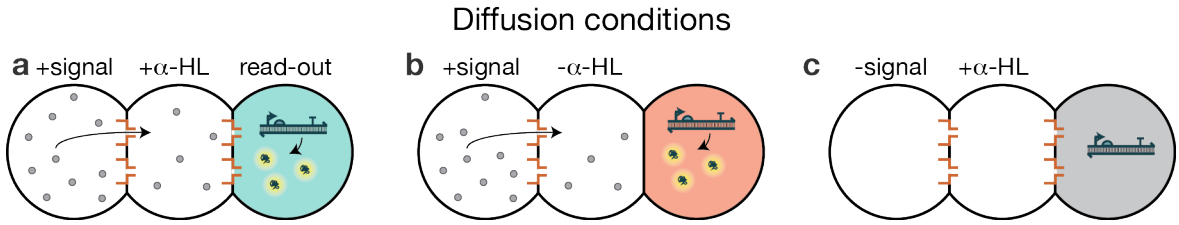

Figure 2.7. Assessing specificity of diffusion in droplet assemblies. **a**, In the first condition, the signal is present in the sender droplet and pores are present in the buffer droplet. If the signal diffuses at all, whether through pores or not, the read-out circuit should be activated. **b**, In the second condition, the signal is present in the sender droplet and pores are absent in the buffer droplet. Signals that diffuse due to the presence of pores will not reach the receiver droplet, but signals that diffuse through the bilayer will. **c**, in the third condition, the signal is absent in the sender droplet and pores are present in the buffer droplet. In this negative control, the read-out should not be activated in the receiver droplet. If it is, this indicates that pores allow the flux of nutrients that increase background activation, and might be an indication that the signal does not diffuse at all.

Assessing diffusion specificity

Our aim was to both assess the diffusion of chemicals and determine its dependence on the presence of α-HL. Naively, we assumed that more hydrophobic chemicals could cross the bilayer with little energy limitation, hydrophilic and small chemicals would only diffuse through the water channels created by pores, and larger chemicals, whether hydrophobic or not, would not diffuse at all. The following droplet assembly was used for diffusion assessment: a receiver droplet contained the read-out circuit and no pores. It was connected to a buffer droplet, which did not contain the chemical, and did or did not contain pores. The buffer droplet was then connected to a sender droplet, which contained pores, and did or did not contain the chemical. The buffer droplet avoided any signal leak between sender and receiver that could occur during bilayer formation

(see Chapter 2.1.2) and cause an increase in read-out independently of the chemical's actual diffusion. Through the presence or absence of pores in the buffer droplet, the pore dependence of diffusion could be assessed. Measuring the read-out when the signal was absent in the sender droplet but pores were present in the buffer droplet was a negative control insuring that any raise in read-out was due to chemical diffusion and not to unrelated effects such as nutrients diffusion from sender to receiver, which could increase background signal. The three conditions that were compared are summarized in Figure 2.7.

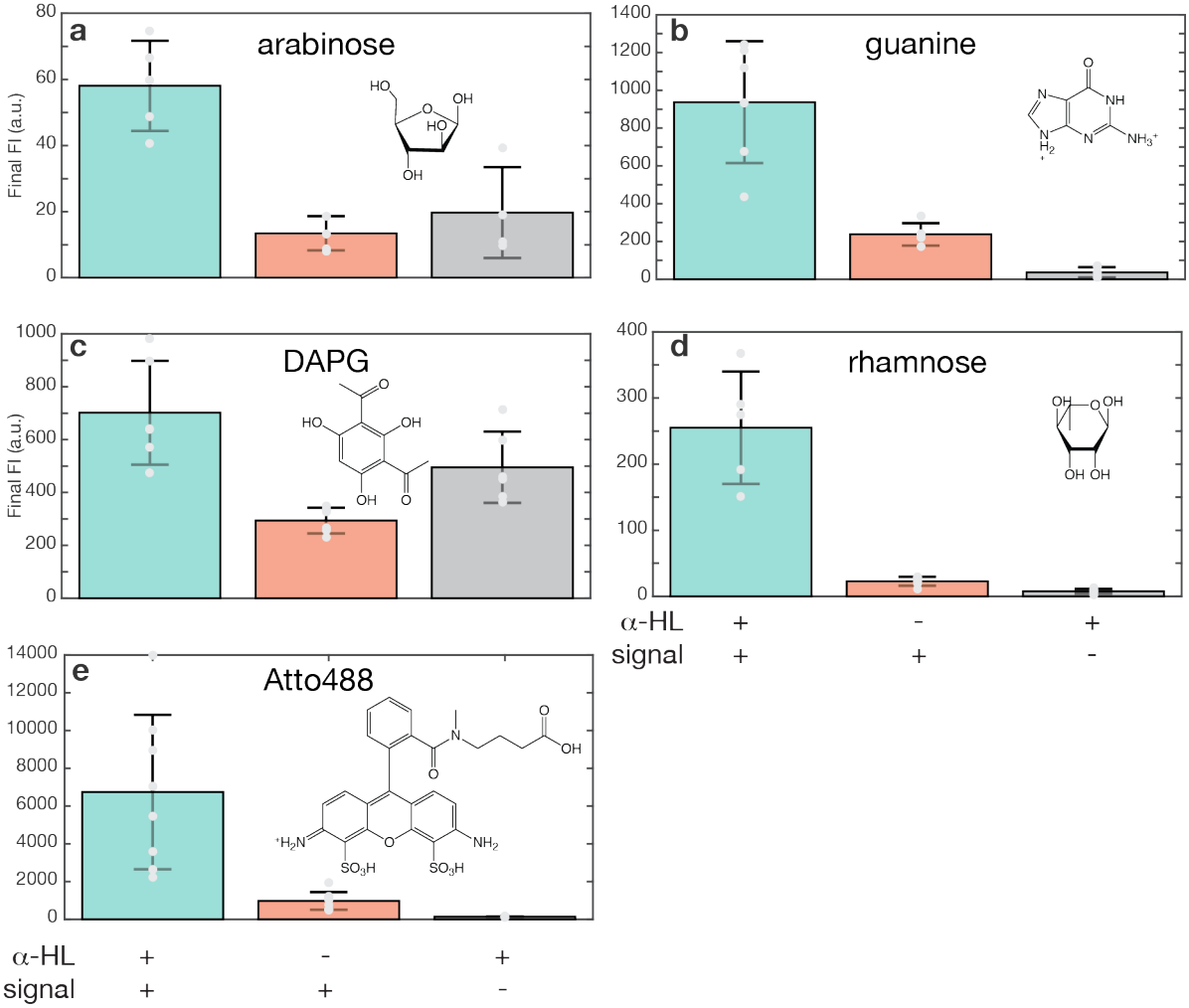

Figure 2.8. Pore-mediated diffusing chemicals. Mean and standard deviation of final fluorescence intensities of read-out are shown for the three conditions listed in Figure 2.7. Single data points are overlaid. Chemical structures are shown. **a**, arabinose, **b**, guanine, **c**, DAPG, **d**, rhamnose, **e**, Atto488.

Three diffusion behaviours could be distinguished, and chemicals are classified according to these below: pore-mediated diffusion (Figure 2.8), where chemicals diffuse faster in presence of pores than in their absence; non-specific diffusion (Figure 2.9), where chemicals diffuse independently of the presence of pores; or absent diffusion (Figure 2.10), where chemicals either partition into the oil or remain in the sender droplet,

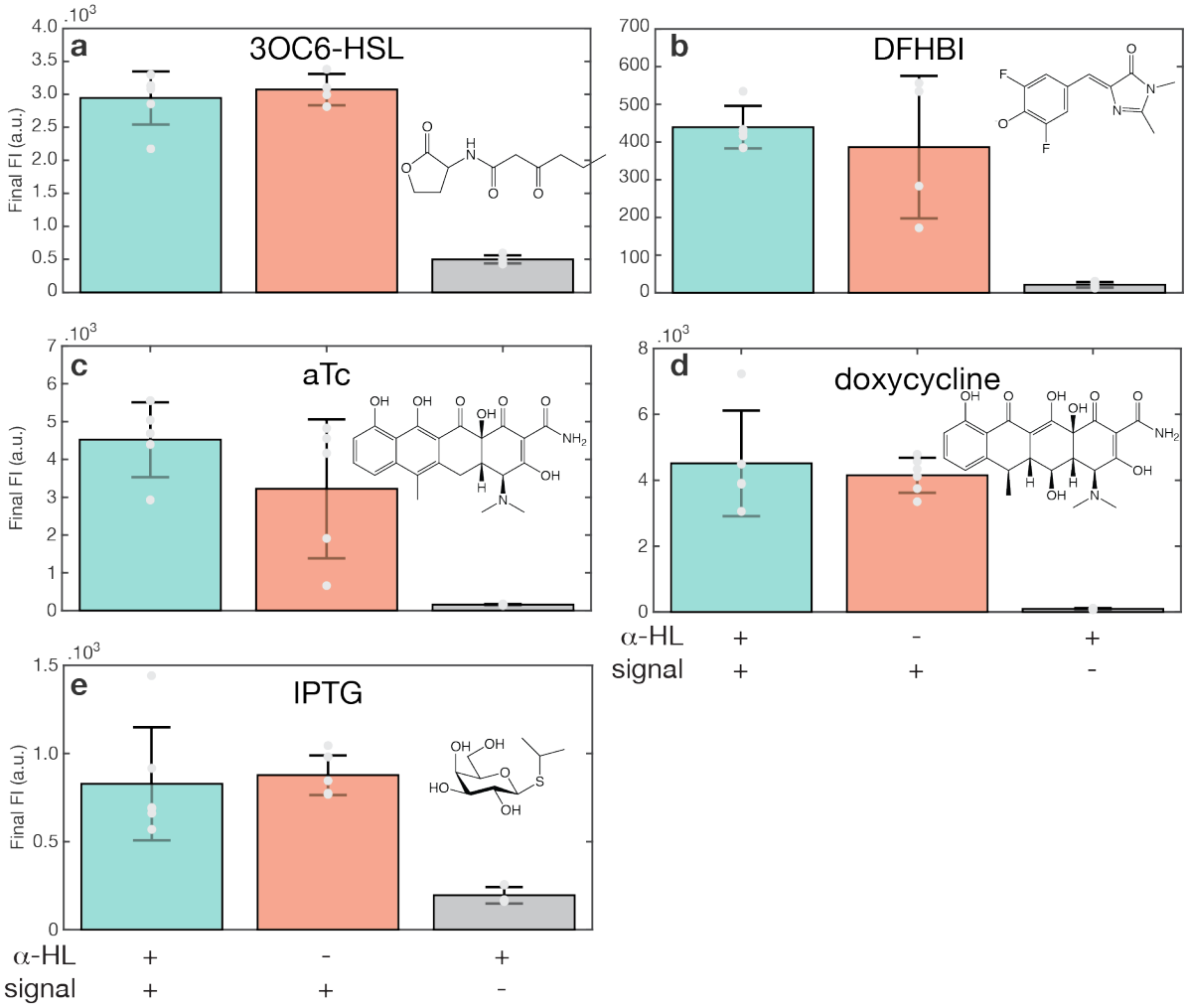

Figure 2.9. Non-specifically diffusing chemicals. Mean and standard deviation of final fluorescence intensities of read-out are shown for the three conditions listed in Figure 2.7. Single data points are overlaid. Chemical structures are shown. **a**, 3OC6-HSL, **b**, DFHBI, **c**, aTc, **d**, doxycycline, **e**, IPTG.

with no compartment-to-compartment diffusion. For each chemical, the read-out signal through time in receiver droplets was measured for at least three different assemblies under each condition in Figure 2.7, and end-measurement values were averaged. The mean and standard deviation, demonstrating the distribution of the read-out circuit, are overlaid with single data points for end values. Chemical structures of the molecules are also indicated.

To clearly visualize the difference between pore-mediated diffusion and non-specific diffusion, 2D assemblies are created where DFHBI (non-specific) or guanine (pore-mediated) is allowed to diffuse. A path of α-HL containing droplets is established in the centre of the assembly, which guanine diffusion follows whereas DFHBI diffuses homogeneously across the assembly (Figure 2.11). This is also studied in more detail with a diffusion comparator circuit in Chapter 3.1.

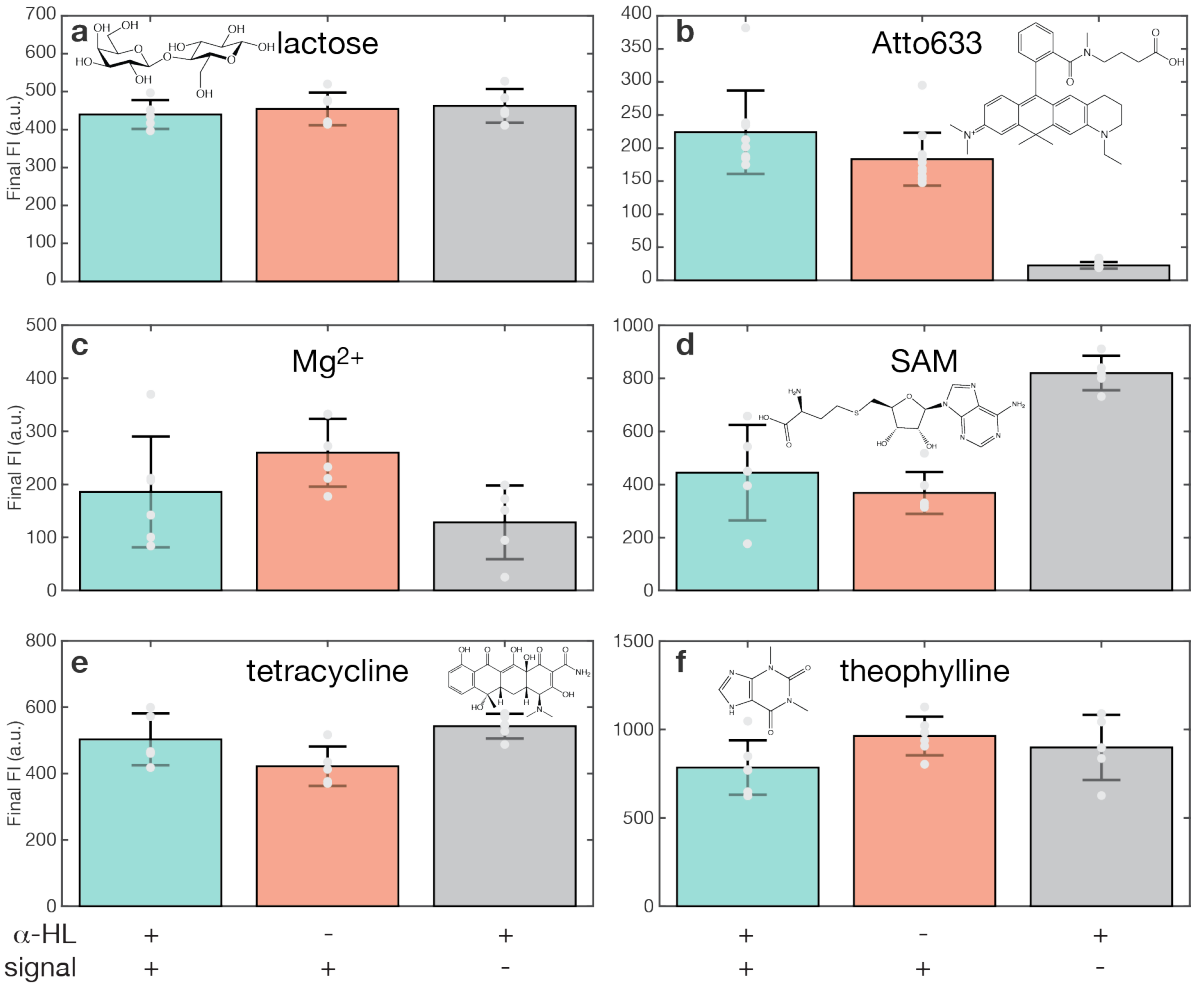

Figure 2.10. Non-diffusing chemicals. Mean and standard deviation of final fluorescence intensities of read-out are shown for the three conditions listed in Figure 2.7. Single data points are overlaid. Chemical structures are shown. **a**, lactose, **b**, Atto633 (although final fluorescence levels seem to indicate non-specific diffusion, the time traces shown in Figure A.2 indicate that the fluorophore diffuses out to the oil), **c**, Mg^{2+}, **d**, SAM, **e**, tetracycline, **f**, theophylline.

Modelling diffusion specificity

For the most part, the diffusion behaviour of chemicals was as naively expected. Rather hydrophobic chemicals such as 3OC6-HSL or DFHBI could easily diffuse in the absence of pores from droplet to droplet. The mechanism for this diffusion could be either bilayer permeation, or partitioning and diffusion into the oil phase followed by partitioning into the receiver droplet. Positioning sender and receiver droplets at close distance without allowing them to form a bilayer could differentiate these mechanisms, but this is beyond the scope of this work. More hydrophilic chemicals, such as sugars (arabinose, rhamnose) or charged molecules (guanine, nucleotides) demonstrated pore-dependent diffusion. However, some structurally similar molecules had drastically different diffusion behaviour: for example, anhydrotetracycline (aTc) could diffuse non-

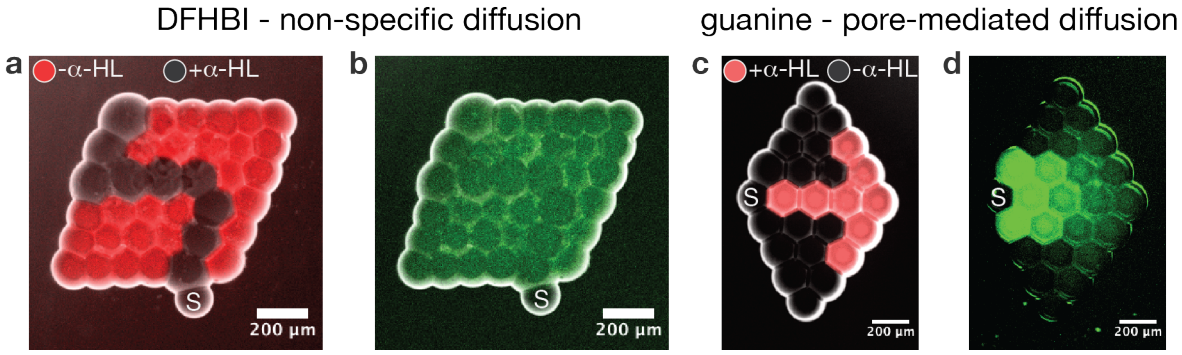

Figure 2.11. Non-specific versus pore-mediated diffusion in 2D assemblies. **a**-**b**, DFHBI diffuses in a 2D assembly from a sender droplet (S) into receiver droplets that either contain (**a**, black) or do not contain (**a**, red) α-HL. Droplets not containing α-HL are marked with a red dye (**a**). DFHBI diffusion is read-out with an RNA aptamer that increases DFHBI fluorescence (**b**, t = 30 min). DFHBI equilibrates homogeneously in the assembly irrespective of the presence of pores in receivers. **c**-**d**, Guanine diffuses in a 2D assembly from a sender droplet (S) into receiver droplets that either contain (**c**, red) or do not contain (**c**, black) α-HL (labelling is inverted compared to **a**). Droplets containing α-HL are marked with a red dye (**c**). Guanine diffusion is read-out with an RNA aptamer that increases DFHBI fluorescence in presence of guanine (**d**, t = 13 h 20 min). Guanine diffuses into droplets that contain α-HL and direct neighbour droplets (α-HL incorporates into every adjacent bilayer to the droplet that contains it), demonstrating an inhomogeneous and directed diffusion pathway across the assembly.

specifically, but tetracycline (Tc) did not diffuse in our experiments.

To elucidate what determines the diffusion behaviour of chemicals, we used molecular modelling to calculate parameters relating to chemical size and hydrophobicity. We focused on criteria affecting bilayer permeation as summarized in the so-called Rule of Five, employed in pharmacology to assess the ability of a molecule to permeate cell membranes [73], [74], [75]. These criteria include for example the molecular weight of the chemical or its number of hydrogen bond donors and acceptors. They predict the ability of a chemical to diffuse non-specifically through bilayers. The calculated parameters from molecular modelling (Chem3D, see Appendix A.3) are summarized in Table 2.1.

We found that generally, the two most relevant parameters to predict the diffusion behaviour of chemicals were molecular weight and partitioning coefficient between water and octanol logP (which predicts partitioning efficiency into the bilayer). Figure 2.12 shows these parameters for all assessed chemicals. Chemicals that satisfied the Rule of Five criteria displayed non-specific diffusion, demonstrating that these criteria are good predictors of bilayer permeation. Pore-mediated diffusion, on the other hand, is affected by the diameter of the chemical compared to that of the pore and interactions within the pore's barrel, and could be more difficult to predict. Indeed, we find that pore-mediated diffusing and none diffusing chemicals do not seem to cluster in specific ranges of logP and molecular weight, other than their lack of fulfilment of the Rule of Five criteria. It seems that hydrophilic and small chemicals such as guanine, rhamnose and arabinose can diffuse through the pore, but an ion such as Mg^{2+} does not diffuse at all, maybe due to its high charge and tight solvation layers. Large and hydrophilic chem-

Chemical	Molecular weight ($g.mol^{-1}$)	Connolly excluded volume ($Å^3$)	Radius (Å)	H-bond acceptors	H-bond donors	logP
Pore-mediated diffusing chemicals						
arabinose	150.130	118.083	3.04	5	4	-1.8245
Atto488*	590.61	N.C.	N.C.	N.C.	N.C.	-1.28
DAPG	210.185	150.8570	3.30	5	3	1.3533
guanine	151.130	85.4350	2.73	3	3	-1.4483
rhamnose	164.160	134.9840	3.18	5	4	-1.3749
Non-specifically diffusing chemicals						
3OC6-HSL	213.233	186.1240	3.54	2	1	1.9708
aTc	462.900	N.C.	N.C.	8	5	1.0686
DFHBI	252.220	172.4380	3.45	5	0	1.0888
doxycycline	444.43	N.C.	N.C.	9	6	-0.6228
IPTG	238.298	204.4620	3.65	5	4	-0.5786
Non-diffusing chemicals						
Atto633*	552.74	N.C.	N.C.	N.C.	N.C.	2.96
lactose	342.300	274.5410	4.03	11	8	-4.4127
Mg^{2+}*	24.31	N.C.	N.C.	N.C.	N.C.	0
SAM	384.411	243.172	3.87	10	5	-3.2196
tetracycline	444.435	N.C.	N.C.	9	6	-0.7617
theophylline	180.164	108.86	2.96	4	1	-0.7462

Table 2.1. Molecular modelling results for diffusing and non-diffusing chemicals. Most chemicals were analysed with Chem3D. Radius is calculated from excluded volume by assuming a spherical volume. Relevant predictors of diffusion behaviour were found to be molecular weight and logP, the log of the partitioning coefficient between octanol and water, which reflects hydrophobicity. N.C.: not calculated. Chemicals marked with * were analysed with the molecular properties module of Cheminfo [76].

icals such as tetracycline, SAM and lactose cannot diffuse through the pores. Pore-mediated transport of a molecule depends on the number and diameter of the pores in the bilayer, as well as on interactions between the translocating molecule and the pore's amino acids. We expect that these interactions are crucial in explaining specifically why each small hydrophilic chemical tested could or could not diffuse through α-HL pores. For example, DNA and RNA molecules have been shown to translocate through α-HL pores in a voltage-dependent manner (see Chapter 2.2.1), demonstrating that the size of a nucleotide is not too large to diffuse through the pore. We however expect that spontaneous diffusion of DNA and RNA is prohibited due to the rigidity of the polymer structure (the persistence length of DNA is around 50 nm). Indeed, in our experiments large hydrophilic chemicals were mostly unable to diffuse across bilayers with or without pores.

In this set of experiments, we assessed the pore-dependent diffusion of a li-

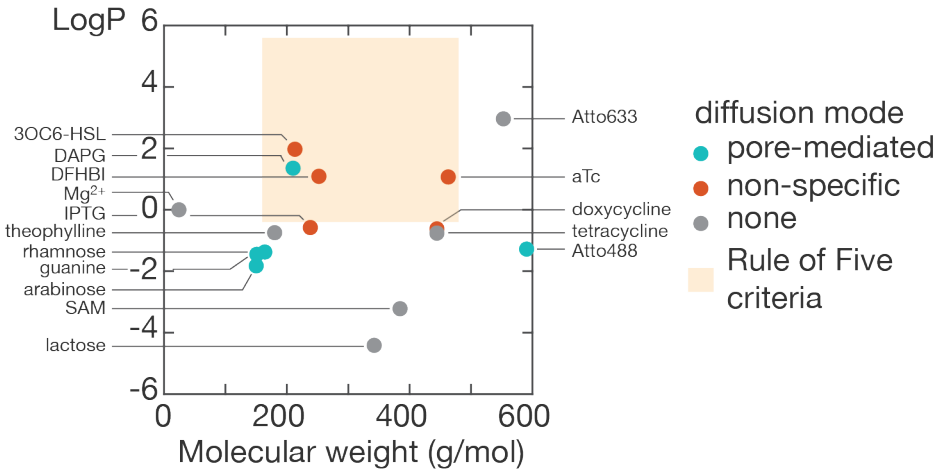

Figure 2.12. Calculated molecular weight and logP for all chemicals tested for diffusion. Chemicals that have pore-mediated diffusion are indicated in blue, chemicals that have non-specific diffusion in red, and chemicals that do not diffuse in grey. The range corresponding to the Rule of Five criteria is indicated with a yellow box. Chemicals are identified with lines.

brary of chemicals by coupling their diffusion to synthetic gene circuit read-outs in our artificial multicellular assemblies (AMA). We therefore established a versatile toolbox for the construction of reaction-diffusion circuits. To understand and predict the dynamics of such circuits, it was important to model diffusion in our assemblies, and to determine the diffusion kinetics of potential chemical signals.

2.3.2 Modelling diffusion

Determining the kinetics of diffusion in our assemblies is a crucial tool to predict the reaction-diffusion circuits' behaviour, their dynamic range and the length scale of pattern formation. To that purpose, we created a simple but effective diffusion model taking into consideration both aqueous diffusion in the compartments and membrane permeation between them. With this model, we determined the permeability of the bilayers to four different chemicals and therefore completely defined their diffusion kinetics in our platform.

Aqueous diffusion and membrane permeation

Considering a linear array of compartments of diameter l, connected via interfaces of thickness $L \ll l$ (the thickness of the bilayer is $L = 5$ nm), an effective diffusion coefficient D_{eff} can be calculated based on the free diffusion in the compartments D, and the permeability of the membrane P [12]:

$$\frac{1}{D_{eff}} = \frac{1}{D} + \frac{1}{Pl} \tag{2.9}$$

For all small molecules considered as signals, the diffusion coefficient in water was estimated using the computed radius (which we approximate to the hydrodynamic radius, although it differs from it) from Chem3D modelling and the Stokes-Einstein equation:

$$D = \frac{k_b T}{6\pi\eta r} \tag{2.10}$$

,assuming T = 37 °C and η = 0.6913 mPa.s for water at T. This diffusion coefficient was typically in the order of D = 1000 µm^2.s^{-1}. Assuming a typical droplet diameter of l = 250 µm (assumed for droplets of volume around 10 nL), $\frac{D}{l} \approx 4 \ . \ 10^{-6}$ m.s^{-1}. From this estimation of the diffusion in water and Equation 2.9, two limit cases can be considered:

- $P \ll \frac{D}{l}$, *i.e.* $P \ll 10^{-6} m.s^{-1}$, $D_{eff} \approx Pl$, and permeation of the bilayer is kinetically limiting. Transport can then be considered as a series of mass transfer processes where molecules hop from one compartment to the next.

- $P \gg \frac{D}{l}$, *i.e.* $P \gg 10^{-6} m.s^{-1}$, $D_{eff} \approx D$, and diffusion through the aqueous compartments is limiting. The diffusion in the assemblies can then be considered equivalent to free diffusion of the signal in a continuous environment, although macromolecules remain localized.

Notes:

- The aqueous diffusion of the signal D can be affected by the chemical's interaction with localized macromolecules, as is detailed here. Let us assume a freely diffusing chemical C with diffusion coefficient D_{free}. This chemical binds a localized macromolecule M (such as a protein or an RNA aptamer) with dissociation constant K_d. The complex MC has a diffusion coefficient D_{bound}. The fraction of free C is:

$$f = \frac{[C]_{free}}{[C]_{tot}} = \frac{[C]_{free}}{[C]_{free} + [MC]} \tag{2.11}$$

  We then assume that the apparent diffusion coefficient of the chemical will be:

$$D = f \times D_{free} + (1 - f) \times D_{bound} \tag{2.12}$$

  f depends on K_d as follows:

$$f = \frac{K_d}{[M]_{free} + K_d} \tag{2.13}$$

  Assuming a large excess of M, we could then write $f \approx \frac{K_d}{[M]_{tot} + K_d}$, but this approximation can rarely be made in our experiments (binding partners are typically present in µM ranges, whether they are proteins or RNAs, and signals are added in ranges from nM to mM). Still, if the fraction of free M is much larger than K_d

(*i.e.* if the K_d is low compared to the concentrations of binding partners present, meaning the binding affinity is strong), we can extrapolate that every C entering the droplet will be bound, and therefore $D = D_{bound}$. Conversely, if the K_d is larger than the amount of free M (either because the binding is weak, or because M is present at low concentrations, for example when it is being expressed on site), we can extrapolate that C will mostly remain in its free form, and $D = D_{free}$. In most of our experiments, C was present in large excess compared to K_d and the binding partner M, therefore we assume that $[C]_{tot} = [C]_{free}$, and $D = D_{free}$.

- The length of the compartments, *i.e.* the diameter of the droplets, will affect which diffusion process is limiting (membrane permeation or aqueous diffusion). As we advanced in the project, we attempted to create droplets of smaller and more reproducible diameters and these efforts culminated in 3D printing where we achieved a droplet diameter of around 100 µm. The reduction in droplet diameter will affect the diffusion as follows: when the compartments are smaller, l is smaller, $\frac{D}{l}$ is larger, and therefore more cases become permeation-limited. Naively speaking, there are more "barriers" over free diffusion on the same total length of an assembly, because there are more droplets. Therefore permeation becomes more frequently the diffusion-limiting step.

In the general case where both membrane permeation and aqueous diffusion contribute to chemical transport across an assembly, diffusion can be described as follows. We first assume an assembly of only two droplets. The diffusion flux from droplet 1 to droplet 2 is:

$$j_{1\to 2} = -D_{eff}\nabla n = -D_{eff}\frac{n_1 - n_2}{l} \tag{2.14}$$

, with n the molar concentration of diffusing molecules, assuming homogeneous concentrations in each droplet. The time derivative of the chemical's concentration n in droplet 1 is then (with N_i the molecule density per unit volume in droplet i and A_{ij} the effective area for transport between droplets i and j, details for the calculation of this area are discussed below):

$$\frac{dn_1}{dt} = \frac{1}{V_1}\frac{dN_1}{dt} = \frac{1}{V_1}j_{1\to 2} \times A_{12} = -\frac{1}{V_1}D_{eff}\frac{n_1 - n_2}{l}A_{12} = -\frac{1}{V_1}A_{12}\frac{DPl}{D + Pl}\frac{n_1 - n_2}{l}$$

$$\frac{dn_1}{dt} = -\frac{1}{V_1}\frac{DPA_{12}}{D + Pl}(n_1 - n_2) \tag{2.15}$$

This can be generalized to any dimension of the assembly:

$$\frac{dn_i}{dt} = \sum_{j\in\{neighbours of i\}} -\frac{1}{V_i}\frac{DPA_{ij}}{D + Pl}(n_i - n_j) \tag{2.16}$$

We used this model to fit the permeability of the membranes to different chemicals, assuming a free diffusion in the aqueous phase. We then determined for each chemical which approximations could be made as to the dominant diffusion process.

A_{ij} is the effective area for transport of the chemical. This corresponds to two different calculations according to the diffusion mechanism. In the case of non-specific diffusion, A_{ij} corresponds to the total area of the bilayer interface. In the case of pore-mediated diffusion it is given approximately by the total cross-section of the pores in the membrane.

The *total area of the bilayer* was estimated from measuring the diameter of the bilayer in standard droplet experiments, and the diameter was found to be on average around 160 µm. From this, the effective area of permeation for non-specific diffusion was calculated to be approximately 2 . 10^{-8} m^2.

The *effective area of pore-mediated permeation* was estimated as follows. The α-HL pore has a maximum outside diameter of 10 nm [37], and we approximate its area on the bilayer to a square, as we expect steric hindrance to keep the pores from having a compact alignment. A fully covered bilayer would therefore have $\frac{\pi r_{bil}^2}{d_{pore}^2}$ = 2 . 10^8 pores. Considering a circular pore area, the bilayer would be covered with maximum 2.6 . 10^8 pores. We assume that this number overestimates the real bilayer occupancy, as diffusion of the pores on the bilayer and other effects reduce the available area, and therefore assumed 1 . 10^8 pores as the maximum occupancy. Other studies have estimated maximum surface coverage by functional α-HL pores at around 1 % due to monomers interacting with the bilayers [77], which would be in the order of 1 . 10^6 pores. In most cases, our droplets contain 1.5 µM of pores, and we can calculate the maximum number of pore monomers in the droplet with $N = \frac{C_m V N_A}{M}$, with C_m the mass concentration, V the volume, N_A Avogadro's number, and M the molecular weight (here approximately 33 kg.mol^{-1}). With N = 9 . 10^9 pore monomers in the droplet, *i.e.* approximately 1.3 . 10^9 potential heptamers, we assume that the bilayer is covered to its maximum occupancy. From this, the effective area of pore-mediated permeation was estimated at 1 . 10^8 pores = 1 . 10^8 x $(10^{-8})^2$ m^2 = 1 . 10^{-8} m^2, half the effective area of non-specific permeation. This ratio may be even lower if monomers interacting with the bilayer affect surface coverage by functional pores, but there is no possible quantification of how strong this effect might be.

These parameters, together with our diffusion model and our transcription or transcription-translation models (see Appendix A.1), were used to fit the permeabilities of a few chemicals.

Permeability fitting

To determine the limiting step in the diffusion of the tested chemicals, we first fitted the bulk kinetics of the read-out circuits (see Figure A.3 and Table A.1 in Appendix A.4) and calculated the aqueous diffusion coefficient of the chemicals from the Stokes-

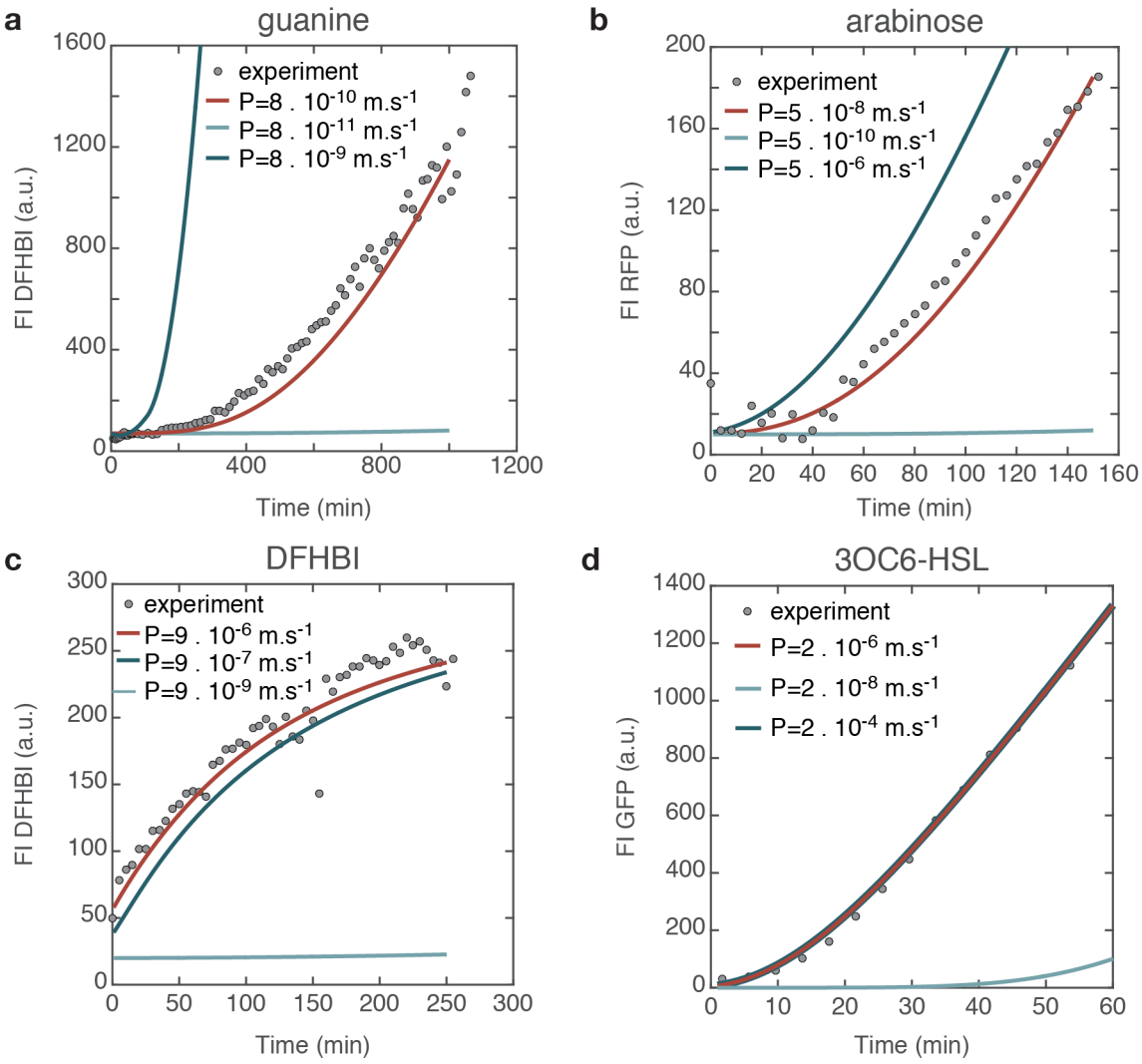

Figure 2.13. Fitting of P from translocation experiments. D was determined for the different species via the Stokes-Einstein equation. All figures show: grey dots, one of six data sets that were fitted; red line, simulation with fitted permeability; light and dark blue lines, simulations with different permeabilities, indicating the significance of the fitted permeability. **a**, guanine, P was fitted at $8 \cdot 10^{-10}$ m.s^{-1} (permeation through the bilayer is limiting). **b**, arabinose, P was fitted at $5 \cdot 10^{-8}$ m.s^{-1} (permeation through the bilayer is limiting). **c**, DFHBI, P was fitted at $9 \cdot 10^{-6}$ m.s^{-1} or above (diffusion across the droplet is limiting). **d**, 3OC6-HSL, P was fitted at $2 \cdot 10^{-6}$ m.s^{-1} or above (diffusion through the droplet is limiting).

Einstein equation, assuming radius values from calculations of Chem3D molecular modelling as approximations for the hydrodynamic radii (Table 2.1). For each chemical, six curves corresponding to six separate assemblies were independently fitted with the permeability as the only fitting parameter, and the values were averaged. Table 2.2 summarizes the fitting results.

The fitted permeabilities were in good agreement with the limit cases of our diffusion model. Guanine and arabinose, pore-mediated diffusing chemicals, had bilayer

Experiment	α (M^{-1})	β	k_{prod} ($M.s^{-1}$)	k_p ($M^{-1}.s^{-1}$)	k_m (s^{-1})	D ($m^2.s^{-1}$)	P ($m.s^{-1}$)	V (L)
guanine permeability (Figure 2.13.a)	$5.0 . 10^8$	70	$5.75 . 10^{-10}$	5.5	$8.25 . 10^{-6}$	$1.2 . 10^{-9}$	$8 . 10^{-10}$	$1.3 . 10^{-8}$
arabinose permeability permeability (Figure 2.13.b)	1000	-10	N.A.	N.A.	N.A.	$9.0 . 10^{-10}$	$5 . 10^{-9}$	$6 . 10^{-9}$
DFHBI permeability permeability (Figure 2.13.c)	$9.4 . 10^7$	-30	$9.83 . 10^{-10}$	$8.17 . 10^4$	0.105	$9.5 . 10^{-10}$	$> 9 . 10^{-6}$	$1.0 . 10^{-8}$
3OC6-HSL permeability permeability (Figure 2.13.d)	$1.9 . 10^{15}$	0	N.A.	N.A.	N.A.	$7.7 . 10^{-10}$	$> 2 . 10^{-6}$	$1.0 . 10^{-8}$

Table 2.2. Permeability fits. Underlined values were fitted in the experiments shown in the corresponding figures. N.A.: not applicable.

permeabilities below 10^{-6} $m.s^{-1}$, corresponding to the membrane permeation limiting case. In this situation, the diffusion can be approximated to "hops" across the bilayer from compartment to compartment. In contrast, 3OC6-HSL and DFHBI had bilayer permeabilities above 10^{-6} $m.s^{-1}$, which corresponds to the aqueous diffusion limiting case. In fact, only a lower limit for the permeability of these chemicals could be fitted, as higher values of the permeabilities did not affect the dynamics of the system anymore. For these chemicals, the reaction-diffusion circuits can be approximated to a continuous environment with localized macromolecules. Figure 2.13 shows for each of these chemicals a typical set of data fitted from one droplet assembly, the simulated model with the fitted permeability value, and the simulated model with extreme permeability values, to demonstrate the range of validity of the fitted permeabilities.

2.3.3 Controlling diffusion kinetics

Our platform relies on spontaneous diffusion through bilayers or through pores to mediate cell-to-cell communication. Although the diffusion kinetics can be partially tuned with protein pore concentrations for pore-mediated chemicals (see Chapter 3.1), a more direct control on diffusion kinetics and diffusion profiles for all signalling chemicals would be of interest. In a number of studies on DIB, this was achieved by imposing voltage across bilayers to accelerate diffusion. However, in large multicellular assemblies, equipping specific droplets with electrodes is not scalable, and would not be fit for

a transfer of the water-in-oil assembly into an aqueous external environment. In living organisms, membrane potential is controlled through a variety of mechanisms, but the Donnan potential is considered one of the main contributors: this effect and attempts to recreate it in droplet assemblies are detailed in the first part of this section. In embryogenesis, constant diffusion gradients could be maintained through a "source-and-sink" mechanism (see Chapter 3.1 and [12]). This approach was also tested and is described in the second part of this section.

Donnan potential

The Donnan potential is an electric potential that arises across a semi-permeable membrane when impermeable ions are present on one side. Let us consider a system where on one side of a membrane, proteins P^{2-} (typically highly negatively charged at physiological pH, we here consider only two negative charges for simplicity) and counter ions K^+ are present (inside the cell), while on the other side of the membrane (outside the cell), C^- and counter ions K^+ are present (Figure 2.14). K^+ and Cl^- can freely diffuse across the membrane with the help of appropriate membrane proteins in biological membranes. We assume that initially, $[K^+]_i = \frac{1}{2}[P^{2-}]_i = [K^+]_o = [Cl^-]_o$ (i and o denoting inside and outside the cell). Cl^- and P^{2-} concentrations are both out of equilibrium, and Cl^- will diffuse along its gradient to equilibrate across the membrane. Meanwhile, the membrane is impermeable to P^{2-}, which remains on the inside of the cell. This results in a net charge imbalance across the membrane, with an excess of negative charges inside the cell. Due to this new electrical gradient, Cl^- will diffuse back outside and K^+ will diffuse inside the cell. This will in turn create a gradient in K^+ concentration, which will diffuse back inside the cell.

At thermodynamic equilibrium, electrical gradient and concentration gradient compensate each other, and the concentrations of ions are not equilibrated across the membrane. There is an excess K^+ in the cell, an excess Cl^- outside the cell, and P^{2-} remains trapped inside the cell. The potential thus established across the membrane at equilibrium is termed the Donnan potential. In living cells, this potential is in the order of tens of millivolts, and affects diffusion kinetics across the bilayer. The membrane potential due to the imbalance of K^+ ions can be calculated by the Nernst equation:

$$E_K = \frac{RT}{ZF} ln \frac{[K^+]_{out}}{[K^+]_{in}} \tag{2.17}$$

, with R the gas constant, T the temperature, Z the charge of the ion (+1 here), and F the Faraday constant. However, as most biological membranes are not at thermodynamic equilibrium and there is a net flux of ions across the membrane, the resting potential can be calculated with the Goldman equation:

$$E = \frac{RT}{F} ln \left(\frac{\sum_i P_{C_i^+} \left[C_i^+\right]_{out} + \sum_j P_{A_j^-} \left[A_j^-\right]_{in}}{\sum_i P_{C_i^+} \left[C_i^+\right]_{in} + \sum_j P_{A_j^-} \left[A_j^-\right]_{out}} \right) \tag{2.18}$$

, with P the permeabilities of the cations C_i^+ and anions A_i^- across the membrane.

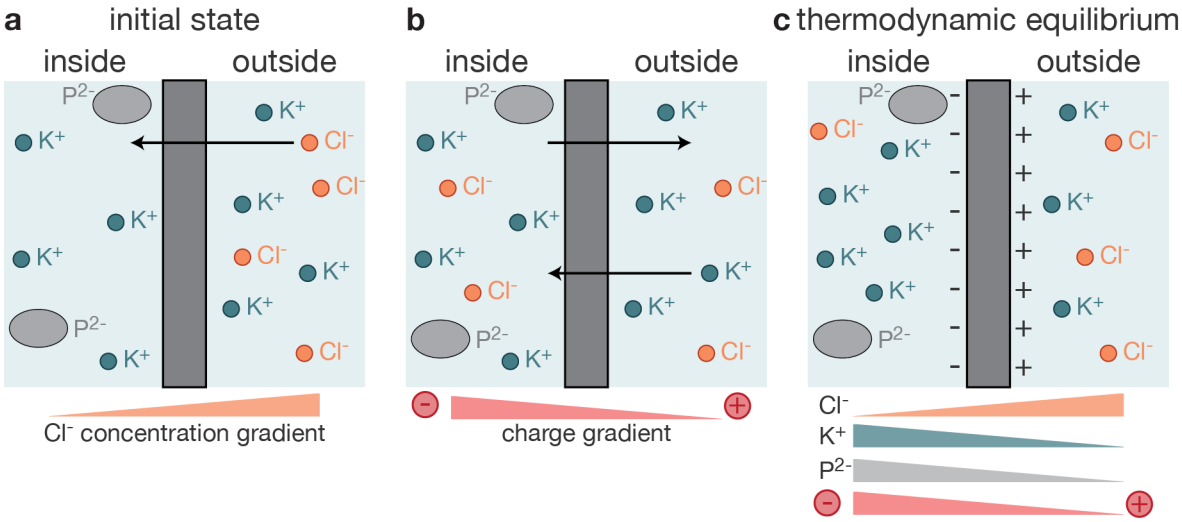

Figure 2.14. Establishment of a Donnan potential. a, Impermeable ions P^{2-} are localized on one side of a semi-permeable membrane (typically inside cells), and permeable ions Cl^{-} on the other side. They are equilibrated on both sides with permeable ions K^{+}. The concentration gradient of Cl^{-} causes them to diffuse inside the cell. b, This induces a charge gradient, which causes K^{+} and Cl^{-} ions to diffuse along it. c, At thermodynamic equilibrium, there is a concentration gradient of K^{+} ions, which induces a polarization of the membrane and the Donnan potential.

We attempted to create a Donnan potential across the bilayer of a droplet pair. We encapsulated bovine serum albumin (BSA), a protein negatively charged at neutral pH, in one droplet and encapsulated monoatomic salts of equal concentration in the adjacent droplet. α-HL pores were present in both droplets to allow the flux of salts. To detect changes in the membrane potential, we used a dye, tetramethylrodhamine ethyl ester (TMRE), which is utilized in cell viability assays to measure depolarization of the membrane. We could not measure any change in the dye concentration in either of the droplets, indicating the absence of a potential. In complementary experiments, we did not measure accelerated diffusion for DFHBI (a non-specifically diffusing chemical) in the BSA-Donnan potential conditions (Figure 2.15.a). These results indicated that we could not establish a significant membrane potential in our systems. Most likely, the α-HL pores are too narrow and too sensitive to cation blockage to allow the flux of small ions and counter ions that is necessary to establish a membrane potential. The membrane may be impermeable to most ions in this system and consequently remain unpolarized. In any case, a Donnan potential would be difficult to scale across droplet assemblies, as droplets would have to be alternatively negatively and positively charged. In biological tissues, all cells are negatively charged and the interstitial fluid is locally positively charged.

Stable gradient

The response of cells to a morphogen gradient is a dominant mechanism for the development of embryos and pattern formation in them (see Chapter 1.1). Under this mechanism, cells are subjected to a stable morphogen gradient during the corre-

sponding differentiation process. Such a gradient can be established if the morphogen is constantly produced from a localized source and degraded at a corresponding constant rate, as in the "source-and-sink" model from Crick (Figure 2.15.b). It is however difficult to imagine how such constant production and degradation could be present in embryo development, as the localized source of the morphogen would eventually stop producing it. The morphogen will then either fully degrade or its concentration will equilibrate and the gradient will dissipate. For example, in the developing *Drosophila* embryo, maternal bicoid mRNA initially localized on one end of the cell in a non-functional form is then released in a functional form and diffuses from this localized source, until it is degraded at cycle 14. It has been suggested that a stable gradient is only necessary during a certain timeframe during which the relevant development processes occur [13]. Establishing stable gradients for controlled periods of time is therefore of key interest to study reaction-diffusion circuits.

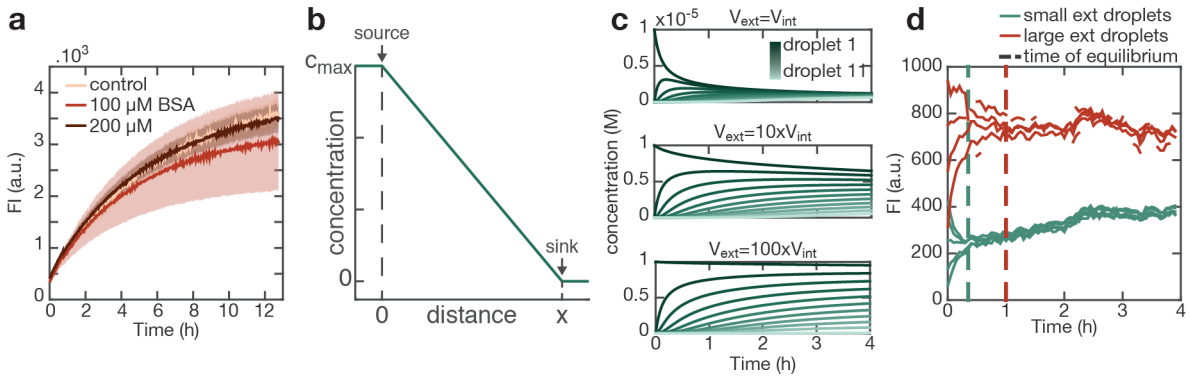

Figure 2.15. Controlling diffusion kinetics. **a**, The diffusion of DFHBI (measured with the transcription of a Spinach aptamer) is not accelerated in presence of different BSA concentrations in one compartment compared to the control, indicating that a Donnan potential could not be established in these assemblies. **b**, In a source-and-sink system as imagined by Crick, a constant source and a constant sink at two positions provided a linear and constant gradient across a system. **c**, Simulations of a signal's concentration in a linear assembly of 11 droplets. The first and last droplets have a volume V_{ext} that is varied compared to the 9 internal droplets with volume V_{int}. The first droplet initially contains 10 µM of a signal that diffuses non-specifically. The volume of a droplet affects diffusion following Equation 2.16. With higher volumes of the external droplets, a somewhat constant concentration in each of the internal droplets is temporarily achieved. **d**, An assembly of 5 droplets is enclosed between two external droplets of identical (blue) or larger (red) volume. A fluorophore diffuses across the assembly. Its concentration is equilibrated later when the enclosing droplets are larger than when they are smaller (estimated time of equilibrium is indicated with dashed vertical lines).

Our assemblies are closed systems and therefore obtaining a constant gradient is difficult, because no flow can be established to provide a constant source of a chemical or to deplete it out of the system. However, droplets of variable sizes can be placed at both sides of a droplet assembly to serve as source and sink. The volume of these droplets will define the time during which a "source-and-sink"-like state can be achieved.

We modelled the diffusion profile in a 9 droplets 1-dimensional array surrounded

by source and sink droplets of varying volume (Figure 2.15.c). A relatively stable gradient can be established for a prolonged period of time using enclosing droplets of much larger size than the droplets in the assembly. We tested this hypothesis by building a similar assembly where the 5 internal droplets contained a purified RNA aptamer (Spinach [78]), the left-most droplet contained DFHBI and the right-most droplet only contained buffer. The size of the enclosing droplets was varied, and the fluorescence of each droplet was measured until equilibrium was reached (*i.e.* equal concentration of the Spinach-DFHBI complex is reached in all droplets). With larger enclosing droplets, the system reached equilibrium later than with smaller enclosing droplets, suggesting that the DFHBI gradient was sustained for a longer period (Figure 2.15.d). This approach to establishing a lasting gradient will be pursued in future experiments in the context of the positional information circuit (Chapter 3.4), to quantify the robustness of the pattern forming circuit against the stability of the gradient.

2.3.4 Automating DIB formation

As addressed in Chapter 1.5, 3D printing strategies to automate the assembly of large droplet systems have been developed [43]. Such an approach is susceptible to give more reproducible droplet volumes, larger assemblies, and permits the construction of 3D assemblies, which is difficult to achieve with the semi-manual technique. 3D printing relies on small droplet volumes, so that the time during which the droplet falls through the oil until reaching the existing assembly is sufficient to allow a lipid monolayer to assemble around it. However, the construction of such a printer is relatively labour-intensive and demands good knowledge of 3D printer building.

To construct our own droplet 3D printer, we therefore turned to the CANTER lab at the Hochschule München, which specializes in building bioprinters. Together with PhD student Sascha Schwarz, preliminary experiments using a regular self-built 3D printer for droplet printing were conducted. Having achieved good initial results regarding droplet extrusion, low droplet volume and bilayer formation, we then designed a bachelor project to systematically explore the reproducibility of droplet printing and assembly formation. The results of this work have been summarized in the bachelor thesis of Nikolas Galensowske [79]. Reproducible droplet diameter of around 100 µm could be achieved, and droplet assemblies could be easily formed by printing droplets on top of each other so that they would form a bilayer upon contact. 2D and 3D assemblies were printed, and the dynamic circuit described in Chapter 3.4 was successfully implemented in these assemblies (Figure 2.16).

However, precise control over geometry proved very difficult to achieve. Two factors were at cause: first, droplets did not fall in a straight vertical line once printed, due to random flow in the oil phase; second, as droplets formed a bilayer by rolling on top of each other, this added randomness to the exact position where they fell after rolling.

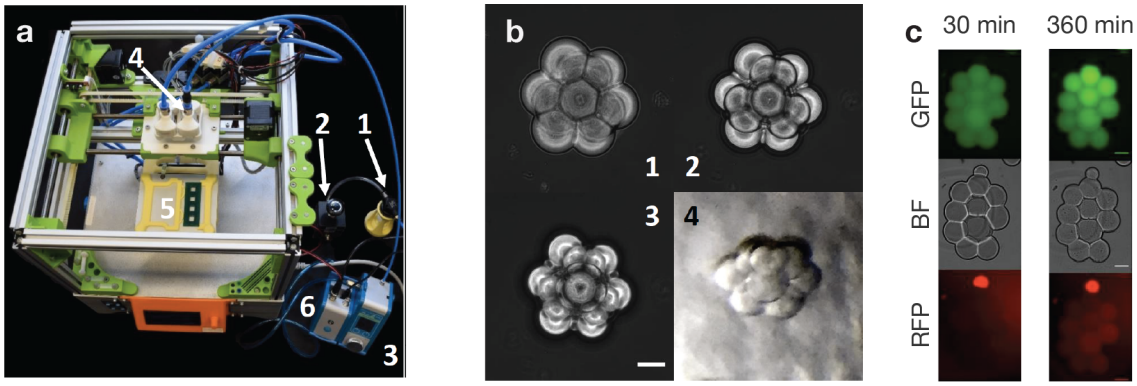

Figure 2.16. 3D printing of AMA. a, 3D printing set-up built by the team of the CANTER lab: (1) air filter, (2) pressure regulator, (3) pressure control module, (4) printhead (printing nozzle is screwed in below), (5) printing plate, (6) communication module. textbfb, 3D-printed small pyramid: (1) first layer, (2) second layer, (3) third layer, (4) picture taken with a phone camera. Scale bar: 100 µm. Reproducible printing of such well-defined structures is difficult to achieve (below 10 % correct yield) due to deviations between calculated printing location and final droplet position. textbfc, Differentiation circuit from Chapter 3.4 implemented in a printed assembly. Due to a co-repression circuit architecture, GFP and RFP express with opposite gradients along the vertical axis of the assembly. Green: GFP, grey: brightfield, red: RFP. Assembly is imaged at t = 30 min and t = 360 min after printing. Scale bar: 100 µm. Images adapted with permission from [79].

The yields of correct assembly decreased as the number of droplets in the assembly increased. This problem is well known for droplet 3D printing, and indeed most printed assemblies to date have been done on large millimetre-scale where local printing defaults can be seen, and only a global geometry is achieved with many irregularities [43]. This presents an important issue for our experiments, as we are interested in precise spatial organization to study reaction-diffusion circuits and in the effects of assembly dimensions on the circuits' dynamics.

To address these challenges, we are exploring the use of physical guides to bring the droplets into specific assemblies. For example, printing the droplets between two rails that are at a one-droplet-diameter distance from each other would easily allow the printing of a 1D assembly of droplets with limited defaults. The "egg-crate" strategy, in which droplets are printed in microfabricated wells with controlled geometrical parameters (droplet-to-droplet distance, square versus honeycomb geometry, etc...), has been investigated in the early days of DIB [80]. We are currently experimenting with droplet printing in such wells with PhD student Benedikt Kaufmann from the CANTER lab, where we expect that the correct assembly of the first layer will then create a similar "egg-crate" structure for the following layers of droplets to assemble, imposing energy-minimizing positions for all droplets to fall into and diminishing printing errors.

In conclusion, we demonstrated that a number of chemicals relevant for the induction of synthetic gene circuits could diffuse in our artificial multicellular assemblies (AMA). The chemicals present a variety of diffusion specificity and kinetics, which we characterized, creating a rich toolbox of diffusion dynamics to engineer reaction-diffusion

circuits.

3 Signal-responsive synthetic circuits

Having characterized our platform for artificial multicellular assemblies, we developed circuits that demonstrate the variety of non-trivial spatiotemporal dynamics that can be implemented with this platform. We first created a simple read-out circuit to compare pore-mediated and non-specific diffusion pathways across the bilayer and tune the diffusion kinetics (Chapter 3.1). We then engineered a circuit based on an ubiquitous gene network motif: the incoherent feed-forward loop. We implemented the topology of this motif with a DNA/RNA circuit and demonstrated that its response can be easily tuned (Chapter 3.2). We went on to explore more complex circuits that are particularly relevant to embryogenesis. We established differentiation based on amplification of noise in stochastic processes (Chapter 3.3) and explored morphogen-gradients-induced differentiation (Chapter 3.4), the two fundamental differentiation processes found in embryos (described in Chapter 1.1). Not only do these circuits show novel spatiotemporal dynamics that cannot be achieved in traditional single-celled artificial cells, they also demonstrate how our assemblies can be used to study intriguing biological questions in simplified artificial environments.

3.1 Diffusion and induction

To study circuit-response to diffusing signals in our droplet assemblies, we first investigated how a simple read-out circuit is affected by variations in the diffusion kinetics of its inducer. We used two signal-inducible genes, *pLux-GFP* inducible by 3OC6-HSL (a non-specific signal), and *pBAD-mScarletI* (an RFP variant [81]) inducible by arabinose (a pore-mediated signal). This double read-out allowed us to directly compare how induction varies with different diffusion modes.

We first investigated the theoretical effects of different permeabilities of the bilayer to a given signal and the consequences for gene induction (Chapter 3.1.1). We then explored experimentally how these effects could be reliably detected in droplet assemblies (Chapter 3.1.2).

3.1.1 Modelling diffusion and induction

We used the diffusion model described in Chapter 2.3 to simulate the time-dependent diffusion profiles of a signal depending on its bilayer permeability. We assumed that the aqueous diffusion constant is on the order of D = 1000 µm^2.s^{-1}, which is the case for the small chemical signals we used (see Chapter 2.3.2). We varied the permeability of the bilayer over several orders of magnitude, and simulated the signal influx in a receiver droplet connected to a sender of fixed concentration. For all permeabilities screened, the signal concentration instantaneously rises in the receiver droplet but the kinetics are slower with lower permeabilities (Figure 3.1.a). The velocity of the signal influx will affect the response of a downstream circuit.

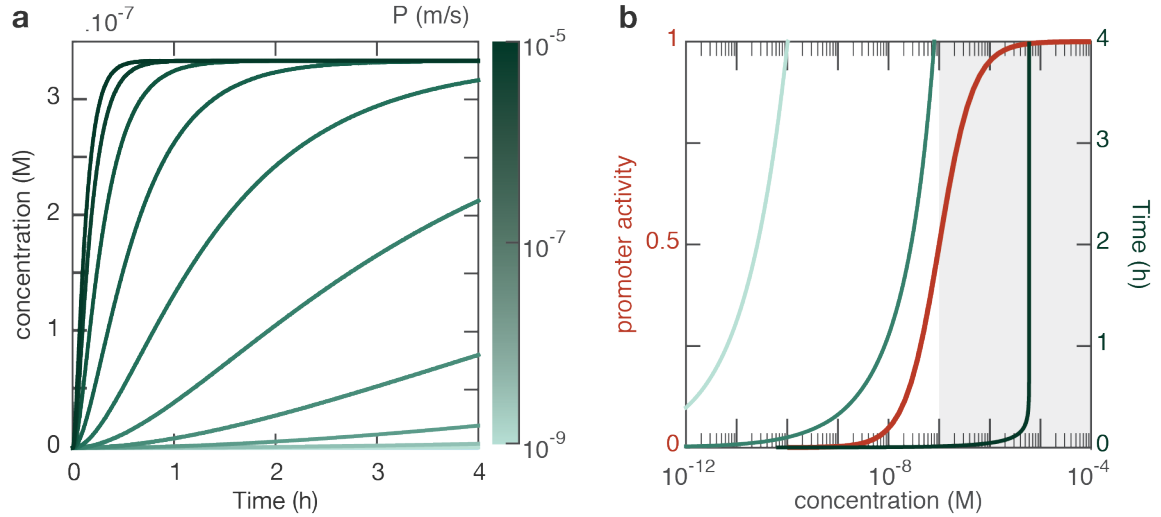

Figure 3.1. Diffusion and induction threshold. **a**, Simulation of the concentration of a signal diffusing into a receiver droplet from a sender droplet for different permeabilities P of the bilayer. The assembly contains a buffer droplet, signal concentration in the sender is initially 1 µM, area of permeation is set at 1 . 10^{-8} m^2. **b**, Overlay of the simulations of the concentration of a diffusing signal (concentration in blue for P = 10^{-5} m.s^{-1}, dark blue, 10^{-7} m.s^{-1} median blue, 10^{-9} m.s^{-1} light blue) and the response function of the promoter it induces (red, Hill function with K_d = 100 nM, n = 1.3). The promoter will be significantly activated for signal concentrations above its threshold, indicated by the shaded grey area.

For a diffusing signal to induce the response of a cooperative biochemical process, its concentration must pass the threshold of this process's induction. We considered a toy-model with an inducer activating the transcription of a gene, so that the promoter's activity p_A responds to the inducer's concentration x with a Hill function dependent on a binding affinity K_d and on a cooperativity n determined by the molecular binding process:

$$p_A = \frac{x^n}{K_d^n + x^n} \tag{3.1}$$

Assuming K_d = 100 nM and n = 1.3 (a cooperativity similar to that found for the

pBAD promoter, see Appendix A.4), we simulated the signal concentration build-up in the receiver droplet for different permeabilities and compared it to the induction threshold (Figure 3.1.b). For high permeabilities, the signal concentration quickly goes over the threshold, leading to a full induction of the downstream process. Intermediate permeabilities cause the signal to rise slowly, leading to a gradual induction of the process, and for the slowest permeabilities, the signal concentration may not induce a response at all.

We have previously determined (see Chapter 2.3) the bilayer permeability and the aqueous diffusion constant of the signals 3OC6-HSL and arabinose used in our diffusion comparison read-out, and are therefore able to fully predict the diffusion kinetics of these signals in our assemblies. We have also determined the thermodynamics and kinetics of their induction of the corresponding *pLux-GFP* and *pBAD-mScarletI* genes (see Appendix A.4). We could therefore model how the diffusion of these signals induces their read-out circuit in our droplet assemblies. We considered an assembly with a sender containing the signal, a receiver containing the read-out, and a variable number of buffer droplets in between. We simulated how the signal concentration rises in the receiver droplet for different numbers of buffer droplets, and compared this to the induction Hill curves of the corresponding promoters. For the non-specific 3OC6-HSL signal, increasing the number of buffer droplets slows down the signal rise in the receiver droplet, but as this chemical diffuses relatively fast it will cross the induction threshold rapidly in all conditions (Figure 3.2.a). This will correspondingly induce an identical response of the promoter independently of the number of buffer droplets in the range tested (Figure 3.2.b). For the pore-mediated arabinose signal, as its diffusion is limited by bilayer permeation, an increase in the number of buffer droplets will increase the number of diffusion barriers and therefore more considerably slow down its concentration build-up in the receiver droplet. Our simulations show that a higher number of buffer droplets indeed slows down the arabinose diffusion so considerably that its concentration in the receiver droplet falls below the activation threshold of the promoter (Figure 3.2.c). The induction of the gene expression is therefore strongly affected by the number of buffer droplets between sender and receiver (Figure 3.2.d).

Our simulations demonstrate how the diffusion of non-specific and pore-mediated signals can be tuned separately with the size of the assemblies. We then investigated if these effects could be measured in experimental set-ups.

3.1.2 Controlling induction with diffusion kinetics

We studied the protein expression of our double read-out when encapsulated in our droplet assemblies. We found that the expression of the pBAD promoter proceeded more slowly in a sender-receiver assembly (Figure 3.3.a) than in bulk (Figure 3.3.b), whereas expression of the pLux promoter seemed only slightly slowed down. In-

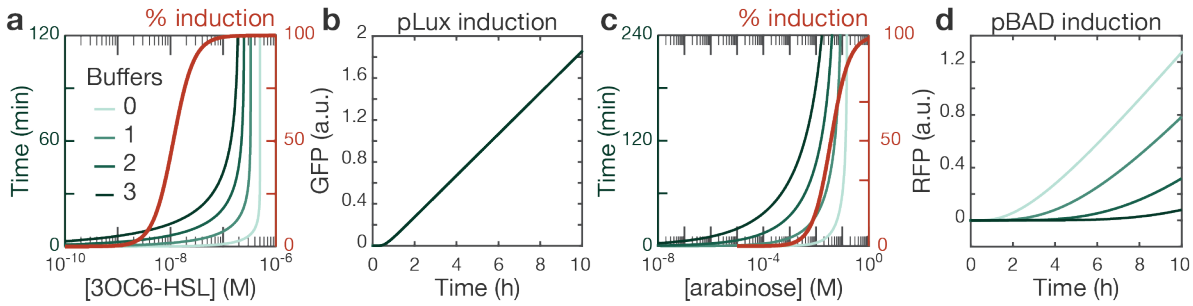

Figure 3.2. Diffusion and induction of the 3OC6-HSL/pLux and arabinose/pBAD pairs. **a**, **c**, Simulations of the concentration of the diffusing signal (**a**, 3OC6-HSL and **c**, arabinose) in a receiver droplet with 0 to 3 buffer droplets and simulation of the induction curve of the corresponding promoter (**a**, pLux and **c**, pBAD). **b**, **d**, Simulations of the consequent protein expression for the different numbers of buffer droplets, from the pLux (**b**) promoter or the pBAD (**d**) promoter. For all simulations, the initial concentration of signal in the sender droplet is 1 µM for 3OC6-HSL and 300 mM for arabinose.

deed, our model predicts that expression of the pBAD promoter in such an assembly would have almost the same kinetics as in bulk if arabinose were to diffuse with the same kinetics as 3OC6-HSL, but that it is slowed down due to the lower permeability of the bilayers to arabinose (Figure 3.3.c, slower expression of mScarletI compared to GFP in bulk is due to the slower protein maturation [82]).

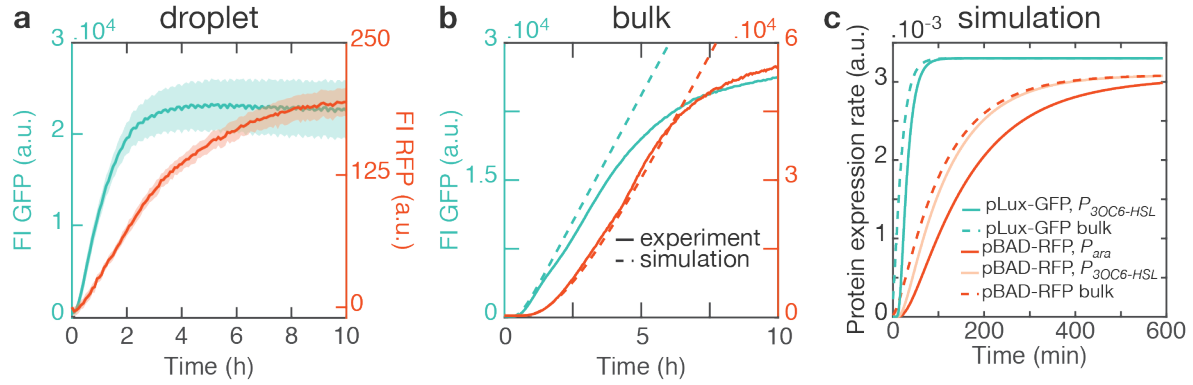

Figure 3.3. Induction of the pLux and pBAD promoters in bulk and in droplet assemblies with 1 buffer droplet. **a**, Expression of *pLux-GFP* and *pBAD-RFP* in droplet assemblies with 1 buffer droplet. Full lines and shaded area represent mean and standard deviation of at least 3 different receivers. **b**, Expression of *pLux-GFP* and *pBAD-RFP* in bulk: continuous lines, experiment and dashed lines, simulation. **c**, Simulation of protein expression rates of *pLux-GFP* and *pBAD-RFP* in bulk (dashed lines, inducer is freely available) and in droplet assemblies where the inducer diffuses from a sender droplet (continuous lines). Expression of *pLux-GFP* in droplets is simulated for a permeability of the bilayer equal to that fitted for 3OC6-HSL. Expression of *pBAD-RFP* in droplets is simulated for a permeability of the bilayer equal to that fitted for arabinose (the realistic case) and for 3OC6-HSL (an ideal case with fast diffusion of the signal). This demonstrates that the delay of expression of RFP in droplets compared to bulk is caused by bilayer permeation.

Varying the amount of pores in the sender droplet correspondingly varies the permeability of the bilayer to pore-mediated signals but does not affect the diffusion of

non-specific signals. Indeed, we found that GFP expression remained mostly unaffected by α-HL concentration, whereas mScarletI expression strongly decreased for lower pore concentrations (Figure 3.4.a and b). We also varied the number of buffer droplets for a fixed α-HL concentration in sender and buffer droplets, and we found that mScarletI expression was reduced with a higher number of buffer droplets whereas GFP expression remained approximately constant (Figure 3.4.c). We could compare this result to our simulations and found that our model correctly predicts the response of both read-outs with increasing number of droplets (mScarletI expression is not reduced as strongly as simulation predicts, which could be due to the model not accounting for background expression of the promoter without inducer).

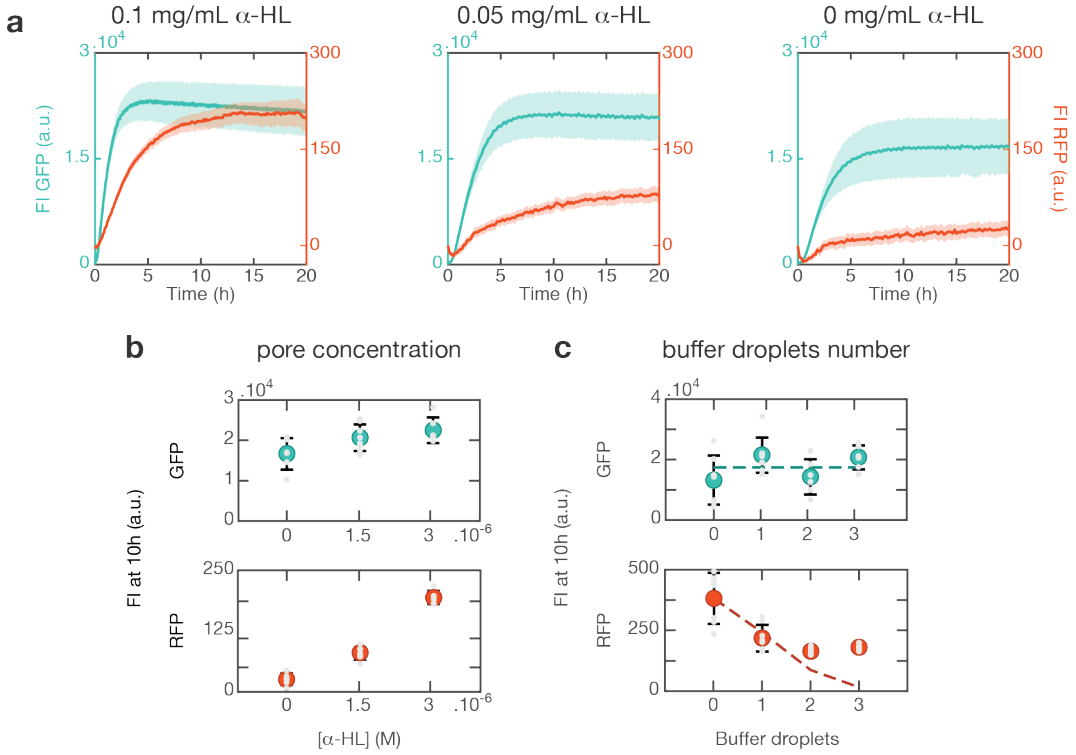

Figure 3.4. Tuning non-specific and pore-mediated diffusion. **a**, Kinetic curves of the expression of *pLux-GFP* and *pBAD-RFP* in a sender-receiver assembly (no buffer droplet) when the concentration of pores is varied. Full lines and shaded area represent mean and standard deviation of at least 3 different receivers. **b**, GFP and RFP levels at 10 h in the conditions listed in **a**, where the concentration of pores in the sender is varied. Circles represent mean and error bars represent standard deviation. Single data points are overlaid in light grey. **c**, GFP and RFP levels at 10 h for varying number of buffer droplets. Mean, standard deviation and single data points are represented as described in **b**. Dashed lines represent simulations.

This simple dual read-out circuit allowed us to gain a better understanding of how bilayer permeability and diffusion barriers affect the kinetics of non-specific and pore-mediated signal diffusion and how this interplays with the induction of downstream circuits.

3.2 Signalling pulse

We were interested in coupling diffusion to a compartmentalized reaction circuit in order to generate assembly-wide signalling. Various processes mediate signalling at different length-scales in living organisms, but some recurring gene network motifs that mediate signal response in cells are of particular interest, both due to their simple architecture and to their overwhelming presence in gene regulation in cells. We focused on a network motif termed the incoherent feed-forward loop (I1-FFL), which typically involves a transcription factor that activates a gene and activates a repressor for this gene (Figure 3.5.a). It is the second most abundant motif of feed-forward loops (network motifs involving three genes where two cascaded genes regulate a third one) in living organisms, accounting for about 35 % of all known transcription network motifs in *E. coli* and about 25 % in *S. cerevisiae* [83]. The I1-FFL motif is suggested to both create a transient pulse of protein expression (Figure 3.5.c) and to accelerate the gene's response to an external signal. It has also been shown to buffer protein expression outputs against extrinsic noise [84]. To our knowledge, our work is the first implementation of a synthetic I1-FFL circuit with spatial dynamics, and although synthetic I1-FFL were since then designed in *in vitro* transcription-translation gene circuits and in *E. coli* [85], the spatial dynamics of such a network motif were so far not addressed.

We chose to implement the I1-FFL motif using a simple and programmable synthetic circuit, and we therefore turned to a category of circuits relying on DNA/RNA base-pairing, termed genelet circuits [86]. DNA templates for transcription by T7 Polymerase are constructed such that the promoter can be turned on and off. The promoter region is partially single-stranded and the template cannot be transcribed, but a single-stranded DNA can turn the template on by binding to its single-stranded region and completing its promoter. Transcription of an output RNA can then be activated or inhibited by the binding or unbinding of this ssDNA activator. The dynamics of circuits based on this principle can be readily tuned [87] due to the programmable thermodynamics and kinetics of nucleic acids base-pairing [88], [89].

We constructed our I1-FFL circuit as follows: the read-out was chosen to be the Spinach fluorescent aptamer, where the Spinach RNA binds the fluorophore DFHBI and increases its fluorescence [78]. Initially, the Spinach RNA is bound to a ssDNA genelet activator. Upon diffusion of DFHBI (**D**) into the droplet, the fluorescent Spinach-DFHBI complex (**C**) forms, and the activator is released by competitive binding of the DFHBI. The activator binds the incomplete DNA template and activates the I1-FFL repressor node (**G**) by turning on the transcription of an inhibitory RNA. This inhibitory RNA is fully complementary to the Spinach RNA and binds it, displacing DFHBI and decreasing fluorescence (Figure 3.5.a and d). This I1-FFL circuit is expected to produce a pulse of the Spinach-DFHBI complex concentration. In the droplet assemblies, the diffusion of DFHBI across the droplets and the activation of the repressor node in each compartment are expected to produce a travelling pulse.

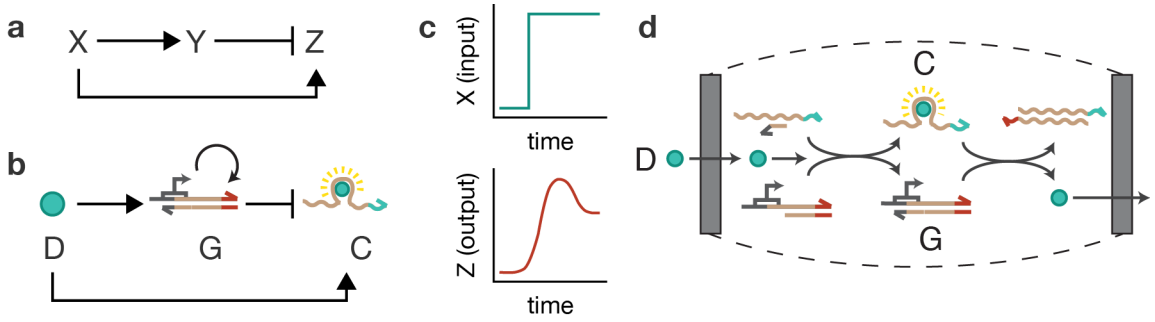

Figure 3.5. The incoherent feed-forward loop. **a**, General schematic of a I1-FFL, where X is the signal, Y the repressor and Z the response. **b**, Implementation of the I1-FFL with a DNA/RNA circuit. DFHBI is the signal, a genelet template is the repressor and the Spinach-DFHBI fluorescent aptamer is the response. **c**, Expected response to a change in signal due to the I1-FFL. **d**, Details of the implementation of the I1-FFL in droplet assemblies: each droplet is loaded with the Spinach RNA bound to the ssDNA activator and with the incomplete genelet template, and DFHBI diffuses across the assembly.

In this section, I will first estimate the kinetic rates of the circuit (Chapter 3.2.1), and describe its bulk characterization (Chapter 3.2.2). The spatial dynamics of the circuit in the droplet assemblies are then addressed in Chapter 3.2.3. Chapter 3.2.4 describes further variations on the pulse circuit, where induction by another diffusing chemical and coupling to a protein expression output were attempted.

3.2.1 Model

We modelled the circuit as a system involving 5 components and 3 reactions (Figure 3.6.a and b). The first reaction, where the DFHBI (**D**) displaces the activator from the Spinach/activator RNA/DNA duplex (**S/A**) and the activator binds the DNA template (**G**), is considered reversible (rates k_{1p} and k_{1m}). The transcription step is considered non-reversible (rate k_2, we neglect RNA degradation here). The final reaction involving the binding of Spinach RNA and inhibitory RNA (**R**) and the release of DFHBI and more activator is also considered non-reversible (rate k_3).

The transcription rate k_2 was measured in the order of 5 . 10^{-3} s^{-1} in separate transcription experiments (which is consistent with previously determined transcription rates from split promoter genelets [87]), and the repression rate k_3 was assumed to be limited by the hybridization of the two RNA strands, and therefore to be in the order of 10^6 $M^{-1}.s^{-1}$ [90].

The kinetics of the first step of the circuit are the most difficult to estimate. Indeed this step is composed of 3 reactions (Figure 3.6.c): the unbinding of the activator DNA and the Spinach RNA (rates k_{11p} and k_{11m}); the binding of the DFHBI to the free Spinach RNA (rates k_{12p} and k_{12m}); and the binding of the activator DNA to the template DNA (rates k_{13p} and k_{13m}). Assuming typical hybridization kinetics, we have $k_{11m} \approx 10^6$

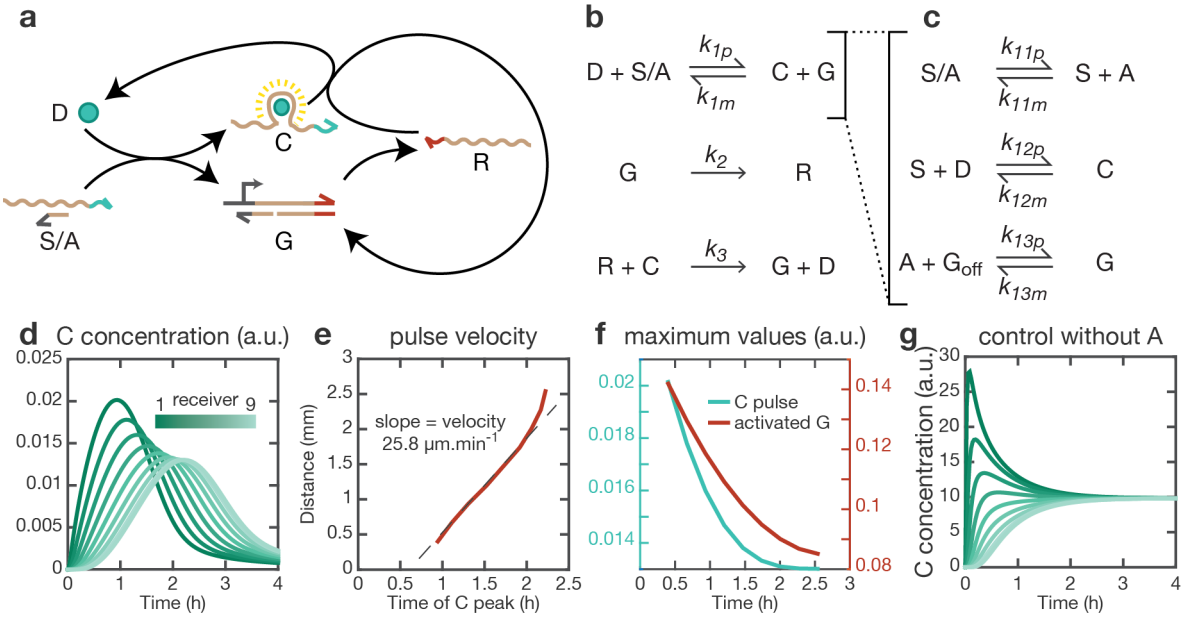

Figure 3.6. Modelling the I1-FFL circuit. **a**, Scheme of the chemicals and reactions taken into consideration in the model. **b**, List of the chemical reactions and their rates in the model of the whole circuit. **c**, The first reaction of the model is subdivided into 3 steps for which the rates can be estimated. **d**, Simulation of the I1-FFL in an assembly of 10 droplets with the sender containing 1 µM **D** and each of the 9 receivers containing 0.15 µM **S/A**. A propagating pulse is observed. **e**, Plotting the time of each peak versus the distance of the corresponding receiver from the sender allows to estimate the velocity of the pulse with a linear fit. In these conditions, the pulse velocity is estimated at 25.8 µm.min^{-1}. **f**, The maximum intensity of the pulse decreases in each droplet as the distance from the sender increases (blue). Similarly, the maximum concentration of **G** activated by the release of **A** decreases with increasing distance. **g**, In a control without activator, all droplets equilibrate at intermediate concentrations of **C**.

M^{-1}.s^{-1}. The off-rate k_{11p} can then be calculated from the equilibrium constant $K_{11} = \frac{k_{11p}}{k_{11m}}$ of the reaction. The stability of the DNA/RNA duplex can be approximated as follows: the stability of RNA/DNA duplexes is typically lower than that of RNA/RNA duplexes of the same sequence but higher than that of corresponding DNA/DNA duplexes [91], and the free energy of non-hybrid duplexes can be calculated with NUPACK [92]. At 37 °C, NUPACK estimates the free energy of the Spinach RNA/activator DNA duplex to be -45.48 kcal.mol^{-1} for RNA/RNA and -33.83 kcal.mol^{-1} for DNA/DNA. We will first assume the highest stability of the duplex (RNA/RNA limit). The equilibrium constant K_{11} can then be calculated by comparing the free energy of the duplex to the free energy of the single components (0 kcal.mol^{-1} for the unstructured activator DNA and -30.40 kcal.mol^{-1} for the Spinach RNA in its equilibrium secondary structure). From this follows that $k_{11p} \approx 2 \cdot 10^{-5}$ s^{-1}. This is a lower limit for the dissociation rate of the duplex, and this rate will increase if the stability of the RNA/DNA duplex is lower than that of the corresponding RNA/RNA duplex.

The kinetics of DFHBI binding to the Spinach RNA have been well described by Wang *et al.* [93], from which we can assume $k_{12p} = 8.1 \cdot 10^4$ M^{-1}.s^{-1} and $k_{11m} = 0.11$ s^{-1}.

Finally, assuming the incomplete template is in excess compared to the free activator, we can make the approximation that $k_{13p} = k_{hybridization} \times [template] \approx 0.15$ s^{-1} for 150 nM of template. We calculate $k_{13m} = \frac{k_{13p}}{K_{13}}$ (K_{13} is calculated from the difference in stability of the incomplete and complete template DNA complexes), which gives us: $k_{13m} = 3.7 \cdot 10^{-18}$ s^{-1}. To estimate the order of magnitude of the rates for the global reaction, we assume that $K_1 = \frac{k_{1p}}{k_{1m}} = K_{11} \times K_{12} \times K_{13}$, and we approximate that $k_{1p} = k_{11p} \times k_{12p} \times k_{13p}$ and $k_{1m} = k_{11m} \times k_{12m} \times k_{13m}$. This gives us $k_{1p} \approx 0.26$ $M^{-1}.s^{-1}$ and $k_{1m} \approx 3.9 \cdot 10^{-13}$ $M^{-1}.s^{-1}$.

Using these estimated reaction rates and our 1-dimensional diffusion model with the fitted DFHBI permeability (Chapter 2.3), we can model the spatial behaviour of the I1-FFL circuit (Figure 3.6.d). A propagating pulse is observed, and the pulse velocity can be estimated by linearly fitting the distance of the receiver from the sender against the time of the peak in this receiver (Figure 3.6.e). The model allows us to estimate at pulse velocity of 25.8 µm.min^{-1} with 1 µM DFHBI in the sender. The maximum intensity of the pulse decreases as the distance from the source increases, and as this determines the amount of activator released, similarly the activity of the repressor node G also decreases as the distance from the DFHBI source increases (Figure 3.6.f). This model confirms that the DFHBI-mediated release of the activator is the mechanism generating the propagating pulse (control without activator, Figure 3.6.g). However, subsequent modelling with continuous DFHBI diffusion found that diffusion within the droplets and not only along the axis of the assembly played a role in the dynamics of the system, which could not be easily approximated with either 1D, 2D or 3D diffusion [3].

3.2.2 Bulk characterization

To establish the proper functionality of the I1-FFL circuit, we tested different subsystems and control circuits in bulk.

First, the binding of the activator to the Spinach RNA and its displacement due to the presence of DFHBI was assessed with screenings using PAGE. A fixed concentration of Spinach RNA (6 µM) was incubated with increasing concentrations of activator (from 0 to 50 µM) (Figure 3.7.a). The smearing of the RNA band as activator concentration increases indicates the formation of a duplex. In a second experiment, fixed concentrations of Spinach RNA and activator DNA were preincubated, and different concentrations of DFHBI were added. No shift of the RNA/DNA duplex band could be observed with higher concentrations of DFHBI (Figure 3.7.b). However, the dissociation rate of DFHBI and Spinach RNA is quite high (estimated at 0.11 s^{-1} in Chapter 3.2.1), and in the absence of an incomplete DNA template capturing the activator, it is possible that the DFHBI unbinds the Spinach, diffuses into the gel buffer and the RNA/DNA duplex forms again. Further experiments were therefore conducted with fluorescence measurements.

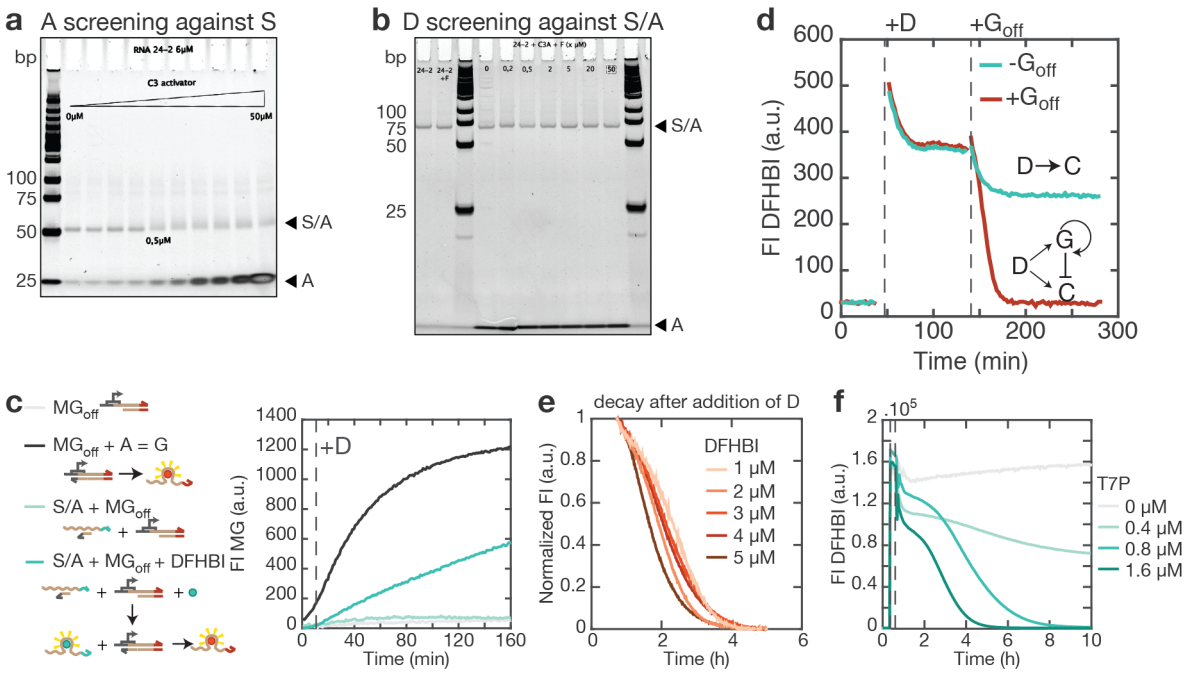

Figure 3.7. Bulk testing of the I1-FFL circuit. **a**, Screening of **A** (labelled C3 activator on the gel) concentrations from 0 to 50 µM against 6 µM of **S** (RNA 24-2). **S** runs at the same height as **S/A**. **b**, Screening of **D** (indicated as F, concentration in µM in each lane) against a preincubated mixture of 6 µM **S** (24-2) and 0.5 µM of **A** (C3A). **c**, The tightness of the RNA-ssDNA duplex is tested with a MG genelet that takes the place of the repressor template **G**. In negative (light grey) and positive (dark grey) controls, the template is either incomplete and off or complete (with **A**) and on. When **A** is preincubated with **S**, the addition of MG_{off} afterwards does not induce any transcription, demonstrating that the activator is tightly blocked by **S** (light blue). If DFHBI (**D**) is added, it binds **S** and releases **A**, therefore activating MG and inducing transcription of the MG aptamer (dark blue). **d**, This experiment shows that **D** is displaced from **C** by the transcription from **G** (see circuit in Figure 3.6.a). **S** is preincubated with **A**, and at 30 min, **D** is added (vertical line +D): **D** partially displaces **A** from **S/A**, forming **C**, and fluorescence increases (decay is due to the equilibration of the reaction). After 55 min, the incomplete G_{off} template is added (red) or not (blue-green). In absence of the template, the fluorescence equilibrates after an initial dilution. When the template is added, the fluorescence quickly drops to zero, indicating that **D** is displaced from **C**. **e**, Higher DFHBI concentrations should cause a release of more **A**, and therefore a stronger activation of **G** and a faster decay. However, when the fluorescence after addition of **G** is normalized, no such effect is observed. **f**, Higher T7 RNA Polymerase concentrations should lead to a faster transcription from activated **G**, and therefore a faster decay rate. This effect is observed clearly.

The release of the activator by addition of DFHBI was tested with a read-out orthogonal to the Spinach-DFHBI aptamer. A genelet template coding for the Malachite Green RNA aptamer (a fluorescent aptamer based on a similar mechanism as Spinach, but using the Malachite Green fluorophore, which emits in the far red spectrum [94]) was constructed that required the same ssDNA activator to turn on its transcription. The Spinach RNA was preincubated with the activator, and then DFHBI and the Malachite Green template were added. In a control sample without DFHBI, transcription from the Malachite Green template did not occur (Figure 3.7.c), indicating that the activator remained sequestered by the Spinach RNA. In the experiment where DFHBI was added,

transcription from the Malachite Green template was restored, indicating that the DFHBI binding to the Spinach RNA had induced the release of the activator.

Finally, the full circuit was assembled in bulk: the Spinach RNA and the activator DNA were preincubated. DFHBI was added and the system was allowed to reach equilibrium. Then, the repressor node template and T7 RNA Polymerase were added. The fluorescence signal decreased strongly in the experiment with the template compared to a control without the template (Figure 3.7.d). Higher DFHBI concentrations should lead to the release of higher activator concentrations, and therefore to faster repression kinetics. This effect could however not be measured in bulk (Figure 3.7.e). As the circuit's dynamics are highly dependent on T7 RNA Polymerase and DFHBI concentrations (see Chapter 3.2.3), effects such as pipetting errors and protein binding to tubes may affect the comparability of different bulk samples. However, the effect of T7 Polymerase on the repression kinetics could be more readily measured (Figure 3.7.f).

Having demonstrated the functionality of the I1-FFL circuit in bulk, we then implemented it in droplet assemblies.

3.2.3 Droplets dynamics

We encapsulated the I1-FFL circuit in our droplet assemblies and first studied its spatial dynamics in 1-dimensional arrays. We created an assembly of 10 droplets with 1 trigger droplet containing the DFHBI signal, and 9 identical receiver droplets containing the circuit. When connecting the trigger droplet to the array, a fluorescent pulse travelling along the assembly could be detected (Figure 3.8.a and b). In each droplet, the fluorescence signal increased until a peak was reached and then decreased with variable kinetics. In contrast, control experiments where the repressor genelet was absent demonstrated simple diffusion and equilibration of the signal across the array, *i.e.* the fluorescence intensity settled at an intermediate value in all droplets (Figure 3.8.d). We measured the typical time to steady state in I1-FFL and control experiments and found that the I1-FFL led to a faster reaching of steady-state (Figure 3.8.e). However it should be noted that in biological experiments addressed in [83], the steady-state reached with and without an I1-FFL loop was identical, whereas in our case the steady-state reached in presence of the I1-FFL is zero fluorescence and in absence of the I1-FFL is an intermediate fluorescence level.

The pulse velocity was determined similarly as with the simulated traces (Figure 3.6.e and Figure 3.8.c). Wave propagation in non-linear reaction-diffusion circuits occurs with a constant velocity $v \propto \sqrt{kD}$, with k being a typical reaction rate and D the signal's diffusion constant (see for example [18]). Our I1-FFL circuit does not fall into this category of RD systems because the amount of diffusing signal is finite and not constantly replenished through a positive feedback loop or other mechanisms. I will, however, ad-

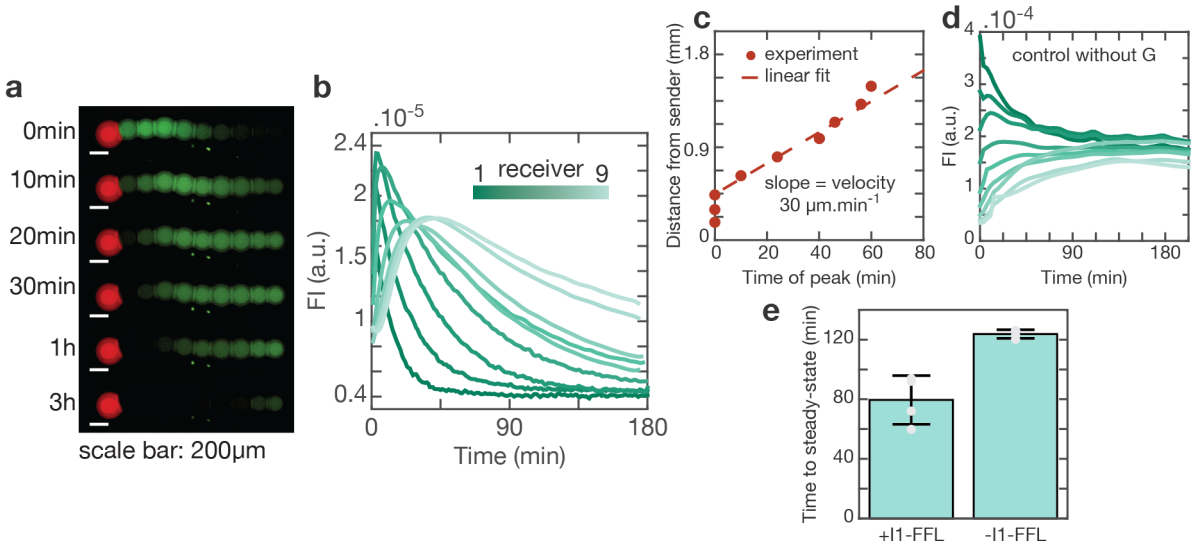

Figure 3.8. Implementation and characterization of the I1-FFL in assemblies. **a**, Propagation of the pulse from a sender droplet (red) to an array of receivers. Fluorescence is shown in green at different time points. Scale bar: 200 µm. **b**, Fluorescence intensity through time for the 9 receivers from **a**. (Curves are smoothed with an fft filter.) **c**, The distance of each receiver's centre (from **a**) to the sender droplet is plotted against the time of the peak in this receiver, and the pulse velocity is estimated with a linear fit. **d**, A control experiment without template **G** shows the equilibration of the fluorescence of all receivers at an intermediate level. **e**, The time to steady-state is estimated by measuring the time at which the derivative of the fluorescence intensity of all droplets of an assembly reaches zero. This is compared between experiments with the template **G** (+I1-FFL) and without. Bars and error bars represent mean and standard deviation, single data points are overlaid.

dress below how diffusion and reaction rates affect the pulse velocity in this system as well. Velocity in this circuit is not constant but decreases with distance from the trigger droplet, therefore a linear fit only provides an estimate of the pulse velocity and allows comparison between experiments only as long as other parameters such as length of the array are kept constant. In the pulse experiment shown in Figure 3.8.a, the pulse velocity was approximately 30 µm.min^{-1}. This is on the order of propagation speeds of biological wave phenomena such as mitotic trigger waves involved in the spatially coordinated division of the fertilized *Xenopus laevis* egg [95].

A back-of-the-envelope calculation with $v \propto \sqrt{kD}$ would give the following velocity: the typical rate here corresponds to the time it takes for the antisense RNA to displace DFHBI from the Spinach RNA (**S**). **S** is initially introduced at a concentration of 1.5 µM, the DNA activator (**A**) at 150 nM (so that in the initial state, there is 150 nM of bound activator-Spinach and 1.35 µM of free Spinach RNA), and the repressor genelet is present at 150 nM. Assuming the DFHBI displaces all **A**, there is then 150 nM of active repressor template and 1.5 µM of DFHBI-Spinach RNA complex (**C**). The rate of transcription of the antisense RNA is then 150 nM $\times$ 0.005 s^{-1} = 0.75 nM.s^{-1}. The typical time it takes for the antisense RNA to bind all the Spinach RNA (with transcription assumed to be the kinetically limiting step) is then $t = \frac{1.5M}{0.75nM.s^{-1}}$ = 2000 s. As addressed in

Chapter 2.3.2, the diffusion rate of all small chemicals used as signals in our experiments is on the order of D = 1000 µm^2.s^{-1}. Therefore $v \approx \sqrt{\frac{D}{t}} = \sqrt{\frac{1000m^2.s^{-1}}{2000s}} \approx 42$ µm.min^{-1}. This is in great agreement with the velocities observed in our experiments.

We further explored how the pulse velocity can be controlled through diffusion and reaction rates. The diffusion of the signal was tuned by the concentration of DFHBI in the trigger droplet and the rate of repression was tuned through activity of the repressor node with the T7 RNA Polymerase concentration. We fitted the pulse velocity of at least three different assemblies for each condition, and found that the velocity of the pulse increased as expected when either DFHBI or T7 RNA Polymerase concentration was increased (Figure 3.9.a and Figure 3.9.b). The velocity of the pulse can therefore be tuned with internal circuit parameters.

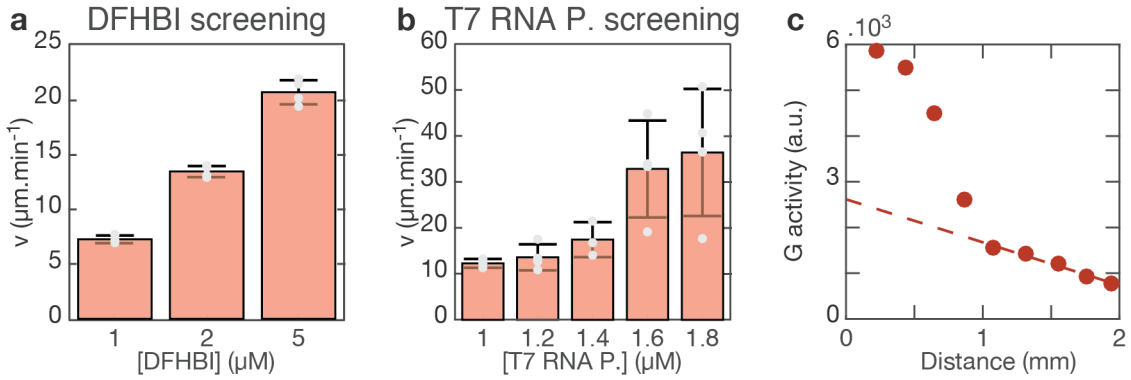

Figure 3.9. Tunable velocity and signalling range. a, Velocity of the pulse for different DFHBI (a) and T7 RNA Polymerase (b) concentrations. Bars and error bars indicate mean and standard deviation, single data points are overlaid. c, Activity of template G (maximum negative slope of fluorescence decay) against distance of the receiver from the sender. Linear fit of the second regime (dashed line) defines the signalling range of the pulse.

The attenuation of the pulse after the peak is reached depends on the activity of the repressor genelet in each compartment. To estimate this activity, we measured the maximum negative slope of fluorescence in each compartment and plotted it against the distance between this compartment and the trigger droplet. We found as expected that the activity of the repressor node was not identical in all compartments but decreased with increasing distance from the trigger droplet (Figure 3.9.c, corresponding to experiment depicted in Figure 3.8.a). We observed two regimes in the decrease of this activity: it first steeply drops over the first 1 mm and then slowly decreases along a line towards zero. As visible in the control experiment (Figure 3.8.d), the DFHBI diffusion from the trigger droplet causes a concentration ”overshoot” in the first droplets where the DFHBI concentration is temporarily above its equilibrium value. This causes more DNA activator to be released in the I1-FFL experiments in the first part of the assembly. Further away from the trigger droplet, the DFHBI concentration slowly rises to its equilibrium value, causing a slow release of the activator, and this is the second regime observed in the activity of the repressor genelet. We interpret the intersection of the fitted line with zero

as the signalling range of the I1-FFL circuit, beyond which DFHBI diffusion will remain below the activation threshold of the genelet. In the experiment depicted in Figure 3.9.c, this is approximately 2.8 mm.

Finally, we studied how dimensionality affects the dynamics of the I1-FFL circuit. We constructed a linear array of 5 receivers and a square array of 5×5 receivers to compare 1-dimensional and 2-dimensional assemblies (Figure 3.10.a and Figure 3.10.b). We first observed that the signalling range was shortened in 2D compared to 1D (Figure 3.10.c): 1.8 mm versus 2.6 mm, approximately. Interestingly, we found that the pulse velocity was higher in 2D than in 1D, but could be similarly tuned with DFHBI and T7 RNA Polymerase concentrations (Figure 3.10.d). Due to the overshoot diffusion effect described above, the peak in the first droplets is controlled by the DFHBI diffusion and only the later decreasing behaviour is controlled by the genelet activity. In the later droplets however, both the peak and the decrease of the signal are due to the genelet activity. In 2D, DFHBI diffuses from the trigger droplet into the first receiver and is then redistributed into two, then three receivers, etc. The diffusion "overshoot" is therefore redistributed faster than in 1D, and this leads to a faster pulse measured. As mentioned earlier, the dynamics of this system cannot be simply approximated with a 1D, 2D or 3D homogeneous diffusion, and the pulse velocity's dependency on dimensionality is therefore complex to predict.

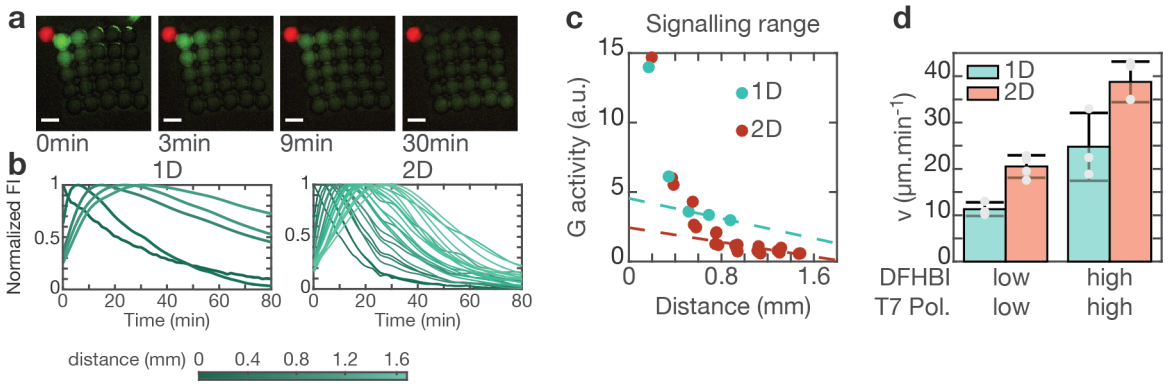

Figure 3.10. Pulse propagation and spatial dimensions. **a**, Fluorescence image of a 2D geometry. The sender is indicated in red, and the fluorescence induced by the circuit is shown in green. Scale bar: 200µm. **b**, Fluorescence intensity through time for the 1D and the 2D assemblies from **a**. **c**, Activity of G as a function of the distance from the sender, for 1D and 2D geometries in the same conditions. Dashed lines represent linear fits. **d**, Velocity compared for 1D and 2D geometries, for slow (low DFHBI, low T7 RNA Polymerase) and fast (high DFHBI, high T7 RNA Polymerase) pulse conditions. Mean, standard deviation and single data points are plotted.

3.2.4 Extension of the circuit

In this section, I describe circuits that were designed to extend the dynamics or controllability of the I1-FFL circuit.

In our original design, the diffusion of DFHBI is non-specific and therefore cannot be readily controlled. We showed how higher concentrations of DFHBI lead to a faster pulse, but the diffusion rate itself could not be addressed. Therefore, we designed a similar I1-FFL circuit based on the diffusion of a pore-specific signal, guanine. Instead of using the Spinach aptamer as read-out, this design uses the bifunctional guanine-DFHBI aptamer, where the binding of guanine to the corresponding RNA aptamer induces a conformation change and the formation of the binding site for DFHBI. Therefore, in the presence of DFHBI, a fluorescence signal will only be detected if guanine is present [96]. Guanine diffusion through our assembly is kinetically limited by the permeation of the bilayer, which depends on the number of pores on the bilayer surface. We could then tune its diffusion rate by tuning the pore concentration, adding a control parameter to the pulse velocity. Although appropriate I1-FFL repression dynamics could be measured in bulk (Figure 3.11.a), the diffusion of guanine in droplet assemblies was too slow for proper functionality of the circuit. The concentration threshold for activation of the repressor genelet could not be reached, and all experiments therefore demonstrated only diffusion and equilibration dynamics (Figure 3.11.b).

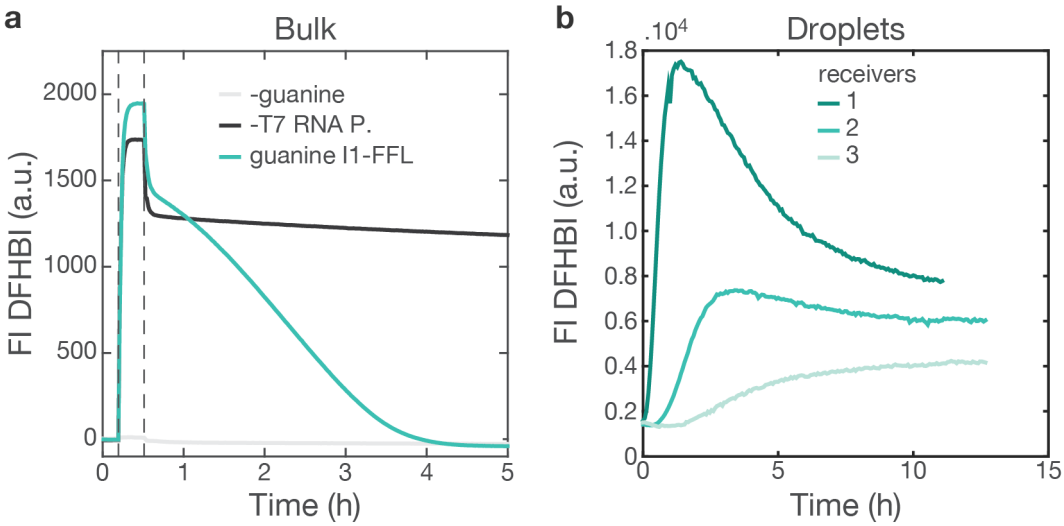

Figure 3.11. Guanine I1-FFL. **a**, Bulk characterization: 24-2-guanine RNA is preincubated with **A**, then guanine and DFHBI are added (left dashed line) and after 30 min incubation, guanine repressor genelet and T7 RNA Polymerase are added (right dashed line). Negative control is without guanine (light grey), positive control without T7 RNA Polymerase so that repressor template cannot be transcribed (dark grey), and complete guanine I1-FFL is functional (blue). **b**, Implementation of guanine I1-FFL in droplets merely shows equilibration of the fluorescence in all receivers at intermediate levels, as in control experiments.

One additional limitation of our pulse design is that the signal diffuses from a finite source without a positive feedback loop to create more signal, and the dynamics can therefore not reach true propagating wave behaviour. We explored the on-site autocatalytic production of a signalling species in experiments described in Chapter 4.

Finally, we considered using our I1-FFL circuit to modulate protein expression. Feedforward and feedback loop motifs regulate gene expression *in vivo*, and as genelet

circuits have thus far never been used in conjunction with protein expression, let alone employed to regulate it, we thought it an interesting challenge. As demonstrated in Chapter 3.2.3, the I1-FFL implementation in droplet assemblies leads to a spatial differentiation in the release of the activator and in the induction of the downstream repressor genelet. We thought these spatial differences could be used to induce a differentiation in protein expression in the array (we used a gene encoding a red-fluorescent protein under the control of a T7 promoter as read-out). In this design, the activator DNA would additionally activate a genelet coding for an RNA repressing protein expression - either a small RNA (sRNA) binding the RBS site of the mRNA and inhibiting ribosome binding and translation, or a short guide RNA (sgRNA) inducing transcription inhibition through the catalytically dead CRISPR-associated dCas9 system (Figure 3.12.a and b). We first verified that the I1-FFL circuit could be implemented in an *in vitro* transcription-translation system free of DNAse, and where RNAse activity is limited with RNAse inhibitors, namely the PURExpress system (Figure 3.12.c).

In the sRNA design, higher concentrations of DFHBI, which cause higher activation of the downstream template, did not lead to a higher repression of protein expression in bulk (Figure 3.12.d) or in droplets (Figure 3.12.e). We hypothesize that the translation interference was not sufficiently effective to lead to significant repression.

In the sgRNA design, significant protein expression repression was achieved with purified sgRNA, but not with activated genelet template (Figure 3.12.f). Accordingly, no difference in protein repression could be detected in droplets (Figure 3.12.g). We hypothesize that with an estimated maximum transcription rate of the sgRNA of 0.75 $nM.s^{-1}$ (see Chapter 3.2.3), concentrations of sgRNA sufficient for protein expression repression could not be transcribed. A version of this circuit using a mutated T7 promoter (leading to slower transcription of the gene and therefore easier repression) had correct functionality in bulk (Figure 3.12.h) but protein expression was overall too low to be detected in droplets.

With the I1-FFL pulse circuit, we demonstrated non-trivial, biomimetic and controllable spatial dynamics that can only be achieved in a spatially organized environment.

3.3 Differentiation

To further demonstrate the biomimicking relevance of our artificial multicellular assemblies, we implemented a fundamental process in embryo development: stochastic differentiation of cells. We constructed a circuit that amplifies natural noise in biological processes with a positive feedback loop, leading to an increased variability of protein expression between compartments. Chapter 3.3.1 discusses the importance of noise in

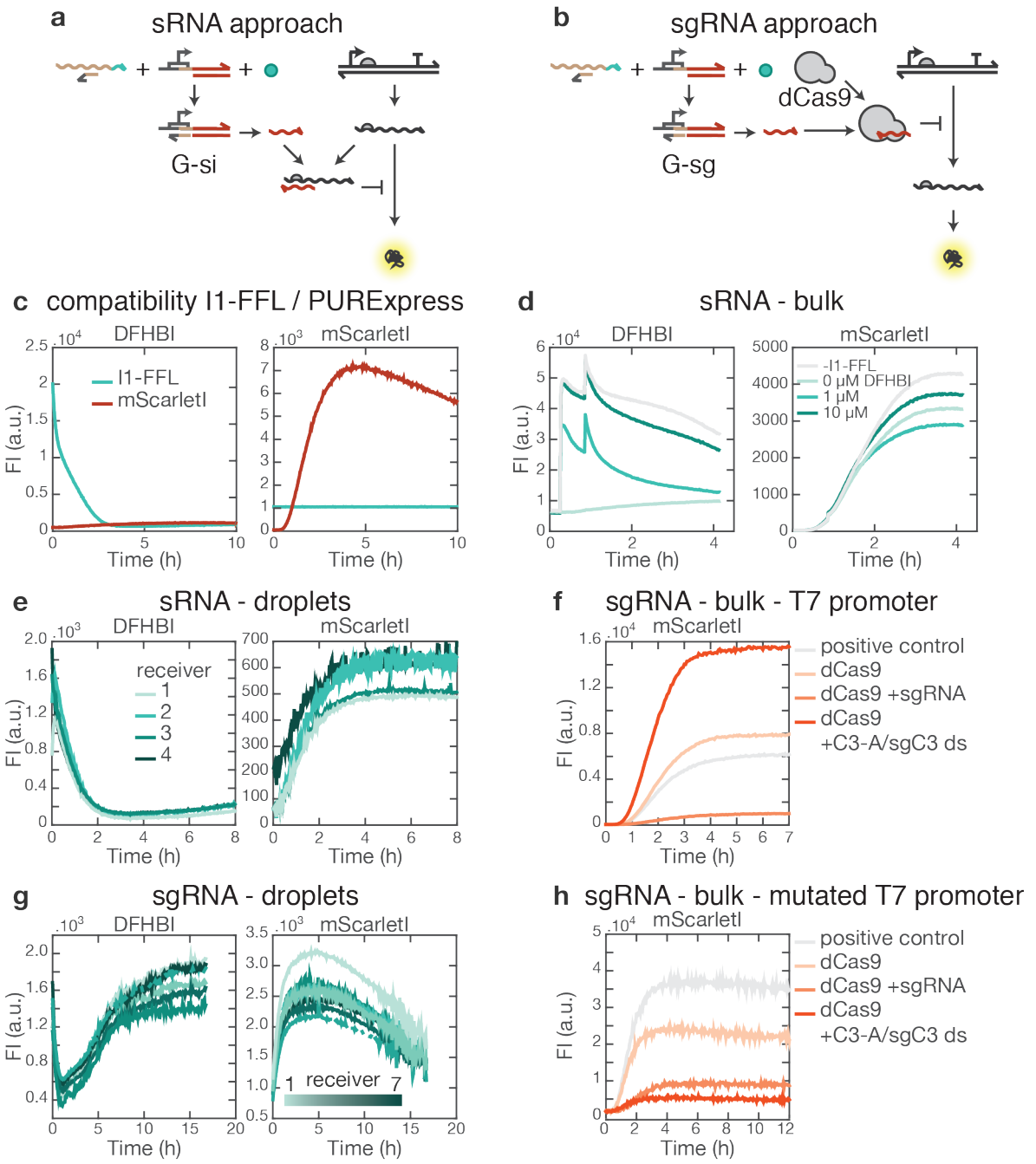

Figure 3.12. Coupling protein expression with I1-FFL. a-b, Two different approaches use the expression a small RNA activated by the I1-FFL to repress protein expression, either at the translational level (sRNA, a) or at the transcriptional level (sgRNA, b). c, The I1-FFL circuit can be implemented in PURExpress, an environment suitable for protein expression. d, Bulk characterization of the sRNA approach. Different concentrations of DFHBI, which should different levels of activation of the sRNA expression and therefore different levels of repression, do not cause a difference in protein expression. e, The sRNA approach also does not lead to different protein expression in droplets. f, Bulk characterization of the sgRNA approach with a normal T7 promoter. Purified sgRNA allows repression, but not the corresponding DNA template (C3-A with sgC3 ds). g, sgRNA approach with the normal T7 promoter does not lead to different protein expression in droplets. h, Bulk characterization of the sgRNA approach with a mutated T7 promoter. Both purified sgRNA and DNA template allow repression of protein expression.

biological processes and its sources. The circuit we engineered and its behaviour in bulk experiment is then described in Chapter 3.3.2, and droplet experiments demonstrating differentiation are discussed in Chapter 3.3.3.

3.3.1 Noise in biological processes

As described in Chapter 1.1, stochasticity of biochemical processes can lead to differentiation in embryos through certain reaction-diffusion processes, as described by Alan Turing. A random small deviation of a chemical concentration from equilibrium can be amplified by a positive feedback loop motif and through subsequent layers of feedback and feedforward motifs, impose the concentration of other components until the cell is differentiated from its neighbours.

Biochemical processes are fundamentally noisy due to low number of molecules, variation in metabolic activity, fluctuations in environmental conditions and other sources of stochasticity. Gene expression is particularly subject to variability since genes are present at low numbers in cells (1 to 2 copies), and the off and on states of promoters are typically long-lived [97]. Consequently, the current model of protein expression considers that mRNA is transcribed in bursts, and these bursts are amplified in the translation step. However, since proteins are typically longer-lived than mRNAs, proteins tend to average out variations in RNA concentrations (Figure 3.13.a). Single-cell measurement techniques, such as flow cytometry, fluorescence microscopy or single-cell sequencing have begun to unravel the cell-to-cell variability of gene expression and other biological processes.

Noise was long considered a nuisance to the correct functioning of gene circuits, and indeed gene regulatory networks need to perform reliably despite biological noise. Many network motifs have been shown to be robust against noise [98], [99], and this is believed to be a cause for their selection in performing certain biological computations. However, more and more studies recognize that noise is also used by biological organisms to perform crucial functions [97]. Examples include cell-state switching, such as in the lac operon that controls the switching between different sugar metabolisms, probabilistic differentiation in stem cells, such as in the Nanog/Gata6 differentiation, and all Turing-based differentiation processes in development (see Chapter 1.1). Models have also suggested that noise could play an important role in evolution, so that increased phenotypic noise would be selected for in periods of adaptation to new environments, whereas lower phenotypic noise would be advantageous in stable environments [97], [100].

The sources of variability in gene expression were classified by Elowitz *et al.* as intrinsic and extrinsic noise sources [101] (Figure 3.13.b). Extrinsic noise encompasses all variations in concentrations, activities and spatial distribution of regulatory molecules

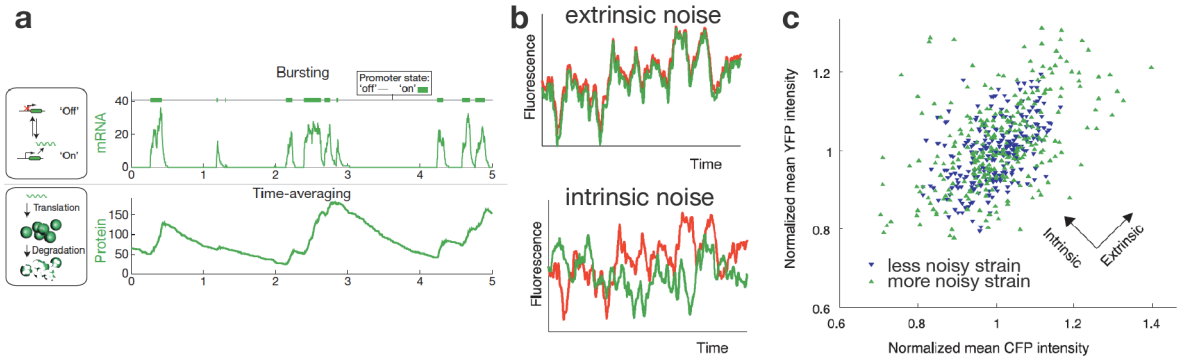

Figure 3.13. Noise in protein expression. a, Switching between long-lived promoter states leads to bursts in mRNA, which are averaged out in the protein concentration due to its longer lifetime. Figure adapted with permission from [97]. b, Two proteins, CFP (green) and YFP (red) are controlled by identical promoters. Extrinsic noise sources will cause both protein levels to fluctuate identically within a cell, whereas intrinsic noise sources will affect each protein level differently. Figure adapted with permission from [101]. c, Consequently, when CFP is plotted against YFP for each cell, the correlated noise is the extrinsic noise, whereas the uncorrelated is the intrinsic noise. Two strains are show, a less noisy strain (blue) and a more noisy strain (green). Figure adapted with permission from [101].

within a cell, such as polymerases or ribosomes. Extrinsic noise is identical for all processes within a cell but may vary from cell to cell. By contrast, intrinsic noise is introduced by the stochasticity of the gene expression process itself (such as random bursts of transcription). In the seminal paper from Elowitz *et al.*, the authors elegantly distinguished between extrinsic and intrinsic noise by measuring the expression of two fluorescent protein genes under identical promoters and in the same copy number in cells. Correlated variation in expression was due to extrinsic (*i.e.* identical for all processes within a cell) noise sources, whereas uncorrelated variation in expression was caused by intrinsic noise in the expression process itself (Figure 3.13.c).

Noise of gene expression is generally quantified by the coefficient of variation η (the standard deviation of the protein concentration between cells divided by its mean):

$$\eta = \frac{\sigma}{\mu} \tag{3.2}$$

In this work, we calculated the mean and standard deviation of a set of N data points x_i with the following formula (applying Bessel's correction):

$$\mu = \frac{1}{N}\sum_{i=1}^{N} x_i \tag{3.3}$$

$$\sigma = \sqrt{\frac{1}{N-1}\sum_{i=1}^{N} |x_i - \mu|^2} \tag{3.4}$$

Although many processes of cell differentiation are deterministic and induced by specific external signals, the importance of stochasticity in cell fate decisions is be-

coming increasingly evident [102]. We have addressed in Chapter 1.1 how the theory of stochastic processes in development is being integrated into the more classical positional information theory. We therefore attempted to build a simple differentiation circuit based on noise amplification.

3.3.2 Noise-based differentiation circuit and bulk response

We constructed a genetic circuit based on protein expression coupled to pore-mediated diffusion that is able to amplify biochemical noise in order to differentiation compartments in our assemblies. The circuit is similar to the lac operon in *E. coli*, which works as follows: the lactose permease LacY is randomly expressed through bursts of transcription of the lac promoter (temporarily de-repressed when the lac repressor stochastically unbinds). The LacY permease allows the uptake of lactose, which displaces the lac repressor. This induces sustained activation of the LacY promoter, increased expression of the LacY permease, and therefore further uptake of lactose in a positive feedback loop [103]. Similarly, we anticipated that expression of the α-HL pore put under the control of a pore-mediated diffusing chemical could lead to a positive feedback loop. As the induction of this loop would depend on random noisy expression of the pore and its insertion in the bilayer, we expected that this would lead to differentiation between different compartments subjected to the same circuit.

Therefore, we constructed a plasmid where a gene coding for α-HL monomers and a reporter mScarletI gene were put under the control of a pBAD, arabinose-inducible promoter (plasmid pSB1A2-AD010, Figure 3.14.a). The two genes are placed on the same transcript so that mScarletI expression accurately records activation of the pBAD promoter for α-HL expression. We placed this circuit in a receiver droplet in contact with an arabinose sender droplet and with initially no pores present. Leaky expression of the pBAD promoter will produce α-HL monomers, and if the threshold for pore incorporation in the bilayer is reached, arabinose will begin to diffuse in, thereby inducing the promoter and the further expression of pores. As a control, we used a construct where only mScarletI was placed under the pBAD promoter (pSB1A2-AD011, Figure 3.14.b).

We tested the expression of both these constructs as a function of arabinose in an *in vitro* transcription-translation (*E. coli* cell-extract) system. The response of both constructs to arabinose could be fitted with a Hill function, demonstrating typical promoter induction behaviour. Figure 3.14.c and d show three independent titration experiments for each construct, with the proportion of induced promoter calculated from final fluorescence intensity values (at 10 h of expression). A Hill equation fit overlays the data points for each experiment, and the mean and standard deviation of the mean (s.e.m.) of these fits is represented by a black line and shaded grey area. The standard deviation quantifies the variability of the biological process measured, such as protein expression. The s.e.m. quantifies the precision of the measurement, which in this case is the induction

response. Hence the s.e.m. is shown for the average of the three measurements of the response function.

On average, the affinity constants of both constructs for arabinose fell within the same range, with K_d = 23.1 ± 13.1 mM for the construct with α-HL (pSB1A2-AD010), and K_d = 28.2 ± 4.8 mM for the construct without α-HL (pSB1A2-AD011). However, the cooperativity of arabinose induction differed between the two constructs, with pSB1A2-AD010 having a lower cooperativity (n = 1.03 ± 0.15) than pSB1A2-AD011 (n = 1.85 ± 0.35). We assume that the difference in cooperativity is due to the sequence-specific context around the pBAD promoter, which may affect binding of the AraC transcription activator.

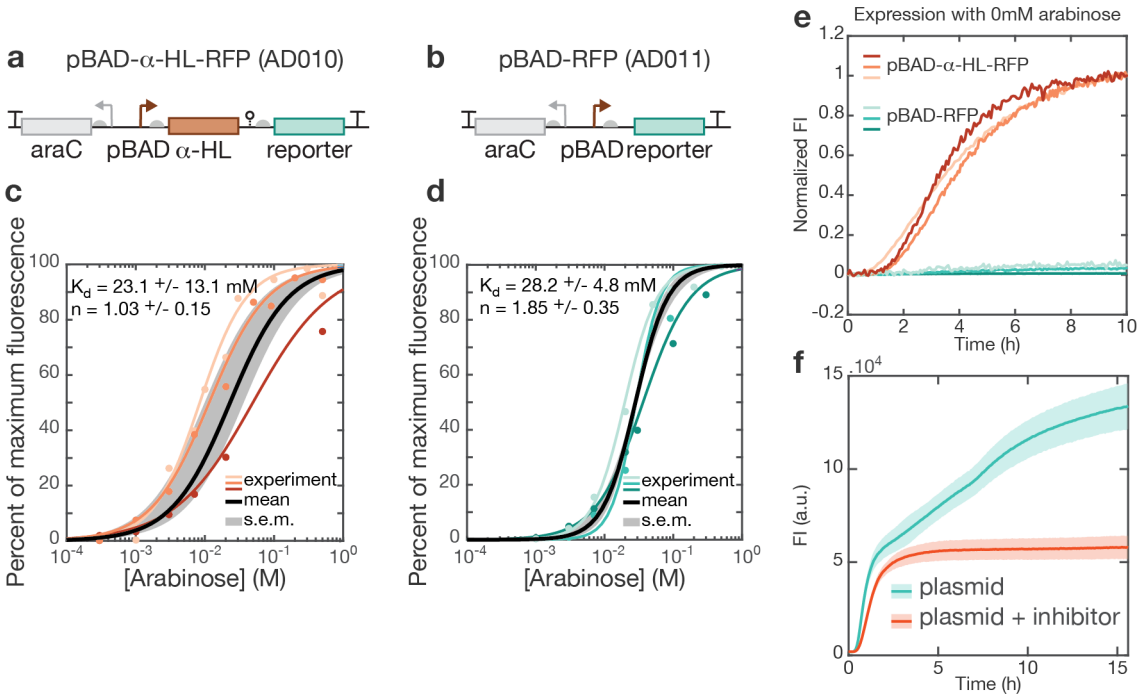

Figure 3.14. Bulk characterization of the noise-based differentiation circuit. **a**, Construct with α-HL and mScarletI under the control of a arabinose-inducible pBAD promoter. **b**, Control construct with mScarletI only under the control of pBAD. **c**-**d**, Arabinose titration and Hill fit for pSB1A2-AD010 (**c**) and pSB1A2-AD011 (**d**). Single data points of normalized fluorescence intensity at 10 h are shown with Hill fits for each experiment and mean and s.e.m. of all 3 experiments for each construct. **e**, Leaky expression of both constructs in the absence of arabinose. **f**, The presence of RNase Inhibitor does not improve protein expression.

In the absence of arabinose, the full construct pSB1A2-AD010 has a significantly higher expression than the mScarletI-only construct pSB1A2-AD011, with around 20 times higher fluorescence intensity (Figure 3.14.e). This higher leaky expression is consistent with the lower cooperativity of arabinose induction, which we assumed to be caused by proximal DNA sequence affecting promoter binding. Another reason for the difference in leakiness between the two constructs could be that pSB1A2-AD010 consists of one bicistronic transcript where mScarletI is in second position. Therefore it is

possible that some internal sequence in the α-HL gene is recognized by endogenous *E. coli* RNA polymerases, causing leaky transcription of a truncated construct still containing the full sequence for mScarletI. Analysis with the SoftBerry software [104]found two potential σ70 promoters in the α-HL gene, with transcription starting at respective positions 94 and 618 in the α-HL coding sequence, which could lead to leaky expression of mScarletI in absence of arabinose, but would not lead to expression of functional α-HL. The observed leakiness would in this case not affect expression of α-HL pores in our circuit, but rather be an artefact of mScarletI reporting. Such a leaky expression would be constant irrespective of the induction state of the pBAD promoter, and therefore simply add to the total fluorescence reported without introducing artificial variability between compartments.

In an early version of the circuit where we used GFP as a reporter for α-HL expression, we tested the effect of RNA stability on the performance of the circuit. We expected that if the mRNA was transcribed in bursts, a longer lifetime of the mRNA would result in higher protein numbers for each mRNA, and that therefore intrinsic noise would be better measured with a higher protein signal when RNA is more stable. We tested this effect in bulk by expressing a *pBAD-α-HL-GFP* (pSB1A2-AD001) construct in the presence and absence of RNAse inhibitor. Surprisingly, we found that GFP expression was higher in the absence of RNAse inhibitor than in its presence (Figure 3.14.f). In the presence of RNAse inhibitor, GFP expression was linear for the first 2 h and reached a plateau after 3 h. In contrast, in the absence of RNAse inhibitor, GFP expression was linear (and slightly faster than with inhibitor) in the first 1.5 h, and then entered a second regime of linear but slower expression. The noise in protein expression was not significantly affected by RNAse inhibitor. We assume that the process dominating protein expression here, rather than RNA stabilization, is resource depletion and regeneration [105]. The degradation of mRNA could be replenishing the cell-extract with free ATP and GTP molecules, which are necessary cofactors in translation, through the glycolysis biochemical pathway [105]. This could allow slow continuous translation of GFP molecules after the resources have been exhausted in the first phase of the expression (the first 1.5 to 2 h). In the presence of RNAse inhibitor, we assume that the RNA is not degraded, and that transcription might eventually consume all GTP and ATP molecules, permitting only translation of GFP in the first phase of the expression when resources are more freely available. Experiments with this GFP construct were not continued as background fluorescence in the GFP channel is quite high in cell-extract, and this rendered droplet experiments difficult to analyse.

This experiment with RNA stability clarified an important point in our experiments. RNA stability is expected to measurably affect protein expression if transcription and translation occur in unaveraged bursts, which is the case with low molecule numbers. However, in the volumes we are using both in bulk and in droplets, molecules are not present in numbers low enough to measure stochastic effects such as bursts of transcription. The number of molecules simultaneously undergoing such stochastic processes will average out these effects. Indeed, if we consider that our plasmid con-

centration is 5 nM, that bulk volume is 15 µL and that typical droplet volume is around 10 nL, we have around $4.5 \cdot 10^{10}$ molecules of DNA in a bulk experiment and $3 \cdot 10^{7}$ molecules of DNA in each droplet. If any noise is to be amplified by our circuit, it therefore cannot be gene expression noise but has to come from other processes.

3.3.3 Differentiation in droplets

We encapsulated the genetic circuit in droplet assemblies of the following geometry: a sender containing 300 mM arabinose (approximately 10 $\times K_d$) was put at the centre of four receivers containing the circuit. Having multiple receivers per assembly allowed us to compare protein expression between receivers in the same environment. Indeed, different locations in the chamber may have slightly different temperatures or local concentrations of lipids, and the volume of the sender droplet will vary from assembly to assembly, so that all of these effects may affect the protein expression in the compartments. We assume that such extrinsic noise sources affect all receivers in a given assembly identically, therefore we compared receivers of an assembly with each other. We also wondered if the presence of several receivers connected to a given sender might lead to competitive effects, where a receiver that stochastically would produce enough pores for arabinose permeation before its neighbours would titrate the arabinose in the sender away from the other receivers and create a lateral repression.

Results

As we expect that even without a noise-amplification circuit, measured protein expression would vary from compartment to compartment due to extrinsic noise sources listed above or to imaging artefacts affecting fluorescence measurements, we had to compare the noise in our circuit to several controls. The differentiation experiment is sketched out in Figure 3.15.a and the four experimental conditions are listed in Figure 3.15.c.

- In the differentiation experiment, the senders contain arabinose and no pores, and the receivers contain the full construct pSB1A2-AD010 so that leaky expression of the construct leads to increased permeability of the sender-receiver bilayer to arabinose and induces a positive feedback loop.

- In the positive control, the senders contain arabinose and purified α-HL pores, and the receivers contain the full construct so that bilayer permeability to arabinose is maximized from the beginning of the experiment and arabinose is distributed between the receivers, fully inducing the constructs.

- In the negative control, the senders contain neither arabinose nor pores, and the receivers contain the full construct so that the construct cannot be induced and measured fluorescence is only caused by leaky, uninduced expression of the pro-

moter.

- In the bilayer leakiness control, the senders contain arabinose and no pores, and the receivers contain the truncated construct pSB1A2-AD011 without α-HL gene, so that the effect of arabinose non-specifically permeating the bilayer in the absence of pores can be measured.

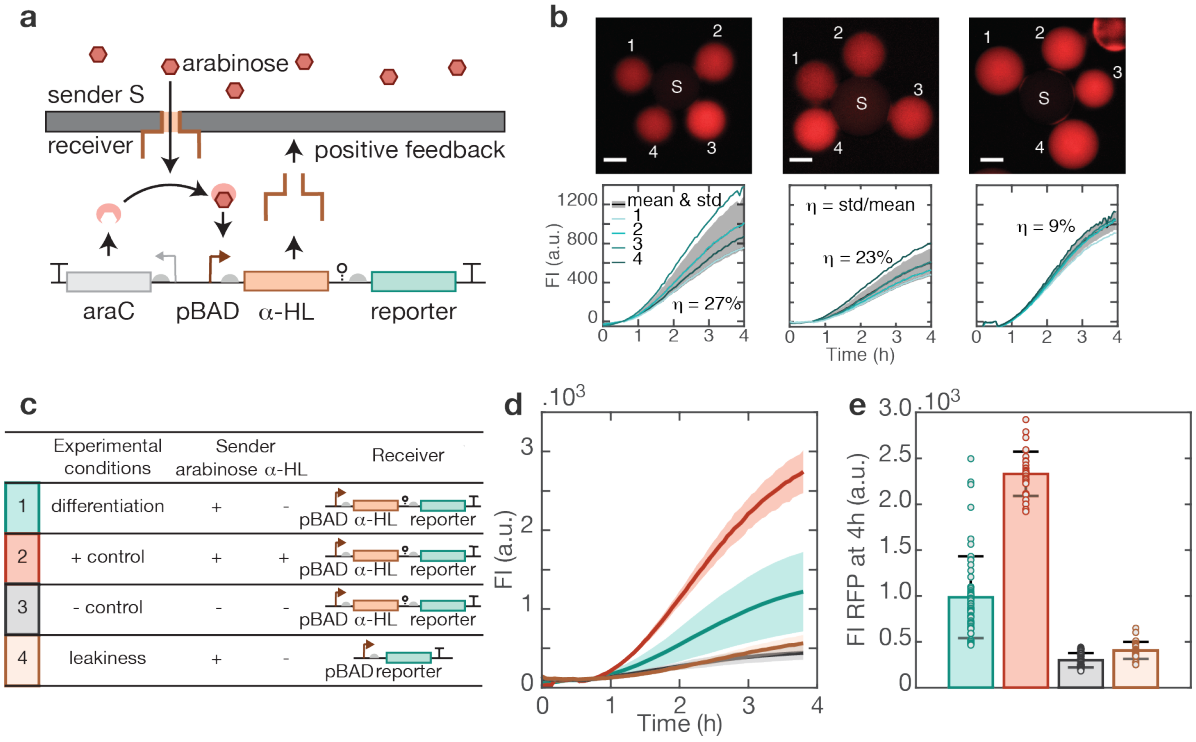

Figure 3.15. Droplet characterization of noise-based differentiation circuit. **a**, Differentiation experiment with positive feedback loop on the production of pores. **b**, Fluorescence images of 3 assemblies and time traces of each of the receivers overlaid with their mean and standard deviation (black line and shaded area). The first two assemblies (left and central panels) are considered high-differentiated as the coefficient of variation between receivers is above 20 %, and this can occur for high mean intensity (left panel) or low mean intensity (central panel), and is therefore not proportional to the intensity of the fluorescence. The third assembly (right panel) is considered not differentiated (coefficient of variation below 10 %) but has a mean high intensity. **c**, List of the four experimental conditions (one differentiation experiment and three controls). **d**, Time traces of the fluorescence intensity in all the droplets of all the assemblies considered. Mean and standard deviation are represented as thick line and shaded area. Colour code is defined in subfigure **c**. **e**, Mean (bars), standard deviation (error bars) and single data points (dots) of the final fluorescence intensity of all droplets for all 4 conditions.

We summarize the measured mean fluorescence intensity and its standard deviation for all droplets in all assemblies for the four experimental conditions (Figure 3.15.d). First, we observe that the mean expression in the differentiation experiment falls in between the positive control and the negative and leakiness controls, suggesting that the promoter is activated above its background leaky expression (negative control) and above its induction by leaky arabinose permeation (leakiness control). Neither of these

processes alone (leaky expression or leaky permeation) can account for the expression levels measured in the differentiation experiment. This demonstrates that the positive feedback loop of the circuit has been activated and that the threshold for pore incorporation has been crossed, causing arabinose to flow in and induce the promoter. The promoter is however not fully induced, since the mean expression in the differentiation experiment is lower than in the positive control. The mean expression in the leakiness control is slightly higher than in the negative control, which could indicate that arabinose indeed non-specifically permeates the bilayer in the absence of pores.

Second, we observe that the distribution of protein expression levels is broader in the differentiation experiment than in the controls, as quantified by the standard deviation of the fluorescence intensity, which is much higher for this experiment than for all controls (Figure 3.15.e shows the final mean fluorescence intensity, its standard deviation, and the single fluorescence values for all receiver droplets in the four experimental conditions). We expect extrinsic noise sources to cause similar variability in protein expression in all experiments. The fact that the variability of expression is much higher in the differentiation experiment than in the controls indicates that our circuit amplifies noise from intrinsic sources. Our positive feedback loop is therefore functional in inducing differentiation between compartments.

The simplest and most employed quantifier for noise is the coefficient of variation η, which measures the standard deviation divided by the mean expression, and will be expressed as a percentage throughout the thesis. As explained above, we wanted to limit artefacts in the quantification of noise and its amplification due to extrinsic noise sources that will vary expression rates from assembly to assembly. We therefore took a conservative approach in our quantification of differentiation, and only measured variation between receivers of the same assembly. The total larger distribution of fluorescence values in our differentiation experiment compared to controls nonetheless suggests that the noise amplification is even larger than will be quantified within single assemblies.

When plotting the coefficient of variation for each assembly (Figure 3.16.a), we find that in the controls, η is overall below 20 %, indicating that this is the upper variation caused by extrinsic noise sources. In the differentiation experiment, we can distinguish two populations of assemblies: for some assemblies, the coefficient of variation remains below 20 %, not exceeding the upper limit of extrinsic-noise-caused variability, whereas for others, the coefficient of variation is between 20 % and 45 %, demonstrating differentiation from internal noise amplification. As an example of these two populations, Figure 3.15.b shows 3 assemblies, two with high differentiation (above 20 %) but different mean intensities and a third with low differentiation (below 10 %) with high mean intensity. In these assemblies, a form of differentiation between receivers has been achieved. When fitting the histogram of η values for each condition with a lognormal distribution, we found that both the mean value and its variance were higher in the differentiation experiment than in the controls (Figure 3.16.b), confirming that the positive feedback loop increases the variability in protein expression.

We finally performed an additional positive control experiment. We used a construct containing only the α-HL gene under the pBAD promoter with no reporter (pSB1A2-AD009), which could induce a positive feedback loop on its own expression similarly to pSB1A2-AD010 by inducing arabinose flux. We then monitored the diffusion of Atto488, a pore-mediated diffusing signal, from a sender droplet to a receiver in three conditions. In all three conditions, the receivers contained the pSB1A2-AD009 construct. In the first condition, the senders contained arabinose and Atto488: here, the positive feedback loop could be induced similarly as in the differentiation experiment, and this would supposedly lead to α-HL pore formation and Atto488 flux. In the second condition, the senders contained Atto488 but no arabinose: the positive feedback loop could not be induced, and only leak amounts of pores might be formed, leading to no significant flux of Atto488. Finally, in the third condition, the senders contained Atto488 and purified α-HL pores, so that Atto488 could diffuse irrespective of the expression of the *pBAD-α-HL* construct. We found that the experiments with arabinose and with purified α-HL showed similar flux of Atto488, and that it was higher than in the absence of arabinose (Figure 3.16.c). This confirms that the positive feedback loop alone is sufficient to create enough α-HL pores to cause an increase in the permeability of the bilayer.

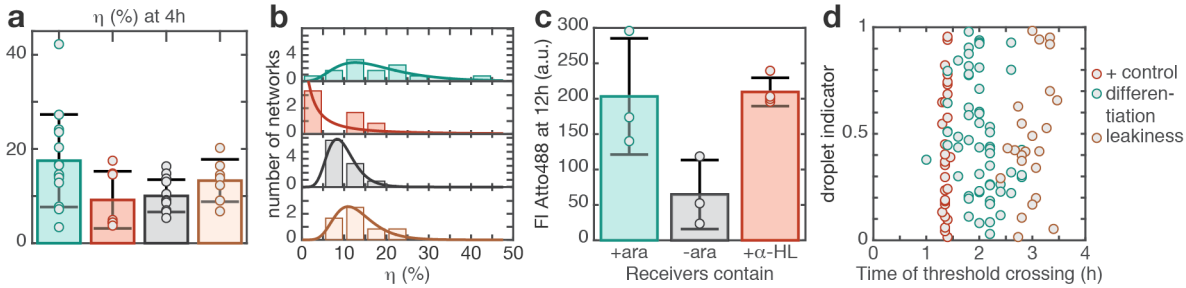

Figure 3.16. Noise quantification. **a**, Coefficient of variation for all assemblies: mean (bars), standard deviation (error bars) between all assemblies and single values for each assembly (dots). **b**, Histogram of the coefficient of variation and lognormal fit for each condition. **c**, Mean (bar), standard deviation (error bar) and single data points (dot) of fluorescence intensity at 12 h in a control experiment where the diffusion of Atto488 is measured, with arabinose, no arabinose or pores in the receiver and a plasmid coding for α-HL under a pBAD promoter. **d**, Time of the crossing of a defined expression threshold for each droplet under three experimental conditions.

Discussion

The circuit we engineered gives rise to an increase in noise and therefore to a significant, albeit not digital, differentiation. However, we have seen (Chapter 3.3.2) that this differentiation cannot be caused by a stochasticity of gene expression between compartments, as the number of molecules is too high for such an effect to occur. So what is the noise source that causes differentiation in our circuit?

We can first consider that leaky crossing of the bilayer by arabinose might be a stochastic process, as there should be a high energy barrier to this event, and that random bilayer permeation of arabinose would induce the pBAD promoter differently in each compartment, causing that noise to be further amplified by different expression

rates of α-HL. There are several arguments to oppose this hypothesis. First of all, we do not expect the spontaneous diffusion of arabinose across the bilayer to be a fast or efficient process, as experiments did not show a significant read-out expression in the absence of pores (see Chapter 2.3, where read-out expression is similar in the absence of arabinose/presence of pores and in the presence of arabinose/absence of pores, and Chapter 3.1). Therefore we can suppose that the concentration of arabinose that can non-specifically diffuse across the bilayers is several orders of magnitude lower than the reservoir concentration, and therefore well below K_d for activating pBAD. Second, as the size of the compartments is not such that numbers of molecules are low, we expect the non-specific permeation of arabinose to be a homogeneous process, dependent only on the area of permeation between senders and receivers. These areas typically diverge about 10 % around a mean value of 2 . 10^{-8} m^2 (see Chapter 2.3.2). Finally, in the leakiness control, induction of the construct is caused by non-specific permeation of arabinose, and we see that the noise in this experiment is not greater than in the other controls (about 20 % variability maximum). Therefore any leaky diffusion of arabinose into the receivers is unlikely to yield a significant differentiation effect such as observed in our experiments.

One process involved in the positive feedback loop of our circuit may be particularly noisy: the threshold for α-HL incorporation into the bilayer. As discussed in Chapter 2.2.1, although α-HL is a widely used pore, there is no consensus on the critical concentration required for its incorporation, and values ranging from the nM to the µM range have been reported. Gene expression and arabinose leakiness might lead to a relatively homogeneous leak expression of α-HL pores between compartments. However, if we assume that membrane incorporation efficiency is an intrinsically noisy process, the threshold concentration at which functional pores will assemble on the bilayers and induce the positive feedback loop might vary significantly from compartment to compartment. This hypothesis is supported by the observation that a given expression threshold is reached at times relatively narrowly distributed for all droplets in control experiments (around 1.5 h for the positive control and between 2.5 h to 3.5 h for the leakiness control, Figure 3.16.d). In the differentiation experiment, the threshold is reached at more distributed time points (from 1 h to 3 h). Modelling of the circuit confirmed that this effect could lead to an increase in variability in the differentiation experiment compared to controls [3].

In embryos, cell differentiation should follow an all-or-nothing mechanism where the cells obtain a clear distinctive phenotype at the end of the differentiation process. In our circuit however, we could so far create a spreading of the distribution and an increase in variability, but we did not see the compartments separate into ”fully-on” and ”fully-off” populations. Stronger coupling and direct lateral repression mechanisms should be introduced so that such effects can take place. Nevertheless, our work is the first to demonstrate a form of noise-based differentiation in artificial cells. These results open the way for biomimicking of developmental processes in non-living multicellular systems.

3.4 Gradient-based differentiation

Having explored stochastic differentiation in our droplet assemblies, we were interested in testing the second theory of cell differentiation in developing embryos: positional information. This theory was addressed in greater detail in Chapter 1.1. Briefly, a pre-existing morphogen gradient affects protein expression in embryos so that each cell reads out its local concentration of the morphogen and interprets it into a differentiated cell state. The morphogen gradient provides positional information to the cells: they ”know” their position in the embryo (and therefore the state they should differentiate into) based on the morphogen concentration they sense. Many factors can render the morphogen gradient and its interpretation noisy, leading to an uncertainty in the positional information. Robust patterning of embryos therefore requires noise-robust gene networks and sharp morphogen gradients.

To explore such gradients and gene networks in the artificial multicellular assemblies, I constructed a synthetic circuit that mimics the cross-repressing gene networks reading out pre-patterned morphogen gradients in embryos. This circuit takes the form of a bistable switch, of which one state can be induced by a morphogen. A gradient of the morphogen therefore induces a gradient in the expression of one of the two states, which induces an opposite gradient in the expression of the second state through repressive interactions, therefore leading to differentiated states in every compartment. In Chapter 3.4.1, I will address how robust positional information is implemented in developing embryos. The characteristics of natural gene networks and morphogen gradients will be detailed. I will then describe the circuit (Chapter 3.4.2) and its implementation in droplet assemblies (Chapter 3.4.3).

3.4.1 Robust positional information

In developmental biology, a central and on-going topic of research is to understand how embryos grow and differentiate reliably in noisy conditions, *i.e.* how they acquire robust patterns laying out their developmental program across a variety of embryo sizes, temperatures, and other environmental conditions. Particularly, induction of patterns by gradients of morphogens has been studied as one of the central mechanisms of embryo development. Precise experimentation is complex in living organisms and particularly in embryos, and artificial multicellular assemblies could provide an interesting platform to study these questions in simplified environments. This section will address how morphogen gradients are established in living organisms and how the concepts of positional information and positional error relate to developmental gene networks. Two archetypical examples of morphogen-based differentiation will then be addressed: the *Drosophila melanogaster* embryo and the development of neural tubes in vertebrates. Finally, the mechanisms that grant developmental processes robustness against a variety

of noise sources will be discussed.

Morphogen gradients and their stability

The synthesis-diffusion-degradation (SDD) model is a simple model describing how morphogen gradients are formed in developing embryos. The morphogens are synthesized at a localized source, they diffuse from that point into the embryo, and they are homogeneously degraded across the embryo (similar to the Crick model of sink-and-source, Figure 3.17.a). If the timescales of diffusion and degradation are similar to the timescale of morphogen synthesis, stable gradients can theoretically be established across embryos. However, establishing steady gradients in developing embryos is not an easy task: embryos can grow while the morphogen concentration profile is developing, resources for synthesis (such as metabolites) might be limited so that the morphogen cannot be synthesized at a constant rate, and embryo metabolism is altogether time dependent, making both the synthesis and the degradation rates vary in time.

Morphogen synthesis often occurs through translation of the corresponding protein from a localized source from which it diffuses. For example in *Drosophila*, a pool of maternal bicoid mRNA is localized on one side of the egg pre-fertilization. Synthesis of the morphogen need only be sustained for the time span during which the downstream differentiation processes occur. In the case of *Drosophila*, the differentiated gap gene pattern is formed in 2 to 3 hours following fertilization. In the vertebrate neural tube, studies show that the morphogen gradient is only stable for the first 30 hours of development after which it collapses, and could only be necessary to induce stable differentiation during the first 15 hours [13].

Many morphogen gradients are not constant over time. The sonic hedgehog (Shh) morphogen, which forms one of the two morphogen gradients critical to vertebrate neural tube development, has a concentration profile growing over time with an increasing maximum concentration [14]. In *Drosophila*, the protein dpERK forms a morphogen gradient in the terminal region of the embryo. This gradient becomes sharper during successive nuclei division cycles, and its maximum also increases over time. Interestingly, this change is due to the growing number of nuclei that present a correspondingly growing number of cell receptors for dpERK. As the number of binding partners increases, dpERK is locally trapped in regions close to the source of the morphogen and cannot diffuse into more distant regions, changing the diffusion profile [106]. Such a trapping mechanism is likely to be involved in the modulation of all morphogen gradient profiles.

In contrast, some morphogens form gradient profiles that remain constant over time. Organisms have evolved intricate mechanisms to maintain such concentration profiles while the embryo undergoes drastic changes. The Bicoid (Bcd) protein of *Drosophila* - one of the most studied morphogens - forms its gradient within the first hour following egg fertilization and remains stable thereafter despite the increasing number of nuclei and the constant breakdown and reformation of nuclei membranes due to mitosis [107]. Following mitosis, Bcd concentration in each nucleus returns to concentration levels be-

fore mitosis with only 10 % variability. Mechanisms involving rapid Bicoid equilibration across the nuclei membrane and possible degradation within the nuclei are believed to be responsible for the stable gradient formation.

Assuming that synthesis of a morphogen is constant during the critical time of pattern formation, the two processes that control the length scale and timescale over which the gradient will be established are the diffusion constant of the morphogen and its degradation kinetics. Localization and trapping mechanisms (such as the one described for dpERK) are suggested to tune the diffusion coefficient of the morphogen to appropriate scales for correct pattern formation [21]. Variable degradation kinetics (either through protease-based degradation or trapping of the morphogen in inactive forms) are thought to allow similar morphogens to establish gradients over varying length scales in different organisms: the Bicoid gradient can induce similar pattern formation in different species between which eggs vary in size by a factor of up to 5 [108]. Many differentiation systems also employ multiple parallel morphogen gradients, possibly leading to more robust pattern formation.

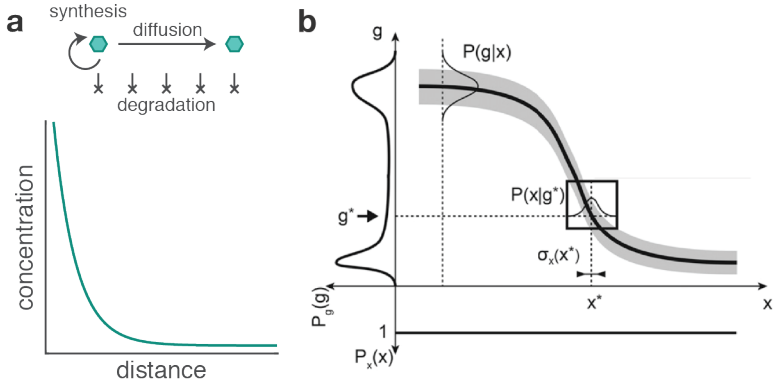

Figure 3.17. Morphogen gradient and positional error. a, The synthesis-diffusion-degradation model describes the formation of a spatial morphogen gradient as the results of its localized synthesis, its diffusion and its homogeneous degradation. b, A gene expression profile will have a certain variability among embryos (mean in thick line, standard deviation in shaded area). The error of the gene expression g at a specific location x can be used to calculate the error in position x at a specific gene expression level g, which is termed the positional error. This error in x corresponds to the region in which the cell could be when measuring expression level g. Figure adapted with permission from [109].

Positional information and positional error

Morphogen gradients induce a position-dependent pattern of gene expression across an embryo. Initially identical cells will then differentiate into various cell fates according to their position. It has therefore been customary to consider that a morphogen gradient provides "positional information", which is processed by the gene networks in the cells to read out their location [11]. The positional information can be quantified: this provides a measurement of the number of differentiable gene expression levels (*i.e.* distinguishable positions in the embryo) that the morphogen gradient induces. Accordingly, a positional error can be measured that reflects the relative position in the embryo that

the cell might interpret based on the morphogen level it senses. A robust pattern-forming gene network should allow for a low positional error in all cells during the critical time of developmental (the error should be lower than a few cells for accurate differentiation). In the case of the vertebrate neural tube, two antiparallel gradients maintain a positional error below 3 cell diameters across the whole tissue for the first 30 hours of development [13].

Although the mathematical description of positional error and positional information calculation is beyond the scope of this work, and the methodology has been laid out in great details in [109], a sense of how positional error depends on the variability of gene expression is given in Figure 3.17.b. If a gene expression profile has a given variability between embryos, the cell needs to be able to determine its position in the embryo given that variability. It should therefore differentiate into a given cell fate not if the measured gene level is exactly g_0, but if the measured gene level is in the range$[g_0 - \sigma_g, g_0 + \sigma_g]$. There is a certain spatial extent that is spanned by this expression range, and therefore a cell measuring a gene level within this range will not know where it is within the span of positions: this will be its positional error. For the cells to reliably interpret the morphogen gradient into a relative position (along the anterior-posterior axis in *Drosophila*, or along the dorsal-ventral axis in vertebrate neural tube for example) and to differentiate accordingly, the positional error needs to be maintained at low values. As the differentiation here is between large areas of the body plan (thorax, abdomen, etc...), the positional error does not need to be below 1 cell, but can be of the order of several cells.

The positional information measures the total information available to the cells due to the morphogen gradient's specific profile - that is, how many differentiated cell fates can be reached based on the gene expression profile and its variance. Formally, the positional information is the mutual information I between the spatial distribution of cells in an embryo and the gene expression distribution [109]. If a gradient provides I bits of positional information, the cells can distinguish 2^I differentiated states from this gradient.

The *Drosophila* blastoderm and the vertebrate neural tube

Two examples of positional information development have been extensively studied and have served as a systematic point of reference when formulating hypotheses about robust pattern development in morphogen gradients. They will be described below.

The embryo of *Drosophila melanogaster* consists of one large egg where, after fertilization, the nuclei divide within one cytoplasm. The nuclei membranes cyclically break down following mitosis cycles, and after the 10^{th} cycle of division the nuclei migrate from the centre to the periphery of the embryo. The maternal bicoid mRNA is localized in the egg before fertilization. After fertilization, its translation is activated and the protein diffuses from this fixed sourced along the anterior-posterior axis of the embryo, forming a

stable morphogen gradient within the first hour following fertilization (Figure 3.18.a) [107]. Bicoid (Bcd) inhibits the translation of Caudal (Cad), which forms an antisense gradient. After the 10th division cycle and the migration of the nuclei to the periphery of the egg, the nuclei internalize local Bcd and Cad morphogen levels based on their position. Diffusion of Bcd and Cad activates the expression of downstream proteins that are part of a gene network based on cross-repression: a/ Bcd activates Giant, Hunchback, Kruppel and Knirps while Cad activates Giant; b/ Giant, Hunchback, Kruppel and Knirps co-repress each other; c/ Tailless, a third morphogen, represses Knirps and Giant [110]. these proteins create expression regions in the embryo and form the gap gene pattern (Figure 3.18.b and c). A downstream gene network of co-repressors (the pair-rule genes) then forms even narrower regions of well-defined protein expression in the form of 7 stripes. After this pattern is established, cell membranes are formed separating the nuclei and gastrulation follows. The gap gene pattern is established very rapidly, over the first 2 to 3 hours following fertilization [14]. This was typically attributed to a supposed fast diffusion of morphogens since the embryo has one cytoplasm and the nuclei membranes break down cyclically. However, a study has shown that Bcd has a surprisingly low diffusion coefficient in the embryo, and suggested that nuclei-localized degradation of Bcd might be responsible for the fast establishment of the gradient and the subsequent pattern [107].

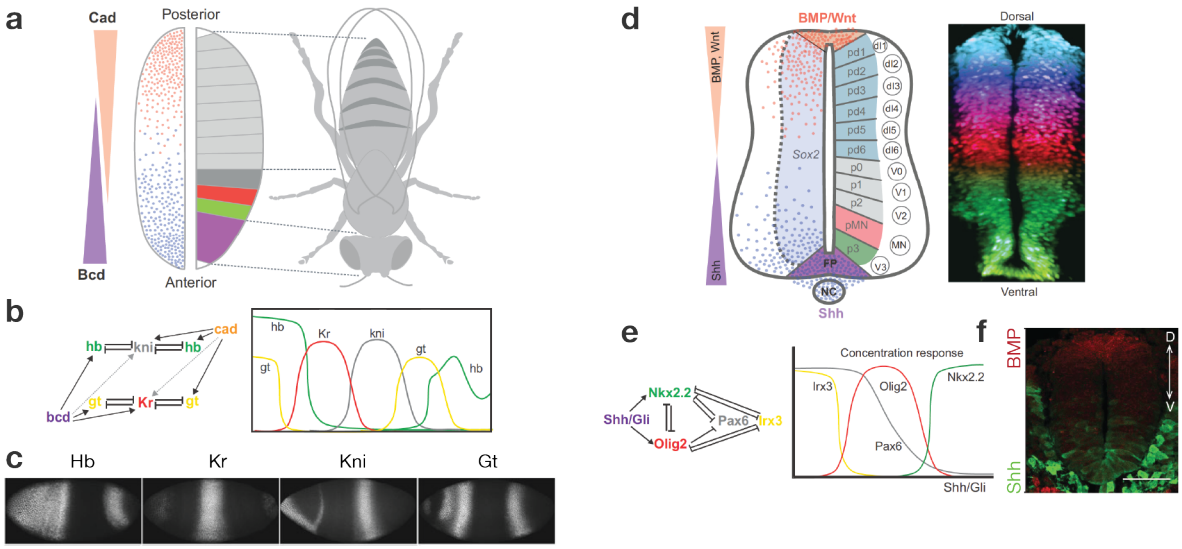

Figure 3.18. Gradients and development in *Drosophila* and the vertebrate neural tube. **a**, Anterio-posterior morphogen gradients (Bcd and Cad) in *Drosophila* result in the differentiation of the cephalic, thoracic and abdominal segments. **b**, Gap-gene network and gradients (in the central region of the embryo) of the different proteins along the anterio-posterior axis (left to right) at the late blastoderm stage. **c**, Microscopy image of the embryo egg at the late blastoderm stage, with gap gene proteins stained. Anterio-posterior axis is from left to right. **d**, Dorso-ventral morphogen gradient (Shh and BMP/Wnt) in the vertebrate neural tube result in the differentiation and segmentation of the tissue. **e**, Gene network of the vertebrate neural tube differentiation and gradients of the different proteins. **f**, Microscopy image of a mouse neural tube stained with reporters for Shh and BMP. Figure adapted with permission from [14] (**a**, **b**, **d**, **e**), [111] (**c**), and [13] (**f**).

By contrast, the vertebrate neural tube differentiation along its dorsal-ventral axis happens over tens of hours (more than 18 h for the mouse, [14]). This process takes place in a large tissue where long-range signalling is necessary and the morphogen needs to be internalized in the cells. The sonic hedgehog (Shh) and the bone morphogenetic proteins (BMPs) form anti-parallel gradients that induce the progressive establishment of a gene expression pattern (Figure 3.18.d, e and f). As described above, the gradients are conserved over the first 30 hours of development and then collapse, at which point the pattern has formed and remains independently of the gradient decay. The reading of both morphogen gradients by each cell is thought to be key to proper differentiation as their joint positional error is below 3 cells length during the first phase of development [13].

These two developmental processes have many similarities. They both occur in approximately one-dimensional tissues, involve anti-parallel gradients and gene networks of transcription factors that co-repress each other, so that sharp boundaries of gene expression are established. Interestingly, these gene networks often have redundancies, which are believed to render the pattern formation more robust. However, the parallels between these two examples of morphogen-based differentiation might introduce a bias and give the impression that they represent a general model for such processes. A neural network study analysed 3-genes network topologies that led to the formation of a strip of protein expression in a morphogen gradient (a simplified version of the classic French flag pattern problem) [112]. They found that six basic topologies could lead to such a sharp profile of protein expression. *Drosophila* and the vertebrate neural tube corresponded to only one of these topologies. these six topologies function with widely different mechanisms and rely on direct single-cell read-out of morphogen levels. Incoherent feed-forward loop motifs extracted from these topologies were implemented with synthetic circuits in *E. coli* and shown to produce stripe patterns in a morphogen gradient [113].

Robustness in pattern formation

Many of the processes involved in positional information based differentiation can be noisy, and the developmental processes in embryo have to mediate these sources of variability.

As addressed above, the morphogen amplitude can vary between embryos or through time (due to overproduction at the source for example). To mediate this noise, the binding of the morphogen to a receptor can be effectively equivalent to degradation and can tune the diffusion kinetics to ensure a reproducible gradient [114]. It has often been remarked that some molecules involved in pattern formation seem to be present in excess, and that an increase in morphogen concentrations by large factors is relatively well buffered by organisms [14]. This is for example the case for the dpERK gradient that remains surprisingly stable when its Torso receptor is overexpressed [106]. Generally speaking, the overexpression of receptors can therefore act as a buffer for variations in morphogen synthesis.

Fluctuations in the morphogen concentration profile are an important source of noise that must be buffered by embryos. This can be caused by noise in diffusion and degradation of the morphogen or by variation in the size of the embryo. Mechanisms might be needed to systematically adapt the morphogen profile if its diffusion kinetics do not match the size of the embryo (if the embryo is large and the morphogen slow diffusing the profile needs to be extended, if the embryo is small and the morphogen fast diffusing, the profile need to be sharpened). A suggested mechanism for the expansion of a diffusion profile that is too narrow involves the expression of an expander with a profile opposite to the morphogen (its expression can for example be repressed by the morphogen). The expander can then block the morphogen from binding its receptors, allowing it to diffuse further and extending the gradient profile, until the morphogen reaches high-enough concentrations at the more distant positions to repress the expression of the expander overall [114]. Maintaining an appropriate morphogen profile if the embryo is simultaneously growing might involve more complex mechanisms.

Redundancy in regulatory elements of the corresponding gene networks is thought to be critical for robust pattern formation [14]. The several layers of co-repression in the *Drosophila* gap gene system is one example of redundancies occurring in gene networks that respond to morphogen positional information. As gene expression at this copy number proceeds through noisy transcriptional bursts, redundancy of activatable or repressible promoters might permit the cells to perform time-averaging of the morphogen level, and therefore buffer variation of diffusion profiles through time. This suggests that morphogen levels varying through time might achieve the same patterns as morphogen levels varying through space [14]. Interestingly, this redundancy of stochastically expressed promoters might simultaneously allow for fast response to changes in morphogen concentrations. Many network motifs involved in such pattern formation resemble multistable switches, which possibly permit induced states to remain stable and an established pattern to be conserved after the morphogen gradient is lost. Stochastic transcription inactivation of the whole nuclei has also been demonstrated in later stages of the *Drosophila* development (14^{th} nuclear cycle) and could allow for spatial and temporal averaging of morphogen levels by stopping their synthesis [115]. Redundant gene motifs may also allow robust patterning if embryos are exposed to a variety of temperatures, as different promoters have different responses to temperature changes. Finally, a redundancy is suggested to be advantageous for evolvability, so that mutations in the gene networks are not systematically lethal to the embryo. Ways in which embryos of a given species might mediate variability were listed above, but it is an equally fascinating topic to determine how similar differentiation processes between species adapt to the large variability in species-specific embryo sizes or environmental conditions.

Having determined the key processes at stake in morphogen-gradient based differentiation, I will now describe the system I designed to study these processes in an artificial set-up.

3.4.2 Bistable circuit and preliminary results

The initial inspiration for building a synthetic circuit to mimic positional information differentiation was the Bicoid/Caudal opposing gradients. A gene network of two co-repressing genes forming a bistable switch and inducible by a morphogen would theoretically create opposing gradient profiles in space, so that subsequent layers of gene expression could be built in similar fashion to the progressive patterning in *Drosophila*. If the first circuit correctly induces the formation of opposing protein expression gradients, a network layer coding for one central stripe could then be added, then several other stripes in a similar manner.

The two-states switch was constructed based on the co-repression of two proteins, LacI and TetR. The expression of TetR is put under the control of a LacI-repressible pLacO promoter, and a GFP reporter is placed on the same transcript. Meanwhile, the expression of LacI is under the control of a TetR-repressible pTetO promoter, with a mCherry reporter on the same transcript (Figure 3.19.a, plasmids were cloned together with student Florian Rothfischer). This circuit architecture should lead to one of two states with either TetR/GFP or LacI/mCherry predominating. Additionally, both promoters are addressable with chemical signals: IPTG can be used to bind LacI and derepress pLacO, while aTc can bind TetR and derepress pTetO. This way, the expression state of either gene can be screened with one inducer gradient, and the two genes then co-regulate the expression of each other through repressive interactions. In our design, a degradation tag is additionally placed on the mCherry, so that if LacI/mCherry initially ”wins”, the proteins do not accumulate but rather this state can be effectively derepressed later on when adding IPTG and expressing TetR. For simplicity, the two constructs will be referred to as ”gene 1” for *pLacO-TetR-GFP* and ”gene 2” for *pTetO-LacI-mCherry*.

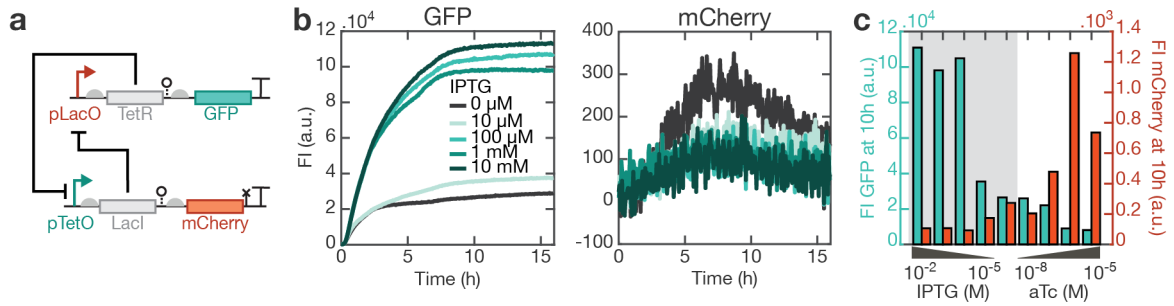

Figure 3.19. Bistable gene circuit and bulk response. **a**, Scheme of the circuit, with two plasmids each repressing the other's promoter. **b**, Time traces of GFP and mCherry expression in an IPTG titration against 5 nM of each plasmid. **c**, Final fluorescence intensities (at 10 h) in IPTG and aTc titrations with 5 nM of each plasmid (IPTG concentrations: 0 µM, 10 µM, 100 µM, 1mM, 10 mM, aTc concentrations: 0 nM, 10 nM, 100 nM, 1 µM, 10 µM). Grey shaded area represents IPTG titration.

The circuit was first tested in bulk, in an *in vitro* transcription-translation system (*E. coli* cell-extract) to verify its correct response to various inducer concentrations. We used equal concentrations of gene 1 and gene 2 (5 nM each) and monitored their expres-

sion in presence of 10 µM to 10 mM of IPTG and 10 nM to 10 µM of aTc. As an example, the time series of protein expression of GFP and mCherry for the IPTG titration are shown in Figure 3.19.b. The final protein levels at 10 hours of expression were compared for the different inducers concentrations (Figure 3.19.c). When no inducer is present, both genes repress each other and are expressed at intermediate-low levels: each gene is expressed normally at the beginning of the reaction, and the expressed proteins repress their corresponding promoter, halting the expression of the other gene.

Addition of IPTG causes a higher expression of gene 1 (TetR and GFP, under the control of pLacO) and a correspondingly lower expression of gene 2 (LacI and mCherry, under the control of pTetO) in a concentration-dependent manner. Indeed, when the reaction is assembled both LacI and TetR are initially expressed. However, binding of LacI to IPTG allows the continued activation of the pLacO promoter, so that TetR is expressed in large amounts and represses the pTetO promoter, and therefore the expression of gene 2. Equivalently, addition of aTc causes a higher expression of gene 2, which in turn causes a lower expression of gene 1.

With the screening of IPTG and aTc, the full spectrum of expression for both proteins can be reached: from high gene 1/low gene 2 at high IPTG concentration to low gene 1/high gene 2 at high aTc concentration. However, a morphogen gradient in droplets would ideally be created from a single inducer diffusing from a reservoir droplet into an assembly. Considering an IPTG gradient, the protein expression levels that could be reached would range from high gene 1/low gene 2 at high IPTG concentration to median gene 1/median gene 2 with no IPTG (corresponding to the shaded area of Figure 3.19.c). However, our goal is to obtain as much positional information as possible from the morphogen gradient, to give rise to the maximum number of differentiated protein expression states. This would mean screening expression profiles from high gene 1/low gene 2 to low gene 1/high gene 2 within a given morphogen gradient. Although the droplet experiments were conducted with the conditions of Figure 3.19, I later screened plasmid concentrations to obtain better conditions for a more differentiated protein expression (results described in Chapter 3.4.3).

I then encapsulated this bistable circuit in the linear assemblies: 5 receiver droplets were arranged in a 1D-array and connected to a reservoir droplet containing either IPTG or aTc. The protein expression was tracked in each droplet following the diffusion of the morphogens into the array. I found that the diffusion of IPTG induced a differentiation in protein expression between the different compartments (Figure 3.20.a): the leftmost compartments demonstrated a high GFP and low mCherry expression, whereas the rightmost compartments showed high mCherry and low GFP levels. A differentiation of protein levels over such a length scale (approximately 500 µm) is reminiscent of the spatial differentiation found in embryonic tissues, such as the *Drosophila* embryo or vertebrate neural tube tissues, and resembles the antiparallel protein gradients that begin the patterning of these systems. On the contrary, when aTc diffused into the droplet array (Figure 3.20.b), I found that on average all compartments showed a high mCherry/low

GFP phenotype. This homogeneous protein expression indicates that the characteristic length of diffusion of aTc is higher than the size of the assembly. All 5 receivers are therefore in a region of high aTc concentration, and express the corresponding protein levels. Indeed, aTc is a highly hydrophobic molecule that likely diffuses through the oil as well as through the bilayer, and might diffuse faster than a relatively more hydrophilic molecule, IPTG (although both are non-specifically diffusing signals). The diffusion constant of aTc might therefore make it an inadequate morphogen for an assembly of that size, but could be more suited for pattern induction in larger assemblies. With our simple circuit, we find ourselves already faced with issues that must be resolved in embryos for correct pattern development: the tuning of the diffusion coefficients of the morphogens to allow patterning over particular tissue sizes. I decided to concentrate on establishing patterns over sub-millimetre length scales, and therefore chose IPTG as the more adequate morphogen.

I then screened the dimensions of the droplet assemblies and measured the effect of tissue size on this morphogen-induced differentiation circuit. I created 1D-assemblies of 5, 7 and 9 receivers, and 2D-assemblies of 10 receivers in a 2×5 array. The protein expressions of both reporters in these arrays were averaged and are represented in respectively Figure 3.20.c, d, e and f. First, it is quite evident that the gradient of GFP expression is sharper, and therefore provides better positional information than that of mCherry. mCherry is indeed a protein with poor fluorescence properties: it has a low quantum yield (ϕ = 0.22 [116]) compared to ϕ = 0.65 for superfolder-GFP used here [117], and a low brightness (17.5 compared to 54.2 for sfGFP). Measurement of mCherry fluorescence is therefore noisier, and this added noise worsens the estimation of the positional information compared to its actual value. The GFP gradient was therefore used for further analysis.

Then, when comparing the 1D-arrays of 5, 7 and 9 receivers (Figure 3.20.c, d and e), the GFP expression gradient seems to spread over 5 to 7 receiver droplets and to reach a plateau of low expression for longer distances. We can estimate that this corresponds to the characteristic diffusion length of IPTG, so that a diffusion gradient can only be established over approximately 500 µm. As IPTG is a non-specifically diffusing chemical, it is quite likely that its diffusion is limited by aqueous diffusion. However, we have seen that it diffuses significantly slower than other non-specifically diffusing chemicals such as aTc, which could indicate that bilayer permeation slows down IPTG diffusion. Further experiments quantifying the exact kinetics of IPTG diffusion should be conducted to understand whether the length of the assembly or the number of bilayers it contains affect most the IPTG diffusion. We find here again an effect that was addressed in Chapter 3.4.1 for living embryos: adjusting the morphogen profile to varying tissue sizes necessitates active mechanisms, such as receptor blocking, trapping or trafficking. The design of similar mechanisms that can affect morphogen diffusion dynamics in artificial environments is an interesting challenge that remains largely unexplored. In the specific context of the cell-extract, the lifetime of the cell-extract and its effect on protein expression when induced with a delay should be quantified and compared to the

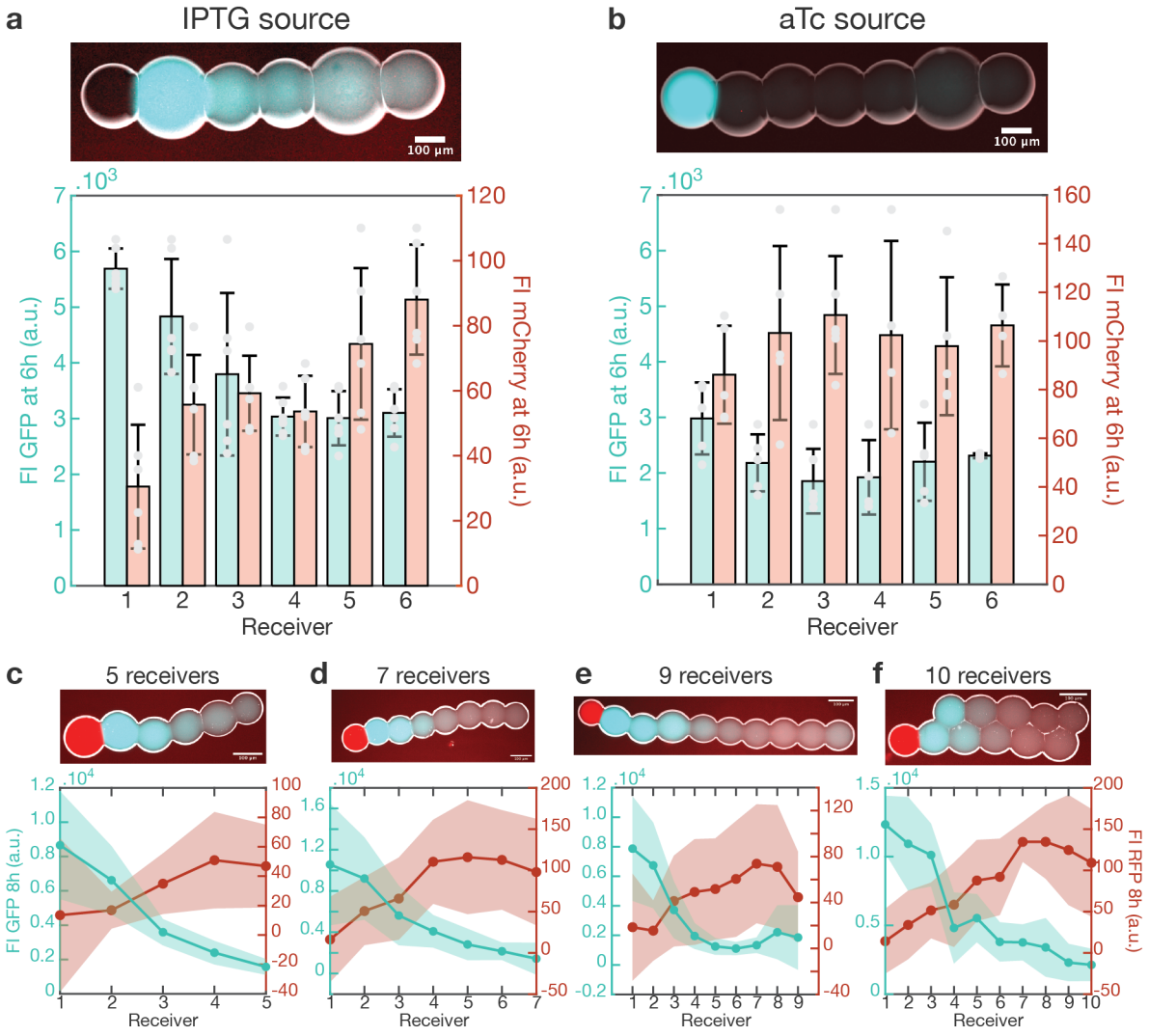

Figure 3.20. Bistable gene circuit in droplets. **a**, Fluorescence in a 5-receivers assembly with 10 mM IPTG in the sender droplet (left-most on microscopy image). Microscopy image: scale bar 100 µm, GFP is indicated in blue, mCherry is indicated in red. Bars and error bars indicate mean and standard deviation, single data points are overlaid. **b**, Fluorescence in a 5-receivers assembly with 10 µM aTc in the sender droplet (marked with a dye, left-most droplet). **c**-**e**, Microscopy image and fluorescence intensity in assemblies of 5 (**c**), 7 (**d**), 9 (**e**) and 10 (**f**, in 2D) receiver droplets, with 10 mM IPTG in the sender droplet (indicated with a red dye, left-most droplet). Lines indicate mean and shaded area indicate standard deviation of at least 6 assemblies.

IPTG-diffusion-dependent expression of the circuit's genes.

Finally, diffusion of IPTG into a 2D array showed a sharp gradient of GFP expression. Due to the geometry of this array, most receivers can be grouped in pairs that are at the same distance from the sender droplet and separated by the same number of bilayers. These pairs of droplets seem to have similar expression levels, as can be seen in Figure 3.20.f. This assembly therefore responds similarly to the 1D-array with 5

receivers, with simply a doubled number of receivers.

Lastly, we were interested in assessing how the circuit responded in environments other than the droplet assemblies. Indeed, protein and plasmid diffusion is limited in the context of our droplets, and morphogen diffusion might be slowed by bilayer permeation as discussed above. This is naively in contrast to a *Drosophila* embryo, for example, where proteins and mRNAs freely diffuse in the cytoplasm of the egg cell and permeate the nuclei. We therefore set our circuit in a low-melting agarose gel (0.88 %) so that proteins, plasmids and morphogens could diffuse freely. IPTG was pipetted at one end of a 2 mm × 2 cm channel and fluorescence was recorded along the whole channel. This experiment was conducted together with PhD student Lukas Aufinger. In the kymograph in Figure 3.21.a, GFP expression can be seen to increase through time and along the length of the channel. A GFP gradient clearly establishes (Figure 3.21.b) across a length of approximately 5 mm. No mCherry expression can be detected across the channel, probably due to the low fluorescence properties addressed above (Figure 3.21.c). In this system, the protein expression differentiation can therefore be established, but the free diffusion of all components smears out the pattern over one order of magnitude (from 500 µm in droplets to 5 mm in gel), therefore increasing positional error. This result is consistent with the hypothesis that the trapping of transcription factors in nuclei due to their binding to the genome effectively slows their diffusion and allows for the establishment of the correct pattern over appropriate length scales [21].

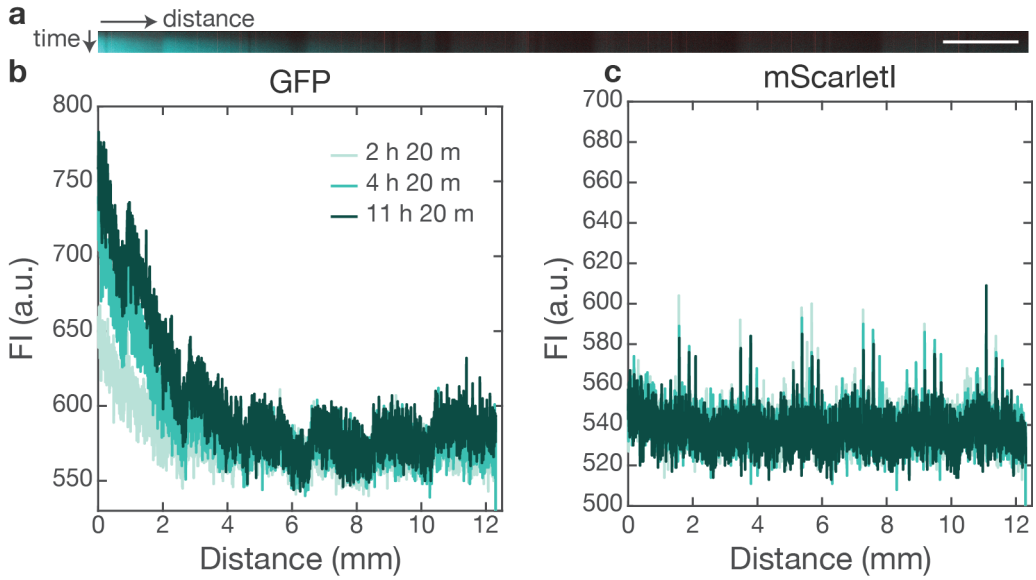

Figure 3.21. Bistable gene circuit in continuous medium. **a**, Kymograph of fluorescence (blue: GFP, red: mScarletI). 10 mM IPTG source is on the left side of the chamber. Time from top to bottom, from 0 h to 12 h. Scale bar: 1 mm. **b-c**, Fluorescence intensity in the chamber at 3 time points, 2 h 20 min, 4h 20 min and 11 h 20 min from light to dark blue (**b**, GFP, **c**, mScarletI).

Characterization of our positional information circuit and its implementation in droplets have demonstrated the possibility to reproduce some of the key dynamic pro-

cesses controlling differentiation in embryos. Although improvements can be made on both the circuit design and the quantification of positional information and positional error, these preliminary results demonstrate that our assemblies can be used to study the second class of development processes, morphogen pre-pattern based differentiation.

3.4.3 Improvement of circuit response

To achieve maximum and reliable positional information, a gene network should span whole ranges of protein expression over the morphogen gradient. In the uninduced state of our circuit (Figure 3.19.c), both gene 1 and gene 2 repress each other so that their expression is at an intermediate-low level. This means that an inducer gradient will only allow to titrate half of the full protein expression range: in the case of an IPTG morphogen gradient, this will range from high gene 1/low gene 2 for high IPTG concentrations to medium-low gene 1/medium-low gene 2 for low IPTG concentrations. To improve this performance of the circuit, the ”zero-state” of the circuit in the absence of inducer should be a ”gene 2 wins” state (that is, if IPTG is chosen as the morphogen), and the fully induced state in presence of maximum morphogen concentration should be a ”gene 1 wins” state.

I prototyped whether this was possible with the initial circuit design by titrating the concentrations of the plasmids of the two genes against each other. I kept the total plasmid concentration below 10 nM to avoid resource depletion effects in the cell-extract. To reach a high mCherry state in the absence of inducers, I kept the concentration of the gene 1 plasmid constant at 3 nM and varied the concentration of the gene 2 plasmid between 4 nM and 6 nM (Figure 3.22.a, b and c). In each of these conditions, I induced the circuit with 1 µM aTc as a positive control (in which gene 2 wins), and screened IPTG concentration between 0.1 mM and 10 mM. I found that a ratio of 3 nM gene 1 to 5 nM gene 2 (Figure 3.22.b) gave the highest GFP expression at high IPTG concentration, while retaining a high mCherry expression in the absence of IPTG, close to the positive control with 1 µM aTc. Appropriate plasmids ratio could similarly be optimized in further iterations of the circuit. In embryos, this could correspond to copy number of the genes or basal expression of the promoters.

The initial circuit design holds several flaws that will be improved in following iterations. First of all, I have addressed the poor fluorescence properties of mCherry. This reporter will be replaced by the brighter mScarletI, which should allow a less noisy measurement of positional information and positional error. Then, a degradation tag will be added to LacI. Indeed, only the reporter mCherry is currently tagged for degradation, so that when the system initially reaches a high gene 2 state, further induction of gene 1 through the IPTG gradient allows the initial mCherry to be degraded. This reports an apparent ”low gene 2” state, but LacI persists in the compartment and this could affect the dynamics of the circuit. Both LacI and the new reporter mScarletI will be tagged

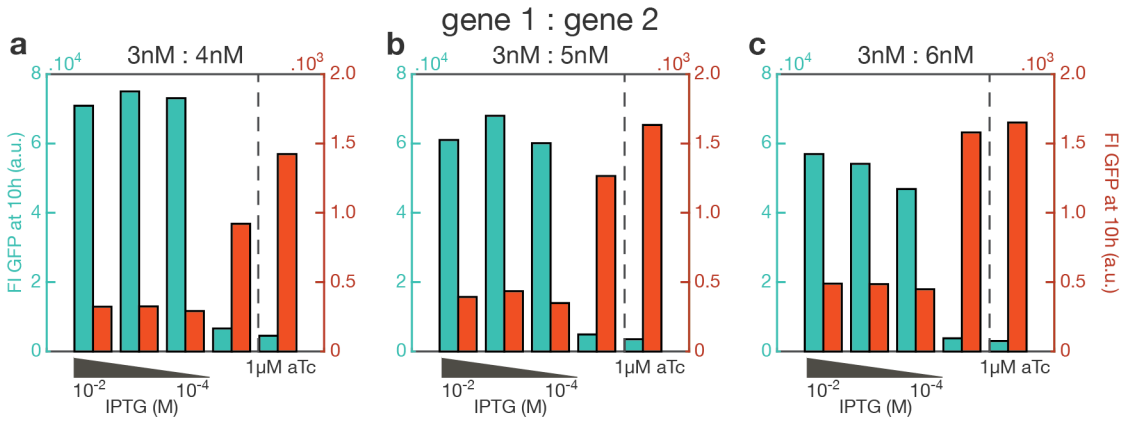

Figure 3.22. Plasmid ratio screening in bistable gene circuit. Fluorescence intensity at 10 h for GFP and mScarletI is shown for different plasmid concentrations, and for 0 mM to 10 mM IPTG and 10 μM aTc (control). **a**, 3 nM gene 1, 4 nM gene 2. **b**, 3 nM gene 1, 5 nM gene 2. **c**, 3 nM gene 1, 6 nM gene 2.

for degradation, so that an initial "high gene 2" state can be fully derepressed with the addition of IPTG. Finally, the GFP reporter will be changed to YFP: this is not critical to the performance of the circuit in its current form, but will be critical for implementing further layers in the gene network. Indeed, once proper opposing gradients of gene 1 and gene 2 can be established through a morphogen gradient, subsequent layers of gene expression will be added to the circuit so that regions of protein expression with sharp boundaries can be formed. Similarly to the stripes that develop in the *Drosophila* embryo due to cascades of gene repression and activation, genes repressed by both gene 1 and gene 2 can become repressors for other genes, which could lead to the formation of stripes of protein levels, and a single-compartment resolution of protein expression states may be achieved.

I have constructed a synthetic circuit that responds to a morphogen gradient with differentiated protein expression, with dynamics similar to many developmental processes in multicellular organisms. This circuit is an interesting platform to study the robust implementation of positional information in morphogen gradient and the reduction of positional error in large assemblies.

4 Signal-sending synthetic circuits

For engineering signalling between artificial cells, the simplest signals to produce are small chemicals that are produced at a low metabolic cost. Quorum sensing signals - used by bacteria to sense their own population density - are ideal because they exist in a variety of sizes and require few genes for their production and detection. Specifically, gram-negative bacteria produce N-acyl-homoserine lactones (HSL) that vary in carbon length chain and acyl chain substituent on the C3 position (Figure 4.1). These HSL signals easily permeate the bacterial cell wall and diffuse into the outer medium, so that their concentration is equilibrated across the bacterial population and rises as the cells grow, thereby providing information about cell density [118]. The quorum sensing operon of gram-negative bacteria often functions in a two-protein system as exemplified in the prototypical organism, *Vibrio fischeri*. In this case, the HSL chemical (3-oxo-C6-homoserine lactone 3OC6-HSL) is produced by LuxI, then binds the transcription inducer LuxR and activates it for the transcription of the pLux promoter (Figure 4.1.a). We focused on two homolog quorum sensing systems: the 3OC6-HSL/LuxR/LuxI system from *Vibrio fischeri* and the 3-oxo-C12-homoserine lactone 3OC12-HSL/LasR/LasI system from *Pseudomonas aeruginosa* (Figure 4.1.b).

4.1 Autocatalysis of signal production

To explore the possibility of producing HSL signals in situ in our droplet assemblies, I first used a quorum-sensing signal producing circuit with an autocatalytic feedback on signal expression. The autocatalysis ensures the production of high concentrations of signal, it is an interesting phenomenon to study in a spatial context, and it is the form of the quorum sensing operon in *Vibrio fischeri* [118]. The circuit consisted of two plasmids that were initially cloned by Dr. Andrea M□ ckl and PhD student Yalan Yi. The read-out plasmid (Figure 4.1.c) carried a LuxR gene (the transcription factor) under the control of a pLacO promoter (constitutively expressed in the cell-extract and IPTG-inducible in *E. coli*), as well as a GFP reporter under the control of a pLux promoter. This read-out could be induced with purified 3OC6-HSL and was used in other circuits (see Chapter 2.3 and Chapter 3.1). The sender plasmid carried a LuxI gene (the signal

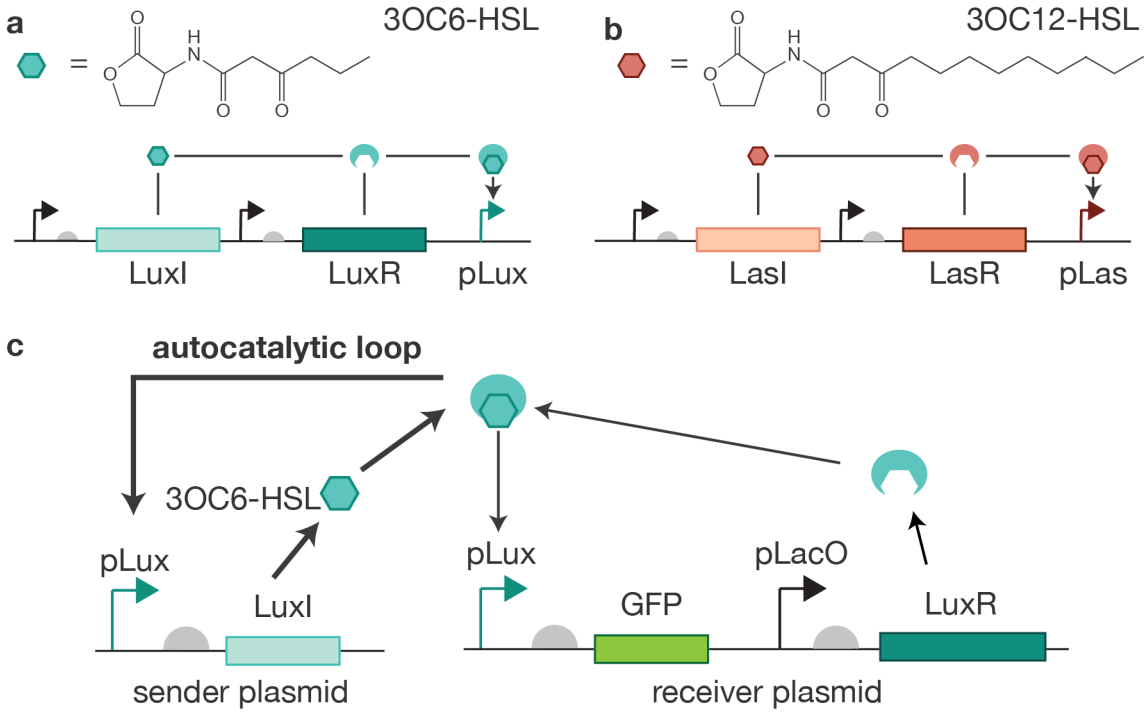

Figure 4.1. Quorum sensing. a-b, Signalling and induction based on quorum sensing signals 3OC6-HSL (a) and 3OC12-HSL (b). LuxI (respectively LasI) produces its cognate signal 3OC6-HSL (respectively 3OC12-HSL). The signal then binds the transcription factor LuxR (respectively LasR) and activates it. This activated transcription factor then activates its cognate promoter pLux (respectively pLas). c, Scheme of the autocatalysis gene circuit, where the production of the signal 3OC6-HSL is placed under the control of its own promoter on a signal-sending plasmid. GFP serves as a reporter of pLux activation, and LuxR is constitutively expressed (receiver plasmid).

synthesizing protein) under the control of a pLux promoter, so that leaky expression of pLux would induce the synthesis of 3OC6-HSL and further induce the expression of LuxI in an autocatalytic fashion.

I will first describe the characterization of this circuit in bulk (Chapter 4.1.1) and its implementation in droplets (Chapter 4.1.2). I will then present variants of this circuit, namely LuxI-RBS variants and a 3OC12-HSL/LasI/LasR based circuit (Chapter 4.1.3).

4.1.1 Autocatalysis response in bulk

To begin, a titration of purified 3OC6-HSL was performed in cell-extract against the read-out plasmid (*pSB1A3-pLacO-T9002-LVA* [119]), to determine the dose-response function of the pLux promoter (Figure 4.2.a and b, see also Figure AA.2.a and b). The promoter showed usual Hill function response to increasing concentrations of 3OC6-HSL, with protein expression starting at the same time in all conditions but with varying

kinetics therefore reaching different protein levels.

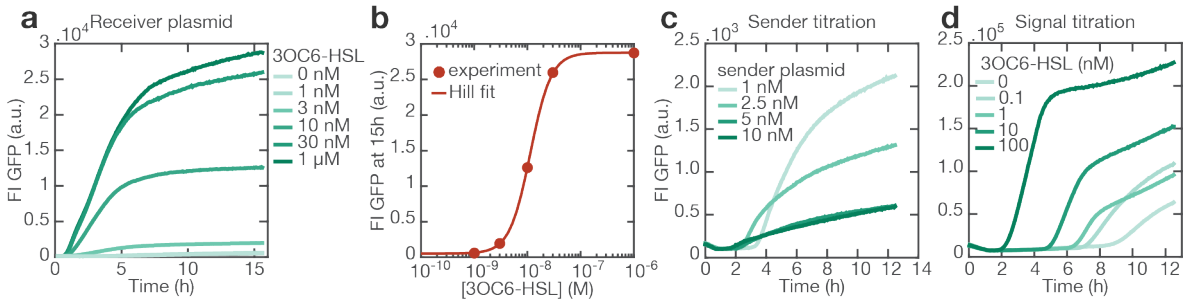

Figure 4.2. Bulk characterization of autocatalysis circuit. a, Time trace of fluorescence intensity in a 3OC6-HSL titration against the receiver plasmid. b, Hill fit of final fluorescence intensity in 3OC6-HSL titration. c, Titration of sender plasmid against 5 nM of receiver plasmid. d, 3OC6-HSL titration against 5 nM of receiver plasmid and 1 nM of sender plasmid.

Then, a titration of the sender plasmid (*pSB4K5-pLux-LuxI*) was performed against the read-out plasmid, in absence of 3OC6-HSL, to verify whether the sender plasmid did produce 3OC6-HSL (Figure4.2.c). First, addition of any amount of sender plasmid led to the induction of GFP expression, demonstrating that the sender plasmid did produce significant amounts of 3OC6-HSL. Second, an interesting relation between concentration of sender plasmid and kinetics of protein expression could be observed. With increasing concentrations of the sender plasmid, GFP expression started at earlier times but surprisingly reached lower final levels. When the read-out plasmid is induced with purified 3OC6-HSL, GFP expression is detectable after 30 minutes to 1 hour (Figure 4.2.a), which is consistent with the delay for expressing the first mRNA and proteins, and the rapid folding time of this protein (7 min for sfGFP [82]). With 1 nM of sender plasmid, detectable GFP expression begins at around 3.5 hours, and this delay can be attributed to the induction of the *pLux-LuxI* autocatalysis. With higher sender plasmid concentrations, the leaky expression of pLux should lead to higher leak concentrations of LuxI, therefore producing more 3OC6-HSL and inducing the autocatalytic loop earlier. This earlier induction with higher concentrations of *pLux-LuxI* plasmid is confirmed by our data. Simultaneously, a higher concentration of sender plasmids will titrate resources away from the *pLux-GFP* gene to the *pLux-LuxI* gene, and will altogether consume resources faster. We can assume that the low total levels of GFP expression at high sender plasmid concentrations are due to this resource competition and depletion effects. The autocatalysis loop already demonstrates non-trivial dynamics with a tuneable delay in protein expression.

We then studied the effect of ”helping” the induction of the autocatalytic loop by adding low amounts of purified 3OC6-HSL to the sender/read-out plasmids circuit (Figure 4.2.d). We chose a low concentration of sender plasmid to avoid resource depletion issues. First, we can see that the induction of the autocatalytic loop may vary from experiment to experiment: in this experiment the control with no 3OC6-HSL (identical to the experiment with 1 nM sender plasmid in Figure 4.2.c) begins detectable GFP

expression after a delay of around 9 hours, more than double the delay seen in the first experiment. Batch-to-batch variability of the cell-extract and intrinsic noise in autocatalytic loops could explain this difference. Second, with higher 3OC6-HSL concentrations, detectable GFP expression begins earlier and reaches higher total protein expression. Interestingly, this effect is seen for 3OC6-HSL concentrations that are too low to induce read-out plasmid expression alone. We can therefore deduct that added 3OC6-HSL helps induce the autocatalytic loop faster, giving a direct control over the delay of the loop without reaching resource depletion issues.

This simple autocatalytic loop shows non-trivial behaviour in bulk, with tuneable critical time of induction. We then investigated its response in a spatial context.

4.1.2 Autocatalysis response in droplet assemblies

The response of the read-out plasmid to a diffusing 3OC6-HSL signal in droplet assemblies was characterized in detail in Chapter 3.1. Here I further explored whether 3OC6-HSL could diffuse through the oil or only permeate the bilayers. This chemical has indeed been shown to partition into fluorinated oils [2], so that there would be a reasonable expectation that it would partition into silicon oil. I used sender droplets containing 10 µM 3OC6-HSL and receiver droplets containing the read-out plasmid in cell-extract, and I either assembled the droplets into linear assemblies or arranged them in linear arrays without connecting them. I attempted to place the droplets at similar distances from the sender whether or not they were in a connected assembly. I found that in non-connected arrays, GFP expression was high in the first receiver and rapidly dropped in following receivers (Figure 4.3.a). This indicates that a/ 3OC6-HSL can diffuse through the oil and b/ that it dissipates quickly in space, probably due to the large dimensions of the chamber and the large volume of oil that acts as a sink. In connected assemblies, GFP expression was noisier but showed intermediate levels in all droplets across the array, suggesting that 3OC6-HSL diffuses and equilibrates between all receivers and induces GFP expression in all of them. This experiment demonstrates that 3OC6-HSL partitions into the oil, but that its diffusion is faster through lipid bilayers and therefore in connected assemblies. Indeed, in connected assemblies we can expect diffusion to occur approximately in 2 dimensions across the bilayers, whereas it occurs in 3 dimensions across the oil between isolated droplets.

Next, I placed sender droplets containing the sender plasmid in cell-extract inside randomly-arranged assemblies of receiver droplets containing the read-out plasmid in cell-extract. I compared the expression in these assemblies to isolated sender and receiver droplets placed at similar distances (Figure 4.4.a, b, c and d). The total dimensions of assembled and isolated droplets observed were around 2 mm $\times$ 2 mm, and the ratio of sender to receiver droplets was similar in all experiments. First, all GFP expression begins after approximately 5 hours, and this delay indicates that expression is due to the

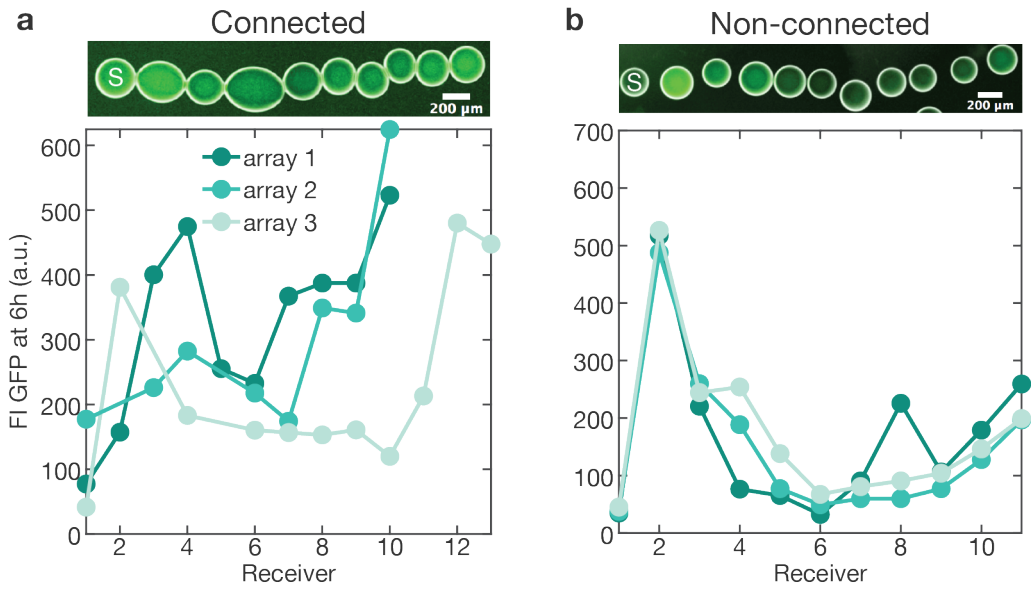

Figure 4.3. Induction of the receiver plasmid in droplet assemblies. Microscopy images with a sender droplet (S) containing 10 µM 3OC6-HSL on the left diffusing into an array of connected (**a**) or non-connected (**b**) droplets. Scale bar: 200 µm. Fluorescence intensity of three different assemblies is plotted.

induction of the autocatalytic loop. Second, the GFP expression is stronger and more synchronized in connected assemblies than in isolated droplets. Isolated droplets start expressing GFP at more distributed time points. The stronger expression in connected assemblies is coherent with experiments in Figure 4.3, and confirms that 3OC6-HSL diffusion is faster and more directed when droplets are connected through bilayer, and that 3OC6-HSL dissipates faster when senders are isolated.

The more synchronized induction of GFP expression in the connected assembly could demonstrate a quorum-sensing type of behaviour. Indeed, the experiments in Figure 4.3 suggest that 3OC6-HSL is quickly equilibrated over connected assemblies. This effect could lead 3OC6-HSL concentrations to remain homogeneous across connected compartments when the signal is produced in dedicated sender droplets, which would mimic the way quorum sensing concentrations are equilibrated in bacterial populations (to allow synchronization of response at high densities). In contrast, 3OC6-HSL sensing in isolated droplets could purely depend on the distance between each droplet and the closest sender droplets, and this would lead to the time-distribution of GFP expression induction that we measure in our experiments.

I also attempted to connect bacterial sender droplets, containing *E. coli* transformed with the sender plasmid, to cell-extract receiver droplets, to establish biological-artificial communication. Bi-directional communication between living and non-living systems through quorum-sensing signals was demonstrated in fluorinated oil emulsions arranged in 1 dimension [2]. However, significant GFP expression was not detected in this system, probably because the initial low density of cells did not allow to produce sig-

nificant 3OC6-HSL concentrations before the expression capabilities of the cell-extract droplets ran out.

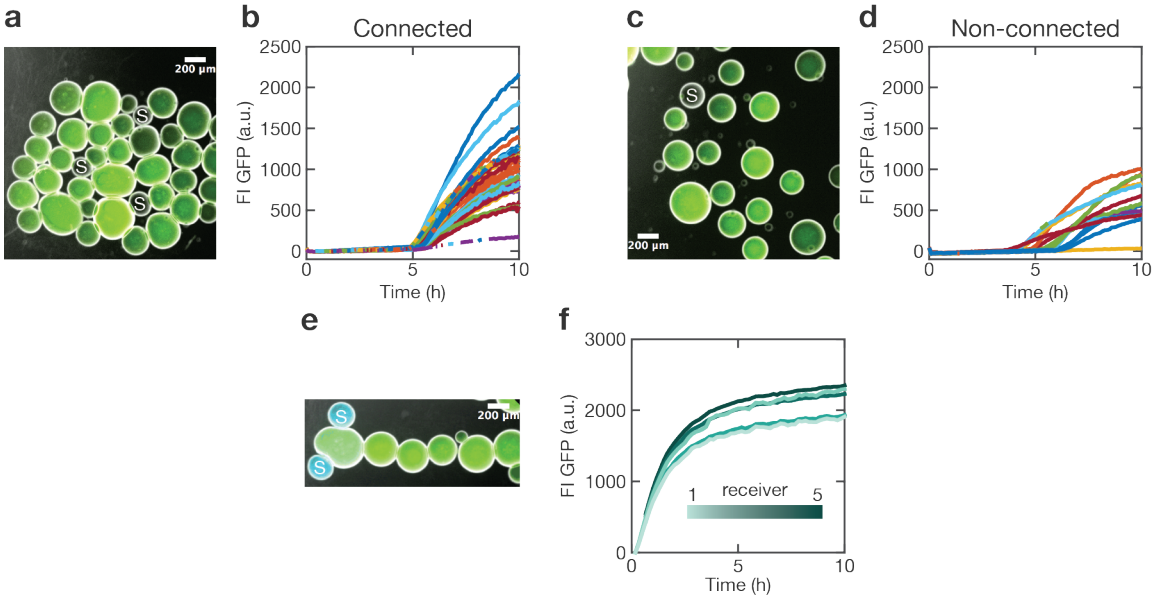

Figure 4.4. **Autocatalysis of signal production in droplet assemblies.** **a-d**, Response of connected (**a-b**) or non-connected (**c-d**) assemblies of droplets containing the receiver plasmid to sender droplets (S) containing the sender plasmid. **e-f**, Response of connected assemblies of droplets containing the receiver plasmid and the sender plasmid to sender droplets (S) containing purified 3OC6-HSL. **a**, **c**, **e**, Microscopy images, scale bar: 200 µm. **b**, **d**, **f**, Time traces of fluorescence intensity in the droplets.

Finally, I was interested in testing in a spatial context the activation of the autocatalytic loop with spiking concentrations of 3OC6-HSL, as was shown in bulk in Figure 4.2.d. I assembled sender droplets containing purified 3OC6-HSL with receiver droplets containing the sender/read-out plasmids in cell-extract in linear assemblies. A possible behaviour of such a system would be a propagating wave of GFP expression, as this was the response of a similar circuit in connected gene chips [18]. However, I instead observed synchronized induction of GFP expression across all receivers in a given array (Figure 4.4.d and e). The 3OC6-HSL diffusing from the sender and the one produced by the autocatalytic loop were homogeneously distributed across the array and induced homogeneous protein expression. This spatial behaviour is a known regime of autocatalytic loops, and a propagating wave can theoretically be produced with the same circuit by tuning the strength of the autocatalysis and the diffusion coefficient of the signal. I attempted to tune both these parameters in further variants of the circuit.

4.1.3 Circuit variants

I engineered variants of the initial autocatalytic circuit with the goal to create a library of circuit versions with different kinetics of autocatalysis and diffusion.

First, I constructed two variants of the initial sender plasmid where the strength of the LuxI ribosome-binding site (RBS) was varied. A stronger RBS should lead to a faster induction of autocatalysis, since a given leakily expressed mRNA will produce more LuxI proteins and consequently more 3OC6-HSL, whereas a weaker RBS should delay the induction. The RBS in the initial sender plasmid, B0064, has a relative strength of 0.35 (RBS Biobricks collection [120]) and a predicted translation rate of 6168.89 a.u. (all predicted translation rates were calculated with the De Novo DNA software [121]). The two variants I constructed, *pSB4K5-AD002* and *pBS4K5-AD003*, had weaker RBS, respectively B0031 with relative strength 0.07 and predicted translation rate 1124.62 a.u., and B0032 with relative strength 0.3 and predicted translation rate 1635.40 a.u. (Table 4.1). Note that the relative strength and predicted translation rate do not match, which could be due to local mRNA secondary structure affecting the effective translation rate of the gene, however both variants should have weaker RBS than the initial construct.

Construct	RBS	Relative strength	Predicted translation rate (a.u.)
pSB4K5-pLux-LuxI	B0064	0.35	6168.89
pSB4K5-AD002	B0031	0.07	1124.62
pSB4K5-AD003	B0032	0.30	1635.40

Table 4.1. RBS variants of the sender plasmid. Relative strength values are taken from[120].

When 3 nM of each sender plasmid were added to the read-out plasmid, the three variants demonstrated quite different kinetics in inducing the autocatalytic loop (Figure 4.5.a). *pSB4K5-AD002* showed the strongest induction of autocatalysis, producing the highest concentration of GFP, and *pSB4K5-AD003* showed the weakest induction of autocatalysis. It is striking that calculated translation rates badly predict the kinetics of the autocatalytic feedback loop. We have seen before that strong induction of autocatalysis may have resource depletion effects and therefore counter-intuitively lead to less GFP expression. Ribosome titration between the three proteins (LuxR, LuxI and GFP) due to their relative RBS strength could explain the behaviour of the three LuxI RBS variants observed here. A future prospect of this project is to explore the spatial behaviour of these different constructs.

As we have explored in Chapter 3.1, tuning the diffusion kinetics of non-specifically diffusing signals is not possible in our assemblies. However, quorum sensing signals have various diffusion kinetics dependent on their chemical structures. Karig *et al.*, estimated the diffusion coefficient of 3OC6-HSL to be 20 times smaller than the diffusion coefficient of C4-HSL [122]. Therefore, to adjust the diffusion in our autocatalytic loop system, I constructed a similar circuit based on another quorum sensing signal, 3OC12-HSL. As the carbon chain of this molecule is twice as long as that of 3OC6-HSL and

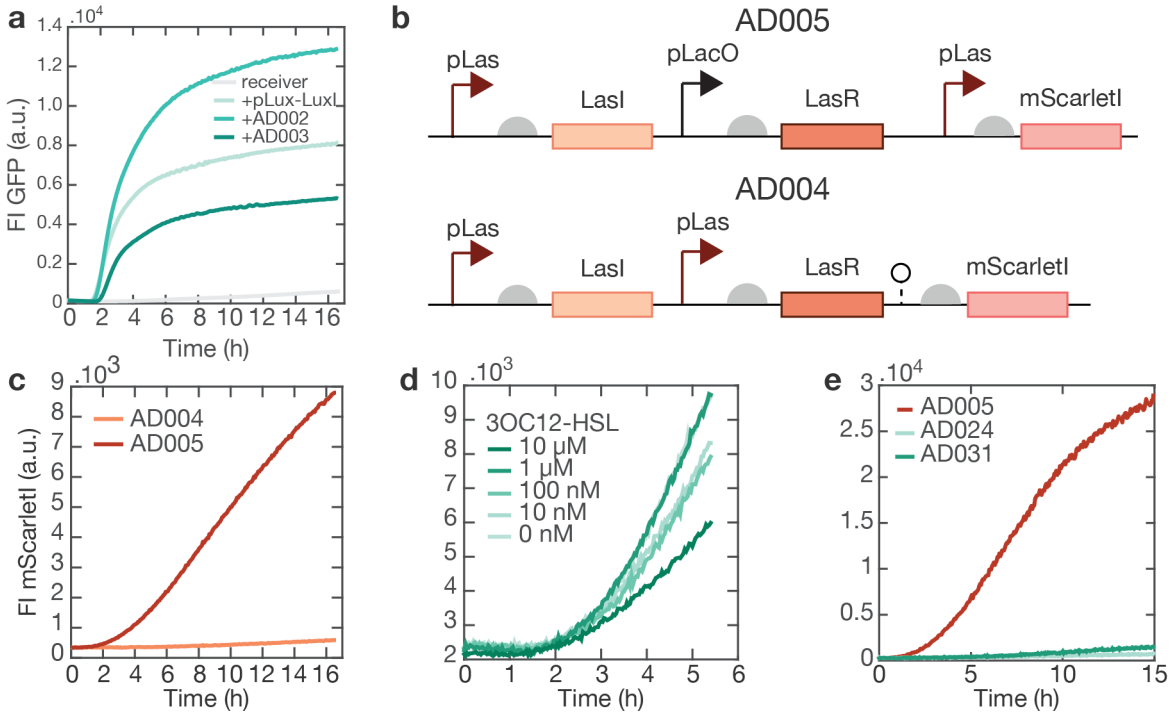

Figure 4.5. Variants of the autocatalytic circuit design. **a**, The receiver plasmid is expressed with 3 RBS variants of the sender plasmid. **b**, Two variants of the initial design for the 3OC12-HSL circuit: AD005, where only LasI and mScarletI are under the control of the pLas promoter, and AD004, where all genes are under the control of a pLas promoter. Ribozymes are represented by a dotted line and circle symbol. **c**, Compared expression of AD004 and AD005. **d**, Induction of AD005 with different concentrations of 3OC12-HSL. **e**, Comparison of the expression of AD005 with two mScarletI RBS variants: AD024 and AD031.

therefore the molecule is much more bulky (due to the free rotation of each carbon-carbon bond), we expect that bilayer permeation or partitioning into the oil will be significantly slower for this signal, although it might be more hydrophobic. The corresponding autocatalytic circuit is therefore based on LasR, LasI and the promoter pLas.

I first constructed two versions of the autocatalytic loop with these elements. A mimic of the first circuit, *pSB4A5-AD005*, has the following genes: *pLacO-LasR*, *pLas-mScarletI* (this is the reporter gene), and *pLas-LasI* (Figure 4.5.b). A more stringent version of the circuit, *pSB4A5-AD004*, has the following genes: *pLas-LasR-mScarletI* (both LasR and the reporter are on the same transcript), and *pLas-LasI* (Figure 4.5.b). In this more stringent version, both LasR and LasI have to be expressed leakily to sufficient concentrations for the autocatalytic loop to be induced, which imposes more strict conditions on the induction of autocatalysis. Indeed, I found that detectable mScarletI expression only occurred after 14 hours and at a very low level for *pSB4A5-AD004*, whereas *pSB4A5-AD005* showed strong induction of the autocatalytic loop after only 2 hours (Figure 4.5.c). However, addition of purified 3OC12-HSL did not produce the acceleration of the autocatalysis induction observed for the Lux system (Figure 4.5.d).

Due to its long carbon chain, 3OC12-HSL is less hydrophilic than 3OC6-HSL and is difficult to dissolve in cell-extract solutions. This may affect its activity when it is added as a purified component, compared to when it is produced on-site by the corresponding proteins.

Finally, I compared three variants of *pSB4A5-AD005* where the mScarletI RBS was varied. *pSB4A5-AD005* contains the RBS N1 for mScarletI (this and the following RBS are taken from [123]), which here has a low predicted expression rate of 13.26. The two variants *pSB4A5-AD024* and *pSB4A5-AD031* have respective RBS B3 (predicted expression rate 179.63) and P1 (predicted expression rate 10882.06). Both these constructs demonstrate very poor induction of autocatalysis, with AD031 being slightly better than AD024, but both giving neglectable mScarletI expression compared to AD005 (Figure 4.5.e). This surprising result is additional evidence that each gene's predicted translation rate is a bad predictor of the overall performance of the autocatalytic circuit. We can explain this behaviour considering that since initially both LasI and mScarletI are expressed leakily (they are both controlled by the pLas promoter), a stronger mScarletI RBS titrates ribosomes away from the LasI mRNA and impedes the production of 3OC12-HSL, thereby inhibiting the autocatalytic loop. The higher expression of AD031 compared to AD024 might simply reflect the higher leak expression of mScarletI due to the stronger RBS in AD031. Unintuitively, a weaker RBS for mScarletI (potentially weaker than the LasI RBS, which has a predicted translation rate of 163.11) might allow the induction of the autocatalytic loop. The AD005 construct should further be tested in droplet assemblies and the putative slower diffusion of 3OC12-HSL compared to 3OC6-HSL should be assessed.

The behaviour of the circuit variants described here allows a better understanding of the delicate response of an autocatalytic circuit. This system involves three genes whose expression must be finely tuned to allow for a proper induction of the whole circuit.

4.2 Ecosystems dynamics probed with quorum sensing

Building up on the autocatalytic circuit described in Chapter refChapter 4.1, I designed a gene network to investigate the consequences of different types of interaction (cooperative or competitive) between two populations on the behaviour of the whole ecosystem. This gene network could be implemented in two populations of bacteria or artificial cells, whose interactions could be freely tuned by response to quorum sensing signals. The dynamics of simplified ecosystems could therefore be probed in both living and artificial cells. Motivation for this circuit and its relevance are further described in Chapter refChapter 4.2.1. The initial design for the circuit is described in Chapter refChapter 4.2.2. The functionality of each part of the circuit is described in

Chapters refChapter 4.2.3, refChapter 4.2.4 and refChapter 4.2.5. Chapter refChapter 4.2.6 addresses the issue of load in a circuit containing numerous simultaneously expressed genes. The integration of the circuit's parts and future directions for the project are described in Chapter refChapter 4.2.7.

4.2.1 Cooperation and competition in living things

By exploring the implementation of multicellularity in artificial cells, the goal of this thesis is to study the specific interactions that permit the synchronized function of separate entities. It is my hypothesis that multicellularity would allow to examine more complex systems than unicellular artificial cells. However, as what makes a system more complex than others has long been a subject of debate, particularly for living organisms, I will review some arguments for the case that complexity increases when units are made to interact, *i.e.* that "structural complexification is produced by spatial differentiation and the selection of fit linkages between compartments" [124].

Cooperation between distinct entities is believed to be a mechanism for the emergence of complexity in the evolutive history of life [125]. For example, cooperation between molecules leads to cells, cooperation between cells leads to multicellular organisms, cooperation between multicellular organisms leads to colonies or groups. These examples give an intuitive impression that complexity increases as evolution goes on, and this is view is widely accepted but some criticism has been raised as to whether this is empirically true, and not simply an anthropomorphic bias [126]. Heylighen [124] addresses these concerns by suggesting that the very definition of "complexity" implies the presence of distinct but connected parts, and thereby demonstrates how evolution and selection indeed induce an increase in complexity. He argues that mutations and variation tend to increase differentiation between entities, but simultaneously selection tends to increase dependency: a new species A will have to adapt to the environment created by an existing species B, and vice-versa, so that they become increasingly dependent on each other's environment or co-dependent (the most striking examples of this phenomenon are symbiosis relations). Heylighen distinguishes two contributions to the increase of complexity that both provide a selective advantage: structural complexity, or internal fitness, has to do with the strength of linkages between parts of a system (and the more connected a system is the more robust it is), and functional complexity, or external fitness, has to do with the variety of environmental variations a system can respond to (and the more adaptable a system is the more robust it is). Heylighen argues that fitness is higher for more integrated systems of parts that are able to survive in a larger variety of environments, so that evolution goes with increasing complexity.

One can therefore argue that evolution does not select the strongest but the most collaborative units. Dupr□ and O'Malley claim that "competitive relations are a transitional state, with multi-lineage metabolic wholes eventually outcompeting selfish

competitors, and that this process sometimes leads to the emergence of new types or levels of wholes." [127]. These "metabolic wholes" made of cooperative parts can be thought of as molecules that cooperate to form cells, cells that form multicellular organisms, etc., each time creating a new type or level of whole.

Understanding the cooperative and competitive dynamics between units of a system therefore provides the basis to understand the fitness advantage of collaborative behaviour. The platform we created, more than simply mimicking multicellular tissues, allows us to study these dynamics in a controllable environment. We can thereby investigate larger and more fundamental questions regarding the emergence of complexity through cooperativity. This is of particular interest because our historical knowledge of such evolutionary transitions through collaboration is extremely limited and the study of whole ecosystems is complex.

We therefore set out to construct simplified ecosystems with controlled interactions and to study their dynamics. We proposed to use quorum sensing signals and repressor/activator gene networks to design artificial cell communities and study how different interactions between these "species" may affect the behaviour of the community as a whole. This project was presented for the First Grant fund of the graduate school GRK2062 and awarded with funding in late 2016.

Many studies have employed multistrain populations of bacteria to prototype ecosystem interactions and implement the resulting dynamics in bulk or in space. Following are a few examples of such studies: predator-prey ecosystem [128], a two-strain ring-pattern forming circuit [35], oscillations in a microbial consortium [129], inter- and intrakingdom synthetic ecosystems [130], implementation of Simpson's paradox [131]. Although this specific project could not be brought to completion within the time of this thesis, its relevance and the interest of the synthetic biology community in these questions is evident from the publication of a similar engineering of ecosystems interactions in microbial communities [132]. This study was conducted *in vivo* using pathways with up to 13 genes, which imposes a large load on the cells. In contrast, the design described here is somewhat less resource consuming and can be easily implemented in cell-extract, as will be described in the following sections.

4.2.2 Circuit design and modularity

The initial design of the circuit consists of a competitive ecosystem, with two populations that activate themselves through an internal positive feedback and repress each other through an external inhibitor interaction. Figure 4.6 represents the abstract and explicit design of the circuit. Each population contains an autocatalytic loop on quorum sensing signal production, similar to the circuit described in Chapter 4.1, with respectively population *A* producing 3OC6-HSL and population *B* producing 3OC12-HSL.

The quorum sensing signals diffuse into the whole ecosystem and are therefore sensed by both populations. When population *A* senses 3OC12-HSL produced by population *B*, this signal will activate the expression of the TetR repressor, which will in turn repress the expression of LuxR and of a reporter protein YPet. As LuxR is tagged for degradation, this will eventually turn off all expression from pLux. Symmetrically, 3OC6-HSL sensing by population *B* will induce the expression of a LacI repressor, and the repression of LasR (and a reporter protein mScarletI). Population *A* therefore contains two plasmids, *Ai* responsible for the internal feedback loop (pTetO-LuxR-YPet and pLux-LuxI expression), *Ae* responsible for the external feedback loop (pJ23106-LasR and pLas-TetR). Population *B* contains *Bi* (pLacO-LasR-mScarletI and pLas-LasI) and *Be* (*pJ23106*-LuxR and pLux-LacI). pJ23106 is a constitutively expressed promoter.

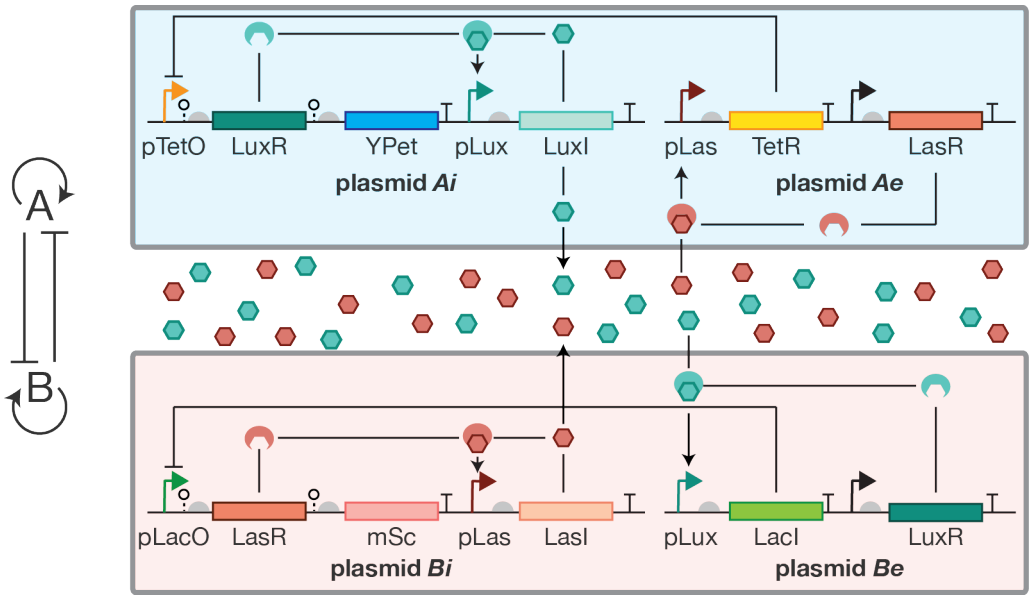

Figure 4.6. Ecosystem circuit design, with populations *A* and *B* containing each an internal feedback plasmid (*Ai* and *Bi*) and an external feedback plasmid (*Ae* and *Be*). pJ23106 promoters are represented in black and not labelled.

The constructs were designed so that a/ inserts could be easily exchanged between plasmids of different copy numbers from the BioBricks library, to tune the respective strength of the internal and external feedbacks *in vivo*, b/ promoters, RBS and degradation tags could be easily changed to modify the types of interactions in the ecosystem. With simple changes in the building blocks of the constructs, network topologies such as mutualism, cooperativity or predator-prey could be easily implemented. Sequences for the ribozymes, ribosome binding sites and terminators were taken from Nielsen *et al.* [123]. Quorum sensing systems demonstrate crosstalk at both the genetic (promoter is transcribed by non-cognate transcription factor, such as pLux is transcribed by LasR) and the chemical (transcription factor is activated non-cognate signal, such as 3OC6-HSL activates LasR) level [133], [134]. Chemical crosstalk can be limited by optimizing the strength of transcription factor expression: LasR binds 3OC12-HSL with a better affinity than 3OC6-HSL. Genetic crosstalk was shown to be drastically reduced

by mutating the sequences of the pLux and pLas promoters [135] and these optimized promoters were used in this circuit design.

We tested the functionality of each part of the circuit as follows: the reporters (Chapter 4.2.3), the HSL expressing genes (Chapter 4.2.4), both present on the internal feedback loop plasmid, and the repressors (Chapter 4.2.5) present on the external feedback loop plasmid. These parts were tested in cell-extract.

4.2.3 Expression of the reporters

We first assessed the proper expression of the reporter modules on the internal feedback loop plasmids. These plasmids (*Ai* and *Bi*) were tested in cell-extract as well as transformed into *E. coli* cells. As each of the reporters (YPet in *Ai* and mScarletI in *Bi*) is under a constitutively expressed promoter (pTetO and pLacO respectively), we expected that plasmids *Ai* and *Bi* would express fluorescent reporters at high level constitutively. We found that this was neither the case in cell-extract nor *in vivo*, and in both environments low to inexistent fluorescence levels were measured.

An *in silico* analysis of the constructs was conducted to determine whether any of the genes had sequence-based defaults that might hinder its expression (such as a weak ribosome binding-site RBS, or an mRNA secondary structure blocking the RBS). The predicted translation rate was 53.28 for YPet and 13.26 for mScarletI. These relatively low translation rates could explain the low fluorescence levels observed even though the promoter is functional.

We therefore constructed a library of RBS sequences. The reporter RBS for the initial versions of *Ai* and *Bi* was N1 [123]. Together with working student Ludwig Bauer, we built 3 variants for each reporter with RBS B3, P1 and S4. Predicted translation rates are summarized in Table 4.2, with predicted relative strengths of the RBS for both constructs: N1<B3<S4<P1. We then tested the expression of these variants (Figure 4.7.a and b). The measured relative strengths of these RBS were: N1<S4<B3<P1. The measured strength of S4 was therefore lower than predicted compared to B3. Constructs with RBS P1 showed the highest level of expression of the reporter, and therefore this RBS was kept for both reporters. Correspondingly, these constructs had high constitutive fluorescence levels *in vivo*.

4.2.4 Expression of the quorum sensing signals

We then tested the functionality of the autocatalytic loop expressing the quorum sensing HSL signals (pLux-LuxI on *Ai* and pLas-LasI on *Bi*). In the circuit designs, the

Plasmid	Reporter RBS	Predicted translation rate (a.u.)	Plasmid	Reporter RBS	Predicted translation rate (a.u.)
Ai (YPet)	N1	53.28	*Bi* (mScarletI)	N1	13.26
	B3	1232.87		B3	266.92
	P1	12177.95		P1	10882.06
	S4	3182.69		S4	2552.84

Table 4.2. Predicted translation rates for RBS variants of the reporter on the internal feedback plasmid.

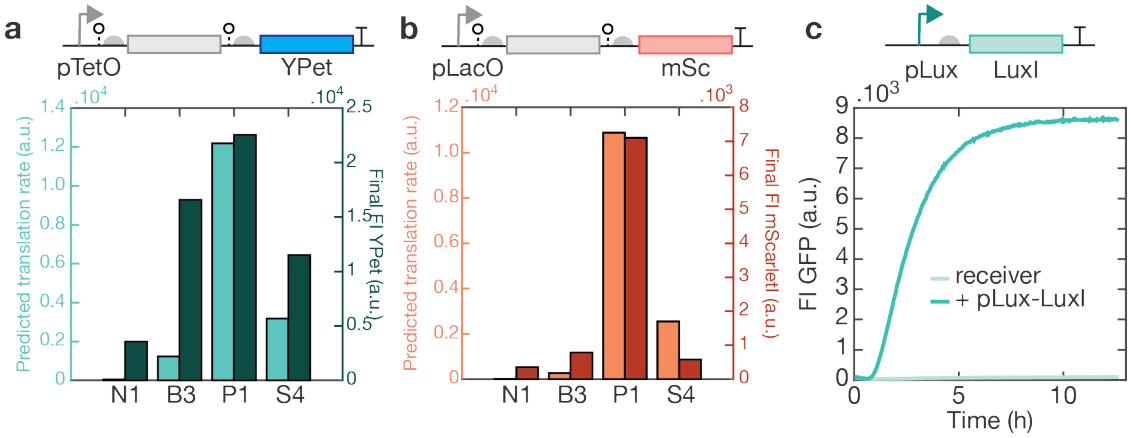

Figure 4.7. Expression of the reporter modules and the sending modules. **a-b**, Predicted translation rates and final fluorescence levels of an expression experiments for the four RBS variants for *Ai* (**a**) and *Bi* (**b**). **c**, Expression of a receiver plasmid in absence and presence of the sending module for *Ai*.

reporters track the expression of the transcription factors proteins LuxR (reported by YPet) and LasR (reported by mScarletI), which are under repressible promoters. There is no direct reporting on the expression of the LuxI and LasI HSL-expressing modules. We therefore isolated these modules and tested them together with appropriate read-outs.

The correct expression of 3OC12-HSL by the pLas-LasI module of *Bi* was confirmed by the autocatalytic loop construct described in Chapter 4.1.3. In this construct, the pLas-LasI module was placed together with the two genes pLacO-LasR and pLas-mScarletI, so that LasR would be expressed constitutively and that mScarletI would report on the expression of LasI and synthesis of 3OC12-HSL. The expression of mScarletI confirmed the correct function of the pLas-LasI module, although this autocatalytic loop was very sensitive to the relative RBS strengths of all genes placed under the pLas promoter.

The correct expression of 3OC6-HSL by the pLux-LuxI module of *Ai* had to be confirmed for this construct, as the LuxI-based autocatalytic loop presented in Chapter 3.1 employed a different pLux promoter. The pLux-LuxI module was isolated and expressed it in cell-extract together with a read-out plasmid (pLacO-LuxR, pLux-GFP). GFP expression was orders of magnitude higher in presence of the pLux-LuxI module,

confirming the correct function of this module (Figure 4.7.c).

4.2.5 Expression of the repressors

Having tested the functionality of both subparts of the internal feedback loop plasmids (reporter and signalling), we tested the repressor modules on the external feedback loop plasmids. These consist of HSL-inducible expression of repressor proteins. We first studied the leakiness of these constructs - that is, their ability to express the repressor proteins in the absence of HSL signal - and then investigated their dosed response to quorum sensing signals.

Leakiness

When expressing together the *Ai* and *Ae* plasmids (respectively the *Bi* and *Be* plasmids), we noticed that the reporter expression was strongly repressed even in the absence of any quorum-sensing signal. This seemed to indicate that our repressor modules are leaky: the pLas (respectively pLux) promoter regulating the expression of the repressor (TetR, respectively LacI) seemed to be active without the presence of their cognate inducer. To verify whether the low reporter expression was indeed caused by a leakiness of the repressor modules - and not, for example, by a load effect - we added a chemical de-repressor corresponding to the repressor proteins (aTc for TetR and IPTG for LacI).

In the presence of the *Ae* plasmid, the *Ai* reporter expression (YPet) was reduced to 5 % of its maximum expression (plasmid concentrations: 6 nM *Ai*, 3 nM *Ae*). With 0.1 µM aTc, its expression was restored to approximately 60 % of its original level (Figure 4.8.a). Concerning the *Bi* reporter expression (mScarletI), it should be noted that it is controlled by a pLacO promoter. As the cell-extract contains traces of LacI from the *E. coli* strain Rosetta, the reporter expression is naturally repressed to about 30 % of its full expression, which can be restored when 0.1 mM of IPTG is added (Figure 4.8.b). When adding the repressor module plasmid *Be*, the expression of the reporter is repressed to 5 % of its maximum expression, and this can be derepressed to about 35 % in the presence of 0.1mM IPTG (Figure 4.8.b).

To circumvent this leakiness issue, we explored the possibility to add decoy, so-called ”sponge” elements to titrate leakily expressed repressors away from the promoters critical for the function of the circuit. We therefore added one or two promoter sites (pTetO, respectively pLacO) containing each two binding sites for TetR, respectively LacI, at the back of the insert region in *Ae* (respectively *Be*). For constructs *Ai* and *Ae*, in the absence of aTc, the addition of 1 and 2 sponge elements restored the expression of YPet to 18 % and 20 % of its maximum expression. The sponge elements therefore only slightly reduced the effect of the leaky repression. In the presence of aTc, the construct with 1 sponge allowed recuperation of YPet expression to 65 % of its maximum level, but the construct with 2 sponges allowed recuperation to only 50 % (Figure 4.8.a).

For constructs *Bi* and *Be*, the addition of 1 sponge element did not significantly affect mScarletI expression in the absence of IPTG, and the addition of 2 sponge elements restored expression to only 7 % of maximum levels (Figure ??.8.b). The sponge elements therefore did not seem to have a significant impact in reducing leaky repression. With the addition of IPTG, the expression of mScarletI with 1 sponge element was restored to 35 % of maximum expression, similarly to the expression measured in absence of sponge elements. With 2 sponge elements and IPTG, expression was restored to approximately 55 %, indicating a possible decoy effect of the sponge elements.

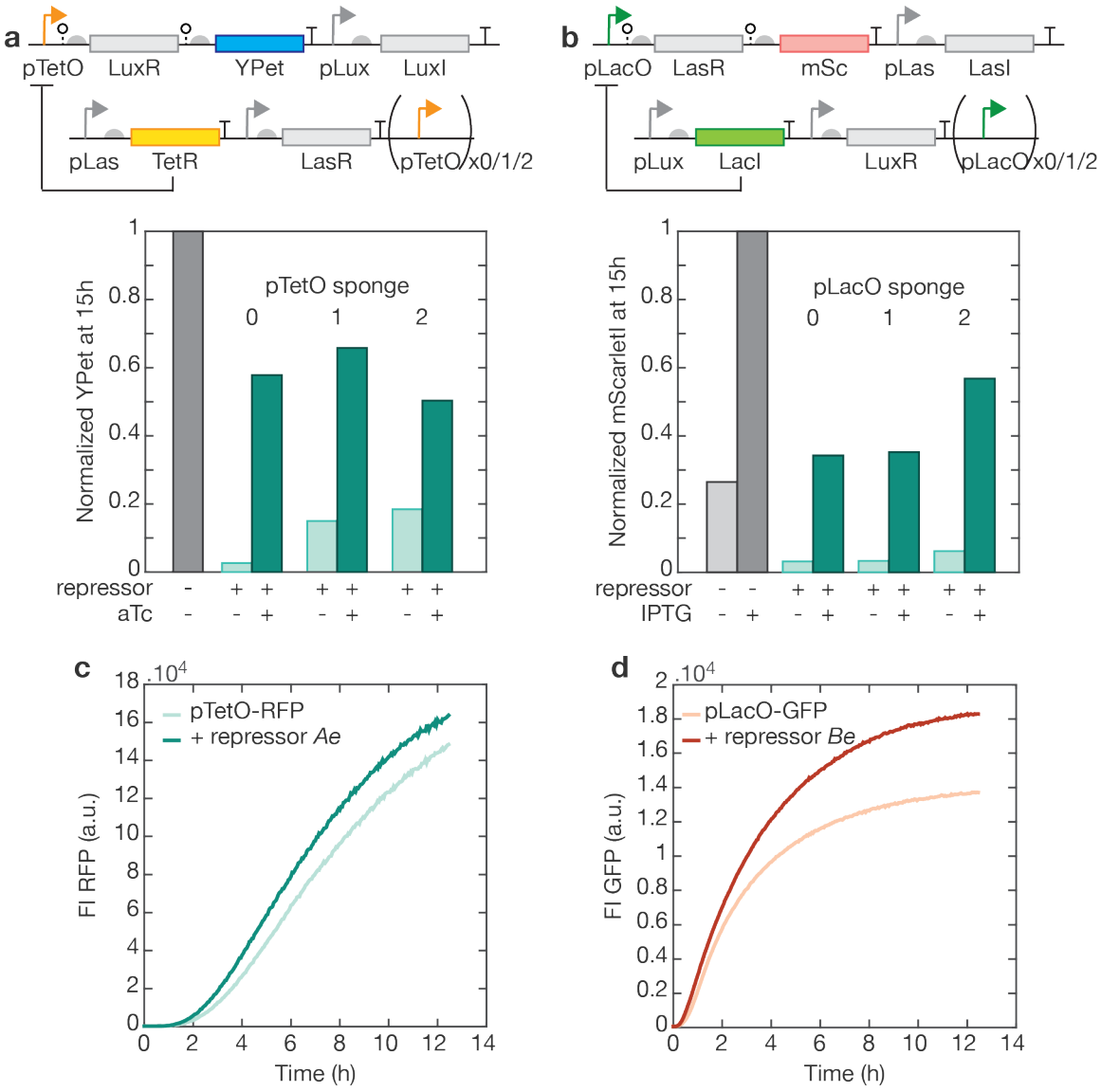

Figure 4.8. Leakiness of the repressor modules. **a-b**, Expression of the reporters in the full *Ai* (**a**) and *Bi* (**b**) plasmids in presence or absence of the repressor modules (*Ae*, respectively *Be*) with 0, 1 or 2 sponge elements. Final fluorescence intensity is normalized to a sample without repressor. Chemical inducers (aTc, respectively IPTG) are added to de-repress the leakily-expressed repressors. **c-d**, Expression of a repressible reporter in presence or absence of the repressor modules *Ae* (**c**) and *Be* (**d**).

This strong leaky repression of the reporter modules by the repressor modules in the absence of the cognate HSL inducer was a significant issue, as we could not expect measurable additional repression when adding the corresponding signal. The strength of the leaky repression was also surprising if we assume that it is caused by an uninduced promoter that would only stochastically be expressed for short periods of time. We therefore tested whether the repressor modules would show a similar leaky repression on other reporter plasmids than Ai and Bi. We expressed the *Ae* plasmid together with a pTetO-RFP reporter (Figure 4.8.c) and the *Be* plasmid together with a pLacO-GFP reporter (Figure 4.8.d). In both cases, we found that the reporter expression was not significantly affected by the presence of the repressor modules. This indicates that the repression seen on the *Ai* and *Bi* plasmids is not due to a leaky expression of the *Ae* and *Be* modules (which would be seen with other reporters), but to a non-cognate induction of the *Ae* and *Be* modules by the HSL signals produced by *Ai* and *Bi*.

Indeed, *Ae* is designed to be induced by 3OC12-HSL, but when both plasmids are present (*Ai* and *Ae*), we have simultaneous expression of LuxR (from *Ai*), LasR (from *Ae*) and 3OC6-HSL (from LuxI on *Ai*). We could therefore imagine two scenarios for the induction of the repressor modules (pLas-TetR in the case of *Ae*): either genetic cross-talk, where LuxR binds 3OC6-HSL and activates pLas (although this should be avoided by the promoters sequences optimized to limit genetic cross-talk [135]), or chemical cross-talk, where LasR binds 3OC6-HSL and activates pLas. The chemical cross-talk is the most probable scenario, as the similarity in structures between LuxR and LasR make them subjectable to activation by their non-cognate signal. *In vivo*, these transcription factors have been shown to respond to different quorum sensing signals in parallel [118].

Induction

To investigate the question of chemical cross-talk, we therefore expressed the repressor modules together with the simple reporters described above, and titrated cognate and non-cognate quorum sensing-signals. We found that *Ae* responded much more strongly to its cognate signal (3OC12-HSL, with a K_d below 0.1 µM) than to its non-cognate signal (3OC6-HSL, with a K_d between 1 µM and 10 µM) (Figure 4.9.a). However, this response to 3OC6-HSL could explain the leaky repression measured when *Ai* and *Ae* are expressed together: *Ai* expresses 3OC6-HSL at high concentrations (under a positive feedback loop) and *Ae* is therefore likely to show a strong response to its non-cognate inducer in these conditions. We also added 3 nM of a pLas-LasI construct (the autocatalytic loop from *Bi*), and measured a significant repression equivalent to the presence of purified 3OC12-HSL, demonstrating that the repressor module of *Ae* can respond to on-site produced HSL.

We also found that *Be* responded somewhat more strongly to its cognate signal (3OC6-HSL, with a K_d around 0.1 µM) than to its non-cognate signal (3OC12-HSL, with a K_d between 0.1 µM and 1 µM) (Figure 4.9.b). However, the chemical cross-talk was more significant here, indicating that LuxR is more likely to be activated by 3OC12-HSL

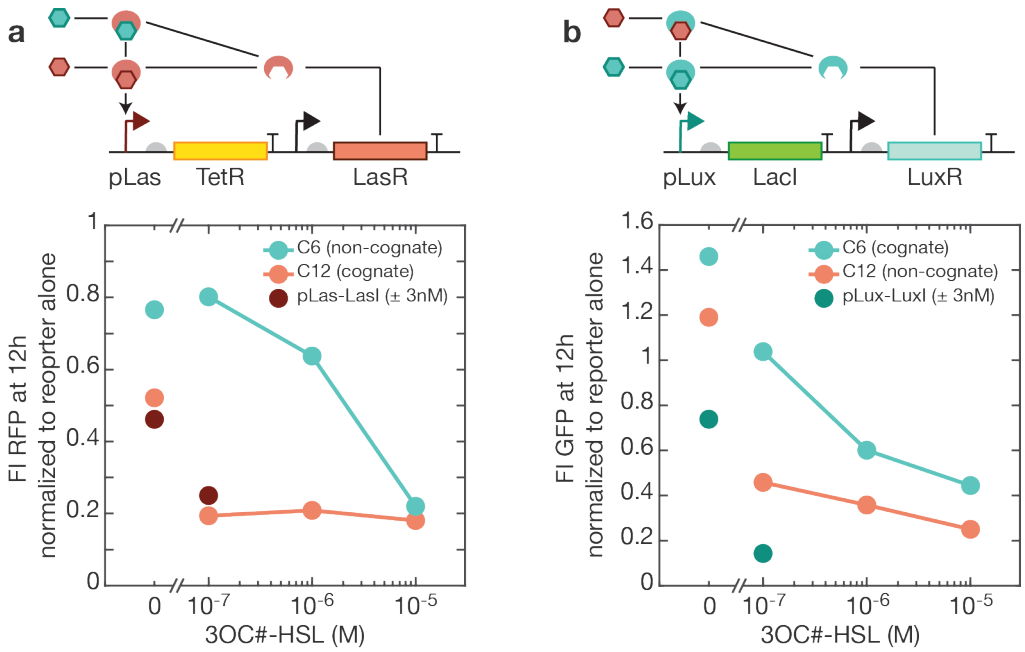

Figure 4.9. Chemical cross-talk for the induction of the repressor modules. Expression of a repressible reporter plasmid (**a**: pTetO-RFP, **b**: pLacO-GFP) in presence of the repressor modules (**a**: *Ae*, **b**: *Be*) induced with their cognate signal, their non-cognate signal, or a plasmid expressing their cognate signal (0 nM plotted at 0 M 3OC#-HSL, 3 nM plotted at 10^{-7} M 3OC#-HSL).

than LasR by 3OC6-HSL. When adding 3 nM of a pLux-LuxI construct (the autocatalytic loop from *Ai*), we measured a significant repression equivalent to high concentrations of purified 3OC6-HSL.

These results indicate that LuxR and LasR are subject to chemical cross-talk, which could be a significant issue in our circuit since each population produces high local concentrations of its autocatalytic signal (for example 3OC6-HSL for *A*) but only receives low concentrations through diffusion of its repressing signal (3OC12-HSL for *A*, produced by *B*). This chemical cross-talk can somewhat be mediated by reducing the expression of LasR (on *Ae*) and LuxR (on *Be*) [135] so that they only respond to their cognate signals.

However, the response of *Ae* to the signal produced from *Bi* and of *Be* to the signal produced from *Ai* suggests that the circuit could be functional. After addressing the issue of load on protein expression (Chapter 4.2.6), we will study the integration of the circuit and its functionality, and discuss future work for this project (Chapter 4.2.7).

4.2.6 Load on protein expression

In the circuit design, each population must express five genes: population *A* must express LuxR, YPet, LuxI, LasR and TetR, while population *B* must express LasR, mScarletI, LasI, LuxR and LacI. We should expect that the simultaneous expression of all these genes will cause a load and affect protein expression - in living cells, a defect in growth can also be expected. A preventive measure to avoid such effects *in vivo* is to use low copy number plasmids, so that the cell's resources are not entirely titrated to expression of the plasmids. We therefore cloned our constructs in plasmids pSB4A5 (origin of replication rep101) and pSB3C5 (origin of replication p15A) with respective copy numbers 5 and 10 approximately.

We quantified the load effect of various modules in the circuit. We first quantified the load exerted by the autocatalytic loop (*A*: pLux-LuxI and *B*: pLas-LasI) on protein expression. We compared the full *Ai* plasmid with a truncated version not containing the pLux-LuxI module, and saw that protein expression of the reporter in cell-extract was not affected, suggesting that 3OC6-HSL expression did not create a load on protein expression (Figure 4.10.a). When comparing *Bi* with a truncated version not containing the pLas-LasI module, the truncated version showed considerably higher protein expression in cell-extract (Figure 4.10.b), indicating that LasI and 3OC12-HSL expressions create a load on protein expression. Reporter expression was also higher *in vivo* (JW0336, M9 medium, 37 °C) with the truncated construct than with the full construct (Figure 4.10.c). This higher load of LasI compared to LuxI is probably not due to a stronger expression, since the predicted translation rate is 163.11 for LasI and 4517.62 for LuxI. Since 3OC12-HSL has a longer carbon chain, it is possible that either the metabolic pathway for its synthesis is more resource consuming, or the chemical is slightly toxic to protein expression, or a combination of both.

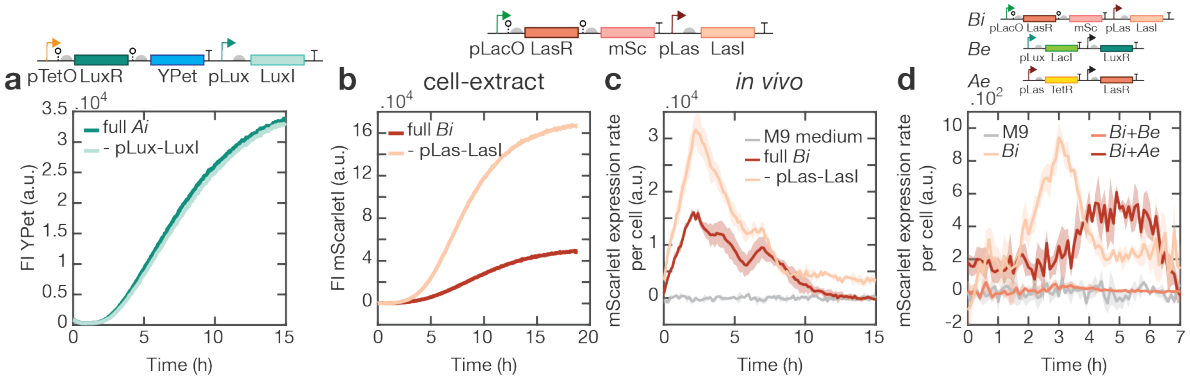

Figure 4.10. Load of simultaneous expression of several genes on total protein expression. **a**, Expression of the full *Ai* plasmid compared with the truncated plasmid without pLux-LuxI in cell-extract. **b-c**, Expression of the full *Bi* plasmid compared with the truncated plasmid without pLas-LasI in cell-extract (**b**) and *in vivo* (protein expression rate, **c**). **d**, Expression rate of the reporter for cells containing the *Bi* plasmid only, the *Bi* and *Be* plasmids (cross-talk induction of the repressor) and the *Bi* and *Ae* plasmids (load).

We also measured the load caused by the presence of both plasmids (for example *Bi* and *Be*) on the total protein expression. We compared reporter expression in cells transformed with *Bi*, *Bi* and *Be*, or *Bi* and *Ae* (Figure 4.10.d, JW0336, M9 medium, 37 °C). Since the presence of *Be* causes a leaky repression of *Bi* in absence of inducer, we wanted to compare this to a pure load effect, measured when *Ae* is present with *Bi*. We found that *Ae* causes a load on reporter expression of *Bi in vivo*, and that by comparison, low expression when *Be* is present must be due to leaky repression of this module, as addressed in Chapter 4.2.5.

We therefore determined that the large number of genes simultaneously expressed can cause a load to the total protein expression, but that this does not suppress correct expression of the circuit entirely.

4.2.7 Functionality of the circuit and future work

We have seen that the reporter modules are functional (Chapter 4.2.3), as well as the signal-expressing modules (Chapter 4.2.4) and the repressor modules (Chapter 4.2.5). The circuit's functionality is therefore demonstrated in the isolated parts, which remain to be assembled. We have seen in Chapter 4.2.5 how this can present some difficulty due to the chemical cross-talk between HSL signals and the difference in signal concentration in each population. As a temporary solution, we reduced the effects of this non-cognate activation of the repressors by adding low concentrations of aTc and IPTG to our experiments, partially relieving the leaky repression. We then attempted to assemble the circuit into two parts: we integrated the full *A* circuit (*Ai* and *Ae*) with the *Bi* plasmid (Figure 4.11.a) on one part, and we integrated the full *B* circuit (*Bi* and *Be*) with the *Ai* plasmid (Figure 4.11.b) on the other part.

We assembled 2 nM of *Ai* with 2 nM of *Ae* and added either 10 µM 3OC12-HSL, 2 nM of the full *Bi* plasmid, 2 nM of the pLas-LasI expressing module of *Bi*, or 2 nM of a load plasmid expressing a protein that does not affect the circuit. We found that although 3OC12-HSL efficiently repressed the expression of *Ai* (Figure 4.11.a), only the isolated pLas-LasI module achieved a repression that was stronger than the load effect. Therefore, although the full *A* construct seems responsive to purified 3OC12-HSL, it seems that *Bi* does not produce 3OC12-HSL concentrations significant enough to induce *A*.

We then assembled 3 nM of *Bi* with 3 nM of *Be* and added either 10 µM 3OC6-HSL, 3 nM of the pLux-LuxI expressing module of *Ai*, or 3 nM of a load plasmid. We found that construct *B* was efficiently repressed by purified 3OC6-HSL as well as 3OC6-HSL producing plasmids (Figure 4.11.b).

These results indicate that some trouble-shooting must be conducted to achieve

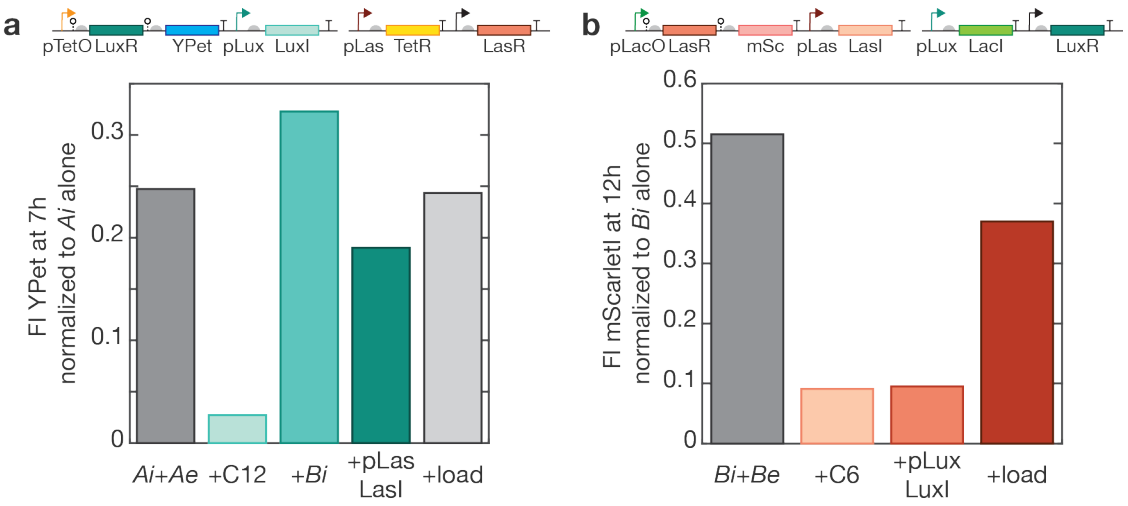

Figure 4.11. Integration of the circuit parts. **a**, Expression of the reporter of *Ai* in presence of *Ae* and of inducers 3OC12-HSL, *Bi*, the isolated signalling module of *Bi*, or a load plasmid. **b**, Expression of the reporter of *Bi* in presence of *Be* and of inducers 3OC6-HSL, the isolated signalling module of *Ai*, or a load plasmid.

a fully functional circuit, but that there is good indication of functionality of the parts and some integration of the parts. However, many unforeseen issues arose during the characterization of this circuit (such as weak RBS, chemical cross-talk, load effects). The initial approach to assemble the full circuit and test it as such was therefore relatively unsuccessful. For future projects, it would be recommended to take a "building blocks" approach, where every part of the circuit is tested and optimized in isolation, and subsequent parts of the circuits are added step-by-step while controlling for functionality. Such a systematic approach would have allowed quickly identifying and fixing the issues raised above. For this circuit specifically, this approach would have been: test the reporter modules, test the repressor modules, integrate the two together, test the signal-expressing modules, integrate to the reporter and repressor modules, then integrate the two populations together.

We have however shown with preliminary experiments the functionality of a circuit based on the co-repression of two populations. This circuit needs to be tested in an encapsulated environment for its spatial dynamics.

5 Tools, collaborations and secondary projects

This chapter summarizes projects that did not relate directly to artificial multicellular assemblies. Here are described: several collaboration projects (Chapter 5.1), a project aiming to produce spontaneously growing peptide vesicles (Chapter 5.2), a library of tags for programmable protein degradation kinetics (Chapter 5.3), a library of mutated T7 promoters (Chapter 5.4), the characterization of fluorescent reporter variants (Chapter 5.5), an analysis of LacI and lactose effects on the functionality of the pLacO promoter *in vivo* (Chapter 5.6), insights on circuit design rules for correct growth and expression *in vivo* (Chapter 5.7), the use of GamS to allow expression from linear templates in cell-extract (Chapter 5.8), the possibility to use genelets in PURExpress (Chapter 5.9), a library of fluorescent aptamers (Chapter 5.10), and finally the characterization of dose-response functions for most inducers used in this thesis (Chapter 5.11).

5.1 Collaborations

This section summarizes collaborations that were conducted during this thesis.

The collaboration most relevant to the main research project of this thesis is the development of a 3D printer for droplet networks assembly. This project was conducted together with the lab of Prof. Dr. Hauke Clausen-Schaumann and Dr. Stefanie Sudhop, which specializes in 3D bioprinting. PhD students Sascha Schwarz and Benedikt Kaufmann and bachelor student Nikolas Galensowske built a 3D printer that allow the fast assembly of 2D and 3D droplet assemblies, although precise positioning remains challenging. The results of this collaboration are addressed in more details in Chapter 2.3.4.

In a collaboration with Dr. Claudia Huber and PhD student Jessica Sobotta, we characterized fatty acids that were synthesized under possible origin-of-life conditions.

These researchers demonstrated the possibility to synthesize fatty acids with 3, 5, 7 and 9 carbons in a one-pot reaction [136]. Together with PhD students Swati Krishnan and Kilian Vogele, we performed a series of tests to assess the possibility to form stable membranes and vesicles with such fatty acids. The one-pot reaction solution was extracted 3 times with a 2:1 v:v mixture of chloroform and methanol, the oil phases were pooled and evaporated under vacuum to yield a dried film. This film was resuspended in 80 mM Tris-HCl at pH 7.5, and water-in-oil droplets were formed in mineral oil and in a 1:1 v:v mixture of hexadecane and AR20 silicone oil. After 30 min incubation, droplets put in contact fused, indicating that no continuous layer of surfactant molecules had been formed at the interface. This does not necessarily indicate that there are no surfactants present in the water phase, but rather that their concentration is too low to form a stable monolayer. Characterization with transmission electron microscopy and dynamic light scattering by Dr. Krishnan and Kilian Vogele did not allow for the unambiguous identification of vesicles, although particles that could be oil droplets or vesicles were detected in the extracted samples.

Prof. Dr. Job Boekhoven and his team have developed a dissipative chemical reaction network where a precursor containing two carboxylic acids reacts to form a cyclic anhydride in the presence of EDC (1-ethyl-3-(3-dimethylaminopropyl)carbodiimide), which is then hydrolysed back into its dicarboxylate form [137]. Our collaboration with Prof. Boekhoven and Dr. Chandan Maity focused on using this chemical reaction network to actuate a conformation shift in a nucleic acid structure. Being that the reaction involves the neutralization of 2 negative charges (the two carboxylic acids), we hypothesized that such a high concentration of negative charges may disturb the folding of a nucleic acid structure by affecting the charge density in the centre of a double helix. We therefore designed single-stranded DNA sequences to form hairpins, and modified the sugar of one nucleotide with a nitrile functional group, which was then clicked with the appropriate dicarboxylate precursor. We assumed that in the precursor state, the charge density in the centre of the helix would be too high to allow for the hairpin to fold, but that in the cyclic anhydride state the hairpin could fold again. This was to be tracked by the FRET of an acceptor/donor pair of fluorophores placed at the ends of the DNA sequence. Although mass spectrometry measurements seemed to indicate that the clicking reaction worked, the change in FRET induced by the chemical reaction network was not consistent, and experiments were not continued.

Experimental support was contributed to a project from PhD student Matthaeus Schwarz-Schilling. This project consisted of assembling an RNA-protein nanostructure, where an RNA sequence was designed with functional regions (structural motifs and aptamers) so that it served as a scaffold for the assembly of a protein pair capable of FRET, of a streptavidin and of a fluorescent reporter. The nanostructure was assembled from isolated purified parts (RNA, proteins and fluorophore), but was also expressed and assembled *in situ* in cell-extract and in *E. coli* cells. The design of gene constructs coding for the two fluorescent proteins involved in FRET was critical to tune the correct expression of each of the assembly's components and the yield of assembly. In the context

of this collaboration, the tasks performed were the design and cloning of gene constructs for the FRET proteins, troubleshooting of potential ribozyme toxicity (described in more details in Chapter 5.7.4) and characterization of the stability of different RNA structures. For this set of experiments, degradation of an RNA sequence in cell-extract was tracked with the fluorescence of an aptamer based on the fluorophore Malachite Green (described in Chapter 3.2.2). The experiment compared the degradation kinetics of a simple Malachite Green aptamer, of the RNA nanostructure with its central stabilizing three-way junction motif and the Malachite Green aptamer in the 5'-end position, in the central position or in the 3'-end position on the RNA, and of the RNA nanostructure without a three-way junction and the Malachite Green aptamer in the 3'-end position. The degradation dynamics could be fitted with first-order kinetics and the half lifetime of each RNA sequence could be determined. These experiments demonstrated that degradation in cell-extract was faster from the 3'-end of the structure, and that the presence of a structural motif such as the three-way junction greatly increased overall RNA stability. The results of this project were published in Nano Letters in 2018 [138].

Finally, I supervised in 2017 a team of students participating in the main international synthetic biology competition, iGEM (international Genetically Engineered Machine). The team of 17 students focused on a novel diagnostics method to limit the abusive prescription of antibiotics, which is causing a rise in resistant bacteria strains and a recrudescence in deaths from relatively benign bacterial infections. Their goal was to establish a diagnostics tool for point-of-care use, so that viral and bacterial infections could be distinguished within a few hours and antibiotics could be prescribed appropriately in point-of-care facilities without costly or non-distributable lab equipment. They built a low-cost fluorescence detector easily assembled from 3D printed parts and coupled to a heating plate allowing for the extraction of RNA or DNA from the patient's sample. The detection mechanism itself was based on a CRISPR-associated protein, Cas13a, which has been shown to develop nuclease activity after the recognition of a target RNA sequence [139], allowing for an amplification of read-out signal compared to the concentration of detected RNA. The iGEM team, CasCAID (Cas13a Controlled Assay for Infectious Diseases) started working using Cas13a as a detection tool for viral and bacterial nucleic acids, and in April 2017, the detection of fM concentrations of nucleic acids from a variety of pathogens using isothermal PCR and Cas13a was demonstrated by the group of Prof. Feng Zhang [140]. The iGEM team reproduced the principal results of this publication and demonstrated orthogonal recognition of RNA from specific viruses and bacteria, the isothermal amplification of DNA extracted from bacteria, the detection of pM concentrations of DNA using amplification and Cas13a, and the live measurement of the read-out signal on paper in a self-built fluorescence detector. At the competition, the team was awarded with 6 awards in the Overgraduate section: First Runner-Up (they were second of the two finalists teams), Best Diagnostics Project, Best Model, Best Hardware, Best Software, Best Applied Design, and they were nominated for 8 other prizes. Their project and results can be seen at http://2017.igem.org/Team:Munich. A paper describing the design and usage of the low-cost fluorescence detector that was built during the project is currently under submission.

In addition, as I developed and improved the protocol for cell-extract preparation from *E. coli* lysate (following on the work of Dr. Andrea M□ ckl and Dr. Matthaeus Schwarz-Schilling, and with the protocol of Prof. Dr. Vincent Noireaux [141]), cell-extract experiments conducted in the lab between 2015 and 2017 were mostly done with batches of my production. I later taught most members of the lab how to produce cell-extract. In addition, I taught cell-extract preparation to collaborators from other synthetic biology labs, namely Francois-Xavier Lehr, a PhD student from the lab of Prof. Dr. Koeppl at the TU Darmstadt, and Gerassimos Kolaitis, a PhD student from the lab of Prof. Dr. Sieber at the TU Munich. An optimized protocol for cell-extract preparation can be found in Appendix A.3.

5.2 Peptide vesicles

The vast majority of artificial cells are based on lipid membranes, as is the case for our artificial multicellular assemblies (AMA). This biomimicking approach allows the incorporation of many natural membrane-bound components such as protein pores. However, the possibility to construct artificial cells with polymer-based or peptide membranes is also being explored, and dynamic circuits were shown in such compartments: DNA circuits were implemented in populations of BSA-based protocells permeable to short single-stranded DNA [142], cascading enzymatic reactions were performed in polymersomes [143] and predator-prey behaviour was demonstrated between coarcervates and BSA-based proteinosomes [24].

With the facility of reconstituted transcription-translation permitted by *E. coli* cell-extract, I considered the possibility of expressing in peptide-based compartments the peptide components of the membrane. If the membrane's building blocks can be produced on site, dynamics such as compartment growth and even budding or division can be expected and studied. By comparison, the complexity of lipid synthesis makes it so far difficult to produce membrane growth in lipid-based compartment.

The self-assembly of amphiphilic peptides into a variety of nanostructures such as nanotubes, filaments, vesicles or membranes has been demonstrated with different peptide sequences [144], [145] and [146], and elastin-like peptides ELPs have even been shown to form organelle-like compartments *in vivo* [147]. I chose a simple 80 amino acid long diblock peptide with a hydrophilic negatively charged sequence of 60 glutamic acid repeats and a hydrophobic sequence of 20 leucine repeats, $E_{60}L_{20}$. This peptide has been shown to form vesicles of approximately 1 µm diameter with a bilayer-like membrane where two layers of peptides face each other with an inner hydrophobic core [148].

I therefore cloned this gene coding sequence in the plasmid pCola-Duet-1,

under the control of a LacI-repressible T7 promoter. The cloning of this insert was challenging due to the sequence's repetitive nature, but correct assembly of the plasmid was achieved and sequencing confirmed the absence of mutation or recombination in the cloned sequence. The plasmid was then purified and expressed in *E. coli* cell-extract. Expression was monitored in microscopy experiments, and aggregates could be seen to form after a few hours (Figure 5.1.a). When stained with TMRE (tetramethylrhodamine ethyl ester, a positively charged dye known to bind to negatively charged mitochondria membranes) and FMN (flavin mononucleotide, a slightly negatively charged dye), the aggregates were specifically stained by TMRE (Figure 5.1.b) but not by FMN (Figure 5.1.c), indicating that they are negatively charged. However, it is not possible to distinguish at this stage whether these aggregates are made specifically of $E_{60}L_{20}$ or whether they are generally produced by aggregation of negatively charged proteins from the cell-extract.

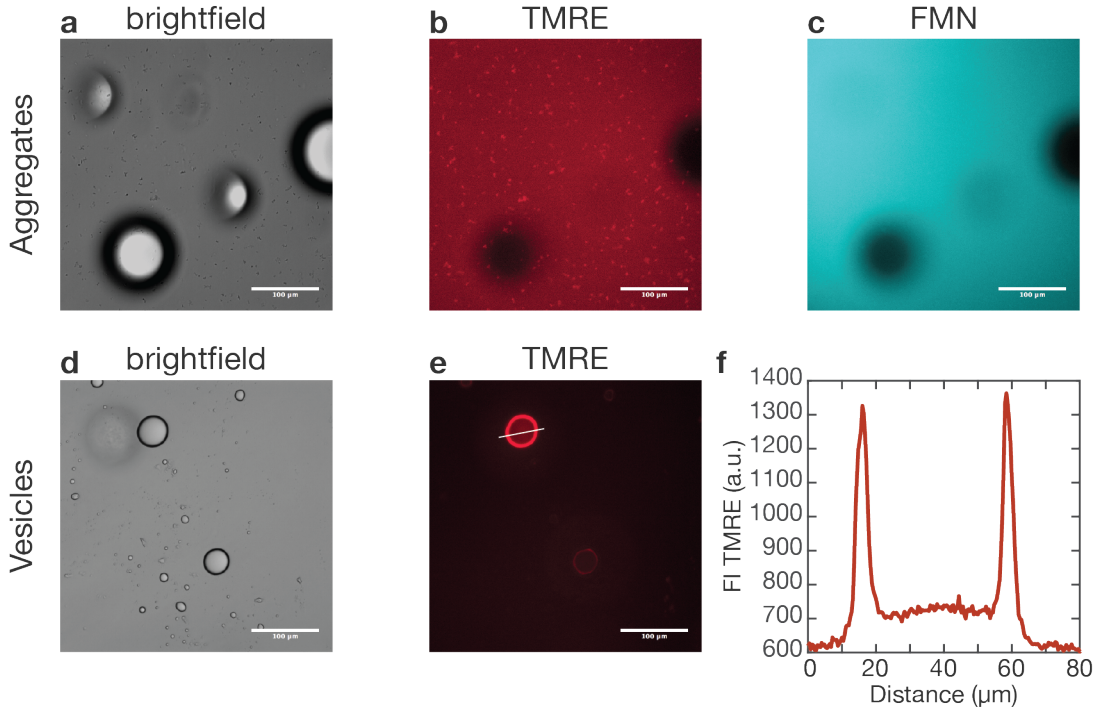

Figure 5.1. Expression of amphiphilic peptides. **a**-**c**, Imaging of aggregates found post-expression in cell-extract: brightfield (**a**), TMRE negative charge staining (**b**), FMN hydrophilic staining (**c**). **d**-**f**, Imaging of vesicles prepared from drying and resuspending a $E_{60}L_{20}$ cell-extract solution: brightfield (**d**) and TMRE negative charge staining (**e**), cross section of a vesicle shown by a white line in **e**, plotted in **f**. Scale bar: 100 µm.

The cell-extract sample in which $E_{60}L_{20}$ was expressed was then dried in a glass vial and resuspended in a sugar solution (200 mM sorbitol). The solution was vortexed, and spherical structures were detected (Figure 5.1.d). The TMRE dye was found inside the compartments, indicating that they are water-in-water compartments, and the membrane showed a higher intensity of TMRE compared to the outer and inner intensities, suggesting that the membrane consists of highly negatively charged components (Figure 5.1.e and f). Although the negative controls lack here as well to determine whether this

membrane is formed specifically from $E_{60}L_{20}$ or from aggregates of negatively charged and amphiphilic cell-extract proteins, these results give some indication that vesicles based on the $E_{60}L_{20}$ peptide could be formed. The subsequent encapsulation of cell-extract containing the genetic material to produce more of the peptide remains to be explored.

This project was halted as focus was put unto the construction of artificial multicellular tissues. However, this project was later pursued by PhD student Kilian Vogele, who used ELPs to demonstrate vesicle growth upon expression of the peptides in the peptide-based vesicles [149].

5.3 Programmable degradation kinetics

In existing biological circuits as well as in synthetic ones, dynamical response is controlled by the ratio of kinetic parameters such as diffusion, production and degradation rates. We explored in Chapter 3.1 how diffusion rates can be tuned with pore concentration in multicellular assemblies and in Chapter 3.2 how transcription rates affect the velocity of a signalling pulse. However, the use of controllable degradation kinetics to affect gene circuit dynamics has been extensively explored. For example, the effect of protease overload by a large number of tagged proteins has been shown to reduce the coupling time of genetic circuits [150].

I therefore characterized a library of degradation tags to provide a toolbox for programmable protein degradation. A gene coding for GFP under the pTetO promoter was tagged with degradation tags recognized by the ClpX protease machinery. The library consisted of 4 variants of the *E. coli* ssrA peptide tag AANDENYALAA (in short, LAA), LVA, AAV and ASV [151], and of 6 variants of the *M. fluorum* ssrA peptide tag AANKNEENTNEVPTFMLNAGQANYLSQ (in short pdt2), pdt2A, pdt2B, pdt2C, pdt2D and pdt2E [152].

The degradation tag library was cloned by overhang PCR at the C terminus of an untagged GFP and transformed in *E. coli* DH5αZ1, a strain with constitutively overexpresses TetR. Cultures were grown overnight from glycerol stocks in LB medium supplemented with antibiotics. The next day, cultures were diluted to OD 0.1 with 214 nM aTc (inducing the pTetO promoter) and grown at 37 °C for 2.5 h. The cells were pelleted with soft conditions (2000 rcf, 5 min) and resuspended in M9 medium twice. This step halts cell growth by transferring the cells to a poor medium. The cells were then diluted in M9 medium to OD 0.45 and 25 µg/mL chloramphenicol was added - this antibiotic inhibits protein chain elongation and thereby halts protein expression. With this approach, the cells stop growing so that the existing GFP is not diluted, which could lead to an apparent degradation, and no additional GFP is expressed - once all the existing GFP has

matured. The absorbance and GFP fluorescence is then monitored over several hours, and the decay of fluorescence is a direct read-out of the degradation kinetics.

The untagged GFP showed no degradation after an initial dilution, probably caused by the completion of division of cells that were dividing when the antibiotic was added (Figure 5.2.a). In contrast, GFP proteins tagged with LAA variants (Figure 5.2.a) and with pdt2 variants (Figure 5.2.c) had decaying signals and were fully degraded after 200 min to 800 min. The initial decay due to dilution was discarded and the remaining normalized fluorescence curves were fitted with a 1st order exponential decay model $x(t) = e^{-kt}$ [153] (Figure 5.2.b and d). The fitted kinetic rates k were averaged over 3 technical replicates (Figure 5.2.e). Tags AAV and LAA had the fastest degradation, followed by LVA, ASV, pdt2A, pdt2B, pdt2, pdt2E, pdt2C and finally pdt2D. Degradation rates ranged over one order of magnitude (Table 5.1).

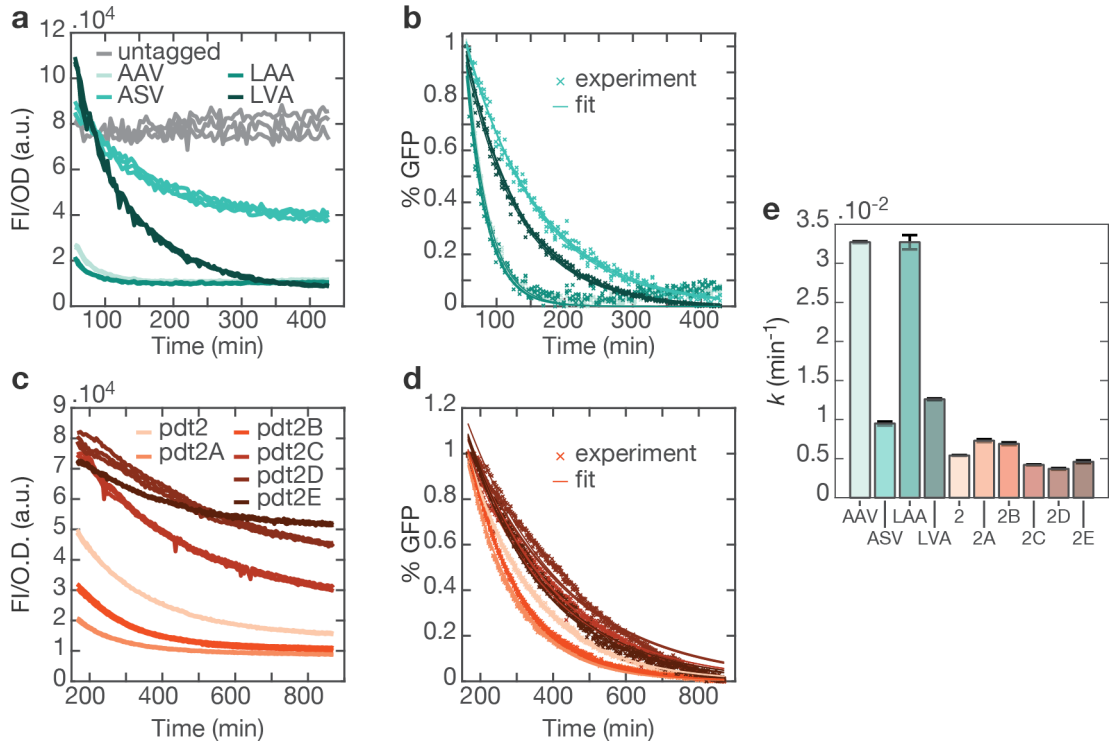

Figure 5.2. Characterization of a library of protein degradation tags. a,c, Fluorescence intensity per cell in strains containing plasmids with GFP tagged with different degradation tags (a: LAA variants, c: pdt2 variants). b,d, Normalized GFP and overlaid first order fits of degradation (data points: crosses, fits: lines, b: LAA variants, d: pdt2 variants). e, Degradation rates for the different degradation tags. Bars and error bars are mean and standard deviation.

The creation and characterization of such parts library is an important resource when building synthetic gene circuits and tuning dynamics.

Degradation tag	$\overline{k}$ (min^{-1})	$\frac{\sigma_k}{\overline{k}}$
AAV	0.0327	0.34 %
ASV	0.0095	2.74 %
LAA	0.0327	2.81 %
LVA	0.0126	0.81 %
pdt2	0.0054	0.90 %
pdt2A	0.0073	2.49 %
pdt2B	0.0069	2.55 %
pdt2C	0.0042	1.57 %
pdt2D	0.0037	2.30 %
pdt2E	0.0046	3.80 %

Table 5.1. Mean and relative standard deviation of degradation rates for each tag.

5.4 T7 RNA Polymerase

T7 RNA Polymerase is an important tool in synthetic biology circuit design as well as in recombinant protein expression. Its high transcription rate makes it particularly useful for DNA/RNA synthetic circuits, and we have used it in our signalling pulse circuit (Chapter 3.2) where the pulse velocity could be tuned with the T7 RNA Polymerase concentration. T7 RNA Polymerase is specific for its 17 base pairs cognate promoter sequence, and mutations in this sequence affect significantly transcription initiation rate. A library of 5 T7 RNA Polymerase mutants was evolved to orthogonally recognize 5 mutated T7 promoters [154], although some cross-talk still existed between T7 RNA Polymerases and non-cognate promoters. As I was interested in weakening the affinity of T7 RNA Polymerase for its promoter for a pulse-induced differentiated CRISPR-interference circuit (Chapter 3.2.4), I placed an mScarletI gene downstream of the wild-type (wt) and 5 mutated T7 promoters: 3 of them were promoters from this library (namely P_{CTGA}, P_{T3}, and P_{K1F}) and 2 of them were 1 base pair mutations of the wt promoter (P_{mut1} and P_{mut2}). I measured the resulting protein expression using the native T7 RNA Polymerase for transcription. These experiments were conducted in PURExpress, a minimal cell-free transcription-translation system where all components necessary for protein expression and T7 RNA Polymerase are reconstituted [155].

The mutated promoter constructs were AD013, AD014, AD015, AD016 and AD017, corresponding respectively to promoters P_{CTGA}, P_{T3}, P_{K1F}, P_{mut1} and P_{mut2}. I found the following efficiencies in expression driven from these promoters by wt T7 RNA Polymerase: P_{mut1}>wt promoter»P_{K1F}>P_{mut2}»P_{T3}>P_{CTGA} (Figure 5.3.a). In the original T7 RNA Polymerase library, the following read-out order for expression from wt T7 RNA Polymerase was found: for GFP expression *in vivo*, wt promoter»P_{K1F}>P_{T3}>P_{CTGA}; and for Spinach transcription *in vitro*, wt promoter»P_{K1F}> P_{T3}»P_{CTGA}. The strength order of the promoters was therefore consistent with the publication, and I introduced two new

promoters, one with similar or higher activity to the wild-type promoter and one with intermediate activity between P_{K1F} and P_{T3}.

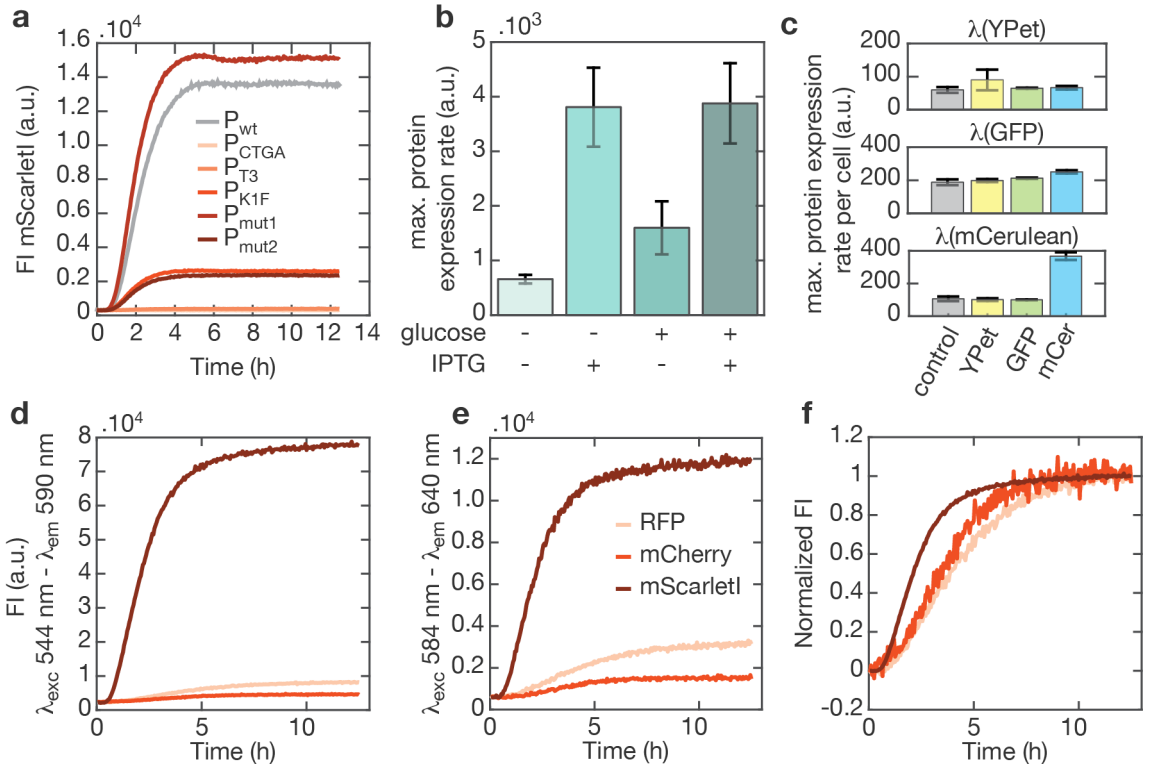

Figure 5.3. Library of T7 promoter and of fluorescent proteins, leakiness of LacI and lactose. **a**, Expression of mScarletI from 5 mutated T7 promoters and the wild-type promoter. **b**, Leakiness of LacI and lactose: expression of pSB1A3-pLacO-GFP in DH5α, LB medium in presence or absence of 1 mM IPTG and 2 mM glucose. **c**, Maximum protein expression rate of cells carrying a control plasmid (pSB4A5-AD026, expressing mScarletI), a plasmid with YPet, a plasmid with GFP or a plasmid with mCerulean (mCer). Maximum expression rate is calculated for different measured wavelengths: that of YPet, GFP or mCerulean. **d-f**, Expression of RFP variants, RFP, mCherry and mScarletI (5 nM plasmid, 400 nM T7 RNA Polymerase in cell-extract). Fluorescence intensity measured at low RFP wavelengths (**c**), high RFP wavelengths (**d**) and normalized low RFP (**e**).

These results are therefore relatively consistent with literature, and this library of T7 promoters provides an interesting way to tune transcription rates in synthetic circuits.

5.5 Fluorescent protein reporter variants

Fluorescent proteins are generally used as reporters for the expression of proteins of interest or the dynamics of a synthetic circuit. However, these fluorescent proteins (which all consist of mutations of the original green fluorescent protein GFP) vary

in their maturation time, their quantum yield and their brightness. As several reporters may be used in parallel to follow two different processes (Chapter 3.4 and Chapter 4.2), it is important to use proteins with distant excitation and emission wavelengths, but with robust fluorescence emission. I therefore studied several fluorescent protein variants in the red and in the blue-to-green emission regions.

First, I studied the effect of replacing a YPet reporter protein by two other fluorescent proteins in the same spectral region, mCerulean and GFP. Indeed, we had found that a constitutively expressed YPet reporter with high-predicted translation rate (12177.95, Table 5.2 summarizes the predicted translation rates and spectral properties of the 3 variants) was not expressed *in vivo* (construct was pSB4A5-AD029 carrying a bicistronic constitutive gene with LuxR and YPet reporter and a monocistronic gene with LuxI under its own promoter pLux, in JW0336 cells, M9 medium, 37 °C). I hypothesized that the reporter may not be expressed highly enough to be detected, although this YPet reporter had been successfully used in a high copy number plasmid (pSB1C3, in the RNA-protein nanostructure project, see Chapter 5.1). I therefore constructed two variants of the pSB4A5-AD029 construct with different reporters, pSB4A5-AD044 with GFP reporter and pSB4A5-AD045 with mCerulean reporter. When these three constructs were transformed in *E. coli* cells, only pSB4A5-AD045 showed significant protein expression of the reporter above background level (measured with the autofluorescence of an *E. coli* strain) (Figure 5.3.c). The proteins' respective quantum yields (in the order YPet, GFP and mCerulean, Table 5.2) are 0.77 [156], 0.65 [117] and 0.64 [157], and their respective brightness are 80.08, 54.2 and 27.52. Therefore we do not expect that the expressed mCerulean was better detected at the same expression level because of its spectral properties. Rather, these results indicate how protein expression is highly dependent on local DNA context (such as flanking sequences and consequent tertiary DNA structure) in a manner that is not fully understood by the current theory. The relative expression of these three fluorescent reporters placed in the same context does not follow their relative fluorescent properties nor their relative predicted expression rate. Predictable reporter expression in a variety of context remains difficult to achieve, as these and the results of Chapter 5.7 indicate.

We have addressed in Chapter 3.4 the issues raised with using red fluorescent proteins as reporters. Proteins emitting in this region typically show a poor quantum yield, but they are interesting reporters as their excitation and emission wavelengths are quite orthogonal to GFP, YFP, CFP and variants. To find out which red fluorescent protein variant had the best spectral properties for our studies, I compared three constructs containing a RFP variant under a T7 promoter: mRFP, mCherry and mScarletI. I expressed these 3 constructs in cell-extract and measured protein expression in two typical RFP channels that can be matched by the majority of fluorescence instruments (particularly microscopes and flow cytometers): excitation 544nm-emission 590nm and excitation 584nm-emission 640nm (Figure 5.3.d and e). The predicted translation rates are similar (Table 5.2, mCherry reference: [116], RFP reference: [158]. mScarletI: [81]). mScarletI expression gave a much higher signal than mCherry, which gave a slightly higher

Construct	Reporter	Predicted translation rate (a.u.)	Quantum yield	Brightness
AD029	YPet	12177.95	0.77	80.08
AD044	GFP	3377.03	0.65	27.52
AD045	mCerulean	2910.06	0.64	54.2
pT7-mCherry	mCherry	1845.2	0.22	17.47
pT7-RFP	RFP	3657.05	0.25	12.5
pT7-mScarletI	mScarletI	1721.39	0.54	56.16

Table 5.2. Predicted translation rate and spectral properties for fluorescent protein variants. Quantum yield and brightness values are taken from: YPet [156], GFP [117], mCerulean [157], mCherry [116], RFP [158], and mScarletI [81].

signal than mRFP in the two wavelengths tested. When normalizing the fluorescence intensities (Figure 5.3.f), mScarletI levels rose faster, which is likely to indicate a faster maturation rate mScarletI was therefore the far superior RFP variant and it was used as an orthogonal reporter in all subsequent circuit designs.

5.6 LacI and lactose background

We have used LacI repressible promoters in many different circuits in this thesis (see Chapters 3 and 4). However, *E. coli* cells natively produce LacI, and correspondingly our cell-extract contains traces of LacI. LB medium, often used for cell experiments, contains lactose that can induce the pLacO promoter. This background concentration of LacI and lactose might hinder the proper function of LacI-containing circuits, and we therefore quantified these effects.

To assess this effect *in vivo*, we transformed a high copy number plasmid *pSB1A3-pLacO-GFP* (copy number 400 to 500, ORI pBM1, [159]) into DH5α, which naturally expresses LacI from its genome. We wanted to quantify the following effects: is the native LacI expression in DH5α sufficient to repress the pLacO promoter of a high copy number plasmid to the same extent as overexpression of LacI in other strains? And does the presence of lactose in LB medium induce the pLacO promoter? (These experiments were conducted together with student Ludwig Bauer). To investigate these questions, we grew the two cultures in LB medium containing or not 2 mM glucose. Indeed, when glucose is available as a sugar source, this is preferred to lactose and *E. coli* cells do not express the lactose permease LacY necessary to important lactose into the cells.

In DH5α (LB medium, 37 °C), we found that in the presence or absence of glucose, GFP expression was repressed (Figure 5.3.b), demonstrating that the native levels of LacI expressed in *E. coli* are sufficient to repress even a high copy number plasmid, and the lactose in LB medium is not sufficient to induce the pLacO promoter. Expression of GFP could be induced with IPTG whether glucose was present or not.

In conclusion, we assessed the strength of genomic LacI repression of the pLacO promoter and its induction by lactose in a variety of strains, which informed our experiments on the appropriate strains to use for the different circuits we constructed.

5.7 Circuit design, growth and protein expression *in vivo*

When implementing gene circuits *in vivo* (Chapter 4.2 and Chapter 5.1), we were faced with issues regarding the growth of cells and the quality of protein expression. I compared different design rules for genetic circuits and their effect in cells. This section presents the insights gained from these experiments: the effect of carbon source on growth and expression (Chapter 5.7.1), the difference between monocistronic and polycistronic transcripts (Chapter 5.7.2), the effect of plasmid copy number (Chapter 5.7.3) and the effect of ribozymes (Chapter 5.7.4). I conclude on design rules for circuit implementation in *E. coli* cells.

5.7.1 Metabolites and protein expression

Cells can use different sugars to fuel their metabolism. In general, glucose and glycerol are preferred carbon sources because contrary to lactose, they don't interfere with gene circuit dynamics such as LacI repression. We measured the growth and expression of JW0336 cells transformed with a constitutive mScarletI-expressing plasmid (pSB4A5-AD026, M9 medium, 37 °C) in the presence of different glucose concentrations. I found that cells saturate at slightly higher ODs with higher glucose concentrations (from around OD 1 for 0.5 mM glucose to around OD 1.5 for 20 mM glucose, Figure 5.4.a).

However, protein expression differed more drastically between growth conditions (Figure 5.4.b): with 0.5 mM glucose, protein expression stopped after 4 hours and with 20 mM glucose, expression continued linearly during the 16 hours of the experiment. With 2 mM and 5 mM glucose, the cells showed a sudden increase of protein expression after 4 and 6 hours respectively, and then saturated. This approximately corresponds to the time where the cells enter saturation growth phase. No similar correlation could be made for 20 mM glucose as protein expression continues linearly after growth saturation.

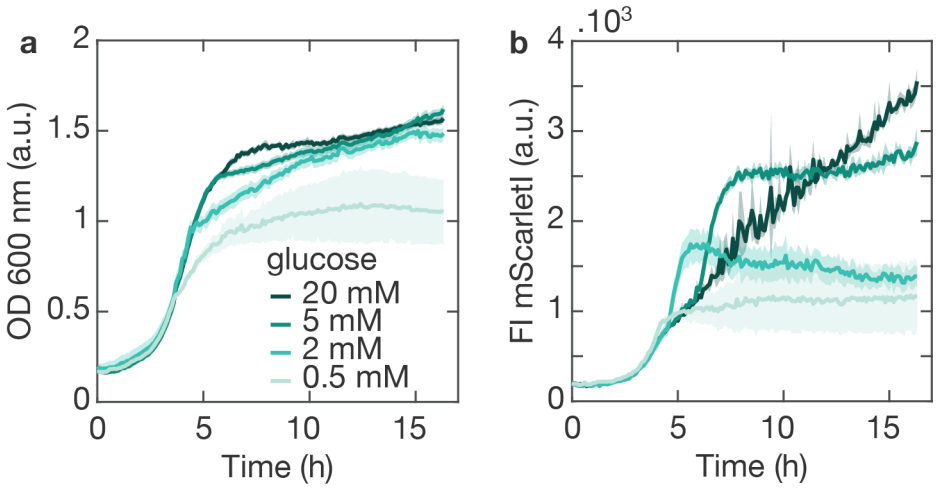

Figure 5.4. Effect of carbon sources on growth and protein expression. Growth (**a**) and protein expression (**b**) in cells grown in M9 medium containing different concentrations of glucose.

We can suppose that this sudden burst in protein expression for 2 and 5 mM glucose corresponds to a change in metabolism, when the cells have run out of glucose and switch to a different carbon source. This could be avoided with 20 mM glucose if the cells reach growth saturation before all the glucose is utilized. These results suggest that protein expression dynamics can be easily modified by activating different metabolisms and sugar usages, but that therefore circuit behaviour might not be reproducible across different growth media.

5.7.2 Monocistronic and polycistronic constructs

Fluorescent reporters are often the fastest method to measure the dynamic behaviour of a circuit. However, a reporter may not always quantitatively report on the concentration of the protein of interest. Several methods exist for the placement of the reporter gene in regard to the gene of interest. The reporter can be placed in the same transcript and open reading frame as the protein of interest, so that a fusion protein is translated, but this approach forms a large protein complex so that the functionality of either protein may be affected or toxicity for the cells may be introduced. Unexpected internal ribosome binding sites have also been shown to cause larger expression levels of the reporter protein compared to the protein of interest (see [160] and Chapter 3.3). The reporter and the protein of interest can be placed under two identical promoters, but due to local DNA context, the two promoters might not be transcribed with the same efficiency, leading to a discrepancy between levels of reporter and protein of interest.

In most of our circuits (Chapters 2, 3 and 4), we placed the protein of interest and the reporter on one transcript (a bicistronic gene), and added ribozymes between

the two open reading frames so that the bicistronic transcript would be cleaved into two transcripts translated independently. This guarantees a faithful reporting at the RNA level while avoiding internal-RBS-artefacts in reporting at the protein level. However, as ribozyme-dependent cleavage can be slow, it is not certain whether a bicistronic construct is advantageous compared to two monocistronic constructs under identical promoters. I therefore compared the expression of bi- and monocistronic constructs with low, intermediate and high predicted translation rates (varied with RBS of different strengths), both in cell-extract and *in vivo*.

I compared a LasR-mScarletI gene under the control of a pLacO promoter in a bicistronic (pSB4A5-QS02i) and a double monocistronic (pSB4A5-AD018) construct (Figure 5.5.a). Both proteins are predicted to have low expression rates (rates are summarized in Table 5.3). The expression of mScarletI was very similar in the two constructs in cell-extract. Therefore in a low protein expression context, reporter reliability seemed identical for bicistronic and double monocistronic constructs.

Plasmid	Cistronicity	Gene 1	TL rate (a.u.)	Gene 2	TL rate (a.u.)
AD018	monocistronic	LasR	4.72	mScarletI	13.26
QS02i	bicistronic	LasR	4.72	mScarletI	13.26
AD022	monocistronic	LasR	4.72	mScarletI	266.92
AD023	bicistronic	LasR	4.72	mScarletI	266.92
AD043	monocistronic	LasR	4.72	mScarletI	10882.06
AD026	bicistronic	LasR	4.72	mScarletI	10882.06
AD042	bicistronic	LuxR	411.87	YPet	12177.95
AD029	monocistronic	LuxR	411.87	YPet	12177.95

Table 5.3. Predicted translation rates for polycistronic and monocistronic constructs.

Copy number	TL rate	Best cistronicity	Experiment
low	low	mono = poly	Figure 5.5.a
low	intermediate	mono > poly	Figure 5.5.b
low	high	mono = poly mono > poly	Figure 5.5.c Figure 5.5.e
medium	high	mono > poly	Figure 5.5.d

Table 5.4. Expression of polycistronic and monocistronic constructs for different copy number plasmids and translation (TL) rates.

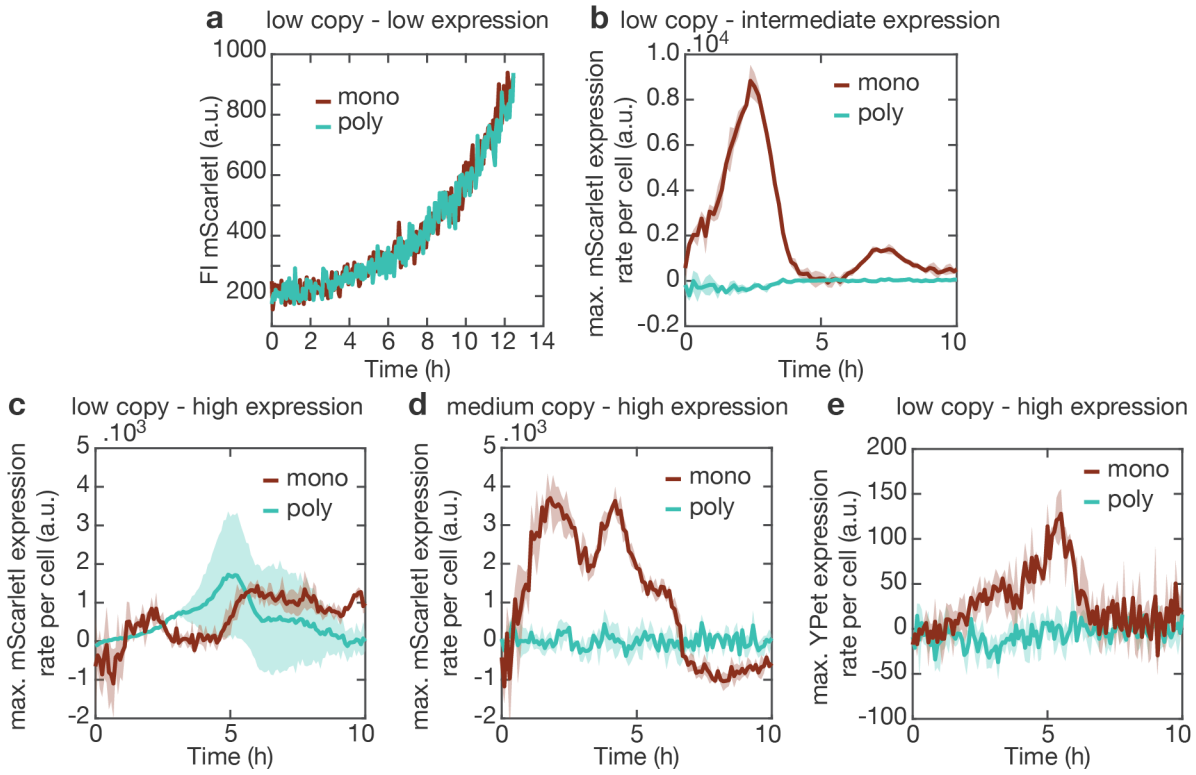

Figure 5.5. Comparison of mono and polycistronic constructs. a, Comparison in low copy number, low translation rate setting, cell-extract. b-d, Comparisons *in vivo*, low copy plasmid with intermediate protein expression (b), low copy plasmid with high protein expression (c: mScarletI, e: YPet), medium copy plasmid with high protein expression (d).

I then compared two similar constructs with intermediate predicted translation rates (Table ??5.3), in low copy number plasmids. In JW0336 cells, the monocistronic construct (two different promoters, pSB4A5-AD022) expressed significantly better than the bicistronic construct although growth was similar (Figure 5.5.b, M9 medium, 37 °C). With low copy number plasmids and high predicted translation rates (Table 5.3), both constructs expressed similarly (Figure 5.5.c, JW0336, M9 medium, 37 °C). With medium copy number plasmids and high predicted translation rates however, expression of the double monocistronic construct was higher than that of the bicistronic construct (Figure 5.5.d, JW0336, M9 medium, 37 °C). For a different gene, LuxR-YPet under the control of a pTetO promoter, expression was higher for a monocistronic construct than for a bicistronic construct in a low-copy-number, high-predicted-expression (Table 5.3) setting (Figure 5.5.e, JW0336, M9 medium, 37 °C).

There seems to be a trend that double monocistronic constructs allow for higher reporter expression than bicistronic constructs, although this is not systematic (Table 5.4). Since predicted translation rates are identical between the monocistronic and bicistronic constructs, this seems to indicate that the expressions differ at the transcription level (besides, an internal RBS would lead to higher reporter levels in the bicistronic con-

struct, which is not the case here). During transcription of a bicistronic gene, RNA polymerase may fall off the gene, which would cause comparatively lower levels of reporter transcript. It is possible that the use of a double monocistronic construct restores the correct transcription of both open reading frames, and therefore high levels of reporter expression. However, other effects such as local DNA context and load might play a role, and it is uncertain whether the trend measured here would be confirmed in more varied constructs.

5.7.3 Plasmid copy number and expression

The interplay between plasmid copy number and effective expression of constructs is complex. Naively, one could assume that a higher copy number means higher protein expression, and changing the plasmid backbone of constructs is often done with this purpose in mind. However, a higher plasmid copy number also entails a higher metabolic load on the cells: more plasmids have to be replicated, the plasmids may titrate proteins away from other binding partners through specific or unspecific interactions (especially for high copy number plasmids that can reach up to 500 copies per cell, compared to one copy of the chromosome), the plasmids can use up resources necessary for transcription-translation if their expression is too high, etc. Plasmids may therefore have toxic effects and affect cell growth, although slower growth of a healthy culture can lead to higher protein expression yields (this effect is typically used in recombinant protein expression). I therefore investigated how growth and protein expression varied when constructs were inserted in low or medium copy number plasmids. I investigated this effect for three plasmids, carrying each three genes (including one constitutively expressed reporter). All experiments were conducted in JW0336 cells in M9 medium at 37 °C. I used pSB4A5 (ORI rep101, copy number 5) for low copy number and pSB3C5 (ORI p15A, copy number 10) for medium copy number.

For construct AD026 (mScarletI constitutively expressed in a bicistronic construct), transformation of the pSB3C5 plasmid into JW0336 cells led to colony formation on plates, but these cells did not grow in liquid medium (Figure 5.6.a and b). In contrast, cells transformed with the pSB4A5 low-copy plasmid grew normally and expressed the reporter (Figure 5.6.a and b). Turbo cells (a strain optimized for fast growth) transformed with the pSB3C5 plasmid did not show any protein expression (Figure 5.6.a and b), and showed a defect in growth: the cells grew slowly and after ten hours, the OD decreased. In summary for the AD026 construct, the data suggests that doubling the number of plasmids per cell is lethal or highly toxic for the cells - this is probably due to unspecific interactions with the cell's fundamental pathways, as the Turbo cells show no reporter expression but defects in growth.

For construct AD042 (expressing YPet constitutively in a monocistronic construct), reporter expression was completely suppressed when the construct was placed

in a medium copy number plasmid, compared to high expression in a low copy number plasmid (Figure 5.6. c and d). Growth was slightly slower for the cells containing the low copy number plasmid, which could be due to the load of protein expression, but cells with a medium copy number plasmid grew normally. For this construct, doubling the copy number of the plasmid did not cause any lethal defects, but protein expression ceased, which could indicate that cell resources are titrated away from plasmid gene expression to fundamental metabolic pathways. No mutation in the plasmid's sequence could be detected. Results for AD042 were reproducible across 4 independent experiments.

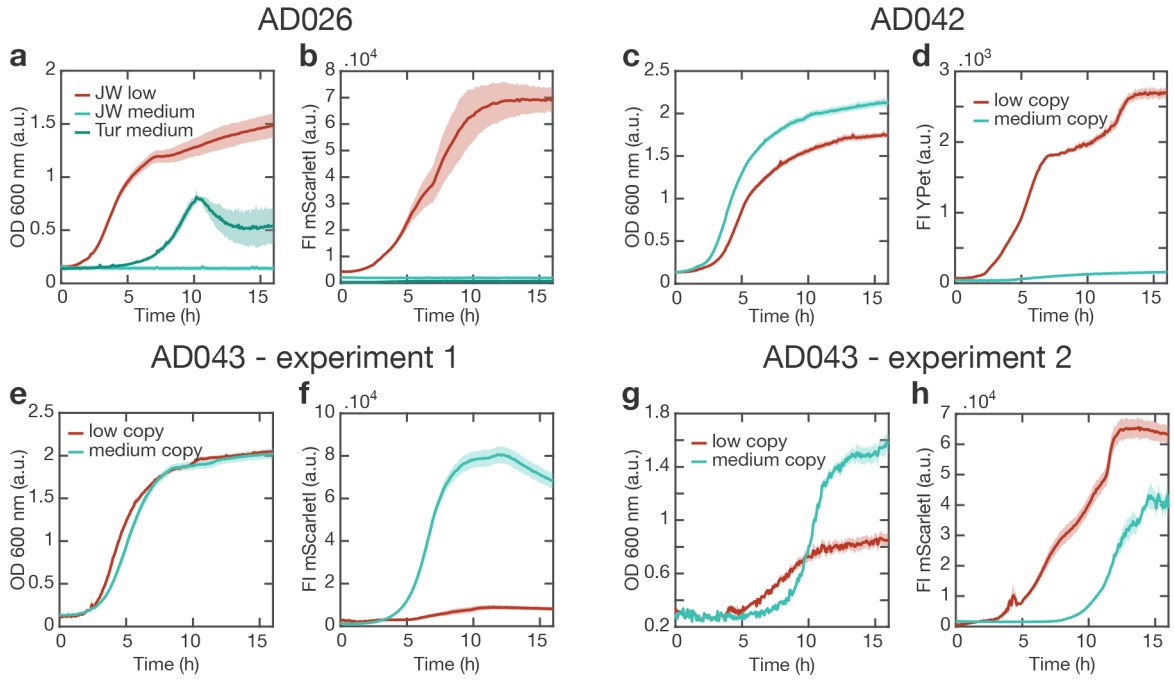

Figure 5.6. Effect of plasmid copy number on growth and protein expression. Growth (**a**, **c**, **e**, **g**) and expression (**b**, **d**, **f**, **h**) compared between low and medium copy number plasmids. **a**-**b**, With construct AD026, in JW0336 and Turbo cells. **c**-**d**, With construct AD042, in JW0336 cells. **e**-**h**, With construct AD043, in JW0336 cells.

Finally, for construct AD043 (expressing mScarletI constitutively in a monocistronic construct), growth and protein expression of the cells varied between experiments. Sometimes, cells transformed with low copy number plasmid grew slower but showed higher protein expression (Figure 5.6.e and f), which could represent a case of slower growth causing higher protein expression, as cells' resources are less titrated to growth pathways and more available for plasmid expression. In other cases, cells transformed with low and medium copy number plasmids grew similarly, but medium copy number plasmid showed faster protein expression (Figure 5.6.g and h).

These results therefore seem to show a trend that expression is facilitated in low copy number plasmids, as this probably results in a lower load to the cells, less toxicity and more resources being available for protein expression. However, this behaviour is not systematic, and in some cases a higher copy number can lead to higher

expression during exponential growth phase. This is likely to depend on the load that a given plasmid imposes on the cells, and plasmids with less genes or weaker RBS may be better expressed at higher copy numbers, whereas constructs with more genes or stronger RBS should preferentially be cloned in lower copy number plasmids.

5.7.4 Ribozymes and toxicity

Ribozymes are self-cleaving RNA motifs that can be used to isolate an mRNA from its promoter context and to split a bicistronic transcript into two mRNAs for independent translation. However, repeated issues with cell growth when using these elements in our circuits led us to investigate the possible toxicity of such motifs.

We first suspected a toxic effect of ribozymes when cloning the mTq2-BivTat construct for the RNA-protein nanostructure project (Chapter 5.1). This construct consists of a simple constitutively expressed fluorescent protein on a high copy number plasmid, and although this could induce some load to the cells, we did not expect this plasmid to have lethal effects on cells. We did not detect any growth defects when cloning *pSB1C3-YPet-PCP*, although this construct also contained a ribozyme. However, when cloning *pSB1C3-mTq2-Biv-Tat*, we found that colonies on plates grew extremely slowly when picked and resuspended in liquid culture. Saturation of the culture could only be reached after 48 hours of incubation if the cells grew at all, which is 4 to 6 times slower than a normal *E. coli* culture.

I therefore constructed a version of *pSB1C3-mTq2-Biv-Tat* where the ribozyme was deleted, *pSB1C3-AD046*. This construct had a slightly higher predicted translation rate (4130.11 vs. 2082.76 for the construct with ribozyme). Colonies of AD046 could be rapidly grown in liquid culture and no growth defect was detected. I therefore compared the growth and expression of these two constructs from 3 initial growth stages: I grew liquid cultures from single colonies for 48 hours, 24 hours, or resuspended colonies in liquid culture and immediately measured their growth and protein expression. Growth was similar for both constructs when they were diluted from a 48 hour or a 24 hour preculture, and that protein expression was slightly slower for AD046 (Figure 5.7.a and b, DH5α, M9 medium, 37 °C). In contrast, single colonies of AD046 grew normally, whereas mTq2-BivTat colonies did not grow at all in the time of the experiment (14 hours). This seems to indicate that ribozymes can cause an initial growth defect, but that normal growth can be rescued if cultures are first grown and then diluted.

I then measured how the presence or absence of ribozymes affected the growth and expression of larger gene constructs (3 genes) in low copy number plasmids (pSB4A5). As moving a construct with ribozymes to higher copy number had shown lethal growth defects (see AD026 growth in Chapter 5.7.3), I suspected that ribozymes used in this library of constructs may cause growth issues. We therefore constructed 2 variants

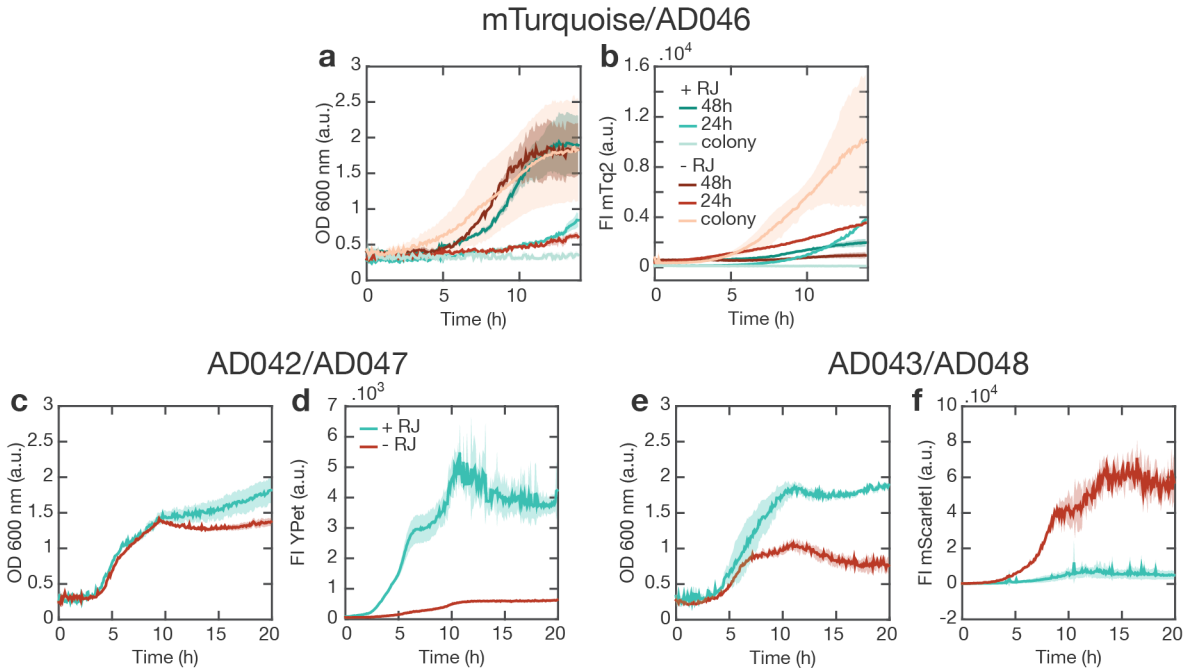

Figure 5.7. Growth and protein expression in constructs with and without ribozymes. a-b, Constitutive mTurquoise construct in high-copy-number plasmid, with (*pSB1C3-mTq2*) or without (*pSB1C3-AD046*) ribozyme, grown from single colonies, 24 h or 48 h precultures. c-d, Constitutive YPet construct in low-copy-number plasmid, with (*pSB4A5-AD042*) or without (*pSB4A5-AD047*) ribozyme. e-f, Constitutive mScarletI construct in low-copy-number plasmid, with (*pSB4A5-AD043*) or without (*pSB4A5-AD048*) ribozyme.

of 2 genes, with and without ribozymes. First, I used AD042 (a three gene construct with monocistronic transcripts and constitutive YPet expression), and constructed a ribozyme-free version (AD047, YPet predicted translation rate was reduced three-fold). The protein expression rate was 10-fold lower for the construct without ribozymes compared to the construct with ribozymes, and no significant growth defect could be detected (Figure 5.7.c and d). Then, I used AD043 (a three genes construct with monocistronic transcripts and constitutive mScarletI expression), and constructed a ribozyme-free version (AD048, mScarletI predicted translation rate was reduced 12 folds). Protein expression rate was 2-fold higher for the construct without ribozymes, contrary to predicted translation rates (Figure 5.7.e and f). The construct without ribozymes had a slower growth but this could be attributed to the stronger protein expression. Overall, deleting the ribozymes had opposite effects on protein expression in these two constructs but had no obvious effect on growth.

Our results therefore do not clearly indicate a toxicity of ribozymes. Other circuit elements, such as local DNA context, poly- or monocistronic transcripts, or plasmid copy numbers, are likely to dominate effects cell growth and protein expression rates. The results presented in Chapters 5.7.2, 5.7.3 and 5.7.4 indicate the following circuit design rules: monocistronic transcripts under identical promoters rather than bicistronic

transcripts, low copy number plasmids and usage of ribozymes.

5.8 GamS

Synthetic circuits often require optimization of the expression levels and of the functionality of all their parts. This was particularly well exemplified with the quorum-sensing ecosystem dynamics described in Chapter 4.2, where many of the genes did not function as designed and needed troubleshooting. When working *in vivo*, the prototyping of circuits' parts can be lengthy and tedious because it necessitates cloning of parts in plasmids and is therefore limited by cell growth. In response to this issue, prototyping of circuits' functionality in cell-extract is becoming more popular as a means of rapidly characterizing library of parts before implementing the optimized design in living cells.

For a fast design-build-test cycle in cell-extract, linear DNA is optimal for quick assembly of parts but its expression is limited since cell-extract typically contains nucleases targeting linear DNA. The lab of Vincent Noireaux, who revived the use of *E. coli* cell-extract for synthetic biology, together with the lab of Richard Murray demonstrated that circuits could be rapidly prototyped with linear DNA in cell-extract using a decoy protein to protect linear DNA from degradation [161]. RecBCD is considered the main exonuclease responsible for DNA degradation in cell-extract, and it can be inhibited with a small protein, gamS, which binds RecBCD and titrates it away from the linear DNA [162].

Together with student Ludwig Bauer, we purified the gamS protein and assessed the expression of fluorescent proteins from linear DNA in cell-extract. On three different titration experiments, we found that the titration of gamS had a Hill-function-like effect on expression from linear DNA, with a K_d in the range of 100 nM to 1 µM (Figure 5.8.a). This dose-response corresponds to the titration of gamS against RecBCD present at a fixed concentration in the cell-extract. In all cases, we found that 10 µM gamS was sufficient to restore maximum expression from linear DNA template. This maximum expression corresponds to about 50 % of the expression obtained from a plasmid DNA template of the same sequence (Figure 5.8.b). This difference can be caused by other nucleases than RecBCD that are not inhibited by gamS, or by DNA topology which affects recognition by RNA Polymerases and expression.

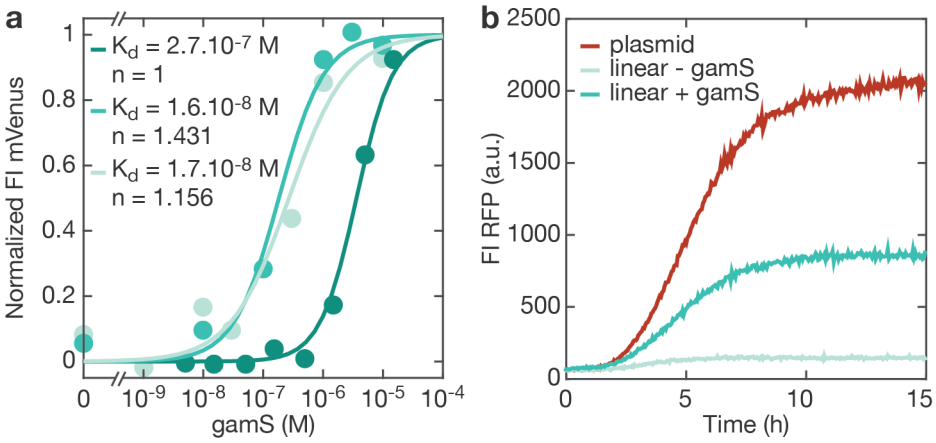

Figure 5.8. Expression of linear DNA in cell-extract with gamS. a, Titration of gamS in three separate experiments and resulting protein expression from a linear template. **b**, Protein expression from a plasmid, and from the corresponding linear template protected or not by gamS.

5.9 Genelets in PURExpress

Genelets are linear DNA templates that form the basis for a class of synthetic circuits involving nucleic acids computation. Since activation and deactivation of these templates can be induced by the annealing of DNA and RNA strands with known kinetics and thermodynamics, they allow for highly programmable circuit dynamics [86]. However, as described in Chapter 5.8, linear DNA is unstable in cell-extracts, as these contain nucleases specific for linear DNA degradation. However, the reconstituted protein expression system PURExpress [155] does not contain DNA or RNA nucleases.

We therefore considered that PURExpress would be the ideal platform to combine the programmability of genelet circuits with the biological relevance of controllable protein expression. We aimed at using our signalling pulse to induce differentiation in the expression of a fluorescent protein (see Chapter 3.2.4). Although our approaches for this gene circuit did not succeed, we demonstrated for the first time that genelet circuits were compatible with a protein expression system.

I first transcribed a fluorescent aptamer, dBroccoli, in PURExpress from a linear template (Figure 5.9.a). Although RNA degradation is apparent after 3 hours, this is likely due to RNAse contamination from pipetting, and good expression of the genelet template can be detected in the first 3 hours. Then, I assembled the circuit for the signalling pulse in PURExpress in the presence or absence of a plasmid coding for the fluorescent protein mTq2 (Figure 5.9.b). I first incubated the ssDNA activator with the Spinach RNA aptamer, then added DFHBI and incubated the reaction for 10 min, after which I added the incomplete repressor node template. I found that the pulse circuit dynamics were similar in PURExpress as in a purified T7 RNA Polymerase buffer, with the Spinach-DFHBI signal being completely repressed within 1 hour. mTq2 expression

was functional in presence of the genelet circuit, and in these conditions the Spinach-DFHBI signal increased again after 2 hours, which is likely due to a bleed-through of the fluorescence from mTq2 into the GFP channel. This therefore demonstrates that genelet circuits and protein expression could be conducted simultaneously in the same environment.

Finally, I tested the possibility to conduct expression from *E. coli* promoters in PURExpress. Indeed, the only RNA Polymerase present in PURExpress is T7 RNA Polymerase, which limits the diversity of genetic circuits that can be implemented in this environment. Promoters that can be detected by *E. coli* RNA Polymerases, such as repressible promoters pTetO and pLacO or inducible promoters pLux and pLas, can be of great interest to construct repression and activation interactions in circuits. I therefore attempted to express a RFP gene under the control of the pLacO promoter in PURExpress by supplementing the system with the *E. coli* RNA Polymerase holoenzyme (the core enzyme saturated with sigma factor 70). I compared the expression of this gene to that of a GFP gene under the control of a T7 promoter (Figure 5.9.c). Although GFP was strongly expressed through the control of the T7 RNA Polymerase, RFP was only expressed at low and noisy levels through the control of the *E. coli* RNA Polymerase. This experiment demonstrated that genes transcribed by endogenous *E. coli* RNA Polymerases could not be expressed in PURExpress.

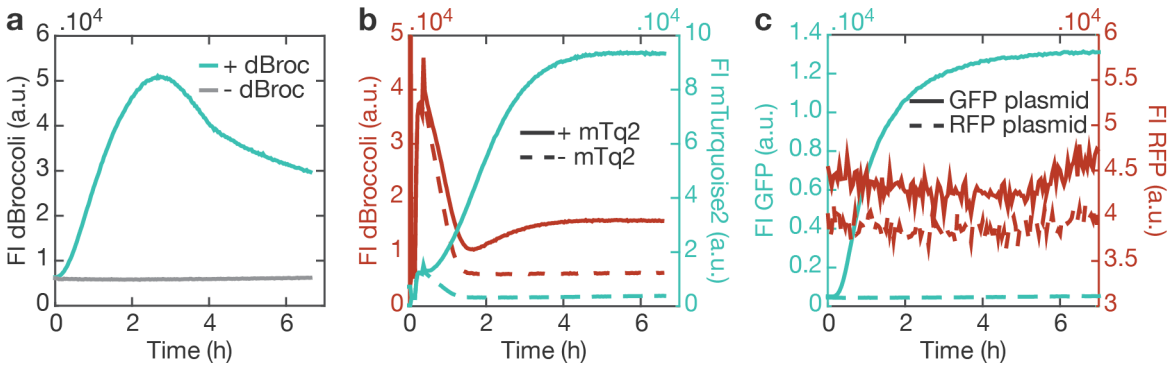

Figure 5.9. Expression of genelet circuits and *E. coli* constitutive promoters in PURExpress. **a**, Expression of a dBroccoli template. **b**, Expression of the signalling pulse circuit in presence or absence of an mTq2 expressing plasmid. **c**, Expression of GFP under a T7 promoter and of RFP under an *E. coli* constitutive promoter.

5.10 Aptamers

Throughout this thesis, RNA aptamers were used as fluorescence reporters and to detect small chemicals. In this section, I present the work conducted on aptamers in more details.

Nucleic acid sequences that recognize and bind a variety of small chemicals (from fluorophores to antibiotics) have been adapted from existing structures *in vivo* or have been engineered and selected *in vitro* [163]. Such sequences, called aptamers, typically bind their ligand through tertiary motifs in their conformation. These conformations can be formed by the nucleic acid alone or induced by the presence of the ligand. *In vivo*, RNA sequences that bind a small molecule, thereby inducing a conformational change in the RNA, often are placed on messenger RNA and switch from non-translatable to translatable states. They are referred to as riboswitches.

Recently, RNA aptamers that increase the fluorescence of fluorophores through their binding have been developed based on the chromophore found in GFP [78], [63]. Typically, these RNA aptamers rely on a G-quadruplex motif to stabilize the planar conformation of the fluorophore through π-stacking, which in turn increases the fluorophore's quantum yield [164]. For example, DFHBI (3,5-difluoro-4-hydroxybenzylidene imidazolinone, which has its excitation peak at 469 nm and its emission peak at 501 nm) has a quantum yield of 0.0007 in absence of the Spinach RNA aptamer and a quantum yield of 0.72 in its presence [78].

All experiments done with the Spinach aptamer in this thesis used the 24-2-min sequence, which we found to have a K_d of around 0.8 µM with DFHBI (Figure 5.10.a), compared to a K_d of approximately 0.5 µM reported in literature [78]. We also worked with the dBroccoli aptamer [63], which contains 2 binding pockets for DFHBI on a sequence length of 107 nucleotides, compared to 1 binding pocket over 94 nucleotides for Spinach. It therefore allows a stronger fluorescence read-out for approximately the same consumption of transcription resources.

Finally, we used the 13-2-min aptamer sequence, which binds the fluorophore DMHBI (3,5-dimethoxy-4-hydroxybenzylidene imidazolinone). This fluorophore has different spectral properties than DFHBI, as its excitation peak is at 394 nm and its emission peak is at 487 nm. As it is not commercially available, I synthesized the fluorophore following the protocol of [78] (NMR spectrum in Figure 5.10.b), and successfully used it to report on the transcription of the 13-2-min RNA (Figure 5.10.c). My goal was to use the DMHBI aptamer together with the DFHBI aptamer to form a FRET pair, to report on the spatial proximity of RNA motifs in certain structures. However, this project was not pursued due to lack of time. A similar RNA FRET pair was later published by the groups of Kurt Gothelf and Ebbe Andersen [165].

We also studied bifunctional RNA aptamers as possible replacements for the Spinach aptamer in the I1-FFL circuit, so that other chemical signals could be employed to induce the circuit (see Chapter 3.2.4). Bifunctional aptamers were developed from the Spinach aptamer by the group of Samie Jaffrey to detect cellular metabolites [96]. These RNA sequences have been designed with two binding pockets, for DFHBI and for another chemical, and so that the binding of the other chemical induces a conformational change in the RNA folding. With this strategy, the binding pocket for DFHBI (which is

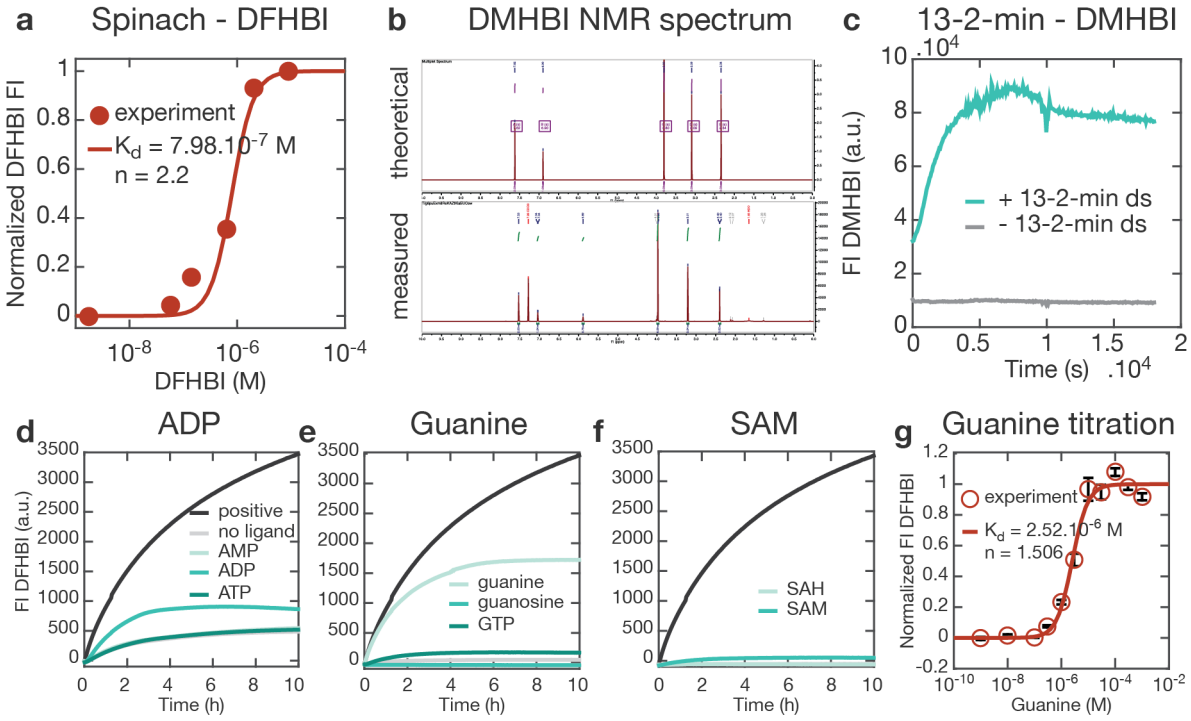

Figure 5.10. Aptamers used in this thesis. a, DFHBI titration against 1 µM 24-2 RNA. b, Theoretical and measured spectrum of DMHBI synthesized in the lab. c, Transcription of 13-2-min (200 nM DNA template) with 10 mM DMHBI. d-f, Transcription of bifunctional in presence of DFHBI and their ligand or related compounds. Dark grey: positive control where 24-2 is transcribed in presence of DFHBI. Light grey: negative control where the bifunctional aptamer is transcribed in absence of its ligand. d,24-2-ADP transcribed in presence of AMP, ADP or ATP. e, 24-2-guanine transcribed in presence of guanine, guanosine or GTP. f, 24-2-SAM transcribed in presence of SAH or SAM. g, Guanine titration against 100 nM 24-2-guanine RNA. Mean and standard deviation are indicated as circles and error bars.

usually constitutively formed by the RNA sequence in absence of the ligand) can only be formed once the first chemical has bound to its corresponding aptamer region. DFHBI fluorescence thereby reports on the binding of other, non-fluorescent, chemicals. I used three of these bifunctional aptamers: the 24-2-ADP aptamer that recognizes adenosine di-phosphate (ADP), the 24-2-guanine aptamer that recognizes guanine and the 24-2-SAM aptamer that recognizes S-adenosyl methionine (SAM). I transcribed the corresponding DNA templates in the presence of DFHBI only, of the appropriate ligand, or of structurally similar chemicals (Figure 5.10.d, ATP, AMP and ADP, Figure 5.10.e, guanine, guanosine and GTP, Figure 5.10.f, SAM and SAH).

Each of the bifunctional aptamer had a low background fluorescence in the absence of the ligand, confirming that the DFHBI binding pocket forms only in presence of the ligand. In addition, each bifunctional aptamer was relatively specific for its ligand compared to structurally similar molecules. The ADP aptamer gave the strongest background fluorescence, which is certainly caused by unspecific binding of the RNA to the high concentration of ATP present in the transcription mix. I also titrated guanine against

its purified bifunctional aptamer and found a K_d of approximately 2.52 µM (Figure 5.10.g), compared to approximately 1 µM in the literature [96].

All RNA aptamers used here were easy to implement and functional, which makes them important tools in synthetic biology.

5.11 Dose-response functions

In this thesis, we used small chemicals as ligands to induce a variety of processes. I have determined the Hill-function responses of these processes to increasing ligand concentrations. This section lists these titration functions and the K_d and cooperativities n that were measured in a variety of environments. K_d and n values are summarized in Table 5.5. Hill functions are fitted from protein expression rate normalized by OD for *in vivo* data and from final fluorescence intensities for cell-extract data.

3OC6-HSL

We measured the response of the pLux promoter to increasing 3OC6-HSL concentrations in 2 contexts *in vivo* and in 1 context in cell-extract. We first used *E. coli* DH5αZi cells transformed with *pSB1A3-pLacO-T9002-LVA* (a construct used in Chapters 2, 3 and 4.1), which consists of a LuxR gene under an IPTG inducible pLacO promoter and a GFP gene under a pLux promoter. In absence of IPTG, leaky expression of LuxR still occurs, and we found a dose-response to increasing concentrations of 3OC6-HSL (Figure 5.11.a, M9 medium, 37 °C), with K_d = 773 pM and a cooperativity n = 1.36. However, when titrating 3OC6-HSL against the plasmid *pSB4A5-AD037* (LuxR under a pTet promoter and YPet under a pLux promoter) in JW0336 (M9 medium, 37 °C), I measured a K_d of 17.1 µM and a cooperativity of 0.8047 indicating a competitive binding (Figure 5.11.b). These results indicate that sequence-specific context might affect the binding affinity and mechanism of LuxR. Finally, I screened 3OC6-HSL in cell-extract against 5 nM of *pSB1A3-pLacO-T9002-LVA*, and found a K_d = 11.36 nM and n = 2.232, indicating a similar response of this plasmid in cell-extract and *in vivo* (Figure 4.2.b and, Figure AA.2.a, for further comparison of the response of this plasmid in the two environments, see [2]).

3OC12-HSL

We measured the response of the pLas promoter to increasing 3OC12-HSL concentrations in 2 contexts *in vivo*. We used *E. coli* JW0336 cells transformed with one of the following 2 plasmids: *pSB4A5-AD032* (pLacO-LasR and pLas-mScarletI) and *pSB4A5-AD036* (pLacO-LasR and pLas-YPet). The range of protein expression rates differed for the two plasmids, but we measured similar Hill responses: for AD032, K_d = 3 µM and n = 17.45, and for AD036, K_d = 3.5 µM and n = 7.665 (Figure 5.11.c, M9 medium, 37 °C). Cooperativity values are excessively high and seem to generally indicate

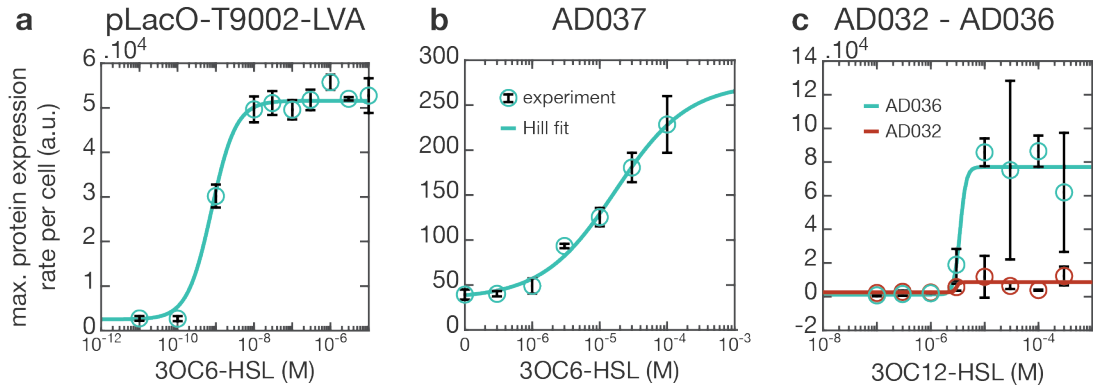

Figure 5.11. 3OC6-HSL and 3OC12-HSL titration curves. Response of LuxR and the pLux promoter to 3OC6-HSL in two constructs (a: pLacO-T9002-LVA, b: AD037), and of LasR and the pLas promoter to 3OC12-HSL in two constructs (c: AD032 and AD036). Mean and standard deviation are indicated as circles and error bars.

a very cooperative binding.

Arabinose

We measured the response of the pBAD promoter to increasing arabinose concentrations in 4 contexts *in vivo* and 2 contexts in cell-extract. In *E. coli* BW27783 transformed with construct *pBAD-dsRedmut* (Figure 5.12.a, M9 medium, 37 °C), in *E. coli* Turbo with construct *pSB1A2-AD001* (*pBAD-α-HL-GFP*) (Figure 5.12.b, LB and M9 medium, 37 °C) and in *E. coli* Turbo with constructs *pSB1A2-AD010* (*pBAD-mScarletI*) or *pSB1A2-AD011* (*pBAD-α-HL-mScarletI*) (Figure 5.12.c, M9 medium, 37 °C). K_d values ranged between 500 µM and 10 mM, and n values showed a cooperative binding. In these experiments, Hill function were sometimes fitted from the final fluorescence intensity normalized by OD, since the protein folding is slow and causes a delay between fluorescence detection and growth. In cell-extract, we measured titration curves for *pSB1A2-AD010* and *pSB1A2-AD011* (Figure 3.14.a and b) and found K_d values around 25 mM and cooperative n values.

DAPG

We measured the response of the pPhlF promoter to increasing DAPG concentrations in 2 contexts *in vivo*. In *E. coli* DH5α transformed with plasmid *pPhlF-P2* (PhlF repressor under the control of the IPTG-inducible pTac promoter and YFP under the control of the DAPG-inducible pPhlF promoter), we performed two separate experiments where we measured K_d = 9.02 µM, n = 1.511 (Figure 5.13.a) and K_d = 35.81 µM, n = 1.153 (Figure 5.13.b) (M9 medium, 1 mM IPTG, 37 °C). However, at DAPG concentrations higher than 100 µM, the ethanol that the inducer was dissolved in had toxicity effects on the cells and affected proper measurement of the dose-response. When measuring the response of the same plasmid in Turbo cells, we measured a similar toxicity effect, and a dose-response with K_d = 10.91 µM and n = 2.309 (Figure 5.13.c). These results indicate generally a K_d in the range of 10 µM and a cooperative binding. In cell-

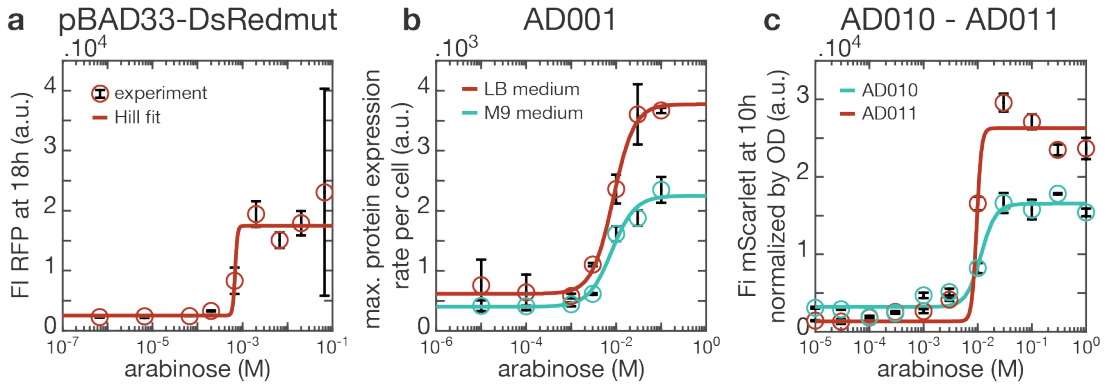

Figure 5.12. Arabinose titration curve. Response of AraC and the pBAD promoter to arabinose in four constructs (a: *pBAD-DsRedmut* in M9 medium, b: *pSB1A2-AD001* in LB and M9 medium, c: *pSB4A5-AD010* and *pSB4A5-AD011* in M9 medium). Mean and standard deviation are indicated as circles and error bars.

extract, the plasmid pPhlF-P2 was not functional. Fluorescence intensity normalized by OD was used for the second and third Hill fits.

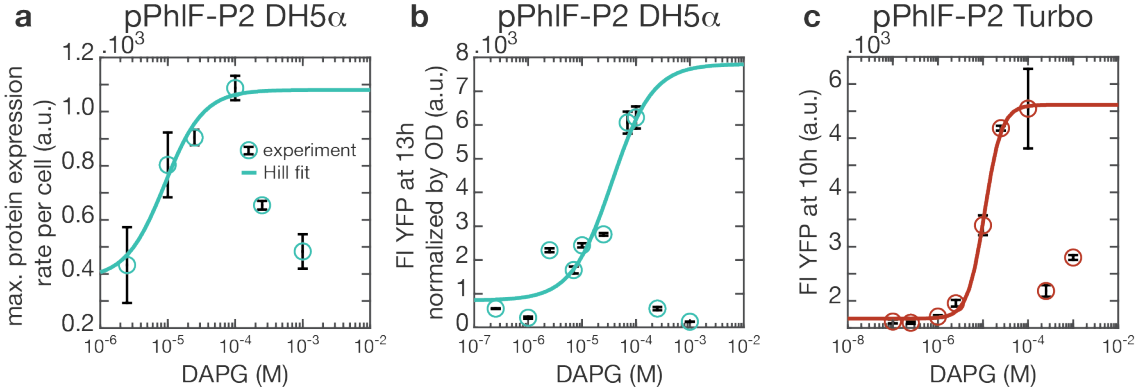

Figure 5.13. DAPG titration curve. Response of PhlF and the pPhlF promoter to DAPG in two strains (a-b: DH5α, c: Turbo). Mean and standard deviation are indicated as circles and error bars.

IPTG

We measured the response of the pLacO promoter to increasing IPTG concentrations in 2 contexts *in vivo*. In *E. coli* DH5αZi cells transformed with *pSB1A3-pLacO-GFP*, we determined a K_d = 28.09 µM and n = 1.356 (Figure 5.14.a, M9 medium, 37 °C, fluorescence at 2 hours normalized by OD). In DH5αZi cells transformed with *pSB4A5-J04450* (*pLacO-RFP*), we measured consistent values with K_d = 26.29 µM and n = 3.342 indicating a strongly cooperative binding (Figure 5.14.b, M9 medium, 37 °C).

Lactose

We measured the response of the pLacO promoter to increasing lactose concentrations in cell-extract, with 5nM *pSB1A3-pLacO-GFP* and 75 nM purified LacI. We could detect an inducible behaviour, but the data was not sufficient to fit a Hill func-

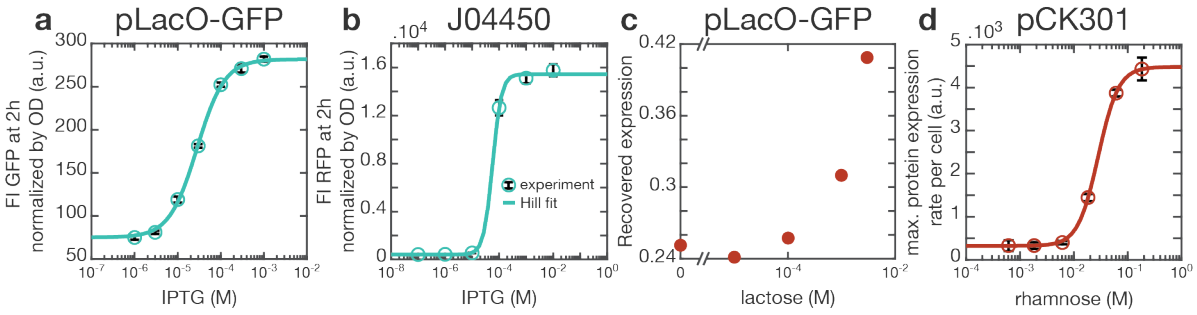

Figure 5.14. IPTG, lactose and rhamnose titration curves. Response of LacI and the pLacO promoter to IPTG in two constructs (**a**: *pSB1A3-pLacO-GFP*, **b**: *pSB4A5-J04450*) and to lactose (**c**: *pSB1A3-pLacO-GFP*), response of RhAS and the prhaBAD promoter to rhamnose (**d**: *pCK301*). Mean and standard deviation are indicated as circles and error bars.

tion (Figure 5.14.c, lactose concentrations sufficient to saturate the activity of the pLacO promoter could not be reached).

Rhamnose

We measured the response of the prhaBAD promoter to increasing rhamnose concentrations *in vivo*: *E. coli* DH5α cells were transformed with *pCK301* (*prhaBAD-GFP*), and a K_d = 28.2 mM was measured, together with n = 2.317 indicating a strongly cooperative binding (Figure 5.14.d, M9 medium, 37 °C). In cell-extract, *pCK301* was not functional and could not be induced with rhamnose.

Tetracycline and anhydrotetracycline

We measured the response of the pTetO promoter to increasing tetracycline (Tc) and anhydrotetracycline (aTc) concentrations *in vivo*: *E. coli* DH5αZ1 cells were transformed with *pSB1A2-I13522* (*pTetO-GFP*) and we measured K_d= 58.78 nM, n = 2.347 for aTc and K_d= 500 nM, n = 3.792 for Tc (Figure 5.15.a, M9 medium, 37 °C, fluorescence at 2 hours normalized by OD). With inducer concentrations above 1 µM, toxicity effects were observed due to the ethanol the inducers were dissolved in. In cell-extract, *pSB1A3-I13522* could be induced by 1 µM aTc, Tc or doxycycline, but not titration experiments were conducted.

Theophylline

We measured the response of the theophylline riboswitch to increasing theophylline concentrations *in vivo* and in cell-extract. *E. coli* BL21star(DE3) cells were transformed with *pSB1A3-pT7-Th-YPet* (YPet translation controlled by an upstream theophylline riboswitch, transcription under a T7 promoter), and we measured K_d = 475.8 nM and n=0.9538 (Figure 5.15.b). Higher theophylline concentrations could not be used due to low solubility of the inducer. In cell-extract, theophylline was screened against 10 nM *pSB1A3-pT7-Th-YPet*, and we measured K_d = 75.36 µM and n = 0.533 (Figure 5.15.c). These results indicate a K_d in the high nM to mid µM range and a negatively cooperative binding (meaning the binding of one theophylline molecule to the RNA de-

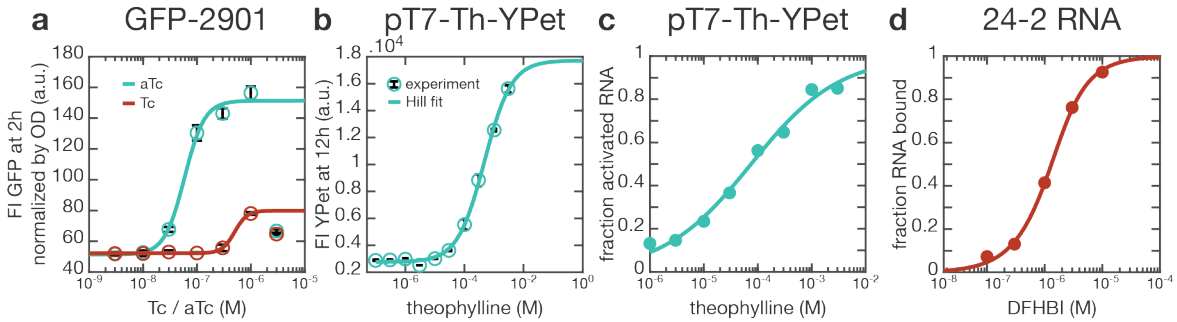

Figure 5.15. Tc, aTc, theophylline and DFHBI titration curves. Response of TetR and the pTetO promoter to aTc or Tc (**a**: *pSB1A2-GFP-2901*), of the theophylline RNA riboswitch *pSB1A3-pT7-Th-YPet* to theophylline *in vivo* (**b**) or in cell-extract (**c**), and of the Spinach RNA aptamer 24-2 RNA to DFHBI (**d**: 1 µM RNA, *in vitro*).

creases the affinity of this RNA for theophylline).

GamS

We measured the expression of a linear DNA fragment in cell-extract when gamS was titrated against RecBCD (gamS is an inhibitor of RecBCD and therefore of linear DNA degradation, see Chapter 5.8). We titrated gamS with 5 nM, 10 nM and 12.5 nM pT7-mVenus linear DNA (Figure 5.8.a). We found respectively K_d = 16.33 nM, 16.46 nM and 268.3 nM, and n = 1.431, 1.156 and 1.

Aptamer ligands

We measured the binding of DFHBI to purified Spinach RNA aptamer *in vitro*, and found in one experiment K_d = 798 nM and n = 2.2 (Figure 5.10.a) and in another experiment K_d= 800 nM and n = 1.11 (Figure 5.15.d). We measured the binding of guanine to purified 24-2-guanine bifunctional aptamer and found K_d = 2.52 µM and n = 1.506 (Figure 5.10.g). Aptamers are described in more detail in Chapter 5.10.

Ligand	Binding partner	Read-out	K_d (M)	n	Experiment
3OC6-HSL	LuxR / pLux	*pSB1A3-pLacO-T9002-LVA*, *in vivo* DH5αZi, M9, 37 °C	7.73 . 10^{-10}	1.36	Figure 5.11.a
		pSB4A5-AD037, *in vivo*, JW0336, M9, 37 °C	1.71 . 10^{-5}	0.8047	Figure 5.11.b
		pSB1A3-pLacO-T9002-LVA, cell-extract, 5 nM	1.136 . 10^{-8}	2.232	Figure 4.2.b
3OC12-HSL	LasR / pLas	*pSB4A5-AD032*, *in vivo*, JW0336, M9, 37 °C	3 . 10^{-6}	17.45	Figure 5.11.c
		pSB4A5-AD036, *in vivo*, JW0336, M9, 37 °C	3.5 . 10^{-6}	7.665	Figure 5.11.c
arabinose	AraC / pBAD	*pBAD-DsRedmut*, *in vivo*, BW27783, M9, 37 °C	6.85 . 10^{-4}	16.39	Figure 5.12.a
		pSB1A2-AD001, *in vivo*, Turbo, LB, 37 °C	8.5 . 10^{-3}	1.86	Figure 5.12.b
		pSB1A2-AD001, *in vivo*, Turbo, M9, 37 °C	7.9 . 10^{-3}	1.696	Figure 5.12.b
		pSB1A2-AD010, *in vivo*, Turbo, M9, 37 °C	1.15 . 10^{-2}	3.229	Figure 5.12.c
		pSB1A2-AD011, *in vivo*, Turbo, M9, 37 °C	9.6 . 10^{-3}	9.972	Figure 5.12.c

Ligand	Binding partner	Read-out	K_d (M)	n	Experiment
arabinose	AraC / pBAD	*pSB4A5-AD010*, cell-extract, 5 nM	2.31 . 10^{-2}	1.03	Figure 3.14.a
		pSB4A5-AD011, cell-extract, 5 nM	2.82 . 10^{-2}	1.85	Figure 3.14.b
DAPG	PhlF / pPhlF	*pPhlF-P2*, *in vivo*, DH5α, M9, 37 °C	9.02 . 10^{-6}	1.511	Figure 5.13.a
			3.581 . 10^{-5}	1.153	Figure 5.13.b
		pPhlF-P2, *in vivo*, Turbo, M9, 37 °C	1.091 . 10^{-5}	2.309	Figure 5.13.c
IPTG	LacI / pLacO	*pSB1A3-pLacO-GFP*, *in vivo*, DH5αZi, M9, 37 °C	2.809 . 10^{-5}	1.356	Figure 5.14.a
		pSB4A5-J04450, *in vivo*, DH5αZi, M9, 37 °C	2.629 . 10^{-5}	3.342	Figure 5.14.b
rhamnose	RhaS / prhaBAD	*pCK301*, *in vivo*, DH5α, M9, 37 °C	2.82 . 10^{-2}	2.317	Figure 5.14.d
Tc	TetR / pTetO	*pSB1A3-I13522*, *in vivo*, DH5αZ1, M9, 37 °C	5.878 . 10^{-8}	2.347	Figure 5.15.a
aTc	TetR / pTetO	*pSB1A3-I13522*, *in vivo*, DH5αZ1, M9, 37 °C	5.0 . 10^{-7}	3.792	Figure 5.15.a
theophylline	theophylline riboswitch	*pSB1A3-pT7-Th-YPet*, *in vivo*, BL21star(DE3), M9, 37 °C	4.758 . 10^{-7}	0.9538	Figure 5.15.b
		pSB1A3-pT7-Th-YPet, cell-extract, 10 nM	7.536 . 10^{-5}	0.533	Figure 5.15.c

Ligand	Binding partner	Read-out	K_d (M)	n	Experiment
gamS	RecBCD / linear DNA	linear mVenus, cell-extract, 5 nM	1.633 . 10^{-8}	1.431	Figure 5.8.a
		linear mVenus, cell-extract, 10 nM	1.646 . 10^{-8}	1.156	Figure 5.8.a
		linear mVenus, cell-extract, 12.5 nM	2.683 . 10^{-7}	1	Figure 5.8.a
DFHBI	24-2 RNA	purified 24-2 RNA, *in vitro*, 1 µM	7.98 . 10^{-7}	2.2	Figure 5.10.a
			8.0 . 10^{-7}	1.11	Figure 5.15.d
guanine	24-2-guanine RNA	purified 24-2-guanine RNA, *in vitro*, 1 µM	2.52 . 10^{-6}	1.506	Figure 5.10.g

Table 5.5. Hill fits for different ligand / binding partner combinations.

Outlook

This thesis has shown the possibility to assemble artificial cells into connected multicellular assemblies and to implement complex gene dynamics in them. The platform developed here is a toy-model to explore the organization, the division of labour, and the integration of a variety of processes in living tissues and organisms. It allows us to address experimentally a fundamental question: what does it take for lower-level parts to form a higher-level system capable of emergent complex behaviour? Following the words of Richard Feynman, "what I cannot create I do not understand", implementing gene networks in communicating multicellular system provides insights on the emergence of multicellularity. This thesis demonstrates the feasibility of assembling artificial multicellular systems, and a few principles of development have been implemented in them, but the scope of the biological processes that can be mimicked and studied in those systems remains largely to explore.

The work presented in this thesis could be extended in several directions that were mentioned in different chapters. The assembly of the artificial cells could be scaled up and automatized. The assemblies could be brought into an aqueous external environment, to be more biocompatible, or solidified into gels for better transportation and study [166]. The communication between compartments could be extended, with mechanisms that allow large molecules, or even macromolecular signals (such as RNA or proteins) to be transported [70]. Continuously providing resources to the assemblies could allow the system to function on long time scales out of equilibrium, as is the case in biological organisms. The division of labour and the separation of incompatible processes in such assemblies was not addressed in this thesis and could be explored.

In term, artificial multicellular assemblies could be employed to study biochemical processes, as is done in mammalian cell cultures today. Specific gene networks or interacting proteins could be isolated and studied in these less noisy, more engineerable environments. Insights about living organisms, how they evolved, how they develop, and how they function could be gained through the use of artificial cells of sufficient complexity.

Bibliography

[1] Rothe, F. *Global Solutions of Reaction-Diffusion Systems*, vol. 1072 of *Lecture Notes in Mathematics* (Springer-Verlag Berlin Heidelberg, 1984), 1 edn.

[2] Schwarz-Schilling, M., Aufinger, L., Mückl, A. & Simmel, F. C. Chemical communication between bacteria and cell-free gene expression systems within linear chains of emulsion droplets. *Integrative Biology* **8**, 564–570 (2016). URL `http://dx.doi.org/10.1039/C5IB00301F`.

[3] Dupin, A. & Simmel, F. C. Signalling and differentiation in emulsion-based multi-compartmentalized in vitro gene circuits. *Nature Chemistry* **11**, 32–39 (2018). URL `http://dx.doi.org/10.1038/s41557-018-0174-9`.

[4] Turing, A. M. The chemical basis of morphogenesis. *Philosophical Transactions of the Royal Society (part B)* **237**, 37–72 (1952). URL `http://dx.doi.org/10.1007/BF02459572`.

[5] Kondo, S. & Miura, T. Reaction-diffusion model as a framework for understanding biological pattern formation. *Science* **329**, 1616 (2010).

[6] Ueda, H. R. Systems biology of mammalian circadian clocks. *Cold Spring Harbor Symposia on Quantitative Biology* **72**, 365–380 (2007). URL `http://dx.doi.org/10.1101/sqb.2007.72.047`.

[7] Cabrera, C. V. Lateral inhibition and cell fate during neurogenesis in drosophila: the interactions between scute, notch and delta. *Development* **110**, 733–742 (1990).

[8] Sardet, C., Roegiers, F., Dumollard, R., Rouviere, C. & McDougall, A. Calcium waves and oscillations in eggs. *Biophysical Chemistry* **72**, 131 – 140 (1998). URL `http://www.sciencedirect.com/science/article/pii/S030146229800129X`.

[9] Yamaguchi, M., Yoshimoto, E. & Kondo, S. Pattern regulation in the stripe of zebrafish suggests an underlying dynamic and autonomous mechanism. *PNAS; Proceedings of the National Academy of Sciences* **104**, 4790–4793 (2007).

[10] Nakamura, T. *et al.* Generation of robust left-right asymmetry in the mouse embryo requires a self-enhancement and lateral-inhibition system. *Developmental Cell* **11**, 495–504 (2006). URL `http://dx.doi.org/10.1016/j.devcel.2006.08.002`.

[11] Wolpert, L. Positional information and the spatial pattern of cellular differentiation. *Journal of Theoretical Biology* **25**, 1 – 47 (1969). URL `http://www.sciencedirect.com/science/article/pii/S0022519369800160`.

[12] Crick, F. Diffusion in embryogenesis. *Nature* **225**, 420–422 (1970). URL `http://dx.doi.org/10.1038/225420a0`.

[13] Zagorski, M. *et al.* Decoding of position in the developing neural tube from antiparallel morphogen gradients. *Science* **356**, 1379–1383 (2017).

[14] Briscoe, J. & Small, S. Morphogen rules: design principles of gradient-mediated embryo patterning. *Development* **142**, 3996–4009 (2015).

[15] Green, J. B. A. & Sharpe, J. Positional information and reaction-diffusion: two big ideas in developmental biology combine. *Development* **142**, 1203–1211 (2015).

[16] Quiñinao, C., Prochiantz, A. & Touboul, J. Local homeoprotein diffusion can stabilize boundaries generated by graded positional cues. *Development* **142**, 1860–1868 (2015).

[17] Zadorin, A. S., Rondelez, Y., Galas, J.-C. & Estevez-Torres, A. Synthesis of programmable reaction-diffusion fronts using dna catalyzers. *Physical Review Letters* **114** (2015).

[18] Tayar, A. M., Karzbrun, E., Noireaux, V. & Bar-Ziv, R. H. Propagating gene expression fronts in a one-dimensional coupled system of artificial cells. *Nature Physics* **11**, 1037–1041 (2015). URL `http://dx.doi.org/10.1038/nphys3469`.

[19] Zadorin, A. S. *et al.* Synthesis and materialization of a reaction–diffusion french flag pattern. *Nature Chemistry* **9**, 990–996 (2017). URL `http://dx.doi.org/10.1038/nchem.2770`.

[20] Chirieleison, S. M., Allen, P. B., Simpson, Z. B., Ellington, A. D. & Chen, X. Pattern transformation with dna circuits. *Nature Chemistry* **5**, 1000–1005 (2013). URL `http://dx.doi.org/10.1038/nchem.1764`.

[21] Isalan, M., Lemerle, C. & Serrano, L. Engineering gene networks to emulate drosophila embryonic pattern formation. *PLoS Biology* **3**, e64 (2005). URL `http://dx.doi.org/10.1371/journal.pbio.0030064`.

[22] Lentini, R. *et al.* Two-way chemical communication between artificial and natural cells. *ACS Central Science* **3**, 117–123 (2017). URL `http://dx.doi.org/10.1021/acscentsci.6b00330`.

[23] Adamala, K. P., Martin-Alarcon, D. A., Guthrie-Honea, K. R. & Boyden, E. S. Engineering genetic circuit interactions within and between synthetic minimal cells. *Nature Chemistry* **9**, 431–439 (2016). URL `http://dx.doi.org/10.1038/nchem.2644`.

[24] Qiao, Y., Li, M., Booth, R. & Mann, S. Predatory behaviour in synthetic protocell communities. *Nature Chemistry* **9**, 110–119 (2016). URL `http://dx.doi.org/10.1038/nchem.2617`.

[25] Aufinger, L. & Simmel, F. C. Artificial gel-based organelles for spatial organization of cell-free gene expression reactions. *Angewandte Chemie International Edition* **57**, 17245–17248 (2018). URL `http://dx.doi.org/10.1002/anie.201809374`.

[26] Niederholtmeyer, H., Chaggan, C. & Devaraj, N. K. Communication and quorum sensing in non-living mimics of eukaryotic cells. *Nature Communications* **9** (2018). URL `http://dx.doi.org/10.1038/s41467-018-07473-7`.

[27] Sokolova, E. *et al.* Enhanced transcription rates in membrane-free protocells formed by coacervation

of cell lysate. *PNAS; Proceedings of the National Academy of Sciences* **110**, 11692–11697 (2013).

[28] Hansen, M. M. K. *et al.* Cell-like nanostructured environments alter diffusion and reaction kinetics in cell-free gene expression. *ChemBioChem* **17**, 228–232 (2016).

[29] Karzbrun, E., Shin, J., Bar-Ziv, R. H. & Noireaux, V. Coarse-grained dynamics of protein synthesis in a cell-free system. *Physical Review Letters* **106** (2011).

[30] Walter, H. & Brooks, D. E. Phase separation in cytoplasm, due to macromolecular crowding, is the basis for microcompartmentation. *FEBS Letters* **361**, 135–139 (1995). URL `http://dx.doi.org/10.1016/0014-5793(95)00159-7`.

[31] Madani, F., Lindberg, S., Langel, Ü., Futaki, S. & Gräslund, A. Mechanisms of cellular uptake of cell-penetrating peptides. *Journal of Biophysics* **2011**, 1–10 (2011). URL `http://dx.doi.org/10.1155/2011/414729`.

[32] Grassl, S. M. *Cell Physiology Source Book (Third Edition)*, chap. 16 - Mechanisms of Carrier-Mediated Transport: Facilitated Diffusion, Cotransport, and Countertransport (Academic Press, 2001), third edition edn.

[33] Johnston, D. S. & Nüsslein-Volhard, C. The origin of pattern and polarity in the drosophila embryo. *Cell* **68**, 201–219 (1992). URL `http://dx.doi.org/10.1016/0092-8674(92)90466-p`.

[34] Danino, T., Mondragón-Palomino, O., Tsimring, L. & Hasty, J. A synchronized quorum of genetic clocks. *Nature* **463**, 326–330 (2010). URL `http://dx.doi.org/10.1038/nature08753`.

[35] Basu, S., Gerchman, Y., Collins, C. H., Arnold, F. H. & Weiss, R. A synthetic multicellular system for programmed pattern formation. *Nature* **434**, 1130–1134 (2005). URL `http://dx.doi.org/10.1038/nature03461`.

[36] Hillman, N., Sherman, M. I. & Graham, C. The effect of spatial arrangement on cell determination during mouse development. *Development* **28**, 263–278 (1972).

[37] Song, L. *et al.* Structure of staphylococcal alpha -hemolysin, a heptameric transmembrane pore. *Science* **274**, 1859–1865 (1996). URL `http://dx.doi.org/10.1126/science.274.5294.1859`.

[38] Simpson, A. A. *et al.* Structure of the bacteriophage ϕ29 dna packaging motor. *Nature* **408**, 745–750 (2000). URL `http://dx.doi.org/10.1038/35047129`.

[39] Elani, Y., Gee, A., Law, R. V. & Ces, O. Engineering multi-compartment vesicle networks. *Chemical Science* **4**, 3332 (2013). URL `http://dx.doi.org/10.1039/C3SC51164B`.

[40] Elani, Y., Law, R. V. & Ces, O. Protein synthesis in artificial cells: using compartmentalisation for spatial organisation in vesicle bioreactors. *Physical Chemistry Chemical Physics* **17**, 15534–15537 (2015). URL `http://dx.doi.org/10.1039/C4CP05933F`.

[41] Elani, Y., Law, R. V. & Ces, O. Vesicle-based artificial cells as chemical microreactors with spatially segregated reaction pathways. *Nature Communications* **5** (2014). URL `http://dx.doi.org/10.1038/ncomms6305`.

[42] Deng, N.-N., Yelleswarapu, M. & Huck, W. T. S. Monodisperse uni- and multicompartment liposomes. *Journal of the American Chemical Society* **138**, 7584–7591 (2016). URL `http:`

//dx.doi.org/10.1021/jacs.6b02107.

[43] Villar, G., Graham, A. D. & Bayley, H. A tissue-like printed material. *Science* **340**, 48–52 (2013). URL http://dx.doi.org/10.1126/science.1229495.

[44] Bayley, H. *et al.* Droplet interface bilayers. *Molecular BioSystems* **4**, 1191 (2008). URL http://dx.doi.org/10.1039/B808893D.

[45] Krishnan, S. *et al.* Molecular transport through large-diameter dna nanopores. *Nature Communications* **7** (2016). URL http://dx.doi.org/10.1038/ncomms12787.

[46] Wauer, T. *et al.* Construction and manipulation of functional three-dimensional droplet networks. *ACS Nano* **8**, 771–779 (2014). URL http://dx.doi.org/10.1021/nn405433y.

[47] Booth, M. J., Restrepo Schild, V., Box, S. J. & Bayley, H. Light-patterning of synthetic tissues with single droplet resolution. *Scientific Reports* **7** (2017). URL http://dx.doi.org/10.1038/s41598-017-09394-9.

[48] Stanley, C. E. *et al.* A microfluidic approach for high-throughput droplet interface bilayer (dib) formation. *Chemical Communications* **46**, 1620 (2010). URL http://dx.doi.org/10.1039/B924897H.

[49] Eeman, M. & Deleu, M. From biological membranes to biomimetic model membranes. *Biotechnology, Agronomy, Society and Environment* **14**, 719–736 (2010).

[50] psen, J. H., Karlström, G., Mourtisen, O., Wennerström, H. & Zuckermann, M. Phase equilibria in the phosphatidylcholine-cholesterol system. *Biochimica et Biophysica Acta (BBA) - Biomembranes* **905**, 162–172 (1987). URL http://dx.doi.org/10.1016/0005-2736(87)90020-4.

[51] Venkatesan, G. A. *et al.* Adsorption kinetics dictate monolayer self-assembly for both lipid-in and lipid-out approaches to droplet interface bilayer formation. *Langmuir* **31**, 12883–12893 (2015). URL http://dx.doi.org/10.1021/acs.langmuir.5b02293.

[52] Poulin, P. & Bibette, J. Adhesion of water droplets in organic solvent. *Langmuir* **14**, 6341–6343 (1998). URL http://dx.doi.org/10.1021/la9801413.

[53] Thiam, A. R. Adhesive emulsion bilayers under an electric field: From unzipping to fusion. *Physical Review Letters* **107** (2011).

[54] Taylor, G. J. *Improving Droplet Interface Bilayers as Models for Cell Membranes*. Ph.D. thesis, University of Tennessee - Knoxville (2016).

[55] Guiselin, B., Law, J. O., Chakrabarti, B. & Kusumaatmaja, H. Dynamic morphologies and stability of droplet interface bilayers. *Physical Review Letters* **120** (2018).

[56] Almén, M., Nordström, K. J., Fredriksson, R. & Schiöth, H. B. Mapping the human membrane proteome: a majority of the human membrane proteins can be classified according to function and evolutionary origin. *BMC Biology* **7**, 50 (2009). URL http://dx.doi.org/10.1186/1741-7007-7-50.

[57] An, N., Fleming, A. M., Middleton, E. G. & Burrows, C. J. Single-molecule investigation of g-quadruplex folds of the human telomere sequence in a protein nanocavity. *Proceedings of the National Academy of Sciences* **111**, 14325–14331 (2014). URL http://dx.doi.org/10.1073/pnas.1415944111.

[58] Hildebrand, A., Pohl, M. & Bhakdi, S. Staphylococcus aureus alpha-toxin. dual mechanism of binding to target cells. *The Journal of Biological Chemistry* **266**, 17195–17200 (1991).

[59] Benz, R., Janko, K., Boos, W. & Läuger, P. Formation of large, ion-permeable membrane channels by the matrix protein (porin) of escherichia coli. *Biochimica et Biophysica Acta (BBA) - Biomembranes* **511**, 305–319 (1978). URL `http://dx.doi.org/10.1016/0005-2736(78)90269-9`.

[60] Yildiz, Ö., Vinothkumar, K. R., Goswami, P. & Kühlbrandt, W. Structure of the monomeric outer-membrane porin ompg in the open and closed conformation. *The EMBO Journal* **25**, 3702–3713 (2006). URL `http://dx.doi.org/10.1038/sj.emboj.7601237`.

[61] Hwang, W. L., Chen, M., Cronin, B., Holden, M. A. & Bayley, H. Asymmetric droplet interface bilayers. *Journal of the American Chemical Society* **130**, 5878–5879 (2008). URL `http://dx.doi.org/10.1021/ja802089s`.

[62] Schwarzer, T. S., Hermann, M., Krishnan, S., Simmel, F. C. & Castiglione, K. Preparative refolding of small monomeric outer membrane proteins. *Protein Expression and Purification* **132**, 171–181 (2017). URL `http://dx.doi.org/10.1016/j.pep.2017.01.012`.

[63] Filonov, G. S., Moon, J. D., Svensen, N. & Jaffrey, S. R. Broccoli: Rapid selection of an rna mimic of green fluorescent protein by fluorescence-based selection and directed evolution. *Journal of the American Chemical Society* **136**, 16299–16308 (2014). URL `http://dx.doi.org/10.1021/ja508478x`.

[64] Sabatini, G., D. D.d Kreibich, Morimoto, T. & M., A. Mechanisms for the incorporation of proteins in membranes and organelles. *The Journal of Cell Biology* **92**, 1–22 (1982). URL `http://dx.doi.org/10.1083/jcb.92.1.1`.

[65] Eifler, N. *et al.* Cytotoxin clya from escherichia coli assembles to a 13-meric pore independent of its redox-state. *The EMBO Journal* **25**, 2652–2661 (2006). URL `http://dx.doi.org/10.1038/sj.emboj.7601130`.

[66] Soskine, M. *et al.* An engineered clya nanopore detects folded target proteins by selective external association and pore entry. *Nano Letters* **12**, 4895–4900 (2012). URL `http://dx.doi.org/10.1021/nl3024438`.

[67] Franceschini, L., Brouns, T., Willems, K., Carlon, E. & Maglia, G. Dna translocation through nanopores at physiological ionic strengths requires precise nanoscale engineering. *ACS Nano* **10**, 8394–8402 (2016). URL `http://dx.doi.org/10.1021/acsnano.6b03159`.

[68] Bayoumi, M., Bayley, H., Maglia, G. & Sapra, K. T. Multi-compartment encapsulation of communicating droplets and droplet networks in hydrogel as a model for artificial cells. *Scientific Reports* **7** (2017). URL `http://dx.doi.org/10.1038/srep45167`.

[69] Bhakdi, S., Tranum-Jensen, J. & Sziegoleit, A. Mechanism of membrane damage by streptolysin-o. *Infection and Immunity* **47**, 52–60 (1985).

[70] Yasuga, H. *et al.* Logic gate operation by dna translocation through biological nanopores. *PLOS ONE* **11**, e0149667 (2016). URL `http://dx.doi.org/10.1371/journal.pone.0149667`.

[71] Matsuzaki, K., Yoneyama, S. & Miyajima, K. Pore formation and translocation of melittin. *Biophysical Journal* **73**, 831–838 (1997). URL `http://dx.doi.org/10.1016/S0006-3495(97)78115-3`.

[72] Ladokhin, A., Selsted, M. & White, S. Sizing membrane pores in lipid vesicles by leakage of co-encapsulated markers: pore formation by melittin. *Biophysical Journal* **72**, 1762–1766 (1997). URL `http://dx.doi.org/10.1016/S0006-3495(97)78822-2`.

[73] Ghose, A. K., Viswanadhan, V. N. & Wendoloski, J. J. A knowledge-based approach in designing combinatorial or medicinal chemistry libraries for drug discovery. 1. a qualitative and quantitative characterization of known drug databases. *Journal of Combinatorial Chemistry* **1**, 55–68 (1999). URL `http://dx.doi.org/10.1021/cc9800071`.

[74] Petit, J., Meurice, N., Kaiser, C. & Maggiora, G. Softening the rule of five—where to draw the line? *Bioorganic and Medicinal Chemistry* **20**, 5343–5351 (2012). URL `http://dx.doi.org/10.1016/j.bmc.2011.11.064`.

[75] Lipinski, C. A. Rule of five in 2015 and beyond: Target and ligand structural limitations, ligand chemistry structure and drug discovery project decisions. *Advanced Drug Delivery Reviews* **101**, 34–41 (2016). URL `http://dx.doi.org/10.1016/j.addr.2016.04.029`.

[76] URL `https://github.com/cheminfo/openchemlib-js`.

[77] Chalmeau, J., Monina, N., Shin, J., Vieu, C. & Noireaux, V. α-hemolysin pore formation into a supported phospholipid bilayer using cell-free expression. *Biochimica et Biophysica Acta (BBA) - Biomembranes* **1808**, 271–278 (2011). URL `http://dx.doi.org/10.1016/j.bbamem.2010.07.027`.

[78] Paige, J. S., Wu, K. Y. & Jaffrey, S. R. Rna mimics of green fluorescent protein. *Science* **333**, 642–646 (2011). URL `http://dx.doi.org/10.1126/science.1207339`.

[79] Galensowske, N. 3d-printing of interconnected networks of micellular micro-reaction chambers to investigate genetic circuits (2018).

[80] Holden, M. A., Needham, D. & Bayley, H. Functional bionetworks from nanoliter water droplets. *Journal of the American Chemical Society* **129**, 8650–8655 (2007). URL `http://dx.doi.org/10.1021/ja072292a`.

[81] Bindels, D. S. *et al.* mscarlet: a bright monomeric red fluorescent protein for cellular imaging. *Nature Methods* **14**, 53–56 (2016). URL `http://dx.doi.org/10.1038/nmeth.4074`.

[82] Iizuka, R., Yamagishi-Shirasaki, M. & Funatsu, T. Kinetic study of de novo chromophore maturation of fluorescent proteins. *Analytical Biochemistry* **414**, 173–178 (2011). URL `http://dx.doi.org/10.1016/j.ab.2011.03.036`.

[83] Mangan, S., Itzkovitz, S., Zaslaver, A. & Alon, U. The incoherent feed-forward loop accelerates the response-time of the gal system of escherichia coli. *Journal of Molecular Biology* **356**, 1073–1081 (2006). URL `http://dx.doi.org/10.1016/j.jmb.2005.12.003`.

[84] Strovas, T. J., Rosenberg, A. B., Kuypers, B. E., Muscat, R. A. & Seelig, G. Microrna-based single-gene circuits buffer protein synthesis rates against perturbations. *ACS Synthetic Biology* **3**, 324–331 (2014). URL `http://dx.doi.org/10.1021/sb4001867`.

[85] Guo, S. & Murray, R. M. Construction of incoherent feedforward loop circuits in a cell-free system and in cells. *ACS Synthetic Biology* **8**, 606–610 (2019). URL `http://dx.doi.org/10.1021/acssynbio.8b00493`.

[86] Kim, J., White, K. S. & Winfree, E. Construction of an in vitro bistable circuit from synthetic transcriptional switches. *Molecular Systems Biology* **2** (2006). URL `http://dx.doi.org/10.1038/msb4100099`.

[87] Franco, E. *et al.* Timing molecular motion and production with a synthetic transcriptional clock. *PNAS; Proceedings of the National Academy of Sciences* **108**, E784–E793 (2011).

[88] SantaLucia, J. & Hicks, D. The thermodynamics of dna structural motifs. *Annual Review of Biophysics and Biomolecular Structure* **33**, 415–440 (2004). URL `http://dx.doi.org/10.1146/annurev.biophys.32.110601.141800`.

[89] Ouldridge, T. E., Šulc, P., Romano, F., Doye, J. P. K. & Louis, A. A. Dna hybridization kinetics: zippering, internal displacement and sequence dependence. *Nucleic Acids Research* **41**, 8886–8895 (2013). URL `http://dx.doi.org/10.1093/nar/gkt687`.

[90] Srinivas, N. *et al.* On the biophysics and kinetics of toehold-mediated dna strand displacement. *Nucleic Acids Research* **41**, 10641–10658 (2013). URL `http://dx.doi.org/10.1093/nar/gkt801`.

[91] Lesnik, E. A. & Freier, S. M. Relative thermodynamic stability of dna, rna, and dna:rna hybrid duplexes: Relationship with base composition and structure. *Biochemistry* **34**, 10807–10815 (1995). URL `http://dx.doi.org/10.1021/bi00034a013`.

[92] Zadeh, J. N. *et al.* Nupack: Analysis and design of nucleic acid systems. *Journal of Computational Chemistry* **32**, 170–173 (2010). URL `http://dx.doi.org/10.1002/jcc.21596`.

[93] Wang, P. *et al.* Photochemical properties of spinach and its use in selective imaging. *Chemical Science* **4**, 2865 (2013). URL `http://dx.doi.org/10.1039/C3SC50729G`.

[94] Babendure, J. R., Adams, S. R. & Tsien, R. Y. Aptamers switch on fluorescence of triphenylmethane dyes. *Journal of the American Chemical Society* **125**, 14716–14717 (2003). URL `http://dx.doi.org/10.1021/ja037994o`.

[95] Chang, J. B. & Ferrell Jr, J. E. Mitotic trigger waves and the spatial coordination of the xenopus cell cycle. *Nature* **500**, 603–607 (2013). URL `http://dx.doi.org/10.1038/nature12321`.

[96] Paige, J. S., Nguyen-Duc, T., Song, W. & Jaffrey, S. R. Fluorescence imaging of cellular metabolites with rna. *Science* **335**, 1194–1194 (2012). URL `http://dx.doi.org/10.1126/science.1218298`.

[97] Eldar, A. & Elowitz, M. B. Functional roles for noise in genetic circuits. *Nature* **467**, 167–173 (2010). URL `http://dx.doi.org/10.1038/nature09326`.

[98] Carignano, A., Mukherjee, S., Singh, A. & Seelig, G. Extrinsic noise suppression in micro rna mediated incoherent feedforward loops. *bioRxiv* (2018).

[99] Averbukh, I., Lai, S.-L., Doe, C. Q. & Barkai, N. A repressor-decay timer for robust temporal patterning in embryonic drosophila neuroblast lineages. *eLife* **7** (2018). URL `http://dx.doi.org/10.7554/eLife.38631`.

[100] Samoilov, M. S., Price, G. & Arkin, A. P. From fluctuations to phenotypes: The physiology of noise. *Science's STKE* **2006**, re17–re17 (2006). URL `http://dx.doi.org/10.1126/stke.3662006re17`.

[101] Elowitz, M. B., Levine, A. J., D., S. E. & S., S. P. Stochastic gene expression in a single cell. *Science*

297, 1183–1186 (2002). URL `http://dx.doi.org/10.1126/science.1070919`.

[102] Losick, R. & Desplan, C. Stochasticity and cell fate. *Science* **320**, 65–68 (2008). URL `http://dx.doi.org/10.1126/science.1147888`.

[103] Ozbudak, E. M., Thattai, M., Lim, H. N., Shraiman, B. I. & van Oudenaarden, A. Multistability in the lactose utilization network of escherichia coli. *Nature* **427**, 737–740 (2004). URL `http://dx.doi.org/10.1038/nature02298`.

[104] Solovyev, V. & Salamov, A. *Automatic Annotation of Microbial Genomes and Metagenomic Sequences. In Metagenomics and its Applications in Agriculture, Biomedicine and Environmental Studies* (Nova Science Publishers, 2011).

[105] Caschera, F. & Noireaux, V. Synthesis of 2.3 mg/ml of protein with an all escherichia coli cell-free transcription–translation system. *Biochimie* **99**, 162–168 (2014). URL `http://dx.doi.org/10.1016/j.biochi.2013.11.025`.

[106] Coppey, M., Boettiger, A. N., Berezhkovskii, A. M. & Shvartsman, S. Y. Nuclear trapping shapes the terminal gradient in the drosophila embryo. *Current Biology* **18**, 915–919 (2008). URL `http://dx.doi.org/10.1016/j.cub.2008.05.034`.

[107] Gregor, T., Wieschaus, E. F., McGregor, A. P., Bialek, W. & Tank, D. W. Stability and nuclear dynamics of the bicoid morphogen gradient. *Cell* **130**, 141–152 (2007). URL `http://dx.doi.org/10.1016/j.cell.2007.05.026`.

[108] Gregor, T., Bialek, W., van Steveninck, R. R. d. R., Tank, D. W. & Wieschaus, E. F. Diffusion and scaling during early embryonic pattern formation. *Proceedings of the National Academy of Sciences* **102**, 18403–18407 (2005). URL `http://dx.doi.org/10.1073/pnas.0509483102`.

[109] Tkacik, G., Dubuis, J. O., Petkova, M. D. & Gregor, T. Positional information, positional error, and readout precision in morphogenesis: A mathematical framework. *Genetics* **199**, 39–59 (2014). URL `http://dx.doi.org/10.1534/genetics.114.171850`.

[110] Papatsenko, D. & Levine, M. The drosophila gap gene network is composed of two parallel toggle switches. *PLoS ONE* **6**, e21145 (2011). URL `http://dx.doi.org/10.1371/journal.pone.0021145`.

[111] Jaeger, J. The gap gene network. *Cellular and Molecular Life Sciences* **68**, 243–274 (2010). URL `http://dx.doi.org/10.1007/s00018-010-0536-y`.

[112] Cotterell, J. & Sharpe, J. An atlas of gene regulatory networks reveals multiple three-gene mechanisms for interpreting morphogen gradients. *Molecular Systems Biology* **6** (2010). URL `http://dx.doi.org/10.1038/msb.2010.74`.

[113] Schaerli, Y. *et al.* A unified design space of synthetic stripe-forming networks. *Nature Communications* **5** (2014). URL `http://dx.doi.org/10.1038/ncomms5905`.

[114] Shilo, B.-Z. & Barkai, N. Buffering global variability of morphogen gradients. *Developmental Cell* **40**, 429–438 (2017). URL `http://dx.doi.org/10.1016/j.devcel.2016.12.012`.

[115] Garcia, H. G., Tikhonov, M., Lin, A. & Gregor, T. Quantitative imaging of transcription in living drosophila embryos links polymerase activity to patterning. *Current Biology* **23**, 2140–2145 (2013).

URL http://dx.doi.org/10.1016/j.cub.2013.08.054.

[116] Shen, Y., Chen, Y., Wu, J., Shaner, N. C. & Campbell, R. E. Engineering of mcherry variants with long stokes shift, red-shifted fluorescence, and low cytotoxicity. *PLOS ONE* **12**, e0171257 (2017). URL http://dx.doi.org/10.1371/journal.pone.0171257.

[117] Pédelacq, J.-D., Cabantous, S., Tran, T., Terwilliger, T. C. & Waldo, G. S. Engineering and characterization of a superfolder green fluorescent protein. *Nature Biotechnology* **24**, 79–88 (2005). URL http://dx.doi.org/10.1038/nbt1172.

[118] Hardman, A. M., Stewart, G. S., Williams, P., Williams, P. & Williams, P. Quorum sensing and the cell-cell communication dependent regulation of gene expression in pathogenic and non-pathogenic bacteria. *Antonie van Leeuwenhoek* **74**, 199–210 (1998). URL http://dx.doi.org/10.1023/A:1001178702503.

[119] Weitz, M. *et al.* Communication and computation by bacteria compartmentalized within microemulsion droplets. *Journal of the American Chemical Society* **136**, 72–75 (2013). URL http://dx.doi.org/10.1021/ja411132w.

[120] URL {http://parts.igem.org/Ribosome_Binding_Sites/Prokaryotic/Constitutive/Community_Collection}.

[121] URL https://www.denovodna.com/software/.

[122] Karig, D. *et al.* Stochastic turing patterns in a synthetic bacterial population. *PNAS; Proceedings of the National Academy of Sciences* **115**, 6572–6577 (2018).

[123] Nielsen, A. A. K. *et al.* Genetic circuit design automation. *Science* **352**, aac7341–aac7341 (2016). URL http://dx.doi.org/10.1126/science.aac7341.

[124] Heylighen, F. The growth of structural and functional complexity during evolution. *The Evolution of Complexity* (1999). URL http://citeseerx.ist.psu.edu/viewdoc/summary?doi=10.1.1.161.5859.

[125] Szathmáry, E. & Smith, J. M. The major evolutionary transitions. *Nature* **374**, 227–232 (1995). URL http://dx.doi.org/10.1038/374227a0.

[126] McShea, D. W. Complexity and evolution: What everybody knows. *Biology and Philosophy* **6**, 303–324 (1991). URL http://dx.doi.org/10.1007/BF00132234.

[127] Dupré, M. A., John; O'Malley. Varieties of living things: Life at the intersection of lineage and metabolism. *Philosophy and Theory in Biology* **1** (2009). URL http://hdl.handle.net/2027/spo.6959004.0001.003.

[128] Balagaddé, F. K. *et al.* A synthetic escherichia coli predator–prey ecosystem. *Molecular Systems Biology* **4** (2008). URL http://dx.doi.org/10.1038/msb.2008.24.

[129] Chen, Y., Kim, J. K., Hirning, A. J., Josi, K. & Bennett, M. R. Emergent genetic oscillations in a synthetic microbial consortium. *Science* **349**, 986–989 (2015). URL http://dx.doi.org/10.1126/science.aaa3794.

[130] Weber, W., Daoud-El Baba, M. & Fussenegger, M. Synthetic ecosystems based on airborne inter-

and intrakingdom communication. *PNAS; Proceedings of the National Academy of Sciences* **104**, 10435–10440 (2007).

[131] Chuang, J. S., Rivoire, O. & Leibler, S. Simpson's paradox in a synthetic microbial system. *Science* **323**, 272–275 (2009). URL `http://www.jstor.org/stable/20402823`.

[132] Kong, W., Meldgin, D. R., Collins, J. J. & Lu, T. Designing microbial consortia with defined social interactions. *Nature Chemical Biology* **14**, 821–829 (2018). URL `http://dx.doi.org/10.1038/s41589-018-0091-7`.

[133] Scott, S. R. & Hasty, J. Quorum sensing communication modules for microbial consortia. *ACS Synthetic Biology* **5**, 969–977 (2016). URL `http://dx.doi.org/10.1021/acssynbio.5b00286`.

[134] Halleran, A. D. & Murray, R. M. Cell-free and in vivo characterization of lux, las, and rpa quorum activation systems in e. coli. *ACS Synthetic Biology* **7**, 752–755 (2017). URL `http://dx.doi.org/10.1021/acssynbio.7b00376`.

[135] Grant, P. K. *et al.* Orthogonal intercellular signaling for programmed spatial behavior. *Molecular Systems Biology* **12**, 849–849 (2016). URL `http://dx.doi.org/10.15252/msb.20156590`.

[136] Scheidler, C., Sobotta, J., Eisenreich, W., Wächtershäuser, G. & Huber, C. Unsaturated c3,5,7,9-monocarboxylic acids by aqueous, one-pot carbon fixation: Possible relevance for the origin of life. *Scientific Reports* **6** (2016). URL `http://dx.doi.org/10.1038/srep27595`.

[137] Rieß, B. *et al.* Dissipative assemblies that inhibit their deactivation. *Soft Matter* **14**, 4852–4859 (2018). URL `http://dx.doi.org/10.1039/C8SM00822A`.

[138] Schwarz-Schilling, M. *et al.* Optimized assembly of a multifunctional rna-protein nanostructure in a cell-free gene expression system. *Nano Letters* **18**, 2650–2657 (2018). URL `http://dx.doi.org/10.1021/acs.nanolett.8b00526`.

[139] Abudayyeh, O. O. *et al.* C2c2 is a single-component programmable rna-guided rna-targeting crispr effector. *Science* **353**, aaf5573 (2016). URL `http://dx.doi.org/10.1126/science.aaf5573`.

[140] Gootenberg, J. S. *et al.* Nucleic acid detection with crispr-cas13a/c2c2. *Science* **356**, 438–442 (2017). URL `http://dx.doi.org/10.1126/science.aam9321`.

[141] Sun, Z. Z. *et al.* Protocols for implementing an escherichia coli based tx-tl cell-free expression system for synthetic biology. *Journal of Visualized Experiments* (2013). URL `http://dx.doi.org/10.3791/50762`.

[142] Joesaar, A. *et al.* Dna-based communication in populations of synthetic protocells. *Nature Nanotechnology* **14**, 369–378 (2019). URL `http://dx.doi.org/10.1038/s41565-019-0399-9`.

[143] Peters, R. J. R. W. *et al.* Cascade reactions in multicompartmentalized polymersomes. *Angewandte Chemie International Edition* **53**, 146–150 (2013). URL `http://dx.doi.org/10.1002/anie.201308141`.

[144] Mandal, D., Nasrolahi Shirazi, A. & Parang, K. Self-assembly of peptides to nanostructures. *Org. Biomol. Chem.* **12**, 3544–3561 (2014). URL `http://dx.doi.org/10.1039/C4OB00447G`.

[145] Vauthey, S., Santoso, S., Gong, H., Watson, N. & Zhang, S. Molecular self-assembly of surfactant-

like peptides to form nanotubes and nanovesicles. *Proceedings of the National Academy of Sciences* **99**, 5355–5360 (2002). URL `http://dx.doi.org/10.1073/pnas.072089599`.

[146] Zhang, S., Holmes, T., Lockshin, C. & Rich, A. Spontaneous assembly of a self-complementary oligopeptide to form a stable macroscopic membrane. *Proceedings of the National Academy of Sciences* **90**, 3334–3338 (1993). URL `http://dx.doi.org/10.1073/pnas.90.8.3334`.

[147] Huber, M. C. *et al.* Designer amphiphilic proteins as building blocks for the intracellular formation of organelle-like compartments. *Nature Materials* **14**, 125–132 (2014). URL `http://dx.doi.org/10.1038/nmat4118`.

[148] Holowka, E. P., Pochan, D. J. & Deming, T. J. Charged polypeptide vesicles with controllable diameter. *Journal of the American Chemical Society* **127**, 12423–12428 (2005). URL `http://dx.doi.org/10.1021/ja053557t`.

[149] Vogele, K. *et al.* Towards synthetic cells using peptide-based reaction compartments. *Nature Communications* **9** (2018). URL `http://dx.doi.org/10.1038/s41467-018-06379-8`.

[150] Prindle, A. *et al.* Rapid and tunable post-translational coupling of genetic circuits. *Nature* **508**, 387–391 (2014). URL `http://dx.doi.org/10.1038/nature13238`.

[151] Andersen, J. B. *et al.* New unstable variants of green fluorescent protein for studies of transient gene expression in bacteria. *Applied and Environmental Microbiology* **64**, 2240–2246 (1998).

[152] Cameron, D. E. & Collins, J. J. Tunable protein degradation in bacteria. *Nature Biotechnology* **32**, 1276–1281 (2014). URL `http://dx.doi.org/10.1038/nbt.3053`.

[153] Wong, W. W., Tsai, T. Y. & Liao, J. C. Single-cell zeroth-order protein degradation enhances the robustness of synthetic oscillator. *Molecular Systems Biology* **3** (2007). URL `http://dx.doi.org/10.1038/msb4100172`.

[154] Meyer, A. J., Ellefson, J. W. & Ellington, A. D. Directed evolution of a panel of orthogonal t7 rna polymerase variants for in vivo or in vitro synthetic circuitry. *ACS Synthetic Biology* **4**, 1070–1076 (2014). URL `http://dx.doi.org/10.1021/sb500299c`.

[155] Shimizu, Y. *et al.* Cell-free translation reconstituted with purified components. *Nature Biotechnology* **19**, 751–755 (2001). URL `http://dx.doi.org/10.1038/90802`.

[156] Nguyen, A. W. & Daugherty, P. S. Evolutionary optimization of fluorescent proteins for intracellular fret. *Nature Biotechnology* **23**, 355–360 (2005). URL `http://dx.doi.org/10.1038/nbt1066`.

[157] Ai, H.-w., Henderson, J. N., Remington, S. J. & Campbell, R. E. Directed evolution of a monomeric, bright and photostable version ofclavulariacyan fluorescent protein: structural characterization and applications in fluorescence imaging. *Biochemical Journal* **400**, 531–540 (2006). URL `http://dx.doi.org/10.1042/BJ20060874`.

[158] Campbell, R. E. *et al.* A monomeric red fluorescent protein. *Proceedings of the National Academy of Sciences* **99**, 7877–7882 (2002). URL `http://dx.doi.org/10.1073/pnas.082243699`.

[159] URL `{http://parts.igem.org/Help:Plasmid_backbones/Nomenclature}`.

[160] Lentini, R. *et al.* Integrating artificial with natural cells to translate chemical messages that direct e.

coli behaviour. *Nature Communications* **5** (2014). URL http://dx.doi.org/10.1038/ncomms5012.

[161] Sun, Z. Z., Yeung, E., Hayes, C. A., Noireaux, V. & Murray, R. M. Linear dna for rapid prototyping of synthetic biological circuits in an escherichia coli based tx-tl cell-free system. *ACS Synthetic Biology* **3**, 387–397 (2014). URL http://dx.doi.org/10.1021/sb400131a.

[162] Court, R., Cook, N., Saikrishnan, K. & Wigley, D. The crystal structure of λ-gam protein suggests a model for recbcd inhibition. *Journal of Molecular Biology* **371**, 25–33 (2007). URL http://dx.doi.org/10.1016/j.jmb.2007.05.037.

[163] Famulok, M. Oligonucleotide aptamers that recognize small molecules. *Current Opinion in Structural Biology* **9**, 324–329 (1999). URL http://dx.doi.org/10.1016/S0959-440X(99)80043-8.

[164] Warner, K. D. *et al.* Structural basis for activity of highly efficient rna mimics of green fluorescent protein. *Nature Structural and Molecular Biology* **21**, 658–663 (2014). URL http://dx.doi.org/10.1038/nsmb.2865.

[165] Jepsen, M. D. E. *et al.* Development of a genetically encodable fret system using fluorescent rna aptamers. *Nature Communications* **9** (2018). URL http://dx.doi.org/10.1038/s41467-017-02435-x.

[166] Challita, E. J., Najem, J. S., Monroe, R., Leo, D. J. & Freeman, E. C. Encapsulating networks of droplet interface bilayers in a thermoreversible organogel. *Scientific Reports* **8** (2018). URL http://dx.doi.org/10.1038/s41598-018-24720-5.

[167] Gatti-Lafranconi, P., Dijkman, W. P., Devenish, S. R. & Hollfelder, F. A single mutation in the core domain of the lac repressor reduces leakiness. *Microbial Cell Factories* **12**, 67 (2013). URL http://dx.doi.org/10.1186/1475-2859-12-67.

[168] Karig, D. K., Iyer, S., Simpson, M. L. & Doktycz, M. J. Expression optimization and synthetic gene networks in cell-free systems. *Nucleic Acids Research* **40**, 3763–3774 (2011). URL http://dx.doi.org/10.1093/nar/gkr1191.

[169] Gibson, D. G. *et al.* Enzymatic assembly of dna molecules up to several hundred kilobases. *Nature Methods* **6**, 343–345 (2009). URL http://dx.doi.org/10.1038/nmeth.1318.

[170] Engler, C., Gruetzner, R., Kandzia, R. & Marillonnet, S. Golden gate shuffling: A one-pot dna shuffling method based on type iis restriction enzymes. *PLoS ONE* **4**, e5553 (2009). URL http://dx.doi.org/10.1371/journal.pone.0005553.

[171] Kelly, C. L. *et al.* Synthetic chemical inducers and genetic decoupling enable orthogonal control of the rhabad promoter. *ACS Synthetic Biology* **5**, 1136–1145 (2016). URL http://dx.doi.org/10.1021/acssynbio.6b00030.

[172] Kapsner, K. *Biomolekulare Reaktionsysteme in Mikrokompartimenten*. Ph.D. thesis, Technische Universität München (2015).

[173] (2015). URL https://github.com/kkapsner/Matlab/tree/master/classes/%2BFit/%40Scharfit.

List of publications

Over the course of this work contributions to the following publications were made:

1. **Dupin A.**, Simmel F. C., Signalling and differentiation in multi-compartmentalized in vitro gene circuits. *Nature Chemistry* **11**, 32-39 (2019).

2. Schwarz-Schilling M., **Dupin A.**, Chizzolini F., Krishnan S., Mansy S. S., Simmel F. C., Optimized Assembly of a Multifunctional RNA-Protein Nanostructure in a Cell-Free Gene Expression System. *Nano Letters* **18**, 2650?2657 (2018).

3. Katzmeier F., Aufinger L., **Dupin A.**, Quinteiro J., Lenz M., Bauer L., Klumpe S., Sherpa D., Dürr B., Honemann M., Styazhkin I., Simmel F. C., Heymann M., A low-cost fluorescence reader for in vitro transcription and nucleic acid detection with Cas13a. *in revision* (2019).

A Appendix

A.1 Models

General considerations regarding modelling of diffusion and reaction in our artificial multicellular assemblies (AMA) are addressed in Chapter 1.1.1 and Chapter 2.3.2. Specific reaction models are described below, as well as how statistical calculations were conducted.

Transcription

We model transcription and aptamer/ligand binding with the following reactions. R is the RNA, Lig is the ligand.

$$\emptyset \xrightarrow{k_{prod}} R \tag{A.1}$$

$$R + Lig \underset{k_m}{\overset{k_p}{\rightleftharpoons}} RLig \tag{A.2}$$

RNA degradation is neglected here because it is not significant on the timescale of the experiments. We assume that binding of T7 RNAP to DNA is fast and estimate RNA production from the equilibrium concentration of the DNA-RNAP complex $[DNA \cdot Pol]_{eq}$, which is given by:

$$\begin{aligned}[DNA \cdot Pol]_{eq} =& \frac{1}{2}([DNA]_{tot} + [Pol]_{tot} + K_d \\ & - \sqrt{([DNA]_{tot} + [Pol]_{tot} + K_d)^2 - 4\,[DNA]_{tot}\,[Pol]_{tot}})\end{aligned} \tag{A.3}$$

with $[D]_{tot}$: total concentration of DNA template, $[P]_{tot}$: total concentration of T7 RNA polymerase and K_d: their dissociation constant. In Equation AA.1, k_{prod} is simply proportional to $[DNA \cdot Pol]_{eq}$ and can be estimated from bulk experiments.

Transcription-translation

We model transcription-translation when induced by a chemical I, which binds a regulatory protein to activate transcription from the DNA template D. The nascent fluorescent protein

is denoted by G and the maturated protein G_{mat}. This model is adapted from [2].

$$\frac{d\,[I]}{dt} = -\frac{[I]}{K+[I]} \tag{A.4}$$

$$\frac{d\,[D_{activated}]}{dt} = \frac{[I]}{K+[I]} \tag{A.5}$$

$$\frac{d\,[G]}{dt} = \alpha_{max}(1-e^{-\frac{t}{t_2}})\frac{[D_{activated}]^n}{K_d^n+[D_{activated}]^n} - \frac{[G]}{t_{mat}} \tag{A.6}$$

$$\frac{[G_{mat}]}{dt} = \frac{[G]}{t_{mat}} \tag{A.7}$$

Equations AA.4 and AA.5 describe binding of the inducer to the repressor or activator protein with a dissociation constant K, which leads to a proportional activation of the promoter. As the inducer is usually the diffusing chemical, Equation AA.4 allows to account for the absence of diffusion of the chemical once it is bound to its corresponding protein. In Equation AA.6, α_{max} is a factor to account for the efficiency of the cell extract, which can vary from batch to batch. However, in our experiments it was found to always converge to ≈ 0.0033 when fitted. t_2 is the lifetime of the RNA, which is typically 15 min in the cell extract used [29]. Protein expression is modelled via a Hill function involving the concentration of the activated promoter, with dissociation constant K_d and cooperativity n. t_{mat} is the protein maturation time.

It should be noted that this model does not account for resource depletion, and is therefore only valid for the beginning of the reaction (ranging from 1 hour to 3 hours, depending on the rate of expression and the maturation time of the protein). The model also does not account for leaky expression in the absence of inducer.

Signalling pulse

In the signalling pulse circuit (Chapter 3.2), diffusion was modelled as described above and reactions were modelled as follows, with F the DFHBI, R the Spinach RNA bound to the ssDNA activator, RF the bound Spinach-DFHBI aptamer, A the activated repressor DNA template, and $antiR$ the RNA transcribed from the repressor template. The concentrations of the ssDNA activator and the incomplete repressor DNA template are not explicitly described, as the incomplete repressor is inactive and the ssDNA activator is either bound to the Spinach RNA or to the template (both of these components are in excess compared to the activator). Values for kinetic rates are estimated in Chapter 3.2.

$$\frac{d\,[F]}{dt} = -k_{1p}\,[F]\,[R] + [RF]\,(k_{1m}\,[A] + k_3\,[antiR]) \tag{A.8}$$

$$\frac{d\,[R]}{dt} = -k1p\,[F]\,[R] + k_{1m}\,[RF]\,[A] \tag{A.9}$$

$$\frac{d\,[RF]}{dt} = k_{1p}\,[F]\,[R] - [RF]\,(k_{1m}\,[A] + k_3\,[antiR]) \tag{A.10}$$

$$\frac{d\,[A]}{dt} = k_{1p}\,[F]\,[R] - k_{1m}\,[RF]\,[A] + k_3\,[RF]\,[antiR] \tag{A.11}$$

$$\frac{d\,[antiR]}{dt} = k_2\,[A] - k_3\,[RF]\,[antiR] \tag{A.12}$$

Statistics

For all calculations of the mean μ and the standard deviation σ for a set of N data points x_i, we used the following formula, applying Bessel's correction:

$$\mu = \frac{1}{N}\sum_{i=1}^{N} x_i \tag{A.13}$$

$$\sigma = \sqrt{\frac{1}{N-1}\sum_{i=1}^{N} |x_i - \mu|^2} \tag{A.14}$$

A.2 Materials

Materials are listed as in [3], and supplementary materials are added where necessary.

The following chemicals were purchased from Sigma-Aldrich (Germany): hexadecane #296317, silicone oil AR20 #10836, α-Hemolysin #H9395, $MgCl_2$ (1M) #63069, arabinose #A3256, rhamnose #R3875, isopropyl β-D-1-thiogalactoside (IPTG) #I6758, N-(β-Ketocaproyl)-L-homoserine lactone (3OC6-HSL) #K3007, N-(3-Oxododecanoyl)-L-homoserine lactone (3OC12-HSL) #O9139, anhydrotetracycline (aTc) #37919, Triton X-100 #X100, Na_2HPO_4 #RES20908, KH_2PO_4 #1551139, NH_4Cl #A9434, Malachite Green #38800, Atto488 #41051, Atto633 #18620, 2-mercaptoethanol (β-ME) #M6250, Sample Buffer Laemmli 2x Concentration #S3401, lysozyme from chicken egg white #L6876, S-Adenosyl-L-homocysteine (SAH) #1012112, S-Adenosyl-L-methionine (SAM) #A7007, adenosine 5'-triphosphate (ATP) #A2383, cytidine 5'-triphosphate (CTP) #C1506, guanosine 5'-triphosphate (GTP) #G8877, uridine 5'-triphosphate #94370, theophylline #T1633, Bovine Serum Albumin (BSA) #A9418, tetramethylrodhamine ethyl ester (TMRE) #87917, low-melting agarose #A9414, sorbitol #S1876, riboflavin 5'-monophosphate (FMN) #F2253, maltose #47288, maltodextrin #419672, adenosine 5'-monophosphate (AMP) #01930, adenosine 5'-diphosphate (ADP) #A2754, guanosine #G6752 and ammonium persulfate (APS) #A3678.

The following chemicals were purchased from Carl Roth (Germany): KCl #P017, nuclease-free water (nf H_2O) #T143, lactose #8921, Roti-Aqua-P/C/I (phenol, chloroform, isoamyl alcohol) #X985, chloroform #3313, ethanol #P076, urea #2317, 10x TBE Buffer #3061, acrylamide #A121, TEMED #2367, agarose #2267, Tris.HCl #9090, NaCl #0962, glycerol #3783, LB Medium #X968, SOB Medium #AE27, LB-Agar #X969, carbenicillin #6344, kanamycin #T832, chloramphenicol #3886, $MgSO_4$ #0682, $CaCl_2$ #A119, glucose #7509, casein hydrolysate (caseinh) #A157, Rotiphorese 10x SDS-PAGE Buffer #3060, Roti-Blue quick 1x solution #4829, agarose #2267, 50x TAE Buffer #CL86, methanol #8388 and thiamine #T911.

The following chemicals and enzymes were purchased from New England Biolabs (NEB, USA): RNAPol Reaction Buffer #M0251, Ribonucleotide Solution Mix #N0466L, DNase I Reaction Buffer #M0303, RNase Inhibitor Murine #M0314, Pyrophosphatase Inorganic (*E. coli*) #M0361, DNase I #M0303, Color Prestained Protein Standard Broad Range (10-250 kDa) #P7719, Phusion High-Fidelity PCR 2X Master Mix #M0531, Q5 High-Fidelity 2X Master Mix #M0492, DpnI #R0176, CutSmart Buffer #B7204, Monarch PCR & DNA Cleanup Kit #T1030, T4 DNA Ligase and Buffer #M0202, T4 Polynucleotide Kinase #M0201, NEB Turbo Competent *E. coli* #C2984H, OneTaq 2x Master Mix with Standard Buffer #M0482, Gel Loading Dye Purple (6X) #B7024, 1

kb Plus DNA Ladder #N3200, Antarctic Phosphatase and buffer #M0289, low molecular weight DNA ladder #N3233, PURExpress *in vitro* protein synthesis kit #E6800, *E. coli* RNA Polymerase Holoenzyme and buffer #M0551 and T7 RNA Polymerase #M0251.

The following chemicals were purchased from Thermo Fisher Scientific (USA): guanine #AC12025, 2,4-diacetylphloroglucinol (DAPG) #AC45280, RNA Gel Loading Dye (2X) #R0641, SybR Green II #S7586, SybR Gold #S11494, RiboRuler Low Range RNA Ladder #SM1831, tetracycline #AAB2140822, doxycycline #J63805 and EDTA (0.5M, pH 8.0) #AM9260G.

The following chemicals were purchased from Avanti Polar Lipids (USA): DPhPC (4ME 16:0 PC) #850356, DOPC (18:1 (Δ9-Cis) PC) #850375, DOPG (18:1 (Δ9-Cis) PG) #840475 and cholesterol (20α-hydroxycholesterol) #700156.

DFHBI #410 was purchased from Lucerna Technologies (USA).

The following chemicals were purchased from Bio-rad (USA): precast polyacrylamide gel 4-20% Mini-PROTEAN TGX Stain-Free Protein Gels #4568095, Microseal® 'B' PCR Plate Sealing Film #MSB1001 and Silver Stain Plus Kit #1610449.

DNA was purchased from Biomers (Germany) or Eurofins (Germany) (single-stranded oligos), or from IDT (USA) (double-stranded gBlocks).

Additionally, T7 RNA Polymerase, LacI, TetR, dCas9 and gamS were expressed and purified in our lab according to standard His-tag nickel purification protocols with Ni-NTA beads, by Dr. Sandra Sagredo (T7 RNA Polymerase), PhD student Elisabeth Falgenhauer (LacI and TetR), Dr. Andrea Mückl and student Katrin Fischer (dCas9), and student Ludwig Bauer (gamS) (with specific buffers for T7 RNA Polymerase [154], LacI [167], TetR [168], and gamS [161]).

JW0336 cells were a gift from Dr. Jürgen Lassak.

A.3 Methods

Methods are described as in [3], and supplementary details and methods are added where necessary. For experiments were conditions differ from the usual protocols, specific experimental conditions are listed at the end of this Appendix.

DNA template assembly

Linear DNA templates for transcription are assembled as follows. ssDNA template and non-template strands are mixed at 5 µM each with 1x RNAPol Reaction Buffer in nf H_2O (total volume 100 µL), in a DNA LoBind Tube (Eppendorf, Germany). The sample is heated at 95 °C for 3 minutes, and then slowly cooled down at a rate of - 1 °C.min^{-1}, until reaching 20 °C. This allows for the two strands to fully anneal into a double-stranded (dsDNA) template.

RNA production

Purified RNA was obtained as follows. 200 nM of the dsDNA template was mixed with 15 mM $MgCl_2$, 125 mM KCl, 4 mM each rNTP, 1x RNAPol Reaction Buffer, 0.4 U.µL^{-1} RNAse Inhibitor, 0.001 U.µL^{-1} Pyrophosphatase and 400 nM T7 RNA Polymerase in nf H_2O (total volume 100 µL) in a Protein LoBind Tube (Eppendorf, Germany). The sample is incubated at 37 °C for at least 4

h, up to overnight. After the transcription, 1x DNAseI Buffer and 0.035 U.µL^{-1} DNAseI are added, and the sample is further incubated at 37 °C for 30 min, up to 1 h, to digest the DNA template. The RNA is then extracted following a phenol-chloroform extraction protocol in a 5'-Phase Lock Gel Heavy (VWR, USA), and precipitated with ethanol. The RNA is resuspended in nf H_2O and stored up to 6 months at -80 °C. RNA concentration is measured by denaturing PAGE gel. The gel consists of 8 M urea, 1x TBE Buffer, 15 % (v/v) Acrylamide 29:1, 0.1 % (v/v) TEMED, 0.1 % (w/v) APS, in double-distilled H_2O (total volume 10 mL). The gel is cast in cassettes (Bolt Empty Mini, Thermo Fisher Scientific, USA), and the running buffer is 1x TBE. The gel is pre-run for 30 min at 12.5 V.cm^{-1} with a running temperature of 40 °C. The RNA samples are mixed with 2x RNA loading dye, denatured at 95 °C for 5 min and directly put on ice to prevent the RNA from refolding. The samples are loaded unto the gel and run at 12.5 V.cm^{-1} for 1 h 15 min at 40 °C. The gel is stained with 1x SybR Green II, a fluorescence image of the gel is acquired, and the intensity of the RNA band is quantified against an RNA ladder (low Range Riboruler) with ImageJ.

In vitro transcription was carried out with 1x RNAPol Buffer, 125 mM KCl, 15 mM $MgCl_2$, 4mM each rNTP, between 100 nM and 200 nM dsDNA template, and either 4 U.µL^{-1} (NEB) or 400 nM T7 RNA Polymerase. Osmolarity between droplets was balanced with a glycerol buffer identical to the storage buffer of T7 RNA Polymerase (5 mM Tris.HCl, 100 mM NaCl, 20 mM β-ME, 1 mM EDTA, 50 % (v/v) glycerol, 0.1 % (v/v) Triton X-100, pH 7.9 at 25 °C).

Native PAGE gel

Complex formation between DNA and RNA strands was assessed with native PAGE gels. The gel consists of 1x TBE Buffer, 10 % (v/v) Acrylamide 29:1, 0.1 % (v/v) TEMED, 0.1 % (w/v) APS, in double-distilled H_2O (total volume 10 mL). The gel is cast in cassettes (Bolt Empty Mini, Thermo Fisher Scientific, USA), and the running buffer is 1x TBE. The samples are preincubated at 37 °C and mixed with 6x purple loading dye. The gel is run at 12.5 V.cm^{-1} for 1 h 15 min and stained with 1x SybR Gold. The bands are compared to a low molecular weight DNA ladder.

Cloning and plasmid purification

All plasmids were cloned using standard strategies and NEB enzymes. Specifically, we alternatively used digestion/ligation, Gibson assembly [169], Golden Gate assembly [170] or PCR with 5'-phosphated primers followed by ligation. The plasmids were transformed into the bacterial strains DH5α, Turbo (NEB, USA, #C2984I) or BW27783. All constructs were cloned in the plasmid backbones pSB1A3, pSB1C3, pSB3C5 or pSB4A5, except for *pCK301* (gift from John Heap, Addgene plasmid #87767 [171]), *pPhlF-P2* (gift from Christopher Voigt, Addgene plasmid #74686 [123]) and *pBAD33-dsRedmut*. The cloned bacteria were stored in glycerol stocks: an overnight culture in LB medium was mixed with glycerol to a final concentration of 25 % (v/v) glycerol and stored at -80 °C. To ensure that the glycerol stocks contained a monoclonal population with the correct sequence of the plasmids, an overnight culture was grown in LB medium from the glycerol stock, Mini-prepped (QIAprep Spin Miniprep Kit, Qiagen, Netherlands) and sequenced (Sanger sequencing, LightRun, GATC Biotech, Germany or TubeSeq, Eurofins, Germany). Plasmids were purified prior to use in cell-extract by Miniprep followed by phenol-chloroform extraction, or by Midiprep (NucleoBond Xtra Midi, Macherey-Nagel, Germany).

The best practice for cloning, optimized during the thesis, is as follows. Preferred cloning methods are overhang PCR (suitable for changing small fragments, such as changing a promoter, a RBS or a degradation tag) and digestion-ligation (for all cloning of large DNA sequences such as whole genes). However, if the appropriate digestion sites cannot be found to clone with digestion-ligation, Golden Gate assembly is preferred over Gibson assembly (the use of specific digestion enzymes, as in Golden Gate, was found to be more reliable than the exonuclease degradation of a random nucleotides length involved in Gibson). Cloning workflows for overhang PCR and

digestion-ligation are listed below.

Overhang PCR

- primer design: primers sequence should flank the region were the insertion/deletion/sequence replacement is occurring as close as possible. Primers-overhang will contain the region to be inserted or replaced (for deletion, no overhang is necessary): if this is below 30 nucleotides (nt), the overhang can be carried by one primer, otherwise it should be split more or less equally between the forward and reverse primers. It should be verified that primers are not partially complementary to sequences on the plasmid other than the one designed, and complementary of the 3'- end should be particularly avoided (this verification is done with Benchling (http://benchling.com), with full primer sequence). The primers should have no secondary structure at the annealing temperature, and should not form duplexes with themselves or with the other primer (this is verified with Nupack [92], with the full primer sequence). The annealing temperature for the PCR is calculated based on the NEB Tm Calculator tool (http://tmcalculator.neb.com/#!/main) with only the part of the primer that binds the template (not the overhang).

- PCR: the PCR is conducted in a final volume of 25 or 50 µL. The components are 0.1 $ng.\mu L^{-1}$ DNA template (on which the PCR occurs), 0.5 µM each primer, 1x Phusion HF MM (Q5 MM is sometimes used if it allows to have closer melting temperatures for both primers or an annealing temperature further from 72 °C). The PCR protocol includes a touch-down over 6 cycles to reach the calculated annealing temperature (if this annealing temperature is close to 72 °C, a lower annealing temperature may be chosen, or 3 % DMSO may be added to the PCR solution and the annealing temperature is lowered by 0.6 °C per 1 % DMSO; if the primers show unspecific binding at other sites on the template, a slightly higher annealing temperature may be chosen to avoid unspecific binding). Amplification time is calculated as 20 s per kilo base pair (kbp). x1 {98 °C - 30 s}, x6 {98 °C - 15 s, Ta + 5 °C (-1 °C per cycle) - 30s, 72 °C - 20 s/kbp}, x29 {98 °C - 15s, Ta - 30s, 72 °C, 20 s/kbp}, x1 {72 °C - 5 min}

- DpnI digestion: the DNA template is typically a plasmid extracted from *E. coli* cells. As this plasmid will have a better transformation efficiency than the newly ligated plasmid, it is important to degrade the DNA template to avoid false positives during transformation. For this, the enzyme DpnI that cuts the sequence GATC when the A is methylated (a process that occurs in cells) is incubated with the PCR reaction. After the PCR protocol and prior to purification, 1 µL DpnI and 5.67 µL CutSmart Buffer are added to 50 µL of the PCR reaction, and the solution is incubated at 37 °C for 30 min and at 80 °C for 20 min (this step allows denaturation of DpnI, but is optional if a PCR clean-up is conducted afterwards).

- PCR cleanup: the PCR product is purified with a PCR cleanup kit and resuspended in 25 µL nf H_2O. The PCR product concentration is measured.

- Phosphorylation and ligation: prior to transformation, the PCR product must be ligated into a plasmid. PCR with non-modified primers leads to unphosphorylated ends of the PCR product, whereas ligation requires at least one phosphorylated end. Therefore, 30 nM of the PCR product (or less if PCR did not yield sufficient product concentration) is mixed with 1x T4 DNA Ligase Buffer and 0.5 $U.\mu L^{-1}$ T4 Polynucleotide Kinase, and incubated for 1 h at 37 °C. Then, 10 $U.\mu L^{-1}$ T4 DNA Ligase is added to the solution, which is incubated at 16 °C overnight (typically 12 to 16 h) and denatured for 15 min at 65 °C.

- Transformation: the plasmid is transformed without additional purification in *E. coli* Turbo cells. Electroporation is preferred over chemical transformation as it leads to less colonies but also less false positive colonies. Typically, electroporation is first attempted. If the transformation leads no colonies or all colonies are negative, chemical transformation is attempted. If again colonies containing the correct plasmid are not found, investigation is conducted into the cloning steps: the PCR and ligation products are analyzed on an agarose gel, and these steps are repeated and optimized if necessary, or another cloning strategy is devised. If a given cloning strategy does not allow to obtain the desired plasmid, optimization of the different cloning steps is to my experience unlikely to yield positive results, and it is advised to choose another cloning strategy. Electroporation is conducted as such: 1.5 µL ligation solution is transformed into 40 µL *E. coli* Turbo electrocompetent cells in a 1 mm gap electroporation cuvette (VWR, #732-1135) with 1700 V for 6 ms. The cells are then resuspended in 300 µL room temperature SOC medium (SOB + 20 mM glucose) and incubated in a shaking incubator at 37 °C for 1 to 3 h (longer incubation allows the cells to produce more antibiotic resistance prior to plating). The whole solution is then plated on an LB-Agar plate with the appropriate antibiotic and incubated at 37 °C overnight.

- Colonies picking: if the plate yields colonies, 1 to 3 colonies per plate are picked with a sterile pipette tip or toothpick and resuspended individually in 50 µL LB medium. Plates are stored at 4 °C for several months and picked colonies are stored at 4 °C for up to 2 weeks.

- Colony PCR: colony PCR (cPCR) can be conducted to quickly screen colonies and detect if they contain an insert of the right size. Typically, this step is only conducted if the first 3 picked colonies did not have the right sequence. The cPCR mix contains 0.2 µM of each primer, 1 µL of the colony in LB medium and 1x OneTaq MM (since cPCR is only conducted for analytic purposes, high fidelity of the polymerase enzyme is not necessary) in a total volume of 10 µL. Primers are chosen so that they yield a product of drastically different size whether the correct insert is present or not. Amplification is 1 min per kbp. The protocol is as follows: x1 {95 °C - 10 min}, x6 {95 °C - 30 s, Ta + 5 °C (-1 °C per cycle) - 30s, 68 °C - 1 min/kbp}, x29 {95 °C - 30s, Ta - 30s, 68 °C - 1 min/kbp}, x1 {68 °C - 5 min} After cPCR, 2 µL of purple loading dye (NEB) is added and the whole sample is loaded into an agarose gel (1 % agarose, x1 TAE Buffer, 15V/cm, 25 min, prestained with Serva DNA Stain G, ladder 1 kb Plus DNA Ladder), and the gel is scanned under UV to verify which colonies contain inserts of the right length.

- Plasmid purification, sequencing and glycerol stock: after colonies have been picked, the correct sequence of their plasmid is verified as follows. 5 µL of the picked colony in medium is grown overnight at 37 °C in 5 mL LB medium supplied with the appropriate antibiotics. A glycerol stock of this colony is made by mixing 1 mL of a 50 % glycerol 50% LB medium solution with 1 mL of the overnight culture. The sample is thoroughly mixed and stored at -80 °C. The rest of the overnight culture is Mini-prepped and sequenced. If the sequencing returns negative, the glycerol stock and the picked colony are discarded and more colonies are picked and analysed. If the sequencing returns positive, it is then verified that the glycerol stock contains the correct plasmid. Indeed, it is rare but possible that the picked colony contains a mixture of plasmids, the one desired and another one with a lower load on the cells (such as a plasmid containing a deletion in a promoter). The first picked colony might have a predominance of the desired plasmid but as the culture is grown longer and longer, the secondary plasmid increases in proportion and ”takes over” the population. In this case, cultures grown from the glycerol stock might predominantly contain the unwanted plasmid. To this purpose, an overnight culture in 5 mL LB medium

with the appropriate antibiotics is grown from the glycerol stock, and the next day this culture is Mini-prepped and sequenced. If the sequencing returns positive, the glycerol stock is stored and all cloning intermediates are discarded. If the sequencing returns negative, the initial picked colony is plated, single colonies are picked, and the process is repeated until a clean glycerol stock can be made.

Digestion-ligation

- digestion: insert and backbone are digested with either the same restriction enzymes or restriction enzymes that lead to complementary sticky ends. Restriction enzymes that cut at their recognition sites are preferred. Digestion reaction are conducted in a total volume of 50 µL with the following reagents: 40 ng.µL^{-1} DNA to be digested, 1x restriction buffer (typically CutSmart Buffer, but the buffer in which both enzymes have optimal activity is preferred), 0.4 U.µL^{-1} each restriction enzyme. Samples are incubated at the enzyme's working temperature (typically 37 °C) for 2 hours, up to 2.5 hours. The enzymes are then denatured by incubating the sample at 80 °C for 20 min, and the DNA is purified by PCR cleanup. When digesting plasmids, a step of dephosphorylation must be conducted to ensure that the digested backbone does not relegate on itself in later steps. Such a backbone would typically only contain the origin of replication and the antibiotic resistance without insert and therefore cause a lower load on transformed cells, therefore it would lead to false positive colonies. To this end, during the last 30 min of digestion of a plasmid, 5.78 µL of antarctic phosphatase buffer and 10 U (2 µL) of antarctic phosphatase are added to the sample, which is incubated at 37 °C for another 30 min.

- ligation: ligation is conducted as described above, with a molar ratio of 3:1 insert:backbone. Typically, 5 nM of backbone and 15 nM of insert will be mixed for ligation. The rest of the cloning and transformation protocol is as described above.

Cell extract preparation

The *E. coli* cell extract was prepared according to the protocol by Sun *et al.* [141]. Shortly, a mid-log phase BL21 Rosetta2(DE3) culture was lysed by bead-beating with 0.1 mm glass beads in a Minilys device (Peqlab, Germany). The extract was incubated at 37 °C for 80 min to allow the digestion of genomic DNA, and was then dialyzed for 3 h at 4 °C with a cut-off of 10 kDa (Slide-A-Lyzer Dialysis Cassettes, Thermo Fisher Scientific). Protein concentration was estimated to be 30 mg/mL with a Bradford essay. In the buffer, instead of 3-phosphoglyceric acid (3-PGA), phosphoenolpyruvate (PEP) was utilized as an energy source [105]. The buffer was composed of 50 mM HEPES pH 8, 1.5 mM ATP and GTP, 0.9 mM CTP and UTP, 0.2 mg.ml-1 tRNA, 0.26 mM coenzyme A, 0.33 mM NAD, 0.75 mM cAMP, 68 µM folinic acid, 1 mM spermidine, 30 mM PEP, 1.25 mM leucine, 1.5 mM other amino acids, 1.5 mM DTT, 3.5 % PEG-8000, 80 mM K-glutamate and 6 mM Mg-glutamate. Buffer and extract were flash-frozen in liquid nitrogen, stored at -80 °C and thawed on ice prior to usage. A cell-free reaction was prepared by mixing 33 % (v/v) cell extract with 42 % (v/v) buffer and 25 % (v/v) DNA, inducers, and other additives. Unless stated otherwise, the cell extract was supplemented with 5 or 10 nM plasmid DNA and when using them 75 nM repressor protein (LacI or TetR). Reactions were conducted at 29 °C.

A few modifications were made to this original protocol. 3 litres of culture were grown instead of 4 due to space restrictions. After the three washing steps with buffer S30A, the pellets containing the cell-extract were flash frozen in liquid nitrogen and stored at -80 °C, and cell-extract preparation was continued on the following day. The cells were lysed by sonication rather than bead-beating, because it was more scalable and yielded a cell-extract of better quality (*i.e.* higher protein expression). The pellet was resuspended in 1 mL S30A buffer per gram of cell-extract and incubated on ice with 1 mg/mL lysozyme for 30 min, and the cells were sonicated in 4 mL

aliquots with 30 kHz, 10 % amplitude, 20 cycles, 10 s per cycle. The normal protocol was then resumed from step 39.

Experiments with bacteria

Cultures were grown overnight from glycerol stock in M9 medium (3.37 mM Na_2HPO_4, 0.2 mM KH_2PO_4, 8.55 mM NaCl, 9.35 mM NH_4Cl, 2 mM $MgSO_4$, 100 µM $CaCl_2$, 20 mM glucose, 0.20 % caseinh, 0.2 $mg.mL^{-1}$ thiamine) supplemented with the appropriate antibiotics (in some cases, LB medium was used). In encapsulation experiments, the culture was diluted the next day in M9 medium to a final OD 600nm ranging between 0.05 and 0.2 in receiver droplets. In *in vivo* expression experiments measured in a Plate Reader, the culture was diluted the next day in M9 medium to a final OD 600 nm of 0.05 with appropriate inducer concentrations were added. In *in vivo* expression experiments analysed on gels, the culture was diluted 100 times (v:v) the next day in M9 medium, and induced with appropriate inducer concentrations when OD reached 0.4. A cell sample was taken every 2 hours, spinned down at 15,000 rcf for 5 min and resuspended in 1x Laemmli Buffer. The different samples were normalized to the same cell quantity by measuring the OD 600nm and taking the equivalent of 200 µL of OD 1 solution.

When analysing bacterial data sets, the protein expression rate per cell is calculated as follows: the rate of protein expression is calculated by the derivative over time of the protein fluorescence, then divided by the OD at each time point. When the protein expression rate is too noisy (for the case of low protein expression), the protein level per cell is calculated by dividing the fluorescence intensity by the OD at each time point.

Protein SDS-PAGE Gel and staining

Protein content of cells is analysed on SDS-PAGE denaturing gels. Precast gels with 4-20 % (v/v) Acrylamide gradient density (Bio-rad, USA) are run in 1x SDS-PAGE Buffer for 18 min at 45 $V.cm^{-1}$, room temperature. The cell samples were mixed in 1x Laemmli Buffer, denatured at 95 °C for 10 min and put on ice before being loaded on the gel. The gel is stained with either Roti-Blue (coomassie staining) for 15 min or with silver staining to detect lower protein concentrations (Silver Stain Plus from Bio-rad). Bands are identified by comparison to a protein ladder (Color Prestained Protein Standard).

Lipid preparation

The lipid-oil mixture was optimized for most experiments to be 0.25 mM cholesterol, 0.25 mM DOPG, 4 mM DOPC, 0.5 mM DPhPC in 1:1 hexadecane:AR20. The signalling pulse experiments (Chapter 3.2) were done in a lipid-oil mixture of 5.9 mM DPhPC in 1:1 hexadecane:AR20. The lipid or cholesterol powder was dissolved in chloroform, and the appropriate amounts of lipids and cholesterol were mixed in a glass vial. The chloroform was evaporated under a nitrogen stream, and the lipid film was dried for an additional hour under vacuum. The lipid film was then resuspended in 1:1 hexadecane:AR20 oil mix to reach the desired lipid and cholesterol concentrations, and the mix was briefly vortexed.

Experiment chambers

For the chambers, rubber O-rings (7-1 FPM 80, Herzer, Germany) were glued (UHU Plus Endfest 3000, UHU, Germany) unto glass slides (VWR, Germany). The chambers were washed before each experiment with soap, ethanol and double-distilled water, and dried at 90 °C for at least 30min, to ensure that all contaminant proteins have been denatured.

Droplet production and assembly

The chamber was filled with 65 µL of the lipid:oil mix. Droplet solutions (such as sender, buffer and receiver) were prepared according to each experiment, and pipetted into heat-pulled glass

capillaries with a tip diameter of around 30 µm (capillaries: 1.050 × 1.50 × 100 mm, GB150T-10, Science Products, Germany, heat-puller: DMZ-Universal Puller, Zeitz, Germany). The glass capillary was then fixed unto a house-built micromanipulator, and connected to a microinjector pump (Femtojet 4i, Eppendorf), which provided pressure pulses in the range of 20 to 100 hPa for 0.1 s. A wipe (Kimtech, USA) was lightly pressed against the tip of the capillary to take out the residual air and allow the regular flow of the solution. The pipette was brought into the lipid:oil mix and pressure injections were applied to create droplets of approximately 260 µm diameter, 10 nL volume on average. The droplets sank at the bottom of the chamber and were incubated for 15 min on average, to allow a monolayer of lipids to form around them. The glass capillary, together with the micromanipulator, was then used to move the droplets in the chamber and bring them into contact, and they spontaneously formed bilayers. The chamber was closed with a glass slide to limit evaporation and shrinking of the droplets.

Bulk experiments

Bulk experiments were often conducted to assess functionality of the circuits priori to encapsulation in droplets assemblies. DNA/RNA circuits and bacteria constructs were assessed at 37 °C, cell-extract circuits were assessed at 29 °C. 15 µL (300 µL for bacteria) of the sample were pipetted in a 384-well (96-well respectively) plate (µ-Plate, IBIDI, Germany). The plate was sealed with an optically transparent film (Microseal 'B'), and centrifuged for 30 s at 700 rcf. Time-fluorescence measurements were then taken in a plate reader (FLUOstar Omega or CLARIOstar, BMG Labtech, Germany) with the appropriate excitation and emission filters corresponding best to the fluorescence measured.

Image Acquisition

The fluorescence of the assemblies was recorded with an inverted fluorescence microscope. Most experiments were recorded with an IX-71 microscope (Olympus, Japan), with LEDs, filters and dichroic mirrors from Thorlabs (USA), camera LucaEM from Andor (Northern Ireland, UK), objectives from Olympus (Japan), heating plate from Tokai Hit (Japan), and acquisition software MicroManager 1.4.16. Some of the signalling pulse experiments were recorded with an Eclipse Ti2 (Nikon, Japan), with white light for excitation SOLA light engine (Lumencor, USA), filters and dichroic mirrors from Thorlabs (USA), camera Neo5.5 from Andor (Northern Ireland, UK), objectives from Nikon (Japan), incubation chamber from Okolab (Italy), and acquisition software NIS-Elements AR from Nikon (Japan). The images were further analyzed with ImageJ and MATLAB_R2015b. Objectives used were x4 or x10, with a binning of 2, and the following filters for IX-71: for detection of Atto655-DNA (far-red), LED 627nm, excitation filter 605nm-648nm, dichroic mirror 667nm and emission filter 672nm-712nm; for detection of GFP, Spinach and all green fluorescent molecules, LED 470nm, excitation filter 450nm-490nm, dichroic mirror 510nm and emission filter 518nm-545nm; for detection of RFP and all red fluorescent molecules, LED 530nm, excitation filter 530nm-550nm, dichroic mirror 576nm and for emission, a long pass filter above 590nm. For the Eclipse Ti2 microscope, the far red filters were excitation filter 608nm-648nm, dichroic mirror 660nm and emission filter 672nm-712nm; the green filters were excitation filter 457nm-487nm, dichroic mirror 458nm and emission filter 467nm-515nm.

Data analysis and simulations

Droplets were tracked either with the droplet tracker software from Dr. Kapsner [172] in MATLAB_R2015b and MATLAB_R2018b, or with the plugin Time Series Analyzer in Fiji/ImageJ. The images were background substracted. The total fluorescence intensity and radius of each droplet was extracted, and the mean intensity was calculated as $\frac{intensitysum}{radius^2}$, assuming that the microscope excited and recorded the emission from a circular slice at the centre of the droplet. For the pulse, the mean intensities were filtered with a fft filter. Models were simulated with an ode23s solver with and absolute tolerance of 10^{-9} and a relative tolerance of 10^{-5}, and fits were

made with a ”lsqnonlin” function, using the Scharfit program from Dr. Kapsner [173].

Chem3D

Molecular structures of the chemicals were constructed using the program ChemDraw Professional (version 16.0.1.4(77)), and loaded unto the molecular modelling program Chem3D (version 16.0.1.14). The lowest energy 3D conformations were determined using the energy minimization function of the program. The following molecular parameters were calculated for each molecule: logP (the logarithm of the octanol/water partition coefficient), hydrogen bond acceptors and donors. The molecular weight was taken from the respective company providing the chemical. To follow the Rule of Five and its recent adjustments [75], [74], we considered the following limits for the parameters: logP from -0.4 to 5.6, molecular weight from 160 to 480 $g.mol^{-1}$, hydrogen bond donors under 5, hydrogen bond acceptors under 10.

Chemical diffusion experiments

Chemical diffusion experiments (Chapter 2.3) are typically conducted as follows: assemblies contain a sender, a buffer and a receiver droplet, unless indicated otherwise in the specific experimental conditions below. Droplets contain buffers or media as indicated below. Sender with signal contains the signal as specified in the experimental conditions below and 0.05 $g.L^{-1}$ α-HL. Sender without signal is identical to Buffer with α-HL and has 0.05 $g.L^{-1}$ α-HL and 5 µM Atto655-DNA. Buffer without α-HL does not contain additional components. Receiver is as specified below.

Signalling pulse experiments

Pulse experiments (Chapter 3.2) are typically conducted as follows: Spinach RNA (24-2 RNA) is incubated with activator (C3-A) in 1X RNAPol Buffer, 125 mM KCl, 15 mM $MgCl_2$, at 37 °C for 30 min. After incubation, 4 mM each rNTP, the incomplete genelet template (C3 ds) and T7 RNA polymerase are added. For bulk experiments, the incubation of Spinach RNA and activator is conducted during measurement, the DFHBI is then added and incubated while measuring for 30 min, then the incomplete template and the T7 RNA Polymerase are added.

Noise-based differentiation experiments

Noise-based differentiation experiments (Chapter 3.3) are typically conducted as follows. All samples contain $\frac{3}{4}$ volume extract-buffer mix. Depending on experimental conditions and as specified, Sender contains $\pm$ 300 mM arabinose, 5 µM Atto488 (as a marker), $\pm$ 0.05 $g.L^{-1}$ α-HL. Receiver contains 5 nM of *pSB1A2-AD010* or 5 nM *pSB1A2-AD011*. In the Atto488 control (Figure 3.16.c), the sender solution contained 15 µM Atto488, and the receiver contained 5 nM of a pBAD-α-HL plasmid (*pSB1A2-AD009*), 100 mM arabinose and 0.05 $g.L^{-1}$ α-HL for positive controls.

Gradient-based differentiation

Gradient-based differentiation experiments (Chapter 3.4) are typically conducted as follows. All samples contain $\frac{3}{4}$ volume extract-buffer mix. Plasmids concentrations are 5 nM *pSB1C3-pLacO-TetR-GFP* and 5 nM *pSB1A3-pTetO-LacI-mCherry*, or as specified in the figure. IPTG and aTc concentrations typically ranger from 0 to 100 mM for IPTG and 0 to 100 µM for aTc, and are specified in the figure. Pores are not used. Atto655-DNA or Atto488 are used as markers of the sender for droplet experiments.

Autocatalysis of signal production

Signal production autocatalysis experiments (Chapter 4.1) are typically conducted as follows. All samples contain $\frac{3}{4}$ volume extract-buffer mix. Receiver plasmid (*pSB1A3-pLacO-T9002-LVA*) is at 5 nM, sender plasmid (*pSB4K5-pLux-LuxI*) is typically at 1 nM or as indicated. 3OC6-HSL

is as indicated. Sender droplets were marked with 5 µM Atto655-DNA in droplet experiments.

Specific experimental conditions

Figure 1.1: Simulations for the Turing reaction-diffusion system were conducted with the following code executed in MATLAB, with reaction-diffusion equations as listed in Chapter 1.1.2, initial conditions are either all concentrations equal to 1 (Figure 1.1.b) or concentrations are as listed in Chapter 1.1.2 with ϵ=0.02. Exact code for other simulations and fits is not given, but follows the architecture of this code with adjustments to the reaction and the diffusion terms.

```
function [t, outcome]=Turing_Diff_1(a)

global DX DY nspecies ncompartment e
nspecies=2;
ncompartment=2;
DX=0.06;
DY=0.18;
e=a;

%initialization
for ispecies=1:1:nspecies;
for icomp=1:1:ncompartment;
x(ispecies, icomp)=0;
end
end

%initial values < > 0
x(1,1)=1+3*a;
x(2,1)=1+a;
x(1,2)=1-3*a;
x(2,2)=1-a;

% create vector for odesolver
icount=0;

for icomp=1:1:ncompartment
for ispecies=1:1:nspecies
icount=icount+1;
x0(icount)=x(ispecies,icomp);
end
end
% duration of experiment
dt=0.1; duration=100;
% simulation run
tspan=[0 : dt : duration}];
options=odeset('AbsTol',1e-9,'RelTol',1e-5); % set tolerances
[t, y}]=ode23s(@Turing_function,tspan,x0,options);
%output
t=t;
outcome=y(:,:);
end
function ydot = Turing_function(t, y, flags)
global DX DY nspecies ncompartment e
```

```
% translate back:
ncount=size(y,1);
for icount=1:1:ncount
icomp=floor((icount-1)/nspecies)+1;
ispecies=icount-(icomp-1)*nspecies;
x(ispecies,icomp)=y(icount);
end
dx=zeros(nspecies,ncompartment);
%reaction-diffusion
dx(1,1)=5*x(1,1)-6*x(2,1)+1+DX*(x(1,2)-x(1,1));
dx(2,1)=6*x(1,1)-7*x(2,1)+1+DY*(x(2,2)-x(2,1));
dx(1,2)=5*x(1,2)-6*x(2,2)+1+DX*(x(1,1)-x(1,2));
dx(2,2)=6*x(1,2)-7*x(2,2)+1+DY*(x(2,1)-x(2,2));

icount=0; % construct derivative vector
for icomp=1:1:ncompartment
for ispecies=1:1:nspecies
icount=icount+1;
dy(icount)=dx(ispecies,icomp);
end end
ydot=dy';
end
```

Figure 2.5: Molecular graphics performed with UCSF Chimera, developed by the Resource for Biocomputing, Visualization, and Informatics at the University of California, San Francisco, with support from NIH P41-GM103311. Protein databank ID numbers were: 7aHL for α-HL (representation of hydrophobicity of surface in Figure 2.5.d and of Coulomb potential in Figure 2.5.c), 2F1C for OmpG, 1GFN for OmpF and 6MRU for ClyA.

Figure 2.6.a: This experiment was done without a buffer droplet. All samples have: 1x RNAPol Reaction Buffer, 125 mM KCl, 15 mM $MgCl_2$, 10 µM DFHBI. Sender with α-HL also has: 5 µM Atto655-DNA as a marker (sequence in Appendix A.5), 500 µM guanine, 0.04x glycerol buffer (composition in Appendix A.1), 0.05 $g.L^{-1}$ α-HL. Sender with OmpF also has: 5 µM Atto655-DNA, 500 µM guanine, 0.04x glycerol buffer, 0.05 $g.L^{-1}$ OmpF. Sender without pores also has: 5 µM Atto655-DNA, 500 µM guanine, 0.04x glycerol buffer. Receiver also has 1 µM purified 24-2-guanine RNA (sequence in Appendix A.5), 0.04x glycerol buffer.

Figure 2.8: a/ All sample volumes are completed with M9 medium instead of water. Sender with signal has: 10 mM arabinose. Receiver has *E. coli* BW27783 pBAD33-DsRedmut at OD 0.2 in M9 medium.
b/ All samples contain 1X RNAPol Reaction Buffer, 125 mM KCl, 15 mM $MgCl_2$, 40 µM DFHBI. Sender with signal has: 0.08x glycerol buffer, 4 mM guanine. Sender without signal and Buffer with α-HL have 0.08x glycerol buffer. Buffer without α-HL has: 0.08x glycerol buffer. Receiver has: 4 mM each rNTP, 100 nM 24-2-guanine dsDNA, 4 $U.\mu L^{-1}$ T7 RNA Polymerase (NEB).
c/ All sample volumes are completed with M9 medium instead of water and contain 1 mM IPTG. Sender with signal has: 0.25 mM DAPG. Receiver has DH5α *pPhlF-P2* at OD 0.05 in M9 medium.
d/ All sample volumes are completed with M9 medium instead of water. Sender with signal has: 40 $g.L^{-1}$ rhamnose. Receiver has DH5α *pCK301* at OD 0.1 in M9 medium.
e/ This assembly does not have a buffer droplet. All samples contain 1x RNAPol Reaction Buffer. Sender with signal and α-HL also has: 5 µM Atto488, 0.05 $g.L^{-1}$ α-HL. Sender with signal and without α-HL also has: 5 µM Atto488. Sender without signal and with α-HL also has: 0.05 $g.L^{-1}$ α-HL. Assemblies do not contain a buffer droplet.

Figure 2.9: a/ All samples contain $\frac{3}{4}$ volume extract/buffer mix. Sender with signal has: 5 µM 3OC6-HSL. Receiver has 10 nM *pSB1A3-pLacO-T9002-LVA*.
b/ All samples contain 1X RNAPol Reaction Buffer, 125 mM KCl, 15 mM $MgCl_2$. Sender with signal has: 4 µM DFHBI, 0.08x glycerol buffer. Sender without signal and Buffer with α-HL have: 0.08x glycerol buffer. Buffer without α-HL has: 0.08x glycerol buffer. Receiver has: 4 mM each rNTP, 200 nM 24-2 dsDNA, 4 $U.\mu L^{-1}$ T7 RNA Polymerase (NEB).
c/ All samples contain $\frac{3}{4}$ volume extract/buffer mix. Sender with signal also has: 2 µM aTc. Receiver also has 10 nM *pSB1A3-I13521*, 75 nM TetR.
d/ All samples contain $\frac{3}{4}$ volume extract/buffer mix. Sender with signal also has: 2 µM doxycycline. Receiver also has 10 nM *pSB1A3-I13521*, 75 nM TetR.
e/ All samples contain $\frac{3}{4}$ volume extract/buffer mix. Sender with signal also has: 4.5 mM IPTG. Receiver also has 10 nM *pSB1A3-pLacO-GFP*, 75 nM LacI.

Figure 2.10: a/ All samples contain $\frac{3}{4}$ volume extract/buffer mix. Sender with signal has: 4.5 mM lactose. Receiver has 10 nM *pSB1A3-pLacO-GFP*, 75 nM LacI.
b/ This assembly does not have a buffer droplet. All samples contain 1x RNAPol Reaction Buffer, 125 mM KCl, 15 mM $MgCl_2$. Sender with signal and α-HL also has: 5 µM Atto633, 0.05 $g.L^{-1}$ α-HL. Sender with signal and without α-HL also has: 5 µM Atto633. Sender without signal and with α-HL also has: 0.05 $g.L^{-1}$ α-HL. Assemblies do not contain a buffer droplet.
c/ This assembly does not have a buffer droplet. All samples contain 1X RNAPol Reaction Buffer, 125 mM KCl, 4 µM DFHBI. Sender with signal and α-HL also has: 20 mM $MgCl_2$, 5 µM Atto655-DNA, 0.04x glycerol buffer, 0.05 $g.L^{-1}$ α-HL. Sender with signal and without α-HL also has: 20 mM $MgCl_2$, 5 µM Atto655-DNA, 0.04x glycerol buffer. Sender without signal and with α-HL also has: 5 µM Atto655-DNA, 0.04x glycerol buffer, 0.05 $g.L^{-1}$ α-HL. Receiver also has: 4 mM each rNTP, 200 nM 24-2 dsDNA, 0.4 µM T7 RNA Polymerase (self-purified).
d/ This assembly does not have a buffer droplet. All samples contain 1X RNAPol Reaction Buffer, 125 mM KCl, 15 mM $MgCl_2$, 10 µM DFHBI. Sender with signal and with α-HL also has: 5 µM Atto655-DNA, 4 mM SAM, 0.04x glycerol buffer, 0.05 $g.L^{-1}$ α-HL. Sender with signal and without α-HL also has: 5 µM Atto655-DNA, 4 mM SAM, 0.04x glycerol buffer. Sender without signal and with α-HL also has: 5 µM Atto655-DNA, 0.04x glycerol buffer, 0.05 $g.L^{-1}$ α-HL. Receiver also has: 4 mM each rNTP, 100 nM 24-2-SAM dsDNA, 0.4 µM T7 RNA Polymerase (self-purified).
e/ All samples contain $\frac{3}{4}$ volume extract/buffer mix. Sender with signal also has: 2 µM tetracycline. Receiver also has 10 nM *pSB1A3-I13521*, 75 nM TetR.
f/ All samples contain $\frac{3}{4}$ volume extract/buffer mix. Sender with signal has: 4 mM theophylline, 0.05x glycerol buffer. Sender without signal and Buffer with α-HL have: 0.05x glycerol buffer. Buffer without α-HL has: 0.05x glycerol buffer. Receiver has: 10 nM *pSB1A3-pT7-Th-YPet*, 0.5 µM T7 RNA Polymerase (self-purified).

Figure 2.11: All samples contain 1X RNAPol Reaction Buffer, 125 mM KCl, 15 mM $MgCl_2$. a-b/ Sender also has: 40 µM DFHBI, 0.04x glycerol buffer, 0.05 $g.L^{-1}$ α-HL. Receiver with α-HL also has: 4 mM each rNTP, 200 nM 24-2 dsDNA, 0.4 µM T7 RNA Polymerase (self-purified), 0.05 $g.L^{-1}$ α-HL. Receiver without α-HL also has: 4 mM each rNTP, 200 nM 24-2 dsDNA, 0.4 µM T7 RNA Polymerase (self-purified), 5 µM Atto655-DNA. c-d/ Sender also has: 1 mM guanine, 0.04x glycerol buffer, 0.05 $g.L^{-1}$ α-HL. Receiver with α-HL also has: 1 µM purified 24-2-guanine RNA, 0.04x glycerol buffer, 5 µM DFHBI, 5 µM Atto655-DNA, 0.05 $g.L^{-1}$ α-HL. Receiver without α-HL also has: 1 µM 24-2-guanine RNA, 0.04x glycerol buffer, 5 µM DFHBI.

Figure 2.15: d/ All samples contain 1X RNAPol Reaction Buffer, 125 mM KCl, 15 mM $MgCl_2$, 0.08x glycerol buffer, 0.05 $g.L^{-1}$ α-HL. Additionally, the external left-most droplet has: 20 µM DFHBI, 5 µM Atto655-DNA; the external right-most droplet has: 5 µM Atto655-DNA; the internal droplets have: 1 µM 24-2 purified RNA.

Figure 3.3: a/ All samples contain $\frac{3}{4}$ volume extract/buffer mix. Sender also has: 300 mM arabinose, 1 µM 3OC6-HSL, 0.05 g.L^{-1} α-HL. Buffer also has: 0.05 g.L^{-1} α-HL. Receiver also has: 5 nM *pSB1A2-AD011*, 5 nM *pSB1A3-pLacO-T9002-LVA*. b/ All samples contain $\frac{3}{4}$ volume extract/buffer mix. Sample with *pLux-GFP* also has: 5 nM *pSB1A3-pLacO-T9002-LVA*, 1 µM 3OC6-HSL. Sample with *pBAD-RFP* also has: 5 nM *pSB1A2-AD011*, 300 mM arabinose. Simulations in b/ and c/ are done with these same initial concentrations.

Figure 3.4: conditions as listed for Figure 3.3.a, with the Buffer containing the varying concentrations of α-HL for a/ and b/, and 0.05 g.L^{-1} α-HL for c/.

Figure 3.7: c/ All samples contain 5 µM Malachite Green, 150 nM MG-C3 ds and 150 nM C3-A. d/ Samples contain the usual TX ingredients with 3 µM 24-2 RNA, 3 µM DFHBI, 150 nM C3-A, 0 or 150 nM C3 ds and 1 µM T7 RNA Polymerase. e/ Samples contain the usual TX ingredients with 1 µM 24-2 RNA, 1 to 5 µM DFHBI, 5 µM MG, 200 nM C3-A, 200 nM C3 ds, 200 nM MG-C3 ds and 0.4 µM T7 RNA Polymerase. f/ Samples contain the usual TX ingredients with 1 µM 24-2 RNA, 10 µM DFHBI, 150 nM C3-A, 150 nM C3 ds and 0 to 1.6 µM T7 RNA Polymerase.

Figure 3.8: a-b-c/ All samples contain the usual TX ingredients (1X RNAPol Reaction Buffer, 125 mM KCl, 15 mM $MgCl_2$, 4 mM each rNTP). Sender also has: 3 µM DFHBI, 1 µM Atto655-DNA, 0.1x glycerol buffer (no rNTPs in the sender). Receiver also has: 1.5 µM 24-2 RNA, 150 nM C3-A, 150 nM C3-ds, 1.2 µM T7 RNA Polymerase. d/ All samples contain the usual TX ingredients. Sender also has: 3 µM DFHBI, 1 µM Atto655-DNA, 0.1x glycerol buffer (no rNTPs in the sender). Receiver also has: 1.5 µM 24-2 RNA, 150 nM C3-A, 1.4 µM T7 RNA Polymerase. e/ -I1-FFL experiments are done in the conditions of d. +I1-FFL experiments are done in identical conditions, and receiver additionally has 150 nM C3 ds.

Figure 3.9: a/ Experiments are conducted with 1.5 µM 24-2 RNA, 150 nM C3-A, 150 nM C3 ds, 1.2 µM T7 RNA Polymerase and DFHBI as indicated in the figure. b/ Experiments are conducted with 1.5 µM 24-2 RNA, 150 nM C3-A, 150 nM C3 ds, 3 µM DFHBI and T7 RNA Polymerase as indicated in the figure.

Figure 3.10: a-b-c/ All samples contain the usual TX ingredients. Sender also has: 12 µM DFHBI, 1 µM Atto655-DNA, 0.12x glycerol buffer. Receiver also has: 3 µM 24-2 RNA, 150 nM C3-A, 150 nM C3 ds, 1.2 µM T7 RNA Polymerase. d/ High DFHBI, high T7 RNA Polymerase condition is identical to a. Low DFHBI, low T7 RNA Polymerase has: 6 µM DFHBI, 1 µM T7 RNA Polymerase.

Figure 3.11: All samples contain usual TX ingredients. a/ All samples additionally have 1 µM 24-2-guanine RNA, 100 µM DFHBI, 200 nM C3-G ds. Negative control also has: 0.08x glycerol buffer. Positive control also has: 0.3 mM guanine, 0.08x glycerol buffer. Guanine I1-FFL sample also has: 200 nM C3-G-A, 0.3 mM guanine, 4 U.µL^{-1} T7 RNA Polymerase (NEB). b/ Sender has: 50 µM DFHBI, 1 mM guanine, 0.05 g.L^{-1} α-HL, 5 µM Atto655-DNA, 0.08x glycerol buffer (no rNTPs). Receiver has: 1 µM 24-2-guanine RNA, 50 µM DFHBI, 200 nM C3-G-A, 200 nM C3-G ds, 0.05 g.L^{-1} α-HL, 0.4 µM T7 RNA Polymerase.

Figure 3.12: c/ All samples contain 40 % volume solution A and 30 % volume solution B of the PURExpress kit. I1-FFL sample also has: 1.5 µM 24-2 RNA, 150 nM C3-A, 150 nM C3 ds, 3 µM DFHBI. mScarletI sample also has: 5 nM *pSB4A5-pT7-mScarletI*. d/ All samples contain 40 % volume solution A, 30 % volume solution B, 1 µM 24-2 RNA, 150 nM C3-A, 2.5 nM pSB4A5-pT7-mScarletI. -I1-FFL sample also has: 10 µM DFHBI. All other samples also have: 150 nM C3 ds, 150 nM C3-asRBS ds, and 0, 1 or 10 µM DFHBI. e/ All samples contain 40 % volume solution A, 30 % volume solution B. Sender also has: 4 µM DFHBI, 0.05 g.L^{-1} α-HL, 5 µM Atto655-DNA.

Receiver also has: 1 µM 24-2 RNA, 150 nM C3-A, 150 nM C3 ds, 150 nM C3-asRBS ds, 0.05 g.L^{-1} α-HL, 1 nM *pSB4A5-pT7-mScarletI*. f/ All samples contain 40 % volume solution A, 30 % volume solution B, 5 nM pSB4A5-pT7-mScarletI. Positive control has nothing else. dCas9 sample also has: 300 nM dCas9. dCas9 +sgRNA also has: 300 nM dCas9, 200 nM sgC3 RNA. dCas9 +C3-A/sgC3 ds also has: 300 nM dCas9, 150 nM C3-A, 150 nM sgC3 ds. g/ All samples contain 40 % volume solution A, 30 % volume solution B. Sender also has: 3 µM DFHBI, 1 µM Atto655-DNA. Receiver also has: 1.5 µM 24-2 RNA, 150 nM C3-A, 150 nM C3 ds, 150 nM sgC3 ds, 5 nM p*SB4A5-pT7-mScarletI*, 300 nM dCas9. h/ Samples are identical to f, except that the plasmid is *pSB4A5-AD015*.

Figure 3.14: c-d/ All samples contain $\frac{3}{4}$ volume extract/buffer mix. All samples in c/ contain 5 nM *pSB1A2-AD010* and all samples in d/ contain 5 nM *pSB1A2-AD011*. Arabinose concentrations range from 0 mM to 500 mM. e/ Experimental conditions are identical as in c-d/. Only samples with 0 mM arabinose are shown. f/ All samples contain $\frac{3}{4}$ volume extract/buffer mix, 5 nM *pSB1A2-AD001*, 30 mM arabinose. Sample with RNase Inhibitor additionally has: 1.33 U.µL^{-1} RNase Inhibitor.

Figure 4.4: a-d/ All samples contain $\frac{3}{4}$ volume extract-buffer mix. Sender also has 2 nM *pSB4K5-pLux-LuxI*. Receiver also has 10 nM *pSB1A3-pLacO-T9002-LVA*. e-f/ All samples contain $\frac{3}{4}$ volume extract-buffer mix. Sender also has 1 nM 3OC6-HSL. Receiver also has 10 nM *pSB4K5-pLux-LuxI* and 10 nM *pSB1A3-pLacO-T9002-LVA*.

Figure 4.5: c-d/ All plasmids are present at 5 nM, extract-buffer mix is $\frac{3}{4}$ of the volume. e/ All samples contain $\frac{3}{4}$ volume extract-buffer mix. All plasmids are present at 3 nM.

Figure 4.7: a/ All samples contain $\frac{3}{4}$ volume extract-buffer mix. All plasmids are present at 3 nM. Plasmids are: *pSB4A5-QS01i* for RBS N1, *pSB4A5-AD028* for RBS B3, *pSB4A5-AD029* for RBS P1 and *pSB4A5-AD030* for RBS S4. b/ All samples contain $\frac{3}{4}$ volume extract-buffer mix, 100 µM IPTG and 5 nM plasmid. Plasmids are: *pSB4A5-QS02i* for RBS N1, *pSB4A5-AD023* for RBS B3, *pSB4A5-AD026* for RBS P1 and *pSB4A5-AD027* for RBS S4. c/ All samples contain $\frac{3}{4}$ volume extract-buffer mix, 100 µM IPTG and 5 nM *pSB1A3-pLacO-T9002-LVA* (the receiver plasmid). The sender plasmid, *pSB4A5-AD020*, is present at 2.5 nM in the corresponding sample.

Figure 4.8: a-b/ All samples contain $\frac{3}{4}$ volume extract-buffer mix. Reporter plasmids are present at 6 nM and are: *pSB4A5-AD029* for *Ai* (a) and *pSB4A5-AD026* for *Bi* (b). aTc is added in the corresponding samples at 100 nM, IPTG is at 100 µM. Repressor module plasmids are present at 3 nM and are: for *Ae* (a), *pSB3C5-QS01e* for 0 sponge element, *pSB3C5-AD034* for 1 sponge, and *pSB3C5-AD039* for 2 sponges, for *Be* (b), *pSB3C5-QS02e* for 0 sponge element, *pSB3C5-AD035* for 1 sponge, and *pSB3C5-AD040* for 2 sponges. c-d/ All samples contain $\frac{3}{4}$ volume extract-buffer mix. Repressible reporter plasmids are present at 5 nM and are: *pSB1A3-I13521* for c (*pTetO-RFP*) and *pSB1A3-pLacO-GFP* for d (*pLacO-GFP*). Repressor module plasmids are present at 5 nM and are: *pSB3C5-QS01e* for c and *pSB3C5-QS02e* for d.

Figure 4.9: All samples contain $\frac{3}{4}$ volume extract-buffer mix. Repressible reporter plasmids are present at 3 nM and are: *pSB1A3-I13521* for a (*pTetO-RFP*) and *pSB1A3-pLacO-GFP* for b (*pLacO-GFP*). All samples in a contain 100 nM aTc, all samples in b contain 100 µM IPTG. Repressor module plasmids are present at 3 nM and are *pSB3C5-QS01e* for a and *pSB3C5-QS02e* for b. 3OC6-HSL and 3OC12-HSL are added at concentrations as indicated. For the experiments with signalling plasmids, reporters are 3 nM *pSB4A5-AD029* for a and 3 nM *pSB4A5-AD026* for b, aTc, IPTG, and repressor module plasmids are as described above, and signalling plasmids are present at 3 nM and are: *pSB4A5-AD020* for a and *pSB4A5-AD007* for b.

Figure 4.10: a/ All samples contain $\frac{3}{4}$ volume extract-buffer mix. Full Ai plasmid is *pSB4A5-AD029*. Truncated plasmid without *pLux-LuxI* is *pSB4A5-AD033*. Each plasmid is present at 3 nM. b/ All samples contain $\frac{3}{4}$ volume extract-buffer mix. All samples have 100 µM IPTG. Full Bi plasmid is *pSB4A5-AD026*. Truncated plasmid without *pLas-LasI* is *pSB4A5-AD041*. Each plasmid is present at 6 nM.

Figure 4.11: a/ All samples contain $\frac{3}{4}$ volume extract-buffer mix, 2 nM *Ai* (*pSB4A5-AD029*), 100 µM IPTG, 50 nM aTc and 2 nM *Ae* (*pSB3C5-QS01e*) (samples are normalized to fluorescence intensity of a sample without *Ae*). +C12 sample also has 10 µM 3OC12-HSL. +*Bi* sample also has 2 nM *pSB4A5-AD026*. +*pLas-LasI* sample also has 2 nM *pSB4A5-AD007*. +load sample also has 2 nM *pSB4A5-AD025* (a plasmid expressing mScarletI under a pLas promoter, therefore expressing a protein in another spectral range with no interference to YPet measurement). b/ All samples contain $\frac{3}{4}$ volume extract-buffer mix, 3 nM *Bi* (*pSB4A5-AD026*), 100 µM IPTG and 3 nM *Be* (*pSB3C5-QS02e*) (samples are normalized to fluorescence intensity of a sample without *Be*). +C6 sample also has 10 µM 3OC6-HSL. +*pLux-LuxI* sample also has 3 nM *pSB4A5-AD020*. +load sample also has 3 nM *pSB1A3-pLacO-T9002-LVA* (a plasmid expressing GFP under a pLux promoter, therefore expressing a protein in another spectral range with no interference to mScarletI measurement).

Figure 5.1: a-c/ Sample contains $\frac{3}{4}$ volume extract-buffer, 1 nM *pCola-Duet-1-E60L20*, 1 mM IPTG, 13.3 mM maltose, 5 nM T7 RNA Polymerase (NEB). Staining was conducted with 1 µM TMRE and 10 µM FMN.

Figure 5.3: a/ All samples contain 40 % volume solution A and 30 % volume solution B of the PURExpress kit. All plasmids are present at 5 nM. Plasmids are: for the wt promoter, *pSB4A5-pT7-mScarletI*, for P_{CTGA}, *pSB4A5-AD013*, for P_{T3}, *pSB4A5-AD014*, for P_{K1F}, *pSB4A5-AD015*, for P_{mut1}, *pSB4A5-AD016*, and for P_{mut2}, *pSB4A5-AD017*.

Figure 5.5: a/ All samples contain $\frac{3}{4}$ volume extract-buffer mix, 100 µM IPTG and 5 nM plasmid. Polycistronic construct is *pSB4A5-QS02i*. Monocistronic construct is *pSB4A5-AD018*. b/ Polycistronic construct is *pSB4A5-AD023*, monocistronic construct is *pSB4A5-AD022*. c/ Polycistronic construct is *pSB4A5-AD026*, monocistronic construct is *pSB4A5-AD043*. d/ Polycistronic construct is *pSB3C5-AD026*, monocistronic construct is *pSB3C5-AD043*. e/ Polycistronic construct is *pSB4A5-AD029*, monocistronic construct is *pSB4A5-AD042*.

Figure 5.8: a/ All samples contain $\frac{3}{4}$ volume extract-buffer mix, 12.5 nM linear DNA template (PCR amplicon from *pET21b(+)-mVenus-Biv-Tat*), 15 mM maltodextrin, 1 mM IPTG, 1 $U.\mu L^{-1}$ T7 RNA Polymerase (NEB). GamS concentration is as indicated in the figure. b/ All samples contain $\frac{3}{4}$ volume extract-buffer mix, 15 mM maltodextrin. Plasmid sample also has 5 nM *pSB1A3-I13521* plasmid. Linear samples also have 5 nM linear DNA template (PCR amplicon from *pSB1A3-I13521*) with 0 µM gamS (- gamS sample) or 5 µM gamS (+ gamS sample).

Figure 5.9: a/ All samples contain 40 % volume solution A and 30 % volume solution B of the PURExpress kit, and 10 µM DFHBI. + dBroccoli sample also has 200 nM dBroccoli ds DNA template. b/ All samples contain 40 % volume solution A and 30 % volume solution B of the PURExpress kit, 1 µM 24-2 RNA, 200 nM C3-A, 200 nM C3-ds, 5 µM DFHBI. + mTq2 sample also has 5 nM pJ431-mTurquoise2-Tat. c/ All samples contain 40 % volume solution A and 30 % volume solution B of the PURExpress kit. GFP plasmid sample also has 5 nM pSB6A1-I746907. RFP plasmid samples also has 5 nM pSB4A5-J04450, 1x *E. coli* RNA Polymerase buffer, 0.05 $U.\mu L^{-1}$ *E. coli* RNA Polymerase, holoenzyme.

Figure 5.10: c-e/ All samples contain the usual TX ingredients, 10 µM DFHBI and 2 $U.\mu L^{-1}$ T7

RNA Polymerase (NEB). Positive control also has 100 nM 24-2 ds. Other samples have 100 nM of their template (24-2-ADP ds for c, 24-2-guanine for d, 24-2-SAM for e). Samples in c have 1 mM AMP, ADP or ATP as indicated. Samples in d have 1 mM guanine, guanosine or GTP as indicated. Samples in e have 1 mM SAH or SAM as indicated. f/ All samples contain the usual TX ingredients, 10 µM DFHBI, 100 nM 24-2-guanine RNA and guanine as indicated.

A.4 Figures and tables

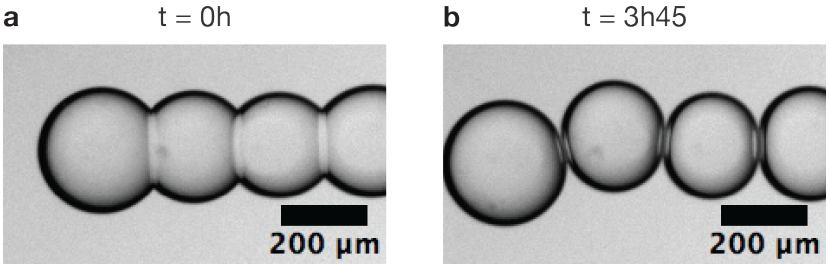

Figure A.1. Surface tension at the bilayer changes over time when cell-extract is encapsulated with lipid mix 4. **a**, Bilayers at 0 h. **b**, Bilayers at 3 h 45 min.

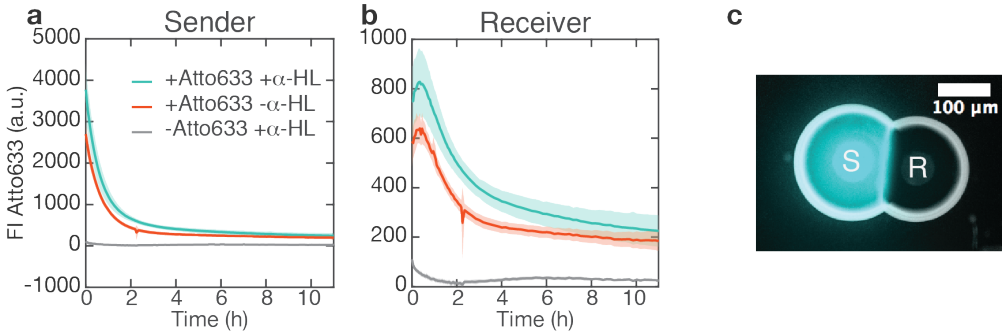

Figure A.2. Diffusion of Atto633 in AMA. a-b, Fluorescence times traces of sender (**a**) and receiver (**b**) droplets in three conditions: sender contains Atto633 and α-HL (blue), Atto633 only (red) or α-HL only (grey). Thick line and shaded area represent mean and standard deviation of at least three assemblies. **c**, Fluorescence image of an assembly where the sender (S) contains Atto633 and α-HL. Diffusion of Atto633 into the oil can be seen in the fluorescence halo around the sender droplet. Scale bar: 100 µm.

Fit	α (M^{-1})	β	K_d (M)	n	K (M)	α_{max}	t_2 (min)	t_{mat} (min)	R^2
pLux induction (Figure AA.2.a)	28220	534.7	$11.36 . 10^{-9}$	2.232					1
pLux kinetics (Figure AA.2.b)	28220	140	$11.36 . 10^{-9}$	2.232	$11.4 . 10^{-9}$	0.0033	15	7	
pBAD induction (Figure AA.2.c)	60530	756.8	$36.4 . 10^{-3}$	1.258					0.9986
pBAD kinetics (Figure AA.2.d)	60530	360	$36.4 . 10^{-3}$	1.258	$18 . 10^{-3}$	0.0033	15	102	

Table A.1. Fitting parameters for pLux and pBAD induction.

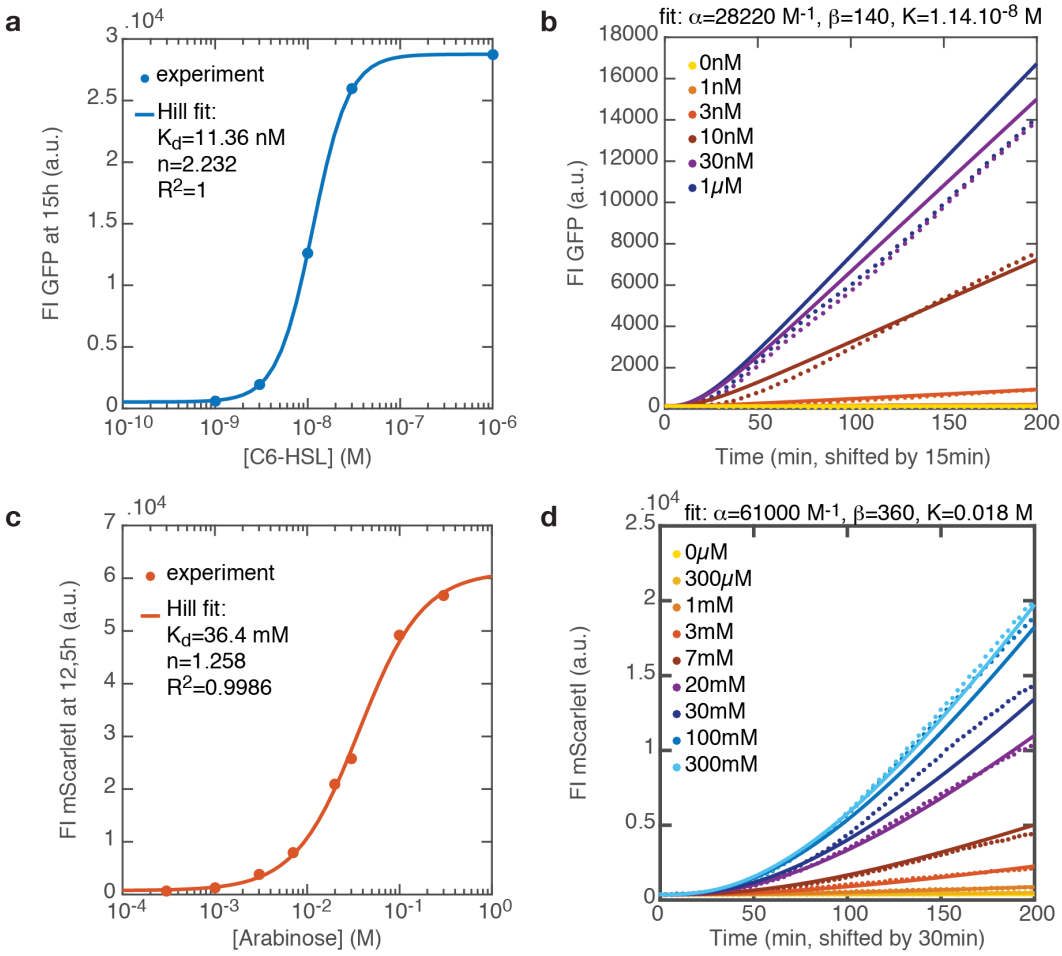

Figure A.3. Comparison of the experimentally determined induction characteristics of the pLux and pBAD promoter. a,c, Final fluorescence intensities from expression of fluorescent proteins under the respective promoters for varying inducer concentrations (cell-extract, 5 nM of either *pSB1A3-pLacO-T9002-LVA* or *pSB1A2-AD011*). Experimental data are fitted with a Hill curve, from which the K_d and Hill exponent were obtained. b,d, Initial protein expression kinetics fitted with an ODE model. Dots represent experimental data and lines represent fits. α and β are parameters relating protein concentration to fluorescence, K is the binding affinity between the chemical (3OC6-HSL or arabinose) and the activator protein (LuxR or AraC), taken from literature and fitted to the experimental data (α has units of M^{-1}).

A.5 Sequences

For all double-stranded sequences, the non-template, (+), coding strand is given. Benchling maps are indicated. Relevant elements (promoters, RBS, coding sequences, degradation tags, etc...) are indicated in capital letters, and separated by double dashes. For plasmid maps, only the insert region containing the genes of interest is shown. Full plasmid maps and backbone sequences can be found in the Benchling links or in plasmid databases. The following plasmids are available on Addgene: pSB1A2-AD009, pSB1A2-AD010, pSB1A2-AD011, pSB1C3-AD050.

Atto655-DNA
Atto655- TTGATGTAT

24-2 ds, from [78]
T7 promoter, Spinach aptamer
GGAATGATAATACGACTCACTATAGGGGACGCGACCGAAATGGTGAAGGACGGGTCCA
GTGCTTCGGCACTGTTGAGTAGAGTGTGAGCTCCGTAACTGGTCGCGTC

24-2-guanine ds, from [96]
T7 promoter, aptamer
GGAATGATAATACGACTCACTATAGGGGACGCGACTGAATGAAATGGTGAAGGACGGGTCCAGATAATCGCGTGGATATGGCACGCAAGTTTCTACCGGGCACC
GTAAATGTCCGACTCTTGTTGAGTAGAGTGTGAGCTCCGTAACTAGTCGCGTC

24-2-SAM ds, from [96]
T7 promoter, aptamer
GGAATGATAATACGACTCACTATAGGGGACGCGACTGAATGAAATGGTGAAGGACGGGTCCACGAAAGGATGGCGGAAACGCCAGATGCCTTGTAACCGAAAG
GGTTGTTGAGTAGAGTGTGAGCTCCGTAACTAGTCGCGTC

24-2-ADP ds, from [96]
T7 promoter, aptamer
GGAATGATAATACGACTCACTATAGGGGACGCGACTGAATGAAATGGTGAAGGACGGGTCCAGCACGAGGGGGAAACCCCGGACAATCAGACACGGTGCTTGT
TGAGTAGAGTGTGAGCTCCGTAACTAGTCGCGTC

dBroccoli ds, from [63]
T7 promoter, dBroccoli aptamer
GGAATGATAATACGACTCACTATAGGGAAGCCTGAGACGGTCGGGTCCATCTGAGACGGTCGGGTCCAGATATTCGTATCTGTCGAGTAGAGTGTGGGCTCAGA
TGTCGAGTAGAGTGTGGGCTCAGGCTT

13-2-min ds, from [78]
T7 promoter, aptamer
TCACGTAATACGACTCACTATAGGGGGGCTATTGCTGGAGGGGCGCCACATGAAAGTGGTGGTTGGGTGCGGTCGGCGATAGCTCATA

C3-A
T7 promoter (part)
TATTACGGAGCTCACACT

C3 ds non-template, complete strand
T7 promoter
AGTGTGAGCTCCGTAATACGACTCACTATAGGGGACTCCAGTTACGGAGCTCACACTCTACTCAACAGTGCCGAAGCACTGGACCCGTCCTTCACCATTTCGGT
CGCGTCTAT

C3 ds template, incomplete strand
T7 promoter (part)
ATAGACGCGACCGAAATGGTGAAGGACGGGTCCAGTGCTTCGGCACTGTTGAGTAGAGTGTGAGCTCCGTAACTGGAGTCCCCTATAGTGAGTCG

MG-C3 ds non template, complete strand
T7 promoter, MG aptamer
AGCACCGTAATACGACTCACTATAGGGATCCCGACTGGCGAGAGCCAGGTAACGAATGGATCCAGTACAT

MG-C3 ds template, incomplete strand
T7 promoter
ATGTACTGGATCCATTCGTTACCTGGCTCTCGCCAGTCGGGATCCCTATAGTGAGTCG

C3-G-A
T7 promoter
TTACGGTGCCCGG

C3-G ds non-template, complete strand
T7 promoter
TTCTACCGGGCACCGTAATACGACTCACTATAGGGCTTGCGTGCCATATCCACGCGATTATCTGGACCCGTCCTTCACCATTTCATTCAGTCGCGTC

C3-G ds template, incomplete strand
T7 promoter
GACGCGACTGAATGAAATGGTGAAGGACGGGTCCAGATAATCGCGTGGATATGGCACGCAAGCCCTATAGTGAGTCGTA

C3-asRBS ds non-template, complete strand
T7 promoter, target sequence
AGTGTGAGCTCCGTAATACGACTCACTATAGGGctagtatttctcctctttctctagtaTAT

C3-asRBS ds template, incomplete strand
T7 promoter, target sequence
ATAtactagagaaagaggagaaatactagCCCTATAGTGAGTCG

sgC3 ds non-template, complete strand
T7 promoter, sgRNA
agtgtgagctccgtaatacgactcactatagtattagaattcgagtcactagttttagagctagaaatagcaagttaaaataaggctagtccgttatcaacttgaaaaagtggcaccgagtcggtgcttttttt

sgC3 ds template, incomplete strand
T7 promoter, sgRNA
aaaaaagcaccgactcggtgccacttttcaagttgataacggactagccttattttaacttgctatttctagctctaaaactagtgactcgaattctaatactatagtgagtcg

pET-Duet-1-OmpG-mRasp-7150, https://benchling.com/s/Gd0ev1qG
T7 promoter, His tag, signal peptide, OmpG, Broccoli, mRaspberry, T7 terminator
taatacgactcactataggggaattgtgagcggataacaattcccctctagaaataaTGCACGATTTACTAGTGCAGTGGTCGGTTGTTCGACCTAGGTAATACGACTCACTATAGGGTCT
ATACTAGAGCCAATACACCCACCGAAGGAGCCGACTCTCCAAATGCATCATCATCACCACCACAAAAAACTCTTGCCGTGCACCGCCTTAGTGATGTGCGCGGG
CATGGCCTGTGCGCAAGCGGAAGAACGTAACGATTGGCATTTCAACATCGGTGCCATGTACGAAATTGAGAATGTAGAAGGTTATGGCGAAGACATGGACGGGC
TGGCCGAACCCTCCGTTTATTTTAATGCAGCTAACGGTCCGTGGCGTATTGCACTGGCATACTATCAAGAGGGACCGGTAGACTACAGTGCCGGTAAACGTGGT
ACGTGGTTTGATCGCCCTGAGCTGGAAGTTCACTACCAGTTCCTGGAAAATGATGATTTCTCATTTGGTCTCACAGGCGGGTTCCGGAACTATGGCTACCATTAC
GTAGATGAACCAGGTAAAGATACTGCAAACATGCAGCGCTGGAAAATTGCACCGGATTGGGATGTGAAGCTGACTGATGATCTTCGTTTTAATGGGTGGCTGTCG
ATGTATAAATTTGCCAATGACCTCAACACTACTGGCTACGCGGACACGCGCGTCGAAACCGAAACAGGTCTGCAGTACACTTTTAATGAGACCGTCGCACTGCGT
GTAAACTACTATTTAGAACGCGGATTTAATATGGATGATTCACGTAACAATGGCGAGTTCTCTACTCAGGAGATCCGCGCATATTTACCGCTGACCCTGGGCAATC
ATAGTGTCACGCCGTACACCCGCATTGGACTGGATCGCTGGAGCAATTGGGATTGGCAGGACGATATCGAGCGCGAATGTCATGATTTCAATCGGGTTGGGCTG
TTCTATGGTTACGATTTCCAGAACGGCCTGTCCGTCTCTCTGGAATATGCGTTTGAATGGCAGGACCATTGTGAAGGGGATTCCGATAAATTTCACTATGCCGGC
GTCGGAGTGAACTATAGCTTCTAGTAAGGTCGGGTCCATCTGAGACGGTCGGGTCCAGATATTCGTATAATGCCAGCAAGCCTGAGACGGTCGGGTCCATCTGA
GACGGTCGGGTCCAGATATTCGTATCTGTCGAGTAGAGTGTGGGCTCAGATGTCGAGTAGAGTGTGGGCTCAGGCTTCTAGCATAACCCCTTGGGGCCTCTAAA
CGGGTCTTGCTTCTTTTATATGCTTCGCCCGCCGGACCGGCCTCGGCATGGCGTAGCAGTGCACAAGCATAATACGACTCACTATAGGGTCTATACTAGAGATC
AAAGATCTTAACACAACTACGGGGAGGAAAGATGGTGTCCAAGGGTGAGGAAGTTATCAAAGAGTTTATGCGCTTCAAAGTTCGCATGGAAGGTAGCGTTAATGG
TCATGAATTCGAGATCGAAGGCGAGGGCGAGGGCCGCCCCGTATGAAGGTACCCAGACAGCGAAACTGAAAGTCACCAAAGGCGGCCCTTTACCTTTCGCCTGG
GATATTCTGTCTCCGCAGTGCATGTATGGTTCTAAAGGATATGTTAAACATCCAGCTGACATTCCCGATTACCTCAAATTAAGCTTCCCTGAGGGGTTCAAGTGGG
AGCGCGTGATGAACTTCGAGGATGGCGGTGTAGTGACGGTTACCCAGGATTCGTCCTTGCAGGATGGTGAATTTATTTATAAAGTTAAACTGCGGGGTACGAATT
TCCCATCAGATGGCCCTGTGATGCAGAAGAAGACAATGGGGTGGGAGGCATCCAGCGAACGTATGTATCCAGAAGATGGTGCGTTAAAAGGAGAAATGAAGATG
CGCTTAAAACTGAAAGACGGCGGTCATTACGATGCTGAAGTGAAAACGACATACATGGCTAAGAAACCGGTACAGCTGCCGGGTGCGTACAAAACGGATATCAA
ACTTGACATCACTTCACATAACGAGGACTATACCATTGTCGAGCAATACGAACGTGCCGAGGGTCGCCACAGCACGGGTGCATAATAACTAGCATAACCCCTTG
GGGCCTCTAAACGGGTCTTGATGAGGTCCACAGGACACTCGTCGCTCTAGAGTCGCTTTCgcagcttaattaacctaggctgctgccaccgctgagcaataactagcataaccccttgggg
cctctaaacgggtcttgaggggttttttg

pET-Duet-1-OmpG-6364, https://benchling.com/s/U8svxQaQ
T7 promoter, His tag, signal peptide, OmpG, Broccoli, T7 terminator
taatacgactcactatagggaattgtgagcggataacaattcccctctagaaataaTGCACGATTTACTAGTGCAGTGGTCGGTTGTTCGACCTAGGTAATACGACTCACTATAGGGTCT
ATACTAGAGCCAATACACCCACCGAAGGAGCCGACTCTCCAAATGCATCATCATCACCACCACAAAAAACTCTTGCCGTGCACCGCCTTAGTGATGTGCGCGGG
CATGGCCTGTGCGCAAGCGGAAGAACGTAACGATTGGCATTTCAACATCGGTGCCATGTACGAAATTGAGAATGTAGAAGGTTATGGCGAAGACATGGACGGGC
TGGCCGAACCCTCCGTTTATTTTAATGCAGCTAACGGTCCGTGGCGTATTGCACTGGCATACTATCAAGAGGGACCGGTAGACTACAGTGCCGGTAAACGTGGT
ACGTGGTTTGATCGCCCTGAGCTGGAAGTTCACTACCAGTTCCTGGAAAATGATGATTTCTCATTTGGTCTCACAGGCGGGTTCCGGAACTATGGCTACCATTAC
GTAGATGAACCAGGTAAAGATACTGCAAACATGCAGCGCTGGAAAATTGCACCGGATTGGGATGTGAAGCTGACTGATGATCTTCGTTTTAATGGGTGGCTGTCG
ATGTATAAATTTGCCAATGACCTCAACACTACTGGCTACGCGGACACGCGCGTCGAAACCGAAACAGGTCTGCAGTACACTTTTAATGAGACCGTCGCACTGCGT
GTAAACTACTATTTAGAACGCGGATTTAATATGGATGATTCACGTAACAATGGCGAGTTCTCTACTCAGGAGATCCGCGCATATTTACCGCTGACCCTGGGCAATC
ATAGTGTCACGCCGTACACCCGCATTGGACTGGATCGCTGGAGCAATTGGGATTGGCAGGACGATATCGAGCGCGAATGTCATGATTTCAATCGGGTTGGGCTG
TTCTATGGTTACGATTTCCAGAACGGCCTGTCCGTCTCTCTGGAATATGCGTTTGAATGGCAGGACCATTGTGAAGGGGATTCCGATAAATTTCACTATGCCGGC
GTCGGAGTGAACTATAGCTTCTAGTAAGGTCGGGTCCATCTGAGACGGTCGGGTCCAGATATTCGTATAATGCCAGCAAGCCTGAGACGGTCGGGTCCATCTGA
GACGGTCGGGTCCAGATATTCGTATCTGTCGAGTAGAGTGTGGGCTCAGATGTCGAGTAGAGTGTGGGCTCAGGCTTCTAGCATAACCCCTTGGGGCCTCTAAA
CGGGTCTTGCTTCTTTTATATGCTTCGCCCGCCGGACCGGCCTCGGCATGGCGTAGCAGTGCACAAGCAATATGAGGTCCACAGGACACTCGTCGCTCTAGAG
TCGCTTTCgcagcttaattaacctaggctgctgccaccgctgagcaataactagcataaccccttggggcctctaaacgggtcttgaggggttttttg

pET-Duet-1-mRasp-5921, https://benchling.com/s/AuH6OeBU
T7 promoter, mRaspberry, T7 terminator
taatacgactcactatagggaattgtgagcggataacaattcccctctagaaataaTGCACGATTTACTAGTGCAGTGGTCGGTTGTTATATGGCGTAGCAGTGCACAAGCATAATACGA
CTCACTATAGGGTCTATACTAGAGATCAAAGATCTTAACACAACTACGGGGAGGAAAGATGGTGTCCAAGGGTGAGGAAGTTATCAAAGAGTTTATGCGCTTCAA
AGTTCGCATGGAAGGTAGCGTTAATGGTCATGAATTCGAGATCGAAGGCGAGGGCGAGGGCCGCCCGTATGAAGGTACCCAGACAGCGAAACTGAAAGTCACC
AAAGGCGGCCCTTTACCTTTCGCCTGGGATATTCTGTCTCCGCAGTGCATGTATGGTTCTAAAGGATATGTTAAACATCCAGCTGACATTCCCGATTACCTCAAAT
TAAGCTTCCCTGAGGGGTTCAAGTGGGAGCGCGTGATGAACTTCGAGGATGGCGGTGTAGTGACGGTTACCCAGGATTCGTCCTTGCAGGATGGTGAATTTATT
TATAAAGTTAAACTGCGGGGTACGAATTTCCCATCAGATGGCCCTGTGATGCAGAAGAAGACAATGGGGTGGGAGGCATCCAGCGAACGTATGTATCCAGAAGA
TGGTGCGTTAAAAGGAGAAATGAAGATGCGCTTAAAACTGAAAGACGGCGGTCATTACGATGCTGAAGTGAAAACGACATACATGGCTAAGAAACCGGTACAGCT
GCCGGGTGCGTACAAAACGGATATCAAACTTGACATCACTTCACATAACGAGGACTATACCATTGTCGAGCAATACGAACGTGCCGAGGGTCGCCACAGCACGG
GTGCATAATAACTAGCATAACCCCTTGGGGCCTCTAAACGGGTCTTGATGAGGTCCACAGGACACTCGTCGCTCTAGAGTCGCTTTCgcagcttaattaacctaggctgctg
ccaccgctgagcaataactagcataaccccttggggcctctaaacgggtcttgaggggttttttg

pBAD33-DsRedmut, https://benchling.com/s/seq-AHfd51V1xqon7sxnsstk

araC, pBAD, dsRedmut

TGACAACTTGACGGCTACATCATTCACTTTTTCTTCACAACCGGCACGGAACTCGCTCGGGCTGGCCCCGGTGCATTTTTTAAATACCCGCGAGAAATAGAGTTG
ATCGTCAAAACCAACATTGCGACCGACGGTGGCGATAGGCATCCGGGTGGTGCTCAAAAGCAGCTTCGCCTGGCTGATACGTTGGTCCTCGCGCCAGCTTAAG
ACGCTAATCCCTAACTGCTGGCGGAAAAGATGTGACAGACGCGACGGCGACAAGCAAACATGCTGTGCGACGCTGGCGATATCAAAATTGCTGTCTGCCAGGT
GATCGCTGATGTACTGACAAGCCTCGCGTACCCGATTATCCATCGGTGGATGGAGCGACTCGTTAATCGCTTCCATGCGCCGCAGTAACAATTGCTCAAGCAGA
TTTATCGCCAGCAGCTCCGAATAGCGCCCTTCCCCTTGCCCGGCGTTAATGATTTGCCCAAACAGGTCGCTGAAATGCGGCTGGTGCGCTTCATCCGGGCGAA
AGAACCCCGTATTGGCAAATATTGACGGCCAGTTAAGCCATTCATGCCAGTAGGCGCGCGGACGAAAGTAAACCCACTGGTGATACCATTCGCGAGCCTCCGG
ATGACGACCGTAGTGATGAATCTCTCCTGGCGGGAACAGCAAAATATCACCCGGTCGGCAAACAAATTCTCGTCCCTGATTTTTCACCACCCCCTGACCGCGAA
TGGTGAGATTGAGAATATAACCTTTCATTCCCAGCGGTCGGTCGATAAAAAAATCGAGATAACCGTTGGCCTCAATCGGCGTTAAACCCGCCACCAGATGGGCAT
TAAACGAGTATCCCGGCAGCAGGGGATCATTTTGCGCTTCAGCCATACTTTTCATACTCCCGCCATTCAGAGAAGAAACCAATTGTCCATATTGCATCAGACATTG
CCGTCACTGCGTCTTTTACTGGCTCTTCTCGCTAACCAAACCGGTAACCCCGCTTATTAAAAGCATTCTGTAACAAAGCGGGACCAAAGCCATGACAAAAACGCG
TAACAAAAGTGTCTATAATCACGGCAGAAAAGTCCACATTGATTATTTGCACGGCGTCACACTTTGCTATGCCATAGCATTTTTATCCATAAGATTAGCGGATCCTA
CCTGACGCTTTTTATCGCAACTCTCTACTGTTTCTCCATACCCGTTTTTTTGGGCTAGCGAATTCGAGCTCGGTACCCGGGGATCCTCTAGAAGGAGATATAACCA
TGGCCTGCGAGCAGTACGTCATCACCGAGTTCATGCGCTTCAAGGTGCGCATGGAGGGCACCGTGAACGGCCACGAGTTCGAGATCGAGGGCGAGGGCGAG
GGCCGCCCCTACGAGGGCCACAACACCGTGAAGCTGAAGGTGACCAAGGGCGGCCCCCTGCCCTTCGCCTGGGACATCCTGTCCCCCCAGTTCATGTACGG
CTCCAAGGTGTACGTGAAGCACCCCGCCGACATCCCCGACTACAAGAAGCTGTCCTTCCCCGAGGGCTTCAAGTGGGAGCGCGTGATGAACTTCGAGGACGG
CGGCGTGGCGACCGTGACCCAGGACTCCTCCCTGCAGGACGGCTGCTTCATCTACAAGGTGAAGTTCATCGGCGTGAACTTCCCCTCCGACGGCCCCGTGAT
GCAGAAGAAGACCATGGGCTGGGAGGCCTCCACCGAGCGCCTGTACCCCCGCGACGGCGTGCTGAAGGGCGAGACCCACAAGGCCCTGAAGCTGAAGGAC
GGCGGCCACTACCTGGTGGAGTTCAAGTCCATCTACATGGCCAAGAAGCCCGTGCAGCTGCCCGGCTACTACTACGTGGACGCCAAGCTGGACATCACCTCC
CACAACGAGGACTACACCATCGTGGAGCAGTACGAGCGCACCGAGGGCCGCCACCACCTGTTCCTGTAGCGGCCGCGACTCTATCTAGAGTCGACCTGCAGG
CATGCAAGCTTGGCTGTTTTGGCGGATGAGAGAAGATTTTCAGCCTGATACAGATTAAATCAGAACGCAGAAGCGGTCTGATAAAACAGAATTTGCCTGGCGGCA
GTAGCGCGGTGGTCCCACCTGACCCCATGCCGAACTCAGAAGTGAAACGCCGTAGCGCCGATGGTAGTGTGGGGTCTCCCCATGCGAGAGTAGGGAACTGCC
AGGCATCAAATAAAACGAAAGGCTCAGTCGAAAGACTGGGCCTTTCGTTTTAT

pCK301, https://benchling.com/s/seq-4YmBvKy6NsJuUAQluTtt, from [171]

pRhaBAD, sfGFP

CCACAATTCAGCAAATTGTGAACATCATCACGTTCATCTTTCCCTGGTTGCCAATGGCCCATTTTCCTGTCAGTAACGAGAAGGTCGCGTATTCAGGCGCTTTTTA
GACTGGTCGTAATGAAACGGTTTCCCTCTAGAAATAATTTTGTTTAACTTTTAGGAGGTAAAACATATGCGTAAAGGCGAAGAGCTGTTCACTGGTGTCGTCCCTAT
TCTGGTGGAACTGGATGGTGATGTCAACGGTCATAAGTTTTCCGTGCGTGGCGAGGGTGAAGGTGACGCAACTAATGGTAAACTGACGCTGAAGTTCATCTGTA
CTACTGGTAAACTGCCGGTACCTTGGCCGACTCTGGTAACGACGCTGACTTATGGTGTTCAGTGCTTTGCTCGTTATCCGGACCATATGAAGCAGCATGACTTCT
TCAAGTCCGCCATGCCGGAAGGCTATGTGCAGGAACGCACGATTTCCTTTAAGGATGACGGCACGTACAAAACGCGTGCGGAAGTGAAATTTGAAGGCGATACC
CTGGTAAACCGCATTGAGCTGAAAGGCATTGACTTTAAAGAAGACGGCAATATCCTGGGCCATAAGCTGGAATACAATTTTAACAGCCACAATGTTTACATCACCG
CCGATAAACAAAAAAATGGCATTAAAGCGAATTTTAAAATTCGCCACAACGTGGAGGATGGCAGCGTGCAGCTGGCTGATCACTACCAGCAAAACACTCCAATCG
GTGATGGTCCTGTTCTGCTGCCAGACAATCACTATCTGAGCACGCAAAGCGTTCTGTCTAAAGATCCGAACGAGAAACGCGATCATATGGTTCTGCTGGAGTTCG
TAACCGCAGCGGGCATCACGCATGGTATGGATGAACTGTACAAAGGCTCCGGCTCCGGCTCCCCATCACCATCACCATTGATAACTCGAGCCCCAAGGGCG
ACACCCCATAATTAGCCCGGGCGAAAGGCCCAGTCTTTCGACTGAGCCTTTCGTTTTATTTGATGCCTGGCAGTTCCCTACTCTCGCATGGGGAGTCCCCACACT
ACCATCGGCGCTACGGCGTTTCACTTCTGAGTTCGGCATGGGGTCAGGTGGGACCACCGCGCTACTGCCGCCAGGCAAACAAGGGGTGTTATGAGCCATATTC
AGGTATAAATGGGCTCGCGATAATGT

pPhlF-P2, https://benchling.com/s/seq-XFd0xQ4JrTRpudYMWtVL, from [122]

pTac, PhlF, pPhlF, YFP

TGTTGACAATTAATCATCGGCTCGTATAATGTGTGGAATTGTGAGCGCTCACAATTAGCGGTCAACGCATGTGCTTTGCGTTCTGATGAGACAGTGATGTCGAAAC
CGCCTCTACAAATAATTTTGTTTAAGGAGCTATGGACTATGTTTGAAAGGCTGAAATACTAGATGGCACGTACCCGAGCCGTAGCAGCATTGGTAGCCTGCGTA
GTCCGCATACCCATAAAGCAATTCTGACCAGCACCATTGAAATCCTGAAAGAATGTGGTTATAGCGGTCTGAGCATTGAAAGCGTTGCACGTCGTGCCGGTGCAA
GCAAACCGACCATTTATCGTTGGTGGACCAATAAAGCAGCACTGATTGCCGAAGTGTATGAAAATGAAAGCGAACAGGTGCGTAAATTTCCGGATCTGGGTAGCT
TTAAAGCCGATCTGGATTTTCTGCTGCGTAATCTGTGGAAAGTTTGGCGTGAAACCATTTGTGGTGAAGCATTTCGTTGTGTTATTGCAGAAGCACAGCTGGACCC
TGCAACCCTGACCCAGCTGAAAGATCAGTTTATGGAACGTCGTCGTGAGATGCCGAAAAAACTGGTTGAAAATGCCATTAGCAATGGTGAACTGCCGAAAGATAC
CAATCGTGAACTGCTGCTGGATATGATTTTTGGTTTTTGTTGGTATCGCCTGCTGACCGAACAGCTGACCGTTGAACAGGATATTGAAGAATTTACCTTCCTGCTG
ATTAATGGTGTTTGTCCGGGTACACAGCGTTAAGGAAACACAGAAAAAAGCCCGCACCTGACAGTGCGGGCTTTTTTTTTCGACCAAAGGTACTCGACGTACGGT
GGAATCTGATTCGTTACCAATTGACATGATACGAAACGTACCGTATCGTTAAGGTAGCTGTCACCGGATGTGCTTTCCGGTCTGATGAGTCCGTGAGGACGAAAC
AGCCTCTACAAATAATTTTGTTTAATACTAGAGAAAGAGGGGAAATACTAGATGGTGAGCAAGGGCGAGGAGCTGTTCACCGGGGTGGTGCCCATCCTGGTCGA
GCTGGACGGCGACGTAAACGGCCACAAGTTCAGCGTGTCCGGCGAGGGCGAGGGCGATGCCACCTACGGCAAGCTGACCCTGAAGTTCATCTGCACCACAG
GCAAGCTGCCCGTGCCCTGGCCCACCCTCGTGACCACCTTCGGCTACGGCCTGCAATGCTTCGCCCGCTACCCCGACCACATGAAGCTGCACGACTTCTTCA
AGTCCGCCATGCCCGAAGGCTACGTCCAGGAGCGCACCATCTTCTTCAAGGACGACGGCAACTACAAGACCCGCGCCGAGGTGAAGTTCGAGGGCGACACCC
TGGTGAACCGCATCGAGCTGAAGGGCATCGACTTCAAGGAGGACGGCAACATCCTGGGGCACAAGCTGGAGTACAACTACAACAGCCACAACGTCTATATCAT
GGCCGACAAGCAGAAGAACGGCATCAAGGTGAACTTCAAGATCCGCCACAACATCGAGGACGGCAGCGTGCAGCTCGCCGACCACTACCAGCAGAACACCCC
AATCGGCGACGGCCCCGTGCTGCTGCCCGACAACCACTACCTTAGCTACCAGTCCGCCCTGAGCAAAGACCCCAACGAGAAGCGCGATCACATGGTCCTGCT
GGAGTTCGTGACCGCCGCCGGGATCACTCTCGGCATGGACGAGCTGTACAAGTAACTCGGTACCAAATTCCAGAAAAGAGGCCTCCCGAAAGGGGGGCCTTTT
TTCGTTTTGGTCCAATGGCGGCGCGCCATCGAATGGCGCAAAACCTTTCGCGGTATGGCATGATAGCGCCCGGAAGAGAGTCAATTCAGGGTGGTGAATATGAA
ACCAGTAACGTTATACGATGTCGCAGAGTATGCCGGTGTCTCTTATCAGACCGTTTCCCGCGTGGTGAACCAGGCCAGCCACGTTTCTGCGAAAACGCGGGAAA
AAGTGGAAGCGGCGATGGCGGAGCTGAATTACATTCCCAACCGCGTGGCACAACAACTGGCGGGCAAACAGTCGTTGCTGATTGGCGTTGCCACCTCCAGTCT
GGCCCTGCACGCGCCGTCGCAAATTGTCGCGGCGATTAAATCTCGCGCCGATCAACTGGGTGCCAGCGTGGTGGTGTCGATGGTAGAACGAAGCGGCGTCGA
AGCCTGTAAAGCGGCGGTGCACAATCTTCTCGCGCAACGCGTCAGTGGGCTGATCATTAACTATCCGCTGGATGACCAGGATGCCATTGCTGTGGAAGCTGCCT
GCACTAATGTTCCGGCGTTATTTCTTGATGTCTCTGACCAGACACCCATCAACAGTATTATTTTCTCCCATGAGGACGGTACGCGACTGGGCGTGGAGCATCTGG
TCGCATTGGGTCACCAGCAAATCGCGCTGTTAGCGGGCCCATTAAGTTCTGTCTCGGCGCGTCTGCGTCTGGCTGGCTGGCATAAATATCTCACTCGCAATCAA
ATTCAGCCGATAGCGGAACGGGAAGGCGACTGGAGTGCCATGTCCGGTTTTCAACAAACCATGCAAATGCTGAATGAGGGCATCGTTCCCACTGCGATGCTGG
TTGCCAACGATCAGATGGCGCTGGGCGCAATGCGCGCCATTACCGAGTCCGGGCTGCGCGTTGGTGCGGATATCTCGGTAGTGGGATACGACGATACCGAAG
ATAGCTCATGTTATATCCCGCCGTTAACCACCATCAAACAGGATTTTCGCCTGCTGGGGCAAACCAGCGTGGACCGCTTGCTGCAACTCTCTCAGGGCCAGGCG
GTGAAGGGCAATCAGCTGTTGCCAGTCTCACTGGTGAAAAGAAAAACCACCCTGGCGCCCAATACGCAAACCGCCTCTCCCCGCGCGTTGGCCGATTCATTAAT
GCAGCTGGCACGACAGGTTTCCCGACTGGAAAGCGGGCAGTGATAATCCAGGAGGAAAAAAATGTCCAGATTAGATAAAAGTAAAGTGATTAACAGCGCATTAG
AGCTGCTTAATGAGGTCGGAATCGAAGGTTTAACAACCCGTAAACTCGCCCAGAAGCTAGGTGTAGAGCAGCCTACATTGTATTGGCATGTAAAAAATAAGCGGG
CTTTGCTCGACGCCTTAGCCATTGAGATGTTAGATAGGCACCATACTCACTTTTGCCCTTTAGAAGGGGAAAGCTGGCAAGATTTTTTACGTAATAACGCTAAAAG
TTTTAGATGTGCTTTACTAAGTCATCGCGATGGAGCAAAAGTACATTTAGGTACACGGCCTACAGAAAAACAGTATGAAACTCTCGAAAATCAATTAGCCTTTTTAT
GCCAACAAGGTTTTTCACTAGAGAATGCATTATATGCACTCAGCGCTGTGGGGCATTTTACTTTAGGTTGCGTATTGGAAGATCAAGAGCATCAAGTCGCTAAAGA
AGAAAGGGAAACACCTACTACTGATAGTATTGCCGCCATTATTACGACAAGCTATCGAATTATTTGATCACCAAGGTGCAGAGCCAGCCTTCTTATTCGGCCTTGAA
TTGATCATATGCGGATTAGAAAAACAACTTAAATGTGAAAGTGGGTCC

pSB1A3-pLacO-T9002-LVA, https://benchling.com/s/seq-YR8htB56EEW6P8wtxZYU, from [119]

pLacO, LuxR, pLux, GFPmut3, LVA degtag

tgccacctgacgtctaagaaaccattattatcatgacattaacctataaaaataggcgtatcacgaggcagaatttcagataaaaaaaatccttagctttcgctaaggatgatttctggaattcgcggccgcttctagagctgataaa
tgtgagcggataacattgacattgtgagcggataacaagatactgagcactagagaaagaggagaaatactagatgaaaaacataaatgccgacgacacatacagaataattaataaaattaaagcttgtagaagcaata
atgatattaatcaatgcttatctgatatgactaaaatggtacattgtgaatattatttactcgcgatcatttatcctcattctatggttaaatctgatatttcaatcctagataattaccctaaaaaatggaggcaatattatgatgacgctaattt
aataaaatatgatcctatagtagattattctaactccaatcattcaccaattaattggaaatatatttgaaaacaatgctgtaaatataaaaatctccaaatgtaattaaagaagcgaaaacatcaggtcttatcactgggtttagtttccctat
tcatacggctaacaatggcttcggaatgcttagttttgcacattcagaaaaagacaactatatagatagtttatttttacatgcgtgtatgaacatacccattaattgttccttctctagttgataatttatcgaaaaataaatatagcaaataat
aaatcaaacaacgatttaaccaaaagagaaaaagaatgtttagcgtgggcatgcgaaggaaaaagctcttgggatatttcaaaaatattaggttgcagtgagcgtactgtcactttccatttaaccaatgcgcaaatgaaactcaa
tacaacaaaccgctgccaaagtatttctaaagcaatttaacaggagcaattgattgcccatactttaaaaattaataacatgatagtgctagtgtagatcactactagagccaggcatcaaataaaacgaaaggctcagtcgaa
agactgggcctttcgttttatctgttgtttgtcggtgaacgctctctactagagtcacactggctcaccttcgggtgggcctttctgcgtttatatactagagacctgtaggatcgtacaggtttacgcaagaaaatggtttgttatagtcg
aataaatactagagtcacacaggaaagtactagatgcgtaaaggagaagaacttttcactggagttgtcccaattcttgttgaattagatggtgatgttaatgggcacaaattttctgtcagtggagagggtgaaggtgatgcaacat
acggaaaacttacccttaaatttatttgcactactggaaaactacctgttccatggccaacacttgtcactactttcggttatggtgttcaatgctttgcgagatacccagatcatatgaaacagcatgactttttcaagagtgccatgcc
cgaaggttatgtacaggaaagaactatatttttcaaagatgacgggaactacaagacacgtgctgaagtcaagtttgaaggtgataccgttgttaatagaatcgagttaaaaggtattgatttaaagaagatggaaacattcttgga
cacaaattggaatacaactataactcacacaatgtatacatcatggcagacaaacaaaagaatggaatcaaagttaacttcaaaattagacacaacattgaagatggaagcgttcaactagcagaccattatcaacaaaatact
ccaattggcgatggccctgtccttttaccagacaaccattacctgtccacacaatctgccctttcgaaagatcccaacgaaaagagagaccacatggtccttcttgagtttgtaacagctgctgggattacacatggcatggatga
actatacaaaAGGCCTGCTGCAAACGACGAAAACtACGCTTTagtagCTTAAtaataatactagtagcggccgctgcagtccggcaaaaaagggcaaggtgtcaccaccctgccctttttcttttaaaaccg
aaaagattacttcgcgttatgcaggcttcctcgctcactgactcgctgcgctcggtcgttcggctgcggcgagcggtatcagctcactcaaaggcggtaat

pSB1A3-pLacO-GFP, https://benchling.com/s/seq-6XyH5h3vss0N7l7OlycL

pLacO-1, GFPmut3 (BBa_E0040)

TGCCACCTGACGTCTAAGAAACCATTATTATCATGACATTAACCTATAAAAATAGGCGTATCACGAGGCAGAATTTCAGATAAAAAAAATCCTTAGCTTTCGCTAAG
GATGATTTCTGGAATTCATTCTGATAAATGTGAGCGGATAACATTGACATTGTGAGCGGATAACAAGATACTGAGCACCTATGGACTATGTTTTCACATACGAGGG
GGATTAGATGCGTAAAGGAGAAGAACTTTTCACTGGAGTTGTCCCAATTCTTGTTGAATTAGATGGTGATGTTAATGGGCACAAATTTTCTGTCAGTGGAGAGGGT
GAAGGTGATGCAACATACGGAAAACTTACCCTTAAATTTATTTGCACTACTGGAAAACTACCTGTTCCATGGCCAACACTTGTCACTACTTTCGGTTATGGTGTTCA
ATGCTTTGCGAGATACCCAGATCATATGAAACAGCATGACTTTTTCAAGAGTGCCATGCCCGAAGGTTATGTACAGGAAAGAACTATATTTTTCAAAGATGACGGG
AACTACAAGACACGTGCTGAAGTCAAGTTTGAAGGTGATACCCTTGTTAATAGAATCGAGTTAAAAGGTATTGATTTTAAAGAAGATGGAAACATTCTTGGACACAA
ATTGGAATACAACTATAACTCACACAATGTATACATCATGGCAGACAAACAAAAGAATGGAATCAAAGTTAACTTCAAAATTAGACACAACATTGAAGATGGAAGCG
TTCAACTAGCAGACCATTATCAACAAAATACTCCAATTGGCGATGGCCCTGTCCTTTTACCAGACAACCATTACCTGTCCACACAATCTGCCCTTTCGAAAGATCC
CAACGAAAAGAGAGACCACATGGTCCTTCTTGAGTTTGTAACAGCTGCTGGGATTACACATGGCATGGATGAACTATACAAATAAGGAAACACAGAAAAAAGCCC
GCACCTGACAGTGCGGGCTTTTTTTTTCGACCAAAGGGGCTTTTTTGTTATTTCTGCAGTCCGGCAAAAAAGGGCAAGGTGTCACCACCCTGCCCTTTTTCTTTAA
AACCGAAAAGATTACTTCGCGTTATGCAGGCTTCCTCGCTCACTGACTCGCTGCGCTCGGTCGTTCGGCTGCGGCGAGCGGTATCAGCTCACTCAAAGGCGGT
AAT

pSB1A3-I13521, https://benchling.com/s/33pnk7Cl

pTetO, mRFP (BBa_E1010)

TGCCACCTGACGTCTAAGAAACCATTATTATCATGACATTAACCTATAAAAATAGGCGTATCACGAGGCAGAATTTCAGATAAAAAAAATCCTTAGCTTTCGCTAAG
GATGATTTCTGGAATTCGCGGCCGCTTCTAGAGTCCCTATCAGTGATAGAGATTGACATCCCTATCAGTGATAGAGATACTGAGCACTACTAGAGAAAGAGGAGA
AATACTAGATGGCTTCCTCCGAAGACGTTATCAAAGAGTTCATGCGTTTCAAAGTTCGTATGGAAGGTTCCGTTAACGGTCACGAGTTCGAAATCGAAGGTGAAG
GTGAAGGTCGTCCGTACGAAGGTACCCAGACCGCTAAACTGAAAGTTACCAAAGGTGGTCCGCTGCCGTTCGCTTGGGACATCCTGTCCCCGCAGTTCCAGTA
CGGTTCCAAAGCTTACGTTAAACACCCGGCTGACATCCCGGACTACCTGAAACTGTCCTTCCCGGAAGGTTTCAAATGGGAACGTGTTATGAACTTCGAAGACG
GTGGTGTTGTTACCGTTACCCAGGACTCCTCCCTGCAAGACGGTGAGTTCATCTACAAAGTTAAACTGCGTGGTACCAACTTCCCGTCCGACGGTCCGGTTATG
CAGAAAAAAACCATGGGTTGGGAAGCTTCCACCGAACGTATGTACCCGGAAGACGGTGCTCTGAAAGGTGAAATCAAAATGCGTCTGAAACTGAAAGACGGTGG
TCACTACGACGCTGAAGTTAAAACCACCTACATGGCTAAAAAACCGGTTCAGCTGCCGGGTGCTTACAAAACCGACATCAAACTGGACATCACCTCCCACAACG
AAGACTACACCATCGTTGAACAGTACGAACCGTGCTGAAGGTCGTCACTCCACCGGTGCTTAATAACGCTGATAGTGCTAGTGTAGATCGCTACTAGAGCCAGGC
ATCAAATAAAACGAAAGGCTCAGTCGAAAGACTGGGCCTTTCGTTTTATCTGTTGTTTGTCGGTGAACGCTCTCTACTAGAGTCACACTGGCTCACCTTCGGGTGG
GCCTTTCTGCGTTTATATACTAGTAGCGGCCGCTGCAGTCCGGCAAAAAAGGGCAAGGTGTCACCACCCTGCCCTTTTTCTTTAAAACCGAAAAGATTACTTCGC
GTTATGCAGGCTTCCTCGCTCACTGACTCGCTGCGCTCGGTCGTTCGGCTGCGGCGAGCGGTATCAGCTCACTCAAAGGCGGTAAT

pSB1A3-pT7-Th-YPet, https://benchling.com/s/seq-39oUNtRZoWH7a6Vxhz87

T7 promoter, theophylline riboswitch, YPet

tgccacctgacgtctaagaaaccattattatcatgacattaacctataaaaataggcgtatcacgaggcagaatttcagataaaaaaaatccttagctttcgctaaggatgatttctgGAATTCATTTAATACGACTCACT
ATAGGGTGATACCAGCATCGTCTTGATGCCCTTGGCAGCACCCTGCTAAGGTAACAACAAGATGGTGTCCAAAGGCGAAGAACTGTTTACCGGTGTGGTTCCGA
TTCTGGTGGAACTGGATGGCGACGTTAACGGTCATAAATTTAGTGTGTCCGGCGAAGGTGAAGGCGATGCGACCTATGGCAAACTGACGCTGAAACTGCTGTGC
ACCACCGGTAAACTGCCGGTCCCGTGGCCGACCCTGGTGACCACGCTGGGTTATGGCGTGCAGTGTTTCGCGCGCTACCCGGACCACATGAAACAACACGAT
TTCTTTAAAAGTGCCATGCCGGAAGGCTATGTTCAGGAACGTACCATCTTTTTCAAAGATGACGGTAACTACAAAACCCGCGCGGAAGTTAAATTTGAAGGCGATA
CGCTGGTCAACCGTATTGAACTGAAAGGTATCGACTTCAAAGAAGATGGCAATATTCTGGGTCATAAACTGGAATATAACTACAATAGCCACAACGTGTATATTAC
CGCGGATAAACAGAAAAACGGCATCAAAGCCAACTTCAAAATCCGCCATAACATCGAAGACGGCGGTGTTCAACTGGCCGATCACTACCAGCAAAACACCCCGA
TTGGTGATGGTCCGGTCCTGCTGCCGGATAATCATTATCTGTCATACCAGTCGAAACTGTTTAAAGACCCGAATGAAAAACGTGATCACATGGTGCTGCTGGAATT
TCTGACCGCGGCCGGCATTACGGAGGGTATGAACGAACTGTATAAATGATAATTAGTTAGTTAGCAGATCCGGCTGCTAACAAAGCCCGAAAGGAAGCTGAGTT
GGCTGCTGCCACCGTAGCAATAAAGAGAATATAAAAAGCCAGATTATTAATCCGGCTTTTTTGTTATTTCTGCAGtccggcaaaaaagggcaaggtgtcaccaccctgccctttttctt
taaaaccgaaaagattacttcgcgttatgcaggcttcctcgctcactgactcgctgcgctcggtcgttcggctgcggcgagcggtatcagctcactcaaaggcggtaat

pSB4A5-pT7-mScarletI, https://benchling.com/s/seq-TTKskZ3WFYl519d95eU6

T7 promoter, mScarletI, AAV degtag

tgccacctgacgtctaagaaaaggaatattcagcaatttgcccgtgccgaagaaaggcccacccgtgaaggtgagccagtgagttgattgctacgtaattagttagttagcccttagtgactcgaattcTAATACGACTCA
CTATAGGGTACTAGAGAAAGAGGAGAAAatggtgtcaaagggagaggcGGTTATCAAGGAATTTATGCGCTTTAAAGTCCACATGGAGGGCAGCATGAACGGGCACGAG
TTTGAAATTGAGGGGGAGGGGGAGGGCCGTCCTTATGAAGGTACTCAGACTGCTAAACTGAAGGTGACAAAAGGTGGCCCCTTGCCTTTCTCGTGGGACATCCT
GTCGCCACAATTCATGTACGGGAGCCGCGCCTTTATCAAACATCCCGCAGATATTCCTGATTACTATAAACAATCTTTCCCGGAAGGTTTCAAATGGGAACGCGT
CATGAATTTTGAGGACGGGGGCGCTGTCACAGTTACTCAGGACACCTCCTTGGAAGACGGCACATTGATTTACAAGGTTAAGTTGCGCGGCACAAACTTCCCCC
CTGACGGGCCAGTAATGCAAAAGAAAACTATGGGTTGGGAGGCGTCTACAGAACGTTTATACCCCGAAGACGGGGTGCTGAAAGGTGACATTAAGATGGCCCT
GCGCCTGAAGGACGGCGGTCGCTATCTTGCCGACTTTAAAACTACTTATAAGGCTAAAAAACCAGTCCAGATGCCAGGCGCCTATAATGTTGACCGCAAGTTAGA
CATCACCTCACATAATGAAGACTATACCGTTGTAGAACAATACGAGCGCAGCGAGGGTCGTCACAGTACCGGGGGGATGGATGAATTATACAAACGTCCTGCTG
CGAACGACGAAAATTATGCGGCTGCGGTTTGATAAGGAAACACAGAAAAAAGCCCGCACCTGACAGTGCGGGCTTTTTTTTTCGACCAAAGGTTAATTAAACCTA
TAGGATCGTATAGGTTTACGCAAGAAAATGGTTTGTTATAGTCGAATAAACCTAGGCCCCCCGAGGAGTAGCACATGATTGTGCAAATCGGCCGCCGTGAGGAGT
TCGATAAAAAGCTGCTTGGGGAAATGCATAAACTTCGTGCTCAGGTGTTCAAGGAGCGTAAGGGGTGGGATGTTTCCGTTATTGACGAAATGGAAATTGATGGGT
ACGATGCATTATCACCTTACTATATGCTGATTCAAGAAGACACACCTGAGGCCCAGGTATTCGGTTGCTGGCGCATTTTTGACACGACGGGGCCTTACATGTTGA
AGAACACGTTTCCTGAATTGTTACACGGCAAAGAAGCTCCCTGCTCACCCCATATTTGGGAACTGAGCCGTTTCGCTATCAATTCCGGTCAAAAGGGCTCCCTGG
GCTTTTCGGACTGCACCCTTGAAGCCATGCGCGCACTTGCCCGTTACTCCCTGCAAAACGACATTCAAACCTTAGTTACTGTTACTACCGTTGGCGTAGAGAAGA
TGATGATCCGTGCGGGTCTTGACGTATCTCGCTTTGGACCGCATCTGAAGATTGGAATCGAGCGTGCGGTGGCGTTGCGCATCGAATTGAACGCAAAAACGCAA
ATTGCGTTATACGGCGGGGTCTTGGTTGAACAGCGTTTAGCCGTGAGTTGATAATCCGGCAATTAAAAAAGCGGCTAACCACGCCGCTTTTTTTACGTCTGCActg
caggagtcactaagggttagttagttagattagcagaaagtcaaaagcctccgaccggaggcttttgactaaaactccctggggttatcattggggctcactcaaaggcggtaat

pSB4A5-pT7-mCherry, https://benchling.com/s/seq-SbUZMbDgailfzlhTo7ou

T7 promoter, mCherry, AAV degtag

tgccacctgacgtctaagaaaaggaatattcagcaatttgcccgtgccgaagaaaggcccacccgtgaaggtgagccagtgagttgattgctacgtaattagttagttagccctagtgactcgaattctactccaccgttggcT
AATACGACTCACTATAGGGTACTAGAGAAAGAGGAGAAAtactagatggtcagcaagggcGAGGAGGATAACATGGCCATCATCAAGGAGTTCATGCGCTTCAAGGTGCA
CATGGAGGGCTCCGTGAACGGCCACGAGTTCGAGATCGAGGGCGAGGGCGAGGGCCGCCCCTACGAGGGCACCCAGACCGCCAAGCTGAAGGTGACCAAG
GGTGGCCCCCTGCCCTTCGCCTGGGACATCCTGTCCCCTCAGTTCATGTACGGCTCCAAGGCCTACGTGAAGCACCCGCCCGACATCCCCGACTACTTGAAG
CTGTCCTTCCCCGAGGGCTTCAAGTGGGAGCGCGTGATGAACTTCGAGGACGGCGGCGTGGTGACCGTGACCCAGGACTCCTCCCTGCAAGACGGCGAGTTC
ATCTACAAGGTGAAGCTGCGCGGCACCAACTTCCCCTCCGACGGCCCCGTAATGCAGAAGAAGACTATGGGCTGGGAGGCCTCCTCCGAGCGGATGTACCCC
GAGGACGGCGCCCTGAAGGGCGAGATCAAGCAGAGGCTGAAGCTGAAGGACGGCGGCCACTACGACGCTGAGGTCAAGACCACCTACAAGGCCAAGAAGCC
CGTGCAGCTGCCCGGCGCCTACAACGTCAACATCAAGTTGGACATCACCTCCCACAACGAGGACTACACCATCGTGGAACAGTACGAACGCGCCGAGGGCCG
CCACTCCACCGGCGGCATGGACGAGCTGTACAAGCGCCCGGCGGCGAACGATGAAAACTATGCGGCAGCGGTTTAATTCAGCCAAAAAACTTAAGACCGCCG
GTCTTGTCCACTACCTTGCAGTAATGCGGTGGACAGGATCGGCGGTTTTCTTTTCTCTTCTCAActgcaggagtcactaagggttagttagttagattagcagaaagtcaaaagcctccga
ccggaggcttttgactaaaacttcccttggggttatcattggggctcactcaaaggcggtaat

pSB4A5-pT7-RFP, https://benchling.com/s/seq-MliKy0nkFBCuHPSQwTl3

T7 promoter, RFP

tgccacctgacgtctaagaaaaggaatattcagcaatttgcccgtgccgaagaaaggcccacccgtgaaggtgagccagtgagttgattgctacgtaattagttagttagcccttagtgactcgaattcgcggccgcttctagag
TAATACGACTCACTATAGGGtactagagaaagaggagaaatactagatggcttcctccgaagacgttatcaaagagttcatgcgtttcaaagttcgtatggaaggttccgttaacggtcacgagttcgaaatcgaaggt
gaaggtgaaggtcgtccgtacgaaggtacccagacgctaaactgaaagttaccaaaggtggtccgctgccgttcgcttgggacatcctgtcccgcagttccagtacggttccaaagcttacgttaaacacccggctgaca
tccggactacctgaaactgtccttcccggaaggtttcaaatgggaacgtgttatgaacttcgaagacggtggtgttgttaccgttacccaggactcctccctgcaagacggtgagttcatctacaaagttaaactgcgtggtacca
acttcccgtccgacggtccggttatgcagaaaaaaaccatgggttgggaagcttccaccgaacgtatgtacccggaagacggtgctctgaaaggtgaaatcaaaatgcgtctgaaactgaaagacggtggtcactacgacgc
tgaagttaaaaccacctacatggctaaaaaaccggttcagctgccgggtgcttacaaaaccgacatcaaactggacatcacctcccacaacgaagactacaccatcgttgaacagtacgaacgtgctgaaggtcgtcactcc
accggtgcttaataacgctgatagtgctagtgtagatcgctactagagccaggcatcaaataaaacgaaaggctcagtcgaaagactgggccttttgttttatctgttgtttgtcggtgaacgctctctactagagtcacactggctc
accttcgggtgggcctttctgcgtttatatactagtagcggccgctgcaggagtcactaagggttagttagttagattagcagaaagtcaaaagcctccgaccggaggcttttgactaaaacttcccttggggttatcattggggctc
actcaaaggcggtaat

pSB1C3-pLacO-TetR-GFP, https://benchling.com/s/seq-sVHoYxNk05eTOolVjQ1V

pLacO, TetR, GFP

tgccacctgacgtctaagaaaccattattatcatgacattaacctataaaaatagGCGTATCACGAGGCAGAATTTCAGATAAAAAAAATCCTTAGCTTTCGCTAAGGATGATTTGAATTCATTctgataaatgtgagcggataa
cattgacattgtgagcggataacaagatactgagcacCTGAGCGCTCAACGGGTGTGCTTCCCGTTCTGATGAGTCCGTGAGGACGAAAGCGCCTCTACAAATAATTTTGTTTAA
CCCCCCGAGGAGTAGCACatgtccagattagataaaagtaaagtgattaacagcgcattagagctgcttaatgaggtcggaatcgaaggtttaacaacccgtaaactcgcccagaagctaggtgtagagcagccta
cattgtattggcatgtaaaaaatgagcgggcttgctcgacgccttagccattgagatgttagataggcaccatactcacttttgcccttagaaggggaaagctggcaagatttttacgtaataacgctaaaagttttagatgtgctttt
actaagtcatcgcgatggagcaaaagtacatttaggtacacggcctacagaaaaacagtatgaaactctcgaaaatcaattagccttttatgccaacaaggttttcactagagaatgcattatatgcactcagcgctgtggggca
ttttacttaggttgcgtattggaagatcaagagcatcaagtcgctaaagaagaaagggaaacacctactactgatagtattgccgccattattacgacaagctatcgaattatttgatcaccaaggtgcagagccagcctttattc
ggccttgaattgatcatatgcggattagaaaaacaacttaaatgtgaaagtgggtcctaaTAAGCTCCGGCAAGCAATATCTGAGTAGTCACCGGCTGTGCTTGCCGGTCTGATGAGCCTGT
GAAGGCGAAACTACCTCTACAAATAATTTTGTTTAACTATGGACTATGTTTTCACATACGAGGGGGATTAGatgcgtaaaggagaagaacttttcactggagttgtcccaattcttgttgaa
ttagatggtgatgttaatgggcacaaattttctgtcagtggagagggtgaaggtgatgcaacatacggaaaacttaccctaaatttatttgcactactggaaaactacctgttccatggccaacacttgtcactactttcggttatggt
gttcaatgctttgcgagatacccagatcatatgaaacagcatgactttttcaagagtgccatgcccgaaggttatgtacaggaaagaactatatttttcaaagatgacgggaactacaagacacgtgctgaagtcaagtttgaaggt
gataccctgttaatagaatcgagttaaaaggtattgattttaaagaagatggaaacattcttggacacaaattggaatacaactataactcacacaatgtatacatcatggcagacaaacaaaagaatggaatcaaagttaacttc
aaaattagacacaacattgaagatggaagcgttcaactagcagaccattatcaacaaaatactccaattggcgatggccctgtccttttaccagacaaccattacctgtccacacaatctgccctttcgaaagatcccaacgaaa
agagagaccacatggtccttcttgagtttgtaacagctgctgggattacacatggcatggatgaactatacaaataaGGAAACACAGAAAAAAGCCCGCACCTGACAGTGCGGGCTTTTTTTTTCGA
CCAAAGGGGCTTTTTTGTTATTTctgcagtccggcaaaaaagggcaaggtgtcaccaccctgccctttttctttaaaaccgaaaagattacttcgcgttatgcaggcttcctcgctcactgactcgctgcgctcggtcg
ttcggctgcggcgagcggtatcagctcactcaaaggcggtaat

pSB1A3-pTetO-LacI-mCherry, https://benchling.com/s/ylv7lOrn

pTetO, LacI, mCherry, AAV-degtag

tgccacctgacgtctaagaaaccattattatcatgacattaacctataaaaatagGCGTATCACGAGGCAGAATTTCAGATAAAAAAAATCCTTAGCTTTCGCTAAGGATGATTTCTGGAATTCTACTCCACCGTTGGCT
TTTTTCCCTATCAGTGATAGAGATTGACATCCCTATCAGTGATAGAGATAATGAGCACCTGAGGGGTCAGTTGATGTGCTTTCAACTCTGATGAGTCAGTGATGAC
GAAACCCCCTCTACAAATAATTTTGTTTAACCCCCCGAGGAGTAGCACATGAAACCAGTAACGTTATACGATGTCGCAGAGTATGCCGGTGTCTCTTATCAGACC
GTTTCCCGCGTGGTGAACCAGGCCAGCCACGTTTCTGCGAAAACGCGGGAAAAAGTGGAAGCGGCGATGGCGGAGCTGAATTACATTCCCAACCGCGTGGCA
CAACAACTGGCGGGCAAACAGTCGTTGCTGATTGGCGTTGCCACCTCCAGTCTGGCCCTGCACGCGCCGTCGCAAATTGTCGCGGCGATTAAATCTCGCGCCG
ATCAACTGGGTGCCAGCGTGGTGGTGTCGATGGTAGAACGAAGCGGCGTCGAAGCCTGTAAAGCGGCGGTGCACAATCTTCTCGCGCAACGCGTCAGTGGGC
TGATCATTAACTATCCGCTGGATGACCAGGATGCCATTGCTGTGGAAGCTGCCTGCACTAATGTTCCGGCGTTATTTCTTGATGTCTCTGACCAGACACCCATCAA
CAGTATTATTTTCTCCCATGAGGACGGTACGCGACTGGGCGTGGAGCATCTGGTCGCATTGGGTCACCAGCAAATCGCGCTGTTAGCGGGCCCATTAAGTTCTG
TCTCGGCGCGTCTGCGTCTGGCTGGCTGGCATAAATATCTCACTCGCAATCAAATTCAGCCGATAGCGGAACGGGAAGGCGACTGGAGTGCCATGTCCGGTTTT
CAACAAACCATGCAAATGCTGAATGAGGGCATCGTTCCCACTGCGATGCTGGTTGCCAACGATCAGATGGCGCTGGGCGCAATGCGCGCCATTACCGAGTCCG
GGCTGCGCGTTGGTGCGGATATCTCGGTAGTGGGATACGACGATACCGAAGATAGCTCATGTTATATCCCGCCGTTAACCACCATCAAACAGGATTTTCGCCTG
CTGGGGCAAACCAGCGTGGACCGCTTGCTGCAACTCTCTCAGGGCCAGGCGGTGAAGGGCAATCAGCTGTTGCCAGTCTCACTGGTGAAAAGAAAAACCACC
CTGGCGCCCAATACGCAAACCGCCTCTCCCCGCGCGTTGGCCGATTCATTAATGCAGCTGGCACGACAGGTTTCCCGACTGGAAAGCGGGCAGTGATAATAAG
CTCCGGCAAGCACcCATGGATATCTGAGAAGTCAATTAATGTGCTTTTAATTCTGATGAGTCGGTGACGACGAAACTTCCTCTACAAATAATTTTGTTTAACTATGG
ACTATGTTTTAACTACTAGATGGTCAGCAAGGGCGAGGAGGATAACATGGCCATCATCAAGGAGTTCATGCGCTTCAAGGTGCACATGGAGGGCTCCGTGAACG
GCCACGAGTTCGAGATCGAGGGCGAGGGCGAGGGCCGCCCCTACGAGGGCACCCAGACCGCCAAGCTGAAGGTGACCAAGGGTGGCCCCCTGCCCTTCGCC
CTGGGACATCCTGTCCCCTCAGTTCATGTACGGCTCCAAGGCCTACGTGAAGCACCCCGCCGACATCCCCGACTACTTGAAGCTGTCCTTCCCCGAGGGCTTC
AAGTGGGAGCGCGTGATGAACTTCGAGGACGGCGGCGTGGTGACCGTGACCCAGGACTCCTCCCTGCAAGACGGCGAGTTCATCTACAAGGTGAAGCTGCGC
GGCACCAACTTCCCCTCCGACGGCCCCGTAATGCAGAAGAAGACTATGGGCTGGGAGGCCTCCTCCGAGCGGATGTACCCCGAGGACGGCGCCCTGAAGGG
CGAGATCAAGCAGAGGCTGAAGCTGAAGGACGGCGGCCACTACGACGCTGAGGTCAAGACCACCTACAAGGCCAAGAAGCCCGTGCAGCTGCCCGGCGCCT
ACAACGTCAACATCAAGTTGGACATCACCTCCCACAACGAGGACTACACCATCGTGGAACAGTACGAACGCGCCGAGGGCCGCCACTCCACCGGCGGCATGG
ACGAGCTGTACAAGCGCCCGGCGGCGAACGATGAAAACTATGCGGCAGCGGTTTAATTCAGCCAAAAAACTTAAGACCGCCGGTCTTGTCCACTACCTTGCAGT
AATGCGGTGGACAGGATCGGCGGTTTTCTTTTCTCTTCTCAAcTGCAgtccggcaaaaaagggcaaggtgtcaccaccctgcccttttttcttaaaaccgaaaagattacttcgcgttatgcaggcttc
ctcgctcactgactcgctgcgctcggtcgttcggctgcggcgagcggtatcagctcactcaaaggcggtaat

pSB4K5-pLux-LuxI, https://benchling.com/s/seq-urxaiBiCjvLAQUhMiLRZ

pLux, RBS B0064, LuxI, LVA degtag

tgccacctgacgtctaagaaaaggaatattcagcaatttgcccgtgccgaagaaaggcccacccgtgaaggtgagccagtgagttgattgctacgtaattagttagttagcccttagtgactcgaattcgcggccgcttctagag
ACCTGTAGGATCGTACAGGTTTACGCAAGAAAATGGTTTGTTATAGTCGAATAAATACTAGAGAAAGAGGGGAAATACTAGATgACTATAATGATAAAAAAATCGGA
TTTTTTGGCAATTCCATCAGAGGAGTATAAAGGTATTCTAAGTCTTCGTTATCAAGTGTTTAAGCAAAGACTTGAGTGGGACTTAGTTGTAGAAAATAACCTCGAATC
AGATGAGTATGATAACTCAAATGCAGAATATATTTATGCTTGTGATGATACTGAAAATGTAAGTGGATGCTGGCGTTTATTACCTACAACAGGTGATTATATGCTGAA
AAGTGTTTTTCCTGAATTGCTTGGTCAACAGAGTGCTCCCAAAGATCCTAATATAGTCGAATTAAGTCGTTTTGCTGTAGGTAAAAATAGCTCAAAGATAAATAACTC
TGCTAGTGAAATTACAATGAAACTATTTGAAGCTATATATAAACACGCTGTTAGTCAAGGTATTACAGAATATGTAACAGTAACATCAACAGCAATAGAGCGATTTTT
AAAGCGTATTAAAGTTCCTTGTCATCGTATTGGAGACAAAGAAATTCATGTATTAGGTGATACTAAATCGGTTGTATTGTCTATGCCTATTAATGAACAGTTTAAAAAa
GCAGTCTTAAATGCTGCAAACGACGAAAaCTACGCTTTAGTAGCTTAATAACTCTGATAGTGCTAGTGTAGATCTctactagagccaggcatcaaataaaacgaaaggctcagtcga
aagactgggcctttcgttttatctgttgtttgtcggtgaacgctctctactagagtcacactggctcaccttcgggtgggcctttctgcgtttatatactagtagcggccgctgcaggagtcactaagggttagttagttagattagcaga
agtcaaaagcctccgaccggaggcttttgactaaaacttcccttggggttatcattggggctcactcaaaggcggtaat

pSB4A5-QS01i, https://benchling.com/s/seq-FA3u2oosvUJJGyFSbzII

pTetO, TetR, AAV degtag, RBS N1, YPet, pLux76, LuxI

tgccacctgacgtctaagaaaaggaatattcagcaatttgcccgtgccgaagaaaggcccacccgtgaaggtgagccagtgagttgattgctacgtaattagttagttagcccttagtgactcgaattcTCCCTATCAGTG
ATAGAGATTGACATCCCTATCAGTGATAGAGATACTGAGCACAAGCTTAGGGTGTCTCAAGGTGCGTACCTTGACTGATGAGTCCGAAAGGACGAAACACCCCTC
TACAAATAATTTTGTTTAAGCGGCCGCACTATGTTTTTCAAAGACGAAAAACTACTAGATGAAGAACATTAATGCTGATGATACATATCGCATTATTAACAAGATCAA
GGCCTGCCGTTCCAACAACGATATTAATCAATGTTTGAGCGACATGACGAAGATGGTCCATTGTGAATACTACCTGCTGGCGATCATTTACCCACATTCGATGGTG
AAATCCGACATCAGTATTCTGGACAACTACCCCAAGAAATGGCGTCAGTATTATGACGATGCGAATCTGATCAAATATGACCCCATTGTAGACTATAGCAATAGCA
ACCATTCTCCGATTAACTGGAACATCTTTGAAAATAATGCAGTTAACAAGAAGAGTCCGAATGTAATCAAGGAAGCAAAAACATCAGGCTTAATCACTGGATTCTCC
TTCCCGATCCACACAGCCAACAACGGGTTTGGAATGTTGTCTTTCGCACACAGTGAAAAGGATAATTACATTGATAGTCTTTTCCTGCACGCGTGCATGAATATTC
CACTGATCGTGCCTAGTTTGGTAGACAATTACCGCAAGATTAATATTGCTAACAACAAATCTAACAACGACCTGACGAAACGCGAAAAAGAGTGCCTTGCGTGGG
CATGTGAAGGCAAGTCCTCCTGGGATATTTCGAAAATCTTAGGTTGCTCTGAGCGCACTGTGACCTTCCATCTTACGAACGCTCAAATGAAGTTAAATACCACCAA
CCGTTGCCAGTCAATCAGTAAGGCCATCCTGACTGGAGCTATCGACTGCCCATATTTCAAGAACCGTCCCGCTGCTAATGACGAGAACTATGCTGCGGCTGTCT
GATAACTCGAGAGCTGTCACCGGATGTGCTTTCCGGTCTGATGAGTCCGTGAGGACGAAACAGCGAGATCAGATAATTCTGACGTATCTAGATACGCTATGGACT
ATGTTTTCTGCTATGGACTATGTTTTCACACACGAGATGCCTCGATGTCAAAGGGAGAAGAATTGTTCACGGGAGTTGTACCCATCTTAGTAGAATTGGACGGAGA
CGTCAATGGACACAAGTTCTCCGTTTCGGGAGAGGGGGAGGGGGATGCGACGTATGGTAAATTGACGCTGAAGCTGTTATGTACCACCGGTAAGTTGCCTGTCC
CTTGGCCCACATTAGTAACAACCCTGGGGTACGGCGTGCAATGCTTCGCGCGTTATCCTGACCATATGAAGCAACATGACTTCTTTAAGTCTGCCATGCCTGAAG
GATATGTTCAAGAGCGCACGATTTTTTTTAAAGATGATGGGAATTATAAAACTCGTGCAGAAGTGAAATTTGAGGGCGACACATTAGTGAACCGCATCGAATTAAAA
GGAATCGACTTTAAAGAAGATGGAAACATTTTGGGGCACAAATTGGAGTACAATTATAACAGCCATAACGTCTATATCACAGCGGATAAGCAGAAGAATGGCATCA
AAGCGAATTTTAAGATTCGTCACAATATTGAAGATGGGGGAGTTCAACTGGCGGACCATTATCAACAAAATACACCGATCGGTGACGGACCGGTGTTGTTGCCGG
ACAACCACTATTTATCATATCAGAGCGCGTTATTTAAGGACCCGAACGAGAAGCGTGACCACATGGTCCTGTTGGAATTTCTGACAGCCGCTGGTATTACTGAGG
GTATGAATGAGCTTTACAAACGTCCTGCTGCGAACGACGAAAATTATGCGGCTGCGGTTTGATAAGGAAACACAGAAAAAAGCCCGCACCTGACAGTGCGGGCT
TTTTTTTTCGACCAAAGGTTAATTAAACCTGTAGGATCGTACAAGTTTACGCAAGAAAATGGTTTGTTATAGTCGAATAAACCTAGGCCCCCCGAGGAGTAGCACAT
GACAATTATGATTAAGAAGAGCGATTTCTTAGCAATCCCCTCCGAGGAATATAAAGGCATCCTGTCTCTTCGCTACCGAGGTGTTCAAACAGCGTCTGGAATGGGAT
TTAGTGGTTGAAAATAATTTGGAATCCGACGAGTACGATAACAGCAACGCTGAGTATATTTATGCCTGCGACGATACAGAAAACGTCAGTGGATGCTGGCGCCTG
CTGCCCACAACCGGTGATTATATGTTGAAGTCAGTATTCCCCGAGCTTCTGGGGCAGCAGTCGGCGCCCAAAGATCCTAACATCGTTGAATTGAGTCGTTTTGCT
GTTGGCAAGAACTCCTCTAAAATCAATAATTCCGCAAGTGAGATCACGATGAAACTGTTTGAAGCTATCTATAAGCATGCAGTAAGTCAAGGGATCACGGAGTACG
TCACGGTCACGTCTACCGCAATTGAACGCTTCTTGAAACGTATCAAAGTTCCCTGCCACCGCATCGGAGATAAGGAAATTCACGTACTGGGCGATACTAAGTCCG
TGGTCCTTTCGATGCCAATCAACGAGCAATTCAAAAAAGCTGTCTTAAATTGATAATCCGGCAATTAAAAAAGCGGCTAACCACGCCGCTTTTTTTACGTCTGCAct
gcaggagtcactaagggttagttagttagattagcagaaagtcaaaagcctccgaccggaggcttttgactaaaacttcccttggggttatcattggggctcactcaaaggcggtaat

pSB4A5-QS02i, https://benchling.com/s/seq-8Ph5hiCJBfKdca5dY24V

pLacO, LasR, AAV degtag, RBS N1, mScarletI, pLas81, LasI

tgccacctgacgtctaagaaaaggaatattcagcaatttgcccgtgccgaagaaaggcccacccgtgaaggtgagccagtgagttgattgctacgtaattagttagttagcccttagtgactcgaattcAATTGTGAGCGG
ATAACAATTGACATTGTGAGCGGATAACAAGATACTGAGCACAAAGCTTAGGGTGTCTCAAGGTGCGTACCTTGACTGATGAGTCCGAAAGGACGAAACACCCCT
CTACAAATAATTTTGTTTAAGCGGCCGCACTATGTTTTTCAAAGACGAAAAACTACTAGATGGCCCTGGTAGACGGCTTCTTGGAATTAGAACGTTCTAGTGGCAA
GTTGGAGTGGTCGGCAATCTTGCAAAAAATGGCTTCTGACTTAGGCTTCTCCAAGATTCTGTTTGGTTTGTTACCGAAGGATTCACAGGATTACGAAAACGCATTC
ATCGTCGGGAATTATCCAGCCGCGTGGCGCGAACACTACGATCGCGCTGGGTATGCGCGCGTTGATCCTACCGTGTCGCATTGCACTCAGTCTGTTCTTCCCAT
TTTTTGGGAACCCTCAATCTACCAGACCCGCAAGCAACATGAGTTCTTTGAGGAAGCCTCGGCCGCGGGGGCTTGTGTATGGCCTTACGATGCCACTTCATGGTG
CCCGTGGGGAATTGGGAGCACTGTCGCTTTCAGTCGAAGCCGAAAACCGCGCTGAGGCCAACCGTTTTATTGAGAGCGTCCTTCCAACTTTATGGATGTTGAAG
GACTATGCCCTTCAATCTGGGGCTGGGTTGGCCTTTGAGCACCCTGTTTCTAAACCAGTAGTTCTTACTTCACGCGAGAAGGAAGTCTTGCAATGGTGTGCTATT
GGAAAGACCTCCTGGGAAATCAGCGTCATTTGCAACTGTTCGGAAGCAAATGTAAATTTTCATATGGGGAACATCCGTCGCAAATTTGGGGTGACGTCCCGTCGT
GTCGCAGCCATCATGGCAGTCAATCTTGGTCTTATCACCTTACGTCCCGCTGCTAATGACGAGAACTATGCTGCGGCTGTCTGATAACTCGAGAGCTGTCACCG
GATGTGCTTTCCGGTCTGATGAGTCCGTGAGGACGAAACAGCGAGATCAGATAATTCTGACGTATCTAGATACGCTATGGACTATGTTTTCTGCTATGGACTATGT
TTTCACACACGAGATGCCTCGATGGTGTCAAAGGGAGAGGCGGTTATCAAGGAATTTATGCGCTTTAAAGTCCACATGGAGGGCAGCATGAACGGGCACGAGTT
TGAAATTGAGGGGGAGGGGGAGGGCCGTCCTTATGAAGGTACTCAGACTGCTAAACTGAAGGTGACAAAAGGTGGCCCCTTGCCTTTCTCGTGGGACATCCTG
TCGCCACAATTCATGTACGGGAGCCGCGCCTTTATCAAACATCCCGCAGATATTCCTGATTACTATAAACAATCTTTCCCGGAAGGTTTCAAATGGGAACGCGTCA
TGAATTTTGAGGACGGGGGCGCTGTCACAGTTACTCAGGACACCTCCTTGGAAGACGGCACATTGATTTACAAGGTTAAGTTGCGCGGCACAAACTTCCCCCCT
GACGGGCCAGTAATGCAAAAGAAAACTATGGGTTGGGAGGCGTCTACAGAACGTTTATACCCCGAAGACGGGGTGCTGAAAGGTGACATTAAGATGGCCCTGC
GCCTGAAGGACGGCGGTCGCTATCTTGCCGACTTTAAAACTACTTATAAGGCTAAAAAACCAGTCCAGATGCCAGGCGCCTATAATGTTGACCGCAAGTTAGACA
TCACCTCACATAATGAAGACTATACCGTTGTAGAACAATACGAGCGCAGCGAGGGTCGTCACAGTACCGGGGGGATGGATGAATTATACAAACGTCCTGCTGCG
AACGACGAAAATTATGCGGCTGCGGTTTGATAAGGAAACACAGAAAAAAGCCCGCACCTGACAGTGCGGGCTTTTTTTTTCGACCAAAGGTTAATTAAACCTATAG
GATCGTATAGGTTTACGCAAGAAAATGGTTTGTTATAGTCGAATAAACCTAGGCCCCCCGAGGAGTAGCACATGATTGTGCAAATCGGCCGCGTGAGGAGTTC
GATAAAAAGCTGCTTGGGGAAATGCATAAACTTCGTGCTCAGGTGTTCAAGGAGCGTAAGGGGTGGGATGTTTCCGTTATTGACGAAATGGAAATTGATGGGTAC
GATGCATTATCACCTTACTATATGCTGATTCAAGAAGACACACCTGAGGCCCAGGTATTCGGTTGCTGGCGCATTTTTGACACGACGGGGCCTTACATGTTGAAG
AACACGTTTCCTGAATTGTTACACGGCAAAGAAGCTCCCTGCTCACCCCATATTTGGGAACTGAGCCGTTTCGCTATCAATTCCGGTCAAAAGGGCTCCCTGGGC
TTTTCGGACTGCACCCTTGAAGCCATGCGCGCACTTGCCCGTTACTCCCTGCAAAACGACATTCAAACCTTAGTTACTGTTACTACCGTTGGCGTAGAGAAGATG
ATGATCCGTGCGGGTCTTGACGTATCTCGCTTTGGACCGCATCTGAAGATTGGAATCGAGCGTGCGGTGGCGTTGCGCATCGAATTGAACGCAAAAACGCAAAT
TGCGTTATACGGCGGGGGTCTTGGTTGAACAGCGTTTAGCCGTGAGTTGATAATCCGGCAATTAAAAAAGCGGCTAACCACGCCGCTTTTTTTACGTCTGCActgcag
gagtcactaagggttagttagttagattagcagaaagtcaaaagcctccgaccggaggcttttgactaaaacttcccttggggttatcattggggctcactcaaaggcggtaat

pSB3C5-QS01e, https://benchling.com/s/seq-09hD8s9xD7T0hxLbTCbZ

pLas81, TetR, pJ23106, LasR

tgccacctgacgtctaagaaaaggaatattcagcaatttgcccgtgccgaagaaaggcccacccgtgaaggtgagccagtgagttgattgctacgtaattagttagttagcccttagtgactcgaattcACCTATAGGATC
GTATAGGTTTACGCAAGAAAATGGTTTGTTATAGTCGAATAAAAAGCTTCTATGGACTATGTTTTCACATACGAGGGGGATTAGATGTCGCGTCTGGACAAGAGTAA
AGTGATTAATTCAGCTCTTGAACTGTTGAATGAAGTTGGAATTGAAGGACTTACAACACGTAAGTTAGCACAGAAATTGGGCGTCGAACAACCTACATTGTACTGG
CATGTCAAGAATAAACGTGCGCTTCTGGATGCTCTTGCTATTGAAATGTTGGACCGTCACCACACTCACTTTTGCCCCTTGGAAGGAGAAAGCTGGCAAGATTTTC
TGCGCAACAACGCTAAGTCATTTCGTTGCGCTCTGTTATCCCACCGTGATGGGGCCAAAGTCCACTTGGGCACTCGCCCCACGGAAAAACAGTATGAAACCCTG
GAAAACCAACTTGCTTTCCTGTGTCAACAAGGATTTAGCCTTGAGAATGCATTGTATGCCCTGTCTGCGGTAGGGCACTTTACGTTGGGCTGTGTCTTAGAGGAC
CAGGAGCATCAGGTTGCCAAGGAGGAGCGTGAGACACCTACGACCGACAGTATGCCACCCTTATTACGTCAGGCGATTGAGCTGTTTGACCACCAAGGTGCGG
AACCTGCCTTTCTTTTTGGTCTTGAACTTATCATCTGTGGGTTGGAAAAACAACTTAAATGCGAGTCCGGCAGCTGATAACCAATTATTGAACACCCTTCGGGGTGT
TTTTTTGTTTCTGGTCTACCCTCGAGtttacggctagctcagtcctaggtatagtgctagcTCTAGAGGAGCTATGGACTATGTTTGAAAGGCTGAAATACTAGATGGCCTTAGTTG
ATGGCTTCTTGGAGTTAGAGCGTAGCTCTGGAAAGTTAGAGTGGTCTGCAATCTTGCAAAAGATGGCTTCCGATTTAGGCTTCTCGAAGATTTTGTTCGGTTTATTA
CCTAAGGACTCACAGGATTACGAAAACGCGTTTATCGTTGGAAACTACCCGGCAGCATGGCGCGAGCATTATGATCGCGCCGGTTATGCGCGTGTAGATCCTAC
GGTAAGTCATTGTACTCAATCGGTCTTACCGATCTTTTGGGAACCTTCAATCTACCAGACACGTAAACAACATGAGTTCTTCGAAGAAGCGTCAGCAGCTGGTTTG
GTGTACGGCCTGACCATGCCTCTGCATGGAGCGCGTGGGGAATTGGGGGCGTTGTCATTGAGTGTAGAAGCTGAGAACCGCGCGGAAGCTAACCGCTTTATCG
AAAGTGTATTGCCTACACTGTGGATGTTGAAAGACTACGCTCTTCAGTCGGGGGCCGGACTTGCGTTCGAACATCCCGTATCGAAGCCTGTCGTACTTACCTCTC
GCGAAAAAGAAGTCTTGCAGTGGTGCGCCATCGGTAAAACGAGCTGGGAAATCTCAGTAATTTGTAACTGCTCAGAAGCTAACGTAAACTTCCACATGGGCAATA
TCCGTCGTAAGTTTGGAGTCACGTCCCGTCGTGTCGCTGCTATCATGGCGGTCAACTTGGGCCTTATTACTTTATGATAATCCGGCAATTAAAAAAGCGGCTAAC
CACGCCGCTTTTTTTACGTCTGCActgcaggagtcactaagggttagttagttagattagcagaaagtcaaaagcctccgaccggaggcttttgactaaaacttcccttggggttatcattggggctcactcaaagg
cggtaat

pSB3C5-QS02e, https://benchling.com/s/seq-a19GXlmZaTvll0dB86RX

pLux76, LacI, pJ23106, LuxR

tgccacctgacgtctaagaaaaggaatattcagcaatttgcccgtgccgaagaaaggcccacccgtgaaggtgagccagtgagttgattgctacgtaattagttagttagcccttagtgactcgaattcACCTGTAGGATC
GTACAAGTTTACGCAAGAAAATGGTTTGTTATAGTCGAATAAAAAGCTTCTATGGACTATGTTTTCACATACGAGGGGGATTAGATGAAACCAGTGACACTTTACGA
TGTCGCCGAATATGCGGGCGTTTCGTACCAGACTGTATCACGTGTAGTGAATCAAGCGTCGCACGTCAGCGCTAAGACTCGTGAAAAAGTGGAAGCTGCGATGG
CCGAGTTGAACTACATTCCGAATCGTGTTGCACAACAACTGGCAGGAAAACAAAGTTTATTAATTGGTGTGGCCACGTCAAGCCTGGCCTTGCACGCACCCTCG
CAAATCGTTGCTGCGATCAAGAGTCGTGCGGATCAGTTAGGAGCATCCGTCGTTGTATCGATGGTCGAACGTAGTGGAGTGGAGGCATGTAAAGCGGCTGTGCA

CAATCTTCTTGCCCAGCGTGTTTCTGGGCTGATTATTAACTACCCTCTGGATGACCAAGACGCGATTGCCGTTGAAGCTGCGTGCACAAACGTTCCGGCCCTGTT
CCTTGACGTATCAGACCAAACACCTATCAACAGTATCATCTTTAGTCACGAAGATGGTACGCGTTTAGGAGTGGAGCATTTAGTAGCTTTGGGTCACCAGCAGATC
GCATTATTAGCGGGGCCGCTTAGTAGCGTATCCGCCCGCCTGCGCCTGGCTGGCTGGCACAAGTACCTTACTCGCAACCAGATCCAGCCGATCGCAGAGCGT
GAAGGTGACTGGTCGGCGATGTCCGGATTTCAACAGACGATGCAAATGTTAAATGAGGGCATTGTACCTACTGCTATGCTGGTGGCCAACGACCAGATGGCACT
GGGGGCGATGCGTGCAATCACTGAATCTGGCCTTCGCGTTGGCGCAGACATTTCCGTCGTTGGCTATGATGATACAGAAGACTCAAGTTGCTATATCCCCCCAC
TTACGACAATCAAACAGGATTTCCGTTTGCTTGGTCAAACCTCCGTTGACCGTTTGCTGCAACTTAGCCAGGGGCAGGCGGTGAAGGGAAATCAGTTACTTCCTG
TGAGTTTAGTAAAACGCAAGACCACGTTAGCACCTAATACTCAGACGGCAAGCCCACGTGCTTTAGCTGACAGTTTAATGCAACTGGCTCGTCAAGTATCTCGTC
TTGAAAGTGGTCAATGATAACCAATTATTGAACACCCTTCGGGGGTGTTTTTTTGTTTCTGGTCTACCCTCGAGttacggctagctcagtcctaggtatagtgctagcTCTAGAGGA
GCTATGGACTATGTTTGAAAGGCTGAAATACTAGATGAAGAATATTAACGCGGACGATACATATCGCATTATCAACAAGATCAAGGCGTGTCGCTCTAATAACGAC
ATCAACCAGTGCTTGAGTGATATGACTAAGATGGTACATTGCGAGTACTATTTGCTGGCGATTATCTATCCGCATTCAATGGTTAAGTCGGATATTTCTATCTTAGAT
AACTATCCCAAAAAATGGCGTCAATACTACGACGACGCCAATCTGATTAAATACGACCCTATCGTGGATTATTCCAATTCCAACCATTCGCCGATCAATTGGAATAT
CTTCGAGAACAATGCTGTGAACAAAAAGTCTCCCAACGTGATTAAGGAGGCTAAAACCTCCGGTTTAATTACCGGTTTTAGTTTCCCAATTCATACCGCAAACAAC
GGTTTCGGAATGTTGTCCTTCGCACATAGCGAGAAAGATAATTATATCGACTCGCTTTTTTTGCACGCGTGTATGAATATTCCCTTGATCGTACCTAGTCTGGTGGA
TAACTACCGTAAAATTAATATTGCGAATAATAAGTCGAACAACGACCTTACAAAACGTGAGAAGGAATGTCTGGCATGGGCGTGTGAAGGTAAGTCCTCGTGGGA
TATTTCTAAGATCCTTGGTTGTAGCGAGCGTACCGTTACCTTTCATTTGACTAATGCCCAAATGAAGTTAAACACGACTAATCGTTGCCAGTCTATCTCAAAAGCAA
TTCTTACCGGGGCCATCGACTGTCCGTACTTCAAGAATTGATAATCCGGCAATTAAAAAAGCGGCTAACCACGCCGCTTTTTTTACGTCTGCActgcaggagtcactaag
ggttagttagttagattagcagaaagtcaaaagcctccgaccggaggcttttgactaaaacttccctgggggttatcattggggctcactcaaaggcggtaat

pCola-Duet-1-$E_{60}L_{20}$, https://benchling.com/s/G6cL3z7S

T7 promoter, LacO (LacI binding sequence), $E_{60}L_{20}$

taatacgactcactatagggaattgtgagcggataacaatttcccctgtagaaataattttgtttaactttaataaggagatatacCATGGAGGAGGAAGAGGAAGAGGAAGAGGAAGAGGAAGAGGAA
GAGGAAGAGGAAGAGGAAGAGGAAGAGGAAGAGGAAGAGGAAGAGGAAGAGGAAGAGGAAGAGGAAGAGGAAGAGGAAGAGGAAGAGGGCGCCGAAGAGGAAGAGG
AAGAGGAAGAGGAAGAGGAAGAGGAAGAGGAAGAGCTTCTCCTACTGTTATTGCTGCTGCTTCTCCTCCTACTATTGTTGCTCCTACTGTTATAGTAAAagcttgcggccgcataatgcttaagtcgaacagaaagtaatcgtattgtacacggccgcataatcgaaattaatacgactcactatagggaattgtgagcggataacaattccccatcttagtatattagttaagtata
agaaggagatatacatatggcagatctcaattggatatcggccggccacgcgatcgctgacgtcggtaccctcgagtctggtaaagaaaccgctgctgcgaaatttgaacgccagcacatggactcgtctactagcgcagctt
aattaacctaggctgctgccaccgctgagcaataactagcataaccccttggggcctctaaacgggtcttgaggggttttttg

pSB1A2-GFP-2901, https://benchling.com/s/wUvyXUjJ

pTetO, GFP

tgccacctgacgtctaagaaaccattattatcatgacattaacctataaaaaataggcgtatcacgaggcagaatttcagataaaaaaaatccttagctttcgctaaggatgatttctggaattcgcggccgcttctagagtccctatca
gtgatagagattgacatccctatcagtgatagagatactgagcactctagagaaagaggagaaatactagatgcgtaaaggagaaggaagacttttcactggagttgtcccaattcttgttgaattagatggtgatgttaatgggcaca
aattttctgtcagtggagagggtgaaggtgatgcaacatacggaaaacttaccctaaatttatttgcacactggaaaactacctgttccatggccaacacttgtcactactttcggttatggtgttcaatgctttgcgagatacccag
atcatatgaaacagcatgactttttcaagagtgccatgcccgaaggttatgtacaggaaagaactatatttttcaaagatgacgggaactacaagacacgtgctgaagtcaagtttgaaggtgataccctttgttaatagaatcgagtt
aaaaggtattgattttaaagaagatggaaacattcttggacacaaattggaatacaactataactcacacaatgtatacatcatggcagacaaacaaaagaatggaatcaaagttaacttcaaaattagacacaacattgaagatg
gaagcgttcaactagcagaccattatcaacaaaatactccaattggcgatggccctgtccttttaccagacaaccattacctgtccacacaatctgccctttcgaaagatcccaacgaaaagagagaccacatggtccttctttga
gtttgtaacagctgctgggattacacatggcatggatgaactatacaaaTcggtatcagctcactcaaaggcggtaat

pSB1A2-GFP-AAV-3055, https://benchling.com/s/eCgYRkVq

pTetO, GFP, AAV degtag

tgccacctgacgtctaagaaaccattattatcatgacattaacctataaaaaataggcgtatcacgaggcagaatttcagataaaaaaaatccttagctttcgctaaggatgatttctggaattcgcggccgcttctagagtccctatca
gtgatagagattgacatccctatcagtgatagagatactgagcactctagagaaagaggagaaatactagatgcgtaaaggagaaggaagacttttcactggagttgtcccaattcttgttgaattagatggtgatgttaatgggcaca
aattttctgtcagtggagagggtgaaggtgatgcaacatacggaaaacttaccctaaatttatttgcacactggaaaactacctgttccatggccaacacttgtcactactttcggttatggtgttcaatgctttgcgagatacccag
atcatatgaaacagcatgactttttcaagagtgccatgcccgaaggttatgtacaggaaagaactatatttttcaaagatgacgggaactacaagacacgtgctgaagtcaagtttgaaggtgataccctttgttaatagaatcgagtt
aaaaggtattgattttaaagaagatggaaacattcttggacacaaattggaatacaactataactcacacaatgtatacatcatggcagacaaacaaaagaatggaatcaaagttaacttcaaaattagacacaacattgaagatg
gaagcgttcaactagcagaccattatcaacaaaatactccaattggcgatggccctgtccttttaccagacaaccattacctgtccacacaatctgccctttcgaaagatcccaacgaaaagagagaccacatggtccttctttga
gtttgtaacagctgctgggattacacatggcatggatgaactatacaaaCGCCCCGGCGGCGAACGATGAAAACTATGCGGCAGCGGTTtaataatactagagccaggcatcaaataaaacgaaaggct
cagtcgaaagactgggcctttcgttttatctgttgtttgtcggtgaacgctctctactagagtcacactggctcaccttcgggtgggcctttctgcgtttatatACTactagtagcggccgctgcaggcttcctcgctcactgactcgctg
cgctcggtcgttcggctgcggcgagcggtatcagctcactcaaaggcggtaat

pSB1A2-GFP-ASV-3055, https://benchling.com/s/w5fbeMzQ

pTetO, GFP, ASV degtag

tgccacctgacgtctaagaaaccattattatcatgacattaacctataaaaaataggcgtatcacgaggcagaatttcagataaaaaaaatccttagctttcgctaaggatgatttctggaattcgcggccgcttctagagtccctatca
gtgatagagattgacatccctatcagtgatagagatactgagcactctagagaaagaggagaaatactagatgcgtaaaggagaaggaagacttttcactggagttgtcccaattcttgttgaattagatggtgatgttaatgggcaca
aattttctgtcagtggagagggtgaaggtgatgcaacatacggaaaacttaccctaaatttatttgcacactggaaaactacctgttccatggccaacacttgtcactactttcggttatggtgttcaatgctttgcgagatacccag
atcatatgaaacagcatgactttttcaagagtgccatgcccgaaggttatgtacaggaaagaactatatttttcaaagatgacgggaactacaagacacgtgctgaagtcaagtttgaaggtgataccctttgttaatagaatcgagtt
aaaaggtattgattttaaagaagatggaaacattcttggacacaaattggaatacaactataactcacacaatgtatacatcatggcagacaaacaaaagaatggaatcaaagttaacttcaaaattagacacaacattgaagatg
gaagcgttcaactagcagaccattatcaacaaaatactccaattggcgatggccctgtccttttaccagacaaccattacctgtccacacaatctgccctttcgaaagatcccaacgaaaagagagaccacatggtccttctttga
gtttgtaacagctgctgggattacacatggcatggatgaactatacaaaCGCCCCGGCGGCGAACGATGAAAACTATGCGGCATCAGTTtaataatactagagccaggcatcaaataaaacgaaaggct
cagtcgaaagactgggcctttcgttttatctgttgtttgtcggtgaacgctctctactagagtcacactggctcaccttcgggtgggcctttctgcgtttatatactagtagcggccgctgcagATgcttcctcgctcactgactcgctg
cgctcggtcgttcggctgcggcgagcggtatcagctcactcaaaggcggtaat

pSB1A2-GFP-LAA-3055, https://benchling.com/s/9bY7WB1X

pTetO, GFP, LAA degtag

tgccacctgacgtctaagaaaccattattatcatgacattaacctataaaaaataggcgtatcacgaggcagaatttcagataaaaaaaatccttagctttcgctaaggatgatttctggaattcgcggccgcttctagagtccctatca
gtgatagagattgacatccctatcagtgatagagatactgagcactctagagaaagaggagaaatactagatgcgtaaaggagaaggaagacttttcactggagttgtcccaattcttgttgaattagatggtgatgttaatgggcaca
aattttctgtcagtggagagggtgaaggtgatgcaacatacggaaaacttaccctaaatttatttgcacactggaaaactacctgttccatggccaacacttgtcactactttcggttatggtgttcaatgctttgcgagatacccag
atcatatgaaacagcatgactttttcaagagtgccatgcccgaaggttatgtacaggaaagaactatatttttcaaagatgacgggaactacaagacacgtgctgaagtcaagtttgaaggtgataccctttgttaatagaatcgagtt
aaaaggtattgattttaaagaagatggaaacattcttggacacaaattggaatacaactataactcacacaatgtatacatcatggcagacaaacaaaagaatggaatcaaagttaacttcaaaattagacacaacattgaagatg
gaagcgttcaactagcagaccattatcaacaaaatactccaattggcgatggccctgtccttttaccagacaaccattacctgtccacacaatctgccctttcgaaagatcccaacgaaaagagagaccacatggtccttctttga
gtttgtaacagctgctgggattacacatggcatggatgaactatacaaaCGCCCCGGCGGCGAACGATGAAAACTATGCGGCATCAGCGtaataatactagagccaggcatcaaataaaacgaaaggct
cagtcgaaagactgggcctttcgttttatctgttgtttgtcggtgaacgctctctactagagtcacactggctcaccttcgggtgggcctttctgcgtttatatactagtagcggccgctgcagATgcttcctcgctcactgactcgctg
cgctcggtcgttcggctgcggcgagcggtatcagctcactcaaaggcggtaat

pSB1A2-GFP-LVA-3055, https://benchling.com/s/iwU8glOu

pTetO, GFP, LVA degtag

tgccacctgacgtctaagaaaccattattatcatgacattaacctataaaaaataggcgtatcacgaggcagaatttcagataaaaaaaatccttagctttcgctaaggatgatttctggaattcgcggccgcttctagagtccctatca
gtgatagagattgacatccctatcagtgatagagatactgagcactctagagaaagaggagaaatactagatgcgtaaaggagaaggaagacttttcactggagttgtcccaattcttgttgaattagatggtgatgttaatgggcaca
aattttctgtcagtggagagggtgaaggtgatgcaacatacggaaaacttaccctaaatttatttgcacactggaaaactacctgttccatggccaacacttgtcactactttcggttatggtgttcaatgctttgcgagatacccag
atcatatgaaacagcatgactttttcaagagtgccatgcccgaaggttatgtacaggaaagaactatatttttcaaagatgacgggaactacaagacacgtgctgaagtcaagtttgaaggtgataccctttgttaatagaatcgagtt
aaaaggtattgattttaaagaagatggaaacattcttggacacaaattggaatacaactataactcacacaatgtatacatcatggcagacaaacaaaagaatggaatcaaagttaacttcaaaattagacacaacattgaagatg

gaagcgttcaactagcagaccattatcaacaaaatactccaattggcgatggccctgtccttttaccagacaaccattacctgtccacacaatctgccctttcgaaagatcccaacgaaaagagagaccacatggtccttcttga
gtttgtaacagctgctgggattacacatggcatggatgaactatacaaaCGCCCGGCGGCGAACGATGAAAACTATGCGCTGGTGGCGtaataatactagagccaggcatcaaataaaacgaaaggct
cagtcgaaagactgggcctttcgttttatctgttgtttgtcggtgaacgctctctactagagtcacactggctcaccttcgggtgggcctttctgcgttatatactagtagcggccgctgcagATgcttcctcgctcactgactcgctg
cgctcggtcgttcggctgcggcgagcggtatcagctcactcaaaggcggtaat

pSB1A2-GFP-pdt2-3097, https://benchling.com/s/neGFEiiJ

pTetO, GFP, pdt2 degtag

tgccacctgacgtctaagaaaccattattatcatgacattaacctataaaaatagggcgtatcacgaggcagaatttcagataaaaaaaatccttagctttcgctaaggatgatttctggaattcgcggccgcttctagagtccctatca
gtgatagagattgacatccctatcagtgatagagatactgagcactactagagaaagaggagaaatactagatgcgtaaaggagaagaacttttcactggagttgtcccaattcttgttgaattagatggtgatgttaatgggcaca
aattttctgtcagtggaagaggtgaaggtgatgcaacatacggaaaacttaccctaaatttattgcactactggaaaactacctgttccatggccaacacttgtcactactttcggttatggtgttcaatgctttgcgagatacccag
atcatatgaaacagcatgacttttcaagagtgccatgcccgaaggttatgtacaggaaagaactatatttttcaaagatgacgggaactacaagacacgtgctgaagtcaagtttgaaggtgatacccttgttaatagaatcgagtt
aaaaggtattgattttaaagaagatggaaacattcttggacacaaattggaatacaactatactcacacaatgtatacatcatggcagacaaacaaaagaatggaatcaaagttaacttcaaaattagacacaacattgaagatg
gaagcgttcaactagcagaccattatcaacaaaatactccaattggcgatggccctgtccttttaccagacaaccattacctgtccacacaatctgccctttcgaaagatcccaacgaaaagagagaccacatggtccttcttga
gtttgtaacagctgctgggattacacatggcatggatgaactatacaaaGCAGCTAACAAAAATGAAGAAAATACTAATGAGGTGCCAACCTTCATGCTGAACGCCGGTCAAGCTAATT
ACCTGAGCCAGtaataatactagagccaggcatcaaataaaacgaaaggctcagtcgaaagactgggccttttgttttatctgttgtttgtcggtgaacgctctctactagagtcacactggctcaccttcgggtgggcctttt
ctgcgtttatatactagtagcggccgctgcagATgcttcctcgctcactgactcgctgcgctcggtcgttcggctgcggcgagcggtatcagctcactcaaaggcggtaat

pSB1A2-GFP-pdt2A-3097, https://benchling.com/s/nr8jYqLv

pTetO, GFP, pdt2A degtag

tgccacctgacgtctaagaaaccattattatcatgacattaacctataaaaatagggcgtatcacgaggcagaatttcagataaaaaaaatccttagctttcgctaaggatgatttctggaattcgcggccgcttctagagtccctatca
gtgatagagattgacatccctatcagtgatagagatactgagcactactagagaaagaggagaaatactagatgcgtaaaggagaagaacttttcactggagttgtcccaattcttgttgaattagatggtgatgttaatgggcaca
aattttctgtcagtggagagggtgaaggtgatgcaacatacggaaaacttaccctaaatttattgcactactggaaaactacctgttccatggccaacacttgtcactactttcggttatggtgttcaatgctttgcgagatacccag
atcatatgaaacagcatgacttttcaagagtgccatgcccgaaggttatgtacaggaaagaactatatttttcaaagatgacgggaactacaagacacgtgctgaagtcaagtttgaaggtgatacccttgttaatagaatcgagtt
aaaaggtattgattttaaagaagatggaaacattcttggacacaaattggaatacaactatactcacacaatgtatacatcatggcagacaaacaaaagaatggaatcaaagttaacttcaaaattagacacaacattgaagatg
gaagcgttcaactagcagaccattatcaacaaaatactccaattggcgatggccctgtccttttaccagacaaccattacctgtccacacaatctgccctttcgaaagatcccaacgaaaagagagaccacatggtccttcttga
gtttgtaacagctgctgggattacacatggcatggatgaactatacaaaGCAGCTAACAAAAATGAAGAAAATACTAATGAGGTGTTCAAGCTCATGCTGAACGCCGGTCAAGCTAATT
ACCTGAGCCAGtaataatactagagccaggcatcaaataaaacgaaaggctcagtcgaaagactgggccttttgttttatctgttgtttgtcggtgaacgctctctactagagtcacactggctcaccttcgggtgggcctttt
ctgcgtttatatactagtagcggccgctgcagATgcttcctcgctcactgactcgctgcgctcggtcgttcggctgcggcgagcggtatcagctcactcaaaggcggtaat

pSB1A2-GFP-pdt2B-3097, https://benchling.com/s/RjXDZtjN

pTetO, GFP, pdt2B degtag

tgccacctgacgtctaagaaaccattattatcatgacattaacctataaaaatagggcgtatcacgaggcagaatttcagataaaaaaaatccttagctttcgctaaggatgatttctggaattcgcggccgcttctagagtccctatca
gtgatagagattgacatccctatcagtgatagagatactgagcactactagagaaagaggagaaatactagatgcgtaaaggagaagaacttttcactggagttgtcccaattcttgttgaattagatggtgatgttaatgggcaca
aattttctgtcagtggagagggtgaaggtgatgcaacatacggaaaacttaccctaaatttattgcactactggaaaactacctgttccatggccaacacttgtcactactttcggttatggtgttcaatgctttgcgagatacccag
atcatatgaaacagcatgacttttcaagagtgccatgcccgaaggttatgtacaggaaagaactatatttttcaaagatgacgggaactacaagacacgtgctgaagtcaagtttgaaggtgatacccttgttaatagaatcgagtt
aaaaggtattgattttaaagaagatggaaacattcttggacacaaattggaatacaactatactcacacaatgtatacatcatggcagacaaacaaaagaatggaatcaaagttaacttcaaaattagacacaacattgaagatg
gaagcgttcaactagcagaccattatcaacaaaatactccaattggcgatggccctgtccttttaccagacaaccattacctgtccacacaatctgccctttcgaaagatcccaacgaaaagagagaccacatggtccttcttga
gtttgtaacagctgctgggattacacatggcatggatgaactatacaaaGCAGCTAACAAAAATGAAGAAAATACTAATGAGGTGAGAGCGATAATGCTGAACGCCGGTCAAGCTAATT
ACCTGAGCCAGtaataatactagagccaggcatcaaataaaacgaaaggctcagtcgaaagactgggccttttgttttatctgttgtttgtcggtgaacgctctctactagagtcacactggctcaccttcgggtgggcctttt
ctgcgtttatatactagtagcggccgctgcagATgcttcctcgctcactgactcgctgcgctcggtcgttcggctgcggcgagcggtatcagctcactcaaaggcggtaat

pSB1A2-GFP-pdt2C-3097, https://benchling.com/s/KlF4vFo7

pTetO, GFP, pdt2C degtag

tgccacctgacgtctaagaaaccattattatcatgacattaacctataaaaatagggcgtatcacgaggcagaatttcagataaaaaaaatccttagctttcgctaaggatgatttctggaattcgcggccgcttctagagtccctatca
gtgatagagattgacatccctatcagtgatagagatactgagcactactagagaaagaggagaaatactagatgcgtaaaggagaagaacttttcactggagttgtcccaattcttgttgaattagatggtgatgttaatgggcaca
aattttctgtcagtggagagggtgaaggtgatgcaacatacggaaaacttaccctaaatttattgcactactggaaaactacctgttccatggccaacacttgtcactactttcggttatggtgttcaatgctttgcgagatacccag
atcatatgaaacagcatgacttttcaagagtgccatgcccgaaggttatgtacaggaaagaactatatttttcaaagatgacgggaactacaagacacgtgctgaagtcaagtttgaaggtgatacccttgttaatagaatcgagtt
aaaaggtattgattttaaagaagatggaaacattcttggacacaaattggaatacaactatactcacacaatgtatacatcatggcagacaaacaaaagaatggaatcaaagttaacttcaaaattagacacaacattgaagatg
gaagcgttcaactagcagaccattatcaacaaaatactccaattggcgatggccctgtccttttaccagacaaccattacctgtccacacaatctgccctttcgaaagatcccaacgaaaagagagaccacatggtccttcttga
gtttgtaacagctgctgggattacacatggcatggatgaactatacaaaGCAGCTAACAAAAATGAAGAAAATACTAATGAGGTGGCTCAGCCTATGCTGAACGCCGGTCAAGCTAATT
ACCTGAGCCAGtaataatactagagccaggcatcaaataaaacgaaaggctcagtcgaaagactgggccttttgttttatctgttgtttgtcggtgaacgctctctactagagtcacactggctcaccttcgggtgggcctttt
ctgcgtttatatactagtagcggccgctgcagATgcttcctcgctcactgactcgctgcgctcggtcgttcggctgcggcgagcggtatcagctcactcaaaggcggtaat

pSB1A2-GFP-pdt2D-3097, https://benchling.com/s/uAtlzljE

pTetO, GFP, pdt2D degtag

tgccacctgacgtctaagaaaccattattatcatgacattaacctataaaaatagggcgtatcacgaggcagaatttcagataaaaaaaatccttagctttcgctaaggatgatttctggaattcgcggccgcttctagagtccctatca
gtgatagagattgacatccctatcagtgatagagatactgagcactactagagaaagaggagaaatactagatgcgtaaaggagaagaacttttcactggagttgtcccaattcttgttgaattagatggtgatgttaatgggcaca
aattttctgtcagtggagagggtgaaggtgatgcaacatacggaaaacttaccctaaatttattgcactactggaaaactacctgttccatggccaacacttgtcactactttcggttatggtgttcaatgctttgcgagatacccag
atcatatgaaacagcatgacttttcaagagtgccatgcccgaaggttatgtacaggaaagaactatatttttcaaagatgacgggaactacaagacacgtgctgaagtcaagtttgaaggtgatacccttgttaatagaatcgagtt
aaaaggtattgattttaaagaagatggaaacattcttggacacaaattggaatacaactatactcacacaatgtatacatcatggcagacaaacaaaagaatggaatcaaagttaacttcaaaattagacacaacattgaagatg
gaagcgttcaactagcagaccattatcaacaaaatactccaattggcgatggccctgtccttttaccagacaaccattacctgtccacacaatctgccctttcgaaagatcccaacgaaaagagagaccacatggtccttcttga
gtttgtaacagctgctgggattacacatggcatggatgaactatacaaaGCAGCTAACAAAAATGAAGAAAATACTAATGAGGTGGCACCCAATATGCTGAACGCCGGTCAAGCTAATT
ACCTGAGCCAGtaataatactagagccaggcatcaaataaaacgaaaggctcagtcgaaagactgggccttttgttttatctgttgtttgtcggtgaacgctctctactagagtcacactggctcaccttcgggtgggcctttt
ctgcgtttatatactagtagcggccgctgcagATgcttcctcgctcactgactcgctgcgctcggtcgttcggctgcggcgagcggtatcagctcactcaaaggcggtaat

pSB1A2-GFP-pdt2E-3097, https://benchling.com/s/y2WontDc

pTetO, GFP, pdt2E degtag

tgccacctgacgtctaagaaaccattattatcatgacattaacctataaaaatagggcgtatcacgaggcagaatttcagataaaaaaaatccttagctttcgctaaggatgatttctggaattcgcggccgcttctagagtccctatca
gtgatagagattgacatccctatcagtgatagagatactgagcactactagagaaagaggagaaatactagatgcgtaaaggagaagaacttttcactggagttgtcccaattcttgttgaattagatggtgatgttaatgggcaca
aattttctgtcagtggagagggtgaaggtgatgcaacatacggaaaacttaccctaaatttattgcactactggaaaactacctgttccatggccaacacttgtcactactttcggttatggtgttcaatgctttgcgagatacccag
atcatatgaaacagcatgacttttcaagagtgccatgcccgaaggttatgtacaggaaagaactatatttttcaaagatgacgggaactacaagacacgtgctgaagtcaagtttgaaggtgatacccttgttaatagaatcgagtt
aaaaggtattgattttaaagaagatggaaacattcttggacacaaattggaatacaactatactcacacaatgtatacatcatggcagacaaacaaaagaatggaatcaaagttaacttcaaaattagacacaacattgaagatg
gaagcgttcaactagcagaccattatcaacaaaatactccaattggcgatggccctgtccttttaccagacaaccattacctgtccacacaatctgccctttcgaaagatcccaacgaaaagagagaccacatggtccttcttga
gtttgtaacagctgctgggattacacatggcatggatgaactatacaaaGCAGCTAACAAAAATGAAGAAAATACTAATGAGGTGCCTGACGGTATGCTGAACGCCGGTCAAGCTAATT
ACCTGAGCCAGtaataatactagagccaggcatcaaataaaacgaaaggctcagtcgaaagactgggccttttgttttatctgttgtttgtcggtgaacgctctctactagagtcacactggctcaccttcgggtgggcctttt
ctgcgtttatatactagtagcggccgctgcagATgcttcctcgctcactgactcgctgcgctcggtcgttcggctgcggcgagcggtatcagctcactcaaaggcggtaat

pSB1C3-mTq2, https://benchling.com/s/CpsPjjW8

pJ23106, PlmJ ribozyme, mTq2, Biv-Tat

tgccacctgacgtctaagaaaccattattatcatgacattaacctataaaaatagggcgtatcacgaggcagaatttcagataaaaaaaatccttagctttcgctaaggatgatttctggaattcgAgTAAgccgcttctagagcac
CGATTGAGAAGAGAAAAGAAAACCGCCGATCCTGTCCACCGCATTACTGCAAGGTAGTGGACAAGACCGGCGGTCTTAAGTTTTTTGGCTGAAagtagtaccaTTAA
CGACGAATGCGACGACCCTTACCGCGGGTACCACGAGGACGCGGACCGCTGCTGCCGCCGCCACCACGGGTCTTGTACAGTTCGTCCATACCCAGCGTGATA
CCCGCCGCGGTAACAAATTCCAGCAGGACCATGTGGTCACGTTTTTCGTTCGGATCTTTGGACAGTTTGGATTGCGTGCTCAAGTAGTGATTATCTGGCAGCAGG
ACCGGACCATCGCCAATCGGGGTGTTCTGTTGATAGTGATCGGCCAATTGCACGCCGCCATCTTCAATATTGTGACGGATCTTGAAGTTTGCTTTAATGCCGTTTT
TCTGTTTATCAGCGGTGATGTACACATTGTCGCTGAAGTAATTATACTCCAGTTTGTGACCCAGGATGTTACCGTCCTCTTTAAAGTCAATACCTTTCAGCTCAATA
CGATTCACCAGCGTGTCACCCTCGAACTTGACTTCTGCGCGGGTCTTATAGTTACCGTCGTCTTTGAAAAAGATCGTACGTTCCTGAACGTAGCCTTCCGGCATC
GCGCTCTTAAAGAAGTCATGCTGTTTCATGTGATCCGGATAGCGCGCGAAACATTGCACGCCCCACGACAGAGTCGTCACCAGGGTCGGCCACGGAACCGGCA
GCTTACCGGTCGTGCAGATAAACTTCAGGGTCAATTTACCGTAGGTGGCGTCGCCCTCGCCCTCACCGCTAACGCTAAACTTGTGACCGTTGACATCACCATCC
AGCTCAACCAGAATCGGCACGACGCCGGTGAACAGTTCTTCACCCTTGCTAACCATGTCTAtttctcctctttACTGACTTTAAACAAAATTATTTGTAGAGGTCATAAGT
TTCGTCGCATTTCAGCGACTCATCAGTGGGCTTAGCCCAGACTTATGACTGAAGCTTCgctagcactatacctaggactgagctagccgtaaagatcctgaatCTCGAGattggtgccttg
cttggattatgaaatgccagcctgatcatacaacgttggacgaagtagcttaccgtccacacggtcggaacttggtgtgccgaatccaAGTCGAGATAATCACtagatgtcctgaGGtgcAtactagtagcggccgct
gcagtccggcaaaaaagggcaaggtgtcaccaccctgccctttttcttttaaaaccgaaaagattacttcgcgttatgcaggcttcctcgctcactgactcgctgcgctcggtcgttcggctgcggcgagcggtatcagctcactc
aaaggcggtaat

pET21b(+)-mVenus-Biv-Tat, https://benchling.com/s/seq-chYaD0eQk9HWC091O3sS

T7 promoter, LacO (LacI binding element), mVenus, Biv-Tat

ggtgatgtcggcgatataggcgccagcaaccgcacctgtggcgccggtgatgccggccacgatgcgtccggcgtagaggatcgagatctcgatcccgcgaaattaatacgactcactatagggggaattgtgagcggataac
aattccctctagaaataatttttgtttaactttaagaaggagatatacatATGAGCAAAGGCGAAGAACTGTTCACGGGTGTGGTTCCGATCCTGGTTGAACTGGATGGCGATGTGAACG
GTCATAAATTTAGCGTGTCTGGTGAAGGCGAAGGTGATGCGACCTACGGCAAACTGACGCTGAAACTGATTTGCACCACGGGTAAACTGCCGGTTCCGTGGCCG
ACCCTGGTGACCACGCTGGGTTATGGTCTGATGTGTTTCGCACGTTACCCGGATCACATGAAACGCCATGATTTCTTTAAATCTGCGATGCCGGAAGGCTATGTG
CAGGAACGTACCATCTTTTTCAAAGATGATGGTAACTACAAAACCCGCGCGGAAGTTAAATTTGAAGGCGATACGCTGGTGAACCGTATTGAACTGAAAGGTATC
GATTTCAAAGAAGATGGCAATATTCTGGGTCACAAACTGGAATACAACTACAACAGTCATAACGTGTACATTACCGCCGATAAACAGAAAAACGGTATCAAAGCAA
ACTTCAAAATCCGTCACAACATCGAAGATGGCGGTGTTCAGCTGGCCGATCATTACCAGCAGAACACCCCGATTGGCGATGGTCCGGTGCTGCTGCCGGATAAT
CATTATCTGAGTTACCAGAGCAAACTGTCTAAAGATCCGAATGAAAAACGCGATCACATGGTTCTGCTGGAATTTGTGACCGCGGCCGGCATTACGCATGGTATG
GATGAACTGTATAAAACTAGAGGAGGAGGAGGATCAGGAGGAGGAGGATCAACTAGAATGTCCGGCCCGCGTCCTCGTGGTACCCGTGGCAAAGGTCGCCGT
ATTCGCCGTGCGGATCCGAATTCGAGCTCCGTCGACAAGCTTGCGGCCGCActcgagcaccaccaccaccaccactgagatccggctgctaacaaagcccgaaaggaagctgagttggct
gctgccaccgctgagcaataactagcataaccctttggggcctctaaacgggtcttgaggggtttttgctgaaaggaggaactatatccggattggcgaatgggacgcgccctgtagcggcgcattaagcgcggcgggtgtg
gtggttacgcgcagcgtgaccgctacacttgcca

pJ431-mTurquoise2-Tat, https://benchling.com/s/qUQh08yE

T7 promoter, LacO (LacI binding element), 6xHis, mTq2, Biv-Tat

AATTTTGTGTCGCCCTTCCGCGAAATTAATACGACTCACTATAGGGGAATTGTGAGCGGATAACAATTCCCCTCTAGAAATAATTTTGTTTAACTTTTAAGGAGGTA
AAAAATGGGTTCTTCTCACCATCATCATCATCACACTCGCGGCGGCGGCGGTTCTATGGTTAGCAAGGGTGAAGAACTGTTCACCGGCGTCGTGCCGATTCTGG
TTGAGCTGGATGGTGATGTCAACGGTCACAAGTTTAGCGTTAGCGGTGAGGGCGAGGGCGACGCCACCTACGGTAAATTGACCCTGAAGTTTATCTGCACGACC
GGTAAGCTGCCGGTTCCGTGGCCGACCCTGGTGACGACTCTGTCGTGGGGCGTGCAATGTTTCGCGCGCTATCCGGATCACATGAAACAGCATGACTTCTTTAA
GAGCGCGATGCCGGAAGGCTACGTTCAGGAACGTACGATCTTTTTCAAAGACGACGGTAACTATAAGACCCGCGCAGAAGTCAAGTTCGAGGGTGACACGCTG
GTGAATCGTATTGAGCTGAAAGGTATTGACTTTAAAGAGGACGGTAACATCCTGGGTCACAAACTGGAGTATAATTACTTCAGCGACAATGTGTACATCACCGCTG
ATAAACAGAAAAACGGCATTAAAGCAAACTTCAAGATCCGTCACAATATTGAAGATGGCGGCGTGCAATTGGCCGATCACTATCAACAGAACACCCCGATTGGCG
ATGGTCCGGTCCTGCTGCCAGATAATCACTACTTGAGCACGCAATCCAAACTGTCCAAAGATCCGAACGAAAAACGTGACCACATGGTCCTGCTGGAATTCGTTA
CCGCGGCGGGTATCACGCTGGGTATGGACGAACTGTACAAGACCCGTGGTGGCGGCGGCAGCAGCGGTCCGCGTCCTCGTGGTACCCGCGGTAAGGGTCGT
CGCATTCGTCGTTAACCCCCTAGCATAACCCCTTGGGGCCTCTAAACGGGTCTTGAGGGGTTTTTTGCCCCTGAGACGCGTCAATCGAGTTCGTACCTAAGGGC
GACACCCCCT

pSB6A1-I746907, https://benchling.com/s/4Oqh5b6h

T7 promoter, GFP

tgccacctgacgtctaagaaaccattattatcatgacattaacctataaaaatagggcgtatcacgaggccctttcgtcttcaagaattcgcggccgcttctagagtaatacgactcactatagggagatactagagaaagaggaga
aatactagatgcgtaaaggagaagaacttttcactggagttgtcccaattcttgttgaattagatggtgacgttaatggacacaaattttctgtcagtggagagggtgaaggtgatgcaacatacggaaaacttaccctaaatttattt
gcactactggaaaactacctgttccatggccaacacttgtcactactctcgcgtatggtcttcaatgctttgcgagatacccagatcatatgaaacagcatgactttttcaagagtgccatgcccgaaggttatgtacaggaaagaa
ctatatttttcaaagatgacgggtactacaagacacgtgctgaagtcaagtttgaaggtgataccctgttaatagaatcgtgttaaaaggtattgattttaaagaagatggaaacattcttggacacaaattggaatacaactttaact
cacacaatgtatacatcatggcagacaaacaaaagaatggaatcaaagttaacttcaaaattagacacaacattgaagatggaagcgttcaactagcagaccattatcaacaaaatactccaattggcgatggccctgtccttt
accagacaaccattacctgtccacacaatctgccctttcgaaagatcccaacgaaaagagagaccacatggtccttcttgagtttgtaacagctgctggaattacacatggcatggatgaactatacaaacatcatcaccatcac
cactaataatactagagccaggcatcaaataaaacgaaaggctcagtcgaaagactgggcctttcgttttatctgttgtttgtcggtgaacgctctctactagagtcacactggctcaccttcgggtgggcctttctgcgttatatact
agtagcggccgctgcagctctacgccggacgcatcg

pSB4A5-J04450, https://benchling.com/s/y8NtsQ4P

pLacO, RFP

tgccacctgacgtctaagaaaaggaatattcagcaatttgcccgtgccgaagaaaggcccacccgtgaaggtgagccagtgagttgattgctacgtaattagttagttagccccttagtgactcgaattcgcggccgcttctagag
caatacgcaaaccgcctctccccgcgcgttggccgattcattaatgcagctggcacgacaggtttcccgactggaaagcgggcagtgagcgcaacgcaattaatgtgagttagctcactcattaggcaccccaggctttacac
tttatgcttccggctcgtatgttgtgtggaattgtgagcggataacaatttcacacatactagagaaagaggagaaatactagatgcttccttcctcgaagacgttatcaaagagttctcgtatgtgaaggttccgtt
aacggtcacgagttcgaaatcgaaggtgaaggtgaaggtcgtccgtacgaaggtacccagaccgctaaactgaaagttaccaaaggtggtccgctgccgttcgcttgggacatcctgtccccgcagttccagtacggttcca
aagcttacgttaaacacccggctgacatcccggactacctgaaactgtccttcccggaaggtttcaaatgggaacgtgttatgaacttcgaagacggtggtgttgttaccgttacccaggactcctccctgcaagacggtgagttc
atctacaaagttaaactgcgtggtaccaacttcccgtccgacggtccggttatgcagaaaaaaccatgggtgggaagcttccaccgaacgtatgtacccggaagacggtgctctgaaaggtgaaatcaaaatgcgtctgaa
actgaaagacggtggtcactacgacgctgaagttaaaaccacctacatggctaaaaaccggttcagctgccgggtgcttacaaaaccgacatcaaactggacatcacctcccacaacgaagactacaccatcgttgaaca
gtacgaacgtgctgaaggtcgtcactccaccggtgcttaataacgctgatagtgctagtgtagatcgctactagagccaggcatcaaataaaacgaaaggctcagtcgaaagactgggcctttcgttttatctgttgtttgtcggtg
aacgctctctactagagtcacactggctcaccttcgggtgggcctttctgcgtttatatactagtagcggccgctgcaggagtcactaagggttagttagttagattagcagaaagtcaaaagcctccgaccggaggcttttgacta
aaacttcccttggggttatcattggggctcactcaaaggcggtaat

pSB1A3-pT7-Th-YPet, https://benchling.com/s/BWq3155p

T7 promoter, theophylline riboswitch, YPet

tgccacctgacgtctaagaaaccattattatcatgacattaacctataaaaataggcgtatcacgaggcagaatttcagataaaaaaaatccttagctttcgctaaggatgatttctgGAATTCATTTAATACGACTCACT
ATAGGGTGATACCAGCATCGTCTTGATGCCCTTGGCAGCACCCTGCTAAGGTAACAACAAGATGGTGTCCAAAGGCGAAGAACTGTTTACCGGTGTGGTTCCGA
TTCTGGTGGAACTGGATGGCGACGTTAACGGTCATAAATTTAGTGTGTCCGGCGAAGGTGAAGGCGATGCGACCTATGGCAAACTGACGCTGAAACTGCTGTGC
ACCACCGGTAAACTGCCGGTCCCGTGGCCGACCCTGGTGACCACGCTGGGTTATGGCGTGCAGTGTTTCGCGCGCTACCCGGACCACATGAAACAACACGAT
TTCTTTAAAAGTGCCATGCCGGAAGGCTATGTTCAGGAACGTACCATCTTTTTCAAAGATGACGGTAACTACAAAACCCGCGCGGAAGTTAAATTTGAAGGCGATA
CGCTGGTCAACCGTATTGAACTGAAAGGTATCGACTTCAAAGAAGATGGCAATATTCTGGGTCATAAACTGGAATATAACTACAATAGCCACAACGTGTATATTAC
CGCGGATAAACAGAAAAACGGCATCAAAGCCAACTTCAAAATCCGCCATAACATCGAAGACGGCGGTGTTCAACTGGCCGATCACTACCAGCAAAACACCCCGA
TTGGTGATGGTCCGGTCCTGCTGCCGGATAATCATTATCTGTCATACCAGTCGAAACTGTTTAAAGACCCGAATGAAAAACGTGATCACATGGTGCTGGAATT
TCTGACCGCGGGCCGGCATTACGGAGGGTATGAACGAACTGTATAAATGATAATTAGTTAGTTAGCAGATCCGGCTGCTAACAAAGCCCGAAAGGAAGCTGAGTT
GGCTGCTGCCACCGTAGCAATAAAGAGAATATAAAAAGCCAGATTATTAATCCGGCTTTTTTGTTATTTCTGCAGtccggcaaaaaagggcaaggtgtcaccaccctgcccttttttctt
taaaaccgaaaagattacttcgcgttatgcaggcttcctcgctcactgactcgctgcgctcggtcgttcggctgcggcgagcggtatcagctcactcaaaggcggtaat

pSB1A2-AD001, https://benchling.com/s/seq-S21D4M3gz2UfOX0GDVPV

araC, pBAD, α-HL, GFP

tgccacctgacgtctaagaaaccattattatcatgacattaacctataaaaataggcgtatcacgaggcagaatttcagataaaaaaaatccttagctttcgctaaggatgatttctggaattcgcggccgcttctagagGAGAG
TTAGGCATAAGGCTGCATGCTACCCTTTGGTCGAAAAAAAAAGCCCGCACTGTCAGGTGCGGGCTTTTTTCTGTGTTTCCttatgacaacttgacggctacatcattcactttttcttc
acaaccggcacggaactcgctcgggctggccccggtgcatttttttaaatacccgcgagaaatagagttgatcgtcaaaaccaacattgcgaccgacggtggcgataggcatccgggtggtgctcaaaagcagcttcgcctg
gctgatacgttggtcctcgcgccagcttaagacgctaatccctaactgctggcggaaaagatgtgacagacgcgacggcgacaagcaaacatgctgtgcgacgctggcgatatcaaaattgctgtctgccaggtgatcgctg
atgtactgacaagcctcgcgtacccgattatccatcggtggatggagcgactcgttaatcgcttccatgcgccgcagtaacaattgctcaagcagatttatcgccagcagctccgaatagcgcccttcccctgcccggcgttaa
tgatttgcccaaacaggtcgctgaaatgcggctggtgcgcttcatccgggcgaaagaaccccgtattggcaaatattgacggccagttaagccattcatgccagtaggcgcgcggacgaaagtaaacccactggtgatacca
ttcgcgagcctccggatgacgaccgtagtgatgaatctctcctggcgggaacagcaaaatatcacccggtcggcaaacaaattctcgtccctgatttttcaccaccccctgaccgcgaatggtgagattgagaatataacctttc
attcccagcggtcggtcgataaaaaaatcgagataaccgttggcctcaatcggcgttaaacccgccaccagatgggcattaaacgagtatcccggcagcaggggatcattttgcgcttcagccatacttttca-
tactcccgccattcagagaagaaaccaattgtccatattgcatcagacattgccgtcactgcgtcttttactggctcttctcgctaacccaaaccggtaaccccgcttattaaaagcattctgtaacaaagcgggaccaaagccatg
acaaaaaacgcgtaacaaaagtgtctataatcacggcagaaaagtccacattgattatttgcacggcgtcacactttgctatgccatagcatttttatccataagattagcggatcctacctgacgctttttatcgcaactctctactgttt
ctccatacccgttttttgggctagcgaattcgagctcggtacccggggatcctctagaagggagatataaccCTATGGACTATGTTTTTCAAAGACGAAAAACTACTAGATGGATTCTGATATCAAT
ATCAAAACCGGCACCACCGATATCGGCTCCAATACCACCGTTAAAACCGGTGATCTGGTGACCTATGATAAAGAAAACGGTATGCATAAAAAAGTGTTTTACTCGT
TTATTGACGATAAAAACCATAACAAAAAACTGCTGGTCATCCGCACCCAAAGGCACCATTGCGGGTCAATACCGTGTGTACTCCGAAGAAGGTGCGAACAAAAGCG
GTCTGGCTTGGCCGTCTGCCTTTAAAGTGCAGCTGCAACTGCCGGATAATGAAGTGGCGCAGATTTCAGATTATTATCCGCGTAATAGCATCGATACCAAAGAAT
ATATGAGTACCCTGACCTATGGTTTTAATGGCAATGTTACCGGTGATGATACGGGTAAAATTGGCGGTCTGATTGGCGCCAATGTGTCCATTGGTCATACGCTGAA
ATACGTGCAACCGGATTTCAAAACCATTCTGGAAAGTCCGACCGATAAAAAAGTGGGTTGGAAAGTTATCTTCAACAACATGGTGAATCAGAACTGGGGTCCGTA
CGATCGCGATTCCTGGAATCCGGTTTATGGCAATCAGCTGTTTATGAAAACCCGCAACGGTAGTATGAAAGCGGCGGATAATTTTCTGGACCCGAACAAAGCCTC
AAGCCTGCTGTCCAGCGGTTTTAGCCCGGATTTTGCCACGGTTATTACCATGGATCGCAAAGCCAGCAAACAGCAGACCAACATTGATGTGATCTACGAACGTGT
GCGTGATGATTATCAACTGCATTGGACCTCAACCAATTGGAAAGGCACCAATACCAAAGATAAATGGACGGATCGCAGTTCAGAACGCTACAAAATTGATTGGGA
AAAAGAAGAAATGACCAACTAAAGCGCTCAACGGGTGTGCTTCCCGTTCTGATGAGTCCGTGAGGACGAAAGCGCCTCTACAAATAATTTTGTTTAAGGAGCTAT
GGACTATGTTTGAAAGGCTGAAATACTAGATGCGCAAGGGTGAGGAACTGTTCACAGGTGTCGTACCTATCTTGGTAGAATTGGATGGGGATGTAAACGGGCACA
AATTTAGTGTACGCGGCGAGGGGGAGGGGGATGCGACCAACGGGAAGCTGACTCTGAAGTTTATTTGCACCACCGGAAAGTTGCCGGTACCCTGGCCGACATT
AGTAACTACACTTACCTACGGCGTTCAATGCTTCGCGCGCTACCCGGATCATATGAAGCAGCATGACTTCTTCAAGTCAGCGATGCCGGAAGGCTACGTTCAAG
AGCGCACCATCTCCTTTAAAGACGACGGGACGTATAAAACACGCGCCGAGGTAAAATTCGAAGGGGATACGTTAGTCAATCGTATTGAGCTGAAGGGAATCGAC
TTCAAAGAAGATGGAAATATCTTAGGGCATAAACTGGAAATATAATTTCAACAGTCACAATGTGTATATCACGGCGGACAAGCAGAAGAATGGAATCAAGGCGAACT
TTAAAATCCGTCACAACGTCGAAGATGGTTCTGTTCAGCTTGCGGATCATTATCAACAAAATACGCCGATTGGCGATGGACCTGTGTTATTACCGGATAATCATTAT
TTATCCACACAGTCAGTATTGTCCAAAGATCCGAACGAGAAGCGTGACCACATGGTATTGCTGGAGTTTGTTACTGCCGCCGGGATTACGCATGGAATGGACGA
GCTGTATAAGTAATAGAACGCATGAGAAAGCCCCCGGAAGATCACCTTCCGGGGGCTTTTTTATTGCGCCTTGTCACACCTACACTGCTCGAAGtaCtactagtagcgg
ccgctgcagtccggcaaaaaagggcaaggtgtcaccaccctgcccttttttcttttaaaaccgaaaagattactcgcgttatgcaggcttcctcgctcactgactcgctgcgctcggtcgttcggctgcggcgagcggtatcagct
cactcaaaggcggtaat

pSB4K5-AD002, https://benchling.com/s/seq-pgYaxr5s1hTfHrS35jrL

pLux, B0031, LuxI, LVA degtag

tgccacctgacgtctaagaaaaggaatattcagcaatttgcccgtgccgaagaaaggcccacccgtgaaggtgagccagtgagttgattgctacgtaattagttagttagcccttagtgactcgaattcgcggccgcttctagag
ACCTGTAGGATCGTACAGGTTTACGCAAGAAAATGGTTTGTTATAGTCGAATAAATACTAGAGTCACACAGGAAACCTACTAGATgACTATAATGATAAAAAAATCG
GATTTTTTGGCAATTCCATCAGAGGAGTATAAAGGTATTCTAAGTCTTCGTTATCAAGTGTTTAAGCAAAGACTTGAGTGGGACTTAGTTGTAGAAAATAACCTCGAA
TCAGATGAGTATGATAACTCAAATGCAGAATATATTTATGCTTGTGATGATACTGAAAATGTAAGTGGATGCTGGCGTTTATTACCTACAACAGGTGATTATATGCTG
AAAAGTGTTTTTCCTGAATTGCTTGGTCAACAGAGTGCTCCCAAAGATCCTAATATAGTCGAATTAAGTCGTTTTGCTGTAGGTAAAAATAGCTCAAAGATAAATAACT
TCTGCTAGTGAAATTACAATGAAACTATTTGAAGCTATATATAAACACGCTGTTAGTCAAGGTATTACAGAATATGTAACAGTAACATCAACAGCAATAGAGCGATTT
TTAAAGCGTATTAAAGTTCCTTGTCATCGTATTGGAGACAAAGAAATTCATGTATTAGGTGATACTAAATCGGTTGTATTGTCTATGCCTATTAATGAACAGTTTAAAA
AaGCAGTCTTAAATGCTGCAAACGACGAAAaCTACGCTTTAGTAGCTTAATAACTCTGATAGTGCTAGTGTAGATCTctactagagccaggcatcaaataaaacgaaaggctcagtc
gaaagactgggcctttcgttttatctgttgtttgtcggtgaacgctctctactagagtcacactggctcaccttcgggtgggcctttctgcgtttatatactagtagcggccgctgcaggagtcactaagggttagttagttagattagca
gaaagtcaaaagcctccgaccggaggcttttgactaaaacttcccttggggttatcattggggctcactcaaaggcggtaat

pSB4K5-AD003, https://benchling.com/s/seq-wfuH5W9zOxSqSxEVBjzr

pLux, B0032, LuxI, LVA degtag

tgccacctgacgtctaagaaaaggaatattcagcaatttgcccgtgccgaagaaaggcccacccgtgaaggtgagccagtgagttgattgctacgtaattagttagttagcccttagtgactcgaattcgcggccgcttctagag
ACCTGTAGGATCGTACAGGTTTACGCAAGAAAATGGTTTGTTATAGTCGAATAAATACTAGAGTCACACAGGAAACGTACTAGATgACTATAATGATAAAAAAATCGG
ATTTTTTGGCAATTCCATCAGAGGAGTATAAAGGTATTCTAAGTCTTCGTTATCAAGTGTTTAAGCAAAGACTTGAGTGGGACTTAGTTGTAGAAAATAACCTCGAAT
CAGATGAGTATGATAACTCAAATGCAGAATATATTTATGCTTGTGATGATACTGAAAATGTAAGTGGATGCTGGCGTTTATTACCTACAACAGGTGATTATATGCTGA
AAAGTGTTTTTCCTGAATTGCTTGGTCAACAGAGTGCTCCCAAAGATCCTAATATAGTCGAATTAAGTCGTTTTGCTGTAGGTAAAAATAGCTCAAAGATAAATAACT
CTGCTAGTGAAATTACAATGAAACTATTTGAAGCTATATATAAACACGCTGTTAGTCAAGGTATTACAGAATATGTAACAGTAACATCAACAGCAATAGAGCGATTTT
TAAAGCGTATTAAAGTTCCTTGTCATCGTATTGGAGACAAAGAAATTCATGTATTAGGTGATACTAAATCGGTTGTATTGTCTATGCCTATTAATGAACAGTTTAAAAA
aGCAGTCTTAAATGCTGCAAACGACGAAAaCTACGCTTTAGTAGCTTAATAACTCTGATAGTGCTAGTGTAGATCTctactagagccaggcatcaaataaaacgaaaggctcagtcg
aaagactgggcctttcgttttatctgttgtttgtcggtgaacgctctctactagagtcacactggctcaccttcgggtgggcctttctgcgtttatatactagtagcggccgctgcaggagtcactaagggttagttagttagattagcag
aaagtcaaaagcctccgaccggaggcttttgactaaaacttcccttggggttatcattggggctcactcaaaggcggtaat

pSB4A5-AD004, https://benchling.com/s/seq-udWFKRJUWkRXAK9lZeY5

pLas81, LasR, AAV degtag, mScarletI, LasI

tgccacctgacgtctaagaaaaggaatattcagcaatttgcccgtgccgaagaaaggcccacccgtgaaggtgagccagtgagttgattgctacgtaattagttagttagcccttagtgactcgaattcACCTATAGGATC
GTATAGGTTTACGCAAGAAAATGGTTTGTTATAGTCGAATAAAAAGCTTAGGGTGTCTCAAGGTGCGTACCTTGACTGATGAGTCCGAAAGGACGAAACACCCCT
CTACAAATAATTTTGTTTAAGCGGCCGCACTATGTTTTCAAAGACGAAAAACTACTAGATGGCCCTGGTAGACGGCTTCTTGGAATTAGAACGTTCTAGTGGCAA
GTTGGAGTGGTCGGCAATCTTGCAAAAAATGGCTTCTGACTTAGGCTTCTCCAAGATTCATGTTTGGTTTGTTACCGAAGGATTCACAGGATTACGAAAACGCATTC
ATCGTCGGGAATTATCCAGCCGCGTGGCGCGAACACTACGATCGCGCTGGGTATGCGCGCGTTGATCCTACCGTGTCGCATTGCACTCAGTCTGTTCTTCCCCAT
TTTTTGGGAACCCTCAATCTACCAGACCCGCAAGCAACATGAGTTCTTTGAGGAAGCCTCGGCCGCGGGGGCTTGTGTATGGCCTTACGATGCCACTTCATGGTG
CCCGTGGGGAATTGGGAGCACTGTCGCTTTCAGTCGAAGCCGAAAACCGCGCTGAGGCCAACCGTTTTATTGAGAGCGTCCTTCCAACTTTATGGATGTTGAAG
GACTATGCCCTTCAATCTGGGGCTGGGTTGGCCTTTGAGCACCCTGTTTCTAAACCAGTAGTTCTTACTTCACGCGAGAAGGAAGTCTTGCAATGGTGTGCTATTT
GGAAAGACCTCCTGGGAAATCAGCGTCATTTGCAACTGTTCGGAAGCAAATGTAAATTTTCATATGGGGAACATCCGTCGCAAATTTGGGGTGACGTCCGGTCGT
GTCGCAGCCATCATGGCAGTCAATCTTGGTCTTATCACCTTACGTCCCGCTGCTAATGACGAGAACTATGCTGCGGCTGTCTGATAACTCGAGAGCTGTCACCG
GATGTGCTTTCCGGTCTGATGAGTCCGTGAGGACGAAACAGCGAGATCAGATAATTCTGACGTATCTAGATACGCTATGGACTATGTTTTCTGCTATGGACTATGT
TTTCACACACGAGATGCCTCGATGGTGTCAAAGGGAGAGGCGGTTATCAAGGAATTTATGCGCTTTAAAGTCCACATGGAGGGCAGCATGAACGGGCACGAGTT
TGAAATTGAGGGGGAGGGGGAGGGCCGTCCTTATGAAGGTACTCAGACTGCTAAACTGAAGGTGACAAAAGGTGGCCCCTTGCCTTTCTCGTGGGACATCCTG
TCGCCACAATTCATGTACGGGAGCCGCGCCTTTATCAAACATCCCGCAGATATTCCTGATTACTATAAACAATCTTTCCCGGAAGGTTTCAAATGGGAACGCGTCA
TGAATTTTGAGGACGGGGGCGCTGTCACAGTTACTCAGGACACCTCCTTGGAAGACGGCACATTGATTTACAAGGTTAAGTTGCGCGGCACAAACTTCCCCCCT
GACGGGCCAGTAATGCAAAAGAAAACTATGGGTTGGGAGGCGTCTACAGAACGTTTATACCCCGAAGACGGGGTGCTGAAAGGTGACATTAAGATGGCCCTGC
GCCTGAAGGACGGCGGTCGCTATCTTGCCGACTTTAAAACTACTTATAAGGCTAAAAAACCAGTCCAGATGCCAGGCGCCTATAATGTTGACCGCAAGTTAGACA
TCACCTCACATAATGAAGACTATACCGTTGTAGAACAATACGAGCGCAGCGAGGGTCGTCACAGTACCGGGGGGATGGATGAATTATACAAACGTCCTGCTGCG
AACGACGAAAATTATGCGGCTGCGGTTTGATAAGGAAACACAGAAAAAAGCCCGCACCTGACAGTGCGGGCTTTTTTTTTCGACCAAAGGTTAATTAAACCTATAG
GATCGTATAGGTTTACGCAAGAAAATGGTTTGTTATAGTCGAATAAACCTAGGCCCCCCGAGGAGTAGCACATGATTGTGCAAATCGGCCGCCGTGAGGAGTTC
GATAAAAAGCTGCTTGGGGAAATGCATAAACTTCGTGCTCAGGTGTTCAAGGAGCGTAAGGGGTGGGATGTTTCCGTTATTGACGAAATGGAAATTGATGGGTAC
GATGCATTATCACCTTACTATATGCTGATTCAAGAAGACACACCTGAGGCCCAGGTATTCGGTTGCTGGCGCATTTTTGACACGACGGGGCCTTACATGTTGAAG
AACACGTTTCCTGAATTGTTACACGGCAAAGAAGCTCCCTGCTCACCCCATATTTGGGAACTGAGCCGTTTCGCTATCAATTCCGGTCAAAAGGGCTCCCTGGGC
TTTTCGGACTGCACCCTTGAAGCCATGCGCGCACTTGCCCGTTACTCCCTGCAAAACGACATTCAAACCTTAGTTACTGTTACTACCGTTGGCGTAGAGAAGATG

ATGATCCGTGCGGGTCTTGACGTATCTCGCTTTGGACCGCATCTGAAGATTGGAATCGAGCGTGCGGTGGCGTTGCGCATCGAATTGAACGCAAAAACGCAAAT
TGCGTTATACGGCGGGGTCTTGGTTGAACAGCGTTTAGCCGTGAGTTGATAATCCGGCAATTAAAAAAGCGGCTAACCACGCCGCTTTTTTTACGTCTGCActgcag
gagtcactaagggttagttagttagattagcagaaagtcaaaagcctccgaccggaggcttttgactaaaacttccctggggttatcattggggctcactcaaaggcggtaat

pSB4A5-AD005, https://benchling.com/s/seq-6Os5pdCBrNtaeceAf5op

pLacO, LasR, AAV degtag, pLas81, RBS N1, mScarletI, LasI

tgccacctgacgtctaagaaaaggaatattcagcaatttgcccgtgccgaagaaaggcccacccgtgaaggtgagccagtgagttgattgctacgtaattagttagttagccctagtgactcgaattcAATTGTGAGCGG
ATAACAATTGACATTGTGAGCGGATAACAAGATACTGAGCACAAAGCTTAGGGTGTCTCAAGGTGCGTACCTTGACTGATGAGTCCGAAAGGACGAAACACCCCT
CTACAAATAATTTTGTTTAAGCGGCCGCACTATGTTTTTCAAAGACGAAAAACTACTAGATGGCCCTGGTAGACGGCTTCTTGGAATTAGAACGTTCTAGTGGCAA
GTTGGAGTGGTCGGCAATCTTGCAAAAAATGGCTTCTGACTTAGGCTTCTCCAAGATTCTGTTTGGTTTGTTACCGAAGGATTCACAGGATTACGAAAACGCATTC
ATCGTCGGGAATTATCCAGCCGCGTGGCGCGAACACTACGATCGCGCTGGGTATGCGCGCGTTGATCCTACCGTGTCGCATTGCACTCAGTCTGTTCTTCCCAT
TTTTTGGGAACCCTCAATCTACCAGACCCGCAAGCAACATGAGTTCTTTGAGGAAGCCTCGGCCGCGGGGCTTGTGTATGGCCTTACGATGCCACTTCATGGTG
CCCGTGGGGAATTGGGAGCACTGTCGCTTTCAGTCGAAGCCGAAAACCGCGCTGAGGCCAACCGTTTTATTGAGAGCGTCCTTCCAACTTTATGGATGTTGAAG
GACTATGCCCTTCAATCTGGGGCTGGGTTGGCCTTTGAGCACCCTGTTTCTAAACCAGTAGTTCTTACTTCACGCGAGAAGGAAGTCTTGCAATGGTGTGCTATT
GGAAAGACCTCCTGGGAAATCAGCGTCATTTGCAACTGTTCGGAAGCAAATGTAAATTTTCATATGGGGAACATCCGTCGCAAATTTGGGGTGACGTCCGTCGT
GTCGCAGCCATCATGGCAGTCAATCTTGGTCTTATCACCTTACGTCCCGCTGCTAATGACGAGAACTATGCTGCGGCTGTCTGTAATACTCGAGTTCAGCCAAAAA
ACTTAAGACCGCCGGTCTTGTCCACTACCTTGCAGTAATGCGGTGGACAGGATCGGCGGTTTTCTTTTCTCTTCTCAATTAATTAAACCTATAGGATCGTATAGGTT
TACGCAAGAAAATGGTTTGTTATAGTCGAATAAAATCCATAGCTGTCACCGGATGTGCTTTCCGGTCTGATGAGTCCGTGAGGACGAAACAGCGAGATCAGATAA
TTCTGACGTATCTAGATACGCTATGGACTATGTTTTCTGCTATGGACTATGTTTTCACACACGAGATGCCTCGATGGTGTCAAAGGGAGAGGCGGTTATCAAGGAA
TTTATGCGCTTTAAAGTCCACATGGAGGGCAGCATGAACGGGCACGAGTTTGAAATTGAGGGGGAGGGGGAGGGCCGTCCTTATGAAGGTACTCAGACTGCTAA
ACTGAAGGTGACAAAAGGTGGCCCCTTGCCTTTCTCGTGGGACATCCTGTCGCCACAATTCATGTACGGGAGCCGCGCCTTTATCAAACATCCCGCAGATATTC
CTGATTACTATAAACAATCTTTCCCGGAAGGTTTCAAATGGGAACGCGTCATGAATTTTGAGGACGGGGGCGCTGTCACAGTTACTCAGGACACCTCCTTGGAAG
ACGGCACATTGATTTACAAGGTTAAGTTGCGCGGCACAAACTTCCCCCCTGACGGGCCAGTAATGCAAAAGAAAACTATGGGTTGGGAGGCGTCTACAGAACGT
TTATACCCCGAAGACGGGGTGCTGAAAGGTGACATTAAGATGGCCCTGCGCCTGAAGGACGGCGGTCGCTATCTTGCCGACTTTAAAACTACTTATAAGGCTAA
AAAACCAGTCCAGATGCCAGGCGCCTATAATGTTGACCGCAAGTTAGACATCACCTCACATAATGAAGACTATACCGTTGTAGAACAATACGAGCGCAGCGAGG
GTCGTCACAGTACCGGGGGGATGGATGAATTATACAAACGTCCTGCTGCGAACGACGAAAATTATGCGGCTGCGGTTTGATAAGGAAACACAGAAAAAAGCCCG
CACCTGACAGTGCGGGCTTTTTTTTTCGACCAAAGGTTAATTAAACCTATAGGATCGTATAGGTTTACGCAAGAAAATGGTTTGTTATAGTCGAATAAACCTAGGCC
CCCCGAGGAGTAGCACATGATTGTGCAAATCGGCCGCCGTGAGGAGTTCGATAAAAAGCTGCTTGGGGAAATGCATAAACTTCGTGCTCAGGTGTTCAAGGAGC
GTAAGGGGTGGGATGTTTCCGTTATTGACGAAATGGAATTGATGGGTACGATGCATTATCACCTTACTATATGCTGATTCAAGAAGACACACCTGAGGCCCAGG
TATTCGGTTGCTGGCGCATTTTTGACACGACGGGGCCTTACATGTTGAAGAACACGTTTCCTGAATTGTTACACGGCAAAGAAGCTCCCTGCTCACCCCATATTTG
GGAACTGAGCCGTTTCGCTATCAATTCCGGTCAAAAGGGCTCCCTGGGCTTTTCGGACTGCACCCTTGAAGCCATGCGCGCACTTGCCCGTTACTCCCTGCAAA
ACGACATTCAAACCTTAGTTACTGTTACTACCGTTGGCGTAGAGAAGATGATGATCCGTGCGGGTCTTGACGTATCTCGCTTTGGACCGCATCTGAAGATTGGAAT
CGAGCGTGCGGTGGCGTTGCGCATCGAATTGAACGCAAAAACGCAAATTGCGTTATACGGCGGGGTCTTGGTTGAACAGCGTTTAGCCGTGAGTTGATAATCCG
GCAATTAAAAAAGCGGCTAACCACGCCGCTTTTTTTACGTCTGCActgcaggagtcactaagggttagttagttagattagcagaaagtcaaaagcctccgaccggaggcttttgactaaaacttccct
tggggttatcattggggctcactcaaaggcggtaat

pSB4A5-AD007, https://benchling.com/s/seq-wDKemQw5MqS0n9aunel6

pLas81, LasI

tgccacctgacgtctaagaaaaggaatattcagcaatttgcccgtgccgaagaaaggcccacccgtgaaggtgagccagtgagttgattgctacgtaattagttagttagccctagtgactcgaattcCGACCAAAGGTT
AATTAAACCTATAGGATCGTATAGGTTTACGCAAGAAAATGGTTTGTTATAGTCGAATAAACCTAGGCCCCCCCGAGGAGTAGCACATGATTGTGCAAATCGGCCG
CCGTGAGGAGTTCGATAAAAAGCTGCTTGGGGAAATGCATAAACTTCGTGCTCAGGTGTTCCAAGGAGCGTAAGGGGTGGGATGTTTCCGTTATTGACGAAATGGA
AATTGATGGGTACGATGCATTATCACCTTACTATATGCTGATTCAAGAAGACACACCTGAGGCCCAGGTATTCGGTTGCTGGCGCATTTTTGACACGACGGGGCC
TTACATGTTGAAGAACACGTTTCCTGAATTGTTACACGGCAAAGAAGCTCCCTGCTCACCCCATATTTGGGAACTGAGCCGTTTCGCTATCAATTCCGGTCAAAAG
GGCTCCCTGGGCTTTTCGGACTGCACCCTTGAAGCCATGCGCGCACTTGCCCGTTACTCCCTGCAAAACGACATTCAAACCTTAGTTACTGTTACTACCGTTGGC
GTAGAGAAGATGATGATCCGTGCGGGTCTTGACGTATCTCGCTTTGGACCGCATCTGAAGATTGGAATCGAGCGTGCGGTGGCGTTGCGCATCGAATTGAACGC
AAAAACGCAAATTGCGTTATACGGCGGGGTCTTGGTTGAACAGCGTTTAGCCGTGAGTTGATAATCCGGCAATTAAAAAAGCGGCTAACCACGCCGCTTTTTTTA
CGTCTGCActgcaggagtcactaagggttagttagttagattagcagaaagtcaaaagcctccgaccggaggcttttgactaaaacttccctggggttatcattggggctcactcaaaggcggtaat

pSB1A2-AD009, https://benchling.com/s/seq-z5pCzemchBIS22npC44x

araC, pBAD, α-HL

tgccacctgacgtctaagaaaccattattatcatgacattaacctataaaaatagGCGTATCACGAGGCAGAATTTCAGATAAAAAAAATCCTTAGCTTTCGCTAAGGATGATTTCTGGAATTCGCGGCCGCTTCTAGAGGAGAG
TTAGGCATAAGGCTGCATGCTACCCTTTGGTCGAAAAAAAAAGCCCGCACTGTCAGGTGCGGGCTTTTTTCTGTGTTTCCttatgacaacttgacggctacatcattcactttttcttc
acaaccggcacggaactcgctcgggctggccccggtgcatttttttaaatacccgcgagaaatagagttgatcgtcaaaaccaacattgcgaccgacggtggcgataggcatccgggtggtgctcaaaagcagcttcgcctg
gctgatacgttggtcctcgcgccagcttaagacgctaatccctaactgctggcggaaaagatgtgacagacgcgacggcgacaagcaaacatgctgtgcgacgctggcgatatcaaaattgctgtctgccaggtgatcgctg
atgtactgacaagcctcgcgtacccgattatccatcggtggatggagcgactcgttaatcgcttccatgcgccgcagtaacaattgctcaagcagatttatcgccagcagctccgaatagcgcccttccccttgcccggcgttaa
tgatttgcccaaacaggtcgctgaaatgcggctggtgcgcttcatccgggcgaaagaaccccgtattggcaaatattgacggccagttaagccattcatgccagtaggcgcgcggacgaaagtaaacccactggtgataccа
ttcgcgagcctccggatgacgaccgtagtgatgaatctctcctggcgggaacagcaaaatatcacccggtcggcaaacaaattctcgtccctgatttttcaccaccccctgaccgcgaatggtgagattgagaatataacctttc
attcccagcggtcggtcgataaaaaaatcgagataaccgttggcctcaatcggcgttaaacccgccaccagatgggcattaaacgagtatcccggcagcaggggatcattttgcgcttcagccatacttttcatactcccgccat
tcagagaagaaaccaattgtccatattgcatcagacattgccgtcactgcgtctttactggctcttctgctaaccaaacccggtaacccccgcttattaaagcattctgtaacaaagcgggaccaaagccatgacaaaaacgcgt
aacaaaagtgtctataatcacggcagaaaagtccacattgattatttgcacggcgtcacactttgctatgccatagcatttttatccataagattagcggatcctacctgacgcttttatcgcaactctctactgttctccatacccgttt
ttttgggctagcgaattcgagctcggtacccggggatcctctagaagggagatataaccCTATGGACTATGTTTTTCAAAGACGAAAAACTACTAGATGGATTCTGATATCAATATCAAAACCG
GCACCACCGATATCGGCTCCAATACCACCGTTAAAACCGGTGATCTGGTGACCTATGATAAAGAAAACGGTATGCATAAAAAAGTGTTTTACTCGTTTATTGACGA
TAAAAACCATAACAAAAAACTGCTGGTCATCCGCACCAAAGGCACCATTGCGGGTCAATACCGTGTGTACTCCGAAGAAGGTGCGAACAAAAGCGGTCTGGCTT
GGCCGTCTGCCTTTAAAGTGCAGCTGCAACTGCCGGATAATGAAGTGGCGCAGATTTCAGATTATTATCCGCGTAATAGCATCGATACCAAGAATATATGAGTA
CCCTGACCTATGGTTTTAATGGCAATGTTACCGGTGATGATACGGGTAAAATTGGCGGTCTGATTGGCGCCAATGTGTCCATTGGTCATACGCTGAAATACGTGC
AACCGGATTTCAAAACCATTCTGGAAAGTCCGACCGATAAAAAAGTGGGTTGGAAAGTTATCTTCAACAACATGGGTGAATCAGAACTGGGGTCCGTACGATCGCG
ATTCCTGGAATCCGGTTTATGGCAATCAGCTGTTTATGAAAACCCGCAACGGTAGTATGAAAGCGGCGGATAATTTTCTGGACCCGAACAAAGCCTCAAGCCTGC
TGTCCAGCGGTTTTAGCCCGGATTTTGCCACGGTTATTACCATGGATCGCAAAGCCAGCAAACAGCAGACCAACATTGATGTGATCTACGAACGTGTGCGTGATG
ATTATCAACTGCATTGGACCTCAACCAATTGGAAAGGCACCAATACCAAAGATAAATGGACGGATCGCAGTTCAGAACGCTACAAAATTGATTGGGAAAAAGAAG
AAATGACCAACTAATAGAACGCATGAGAAAGCCCCCGGAAGATCACCTTCCGGGGGCTTTTTTATTGCGCCTTGTCACACCTACACTGCTCGAAGtaCtactagtagc
ggccgctgcaggcttcctcgctcactgactcgctgcgctcggtcgttcggctgcggcgagcggtatcagctcactcaaaggcggtaat

pSB1A2-AD010, https://benchling.com/s/seq-k42mlMyPUOepkZctrNRg

araC, pBAD, α-HL, mScarletI

tgccacctgacgtctaagaaaccattattatcatgacattaacctataaaaatagGCGTATCACGAGGCAGAATTTCAGATAAAAAAAATCCTTAGCTTTCGCTAAGGATGATTTCTGGAATTCGCGGCCGCTTCTAGAGGAGAG
TTAGGCATAAGGCTGCATGCTACCCTTTGGTCGAAAAAAAAAGCCCGCACTGTCAGGTGCGGGCTTTTTTCTGTGTTTCCttatgacaacttgacggctacatcattcactttttcttc
acaaccggcacggaactcgctcgggctggccccggtgcatttttttaaatacccgcgagaaatagagttgatcgtcaaaaccaacattgcgaccgacggtggcgataggcatccgggtggtgctcaaaagcagcttcgcctg
gctgatacgttggtcctcgcgccagcttaagacgctaatccctaactgctggcggaaaagatgtgacagacgcgacggcgacaagcaaacatgctgtgcgacgctggcgatatcaaaattgctgtctgccaggtgatcgctg
atgtactgacaagcctcgcgtacccgattatccatcggtggatggagcgactcgttaatcgcttccatgcgccgcagtaacaattgctcaagcagatttatcgccagcagctccgaatagcgcccttccccttgcccggcgttaa
tgatttgcccaaacaggtcgctgaaatgcggctggtgcgcttcatccgggcgaaagaaccccgtattggcaaatattgacggccagttaagccattcatgccagtaggcgcgcggacgaaagtaaacccactggtgataccа
ttcgcgagcctccggatgacgaccgtagtgatgaatctctcctggcgggaacagcaaaatatcacccggtcggcaaacaaattctcgtccctgatttttcaccaccccctgaccgcgaatggtgagattgagaatataacctttc
attcccagcggtcggtcgataaaaaaatcgagataaccgttggcctcaatcggcgttaaacccgccaccagatgggcattaaacgagtatcccggcagcaggggatcattttgcgcttcagccatacttttcatactcccgccat
tcagagaagaaaccaattgtccatattgcatcagacattgccgtcactgcgtctttactggctcttctgctaaccaaacccggtaacccccgcttattaaagcattctgtaacaaagcgggaccaaagccatgacaaaaacgcgt
aacaaaagtgtctataatcacggcagaaaagtccacattgattatttgcacggcgtcacactttgctatgccatagcatttttatccataagattagcggatcctacctgacgcttttatcgcaactctctactgttctccatacccgttt
ttttgggctagcgaattcgagctcggtacccggggatcctctagaagggagatataaccCTATGGACTATGTTTTTCAAAGACGAAAAACTACTAGATGGATTCTGATATCAATATCAAAACCG
GCACCACCGATATCGGCTCCAATACCACCGTTAAAACCGGTGATCTGGTGACCTATGATAAAGAAAACGGTATGCATAAAAAAGTGTTTTACTCGTTTATTGACGA

TAAAAACCATAACAAAAAACTGCTGGTCATCCGCACCAAAGGCACCATTGCGGGTCAATACCGTGTGTACTCCGAAGAAGGTGCGAACAAAAGCGGTCTGGCTT
GGCCGTCTGCCTTTAAAGTGCAGCTGCAACTGCCGGATAATGAAGTGGCGCAGATTTCAGATTATTATCCGCGTAATAGCATCGATACCAAAGAATATATGAGTA
CCCTGACCTATGGTTTTAATGGCAATGTTACCGGTGATGATACGGGTAAAATTGGCGGTCTGATTGGCGCCAATGTGTCCATTGGTCATACGCTGAAATACGTGC
AACCGGATTTCAAAACCATTCTGGAAAGTCCGACCGATAAAAAAGTGGGTTGGAAAGTTATCTTCAACAACATGGGTGAATCAGAACTGGGGTCCGTACGATCGCG
ATTCCTGGAATCCGGTTTATGGCAATCAGCTGTTTATGAAAACCCGCAACGGTAGTATGAAAGCGGCGGATAATTTTCTGGACCCGAACAAAGCCTCAAGCCTGC
TGTCCAGCGGTTTTAGCCCGGATTTTGCCACGGTTATTACCATGGATCGCAAAGCCAGCAAACAGCAGACCAACATTGATGTGATCTACGAACGTGTGCGTGATG
ATTATCAACTGCATTGGACCTCAACCAATTGGAAAGGCACCAATACCAAAGATAAATGGACGGATCGCAGTTCAGAACGCTACAAAATTGATTGGGAAAAAGAAG
AAATGACCAACTAAAGCGCTCAACGGGTGTGCTTCCCGTTCTGATGAGTCCGTGAGGACGAAAGCGCCTCTACAAATAATTTTGTTTAAGGAgctatggactatgtttgaa
aggctgCTCGAGaaagaggagaaaatggtgtcaaagggagaggcGGTTATCAAGGAATTTATGCGCTTTAAAGTCCACATGGAGGGCAGCATGAACGGGCACGAGTTTGAAAT
TGAGGGGGAGGGGGAGGGCCGTCCTTATGAAGGTACTCAGACTGCTAAACTGAAGGTGACAAAAGGTGGCCCCTTGCCTTTCTCGTGGGACATCCTGTCGCCA
CAATTCATGTACGGGAGCCGCGCCTTTATCAAACATCCCGCAGATATTCCTGATTACTATAAACAATCTTTCCCGGAAGGTTTCAAATGGGAACGCGTCATGAATT
TTGAGGACGGGGGCGCTGTCACAGTTACTCAGGACACCTCCTTGGAAGACGGCACATTGATTTACAAGGTTAAGTTGCGCGGCACAAACTTCCCCCCTGACGG
GCCAGTAATGCAAAAGAAAACTATGGGTTGGGAGGCGTCTACAGAACGTTTATACCCCGAAGACGGGGTGCTGAAAGGTGACATTAAGATGGCCCTGCGCCTGA
AGGACGGCGGTCGCTATCTTGCCGACTTTAAAACTACTTATAAGGCTAAAAAACCAGTCCAGATGCCAGGCGCCTATAATGTTGACCGCAAGTTAGACATCACCT
CACATAATGAAGACTATACCGTTGTAGAACAATACGAGCGCAGCGAGGGTCGTCACAGTACCGgggggatggatgaattatacaaaTAAAAGCTTtagaacgcatgagaaagccc
CCGGAAGATCACCTTCCGGGGGCTTTTTTATTGCGCCTTGTCACACCTACACTGCTCGAAGtaCtactagtagcggccgctgcaggcttcctcgctcactgactcgctgcgctcggtcgttc
ggctgcggcgagcggtatcagctcactcaaaggcggtaat

pSB1A2-AD011, https://benchling.com/s/seq-rXZ5ZdhlErF5p7e3Uj0t

araC, pBAD, mScarletI

TGCCACCTGACGTCTAAGAAACCATTATTATCATGACATTAACCTATAAAAATAGGCGTATCACGAGGCAGAATTTCAGATAAAAAAAATCCTTAGCTTTCGCTAAG
GATGATTTCTGGAATTCGCGGCCGCTTCTAGAGGAGAGTTAGGCATAAGGCTGCATGCTACCCTTTGGTCGAAAAAAAAAGCCCGCACTGTCAGGTGCGGGCTT
TTTTCTGTGTTTCCTTATGACAACTTGACGGCTACATCATTCACTTTTTCTTCACAACCGGCACGGAACTCGCTCGGGCTGGCCCCGGTGCATTTTTTAAATACCC
GCGAGAAATAGAGTTGATCGTCAAAACCAACATTGCGACCGACGGTGGCGATAGGCATCCGGGTGGTGCTCAAAAGCAGCTTCGCCTGGCTGATACGTTGGTC
CTCGCGCCAGCTTAAGACGCTAATCCCTAACTGCTGGCGGAAAAGATGTGACAGACGCGACGGCGACAAGCAAACATGCTGTGCGACGCTGGCGATATCAAAA
TTGCTGTCTGCCAGGTGATCGCTGATGTACTGACAAGCCTCGCGTACCCGATTATCCATCGGTGGATGGAGCGACTCGTTAATCGCTTCCATGCGCCGCAGTAA
CAATTGCTCAAGCAGATTTATCGCCAGCAGCTCCGAATAGCGCCCTTCCCCTTGCCCGGCGTTAATGATTTGCCCAAACAGGTCGCTGAAATGCGGCTGGTGCG
CTTCATCCGGGCGAAAGAACCCCGTATTGGCAAATATTGACGGCCAGTTAAGCCATTCATGCCAGTAGGCGCGCGGACGAAAGTAAACCCACTGGTGATACCAT
TCGCGAGCCTCCGGATGACGACCGTAGTGATGAATCTCTCCTGGCGGGAACAGCAAAATATCACCCGGTCGGCAAACAAATTCTCGTCCCTGATTTTTCACCAC
CCCCTGACCGCGAATGGTGAGATTGAGAATATAACCTTTCATTCCCAGCGGTCGGTCGATAAAAAAATCGAGATAACCGTTGGCCTCAATCGGCGTTAAACCCG
CCACCAGATGGGCATTAAACGAGTATCCCGGCAGCAGGGGATCATTTTGCGCTTCAGCCATACTTTTCATACTCCCGCCATTCAGAGAAGAAACCAATTGTCCAT
ATTGCATCAGACATTGCCGTCACTGCGTCTTTTACTGGCTCTTCTCGCTAACCAAACCGGTAACCCCGCTTATTAAAAGCATTCTGTAACAAAGCGGGACCAAAG
CCATGACAAAAACGCGTAACAAAAGTGTCTATAATCACGGCAGAAAAGTCCACATTGATTATTTGCACGGCGTCACACTTTGCTATGCCATAGCATTTTTATCCATA
AGATTAGCGGATCCTACCTGACGCTTTTTATCGCAACTCTCTACTGTTTCTCCATACCCGTTTTTTTGGGCTAGCGAATTCGAGCTCGGTACCCGGGGATCCTCTA
GAAGGAGATATAACCAGCGCTCAACGGGTGTGCTTCCCGTTCTGATGAGTCCGTGAGGACGAAAGCGCCTCTACAAATAATTTTGTTTAAGGAGCTATGGACTAT
GTTTGAAAGGCTGCTCGAGAAAGAGGAGAAAATGGTGTCAAAGGGAGAGGCGGTTATCAAGGAATTTATGCGCTTTAAAGTCCACATGGAGGGCAGCATGAACG
GGCACGAGTTTGAAATTGAGGGGGAGGGGGAGGGCCGTCCTTATGAAGGTACTCAGACTGCTAAACTGAAGGTGACAAAAGGTGGCCCCTTGCCTTTCTCGTG
GGACATCCTGTCGCCACAATTCATGTACGGGAGCCGCGCCTTTATCAAACATCCCGCAGATATTCCTGATTACTATAAACAATCTTTCCCGGAAGGTTTCAAATGG
GAACGCGTCATGAATTTTGAGGACGGGGGCGCTGTCACAGTTACTCAGGACACCTCCTTGGAAGACGGCACATTGATTTACAAGGTTAAGTTGCGCGGCACAAA
CTTCCCCCCTGACGGGCCAGTAATGCAAAAGAAAACTATGGGTTGGGAGGCGTCTACAGAACGTTTATACCCCGAAGACGGGGTGCTGAAAGGTGACATTAAGA
TGGCCCTGCGCCTGAAGGACGGCGGTCGCTATCTTGCCGACTTTAAAACTACTTATAAGGCTAAAAAACCAGTCCAGATGCCAGGCGCCTATAATGTTGACCGC
AAGTTAGACATCACCTCACATAATGAAGACTATACCGTTGTAGAACAATACGAGCGCAGCGAGGGTCGTCACAGTACCGGGGGGATGGATGAATTATACAAATAA
AAGCTTTAGAACGCATGAGAAAGCCCCCGGAAGATCACCTTCCGGGGGCTTTTTTATTGCGCCTTGTCACACCTACACTGCTCGAAGTACTACTAGTAGCGGCC
GCTGCAGTCCGGCAAAAAAGGGCAAGGTGTCACCACCCTGCCCTTTTTCTTTAAAACCGAAAAGATTACTTCGCGTTATGCAGGCTTCCTCGCTCACTGACTCGC
TGCGCTCGGTCGTTCGGCTGCGGCGAGCGGTATCAGCTCACTCAAAGGCGGTAAT

pSB4A5-AD013, https://benchling.com/s/seq-IVaHN64wLjVoZif0a1gw

mutated T7 promoter P_{CTGA} (pT7-CTGA-R13), mScarletI, AAV degtag

tgccacctgacgtctaagaaaaggaatattcagcaatttgcccgtgccgaagaaaggcccacccgtgaaggtgaccagtgagttgattgctacgtaattagttagtagcccttagtgactcgaattcTAATACCTGACA
CTATAGGGTACTAGAGAAAGAGGAGAAAatggtgtcaaagggagaggcGGTTATCAAGGAATTTATGCGCTTTAAAGTCCACATGGAGGGCAGCATGAACGGGCACGAG
TTTGAAATTGAGGGGGAGGGGGAGGGCCGTCCTTATGAAGGTACTCAGACTGCTAAACTGAAGGTGACAAAAGGTGGCCCCTTGCCTTTCTCGTGGGACATCCT
GTCGCCACAATTCATGTACGGGAGCCGCGCCTTTATCAAACATCCCGCAGATATTCCTGATTACTATAAACAATCTTTCCCGGAAGGTTTCAAATGGGAACGCGT
CATGAATTTTGAGGACGGGGGCGCTGTCACAGTTACTCAGGACACCTCCTTGGAAGACGGCACATTGATTTACAAGGTTAAGTTGCGCGGCACAAACTTCCCCC
CTGACGGGCCAGTAATGCAAAAGAAAACTATGGGTTGGGAGGCGTCTACAGAACGTTTATACCCCGAAGACGGGGTGCTGAAAGGTGACATTAAGATGGCCCT
GCGCCTGAAGGACGGCGGTCGCTATCTTGCCGACTTTAAAACTACTTATAAGGCTAAAAAACCAGTCCAGATGCCAGGCGCCTATAATGTTGACCGCAAGTTAGA
CATCACCTCACATAATGAAGACTATACCGTTGTAGAACAATACGAGCGCAGCGAGGGTCGTCACAGTACCGGGGGGATGGATGAATTATACAAACGTCCTGCTG
CGAACGACGAAAATTATGCGGCTGCGGTTTGATAAGGAAACACAGAAAAAAGCCCGCACCTGACAGTGCGGGCTTTTTTTTTCGACCAAAGGTTAATTAAACCTA
TAGGATCGTATAGGTTTACGCAAGAAAATGGTTTGTTATAGTCGAATAAACCTAGGCCCCCCGAGGAGTAGCACATGATTGTGCAAATCGGCCGCCGTGAGGAGT
TCGATAAAAAGCTGCTTGGGGAAATGCATAAACTTCGTGCTCAGGTGTTCAAGGAGCGTAAGGGGTGGGATGTTTCCGTTATTGACGAAATGGAAATTGATGGGT
ACGATGCATTATCACCTTACTATATGCTGATTCAAGAAGACACACCTGAGGCCCAGGTATTCGGTTGCTGGCGCATTTTTGACACGACGGGGCCTTACATGTTGA
AGAACACGTTTCCTGAATTGTTACACGGCAAAGAAGCTCCCTGCTCACCCCATATTTGGGAACTGAGCCGTTTCGCTATCAATTCCGGTCAAAAGGGCTCCCTGG
GCTTTTCGGACTGCACCCTTGAAGCCATGCGCGCACTTGCCCGTTACTCCCTGCAAAACGACATTCAAACCTTAGTTACTGTTACTACCGTTGGCGTAGAGAAGA
TGATGATCCGTGCGGGTCTTGACGTATCTCGCTTTGGACCGCATCTGAAGATTGGAATCGAGCGTGCGGTGGCGTTGCGCATCGAATTGAACGCAAAAACGCAA
ATTGCGTTATACGGCGGGGTCTTGGTTGAACAGCGTTTAGCCGTGAGTTGATAATCCGGCAATTAAAAAAGCGGCTAACCACGCCGCTTTTTTTACGTCTGCActg
caggagtcactaagggttagttagttagattagcagaaagtcaaaagcctccgaccggaggcttttgactaaaacttcccttggggttatcattggggctcactcaaaggcggtaat

pSB4A5-AD014, https://benchling.com/s/seq-9yED5ruUKXn0wwNfeETC

mutated T7 promoter P_{T3} (pT7-T3-R5), mScarletI, AAV degtag

tgccacctgacgtctaagaaaaggaatattcagcaatttgcccgtgccgaagaaaggcccacccgtgaaggtgagccagtgagttgattgctacgtaattagttagtagcccttagtgactcgaattcTAATAACCCTCA
CTATAGGGTACTAGAGAAAGAGGAGAAAatggtgtcaaagggagaggcGGTTATCAAGGAATTTATGCGCTTTAAAGTCCACATGGAGGGCAGCATGAACGGGCACGAG
TTTGAAATTGAGGGGGAGGGGGAGGGCCGTCCTTATGAAGGTACTCAGACTGCTAAACTGAAGGTGACAAAAGGTGGCCCCTTGCCTTTCTCGTGGGACATCCT
GTCGCCACAATTCATGTACGGGAGCCGCGCCTTTATCAAACATCCCGCAGATATTCCTGATTACTATAAACAATCTTTCCCGGAAGGTTTCAAATGGGAACGCGT
CATGAATTTTGAGGACGGGGGCGCTGTCACAGTTACTCAGGACACCTCCTTGGAAGACGGCACATTGATTTACAAGGTTAAGTTGCGCGGCACAAACTTCCCCC
CTGACGGGCCAGTAATGCAAAAGAAAACTATGGGTTGGGAGGCGTCTACAGAACGTTTATACCCCGAAGACGGGGTGCTGAAAGGTGACATTAAGATGGCCCT
GCGCCTGAAGGACGGCGGTCGCTATCTTGCCGACTTTAAAACTACTTATAAGGCTAAAAAACCAGTCCAGATGCCAGGCGCCTATAATGTTGACCGCAAGTTAGA
CATCACCTCACATAATGAAGACTATACCGTTGTAGAACAATACGAGCGCAGCGAGGGTCGTCACAGTACCGGGGGGATGGATGAATTATACAAACGTCCTGCTG
CGAACGACGAAAATTATGCGGCTGCGGTTTGATAAGGAAACACAGAAAAAAGCCCGCACCTGACAGTGCGGGCTTTTTTTTTCGACCAAAGGTTAATTAAACCTA
TAGGATCGTATAGGTTTACGCAAGAAAATGGTTTGTTATAGTCGAATAAACCTAGGCCCCCCGAGGAGTAGCACATGATTGTGCAAATCGGCCGCCGTGAGGAGT
TCGATAAAAAGCTGCTTGGGGAAATGCATAAACTTCGTGCTCAGGTGTTCAAGGAGCGTAAGGGGTGGGATGTTTCCGTTATTGACGAAATGGAAATTGATGGGT
ACGATGCATTATCACCTTACTATATGCTGATTCAAGAAGACACACCTGAGGCCCAGGTATTCGGTTGCTGGCGCATTTTTGACACGACGGGGCCTTACATGTTGA
AGAACACGTTTCCTGAATTGTTACACGGCAAAGAAGCTCCCTGCTCACCCCATATTTGGGAACTGAGCCGTTTCGCTATCAATTCCGGTCAAAAGGGCTCCCTGG
GCTTTTCGGACTGCACCCTTGAAGCCATGCGCGCACTTGCCCGTTACTCCCTGCAAAACGACATTCAAACCTTAGTTACTGTTACTACCGTTGGCGTAGAGAAGA
TGATGATCCGTGCGGGTCTTGACGTATCTCGCTTTGGACCGCATCTGAAGATTGGAATCGAGCGTGCGGTGGCGTTGCGCATCGAATTGAACGCAAAAACGCAA
ATTGCGTTATACGGCGGGGTCTTGGTTGAACAGCGTTTAGCCGTGAGTTGATAATCCGGCAATTAAAAAAGCGGCTAACCACGCCGCTTTTTTTACGTCTGCActg
caggagtcactaagggttagttagttagattagcagaaagtcaaaagcctccgaccggaggcttttgactaaaacttcccttggggttatcattggggctcactcaaaggcggtaat

pSB4A5-AD015, https://benchling.com/s/seq-MmaF18QAvaiWRTlBti9n

mutated T7 promoter P_{K1F} (pT7-K1F-R5), mScarletI, AAV degtag

tgccacctgacgtctaagaaaaggaatattcagcaatttgcccgtgccgaagaaaggcccacccgtgaaggtgagccagtgagttgattgctacgtaattagttagttagccctagtgactcgaattcTAATAACTATCAC
TATAGGGTACTAGAGAAAGAGGAGAAAatggtgtcaaagggagaggcGGTTATCAAGGAATTTATGCGCTTTAAAGTCCACATGGAGGGCAGCATGAACGGGCACGAGT
TTGAAATTGAGGGGGAGGGGGAGGGGCCGTCCTTATGAAGGTACTCAGACTGCTAAACTGAAGGTGACAAAAGGTGGCCCCTTGCCTTTCTCGTGGGACATCCT
GTCGCCACAATTCATGTACGGGAGCCGCGCCTTTATCAAACATCCCGCAGATATTCCTGATTACTATAAACAATCTTTCCCGGAAGGTTTCAAATGGGAACGCGT
CATGAATTTTGAGGACGGGGGCGCTGTCACAGTTACTCAGGACACCTCCTTGGAAGACGGCACATTGATTTACAAGGTTAAGTTGCGCGGCACAAACTTCCCCC
CTGACGGGCCAGTAATGCAAAAGAAAACTATGGGTTGGGAGGCGTCTACAGAACGTTTATACCCCGAAGACGGGGTGCTGAAAGGTGACATTAAGATGGCCCT
GCGCCTGAAGGACGGCGGTCGCTATCTTGCCGACTTTAAAACTACTTATAAGGCTAAAAAACCAGTCCAGATGCCAGGCGCCTATAATGTTGACCGCAAGTTAGA
CATCACCTCACATAATGAAGACTATACCGTTGTAGAACAATACGAGCGCAGCGAGGGTCGTCACAGTACCGGGGGGGATGGATGAATTATACAAACGTCCTGCTG
CGAACGACGAAAATTATGCGGCTGCGGTTTGATAAGGAAACACAGAAAAAAGCCCGCACCTGACAGTGCGGGCTTTTTTTTTCGACCAAAGGTTAATTAAACCTA
TAGGATCGTATAGGTTTACGCAAGAAAATGGTTTGTTATAGTCGAATAAACCTAGGCCCCCCGAGGAGTAGCACATGATTGTGCAAATCGGCCGCCGTGAGGAGT
TCGATAAAAAGCTGCTTGGGGAAATGCATAAACTTCGTGCTCAGGTGTTCAAGGAGCGTAAGGGGTGGGATGTTTCCGTTATTGACGAAATGGAAATTGATGGGT
ACGATGCATTATCACCTTACTATATGCTGATTCAAGAAGACACACCTGAGGCCCAGGTATTCGGTTGCTGGCGCATTTTTGACACGACGGGGCCTTACATGTTGA
AGAACACGTTTCCTGAATTGTTACACGGCAAAGAAGCTCCCTGCTCACCCCATATTTGGGAACTGAGCCGTTTCGCTATCAATTCCGGTCAAAAGGGCTCCCTGG
GCTTTTCGGACTGCACCCTTGAAGCCATGCGCGCACTTGCCCGTTACTCCCTGCAAAACGACATTCAAACCTTAGTTACTGTTACTACCGTTGGCGTAGAGAAGA
TGATGATCCGTGCGGGTCTTGACGTATCTCGCTTTGGACCGCATCTGAAGATTGGAATCGAGCGTGCGGTGGCGTTGCGCATCGAATTGAACGCAAAAACGCAA
ATTGCGTTATACGGCGGGGTCTTGGTTGAACAGCGTTTAGCCGTGAGTTGATAATCCGGCAATTAAAAAAGCGGCTAACCACGCCGCTTTTTTTACGTCTGCActg
caggagtcactaagggttagttagttagattagcagaaagtcaaaagcctccgaccggaggcttttgactaaaacttccctggggttatcattggggctcactcaaaggcggtaat

pSB4A5-AD016, https://benchling.com/s/seq-jcaCkxOPuV12jElk2FJE
mutated T7 promoter P_{mut1}, mScarletI, AAV degtag

tgccacctgacgtctaagaaaaggaatattcagcaatttgcccgtgccgaagaaaggcccacccgtgaaggtgagccagtgagttgattgctacgtaattagttagttagccctagtgactcgaattcTAATACGTCTCA
CTATAGGGTACTAGAGAAAGAGGAGAAAatggtgtcaaagggagaggcGGTTATCAAGGAATTTATGCGCTTTAAAGTCCACATGGAGGGCAGCATGAACGGGCACGAG
TTTGAAATTGAGGGGGAGGGGGAGGGGCCGTCCTTATGAAGGTACTCAGACTGCTAAACTGAAGGTGACAAAAGGTGGCCCCTTGCCTTTCTCGTGGGACATCCT
GTCGCCACAATTCATGTACGGGAGCCGCGCCTTTATCAAACATCCCGCAGATATTCCTGATTACTATAAACAATCTTTCCCGGAAGGTTTCAAATGGGAACGCGT
CATGAATTTTGAGGACGGGGGCGCTGTCACAGTTACTCAGGACACCTCCTTGGAAGACGGCACATTGATTTACAAGGTTAAGTTGCGCGGCACAAACTTCCCCC
CTGACGGGCCAGTAATGCAAAAGAAAACTATGGGTTGGGAGGCGTCTACAGAACGTTTATACCCCGAAGACGGGGTGCTGAAAGGTGACATTAAGATGGCCCT
GCGCCTGAAGGACGGCGGTCGCTATCTTGCCGACTTTAAAACTACTTATAAGGCTAAAAAACCAGTCCAGATGCCAGGCGCCTATAATGTTGACCGCAAGTTAGA
CATCACCTCACATAATGAAGACTATACCGTTGTAGAACAATACGAGCGCAGCGAGGGTCGTCACAGTACCGGGGGGGATGGATGAATTATACAAACGTCCTGCTG
CGAACGACGAAAATTATGCGGCTGCGGTTTGATAAGGAAACACAGAAAAAAGCCCGCACCTGACAGTGCGGGCTTTTTTTTTCGACCAAAGGTTAATTAAACCTA
TAGGATCGTATAGGTTTACGCAAGAAAATGGTTTGTTATAGTCGAATAAACCTAGGCCCCCCGAGGAGTAGCACATGATTGTGCAAATCGGCCGCCGTGAGGAGT
TCGATAAAAAGCTGCTTGGGGAAATGCATAAACTTCGTGCTCAGGTGTTCAAGGAGCGTAAGGGGTGGGATGTTTCCGTTATTGACGAAATGGAAATTGATGGGT
ACGATGCATTATCACCTTACTATATGCTGATTCAAGAAGACACACCTGAGGCCCAGGTATTCGGTTGCTGGCGCATTTTTGACACGACGGGGCCTTACATGTTGA
AGAACACGTTTCCTGAATTGTTACACGGCAAAGAAGCTCCCTGCTCACCCCATATTTGGGAACTGAGCCGTTTCGCTATCAATTCCGGTCAAAAGGGCTCCCTGG
GCTTTTCGGACTGCACCCTTGAAGCCATGCGCGCACTTGCCCGTTACTCCCTGCAAAACGACATTCAAACCTTAGTTACTGTTACTACCGTTGGCGTAGAGAAGA
TGATGATCCGTGCGGGTCTTGACGTATCTCGCTTTGGACCGCATCTGAAGATTGGAATCGAGCGTGCGGTGGCGTTGCGCATCGAATTGAACGCAAAAACGCAA
ATTGCGTTATACGGCGGGGTCTTGGTTGAACAGCGTTTAGCCGTGAGTTGATAATCCGGCAATTAAAAAAGCGGCTAACCACGCCGCTTTTTTTACGTCTGCActg
caggagtcactaagggttagttagttagattagcagaaagtcaaaagcctccgaccggaggcttttgactaaaacttccctggggttatcattggggctcactcaaaggcggtaat

pSB4A5-AD017, https://benchling.com/s/seq-mUhLP9oYkdW3hrDzb2o4
mutated T7 promoter P_{mut2}, mScarletI, AAV degtag

tgccacctgacgtctaagaaaaggaatattcagcaatttgcccgtgccgaagaaaggcccacccgtgaaggtgagccagtgagttgattgctacgtaattagttagttagccctagtgactcgaattcTAATACGACTTA
CTATAGGGTACTAGAGAAAGAGGAGAAAatggtgtcaaagggagaggcGGTTATCAAGGAATTTATGCGCTTTAAAGTCCACATGGAGGGCAGCATGAACGGGCACGAG
TTTGAAATTGAGGGGGAGGGGGAGGGGCCGTCCTTATGAAGGTACTCAGACTGCTAAACTGAAGGTGACAAAAGGTGGCCCCTTGCCTTTCTCGTGGGACATCCT
GTCGCCACAATTCATGTACGGGAGCCGCGCCTTTATCAAACATCCCGCAGATATTCCTGATTACTATAAACAATCTTTCCCGGAAGGTTTCAAATGGGAACGCGT
CATGAATTTTGAGGACGGGGGCGCTGTCACAGTTACTCAGGACACCTCCTTGGAAGACGGCACATTGATTTACAAGGTTAAGTTGCGCGGCACAAACTTCCCCC
CTGACGGGCCAGTAATGCAAAAGAAAACTATGGGTTGGGAGGCGTCTACAGAACGTTTATACCCCGAAGACGGGGTGCTGAAAGGTGACATTAAGATGGCCCT
GCGCCTGAAGGACGGCGGTCGCTATCTTGCCGACTTTAAAACTACTTATAAGGCTAAAAAACCAGTCCAGATGCCAGGCGCCTATAATGTTGACCGCAAGTTAGA
CATCACCTCACATAATGAAGACTATACCGTTGTAGAACAATACGAGCGCAGCGAGGGTCGTCACAGTACCGGGGGGGATGGATGAATTATACAAACGTCCTGCTG
CGAACGACGAAAATTATGCGGCTGCGGTTTGATAAGGAAACACAGAAAAAAGCCCGCACCTGACAGTGCGGGCTTTTTTTTTCGACCAAAGGTTAATTAAACCTA
TAGGATCGTATAGGTTTACGCAAGAAAATGGTTTGTTATAGTCGAATAAACCTAGGCCCCCCGAGGAGTAGCACATGATTGTGCAAATCGGCCGCCGTGAGGAGT
TCGATAAAAAGCTGCTTGGGGAAATGCATAAACTTCGTGCTCAGGTGTTCAAGGAGCGTAAGGGGTGGGATGTTTCCGTTATTGACGAAATGGAAATTGATGGGT
ACGATGCATTATCACCTTACTATATGCTGATTCAAGAAGACACACCTGAGGCCCAGGTATTCGGTTGCTGGCGCATTTTTGACACGACGGGGCCTTACATGTTGA
AGAACACGTTTCCTGAATTGTTACACGGCAAAGAAGCTCCCTGCTCACCCCATATTTGGGAACTGAGCCGTTTCGCTATCAATTCCGGTCAAAAGGGCTCCCTGG
GCTTTTCGGACTGCACCCTTGAAGCCATGCGCGCACTTGCCCGTTACTCCCTGCAAAACGACATTCAAACCTTAGTTACTGTTACTACCGTTGGCGTAGAGAAGA
TGATGATCCGTGCGGGTCTTGACGTATCTCGCTTTGGACCGCATCTGAAGATTGGAATCGAGCGTGCGGTGGCGTTGCGCATCGAATTGAACGCAAAAACGCAA
ATTGCGTTATACGGCGGGGTCTTGGTTGAACAGCGTTTAGCCGTGAGTTGATAATCCGGCAATTAAAAAAGCGGCTAACCACGCCGCTTTTTTTACGTCTGCActg
caggagtcactaagggttagttagttagattagcagaaagtcaaaagcctccgaccggaggcttttgactaaaacttccctggggttatcattggggctcactcaaaggcggtaat

pSB4A5-AD018, https://benchling.com/s/seq-gyaQD5uoEht1LuS8uYYj
pLacO, LasR, AAV degtag, RBS N1, mScarletI, pLas81, LasI

tgccacctgacgtctaagaaaaggaatattcagcaatttgcccgtgccgaagaaaggcccacccgtgaaggtgagccagtgagttgattgctacgtaattagttagttagccctagtgactcgaattcAATTGTGAGCGG
ATAACAATTGACATTGTGAGCGGATAACAAGATACTGAGCACAAAGCTTAGGGTGTCTCAAGGTGCGTACCTTGACTGATGAGTCCGAAAGGACGAAACACCCCT
CTACAAATAATTTTGTTTAAGCGGCCGCACTATGTTTTTCAAAGACGAAAAACTACTAGATGGCCCTGGTAGACGGCTTCTTGGAATTAGAACGTTCTAGTGGCAA
GTTGGAGTGGTCGGCAATCTTGCAAAAAATGGCTTCTGACTTAGGCTTCTCCAAGATTCTGTTGGTTTGTTACCGAAGGATTCACAGGATTACGAAAACGCATTC
ATCGTCGGGAATTATCCAGCCGCGTGGCGCGAACACTACGATCGCGCTGGGTATGCGCGCGTTGATCCTACCGTGTCGCATTGCACTCAGTCTGTTCTTCCCAT
TTTTTGGGAACCCTCAATCTACCAGACCCGCAAGCAACATGAGTTCTTTGAGGAAGCCTCGGCCGCGGGGCTTGTGTATGGCCTTACGATGCCACTTCATGGTG
CCCGTGGGGAATTGGGAGCACTGTCGCTTTCAGTCGAAGCCGAAAACCGCGCTGAGGCCAACCGTTTTATTGAGAGCGTCCTTCCAACTTTATGGATGTTGAAG
GACTATGCCCTTCAATCTGGGGCTGGGTTGGCCTTTGAGCACCCTGTTTCTAAACCAGTAGTTCTTACTTCACGCGAGAAGGAAGTCTTGCAATGGTGTGCTATT
GGAAAGACCTCCTGGGAAATCAGCGTCATTTGCAACTGTTCGGAAGCAAATGTAAATTTTCATATGGGGAACATCCGTCGCAAATTTGGGGTGACGTCCGTCGT
GTCGCAGCCATCATGGCAGTCAATCTTGGTCTTATCACCTTACGTCCCGCTGCTAATGACGAGAACTATGCTGCGGCTGTCTGATAACTCGAGTTCAGCCAAAAA
ACTTAAGACCGCCGGTCTTGTCCACTACCTTGCAGTAATGCGGTGGACAGGATCGGCGGTTTTCTTTTCTCTCTCAATTAATTAAAATTGTGAGCGGATAACAATT
GACATTGTGAGCGGATAACAAGATACTGAGCACAATCCATAGCTGTCACCGGATGTGCTTTCCGGTCTGATGAGTCCGTGAGGACGAAACAGCGAGATCAGATA
ATTCTGACGTATCTAGATACGCTATGGACTATGTTTTCTGCTATGGACTATGTTTTCACACACGAGATGCCTCGATGGTGTCAAAGGGAGAGGCGGTTATCAAGGA
ATTTATGCGCTTTAAAGTCCACATGGAGGGCAGCATGAACGGGCACGAGTTTGAAATTGAGGGGGAGGGGGAGGGCCGTCCTTATGAAGGTACTCAGACTGCTA
AACTGAAGGTGACAAAAGGTGGCCCCTTGCCTTTCTCGTGGGACATCCTGTCGCCACAATTCATGTACGGGAGCCGCGCCTTTATCAAACATCCCGCAGATATT
CCTGATTACTATAAACAATCTTTCCCGGAAGGTTTCAAATGGGAACGCGTCATGAATTTTGAGGACGGGGGCGCTGTCACAGTTACTCAGGACACCTCCTTGGAA
GACGGCACATTGATTTACAAGGTTAAGTTGCGCGGCACAAACTTCCCCCCTGACGGGCCAGTAATGCAAAAGAAAACTATGGGTTGGGAGGCGTCTACAGAACG
TTTATACCCCGAAGACGGGGTGCTGAAAGGTGACATTAAGATGGCCCTGCGCCTGAAGGACGGCGGTCGCTATCTTGCCGACTTTAAAACTACTTATAAGGCTA
AAAAACCAGTCCAGATGCCAGGCGCCTATAATGTTGACCGCAAGTTAGACATCACCTCACATAATGAAGACTATACCGTTGTAGAACAATACGAGCGCAGCGAG
GGTCGTCACAGTACCGGGGGGATGGATGAATTATACAAACGTCCTGCTGCTGCGAACGACGAAAATTATGCGGCTGCGGTTTGATAAGGAAACACAGAAAAAAGCCC
GCACCTGACAGTGCGGGCTTTTTTTTTCGACCAAAGGTTAATTAAACCTATAGGATCGTATAGGTTTACGCAAGAAAATGGTTTGTTATAGTCGAATAAACCTAGGC
CCCCCGAGGAGTAGCACATGATTGTGCAAATCGGCCGCCGTGAGGAGTTCGATAAAAAGCTGCTTGGGGAAATGCATAAACTTCGTGCTCAGGTGTTCAAGGAG
CGTAAGGGGTGGGATGTTTCCGTTATTGACGAAATGGAAATTGATGGGTACGATGCATTATCACCTTACTATATGCTGATTCAAGAAGACACACCTGAGGCCCAG
GTATTCGGTTGCTGGCGCATTTTTGACACGACGGGGCCTTACATGTTGAAGAACACGTTTCCTGAATTGTTACACGGCAAAGAAGCTCCCTGCTCACCCCATATTT
GGGAACTGAGCCGTTTCGCTATCAATTCCGGTCAAAAGGGCTCCCTGGGCTTTTCGGACTGCACCCTTGAAGCCATGCGCGCACTTGCCCGTTACTCCCTGCAA
AACGACATTCAAACCTTAGTTACTGTTACTACCGTTGGCGTAGAGAAGATGATGATCCGTGCGGGTCTTGACGTATCTCGCTTTGGACCGCATCTGAAGATTGGA

ATCGAGCGTGCGGTGGCGTTGCGCATCGAATTGAACGCAAAAACGCAAATTGCGTTATACGGCGGGGTCTTGGTTGAACAGCGTTTAGCCGTGAGTTGATAATC
CGGCAATTAAAAAAGCGGCTAACCACGCCGCTTTTTTTACGTCTGCActgcaggagtcactaagggttagttagttagattagcagaaagtcaaaagcctccgaccggaggcttttgactaaaacttc
ccttggggttatcattggggctcactcaaaggcggtaat

pSB4A5-AD020, https://benchling.com/s/seq-12Q7wAlnhZ8SStOFLQpP

pLux76, LuxI

tgccacctgacgtctaagaaaaggaatattcagcaatttgcccgtgccgaagaaaggcccacccgtgaaggtgagccagtgagttgattgctacgtaattagttagttagcccttagtgactcgaattcCGACCAAAGGTT
AATTAAACCTGTAGGATCGTACAAGTTTACGCAAGAAAATGGTTTGTTATAGTCGAATAAACCTAGGCCCCCCGAGGAGTAGCACATGACAATTATGATTAAGAAG
AGCGATTTCTTAGCAATCCCCTCCGAGGAATATAAAGGCATCCTGTCTCTTCGCTACCAGGTGTTCAAACAGCGTCTGGAATGGGATTTAGTGGTTGAAAATAATT
TGGAATCCGACGAGTACGATAACAGCAACGCTGAGTATATTTATGCCTGCGACGATACAGAAAACGTCAGTGGATGCTGGCGCCTGCTGCCCACAACCGGTGAT
TATATGTTGAAGTCAGTATTCCCCGAGCTTCTGGGGCAGCAGTCGGCGCCCAAAGATCCTAACATCGTTGAATTGAGTCGTTTTGCTGTTGGCAAGAACTCCTCT
AAAATCAATAATTCCGCAAGTGAGATCACGATGAAACTGTTTGAAGCTATCTATAAGCATGCAGTAAGTCAAGGGATCACGGAGTACGTCACGGTCACGTCTACC
GCAATTGAACGCTTCTTGAAACGTATCAAAGTTCCCTGCCACCGCATCGGAGATAAGGAAATTCACGTACTGGGCGATACTAAGTCCGTGGTCCTTTCGATGCCA
ATCAACGAGCAATTCAAAAAAGCTGTCTTAAATTGTAATAATCCGGCAATTAAAAAAGCGGCTAACCACGCCGCTTTTTTTACGTCTGCActgcaggagtcactaagggttagtta
gttagattagcagaaagtcaaaagcctccgaccggaggcttttgactaaaacttccctggggttatcattggggctcactcaaaggcggtaat

pSB4A5-AD022, https://benchling.com/s/seq-6EgqsajDzBFw67w2mP4E

pLacO, LasR, AAV degtag, RBS B3, mScarletI, pLas81, LasI

tgccacctgacgtctaagaaaaggaatattcagcaatttgcccgtgccgaagaaaggcccacccgtgaaggtgagccagtgagttgattgctacgtaattagttagttagcccttagtgactcgaattcAATTGTGAGCGG
ATAACAATTGACATTGTGAGCGGATAACAAGATACTGAGCACAAAGCTTAGGGTGTCTCAAGGTGCGTACCTTGACTGATGAGTCCGAAAGGACGAAACACCCCT
CTACAAATAATTTTGTTTAAGCGGCCGCACTATGTTTTTCAAAGACGAAAAACTACTAGATGGCCCTGGTAGACGGCTTCTTGGAATTAGAACGTTCTAGTGGCAA
GTTGGAGTGGTCGGCAATCTTGCAAAAAATGGCTTCTGACTTAGGCTTCTCCAAGATTCTGTTTGGTTTGTTACCGAAGGATTCACAGGATTACGAAAACGCATTC
ATCGTCGGGAATTATCCAGCCGCGTGGCGCGAACACTACGATCGCGCTGGGTATGCGCGCGTTGATCCTACCGTGTCGCATTGCACTCAGTCTGTTCTTCCCAT
TTTTTGGGAACCCTCAATCTACCAGACCCGCAAGCAACATGAGTTCTTTGAGGAAGCCTCGGCCGCGGGGCTTGTGTATGGCCTTACGATGCCACTTCATGGTG
CCCGTGGGGAATTGGGAGCACTGTCGCTTTCAGTCGAAGCCGAAAACCGCGCTGAGGCCAACCGTTTTATTGAGAGCGTCCTTCCAACTTTATGGATGTTGAAG
GACTATGCCCTTCAATCTGGGGCTGGGTTGGCCTTTGAGCACCCTGTTTCTAAACCAGTAGTTCTTACTTCACGCGAGAAGGAAGTCTTGCAATGGTGTGCTATT
GGAAAGACCTCCTGGGAAATCAGCGTCATTTGCAACTGTTCGGAAGCAAATGTAAATTTTCATATGGGGAACATCCGTCGCAAATTTGGGGTGACGTCCGTCGT
GTCGCAGCCATCATGGCAGTCAATCTTGGTCTTATCACCTTACGTCCCGCTGCTAATGACGAGAACTATGCTGCGGCTGTCTGATAACTCGAGTTCAGCCAAAAA
ACTTAAGACCGCCGGTCTTGTCCACTACCTTGCAGTAATGCGGTGGACAGGATCGGCGGTTTCTTTTCTCTTCTCAATTAATTAAAATTGTGAGCGGATAACAATT
GACATTGTGAGCGGATAACAAGATACTGAGCACAATCCATAGCTGTCACCGGATGTGCTTTCCGGTCTGATGAGTCCGTGAGGACGAAACAGCGAGATCAGATA
ATTCTGACGTATCTAGAccaaacgaggccgggaggATGGTGTCAAAGGGAGAGGCGGTTATCAAGGAATTTATGCGCTTTAAAGTCCACATGGAGGGCAGCATGAACG
GGCACGAGTTTGAAATTGAGGGGAGGGGGAGGGCCGTCCTTATGAAGGTACTCAGACTGCTAAACTGAAGGTGACAAAAGGTGGCCCCTTGCCTTTCTCGTG
GGACATCCTGTCGCCACAATTCATGTACGGGAGCCGCGCCTTTATCAAACATCCCGCAGATATTCCTGATTACTATAAACAATCTTTCCCGGAAGGTTTCAAATGG
GAACGCGTCATGAATTTTGAGGACGGGGGCGCTGTCACAGTTACTCAGGACACCTCCTTGGAAGACGGCACATTGATTTACAAGGTTAAGTTGCGCGGCACAAA
CTTCCCCCCCTGACGGGCCAGTAATGCAAAAGAAAACTATGGGTTGGGAGGCGTCTACAGAACGTTTATACCCCGAAGACGGGGTGCTGAAAGGTGACATTAAGA
TGGCCCTGCGCCTGAAGGACGGCGGTCGCTATCTTGCCGACTTTAAAACTACTTATAAGGCTAAAAAACCAGTCCAGATGCCAGGCGCCTATAATGTTGACCGC
AAGTTAGACATCACCTCACATAATGAAGACTATACCGTTGTAGAACAATACGAGCGCAGCGAGGGTCGTCACAGTACCGGGGGGATGGATGAATTATACAAACGT
CCTGCTGCGAACGACGAAAATTATGCGGCTGCGGTTTGATAAGGAAACACAGAAAAAAGCCCGCACCTGACAGTGCGGGCTTTTTTTTCGACCAAAGGTTAATT
AAACCTATAGGATCGTATAGGTTTACGCAAGAAAATGGTTTGTTATAGTCGAATAAACCTAGGCCCCCCGAGGAGTAGCACATGATTGTGCAAATCGGCCGCCGT
GAGGAGTTCGATAAAAAGCTGCTTGGGGAAATGCATAAACTTCGTGCTCAGGTGTTCAAGGAGCGTAAGGGGTGGGATGTTTCCGTTATTGACGAAATGGAAATT
GATGGGTACGATGCATTATCACCTTACTATATGCTGATTCAAGAAGACACACCTGAGGCCCAGGTATTCGGTTGCTGGCGCATTTTGACACGACGGGGCCTTAC
ATGTTGAAGAACACGTTTCCTGAATTGTTACACGGCAAAGAAGCTCCCTGCTCACCCCATATTTGGGAACTGAGCCGTTTCGCTATCAATTCCGGTCAAAAGGGC
TCCCTGGGCTTTTCGGACTGCACCCTTGAAGCCATGCGCGCACTTGCCCGTTACTCCCTGCAAAACGACATTCAAACCTTAGTTACTGTTACTACCGTTGGCGTA
GAGAAGATGATGATCCGTGCGGGTCTTGACGTATCTCGCTTTGGACCGCATCTGAAGATTGGAATCGAGCGTGCGGTGGCGTTGCGCATCGAATTGAACGCAAA
AACGCAAATTGCGTTATACGGCGGGGTCTTGGTTGAACAGCGTTTAGCCGTGAGTTGATAATCCGGCAATTAAAAAAGCGGCTAACCACGCCGCTTTTTTTACGT
CTGCActgcaggagtcactaagggttagttagttagattagcagaaagtcaaaagcctccgaccggaggcttttgactaaaacttccctggggttatcattggggctcactcaaaggcggtaat

pSB4A5-AD023, https://benchling.com/s/seq-exnDXykmZP8de5k7dgF3

pLacO, LasR, AAV degtag, RBS B3, mScarletI, pLas81, LasI

tgccacctgacgtctaagaaaaggaatattcagcaatttgcccgtgccgaagaaaggcccacccgtgaaggtgagccagtgagttgattgctacgtaattagttagttagcccttagtgactcgaattcAATTGTGAGCGG
ATAACAATTGACATTGTGAGCGGATAACAAGATACTGAGCACAAAGCTTAGGGTGTCTCAAGGTGCGTACCTTGACTGATGAGTCCGAAAGGACGAAACACCCCT
CTACAAATAATTTTGTTTAAGCGGCCGCACTATGTTTTTCAAAGACGAAAAACTACTAGATGGCCCTGGTAGACGGCTTCTTGGAATTAGAACGTTCTAGTGGCAA
GTTGGAGTGGTCGGCAATCTTGCAAAAAATGGCTTCTGACTTAGGCTTCTCCAAGATTCTGTTTGGTTTGTTACCGAAGGATTCACAGGATTACGAAAACGCATTC
ATCGTCGGGAATTATCCAGCCGCGTGGCGCGAACACTACGATCGCGCTGGGTATGCGCGCGTTGATCCTACCGTGTCGCATTGCACTCAGTCTGTTCTTCCCAT
TTTTTGGGAACCCTCAATCTACCAGACCCGCAAGCAACATGAGTTCTTTGAGGAAGCCTCGGCCGCGGGGCTTGTGTATGGCCTTACGATGCCACTTCATGGTG
CCCGTGGGGAATTGGGAGCACTGTCGCTTTCAGTCGAAGCCGAAAACCGCGCTGAGGCCAACCGTTTTATTGAGAGCGTCCTTCCAACTTTATGGATGTTGAAG
GACTATGCCCTTCAATCTGGGGCTGGGTTGGCCTTTGAGCACCCTGTTTCTAAACCAGTAGTTCTTACTTCACGCGAGAAGGAAGTCTTGCAATGGTGTGCTATT
GGAAAGACCTCCTGGGAAATCAGCGTCATTTGCAACTGTTCGGAAGCAAATGTAAATTTTCATATGGGGAACATCCGTCGCAAATTTGGGGTGACGTCCGTCGT
GTCGCAGCCATCATGGCAGTCAATCTTGGTCTTATCACCTTACGTCCCGCTGCTAATGACGAGAACTATGCTGCGGCTGTCTGATAACTCGAGAGCTGTCACCG
GATGTGCTTTCCGGTCTGATGAGTCCGTGAGGACGAAACAGCGAGATCAGATAATTCTGACGTATCTAGAccaaacgaggccgggaggATGGTGTCAAAGGGAGAGGC
GGTTATCAAGGAATTTATGCGCTTTAAAGTCCACATGGAGGGCAGCATGAACGGGCACGAGTTTGAAATTGAGGGGAGGGGGAGGGCCGTCCTTATGAAGGTA
CTCAGACTGCTAAACTGAAGGTGACAAAAGGTGGCCCCTTGCCTTTCTCGTGGGACATCCTGTCGCCACAATTCATGTACGGGAGCCGCGCCTTTATCAAACAT
CCCGCAGATATTCCTGATTACTATAAACAATCTTTCCCGGAAGGTTTCAAATGGGAACGCGTCATGAATTTTGAGGACGGGGGCGCTGTCACAGTTACTCAGGAC
ACCTCCTTGGAAGACGGCACATTGATTTACAAGGTTAAGTTGCGCGGCACAAACTTCCCCCCTGACGGGCCAGTAATGCAAAAGAAAACTATGGGTTGGGAGGC
GTCTACAGAACGTTTATACCCCGAAGACGGGGTGCTGAAAGGTGACATTAAGATGGCCCTGCGCCTGAAGGACGGCGGTCGCTATCTTGCCGACTTTAAAACTA
CTTATAAGGCTAAAAAACCAGTCCAGATGCCAGGCGCCTATAATGTTGACCGCAAGTTAGACATCACCTCACATAATGAAGACTATACCGTTGTAGAACAATACGA
GCGCAGCGAGGGTCGTCACAGTACCGGGGGGATGGATGAATTATACAAACGTCCTGCTGCGAACGACGAAAATTATGCGGCTGCGGTTTGATAAGGAAACACA
GAAAAAAGCCCGCACCTGACAGTGCGGGCTTTTTTTTTCGACCAAAGGTTAATTAAACCTATAGGATCGTATAGGTTTACGCAAGAAAATGGTTTGTTATAGTCGAA
TAAACCTAGGCCCCCCGAGGAGTAGCACATGATTGTGCAAATCGGCCGCCGTGAGGAGTTCGATAAAAAGCTGCTTGGGGAAATGCATAAACTTCGTGCTCAGG
TGTTCAAGGAGCGTAAGGGGTGGGATGTTTCCGTTATTGACGAAATGGAAATTGATGGGTACGATGCATTATCACCTTACTATATGCTGATTCAAGAAGACACACC
TGAGGCCCAGGTATTCGGTTGCTGGCGCATTTTTGACACGACGGGGCCTTACATGTTGAAGAACACGTTTCCTGAATTGTTACACGGCAAAGAAGCTCCCTGCTC
ACCCCATATTTGGGAACTGAGCCGTTTCGCTATCAATTCCGGTCAAAAGGGCTCCCTGGGCTTTTCGGACTGCACCCTTGAAGCCATGCGCGCACTTGCCCGTT
ACTCCCTGCAAAACGACATTCAAACCTTAGTTACTGTTACTACCGTTGGCGTAGAGAAGATGATGATCCGTGCGGGTCTTGACGTATCTCGCTTTGGACCGCATC
TGAAGATTGGAATCGAGCGTGCGGTGGCGTTGCGCATCGAATTGAACGCAAAAACGCAAATTGCGTTATACGGCGGGGTCTTGGTTGAACAGCGTTTAGCCGTG
AGTTGATAATCCGGCAATTAAAAAAGCGGCTAACCACGCCGCTTTTTTTACGTCTGCActgcaggagtcactaagggttagttagttagattagcagaaagtcaaaagcctccgaccggaggc
ttttgactaaaacttccctggggttatcattggggctcactcaaaggcggtaat

pSB4A5-AD024, https://benchling.com/s/seq-ldf6mmUJQB7D5sLEzd8I

pLacO, LasR, AAV degtag, pLas81, RBS B3, mScarletI, LasI

tgccacctgacgtctaagaaaaggaatattcagcaatttgcccgtgccgaagaaaggcccacccgtgaaggtgagccagtgagttgattgctacgtaattagttagttagcccttagtgactcgaattcAATTGTGAGCGG
ATAACAATTGACATTGTGAGCGGATAACAAGATACTGAGCACAAAGCTTAGGGTGTCTCAAGGTGCGTACCTTGACTGATGAGTCCGAAAGGACGAAACACCCCT
CTACAAATAATTTTGTTTAAGCGGCCGCACTATGTTTTTCAAAGACGAAAAACTACTAGATGGCCCTGGTAGACGGCTTCTTGGAATTAGAACGTTCTAGTGGCAA
GTTGGAGTGGTCGGCAATCTTGCAAAAAATGGCTTCTGACTTAGGCTTCTCCAAGATTCTGTTTGGTTTGTTACCGAAGGATTCACAGGATTACGAAAACGCATTC
ATCGTCGGGAATTATCCAGCCGCGTGGCGCGAACACTACGATCGCGCTGGGTATGCGCGCGTTGATCCTACCGTGTCGCATTGCACTCAGTCTGTTCTTCCCAT
TTTTTGGGAACCCTCAATCTACCAGACCCGCAAGCAACATGAGTTCTTTGAGGAAGCCTCGGCCGCGGGGCTTGTGTATGGCCTTACGATGCCACTTCATGGTG
CCCGTGGGGAATTGGGAGCACTGTCGCTTTCAGTCGAAGCCGAAAACCGCGCTGAGGCCAACCGTTTTATTGAGAGCGTCCTTCCAACTTTATGGATGTTGAAG
GACTATGCCCTTCAATCTGGGGCTGGGTTGGCCTTTGAGCACCCTGTTTCTAAACCAGTAGTTCTTACTTCACGCGAGAAGGAAGTCTTGCAATGGTGTGCTATT
GGAAAGACCTCCTGGGAAATCAGCGTCATTTGCAACTGTTCGGAAGCAAATGTAAATTTTCATATGGGGAACATCCGTCGCAAATTTGGGGTGACGTCCGTCGT
GTCGCAGCCATCATGGCAGTCAATCTTGGTCTTATCACCTTACGTCCCGCTGCTAATGACGAGAACTATGCTGCGGCTGTCTGATAACTCGAGAGCTGTCACCG
GATGTGCTTTCCGGTCTGATGAGTCCGTGAGGACGAAACAGCGAGATCAGATAATTCTGACGTATCTAGAccaaacgaggccgggaggATGGTGTCAAAGGGAGAGGC
GGTTATCAAGGAATTTATGCGCTTTAAAGTCCACATGGAGGGCAGCATGAACGGGCACGAGTTTGAAATTGAGGGGAGGGGGAGGGCCGTCCTTATGAAGGTA
CTCAGACTGCTAAACTGAAGGTGACAAAAGGTGGCCCCTTGCCTTTCTCGTGGGACATCCTGTCGCCACAATTCATGTACGGGAGCCGCGCCTTTATCAAACAT
CCCGCAGATATTCCTGATTACTATAAACAATCTTTCCCGGAAGGTTTCAAATGGGAACGCGTCATGAATTTTGAGGACGGGGGCGCTGTCACAGTTACTCAGGAC
ACCTCCTTGGAAGACGGCACATTGATTTACAAGGTTAAGTTGCGCGGCACAAACTTCCCCCCTGACGGGCCAGTAATGCAAAAGAAAACTATGGGTTGGGAGGC
GTCTACAGAACGTTTATACCCCGAAGACGGGGTGCTGAAAGGTGACATTAAGATGGCCCTGCGCCTGAAGGACGGCGGTCGCTATCTTGCCGACTTTAAAACTA
CTTATAAGGCTAAAAAACCAGTCCAGATGCCAGGCGCCTATAATGTTGACCGCAAGTTAGACATCACCTCACATAATGAAGACTATACCGTTGTAGAACAATACGA
GCGCAGCGAGGGTCGTCACAGTACCGGGGGGATGGATGAATTATACAAACGTCCTGCTGCGAACGACGAAAATTATGCGGCTGCGGTTTGATAAGGAAACACA
GAAAAAAGCCCGCACCTGACAGTGCGGGCTTTTTTTTTCGACCAAAGGTTAATTAAACCTATAGGATCGTATAGGTTTACGCAAGAAAATGGTTTGTTATAGTCGAA
TAAACCTAGGCCCCCCGAGGAGTAGCACATGATTGTGCAAATCGGCCGCCGTGAGGAGTTCGATAAAAAGCTGCTTGGGGAAATGCATAAACTTCGTGCTCAGG
TGTTCAAGGAGCGTAAGGGGTGGGATGTTTCCGTTATTGACGAAATGGAAATTGATGGGTACGATGCATTATCACCTTACTATATGCTGATTCAAGAAGACACACC
TGAGGCCCAGGTATTCGGTTGCTGGCGCATTTTTGACACGACGGGGCCTTACATGTTGAAGAACACGTTTCCTGAATTGTTACACGGCAAAGAAGCTCCCTGCTC
ACCCCATATTTGGGAACTGAGCCGTTTCGCTATCAATTCCGGTCAAAAGGGCTCCCTGGGCTTTTCGGACTGCACCCTTGAAGCCATGCGCGCACTTGCCCGTT
ACTCCCTGCAAAACGACATTCAAACCTTAGTTACTGTTACTACCGTTGGCGTAGAGAAGATGATGATCCGTGCGGGTCTTGACGTATCTCGCTTTGGACCGCATC
TGAAGATTGGAATCGAGCGTGCGGTGGCGTTGCGCATCGAATTGAACGCAAAAACGCAAATTGCGTTATACGGCGGGGTCTTGGTTGAACAGCGTTTAGCCGTG
AGTTGATAATCCGGCAATTAAAAAAGCGGCTAACCACGCCGCTTTTTTTACGTCTGCActgcaggagtcactaagggttagttagttagattagcagaaagtcaaaagcctccgaccggaggc
ttttgactaaaacttccctggggttatcattggggctcactcaaaggcggtaat

GACTATGCCCTTCAATCTGGGGCTGGGTTGGCCTTTGAGCACCCTGTTTCTAAACCAGTAGTTCTTACTTCACGCGAGAAGGAAGTCTTGCAATGGTGTGCTATT
GGAAAGACCTCCTGGGAAATCAGCGTCATTTGCAACTGTTCGGAAGCAAATGTAAATTTTCATATGGGGAACATCCGTCGCAAATTTGGGGTGACGTCCCGTCGT
GTCGCAGCCATCATGGCAGTCAATCTTGGTCTTATCACCTTACGTCCCGCTGCTAATGACGAGAACTATGCTGCGGCTGTCTGATAACTCGAGTTCAGCCAAAAA
ACTTAAGACCGCCGGTCTTGTCCACTACCTTGCAGTAATGCGGTGGACAGGATCGGCGGTTTTCTTTTCTCTTCTCAATTAATTAAACCTATAGGATCGTATAGGTT
TACGCAAGAAAATGGTTTGTTATAGTCGAATAAAATCCATAGCTGTCACCGGATGTGCTTTCCGGTCTGATGAGTCCGTGAGGACGAAACAGCGAGATCAGATAA
TTCTGACGTATCTAGAccaaacgaggccgggaggATGGTGTCAAAGGGAGAGGCGGTTATCAAGGAATTTATGCGCTTTAAAGTCCACATGGAGGGCAGCATGAACGG
GCACGAGTTTGAAATTGAGGGGGAGGGGGAGGGCCGTCCTTATGAAGGTACTCAGACTGCTAAACTGAAGGTGACAAAAGGTGGCCCCTTGCCTTTCTCGTGC
GACATCCTGTCGCCACAATTCATGTACGGGAGCCGCGCCTTTATCAAACATCCCGCAGATATTCCTGATTACTATAAACAATCTTTCCCGGAAGGTTTCAAATGGG
AACGCGTCATGAATTTTGAGGACGGGGGCGCTGTCACAGTTACTCAGGACACCTCCTTGGAAGACGGCACATTGATTTACAAGGTTAAGTTGCGCGGCACAAAC
TTCCCCCCTGACGGGCCAGTAATGCAAAAGAAAACTATGGGTTGGGAGGCGTCTACAGAACGTTTATACCCCGAAGACGGGGTGCTGAAAGGTGACATTAAGAT
GGCCCTGCGCCTGAAGGACGGCGGTCGCTATCTTGCCGACTTTAAAACTACTTATAAGGCTAAAAAACCAGTCCAGATGCCAGGCGCCTATAATGTTGACCGCA
AGTTAGACATCACCTCACATAATGAAGACTATACCGTTGTAGAACAATACGAGGGCAGCGAGGGTCGTCACAGTACCGGGGGGGATGGATGAATTATACAAACGT
CCTGCTGCGAACGACGAAAATTATGCGGCTGCGGTTTGATAAGGAAACACAGAAAAAAGCCCGCACCTGACAGTGCGGGCTTTTTTTTTCGACCAAAGGTTAATT
AAACCTATAGGATCGTATAGGTTTACGCAAGAAAATGGTTTGTTATAGTCGAATAAACCTAGGCCCCCCGAGGAGTAGCACATGATTGTGCAAATCGGCCGCCGT
GAGGAGTTCGATAAAAAGCTGCTTGGGGAAATGCATAAACTTCGTGCTCAGGTGTTCAAGGAGCGTAAGGGGTGGGATGTTTCCGTTATTGACGAAATGGAAATT
GATGGGTACGATGCATTATCACCTTACTATATGCTGATTCAAGAAGACACACCTGAGGCCCAGGTATTCGGTTGCTGGCGCATTTTTGACACGACGGGGCCTTAC
ATGTTGAAGAACACGTTTCCTGAATTGTTACACGGCAAAGAAGCTCCCTGCTCACCCCATATTTGGGAACTGAGCCGTTTCGCTATCAATTCCGGTCAAAAGGGC
TCCCTGGGCTTTTCGGACTGCACCCTTGAAGCCATGCGCGCACTTGCCCGTTACTCCCTGCAAAACGACATTCAAACCTTAGTTACTGTTACTACCGTTGGCGTA
GAGAAGATGATGATCCGTGCGGGTCTTGACGTATCTCGCTTTGGACCGCATCTGAAGATTGGAATCGAGCGTGCGGTGGCGTTGCGCATCGAATTGAACGCAAA
AACGCAAATTGCGTTATACGGCGGGGGTCTTGGTTGAACAGCGTTTAGCCGTGAGTTGATAATCCGGCAATTAAAAAAGCGGCTAACCACGCCGCTTTTTTTACGT
CTGCActgcaggagtcactaagggttagttagttagattagcagaaagtcaaaagcctccgaccggaggcttttgactaaaacttccttggggttatcattggggctcactcaaaggcggtaat

pSB4A5-AD025, https://benchling.com/s/seq-rbhjUuWxF366ndyE8Zmz

pLacO, LasR, AAV degtag, pLas81, RBS B3, mScarletI

tgccacctgacgtctaagaaaaggaatattcagcaatttgcccgtgccgaagaaaggcccaccccgtgaaggtgagccagtgagttgattgctacgtaattagttagttagccccttagtgactcgaattcAATTGTGAGCGG
ATAACAATTGACATTGTGAGCGGATAACAAGATACTGAGCACAAAGCTTAGGGTGTCTCAAGGTGCGTACCTTGACTGATGAGTCCGAAAGGACGAAACACCCCT
CTACAAATAATTTTGTTTAAGCGGCCGCACTATGTTTTTCAAAGACGAAAAACTACTAGATGGCCCTGGTAGACGGCTTCTTGGAATTAGAACGTTCTAGTGGCAA
GTTGGAGTGGTCGGCAATCTTGCAAAAAATGGCTTCTGACTTAGGCTTCTCCAAGATTCTGTTTGGTTTGTTACCGAAGGATTCACAGGATTACGAAAACGCATTC
ATCGTCGGGAATTATCCAGCCGCGTGGCGCGAACACTACGATCGCGCTGGGTATGCGCGCGTTGATCCTACCGTGTCGCATTGCACTCAGTCTGTTCTTCCCAT
TTTTTGGGAACCCTCAATCTACCAGACCCGCAAGCAACATGAGTTCTTTGAGGAAGCCTCGGCCGCGGGGCTTGTGTATGGCCTTACGATGCCACTTCATGGTG
CCCGTGGGGAATTGGGAGCACTGTCGCTTTCAGTCGAAGCCGAAAACCGCGCTGAGGCCAACCGTTTTATTGAGAGCGTCCTTCCAACTTTATGGATGTTGAAG
GACTATGCCCTTCAATCTGGGGCTGGGTTGGCCTTTGAGCACCCTGTTTCTAAACCAGTAGTTCTTACTTCACGCGAGAAGGAAGTCTTGCAATGGTGTGCTATT
GGAAAGACCTCCTGGGAAATCAGCGTCATTTGCAACTGTTCGGAAGCAAATGTAAATTTTCATATGGGGAACATCCGTCGCAAATTTGGGGTGACGTCCCGTCGT
GTCGCAGCCATCATGGCAGTCAATCTTGGTCTTATCACCTTACGTCCCGCTGCTAATGACGAGAACTATGCTGCGGCTGTCTGATAACTCGAGTTCAGCCAAAAA
ACTTAAGACCGCCGGTCTTGTCCACTACCTTGCAGTAATGCGGTGGACAGGATCGGCGGTTTTCTTTTCTCTTCTCAATTAATTAAACCTATAGGATCGTATAGGTT
TACGCAAGAAAATGGTTTGTTATAGTCGAATAAAATCCATAGCTGTCACCGGATGTGCTTTCCGGTCTGATGAGTCCGTGAGGACGAAACAGCGAGATCAGATAA
TTCTGACGTATCTAGAccaaacgaggccgggaggATGGTGTCAAAGGGAGAGGCGGTTATCAAGGAATTTATGCGCTTTAAAGTCCACATGGAGGGCAGCATGAACGG
GCACGAGTTTGAAATTGAGGGGGAGGGGGAGGGCCGTCCTTATGAAGGTACTCAGACTGCTAAACTGAAGGTGACAAAAGGTGGCCCCTTGCCTTTCTCGTGC
GACATCCTGTCGCCACAATTCATGTACGGGAGCCGCGCCTTTATCAAACATCCCGCAGATATTCCTGATTACTATAAACAATCTTTCCCGGAAGGTTTCAAATGGG
AACGCGTCATGAATTTTGAGGACGGGGGCGCTGTCACAGTTACTCAGGACACCTCCTTGGAAGACGGCACATTGATTTACAAGGTTAAGTTGCGCGGCACAAAC
TTCCCCCCTGACGGGCCAGTAATGCAAAAGAAAACTATGGGTTGGGAGGCGTCTACAGAACGTTTATACCCCGAAGACGGGGTGCTGAAAGGTGACATTAAGAT
GGCCCTGCGCCTGAAGGACGGCGGTCGCTATCTTGCCGACTTTAAAACTACTTATAAGGCTAAAAAACCAGTCCAGATGCCAGGCGCCTATAATGTTGACCGCA
AGTTAGACATCACCTCACATAATGAAGACTATACCGTTGTAGAACAATACGAGCGCAGCGAGGGTCGTCACAGTACCGGGGGGATGGATGAATTATACAAACGT
CCTGCTGCGAACGACGAAAATTATGCGGCTGCGGTTTGATAAGGAAACACAGAAAAAAGCCCGCACCTGACAGTGCGGGCTTTTTTTTTCGACCAAAGGTTAATT
AAACCctgcaggagtcactaagggttagttagttagattagcagaaagtcaaaagcctccgaccggaggcttttgactaaaacttccttggggttatcattggggctcactcaaaggcggtaat

pSB4A5-AD026, https://benchling.com/s/seq-e9epefwFIA4MkN6Xhp5Q

pLacO, LasR, AAV degtag, RBS P1, mScarletI, pLas81, LasI

tgccacctgacgtctaagaaaaggaatattcagcaatttgcccgtgccgaagaaaggcccaccccgtgaaggtgagccagtgagttgattgctacgtaattagttagttagccccttagtgactcgaattcAATTGTGAGCGG
ATAACAATTGACATTGTGAGCGGATAACAAGATACTGAGCACAAAGCTTAGGGTGTCTCAAGGTGCGTACCTTGACTGATGAGTCCGAAAGGACGAAACACCCCT
CTACAAATAATTTTGTTTAAGCGGCCGCACTATGTTTTTCAAAGACGAAAAACTACTAGATGGCCCTGGTAGACGGCTTCTTGGAATTAGAACGTTCTAGTGGCAA
GTTGGAGTGGTCGGCAATCTTGCAAAAAATGGCTTCTGACTTAGGCTTCTCCAAGATTCTGTTTGGTTTGTTACCGAAGGATTCACAGGATTACGAAAACGCATTC
ATCGTCGGGAATTATCCAGCCGCGTGGCGCGAACACTACGATCGCGCTGGGTATGCGCGCGTTGATCCTACCGTGTCGCATTGCACTCAGTCTGTTCTTCCCAT
TTTTTGGGAACCCTCAATCTACCAGACCCGCAAGCAACATGAGTTCTTTGAGGAAGCCTCGGCCGCGGGGCTTGTGTATGGCCTTACGATGCCACTTCATGGTG
CCCGTGGGGAATTGGGAGCACTGTCGCTTTCAGTCGAAGCCGAAAACCGCGCTGAGGCCAACCGTTTTATTGAGAGCGTCCTTCCAACTTTATGGATGTTGAAG
GACTATGCCCTTCAATCTGGGGCTGGGTTGGCCTTTGAGCACCCTGTTTCTAAACCAGTAGTTCTTACTTCACGCGAGAAGGAAGTCTTGCAATGGTGTGCTATT
GGAAAGACCTCCTGGGAAATCAGCGTCATTTGCAACTGTTCGGAAGCAAATGTAAATTTTCATATGGGGAACATCCGTCGCAAATTTGGGGTGACGTCCCGTCGT
GTCGCAGCCATCATGGCAGTCAATCTTGGTCTTATCACCTTACGTCCCGCTGCTAATGACGAGAACTATGCTGCGGCTGTCTGATAACTCGAGTTCTTACTTCACGC
GATGTGCTTTCCGGTCTGATGAGTCCGTGAGGACGAAACAGCGAGATCAGATAATTCTGACGTATCTAGActatggactatgtttgaaaggagaaatactagATGGTGTCAAA
GGGAGAGGCGGTTATCAAGGAATTTATGCGCTTTAAAGTCCACATGGAGGGCAGCATGAACGGGCACGAGTTTGAAATTGAGGGGGAGGGGGAGGGCCGTCCT
TATGAAGGTACTCAGACTGCTAAACTGAAGGTGACAAAAGGTGGCCCCTTGCCTTTCTCGTGGGACATCCTGTCGCCACAATTCATGTACGGGAGCCGCGCCTT
TATCAAACATCCCGCAGATATTCCTGATTACTATAAACAATCTTTCCCGGAAGGTTTCAAATGGGAACGCGTCATGAATTTTGAGGACGGGGGCGCTGTCACAGTT
ACTCAGGACACCTCCTTGGAAGACGGCACATTGATTTACAAGGTTAAGTTGCGCGGCACAAACTTCCCCCCTGACGGGCCAGTAATGCAAAAGAAAACTATGGG
TTGGGAGGCGTCTACAGAACGTTTATACCCCGAAGACGGGGTGCTGAAAGGTGACATTAAGATGGCCCTGCGCCTGAAGGACGGCGGTCGCTATCTTGCCGAC
TTTAAAACTACTTATAAGGCTAAAAAACCAGTCCAGATGCCAGGCGCCTATAATGTTGACCGCAAGTTAGACATCACCTCACATAATGAAGACTATACCGTTGTAG
AACAATACGAGCGCAGCGAGGGTCGTCACAGTACCGGGGGGATGGATGAATTATACAAACGTCCTGCTGCGAACGACGAAAATTATGCGGCTGCGGTTTGATAA
GGAAACACAGAAAAAAGCCCGCACCTGACAGTGCGGGCTTTTTTTTTCGACCAAAGGTTAATTAAACCTATAGGATCGTATAGGTTTACGCAAGAAAATGGTTTGT
TATAGTCGAATAAACCTAGGCCCCCCGAGGAGTAGCACATGATTGTGCAAATCGGCCGCCGTGAGGAGTTCGATAAAAAGCTGCTTGGGGAAATGCATAAACTT
CGTGCTCAGGTGTTCAAGGAGCGTAAGGGGTGGGATGTTTCCGTTATTGACGAAATGGAAATTGATGGGTACGATGCATTATCACCTTACTATATGCTGATTCAAG
AAGACACACCTGAGGCCCAGGTATTCGGTTGCTGGCGCATTTTTGACACGACGGGGCCTTACATGTTGAAGAACACGTTTCCTGAATTGTTACACGGCAAAGAA
GCTCCCTGCTCACCCCATATTTGGGAACTGAGCCGTTTCGCTATCAATTCCGGTCAAAAGGGCTCCCTGGGCTTTTCGGACTGCACCCTTGAAGCCATGCGCGC
ACTTGCCCGTTACTCCCTGCAAAACGACATTCAAACCTTAGTTACTGTTACTACCGTTGGCGTAGAGAAGATGATGATCCGTGCGGGTCTTGACGTATCTCGCTTT
GGACCGCATCTGAAGATTGGAATCGAGCGTGCGGTGGCGTTGCGCATCGAATTGAACGCAAAAACGCAAATTGCGTTATACGGCGGGGTCTTGGTTGAACAGC
GTTTAGCCGTGAGTTGATAATCCGGCAATTAAAAAAGCGGCTAACCACGCCGCTTTTTTTACGTCTGCActgcaggagtcactaagggttagttagttagattagcagaaagtcaaaagc
ctccgaccggaggcttttgactaaaacttccttggggttatcattggggctcactcaaaggcggtaat

pSB4A5-AD027, https://benchling.com/s/seq-sz4BQB5R8LqDbhFPJncL

pLacO, LasR, AAV degtag, RBS S4, mScarletI, pLas81, LasI

tgccacctgacgtctaagaaaaggaatattcagcaatttgcccgtgccgaagaaaggcccaccccgtgaaggtgagccagtgagttgattgctacgtaattagttagttagccccttagtgactcgaattcAATTGTGAGCGG
ATAACAATTGACATTGTGAGCGGATAACAAGATACTGAGCACAAAGCTTAGGGTGTCTCAAGGTGCGTACCTTGACTGATGAGTCCGAAAGGACGAAACACCCCT
CTACAAATAATTTTGTTTAAGCGGCCGCACTATGTTTTTCAAAGACGAAAAACTACTAGATGGCCCTGGTAGACGGCTTCTTGGAATTAGAACGTTCTAGTGGCAA
GTTGGAGTGGTCGGCAATCTTGCAAAAAATGGCTTCTGACTTAGGCTTCTCCAAGATTCTGTTTGGTTTGTTACCGAAGGATTCACAGGATTACGAAAACGCATTC
ATCGTCGGGAATTATCCAGCCGCGTGGCGCGAACACTACGATCGCGCTGGGTATGCGCGCGTTGATCCTACCGTGTCGCATTGCACTCAGTCTGTTCTTCCCAT
TTTTTGGGAACCCTCAATCTACCAGACCCGCAAGCAACATGAGTTCTTTGAGGAAGCCTCGGCCGCGGGGCTTGTGTATGGCCTTACGATGCCACTTCATGGTG
CCCGTGGGGAATTGGGAGCACTGTCGCTTTCAGTCGAAGCCGAAAACCGCGCTGAGGCCAACCGTTTTATTGAGAGCGTCCTTCCAACTTTATGGATGTTGAAG
GACTATGCCCTTCAATCTGGGGCTGGGTTGGCCTTTGAGCACCCTGTTTCTAAACCAGTAGTTCTTACTTCACGCGAGAAGGAAGTCTTGCAATGGTGTGCTATT
GGAAAGACCTCCTGGGAAATCAGCGTCATTTGCAACTGTTCGGAAGCAAATGTAAATTTTCATATGGGGAACATCCGTCGCAAATTTGGGGTGACGTCCCGTCGT
GTCGCAGCCATCATGGCAGTCAATCTTGGTCTTATCACCTTACGTCCCGCTGCTAATGACGAGAACTATGCTGCGGCTGTCTGATAACTCGAGAGCTGTCACCG

GATGTGCTTTCCGGTCTGATGAGTCCGTGAGGACGAAACAGCGAGATCAGATAATTCTGACGTATCTAGActatggactatgttttcacacaggaaataccaggATGGTGTCAAA
GGGAGAGGCGGTTATCAAGGAATTTATGCGCTTTAAAGTCCACATGGAGGGCAGCATGAACGGGCACGAGTTTGAAATTGAGGGGGAGGGGGAGGGCCGTCCT
TATGAAGGTACTCAGACTGCTAAACTGAAGGTGACAAAAGGTGGCCCCTTGCCTTTCTCGTGGGACATCCTGTCGCCACAATTCATGTACGGGAGCCGCGCCTT
TATCAAACATCCCGCAGATATTCCTGATTACTATAAACAATCTTTCCCGGAAGGTTTCAAATGGGAACGCGTCATGAATTTTGAGGACGGGGGCGCTGTCACAGTT
ACTCAGGACACCTCCTTGGAAGACGGCACATTGATTTACAAGGTTAAGTTGCGCGGCACAAACTTCCCCCCTGACGGGCCAGTAATGCAAAAGAAAACTATGGG
TTGGGAGGCGTCTACAGAACGTTTATACCCCGAAGACGGGGTGCTGAAAGGTGACATTAAGATGGCCCTGCGCCTGAAGGACGGCGGTCGCTATCTTGCCGAC
TTTAAAACTACTTATAAGGCTAAAAAACCAGTCCAGATGCCAGGCGCCTATAATGTTGACCGCAAGTTAGACATCACCTCACATAATGAAGACTATACCGTTGTAG
AACAATACGAGCGCAGCGAGGGTCGTCACAGTACCGGGGGGATGGATGAATTATACAAACGTCCTGCTGCGAACGACGAAAATTATGCGGCTGCGGTTTGATAA
GGAAACACAGAAAAAAGCCCGCACCTGACAGTGCGGGCTTTTTTTTTCGACCAAAGGTTAATTAAACCTATAGGATCGTATAGGTTTACGCAAGAAAATGGTTTGT
TATAGTCGAATAAACCTAGGCCCCCCGAGGAGTAGCACATGATTGTGCAAATCGGCCGCCGTGAGGAGTTCGATAAAAAGCTGCTTGGGGAAATGCATAAACTT
CGTGCTCAGGTGTTCAAGGAGCGTAAGGGGTGGGATGTTTCCGTTATTGACGAAATGGAAATTGATGGGTACGATGCATTATCACCTTACTATATGCTGATTCAAG
AAGACACACCTGAGGCCCAGGTATTCGGTTGCTGGCGCATTTTTGACACGACGGGGCCTTACATGTTGAAGAACACGTTTCCTGAATTGTTACACGGCAAAGAA
GCTCCCTGCTCACCCCATATTTGGGAACTGAGCCGTTTCGCTATCAATTCCGGTCAAAAGGGCTCCCTGGGCTTTTCGGACTGCACCCTTGAAGCCATGCGCGC
ACTTGCCCGTTACTCCCTGCAAAACGACATTCAAACCTTAGTTACTGTTACTACCGTTGGCGTAGAGAAGATGATGATCCGTGCGGGTCTTGACGTATCTCGCTTT
GGACCGCATCTGAAGATTGGAATCGAGCGTGCGGTGGCGTTGCGCATCGAATTGAACGCAAAAACGCAAATTGCGTTATACGGCGGGGTCTTGGTTGAACAGC
GTTTAGCCGTGAGTTGATAATCCGGCAATTAAAAAAGCGGCTAACCACGCCGCTTTTTTTACGTCTGCActgcaggagtcactaagggttagttagttagattagcagaaagtcaaaagc
ctccgaccggaggcttttgactaaaacttccctggggttatcattggggctcactcaaaggcggtaat

pSB4A5-AD028, https://benchling.com/s/seq-c29oDxVpbcfLlHMX5Gbr

pTetO, LuxR, AAV degtag, RBS B3, YPet, pLux76, LuxI

tgccacctgacgtctaagaaaaggaatattcagcaatttgcccgtgccgaagaaaggcccacccgtgaaggtgagccagtgagttgattgctacgtaattagttagttagccccttagtgactcgaattcTCCCTATCAGTG
ATAGAGATTGACATCCCTATCAGTGATAGAGATACTGAGCACAAGCTTAGGGTGTCTCAAGGTGCGTACCTTGACTGATGAGTCCGAAAGGACGAAACACCCCTC
TACAAATAATTTTGTTTAAGCGGCCGCACTATGTTTTTCAAAGACGAAAAACTACTAGATGAAGAACATTAATGCTGATGATACATATCGCATTATTAACAAGATCAA
GGCCTGCCGTTCCAACAACGATATTAATCAATGTTTGAGCGACATGACGAAGATGGTCCATTGTGAATACTACCTGCTGGCGATCATTTACCCACATTCGATGGTG
AAATCCGACATCAGTATTCTGGACAACTACCCCAAGAAATGGCGTCAGTATTATGACGATGCGAATCTGATCAAATATGACCCCATTGTAGACTATAGCAATAGCA
ACCATTCTCCGATTAACTGGAACATCTTTGAAAATAATGCAGTTAACAAGAAGAGTCCGAATGTAATCAAGGAAGCAAAAACATCAGGCTTAATCACTGGATTCTCC
TTCCCGATCCACACAGCCAACAACGGGTTTGGAATGTTGTCTTTCGCACACAGTGAAAAGGATAATTACATTGATAGTCTTTTCCTGCACGCGTGCATGAATATTC
CACTGATCGTGCCTAGTTTGGTAGACAATTACCGCAAGATTAATATTGCTAACAACAAATCTAACAACGACCTGACGAAACGCGAAAAAGAGTGCCTTGCGTGGG
CATGTGAAGGCAAGTCCTCCTGGGATATTTCGAAAATCTTAGGTTGCTCTGAGCGCACTGTGACCTTCCATCTTACGAACGCTCAAATGAAGTTAAATACCACCAA
CCGTTGCCAGTCAATCAGTAAGGCCATCCTGACTGGAGCTATCGACTGCCCATATTTCAAGAACCGTCCCGCTGCTAATGACGAGAACTATGCTGCGGCTGTCT
GATAACTCGAGAGCTGTCACCGGATGTGCTTTCCGGTCTGATGAGTCCGTGAGGACGAAACAGCGAGATCAGATAATTCTGACGTATCTAGAccaaacgaggccgggga
ggATGTCAAAGGGAGAAGAATTGTTCACGGGAGTTGTACCCATCTTAGTAGAATTGGACGGAGACGTCAATGGACACAAGTTCTCCGTTTCGGGAGAGGGGGAG
GGGGATGCGACGTATGGTAAATTGACGCTGAAGCTGTTATGTACCACCGGTAAGTTGCCTGTCCCTTGGCCCACATTAGTAACAACCCTGGGGTACGGCGTGCA
ATGCTTCGCGCGTTATCCTGACCATATGAAGCAACATGACTTCTTTAAGTCTGCCATGCCTGAAGGATATGTTCAAGAGCGCACGATTTTTTTTAAAGATGATGGG
AATTATAAAACTCGTGCAGAAGTGAAATTTGAGGGCGACACATTAGTGAACCGCATCGAATTAAAAGGAATCGACTTTAAAGAAGATGGAAACATTTTGGGGCACA
AATTGGAGTACAATTATAACAGCCATAACGTCTATATCACAGCGGATAAGCAGAAGAATGGCATCAAAGCGAATTTTAAGATTCGTCACAATATTGAAGATGGGGG
AGTTCAACTGGCGGACCATTATCAACAAAATACACCGATCGGTGACGGACCGGTGTTGTTGCCGGACAACCACTATTTATCATATCAGAGCGCGTTATTTAAGGA
CCCGAACGAGAAGCGTGACCACATGGTCCTGTTGGAATTTCTGACAGCCGCTGGTATTACTGAGGGTATGAATGAGCTTTACAAACGTCCTGCTGCGAACGACG
AAAATTATGCGGCTGCGGTTTGATAAGGAAACACAGAAAAAAGCCCGCACCTGACAGTGCGGGCTTTTTTTTTCGACCAAAGGTTAATTAAACCTGTAGGATCGTA
CAAGTTTACGCAAGAAAATGGTTTGTTATAGTCGAATAAACCTAGGCCCCCCGAGGAGTAGCACATGACAATTATGATTAAGAAGAGCGATTTCTTAGCAATCCCC
TCCGAGGAATATAAAGGCATCCTGTCTCTTCGCTACCAGGTGTTCAAACAGCGTCTGGAATGGGATTTAGTGGTTGAAAATAATTTGGAATCCGACGAGTACGATA
ACAGCAACGCTGAGTATATTTATGCCTGCGACGATACAGAAAACGTCAGTGGATGCTGGCGCCTGCTGCCCACAACCGGTGATTATATGTTGAAGTCAGGTATTCC
CCGAGCTTCTGGGGCAGCAGTCGGCGCCCAAAGATCCTAACATCGTTGAATTGAGTCGTTTGCTGTTGGCAAGAACTCCTCTAAAATCAATAATTCCGCAAGTG
AGATCACGATGAAACTGTTTGAAGCTATCTATAAGCATGCAGTAAGTCAAGGGATCACGGAGTACGTCACGGTCACGTCTACCGCAATTGAACGCTTCTTGAAAC
GTATCAAAGTTCCCTGCCACCGCATCGGAGATAAGGAAATTCACGTACTGGGCGATACTAAGTCCGTGGTCCTTTCGATGCCAATCAACGAGCAATTCAAAAAAG
CTGTCTTAAATTGATAATCCGGCAATTAAAAAAGCGGCTAACCACGCCGCTTTTTTTACGTCTGCActgcaggagtcactaagggttagttagttagattagcagaaagtcaaaagcctcc
gaccggaggcttttgactaaaacttccctggggttatcattggggctcactcaaaggcggtaat

pSB4A5-AD029, https://benchling.com/s/seq-UDZ4daitOG0heAlShvos

pTetO, LuxR, AAV degtag, RBS P1, YPet, pLux76, LuxI

tgccacctgacgtctaagaaaaggaatattcagcaatttgcccgtgccgaagaaaggcccacccgtgaaggtgagccagtgagttgattgctacgtaattagttagttagccccttagtgactcgaattcTCCCTATCAGTG
ATAGAGATTGACATCCCTATCAGTGATAGAGATACTGAGCACAAGCTTAGGGTGTCTCAAGGTGCGTACCTTGACTGATGAGTCCGAAAGGACGAAACACCCCTC
TACAAATAATTTTGTTTAAGCGGCCGCACTATGTTTTTCAAAGACGAAAAACTACTAGATGAAGAACATTAATGCTGATGATACATATCGCATTATTAACAAGATCAA
GGCCTGCCGTTCCAACAACGATATTAATCAATGTTTGAGCGACATGACGAAGATGGTCCATTGTGAATACTACCTGCTGGCGATCATTTACCCACATTCGATGGTG
AAATCCGACATCAGTATTCTGGACAACTACCCCAAGAAATGGCGTCAGTATTATGACGATGCGAATCTGATCAAATATGACCCCATTGTAGACTATAGCAATAGCA
ACCATTCTCCGATTAACTGGAACATCTTTGAAAATAATGCAGTTAACAAGAAGAGTCCGAATGTAATCAAGGAAGCAAAAACATCAGGCTTAATCACTGGATTCTCC
TTCCCGATCCACACAGCCAACAACGGGTTTGGAATGTTGTCTTTCGCACACAGTGAAAAGGATAATTACATTGATAGTCTTTTCCTGCACGCGTGCATGAATATTC
CACTGATCGTGCCTAGTTTGGTAGACAATTACCGCAAGATTAATATTGCTAACAACAAATCTAACAACGACCTGACGAAACGCGAAAAAGAGTGCCTTGCGTGGG
CATGTGAAGGCAAGTCCTCCTGGGATATTTCGAAAATCTTAGGTTGCTCTGAGCGCACTGTGACCTTCCATCTTACGAACGCTCAAATGAAGTTAAATACCACCAA
CCGTTGCCAGTCAATCAGTAAGGCCATCCTGACTGGAGCTATCGACTGCCCATATTTCAAGAACCGTCCCGCTGCTAATGACGAGAACTATGCTGCGGCTGTCT
GATAACTCGAGAGCTGTCACCGGATGTGCTTTCCGGTCTGATGAGTCCGTGAGGACGAAACAGCGAGATCAGATAATTCTGACGTATCTAGActatggactatgtttgaaa
gggagaaatactagATGTCAAAGGGAGAAGAATTGTTCACGGGAGTTGTACCCATCTTAGTAGAATTGGACGGAGACGTCAATGGACACAAGTTCTCCGTTTCGGGAG
AGGGGGAGGGGGATGCGACGTATGGTAAATTGACGCTGAAGCTGTTATGTACCACCGGTAAGTTGCCTGTCCCTTGGCCCACATTAGTAACAACCCTGGGGTAC
GGCGTGCAATGCTTCGCGCGTTATCCTGACCATATGAAGCAACATGACTTCTTTAAGTCTGCCATGCCTGAAGGATATGTTCAAGAGCGCACGATTTTTTTTAAAG
ATGATGGGAATTATAAAACTCGTGCAGAAGTGAAATTTGAGGGCGACACATTAGTGAACCGCATCGAATTAAAAGGAATCGACTTTAAAGAAGATGGAAACATTTT
GGGGCACAAATTGGAGTACAATTATAACAGCCATAACGTCTATATCACAGCGGATAAGCAGAAGAATGGCATCAAAGCGAATTTTAAGATTCGTCACAATATTGAA
GATGGGGGAGTTCAACTGGCGGACCATTATCAACAAAATACACCGATCGGTGACGGACCGGTGTTGTTGCCGGACAACCACTATTTATCATATCAGAGCGCGTT
ATTTAAGGACCCGAACGAGAAGCGTGACCACATGGTCCTGTTGGAATTTCTGACAGCCGCTGGTATTACTGAGGGTATGAATGAGCTTTACAAACGTCCTGCTGC
GAACGACGAAAATTATGCGGCTGCGGTTTGATAAGGAAACACAGAAAAAAGCCCGCACCTGACAGTGCGGGCTTTTTTTTTCGACCAAAGGTTAATTAAACCTGT
AGGATCGTACAAGTTTACGCAAGAAAATGGTTTGTTATAGTCGAATAAACCTAGGCCCCCCGAGGAGTAGCACATGACAATTATGATTAAGAAGAGCGATTTCTTA
GCAATCCCCTCCGAGGAATATAAAGGCATCCTGTCTCTTCGCTACCAGGTGTTCAAACAGCGTCTGGAATGGGATTTAGTGGTTGAAAATAATTTGGAATCCGAC
GAGTACGATAACAGCAACGCTGAGTATATTTATGCCTGCGACGATACAGAAAACGTCAGTGGATGCTGGCGCCTGCTGCCCACAACCGGTGATTATATGTTGAA
GTCAGTATTCCCCGAGCTTCTGGGGCAGCAGTCGGCGCCCAAAGATCCTAACATCGTTGAATTGAGTCGTTTGCTGTTGGCAAGAACTCCTCTAAAATCAATAA
TTCCGCAAGTGAGATCACGATGAAACTGTTTGAAGCTATCTATAAGCATGCAGTAAGTCAAGGGATCACGGAGTACGTCACGGTCACGTCTACCGCAATTGAACG
CTTCTTGAAACGTATCAAAGTTCCCTGCCACCGCATCGGAGATAAGGAAATTCACGTACTGGGCGATACTAAGTCCGTGGTCCTTTCGATGCCAATCAACGAGCA
ATTCAAAAAAGCTGTCTTAAATTGATAATCCGGCAATTAAAAAAGCGGCTAACCACGCCGCTTTTTTTACGTCTGCActgcaggagtcactaagggttagttagttagattagcagaa
agtcaaaagcctccgaccggaggcttttgactaaaacttccctggggttatcattggggctcactcaaaggcggtaat

pSB4A5-AD030, https://benchling.com/s/seq-HgTr1CVQrECxeqREZLke

pTetO, LuxR, AAV degtag, RBS S4, YPet, pLux76, LuxI

tgccacctgacgtctaagaaaaggaatattcagcaatttgcccgtgccgaagaaaggcccacccgtgaaggtgagccagtgagttgattgctacgtaattagttagttagccccttagtgactcgaattcTCCCTATCAGTG
ATAGAGATTGACATCCCTATCAGTGATAGAGATACTGAGCACAAGCTTAGGGTGTCTCAAGGTGCGTACCTTGACTGATGAGTCCGAAAGGACGAAACACCCCTC
TACAAATAATTTTGTTTAAGCGGCCGCACTATGTTTTTCAAAGACGAAAAACTACTAGATGAAGAACATTAATGCTGATGATACATATCGCATTATTAACAAGATCAA
GGCCTGCCGTTCCAACAACGATATTAATCAATGTTTGAGCGACATGACGAAGATGGTCCATTGTGAATACTACCTGCTGGCGATCATTTACCCACATTCGATGGTG
AAATCCGACATCAGTATTCTGGACAACTACCCCAAGAAATGGCGTCAGTATTATGACGATGCGAATCTGATCAAATATGACCCCATTGTAGACTATAGCAATAGCA
ACCATTCTCCGATTAACTGGAACATCTTTGAAAATAATGCAGTTAACAAGAAGAGTCCGAATGTAATCAAGGAAGCAAAAACATCAGGCTTAATCACTGGATTCTCC
TTCCCGATCCACACAGCCAACAACGGGTTTGGAATGTTGTCTTTCGCACACAGTGAAAAGGATAATTACATTGATAGTCTTTTCCTGCACGCGTGCATGAATATTC
CACTGATCGTGCCTAGTTTGGTAGACAATTACCGCAAGATTAATATTGCTAACAACAAATCTAACAACGACCTGACGAAACGCGAAAAAGAGTGCCTTGCGTGGG

CATGTGAAGGCAAGTCCTCCTGGGATATTTCGAAAATCTTAGGTTGCTCTGAGCGCACTGTGACCTTCCATCTTACGAACGCTCAAATGAAGTTAAATACCACCAA
CCGTTGCCAGTCAATCAGTAAGGCCATCCTGACTGGAGCTATCGACTGCCCATATTTCAAGAACCGTCCCGCTGCTAATGACGAGAACTATGCTGCGGCTGTCT
GATAACTCGAGAGCTGTCACCGGATGTGCTTTCCGGTCTGATGAGTCCGTGAGGACGAAACAGCGAGATCAGATAATTCTGACGTATCTAGACtatggactatgttttcac
acaggaaataccaggATGTCAAAGGGAGAAGAAGTTGTTCACGGGAGTTGTACCCATCTTAGTAGAATTGGACGGAGACGTCAATGGACACAAGTTCTCCGTTTCGGGA
GAGGGGGAGGGGGATGCGACGTATGGTAAATTGACGCTGAAGCTGTTATGTACCACCGGTAAGTTGCCTGTCCCTTGGCCCACATTAGTAACAACCCTGGGGTA
CGGCGTGCAATGCTTCGCGCGTTATCCTGACCATATGAAGCAACATGACTTCTTTAAGTCTGCCATGCCTGAAGGATATGTTCAAGAGCGCACGATTTTTTTAAA
GATGATGGGAATTATAAAACTCGTGCAGAAGTGAAATTTGAGGGCGACACATTAGTGAACCGCATCGAATTAAAAGGAATCGACTTTAAAGAAGATGGAAACATTT
TGGGGCACAAATTGGAGTACAATTATAACAGCCATAACGTCTATATCACAGCGGATAAGCAGAAGAATGGCATCAAAGCGAATTTTAAGATTCGTCACAATATTGA
AGATGGGGGAGTTCAACTGGCGGACCATTATCAACAAAATACACCGATCGGTGACGGACCGGTGTTGTTGCCGGACAACCACTATTTATCATATCAGAGCGCGT
TATTTAAGGACCCGAACGAGAAGCGTGACCACATGGTCCTGTTGGAATTTCTGACAGCCGCTGGTATTACTGAGGGTATGAATGAGCTTTACAAACGTCCTGCTG
CGAACGACGAAAATTATGCGGCTGCGGTTTGATAAGGAAACACAGAAAAAAGCCCGCACCTGACAGTGCGGGCTTTTTTTTTCGACCAAAGGTTAATTAAACCTG
TAGGATCGTACAAGTTTACGCAAGAAAATGGTTTGTTATAGTCGAATAAACCTAGGCCCCCCGAGGAGTAGCACATGACAATTATGATTAAGAAGAGCGATTTCTT
AGCAATCCCCTCCGAGGAATATAAAGGCATCCTGTCTCTTCGCTACCAGGTGTTCAAACAGCGTCTGGAATGGGATTTAGTGGTTGAAAATAATTTGGAATCCGA
CGAGTACGATAACAGCAACGCTGAGTATATTTATGCCTGCGACGATACAGAAAACGTCAGTGGATGCTGGCGCCTGCTGCCCACAACCGGTGATTATATGTTGAA
GTCAGTATTCCCCGAGCTTCTGGGGCAGCAGTCGGCGCCCAAAGATCCTAACATCGTTGAATTGAGTCGTTTTGCTGTTGGCAAGAACTCCTCTAAAATCAATAA
TTCCGCAAGTGAGATCACGATGAAACTGTTTGAAGCTATCTATAAGCATGCAGTAAGTCAAGGGATCACGGAGTACGTCACGGTCACGTCTACCGCAATTGAACG
CTTCTTGAAACGTATCAAAGTTCCCTGCCACCGCATCGGAGATAAGGAAATTCACGTACTGGGCGATACTAAGTCCGTGGTCCTTTCGGATGCCAATCAACGAGCA
ATTCAAAAAAGCTGTCTTAAATTGATAATCCGGCAATTAAAAAAGCGGCTAACCACGCCGCTTTTTTTACGTCTGCActgcaggagtcactaagggttagttagttagattagcagaaa
agtcaaaagcctccgaccggaggcttttgactaaaacttccctggggttatcattggggctcactcaaaggcggtaat

pSB4A5-AD031, https://benchling.com/s/seq-xNyxZkr0UWWS492dSOx9

pLacO, LasR, AAV degtag, pLas81, RBS P1, mScarletI, LasI

tgccacctgacgtctaagaaaaggaatatttcagcaatttgcccgtgccgaagaaaggcccacccgtgaaggtgagccagtgagttgattgctacgtaattagttagttagcccttagtgactcgaattcAATTGTGAGCGG
ATAACAATTGACATTGTGAGCGGATAACAAGATACTGAGCACAAAGCTTAGGGTGTCTCAAGGTGCGTACCTTGACTGATGAGTCCGAAAGGACGAAACACCCCT
CTACAAATAATTTTGTTTAAGCGGCCGCACTATGTTTTTCAAAGACGAAAAACTACTAGATGGCCCTGGTAGACGGCTTCTTGGAATTAGAACGTTCTAGTGGCAA
GTTGGAGTGGTCGGCAATCTTGCAAAAAATGGCTTCTGACTTAGGCTTCTCCAAGATTCTGTTTGGTTTGTTACCGAAGGATTCACAGGATTACGAAAACGCATTC
ATCGTCGGGAATTATCCAGCCGCGTGGCGCGAACACTACGATCGCGCTGGGTATGCGCGCGTTGATCCTACCGTGTCGCATTGCACTCAGTCTGTTCTTCCCAT
TTTTTGGGAACCCTCAATCTACCAGACCCGCAAGCAACATGAGTTCTTTGAGGAAGCCTCGGCCGCGGGGCTTGTGTATGGCCTTACGATGCCACTTCATGGTG
CCCGTGGGGAATTGGGAGCACTGTCGCTTTCAGTCGAAGCCGAAAACCGCGCTGAGGCCAACCGTTTTATTGAGAGCGTCCTTCCAACTTTATGGATGTTGAAG
GACTATGCCCTTCAATCTGGGGCTGGGTTGGCCTTTGAGCACCCTGTTTCTAAACCAGTAGTTCTTACTTCACGCGAGAAGGAAGTCTTGCAATGGTGTGCTATT
GGAAAGACCTCCTGGGAAATCAGCGTCATTTGCAACTGTTCGGAAGCAAATGTAAATTTTCATATGGGGAACATCCGTCGCAAATTTGGGGTGACGTCCGTCGT
GTCGCAGCCATCATGGCAGTCAATCTTGGTCTTATCACCTTACGTCCCGCTGCTAATGACGAGAACTATGCTGCGGCTGTCTGATAACTCGAGTTCAGCCAAAAA
ACTTAAGACCGCCGGTCTTGTCCACTACCTTGCAGTAATGCGGTGGACAGGATCGGCGGTTTTCTTTTCTCTTCTCAATTAATTAAACCTATAGGATCGTATAGGTT
TACGCAAGAAAATGGTTTGTTATAGTCGAATAAAATCCATAGCTGTCACCGGATGTGCTTTCCGGTCTGATGAGTCCGTGAGGACGAAACAGCGAGATCAGATAA
TTCTGACGTATCTAGACTATGGACTATGTTTGAAAGGGAGAAATACTAGATGGTGTCAAAGGGAGAGGCGGTTATCAAGGAATTTATGCGCTTTAAAGTCCACATG
GAGGGCAGCATGAACGGGCACGAGTTTGAAATTGAGGGGGAGGGGGAGGGCCGTCCTTATGAAGGTACTCAGACTGCTAAACTGAAGGTGACAAAAGGTGGC
CCCTTGCCTTTCTCGTGGGACATCCTGTCGCCACAATTCATGTACGGGAGCCGCGCCTTTATCAAACATCCCGCAGATATTCCTGATTACTATAAACAATCTTTCC
CGGAAGGTTTCAAATGGGAACGCGTCATGAATTTTGAGGACGGGGGCGCTGTCACAGTTACTCAGGACACCTCCTTGGAAGACGGCACATTGATTTACAAGGTT
AAGTTGCGCGGCACAAACTTCCCCCCTGACGGGCCAGTAATGCAAAAGAAAACTATGGGTTGGGAGGCGTCTACAGAACGTTTATACCCCGAAGACGGGGTGC
TGAAAGGTGACATTAAGATGGCCCTGCGCCTGAAGGACGGCGGTCGCTATCTTGCCGACTTTAAAACTACTTATAAGGCTAAAAAACCAGTCCAGATGCCAGGC
GCCTATAATGTTGACCGCAAGTTAGACATCACCTCACATAATGAAGACTATACCGTTGTAGAACAATACGAGCGCAGCGAGGGTCGTCACAGTACCGGGGGGAT
GGATGAATTATACAAACGTCCTGCTGCGAACGACGAAAATTATGCGGCTGCGGTTTGATAAGGAAACACAGAAAAAAGCCCGCACCTGACAGTGCGGGCTTTTTT
TTTCGACCAAAGGTTAATTAAACCTATAGGATCGTATAGGTTTACGCAAGAAAATGGTTTGTTATAGTCGAATAAACCTAGGCCCCCCGAGGAGTAGCACATGATT
GTGCAAATCGGCCGCCGTGAGGAGTTCGATAAAAAGCTGCTTGGGGAAATGCATAAACTTCGTGCTCAGGTGTTCAAGGAGCGTAAGGGGTGGGATGTTTCCGT
TATTGACGAAATGGAAATTGATGGGTACGATGCATTATCACCTTACTATATGCTGATTCAAGAAGACACACCTGAGGCCCAGGTATTCGGTTGCTGGCGCATTTTT
GACACGACGGGGCCTTACATGTTGAAGAACACGTTCCTGAATTGTTACACGGCAAAGAAGCTCCCTGCTCACCCCATATTTGGGAACTGAGCCGTTTCGCTATC
AATTCCGGTCAAAAGGGCTCCCTGGGCTTTTCGGACTGCACCCTTGAAGCCATGCGCGCACTTGCCCGTTACTCCCTGCAAAACGACATTCAAACCTTAGTTACT
GTTACTACCGTTGGCGTAGAGAAGATGATGATCCGTGCGGGTCTTGACGTATCTCGCTTTGGACCGCATCTGAAGATTGGAATCGAGCGTGCGGTGGCGTTGCG
CATCGAATTGAACGCAAAAACGCAAATTGCGTTATACGGCGGGGTCTTGGTTGAACAGCGTTTAGCCGTGAGTTGATAATCCGGCAATTAAAAAAGCGGCTAACC
ACGCCGCTTTTTTTACGTCTGCActgcaggagtcactaagggttagttagttagattagcagaaagtcaaaagcctccgaccggaggcttttgactaaaacttccctggggttatcattggggctcactcaaaggcg
gtaat

pSB4A5-AD032, https://benchling.com/s/seq-0tS1t63hLejNnedtoncJ

pLacO, LasR, AAV degtag, pLas81, mScarletI

tgccacctgacgtctaagaaaaggaatatttcagcaatttgcccgtgccgaagaaaggcccacccgtgaaggtgagccagtgagttgattgctacgtaattagttagttagcccttagtgactcgaattcAATTGTGAGCGG
ATAACAATTGACATTGTGAGCGGATAACAAGATACTGAGCACAAAGCTTAGGGTGTCTCAAGGTGCGTACCTTGACTGATGAGTCCGAAAGGACGAAACACCCCT
CTACAAATAATTTTGTTTAAGCGGCCGCACTATGTTTTTCAAAGACGAAAAACTACTAGATGGCCCTGGTAGACGGCTTCTTGGAATTAGAACGTTCTAGTGGCAA
GTTGGAGTGGTCGGCAATCTTGCAAAAAATGGCTTCTGACTTAGGCTTCTCCAAGATTCTGTTTGGTTTGTTACCGAAGGATTCACAGGATTACGAAAACGCATTC
ATCGTCGGGAATTATCCAGCCGCGTGGCGCGAACACTACGATCGCGCTGGGTATGCGCGCGTTGATCCTACCGTGTCGCATTGCACTCAGTCTGTTCTTCCCAT
TTTTTGGGAACCCTCAATCTACCAGACCCGCAAGCAACATGAGTTCTTTGAGGAAGCCTCGGCCGCGGGGCTTGTGTATGGCCTTACGATGCCACTTCATGGTG
CCCGTGGGGAATTGGGAGCACTGTCGCTTTCAGTCGAAGCCGAAAACCGCGCTGAGGCCAACCGTTTTATTGAGAGCGTCCTTCCAACTTTATGGATGTTGAAG
GACTATGCCCTTCAATCTGGGGCTGGGTTGGCCTTTGAGCACCCTGTTTCTAAACCAGTAGTTCTTACTTCACGCGAGAAGGAAGTCTTGCAATGGTGTGCTATT
GGAAAGACCTCCTGGGAAATCAGCGTCATTTGCAACTGTTCGGAAGCAAATGTAAATTTTCATATGGGGAACATCCGTCGCAAATTTGGGGTGACGTCCGTCGT
GTCGCAGCCATCATGGCAGTCAATCTTGGTCTTATCACCTTACGTCCCGCTGCTAATGACGAGAACTATGCTGCGGCTGTCTGATAACTCGAGTTCAGCCAAAAA
ACTTAAGACCGCCGGTCTTGTCCACTACCTTGCAGTAATGCGGTGGACAGGATCGGCGGTTTTCTTTTCTCTTCTCAATTAATTAAACCTATAGGATCGTATAGGTT
TACGCAAGAAAATGGTTTGTTATAGTCGAATAAAATCCATAGCTGTCACCGGATGTGCTTTCCGGTCTGATGAGTCCGTGAGGACGAAACAGCGAGATCAGATAA
TTCTGACGTATCTAGACTATGGACTATGTTTGAAAGGGAGAAATACTAGATGGTGTCAAAGGGAGAGGCGGTTATCAAGGAATTTATGCGCTTTAAAGTCCACATG
GAGGGCAGCATGAACGGGCACGAGTTTGAAATTGAGGGGGAGGGGGAGGGCCGTCCTTATGAAGGTACTCAGACTGCTAAACTGAAGGTGACAAAAGGTGGC
CCCTTGCCTTTCTCGTGGGACATCCTGTCGCCACAATTCATGTACGGGAGCCGCGCCTTTATCAAACATCCCGCAGATATTCCTGATTACTATAAACAATCTTTCC
CGGAAGGTTTCAAATGGGAACGCGTCATGAATTTTGAGGACGGGGGCGCTGTCACAGTTACTCAGGACACCTCCTTGGAAGACGGCACATTGATTTACAAGGTT
AAGTTGCGCGGCACAAACTTCCCCCCTGACGGGCCAGTAATGCAAAAGAAAACTATGGGTTGGGAGGCGTCTACAGAACGTTTATACCCCGAAGACGGGGTGC
TGAAAGGTGACATTAAGATGGCCCTGCGCCTGAAGGACGGCGGTCGCTATCTTGCCGACTTTAAAACTACTTATAAGGCTAAAAAACCAGTCCAGATGCCAGGC
GCCTATAATGTTGACCGCAAGTTAGACATCACCTCACATAATGAAGACTATACCGTTGTAGAACAATACGAGCGCAGCGAGGGTCGTCACAGTACCGGGGGGAT
GGATGAATTATACAAACGTCCTGCTGCGAACGACGAAAATTATGCGGCTGCGGTTTGATAAGGAAACACAGAAAAAAGCCCGCACCTGACAGTGCGGGCTTTTTT
TTTCGACCAAAGGTTAATTAAACCTATAGGgctcactcaaaggcggtaat

pSB4A5-AD033, https://benchling.com/s/seq-moy0kf1rcN6QUhT8zLLd

pTetO, LuxR, AAV degtag, YPet

tgccacctgacgtctaagaaaaggaatatttcagcaatttgcccgtgccgaagaaaggcccacccgtgaaggtgagccagtgagttgattgctacgtaattagttagttagcccttagtgactcgaattcTCCCTATCAGTG
ATAGAGATTGACATCCCTATCAGTGATAGAGATACTGAGCACAAGCTTAGGGTGTCTCAAGGTGCGTACCTTGACTGATGAGTCCGAAAGGACGAAACACCCCCTC
TACAAATAATTTTGTTTAAGCGGCCGCACTATGTTTTTCAAAGACGAAAAACTACTAGATGAAGAACATTAATGCTGATGATACATATCGCATTATTAACAAGATCAA
GGCCTGCCGTTCCAACAACGATATTAATCAATGTTTGAGCGACATGACGAAGATGGTCCATTGTGAATACTACCTGCTGGCGATCATTTACCCACATTCGATGGTG
AAATCCGACATCAGTATTCTGGACAACTACCCCAAGAAATGGCGTCAGTATTATGACGATGCGAATCTGATCAAATATGACCCCATTGTAGACTATAGCAATAGCA
ACCATTCTCCGATTAACTGGAACATCTTTGAAAATAATGCAGTTAACAAGAAGAGTCCGAATGTAATCAAGGAAGCAAAAACATCAGGCTTAATCACTGGATTCTCC
TTCCCGATCCACACAGCCAACAACGGGTTTGGAATGTTGTCTTTCGCACACAGTGAAAAGGATAATTACATTGATAGTCTTTTCCTGCACGCGTGCATGAATATTC
CACTGATCGTGCCTAGTTTGGTAGACAATTACCGCAAGATTAATATTGCTAACAACAAATCTAACAACGACCTGACGAAACGCGAAAAAGAGTGCCTTGCGTGGG
CATGTGAAGGCAAGTCCTCCTGGGATATTTCGAAAATCTTAGGTTGCTCTGAGCGCACTGTGACCTTCCATCTTACGAACGCTCAAATGAAGTTAAATACCACCAA
CCGTTGCCAGTCAATCAGTAAGGCCATCCTGACTGGAGCTATCGACTGCCCATATTTCAAGAACCGTCCCGCTGCTAATGACGAGAACTATGCTGCGGCTGTCT

GATAACTCGAGAGCTGTCACCGGATGTGCTTTCCGGTCTGATGAGTCCGTGAGGACGAAACAGCGAGATCAGATAATTCTGACGTATCTAGActatggactatgtttgaaa
gggagaaatactagATGTCAAAGGGAGAAGAATTGTTCACGGGAGTTGTACCCATCTTAGTAGAATTGGACGGAGACGTCAATGGACACAAGTTCTCCGTTTCGGGAG
AGGGGGAGGGGGATGCGACGTATGGTAAATTGACGCTGAAGCTGTTATGTACCACCGGTAAGTTGCCTGTCCCTTGGCCCACATTAGTAACAACCCTGGGGTAC
GGCGTGCAATGCTTCGCGCGTTATCCTGACCATATGAAGCAACATGACTTCTTTAAGTCTGCCATGCCTGAAGGATATGTTCAAGAGCGCACGATTTTTTTAAAG
ATGATGGGAATTATAAAACTCGTGCAGAAGTGAAATTTGAGGGCGACACATTAGTGAACCGCATCGAATTAAAAGGAATCGACTTTAAAGAAGATGGAAACATTTT
GGGGCACAAATTGGAGTACAATTATAACAGCCATAACGTCTATATCACAGCGGATAAGCAGAAGAATGGCATCAAAGCGAATTTTAAGATTCGTCACAATATTGAA
GATGGGGGAGTTCAACTGGCGGACCATTATCAACAAAATACACCGATCGGTGACGGACCGGTGTTGTTGCCGGACAACCACTATTTATCATATCAGAGCGCGTT
ATTTAAGGACCCGAACGAGAAGCGTGACCACATGGTCCTGTTGGAATTTCTGACAGCCGCTGGTATTACTGAGGGTATGAATGAGCTTTACAAACGTCCTGCTGC
GAACGACGAAAATTATGCGGCTGCGGTTTGATAAGGAAACACAGAAAAAAGCCCGCACCTGACAGTGCGGGCTTTTTTTTTCGACCAAAGGTTAATTAAACCgctc
actcaaaggcggtaat

pSB3C5-AD034, https://benchling.com/s/seq-VapMMn2Bl9gsX2hdmD6o

pLas81, TetR, pJ23106, LasR, pTetO

tgccacctgacgtctaagaaaaggaatattcagcaatttgcccgtgccgaagaaaggcccacccgtgaaggtgagccagtgagttgattgctacgtaattagttagttagcccttagtgactcgaattcACCTATAGGATC
GTATAGGTTTACGCAAGAAAATGGTTTGTTATAGTCGAATAAAAAGCTTCTATGGACTATGTTTTCACATACGAGGGGGATTAGATGTCGCGTCTGGACAAGAGTAA
AGTGATTAATTCAGCTCTTGAACTGTTGAATGAAGTTGGAATTGAAGGACTTCACAACACGTAAGTTAGCACAGAAATTGGGCGTCGAACAACCTACATTGTACTGG
CATGTCAAGAATAAACGTGCGCTTCTGGATGCTCTTGCTATTGAAATGTTGGACCGTCACCACACTCACTTTGCCCCTTGGAAGGAGAAAGCTGGCAAGATTTTC
TGCGCAACAACGCTAAGTCATTTCGTTGCGCTCTGTTATCCCACCGTGATGGGGCCAAAGTCCACTTGGGCACTCGCCCCACGGAAAAACAGTATGAAACCCTG
GAAAACCAACTTGCTTTCCTGTGTCAACAAGGATTTAGCCTTGAGAATGCATTGTATGCCCTGTCTGCGGTAGGGCACTTTACGTTGGGCTGTGTCTTAGAGGAC
CAGGAGCATCAGGTTGCCAAGGAGGAGCGTGAGACACCTACGACCGACAGTATGCCACCCTTATTACGTCAGGCGATTGAGCTGTTTGACCACCAAGGTGCGG
AACCTGCCTTTCTTTTTGGTCTTGAACTTATCATCTGTGGGTTGGAAAAACAACTTAAATGCGAGTCCGGCAGCTGATAACCAATTATTGAACACCCTTCGGGGTGT
TTTTTTGTTTCTGGTCTACCCTCGAGtttacggctagctcagtcctaggtatagtgctagcTCTAGAGGAGCTATGGACTATGTTTGAAAGGCTGAAATACTAGATGGCCTTAGTTG
ATGGCTTCTTGGAGTTAGAGCGTAGCTCTGGAAAGTTAGAGTGGTCTGCAATCTTGCAAAAGATGGCTTCCGATTTAGGCTTCTCGAAGATTTTGTTCGGTTTATTA
CCTAAGGACTCACAGGATTACGAAAACGCGTTTATCGTTGGAAACTACCCGGCAGCATGGCGCGAGCATTATGATCGCGCCGGTTATGCGCGTGTAGATCCTAC
GGTAAGTCATTGTACTCAATCGGTCTTACCGATCTTTTGGGAACCTTCAATCTACCAGACACGTAAACAACATGAGTTCTTCGAAGAAGCGTCAGCAGCTGGTTTG
GTGTACGGCCTGACCATGCCTCTGCATGGAGCGCGTGGGGAATTGGGGGCGTTGTCATTGAGTGTAGAAGCTGAAGAACCGCGCGGAAGCTAACCGCTTTATCG
AAAGTGTATTGCCTACACTGTGGATGTTGAAAGACTACGCTCTTCAGTCGGGGGCCGGACTTGCGTTCGAACATCCCGTATCGAAGCCTGTCGTACTTACCTCTC
GCGAAAAAGAAGTCTTGCAGTGGTGCGCCATCGGTAAAACGAGCTGGGAAATCTCAGTAATTTGTAACTGCTCAGAAGCTAACGTAAACTTCCACATGGGCAATA
TCCGTCGTAAGTTTGGAGTCACGTCCCGTCGTGTCGCTGCTATCATGGCGGTCAACTTGGGCCTTATTACTTTATGATAATCCGGCAATTAAAAAGCGGCTAAC
CACGCCGCTTTTTTTACGTCTGCActgcaTTCCCTATCAGTGATAGAGACAAGGCTCCCTATCAGTGATAGAGAAGCTGGGCACCTGCAggagtcactaagggttagttagtta
gattagcagaaagtcaaaagcctccgaccggaggcttttgactaaaacttccctggggttatcattggggctcactcaaaggcggtaat

pSB3C5-AD035, https://benchling.com/s/seq-catw2mGgeBA44Me0YDj6

pLux76, LacI, pJ23106, LuxR, pLacO

tgccacctgacgtctaagaaaaggaatattcagcaatttgcccgtgccgaagaaaggcccacccgtgaaggtgagccagtgagttgattgctacgtaattagttagttagcccttagtgactcgaattcACCTGTAGGATC
GTACAAGTTTACGCAAGAAAATGGTTTGTTATAGTCGAATAAAAAGCTTCTATGGACTATGTTTTCACATACGAGGGGGATTAGATGAAACCAGTGACACTTTACGA
TGTCGCCGAATATGCGGGCGTTTCGTACCAGACTGTATCACGTGTAGTGAATCAAGCGTCGCACGTCAGCGCTAAGACTCGTGAAAAAGTGGAAGCTGCGATGG
CCGAGTTGAACTACATTCCGAATCGTGTTGCACAACAACTGGCAGGAAAACAAAGTTTATTAATTGGTGTGGCCACGTCAAGCCTGGCCTTGCACGCACCCTCG
CAAATCGTTGCTGCGATCAAGAGTCGTGCGGATCAGTTAGGAGCATCCGTCGTTGTATCGATGGTCGAACGTAGTGGAGTGGAGGCATGTAAAGCGGCTGTGCA
CAATCTTCTTGCCCAGCGTGTTTCTGGGCTGATTATTAACTACCCTCTGGATGACCAAGACGCGATTGCCGTTGAAGCTGCGTGCACAAACGTTCCGGCCCTGTT
CCTTGACGTATCAGACCAAACACCTATCAACAGTATCATCCTTTAGTCACGAAGATGGTACGCGTTTAGGAGTGGAGCATTTAGTAGCTTTGGGTCACCAGCAGATC
GCATTATTAGCGGGGCCGCTTAGTAGCGTATCCGCCCGCCTGCGCCTGGCTGGCTGGCACAAGTACCTTACTCGCAACCAGATCCAGCCGATCGCAGAGCGT
GAAGGTGACTGGTCGGCGATGTCCGGATTTCAACAGACGATGCAAATGTTAAATGAGGGCATTGTACCTACTGCTATGCTGGTGGCCAACGACCAGATGGCACT
GGGGGCGATGCGTGCAATCACTGAATCTGGCCTTCGCGTTGGCGCAGACATTTCCGTCGTTGGCTATGATGATACAGAAGACTCAAGTTGCTATATCCCCCCAC
TTACGACAATCAAACAGGATTTCCGTTTGCTTGGTCAAACCTCCGTTGACCGTTTGCTGCAACTTAGCCAGGGGCAGGCGGTGAAGGGAAATCAGTTACTTCCTG
TGAGTTTAGTAAAACGCAAGACCACGTTAGCACCTAATACTCAGACGGCAAGCCCACGTGCTTTAGCTGACAGTTTAATGCAACTGGCTCGTCAAGTATCTCGTC
TTGAAAGTGGTCAATGATAACCAATTATTGAACACCCTTCGGGGGTGTTTTTTTGTTTCTGGTCTACCCTCGAGtttacggctagctcagtcctaggtatagtgctagcTCTAGAGGA
GCTATGGACTATGTTTGAAAGGCTGAAATACTAGATGAAGAATATTAACGCGGACGATACATATCGCATTATCAACAAGATCAAGGCGTGTCGCTCTAATAACGAC
ATCAACCAGTGCTTGAGTGATATGACTAAGATGGTACATTGCGAGTACTATTTGCTGGCGATTATCTATCCGCATTCAATGGTTAAGTCGGATATTTCTATCTTAGAT
AACTATCCCAAAAAATGGCGTCAATACTACGACGACGCCAATCTGATTAAATACGACCCTATCGTGGATTATTCCAATTCCAACCATTCGCCGATCAATTGGAATAT
CTTCGAGAACAATGCTGTGAACAAAAAGTCTCCCAACGTGATTAAGGAGGCTAAAACCTCCGGTTTAATTACCGGTTTTAGTTTCCCAATTCATACCGCAAACAAC
GGTTTCGGAATGTTGTCCTTCGCACATAGCGAGAAAGATAATTATATCGACTCGCTTTTTTTGCACGCGTGTATGAATATTCCCTTGATCGTACCTAGTCTGGTGGA
TAACTACCGTAAAATTAATATTGCGAATAATAAGTCGAACAACGACCTTACAAAACGTGAGAAGGAATGTCTGGCATGGGCGTGTGAAGGTAAGTCCTCGTGGGA
TATTTCTAAGATCCTTGGTTGTAGCGAGCGTACCGTTACCTTTCATTTGACTAATGCCCAAATGAAGTTAAACACGACTAATCGTTGCCAGTCTATCTCAAAGGCAA
TTCTTACCGGGGCCATCGACTGTCCGTACTTCAAGAATTGATAATCCGGCAATTAAAAAAGCGGCTAACCACGCCGCTTTTTTTACGTCTGCActgcaTAATTGTGA
GCGGATAACAACAAGGCTTGTGAGCGGATAACAAAGCTGGGAGCACACTGCAggagtcactaagggttagttagttagattagcagaaagtcaaaagcctccgaccggaggcttttgactaaaa
cttccctggggttatcattggggctcactcaaaggcggtaat

pSB4A5-AD036, https://benchling.com/s/seq-UjUkSIjGVDMxUO5WwRMB

pLacO, LasR, AAV degtag, pLas81, YPet

tgccacctgacgtctaagaaaaggaatattcagcaatttgcccgtgccgaagaaaggcccacccgtgaaggtgagccagtgagttgattgctacgtaattagttagttagcccttagtgactcgaattcAATTGTGAGCGG
ATAACAATTGACATTGTGAGCGGATAACAAGATACTGAGCACAAAGCTTAGGGTGTCTCAAGGTGCGTACCTTGACTGATGAGTCCGAAAGGACGAAACACCCCT
CTACAAATAATTTTGTTTAAGCGGCCGCACTATGTTTTTCAAAGACGAAAAACTACTAGATGGCCCTGGTAGACGGCTTCTTGGAATTAGAACGTTCTAGTGGCAA
GTTGGAGTGGTCGGCAATCTTGCAAAAAATGGCTTCTGACTTAGGCTTCTCCAAGATTCTGTTTGGTTTGTTACCGAAGGATTCACAGGATTACGAAAACGCATTC
ATCGTCGGGAATTATCCAGCCGCGTGGCGCGAACACTACGATCGCGCTGGGTATGCGCGCGTTGATCCTACCGTGTCGCATTGCACTCAGTCTGTTCTTCCCAT
TTTTTGGGAACCCTCAATCTACCAGACCCGCAAGCAACATGAGTTCTTTGAGGAAGCCTCGGCCGCGGGGCTTGTGTATGGCCTTACGATGCCACTTCATGGTG
CCCGTGGGGAATTGGGAGCACTGTCGCTTCAGTCGAAGCCGAAAACCGCGCTGAGGCCAACCGTTTTATTGAGAGCGTCCTTCCAACTTTATGGATGTTGAAG
GACTATGCCCTTCAATCTGGGGCTGGGTTGGCCTTTGAGCACCCTGTTTCTAAACCAGTAGTTCTTACTTCACGCGAGAAGGAAGTCTTGCAATGGTGTGCTATT
GGAAAGACCTCCTGGGAAATCAGCGTCATTTGCAACTGTTCGGAAGCAAATGTAAATTTTCATATGGGGAACATCCGTCGCAAATTTGGGGTGACGTCCCGTCGT
GTCGCAGCCATCATGGCAGTCAATCTTGGTCTTATCACCTTACGTCCGCCTGCTAATGACGAGAACTATGCTGCGGCTGTCTGATAACTCGAGTTCAGCCAAAAA
ACTTAAGACCGCCGGTCTTGTCCACTACCTTGCAGTAATGCGGTGGACAGGATCGGCGGTTTTCTTTTCTCTTCTCAATTAATTAAACCTATAGGATCGTATAGGTT
TACGCAAGAAAATGGTTTGTTATAGTCGAATAAAATCCATAGCTGTCACCGGATGTGCTTTCCGGTCTGATGAGTCCGTGAGGACGAAACAGCGAGATCAGATAA
TTCTGACGTATCTAGActatggactatgtttgaaagggagaaatactagATGTCAAAGGGAGAAGAATTGTTCACGGGAGTTGTACCCATCTTAGTAGAATTGGACGGAGACGTC
AATGGACACAAGTTCTCCGTTTCGGGAGAGGGGGAGGGGGATGCGACGTATGGTAAATTGACGCTGAAGCTGTTATGTACCACCGGTAAGTTGCCTGTCCCTTG
GCCCACATTAGTAACAACCCTGGGGTACGGCGTGCAATGCTTCGCGCGTTATCCTGACCATATGAAGCAACATGACTTCTTTAAGTCTGCCATGCCTGAAGGATA
TGTTCAAGAGCGCACGATTTTTTTTAAAGATGATGGGAATTATAAAACTCGTGCAGAAGTGAAATTTGAGGGCGACACATTAGTGAACCGCATCGAATTAAAAGGA
ATCGACTTTAAAGAAGATGGAAACATTTTGGGGCACAAATTGGAGTACAATTATAACAGCCATAACGTCTATATCACAGCGGATAAGCAGAAGAATGGCATCAAAG
CGAATTTTAAGATTCGTCACAATATTGAAGATGGGGGAGTTCAACTGGCGGACCATTATCAACAAAATACACCGATCGGTGACGGACCGGTGTTGTTGCCGGACA
ACCACTATTTATCATATCAGAGCGCGTTATTTAAGGACCCGAACGAGAAGCGTGACCACATGGTCCTGTTGGAATTTCTGACAGCCGCTGGTATTACTGAGGGTA
TGAATGAGCTTTACAAACGTCCTGCTGCGAACGACGAAAATTATGCGGCTGCGGTTTGATAAGGAAACACAGAAAAAAGCCCGCACCTGACAGTGCGGGCTTTTT
TTTTCGACCAAAGGTTAATTAAACCgctcactcaaaggcggtaat

pSB4A5-AD037, https://benchling.com/s/seq-hSS4UvilLjOEf0iwKE4k

pTetO, LuxR, AAV degtag, pLux76, YPet

tgccacctgacgtctaagaaaaggaatattcagcaatttgcccgtgccgaagaaaggcccacccgtgaaggtgagccagtgagttgattgctacgtaattagttagttagcccttagtgactcgaattcTCCCTATCAGTG
ATAGAGATTGACATCCCTATCAGTGATAGAGATACTGAGCACAAGCTTAGGGTGTCTCAAGGTGCGTACCTTGACTGATGAGTCCGAAAGGACGAAACACCCCTC

TACAAATAATTTTGTTTAAGCGGCCGCACTATGTTTTTCAAAGACGAAAAACTACTAGATGAAGAACATTAATGCTGATGATACATATCGCATTATTAACAAGATCAA
GGCCTGCCGTTCCAACAACGATATTAATCAATGTTTGAGCGACATGACGAAGATGGTCCATTGTGAATACTACCTGCTGGCGATCATTTACCCACATTCGATGGTG
AAATCCGACATCAGTATTCTGGACAACTACCCCAAGAAATGGCGTCAGTATTATGACGATGCGAATCTGATCAAATATGACCCCATTGTAGACTATAGCAATAGCA
ACCATTCTCCGATTAACTGGAACATCTTTGAAAATAATGCAGTTAACAAGAAGAGTCCGAATGTAATCAAGGAAGCAAAAACATCAGGCTTAATCACTGGATTCTCC
TTCCCGATCCACACAGCCAACAACGGGTTTGGAATGTTGTCTTTCGCACACAGTGAAAAGGATAATTACATTGATAGTCTTTTCCTGCACGCGTGCATGAATATTC
CACTGATCGTGCCTAGTTTGGTAGACAATTACCGCAAGATTAATATTGCTAACAACAAATCTAACAACGACCTGACGAAACGCGAAAAAGAGTGCCTTGCGTGGG
CATGTGAAGGCAAGTCCTCCTGGGATATTTCGAAAATCTTAGGTTGCTCTGAGCGCACTGTGACCTTCCATCTTACGAACGCTCAAATGAAGTTAAATACCACCAA
CCGTTGCCAGTCAATCAGTAAGGCCATCCTGACTGGAGCTATCGACTGCCCATATTTCAAGAACCGTCCCGCTGCTAATGACGAGAACTATGCTGCGGCTGTCT
GATAACTCGAGTTCAGCCAAAAAACTTAAGACCGCCGGTCTTGTCCACTACCTTGCAGTAATGCGGTGGACAGGATCGGCGGTTTTCTTTTCTCTTCTCAACCAT
GGACCTGTAGGATCGTACAAGTTTACGCAAGAAAATGGTTTGTTATAGTCGAATAAAATCCATAGCTGTCACCGGATGTGCTTTCCGGTCTGATGAGTCCGTGAG
GACGAAACAGCGAGATCAGATAATTCTGACGTATCTAGActatggactatgtttgaaagggagaaatactagATGTCAAAGGGAGAAGAATTGTTCACGGGAGTTGTACCCATCT
TAGTAGAATTGGACGGAGACGTCAATGGACACAAGTTCTCCGTTTCGGGAGAGGGGGAGGGGGATGCGACGTATGGTAAATTGACGCTGAAGCTGTTATGTACC
ACCGGTAAGTTGCCTGTCCCTTGGCCCACATTAGTAACAACCCTGGGGTACGGCGTGCAATGCTTCGCGCGTTATCCTGACCATATGAAGCAACATGACTTCTTT
AAGTCTGCCATGCCTGAAGGATATGTTCAAGAGCGCACGATTTTTTTTAAAGATGATGGGAATTATAAAACTCGTGCAGAAGTGAAATTTGAGGGCGACACATTAG
TGAACCGCATCGAATTAAAAGGAATCGACTTTAAAGAAGATGGAAACATTTTGGGGCACAAATTGGAGTACAATTATAACAGCCATAACGTCTATATCACAGCGGA
TAAGCAGAAGAATGGCATCAAAGCGAATTTTAAGATTCGTCACAATATTGAAGATGGGGGAGTTCAACTGGCGGACCATTATCAACAAAATACACCGATCGGTGA
CGGACCGGTGTTGTTGCCGGACAACCACTATTTATCATACAGAGCGCGTTATTTAAGGACCCGAACGAGAAGCGTGACCACATGGTCCTGTTGGAATTCCTCGAC
AGCCGCTGGTATTACTGAGGGTATGAATGAGCTTTACAACGTCCTGCTGCGAACGACGAAAATTATGCGGCTGCGGTTTGATAAGGAAACACAGAAAAAAGCC
CGCACCTGACAGTGCGGGCTTTTTTTTTCGACCAAAGGTTAATTAAACCgctcactcaaaggcggtaat

pSB3C5-AD039, https://benchling.com/s/seq-b2zDOs3i0pDa9QRr3FYb

pLas81, TetR, pJ23106, LasR, pTetO

tgccacctgacgtctaagaaaaggaatatttcagcaatttgcccgtgccgaagaaaggcccacccgtgaaggtgagccagtgagttgattgctacgtaattagttagttagcccttagtgactcgaattcACCTATAGGATC
GTATAGGTTTACGCAAGAAAATGGTTTGTTATAGTCGAATAAAAAGCTTCTATGGACTATGTTTTCACATACGAGGGGGATTAGATGTCGCGTCTGGACAAGAGTAA
AGTGATTAATTCAGCTCTTGAACTGTTGAATGAAGTTGGAATTGAAGGACTTACAACACGTAAGTTAGCACAGAAATTGGGCGTCGAACAACCTACATTGTACTGG
CATGTCAAGAATAAACGTGCGCTTCTGGATGCTCTTGCTATTGAAATGTTGGACCGTCACCACACTCACTTTTGCCCCTTGGAAGGAGAAAGCTGGCAAGATTTTC
TGCGCAACAACGCTAAGTCATTTCGTTGCGCTCTGTTATCCCACCGTGATGGGGCCAAAGTCCACTTGGGCACTCGCCCCACGGAAAAACAGTATGAAACCCTG
GAAAACCAACTTGCTTTCCTGTGTCAACAAGGATTTAGCCTTGAGAATGCATTGTATGCCCTGTCTGCGGTAGGGCACTTTACGTTGGGCTGTGTCTTAGAGGAC
CAGGAGCATCAGGTTGCCAAGGAGGAGCGTGAGACACCTACGACCGACAGTATGCCACCCTTATTACGTCAGGCGATTGAGCTGTTTGACCACCAAGGTGCGG
AACCTGCCTTTCTTTTTGGTCTTGAACTTATCATCTGTGGGTTGGAAAAACAACTTAAATGCGAGTCCGGCAGCTGATAACCAATTATTGAACACCCTTCGGGGTGT
TTTTTTGTTTCTGGTCTACCCTCGAGtttacggctagctcagtcctaggtatagtgctagcTCTAGAGGAGCTATGGACTATGTTTGAAAGGCTGAAATACTAGATGGCCTTAGTTG
ATGGCTTCTTGGAGTTAGAGCGTAGCTCTGGAAAGTTAGAGTGGTCTGCAATCTTGCAAAAGATGGCTTCCGATTTAGGCTTCTCGAAAGATTTTGTTCGGTTTATTA
CCTAAGGACTCACAGGATTACGAAAACGCGTTTATCGTTGGAAACTACCCGGCAGCATGGCGCGAGCATTATGATCGCGCCGGTTATGCGCGTGTAGATCCTAC
GGTAAGTCATTGTACTCAATCGGTCTTACCGATCTTTTGGGAACCTTCAATCTACCAGACACGTAAACAACATGAGTTCTTCGAAGAAGCGTCAGCAGCTGGTTTG
GTGTACGGCCTGACCATGCCTCTGCATGGAGCGCGTGGGGAATTGGGGGCGTTGTCATTGAGTGTAGAAGCTGAGAACCGCGCGGAAGCTAACCGCTTTATCG
AAAGTGTATTGCCTACACTGTGGATGTTGAAAGACTACGCTCTTCAGTCGGGGGCCGGACTTGCGTTCGAACATCCCGTATCGAAGCCTGTCGTACTTACCTCTC
GCGAAAAAGAAGTCTTGCAGTGGTGCGCCATCGGTAAAACGAGCTGGGAAATCTCAGTAATTTGTAACTGCTCAGAAGCTAACGTAAACTTCCACATGGGCAATA
TCCGTCGTAAGTTTGGAGTCACGTCCCGTCGTGTCGCTGCTATCATGGCGGTCAACTTGGGCCTTATTACTTTATGATAATCCGGCAATTAAAAAAGCGGCTAAC
CACGCCGCTTTTTTTACGTCTGCActgcaTTCCCTATCAGTGATAGAGACAAGGCTCCCTATCAGTGATAGAGAAGCTGGGCACCTGCATTCCCTATCAGTGATAGA
GACAAGGCTCCCTATCAGTGATAGAGAAGCTGGGCACCTGCAggagtcactaagggttagttagttagattagcagaaagtcaaaagcctccgaccggaggcttttgactaaaacttccctggggttta
tcattggggctcactcaaaggcggtaat

pSB3C5-AD040, https://benchling.com/s/seq-pS3Xzkw80aTHUJ3vgWIw

pLux76, LacI, pJ23106, LuxR, pLacO

tgccacctgacgtctaagaaaaggaatatttcagcaatttgcccgtgccgaagaaaggcccacccgtgaaggtgagccagtgagttgattgctacgtaattagttagttagcccttagtgactcgaattcACCTGTAGGATC
GTACAAGTTTACGCAAGAAAATGGTTTGTTATAGTCGAATAAAAAGCTTCTATGGACTATGTTTTCACATACGAGGGGGATTAGATGAAACCAGTGACACTTTACGA
TGTCGCCGAATATGCGGGCGTTTCGTACCAGACTGTATCACGTGTAGTGAATCAAGCGTCGCACGTCAGCGCTAAGACTCGTGAAAAAGTGGAAGCTGCGATGG
CCGAGTTGAACTACATTCCGAATCGTGTTGCACAACAACTGGCAGGAAAACAAAGTTTATTAATTGGTGTGGCCACGTCAAGCCTGGCCTTGCACGCACCCTCG
CAAATCGTTGCTGCGATCAAGAGTCGTGCGGATCAGTTAGGAGCATCCGTCGTTGTATCGATGGTCGAACGTAGTGGAGTGGAGGCATGTAAAGCGGCTGTGCA
CAATCTTCTTGCCCAGCGTGTTTCTGGGCTGATTATTAACTACCCTCTGGATGACCAAGACGCGATTGCCGTTGAAGCTGCGTGCACAAACGTTCCGGCCCTGTT
CCTTGACGTATCAGACCAAACACCTATCAACAGTATCATCTTTAGTCACGAAGATGGTACGCGTTTAGGAGTGGAGCATTTAGTAGCTTTGGGTCACCAGCAGATC
GCATTATTAGCGGGGCCGCTTAGTAGCGTATCCGCCCGCCTGCGCCTGGCTGGCTGGCACAAGTACCTTACTCGCAACCAGATCCAGCCGATCGCAGAGCGT
GAAGGTGACTGGTCGGCGATGTCCGGATTTCAACAGACGATGCAAATGTTAAATGAGGGCATTGTACCTACTGCTATGCTGGTGGCCAACGACCAGATGGCACT
GGGGGCGATGCGTGCAATCACTGAATCTGGCCTTCGCGTTGGCGCAGACATTTCCGTCGTTGGCTATGATGATACAGAAGACTCAAGTTGCTATATCCCCCCAC
TTACGACAATCAAACAGGATTTCCGTTTGCTTGGTCAAACCTCCGTTGACCGTTTGCTGCAACTTAGCCAGGGGCAGGCGGTGAAGGGAAATCAGTTACTTCCTG
TGAGTTTAGTAAAACGCAAGACCACGTTAGCACCTAATACTCAGACGGCAAGCCCACGTGCTTTAGCTGACAGTTTAATGCAACTGGCTCGTCAAGTATCTCGTC
TTGAAAGTGGTCAATGATAACCAATTATTGAACACCCTTCGGGGTGTTTTTTTGTTTCTGGTCTACCCTCGAGtttacggctagctcagtcctaggtatagtgctagcTCTAGAGGA
GCTATGGACTATGTTTGAAAGGCTGAAATACTAGATGAAGAATATTAACGCGGACGATACATATCGCATTATCAACAAGATCAAGGCGTGTCGCTCTAATAACGAC
ATCAACCAGTGCTTGAGTGATATGACTAAGATGGTACATTGCGAGTACTATTTGCTGGCGATTATCTATCCGCATTCAATGGTTAAGTCGGATATTTCTATCTTAGAT
AACTATCCCAAAAAATGGCGTCAATACTACGACGACGCCAATCTGATTAAATACGACCCTATCGTGGATTATTCCAATTCCAACCATTCGCCGATCAATTGGAATAT
CTTCGAGAACAATGCTGTGAACAAAAAGTCTCCCAACGTGATTAAGGAGGCTAAAACCTCCGGTTTAATTACCGGTTTTAGTTTCCCAATTCATACCGCAAACAAC
GGTTTCGGAATGTTGTCCTTCGCACATAGCGAGAAAGATAATTATATCGACTCGCTTTTTTTGCACGCGTGTATGAATATTCCCTTGATCGTACCTAGTCTGGTGGA
TAACTACCGTAAAATTAATATTGCGAATAATAAGTCGAACAACGACCTTACAAAACGTGAGAAGGAATGTCTGGCATGGGCGTGTGAAGGTAAGTCCTCGTGGGA
TATTTCTAAGATCCTTGGTTGTAGCGAGCGTACCGTTACCTTTCATTTGACTAATGCCCAAATGAAGTTAAACACGACTAATCGTTGCCAGTCTATCTCAAAAGCAA
TTCTTACCGGGGCCATCGACTGTCCGTACTTCAAGAATTGATAATCCGGCAATTAAAAAAGCGGCTAACCACGCCGCTTTTTTTACGTCTGCActgcaTAATTGTGA
GCGGATAACAACAAGGCTTGTGAGCGGATAACAAAGCTGGGAGCACACTGCATAATTGTGAGCGGATAACAACAAGGCTTGTGAGCGGATAACAAAGCTGGGA
GCACACTGCAggagtcactaagggttagttagttagattagcagaaagtcaaaagcctccgaccggaggcttttgactaaaacttccctggggttatcattggggctcactcaaaggcggtaat

pSB4A5-AD041, https://benchling.com/s/seq-ObuMhhs5BgYdfZVK1ysm

pLacO, LasR, AAV degtag, mScarletI

tgccacctgacgtctaagaaaaggaatatttcagcaatttgcccgtgccgaagaaaggcccacccgtgaaggtgagccagtgagttgattgctacgtaattagttagttagcccttagtgactcgaattcAATTGTGAGCGG
ATAACAATTGACATTGTGAGCGGATAACAAGATACTGAGCACAAAGCTTAGGGTGTCTCAAGGTGCGTACCTTGACTGATGAGTCCGAAAGGACGAAACACCCCT
CTACAAATAATTTTGTTTAAGCGGCCGCACTATGTTTTTCAAAGACGAAAAACTACTAGATGGCCCTGGTAGACGGCTTCTTGGAATTAGAACGTTCTAGTGGCAA
GTTGGAGTGGTCGGCAATCTTGCAAAAAATGGCTTCTGACTTAGGCTTCTCCAAGATTCTGTTTGGTTTGTTACCGAAGGATTCACAGGATTACGAAAACGCATTC
ATCGTCGGGAATTATCCAGCCGCGTGGCGCGAACACTACGATCGCGCTGGGTATGCGCGCGTTGATCCTACCGTGTCGCATTGCACTCAGTCTGTTCTTCCCAT
TTTTTGGGAACCCTCAATCTACCAGACCCGCAAGCAACATGAGTTCTTTGAGGAAGCCTCGGCCGCGGGGCTTGTGTATGGCCTTACGATGCCACTTCATGGTG
CCCGTGGGGAATTGGGAGCACTGTCGCTTTCAGTCGAAGCCGAAAACCGCGCTGAGGCCAACCGTTTTATTGAGAGCGTCCTTCCAACTTTATGGATGTTGAAG
GACTATGCCCTTCAATCTGGGGCTGGGTTGGCCTTGAGCACCCTGTTTCTAAACCAGTAGTTCTTACTTCACGCGAGAAGGAAGTCTTGCAATGGTGTGCTATT
GGAAAGACCTCCTGGGAAATCAGCGTCATTTGCAACTGTTCGGAAGCAAATGTAAATTTTCATATGGGGAACATCCGTCGCAAATTTGGGGTGACGTCCCGTCGT
GTCGCAGCCATCATGGCAGTCAATCTTGGTCTTATCACCTTACGTCCCGCTGCTAATGACGAGAACTATGCTGCGGCTGTCTGATAACTCGAGAGCTGTCACCG
GATGTGCTTTCCGGTCTGATGAGTCCGTGAGGACGAAACAGCGAGATCAGATAATTCTGACGTATCTAGActatggactatgtttgaaagggagaaatactagATGGTGTCAAA
GGGAGAGGCGGTTATCAAGGAATTTATGCGCTTTAAAGTCCACATGGAGGGCAGCATGAACGGGCACGAGTTTGAAATTGAGGGGGAGGGGGAGGGCCGTCCT
TATGAAGGTACTCAGACTGCTAAACTGAAGGTGACAAAAGGTGGCCCCTTGCCTTTCTCGTGGGACATCCTGTCGCCACAATTCATGTACGGGAGCCGCGCCTT
TATCAAACATCCCGCAGATATTCCTGATTACTATAAACAATCTTTCCCGGAAGGTTTCAAATGGGAACGCGTCATGAATTTTGAGGACGGGGGCGCTGTCACAGTT
ACTCAGGACACCTCCTTGGAAGACGGCACATTGATTTACAAGGTTAAGTTGCGCGGCACAAACTTCCCCCCTGACGGGCCAGTAATGCAAAAGAAAACTATGGG
TTGGGAGGCGTCTACAGAACGTTTATACCCCGAAGACGGGGTGCTGAAAGGTGACATTAAGATGGCCCTGCGCCTGAAGGACGGCGGTCGCTATCTTGCCGAC
TTTAAAACTACTTATAAGGCTAAAAAACCAGTCCAGATGCCAGGCGCCTATAATGTTGACCGCAAGTTAGACATCACCTCACATAATGAAGACTATACCGTTGTAG

AACAATACGAGCGCAGCGAGGGTCGTCACAGTACCGGGGGGGATGGATGAATTATACAAACGTCCTGCTGCGAACGACGAAAATTATGCGGCTGCGGTTTGATAA
GGAAACACAGAAAAAAGCCCGCACCTGACAGTGCGGGCTTTTTTTTTCGACCAAAGGTTAATTAAACCgctcactcaaaggcggtaat

pSB4A5-AD042, https://benchling.com/s/seq-wJ9Q2f5rRjOwJwTSo95l

pTetO, ribozymes, LuxR, AAV degtag, RBS P1, YPet, pLux76, LuxI

tgccacctgacgtctaagaaaaggaatattcagcaatttgcccgtgccgaagaaaggcccacccgtgaaggtgagccagtgagttgattgctacgtaattagttagttagcccttagtgactcgaattcTCCCTATCAGTG
ATAGAGATTGACATCCCTATCAGTGATAGAGATACTGAGCACAAGCTTAGGGTGTCTCAAGGTGCGTACCTTGACTGATGAGTCCGAAAGGACGAAACACCCCTC
TACAAATAATTTTGTTTAAGCGGCCGCACTATGTTTTTCAAAGACGAAAAACTACTAGATGAAGAACATTAATGCTGATGATACATATCGCATTATTAACAAGATCAA
GGCCTGCCGTTCCAACAACGATATTAATCAATGTTTGAGCGACATGACGAAGATGGTCCATTGTGAATACTACCTGCTGGCGATCATTTACCCACATTCGATGGTG
AAATCCGACATCAGTATTCTGGACAACTACCCCAAGAAATGGCGTCAGTATTATGACGATGCGAATCTGATCAAATATGACCCCATTGTAGACTATAGCAATAGCA
ACCATTCTCCGATTAACTGGAACATCTTTGAAAATAATGCAGTTAACAAGAAGAGTCCGAATGTAATCAAGGAAGCAAAAACATCAGGCTTAATCACTGGATTCTCC
TTCCCGATCCACACAGCCAACAACGGGTTTGGAATGTTGTCTTTCGCACACAGTGAAAAGGATAATTACATTGATAGTCTTTTCCTGCACGCGTGCATGAATATTC
CACTGATCGTGCCTAGTTTGGTAGACAATTACCGCAAGATTAATATTGCTAACAACAAATCTAACAACGACCTGACGAAACGCGAAAAAGAGTGCCTTGCGTGGG
CATGTGAAGGCAAGTCCTCCTGGGATATTTCGAAAATCTTAGGTTGCTCTGAGCGCACTGTGACCTTCCATCTTACGAACGCTCAAATGAAGTTAAATACCACCAA
CCGTTGCCAGTCAATCAGTAAGGCCATCCTGACTGGAGCTATCGACTGCCCATATTTCAAGAACCGTCCCGCTGCTAATGACGAGAACTATGCTGCGGCTGTCT
GATAACTCGAGTTCAGCCAAAAAACTTAAGACCGCCGGTCTTGTCCACTACCTTGCAGTAATGCGGTGGACAGGATCGGCGGTTTTCTTTTCTCTTCTCAACCAT
GGTCCCTATCAGTGATAGAGATTGACATCCCTATCAGTGATAGAGATACTGAGCACATCCATAGCTGTCACCGGATGTGCTTTCCGGTCTGATGAGTCCGTGAGG
ACGAAACAGCGAGATCAGATAATTCTGACGTATCTAGActatggactatgtttgaaaggagaaatactagATGTCAAAGGGAGAAGAATTGTTCACGGGAGTTGTACCCATCTT
AGTAGAATTGGACGGAGACGTCAATGGACACAAGTTCTCCGTTTCGGGAGAGGGGGAGGGGGATGCGACGTATGGTAAATTGACGCTGAAGCTGTTATGTACCA
CCGGTAAGTTGCCTGTCCCTTGGCCACATTAGTAACAACCCTGGGGTACGGCGTGCAATGCTTCCGCGCGTTATCCTGACCATATGAAGCAACATGACTTCTTTA
AGTCTGCCATGCCTGAAGGATATGTTCAAGAGCGCACGATTTTTTTTAAAGATGATGGGAATTATAAAACTCGTGCAGAAGTGAAATTTGAGGGCGACACATTAGT
GAACCGCATCGAATTAAAAGGAATCGACTTTAAAGAAGATGGAAACATTTTGGGGCACAAATTGGAGTACAATTATAACAGCCATAACGTCTATATCACAGCGGAT
AAGCAGAAGAATGGCATCAAAGCGAATTTTAAGATTCGTCACAATATTGAAGATGGGGGAGTTCAACTGGCGGACCATTATCAACAAAATACACCGATCGGTGAC
GGACCGGTGTTGTTGCCGGACAACCACTATTTATCATATCAGAGCGCGTTATTTAAGGACCCGAACGAGAAGCGTGACCACATGGTCCTGTTGGAATTTCTGACA
GCCGCTGGTATTACTGAGGGTATGAATGAGCTTTACAAACGTCCTGCTGCGAACGACGAAAATTATGCGGCTGCGGTTTGATAAGGAAACACAGAAAAAAGCCC
GCACCTGACAGTGCGGGCTTTTTTTTTCGACCAAAGGTTAATTAAACCTGTAGGATCGTACAAGTTTACGCAAGAAAATGGTTTGTTATAGTCGAATAAACCTAGGC
CCCCCGAGGAGTAGCACATGACAATTATGATTAAGAAGAGCGATTTCTTAGCAATCCCCTCCGAGGAATATAAAGGCATCCTGTCTCTTCGCTACCAGGTGTTCA
AACAGCGTCTGGAATGGGATTTAGTGGTTGAAAATAATTTGGAATCCGACGAGTACGATAACAGCAACGCTGAGTATATTTATGCCTGCGACGATACAGAAAACGT
CAGTGGATGCTGGCGCCTGCTGCCCACAACCGGTGATTATATGTTGAAGTCAGTATTCCCCGAGCTTCTGGGGCGAGCAGTCGGCGCCCAAAGATCCTAACATC
GTTGAATTGAGTCGTTTTGCTGTTGGCAAGAACTCCTCTAAAATCAATAATTCCGCAAGTGAGATCACGATGAAACTGTTTGAAGCTATCTATAAGCATGCAGTAAG
TCAAGGGATCACGGAGTACGTCACGGTCACGTCTACCGCAATTGAACGCTTCTTGAAACGTATCAAAGTTCCCTGCCACCGCATCGGAGATAAGGAAATTCACG
TACTGGGCGATACTAAGTCCGTGGTCCTTTCGATGCCAATCAACGAGCAATTCAAAAAAGCTGTCTTAAATTGATAATCCGGCAATTAAAAAAGCGGCTAACCACG
CCGCTTTTTTTACGTCTGCActgcaggagtcactaagggttagttagttagattagcagaaagtcaaaagcctccgaccggaggcttttgactaaaacttcccttggggttatcattggggctcactcaaaggcggtaa
t

pSB4A5-AD043, https://benchling.com/s/seq-zJuluQvDtlU4d6iTV7QB

pLacO, ribozymes, LasR, AAV degtag, RBS P1, mScarletI, pLas81, LasI

tgccacctgacgtctaagaaaaggaatattcagcaatttgcccgtgccgaagaaaggcccacccgtgaaggtgagccagtgagttgattgctacgtaattagttagttagcccttagtgactcgaattcAATTGTGAGCGG
ATAACAATTGACATTGTGAGCGGATAACAAGATACTGAGCACAAAGCTTAGGGTGTCTCAAGGTGCGTACCTTGACTGATGAGTCCGAAAGGACGAAACACCCCT
CTACAAATAATTTTGTTTAAGCGGCCGCACTATGTTTTTCAAAGACGAAAAACTACTAGATGGCCCTGGTAGACGGCTTCTTGGAATTAGAACGTTCTAGTGGCAA
GTTGGAGTGGTCGGCAATCTTGCAAAAAATGGCTTCTGACTTAGGCTTCTCCAAGATTCTGTTTGGTTTGTTACCGAAGGATTCACGAAAACGCATTC
ATCGTCGGGAATTATCCAGCCGCGTGGCGCGAACACTACGATCGCGCTGGGTATGCGCGCGTTGATCCTACCGTGTCGCATTGCACTCAGTCTGTTCTTCCCAT
TTTTTGGGAACCCTCAATCTACCAGACCCGCAAGCAACATGAGTTCTTTGAGGAAGCCTCGGCCGCGGGGCTTGTGTATGGCCTTACGATGCCACTTCATGGTG
CCCGTGGGGAATTGGGAGCACTGTCGCTTTCAGTCGAAGCCGAAAACCGCGCTGAGGCCAACCGTTTTATTGAGAGCGTCCTTCCAACTTTATGGATGTTGAAG
GACTATGCCCTTCAATCTGGGGCTGGGTTGGCCTTTGAGCACCCTGTTTCTAAACCAGTAGTTCTTACTTCACGCGAGAAGGAAGTCTTGCAATGGTGTGCTATT
GGAAAGACCTCCTGGGAAATCAGCGTCATTTGCAACTGTTCGGAAGCAAATGTAAATTTTCATATGGGGAACATCCGTCGCAAATTTGGGGTGACGTCCGTCGT
GTCGCAGCCATCATGGCAGTCAATCTTGGTCTTATCACCTTACGTCCCGCTGCTAATGACGAGAACTATGCTGCGGCTGTCTGATAACTCGAGTTCAGCCAAAAA
ACTTAAGACCGCCGGTCTTGTCCACTACCTTGCAGTAATGCGGTGGACAGGATCGGCGGTTTTCTTTTCTCTTCTCAATTAATTAAAATTGTGAGCGGATAACAATT
GACATTGTGAGCGGATAACAAGATACTGAGCACAATCCATAGCTGTCACCGGATGTGCTTTCCGGTCTGATGAGTCCGTGAGGACGAAACAGCGAGATCAGATA
ATTCTGACGTATCTAGActatggactatgtttgaaaggagaaatactagATGGTGTCAAAGGGAGAGGCGGTTATCAAGGAATTTATGCGCTTTAAAGTCCACATGGAGGGCA
GCATGAACGGGCACGAGTTTGAAATTGAGGGGGAGGGGGAGGGCCGTCCTTATGAAGGTACTCAGACTGCTAAACTGAAGGTGACAAAAGGTGGCCCCTTGCC
TTTCTCGTGGGACATCCTGTCGCCACAATTCATGTACGGGAGCCGCGCCTTTATCAAACATCCCGCAGATATTCCTGATTACTATAAACAATCTTTCCCGGAAGGT
TTCAAATGGGAACGCGTCATGAATTTTGAGGACGGGGGCGCTGTCACAGTTACTCAGGACACCTCCTTGGAAGACGGCACATTGATTTACAAGGTTAAGTTGCG
CGGCACAAACTTCCCCCCTGACGGGCCAGTAATGCAAAAGAAAACTATGGGTTGGGAGGCGTCTACAGAACGTTTATACCCCGAAGACGGGGTGCTGAAAGGT
GACATTAAGATGGCCCTGCGCCTGAAGGACGGCGGTCGCTATCTTGCCGACTTTAAAACTACTTATAAGGCTAAAAAACCAGTCCAGATGCCAGGCGCCTATAAT
GTTGACCGCAAGTTAGACATCACCTCACATAATGAAGACTATACCGTTGTAGAACAATACGAGCGCAGCGAGGGTCGTCACAGTACCGGGGGGATGGATGAATTT
ATACAAACGTCCTGCTGCGAACGACGAAAATTATGCGGCTGCGGTTTGATAAGGAAACACAGAAAAAAGCCCGCACCTGACAGTGCGGGCTTTTTTTTTCGACCA
AAGGTTAATTAAACCTATAGGATCGTATAGGTTTACGCAAGAAAATGGTTTGTTATAGTCGAATAAACCTAGGCCCCCCGAGGAGTAGCACATGATTGTGCAAATC
GGCCGCCGTGAGGAGTTCGATAAAAAGCTGCTTGGGGAAATGCATAAACTTCGTGCTCAGGTGTTCAAGGAGCGTAAGGGGTGGGATGTTTCCGTTATTGACGA
AATGGAAATTGATGGGTACGATGCATTATCACCTTACTATATGCTGATTCAAGAAGACACACCTGAGGCCCAGGTATTCGGTTGCTGGCGCATTTTGACACGACG
GGGCCTTACATGTTGAAGAACACGTTTCCTGAATTGTTACACGGCAAAGAAGCTCCCTGCTCACCCCATATTTGGGAACTGAGCCGTTTCGCTATCAATTCCGGT
CAAAAGGGCTCCCTGGGCTTTTCGGACTGCACCCTTGAAGCCATGCGCGCACTTGCCCGTTACTCCCTGCAAAACGACATTCAAACCTTAGTTACTGTTACTACC
GTTGGCGTAGAGAAGATGATGATCCGTGCGGGTCTTGACGTATCTCGCTTTGGACCGCATCTGAAGATTGGAATCGAGCGTGCGGTGGCGTTGCGCATCGAATT
GAACGCAAAAACGCAAATTGCGTTATACGGCGGGGTCTTGGTTGAACAGCGTTTAGCCGTGAGTTGATAATCCGGCAATTAAAAAAGCGGCTAACCACGCCGCT
TTTTTTACGTCTGCActgcaggagtcactaagggttagttagttagattagcagaaagtcaaaagcctccgaccggaggcttttgactaaaacttcccttggggttatcattggggctcactcaaaggcggtaat

pSB4A5-AD044, https://benchling.com/s/seq-qs9W2Wp3Lr3wSYGjYKFB

pTetO, LuxR, AAV degtag, GFP, pLux76, LuxI

tgccacctgacgtctaagaaaaggaatattcagcaatttgcccgtgccgaagaaaggcccacccgtgaaggtgagccagtgagttgattgctacgtaattagttagttagcccttagtgactcgaattcTCCCTATCAGTG
ATAGAGATTGACATCCCTATCAGTGATAGAGATACTGAGCACAAGCTTAGGGTGTCTCAAGGTGCGTACCTTGACTGATGAGTCCGAAAGGACGAAACACCCCTC
TACAAATAATTTTGTTTAAGCGGCCGCACTATGTTTTTCAAAGACGAAAAACTACTAGATGAAGAACATTAATGCTGATGATACATATCGCATTATTAACAAGATCAA
GGCCTGCCGTTCCAACAACGATATTAATCAATGTTTGAGCGACATGACGAAGATGGTCCATTGTGAATACTACCTGCTGGCGATCATTTACCCACATTCGATGGTG
AAATCCGACATCAGTATTCTGGACAACTACCCCAAGAAATGGCGTCAGTATTATGACGATGCGAATCTGATCAAATATGACCCCATTGTAGACTATAGCAATAGCA
ACCATTCTCCGATTAACTGGAACATCTTTGAAAATAATGCAGTTAACAAGAAGAGTCCGAATGTAATCAAGGAAGCAAAAACATCAGGCTTAATCACTGGATTCTCC
TTCCCGATCCACACAGCCAACAACGGGTTTGGAATGTTGTCTTTCGCACACAGTGAAAAGGATAATTACATTGATAGTCTTTTCCTGCACGCGTGCATGAATATTC
CACTGATCGTGCCTAGTTTGGTAGACAATTACCGCAAGATTAATATTGCTAACAACAAATCTAACAACGACCTGACGAAACGCGAAAAAGAGTGCCTTGCGTGGG
CATGTGAAGGCAAGTCCTCCTGGGATATTTCGAAAATCTTAGGTTGCTCTGAGCGCACTGTGACCTTCCATCTTACGAACGCTCAAATGAAGTTAAATACCACCAA
CCGTTGCCAGTCAATCAGTAAGGCCATCCTGACTGGAGCTATCGACTGCCCATATTTCAAGAACCGTCCCGCTGCTAATGACGAGAACTATGCTGCGGCTGTCT
GATAACTCGAGAGCTGTCACCGGATGTGCTTTCCGGTCTGATGAGTCCGTGAGGACGAAACAGCGAGATCAGATAATTCTGACGTATCTAGActatgtttgaaa
gggagaaatactagATGcgtaaaggagaagaacttttcactggagttgtcccaattcttgttgaattagatggtgatgttaatgggcacaaatttttctgtcagtggagagggtgaaggtgatgcaacatacggaaaacttaccctt
aaatttatttgcacactgtggaaaactacctgttccatggccaacacttgtcactactttcggttatggtgttcaatgctttgcgagatacccagatcatatgaaacagcatgactttttcaagagtgccatgcccgaaggttatgtacag
gaaagaactatatttttcaaagatgacgggaactacaagcacacgtgctgaagtcaagtttgaaggtgataccctgttaatagaatcgagttaaaaggtattgattttaaagaagatggaaacattcttggacacaaattggaatac
actataactcacacaatgtatacatcatggcagacaaacaaaagaatggaatcaaagttaacttcaaaattagacacaacattgaagatggaagcgttcaactagcagaccattatcaacaaaatactccaattggcgatggcc
ctgtcctttaccagacaaccattacctgtccacacaatctgccctttcgaaagatcccaacgaaaagagagaccacatgtccttcttgagtttgtaacagctgctgggattacacatggcatggatgaactatacaaaTAAGG
AAACACAGAAAAAAGCCCGCACCTGACAGTGCGGGCTTTTTTTTTCGACCAAAGGTTAATTAAACCTGTAGGATCGTACAAGTTTACGCAAGAAAATGGTTTGTTA
TAGTCGAATAAACCTAGGCCCCCCGAGGAGTAGCACATGACAATTATGATTAAGAAGAGCGATTTCTTAGCAATCCCCTCCGAGGAATATAAAGGCATCCTGTCT
CTTCGCTACCAGGTGTTCAAACAGCGTCTGGAATGGGATTTAGTGGTTGAAAATAATTTGGAATCCGACGAGTACGATAACAGCAACGCTGAGTATATTTATGCCT
GCGACGATACAGAAAACGTCAGTGGATGCTGGCGCCTGCTGCCCACAACCGGTGATTATATGTTGAAGTCAGTATTCCCCGAGCTTCTGGGGCAGCAGTCGGC

GCCCAAAGATCCTAACATCGTTGAATTGAGTCGTTTTGCTGTTGGCAAGAACTCCTCTAAAATCAATAATTCCGCAAGTGAGATCACGATGAAACTGTTTGAAGCTA
TCTATAAGCATGCAGTAAGTCAAGGGATCACGGAGTACGTCACGGTCACGTCTACCGCAATTGAACGCTTCTTGAAACGTATCAAAGTTCCCTGCCACCGCATCG
GAGATAAGGAAATTCACGTACTGGGCGATACTAAGTCCGTGGTCCTTTCGATGCCAATCAACGAGCAATTCAAAAAAGCTGTCTTAAATTGATAATCCGGCAATTA
AAAAAGCGGCTAACCACGCCGCTTTTTTTACGTCTGCActgcaggagtcactaagggttagttagtagattagcagaaagtcaaaagcctccgaccggaggcttttgactaaaacttccctgggggttatc
attggggctcactcaaaggcggtaat

pSB4A5-AD045, https://benchling.com/s/seq-zsxhO2w22tCmc23L0AZB

pTetO, LuxR, AAV degtag, mCerulean, pLux76, LuxI

tgccacctgacgtctaagaaaaggaatattcagcaatttgcccgtgccgaagaaaggcccacccgtgaaggtgagccagtgagttgattgctacgtaattagttagttagcccttagtgactcgaattcTCCCTATCAGTG
ATAGAGATTGACATCCCTATCAGTGATAGAGATACTGAGCACAAGCTTAGGGTGTCTCAAGGTGCGTACCTTGACTGATGAGTCCGAAAGGACGAAACACCCCTC
TACAAATAATTTTGTTTAAGCGGCCGCACTATGTTTTTCAAAGACGAAAAACTACTAGATGAAGAACATTAATGCTGATGATACATATCGCATTATTAACAAGATCAA
GGCCTGCCGTTCCAACAACGATATTAATCAATGTTTGAGCGACATGACGAAGATGGTCCATTGTGAATACTACCTGCTGGCGATCATTTACCCACATTCGATGGTG
AAATCCGACATCAGTATTCTGGACAACTACCCCAAGAAATGGCGTCAGTATTATGACGATGCGAATCTGATCAAATATGACCCCATTGTAGACTATAGCAATAGCA
ACCATTCTCCGATTAACTGGAACATCTTTGAAAATAATGCAGTTAACAAGAAGAGTCCGAATGTAATCAAGGAAGCAAAAACATCAGGCTTAATCACTGGATTCTCG
TTCCCGATCCACACAGCCAACAACGGGTTTGGAATGTTGTCTTTCGCACACAGTGAAAAGGATAATTACATTGATAGTCTTTTCCTGCACGCGTGCATGAATATTC
CACTGATCGTGCCTAGTTTGGTAGACAATTACCGCAAGATTAATATTGCTAACAACAAATCTAACAACGACCTGACGAAACGCGAAAAAGAGTGCCTTGCGTGGG
CATGTGAAGGCAAGTCCTCCTGGGATATTTCGAAAATCTTAGGTTGCTCTGAGCGCACTGTGACCTTCCATCTTACGAACGCTCAAATGAAGTTAAATACCACCAA
CCGTTGCCAGTCAATCAGTAAGGCCATCCTGACTGGAGCTATCGACTGCCCATATTTCAAGAACCGTCCCGCTGCTAATGACGAGAACTATGCTGCGGCTGTCT
GATAACTCGAGAGCTGTCACCGGATGTGCTTTCCGGTCTGATGAGTCCGTGAGGACGAAACAGCGAGATCAGATAATTCTGACGTATCTAGActatggactatgtttgaaa
gggagaaatactagATGGTGAGTAAAGGCGAAGAGCTGTTCACAGGGGTTGTTCCGATTCTGGTCGAACTGGACGGGGACGTTAATGGTCACAAATTCAGCGTTAGC
GGTGAGGGCGAGGGTGATGCCACTTATGGTAAACTGACCCTGAAATTCATCTGTACCACCGGCAAACTGCCTGTTCCTTGGCCTACACTGGTTACAACACTGAC
TTGGGGTGTTCAATGTTTTGCTCGCTATCCGGATCACATGAAACAGCACGATTTCTTCAAAAGCGCCATGCCTGAAGGTTATGTCCAAGAGCGTACGATCTTCTTT
AAAGACGACGGCAACTATAAAACCCGTGCCGAGGTGAAATTCGAAGGTGATACCCTGGTAAACCGTATCGAACTGAAAGGGATCGACTTCAAAGAGGACGGGAA
CATTCTGGGCCATAAACTGGAGTATAACGCCATCAGCGATAATGTGTATATTACCGCCGACAAACAGAAAAACGGGATCAAAGCCAACTTCAAAATCCGCCACAA
CATCGAGGATGGTAGCGTTCAACTGGCCGATCACTATCAACAGAATACCCCGATTGGTGATGGTCCTGTTCTGCTGCCTGATAACCACTATCTGAGCACCCAGTC
TAAACTGTCCAAAGACCCGAACGAGAAACGTGATCACATGGTTCTGCTGGAGTTTGTTACCGCTGCCGGCATTACTCTGGAGTATGGATGAACTGTATAAATAAGG
AAACACAGAAAAAAGCCCGCACCTGACAGTGCGGGCTTTTTTTTTCGACCAAAGGTTAATTAAACCTGTAGGATCGTACAAGTTTACGCAAGAAAATGGTTTGTTA
TAGTCGAATAAACCTAGGCCCCCCGAGGAGTAGCACATGACAATTATGATTAAGAAGAGCGATTTCTTAGCAATCCCCTCCGAGGAATATAAAGGCATCCTGTCT
CTTCGCTACCAGGTGTTCAAACAGCGTCTGGAATGGGATTTAGTGGTTGAAAATAATTTGGAATCCGAGATACGATAACAGCAACGCTGAGTATATTTATGCCT
GCGACGATACAGAAAACGTCAGTGGATGCTGGCGCCTGCTGCCCACAACCGGTGATTATATGTTGAAGTCAGTATTCCCCGAGCTTCTGGGGCAGCAGTCGGC
GCCCAAAGATCCTAACATCGTTGAATTGAGTCGTTTTGCTGTTGGCAAGAACTCCTCTAAAATCAATAATTCCGCAAGTGAGATCACGATGAAACTGTTTGAAGCTA
TCTATAAGCATGCAGTAAGTCAAGGGATCACGGAGTACGTCACGGTCACGTCTACCGCAATTGAACGCTTCTTGAAACGTATCAAAGTTCCCTGCCACCGCATCG
GAGATAAGGAAATTCACGTACTGGGCGATACTAAGTCCGTGGTCCTTTCGATGCCAATCAACGAGCAATTCAAAAAAGCTGTCTTAAATTGATAATCCGGCAATTA
AAAAAGCGGCTAACCACGCCGCTTTTTTTACGTCTGCActgcaggagtcactaagggttagttagtagattagcagaaagtcaaaagcctccgaccggaggcttttgactaaaacttccctgggggttatc
attggggctcactcaaaggcggtaat

pSB1C3-AD046, https://benchling.com/s/seq-Zn8wTqtM7l3XK4ukdn9k

pJ23106, mTq2, Biv-Tat

tgccacctgacgtctaagaaaccattattatcatgacattaacctataaaaatagggcgtatcacgaggcagaatttcagataaaaaaaatccttagcttttcgctaaggatgatttctggaattcgAgTAAgccgcttctagagcac
CGATTGAGAAGAGAAAAGAAAACCGCCGATCCTGTCCACCGCATTACTGCAAGGTAGTGGACAAGACCGGCGGTCTTAAGTTTTTTGGCTGAAagtagtaccaTTAA
CGACGAATGCGACGACCCTTACCGCGGGTACCACGAGGACGCGGACCGCTGCTGCCGCCGCCACCACGGGTCTTGTACAGTTCGTCCATACCCAGCGTGATA
CCCGCCGCGGTAACAAATTCCAGCAGGACCATGTGGTCACGTTTTTCGTTCGGATCTTTGGACAGTTTGGATTGCGTGCTCAAGTAGTGATTATCTGGCAGCAGG
ACCGGACCATCGCCAATCGGGGGTGTTCTGTTGATAGTGATCGGCCAATTGCACGCCGCCATCTTCAATATTGTGACGGATCTTGAAGTTTGCTTTAATGCCGTTTT
TCTGTTTATCAGCGGTGATGTACACATTGTCGCTGAAGTAATTATACTCCAGTTTGTGACCCAGGATGTTACCGTCCTCTTTAAAGTCAATACCTTTCAGCTCAATA
CGATTCACCAGCGTGTCACCCTCGAACTTGACTTCTGCGCGGGTCTTATAGTTACCGTCGTCTTTGAAAAAGATCGTACGTTCCTGAACGTAGCCTTCCGGCATC
GCGCTCTTAAAGAAGTCATGCTGTTTCATGTGATCCGGATAGCGCGCGAAACATTGCACGCCCCACGACAGAGTCGTCACCAGGGTCGGCCACGGAACCGGCA
GCTTACCGGTCGTGCAGATAAACTTCAGGGTCAATTTACCGTAGGTGGCGTCGCCCTCGCCCTCACCGCTAACGCTAAACTTGTGACCGTTGACATCACCATCC
AGCTCAACCAGAATCGGCACGACGCCGGTGAACAGTTCTTCACCCTTGCTAACCATGTCTAtttctcctctttACTGACTGAAGCTTCgctagcactatacctaggactgagctagcc
gtaaagatcctgaatCTCGAGattggtgccttgcttggattatgaaatgccagcctgatcatacaacgttggacgaagtagctttaccgtccacacggtcggaacttggtgtgccgaatccaAGTCGAGATAATCACta
gatgtcctgaGGtgcAtactagtagcggccgctgcagtccggcaaaaaagggcaaggtgtcaccaccctgcccttttttcttaaaaccgaaaagattacttcgcgttatgcaggcttcctcgctcactgactcgctgcgctcggt
cgttcggctgcggcgagcggtatcagctcactcaaaggcggtaat

pSB4A5-AD047, https://benchling.com/s/seq-HKWYujGsFRtkhUCMxqWr

pTetO, LuxR, AAV degtag, YPet, pLux76, LuxI

tgccacctgacgtctaagaaaaggaatattcagcaatttgcccgtgccgaagaaaggcccacccgtgaaggtgagccagtgagttgattgctacgtaattagttagttagcccttagtgactcgaattcTCCCTATCAGTG
ATAGAGATTGACATCCCTATCAGTGATAGAGATACTGAGCACAAGCTTAGGGTGTCTCAAGGTGGCCGCACTATGTTTTTCAAAGACGAAAAACTACTAGATGAAG
AACATTAATGCTGATGATACATATCGCATTATTAACAAGATCAAGGCCTGCCGTTCCAACAACGATATTAATCAATGTTTGAGCGACATGACGAAGATGGTCCATTG
TGAATACTACCTGCTGGCGATCATTTACCCACATTCGATGGTGAAATCCGACATCAGTATTCTGGACAACTACCCCAAGAAATGGCGTCAGTATTATGACGATGCG
AATCTGATCAAATATGACCCCATTGTAGACTATAGCAATAGCAACCATTCTCCGATTAACTGGAACATCTTTGAAAATAATGCAGTTAACAAGAAGAGTCCGAATGT
AATCAAGGAAGCAAAAACATCAGGCTTAATCACTGGATTCTCCTTCCCGATCCACACAGCCAACAACGGGTTTGGAATGTTGTCTTTCGCACACAGTGAAAAGGA
TAATTACATTGATAGTCTTTTCCTGCACGCGTGCATGAATATTCCACTGATCGTGCCTAGTTTGGTAGACAATTACCGCAAGATTAATATTGCTAACAACAAATCTAA
CAACGACCTGACGAAACGCGAAAAAGAGTGCCTTGCGTGGGCATGTGAAGGCAAGTCCTCCTGGGATATTTCGAAAATCTTAGGTTGCTCTGAGCGCACTGTGA
CCTTCCATCTTACGAACGCTCAAATGAAGTTAAATACCACCAACCGTTGCCAGTCAATCAGTAAGGCCATCCTGACTGGAGCTATCGACTGCCCATATTTCAAGAA
CCGTCCCGCTGCTAATGACGAGAACTATGCTGCGGCTGTCTGATAACTCGAGTTCAGCCAAAAAACTTAAGACCGCCGGTCTTGTCCACTACCTTGCAGTAATGC
GGTGGACAGGATCGGCGGTTTTCTTTTCTCTTCTCAACCATGGTCCCTATCAGTGATAGAGATTGACATCCCTATCAGTGATAGAGATACTGAGCACATCCATAGC
TGTCACCGGATTCTAGActatggactatgtttgaaagggagaaatactagATGTCAAAGGGAGAAGAATTGTTCACGGGAGTTGTACCCATCTTAGTAGAATTGGACGGAGACGG
TCAATGGACACAAGTTCTCCGTTTCGGGAGAGGGGGAGGGGGATGCGACGTATGGTAAATTGACGCTGAAGCTGTTATGTACCACCGGTAAGTTGCCTGTCCCT
TGGCCCACATTAGTAACAACCCTGGGGTACGGCGTGCAATGCTTCGCGCGTTATCCTGACCATATGAAGCAACATGACTTCTTTAAGTCTGCCATGCCTGAAGGA
TATGTTCAAGAGCGCACGATTTTTTTTAAAGATGATGGGAATTATAAAACTCGTGCAGAAGTGAAATTTGAGGGCGACACATTAGTGAACCGCATCGAATTAAAAG
GAATCGACTTTAAAGAAGATGGAAACATTTTGGGGCACAAATTGGAGTACAATTATAACAGCCATAACGTCTATATCACAGCGGATAAGCAGAAGAATGGCATCAA
AGCGAATTTTAAGATTCGTCACAATATTGAAGATGGGGGAGTTCAACTGGCGGACCATTATCAACAAAATACACCGATCGGTGACGGACCGGTGTTGTTGCCGGA
CAACCACTATTTATCATATCAGAGCGCGTTATTTAAGGACCCGAACGAGAAGCGTGACCACATGGTCCTGTTGGAATTTCTGACAGCCGCTGGTATTACTGAGGG
TATGAATGAGCTTTACAAACGTCCTGCTGCGAACGACGAAAATTATGCGGCTGCGGTTTGATAAGGAAACACAGAAAAAAGCCCGCACCTGACAGTGCGGGCTT
TTTTTTTCGACCAAAGGTTAATTAAACCTGTAGGATCGTACAAGTTTACGCAAGAAAATGGTTTGTTATAGTCGAATAAACCTAGGCCCCCCGAGGAGTAGCACAT
GACAATTATGATTAAGAAGAGCGATTTCTTAGCAATCCCCTCCGAGGAATATAAAGGCATCCTGTCTCTTCGCTACCAGGTGTTCAAACAGCGTCTGGAATGGGAT
TTAGTGGTTGAAAATAATTTGGAATCCGAGATACGATAACAGCAACGCTGAGTATATTTATGCCTGCGACGATACAGAAAACGTCAGTGGATGCTGGCGCCTG
CTGCCCACAACCGGTGATTATATGTTGAAGTCAGTATTCCCCGAGCTTCTGGGGCAGCAGTCGGCGCCCAAAGATCCTAACATCGTTGAATTGAGTCGTTTTGCT
GTTGGCAAGAACTCCTCTAAAATCAATAATTCCGCAAGTGAGATCACGATGAAACTGTTTGAAGCTATCTATAAGCATGCAGTAAGTCAAGGGATCACGGAGTACG
TCACGGTCACGTCTACCGCAATTGAACGCTTCTTGAAACGTATCAAAGTTCCCTGCCACCGCATCGGAGATAAGGAAATTCACGTACTGGGCGATACTAAGTCCG
TGGTCCTTTCGATGCCAATCAACGAGCAATTCAAAAAAGCTGTCTTAAATTGATAATCCGGCAATTAAAAAAGCGGCTAACCACGCCGCTTTTTTTACGTCTGCAct
gcaggagtcactaagggttagttagtagattagcagaaagtcaaaagcctccgaccggaggcttttgactaaaacttccctgggggttatcattggggctcactcaaaggcggtaat

pSB4A5-AD048, https://benchling.com/s/seq-UgkjoZpizkJ2GJjBpnCZ

pLacO, LasR, AAV degtag, mScarletI, pLas81, LasI

tgccacctgacgtctaagaaaaggaatattcagcaatttgcccgtgccgaagaaaggcccacccgtgaaggtgagccagtgagttgattgctacgtaattagttagttagcccttagtgactcgaattcAATTGTGAGCGG
ATAACAATTGACATTGTGAGCGGATAACAAGATACTGAGCACAAGCTTAGGGTGTCTCAAGGTGGCCGCACTATGTTTTTCAAAGACGAAAAACTACTAGATGGC

CCTGGTAGACGGCTTCTTGGAATTAGAACGTTCTAGTGGCAAGTTGGAGTGGTCGGCAATCTTGCAAAAAATGGCTTCTGACTTAGGCTTCTCCAAGATTCTGTTT
GGTTTGTTACCGAAGGATTCACAGGATTACGAAAACGCATTCATCGTCGGGAATTATCCAGCCGCGTGGCGCGAACACTACGATCGCGCTGGGTATGCGCGCG
TTGATCCTACCGTGTCGCATTGCACTCAGTCTGTTCTTCCCATTTTTTGGGAACCCTCAATCTACCAGACCCGCAAGCAACATGAGTTCTTTGAGGAAGCCTCGG
CCGCGGGGCTTGTGTATGGCCTTACGATGCCACTTCATGGTGCCCGTGGGGAATTGGGAGCACTGTCGCTTTCAGTCGAAGCCGAAAACCGCGCTGAGGCCAA
CCGTTTTATTGAGAGCGTCCTTCCAACTTTATGGATGTTGAAGGACTATGCCCTTCAATCTGGGGCTGGGTTGGCCTTTGAGCACCCTGTTTCTAAACCAGTAGTT
CTTACTTCACGCGAGAAGGAAGTCTTGCAATGGTGTGCTATTGGAAAGACCTCCTGGGAAATCAGCGTCATTTGCAACTGTTCGGAAGCAAATGTAAATTTTCATA
TGGGGAACATCCGTCGCAAATTTGGGGTGACGTCCCGTCGTGTCGCAGCCATCATGGCAGTCAATCTTGGTCTTATCACCTTACGTCCCGCTGCTAATGACGAG
AACTATGCTGCGGCTGTCTGATAACTCGAGTTCAGCCAAAAAACTTAAGACCGCCGGTCTTGTCCACTACCTTGCAGTAATGCGGTGGACAGGATCGGCGGTTTT
CTTTTCTCTTCTCAATTAATTAAAATTGTGAGCGGATAACAATTGACATTGTGAGCGGATAACAAGATACTGAGCACAATCCATAGCTGTCACCGGATTCTAGActatg
gactatgtttgaaagggagaaatactagATGGTGTCAAAGGGAGAGGCGGTTATCAAGGAATTTATGCGCTTTAAAGTCCACATGGAGGGCAGCATGAACGGGCACGAGTTT
GAAATTGAGGGGGAGGGGGAGGGCCGTCCTTATGAAGGTACTCAGACTGCTAAACTGAAGGTGACAAAAGGTGGCCCCTTGCCTTTCTCGTGGGACATCCTGT
CGCCACAATTCATGTACGGGAGCCGCGCCTTTATCAAACATCCCGCAGATATTCCTGATTACTATAAACAATCTTTCCCGGAAGGTTTCAAATGGGAACGCGTCAT
GAATTTTGAGGACGGGGGCGCTGTCACAGTTACTCAGGACACCTCCTTGGAAGACGGCACATTGATTTACAAGGTTAAGTTGCGCGGCACAAACTTCCCCCCTG
ACGGGCCAGTAATGCAAAAGAAAACTATGGGTTGGGAGGCGTCTACAGAACGTTTATACCCCGAAGACGGGGTGCTGAAAGGTGACATTAAGATGGCCCTGCG
CCTGAAGGACGGCGGTCGCTATCTTGCCGACTTTAAAACTACTTATAAGGCTAAAAAACCAGTCCAGATGCCAGGCGCCTATAATGTTGACCGCAAGTTAGACAT
CACCTCACATAATGAAGACTATACCGTTGTAGAACAATACGAGCGCAGCGAGGGTCGTCACAGTACCGGGGGGATGGATGAATTATACAAACGTCCTGCTGCGA
ACGACGAAAATTATGCGGCTGCGGTTTGATAAGGAAACACAGAAAAAAGCCCGCACCTGACAGTGCGGGCTTTTTTTTTCGACCAAAGGTTAATTAAACCTATAG
GATCGTATAGGTTTACGCAAGAAAATGGTTTGTTATAGTCGAATAAACCTAGGCCCCCCGAGGAGTAGCACATGATTGTGCAAATCGGCCGCCGTGAGGAGTTC
GATAAAAAGCTGCTTGGGGAAATGCATAAACTTCGTGCTCAGGTGTTCAAGGAGCGTAAGGGGTGGGATGTTTCCGTTATTGACGAAATGGAAATTGATGGGTAC
GATGCATTATCACCTTACTATATGCTGATTCAAGAAGACACACCTGAGGCCCAGGTATTCGGTTGCTGGCGCATTTTTGACACGACGGGGCCTTACATGTTGAAG
AACACGTTTCCTGAATTGTTACACGGCAAAGAAGCTCCCTGCTCACCCCATATTTGGGAACTGAGCCGTTTCGCTATCAATTCCGGTCAAAAGGGCTCCCTGGGC
TTTTCGGACTGCACCCTTGAAGCCATGCGCGCACTTGCCCGTTACTCCCTGCAAAACGACATTCAAACCTTAGTTACTGTTACTACCGTTGGCGTAGAGAAGATG
ATGATCCGTGCGGGTCTTGACGTATCTCGCTTTGGACCGCATCTGAAGATTGGAATCGAGCGTGCGGTGGCGTTGCGCATCGAATTGAACGCAAAAACGCAAAT
TGCGTTATACGGCGGGGTCTTGGTTGAACAGCGTTTAGCCGTGAGTTGATAATCCGGCAATTAAAAAAGCGGCTAACCACGCCGCTTTTTTTACGTCTGCActgcag
gagtcactaagggttagttagttagattagcagaaagtcaaaagcctccgaccggaggcttttgactaaaacttcccttggggttatcattggggctcactcaaaggcggtaat

Acknowledgments

I would like to thank those who have made possible this thesis, this adventure and this journey.

First, I want to thank Fritz Simmel for giving me the opportunity to do this thesis, to come to Munich, and to become a synthetic biologist. I found the freedom I was looking for while being challenged enough to grow as a scientist. I was inspired not only by the science done in the lab, but by the approach and the philosophy in which this science is done.

A big thank you to Susanne and Helene for being constant facilitators, making administrative and lab tasks seem much simpler than they actually are. Thank you to Andrea and to Korbinian for teaching so patiently when I joined.

Thank you to the GRK2062, which was the best graduate school I could have hoped for and brought me much more than the appreciated travelling and research funds. Thank you to Kirsten Jung for her advice and support, which every time gave me a boost of motivation. Thank you to Beate for always being available and offering us many opportunities by organizing seminars, conferences and workshops. Thank you to all the students of the GRK for the fun and fascinating meetings and the enriching conversations, particularly Karsten, Mona, Martin and Philipp.

Thanks to the CANTER lab guys, particularly to Sascha, for being such enthusiastic collaborators, it was always fun to work with you.

Thank you to all my students, from Berta to Ariane: Ludwig, Igor, Benedikt, Dawa, and everyone else. Your talent and creativity amazed me, and you showed me how rewarding it is to work with good people. You taught me more than you know about research and about myself. Thank you to the 2017 iGEM team for this incredible adventure.

Thank you to all the E14 lab, for being a beehive of interesting and passionate people. A particular thanks to Daniela, Aradhana, Ali and Swati, for all the discussions, all the advice, all the laughs. You were there in the bad times and the good. Thank you

for always making me feel like I could do it.

Thank you to Dr. Leonora Henault-Mezaize for being an amazing supervisor, working with you made me want to do a PhD. Thank you to Prof. Jean Gayon, for treating me on an equal footing, and inspiring my research interests. You were an exceptional professor.

Pauline, Mélissa, you don't know how many evenings I wanted to teleport to Paris and meet you for a beer. I missed living in the same city as you all these five years. Thank you for your down-to-earth advices when I needed them.

Thank you Matthaeus for your never-ending support and trust during this crazy rollercoaster ride.

À Antoine - j'aurai bien aimé que tu lises cette thèse.

My biggest thanks must go to my parents Laure et Jean-Charles. Thank you for always setting me on the right track without pushing me, thank you for making me travel from such a young age, for giving me values and a solid foundation. Thank you to my sisters, Clairelyne et Anne-Louise, for listening to me when I needed to talk, for your kindness. Your advice got me un-stuck. Thank you to all four of you - home is wherever we are together.

I must also thank all the podcasts - particularly Hidden Brain - that informed me about a variety of fascinating topics and accompanied long hours in the lab.

» Que pour examiner la vérité, il est besoin, une fois dans sa vie,
de mettre toutes choses en doute autant qu'il se peut. «

» If you would be a real seeker after truth, it is necessary
that at least once in your life you doubt, as far as possible, all things. «

– René Descartes, Les Principes de la philosophie, 1644

The cover image is an artistic representation of the artificial multicellular assemblies,
and is the work of Jürgen Gawron from the grafikcafé, Munich.